

Quantum Theory of Solids

Edited by I. M. LIFSHITS

Advances
in
Science
and
Technology
in
the USSR

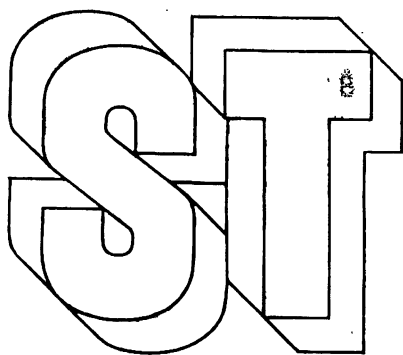


Physics Series

Mir Publishers
Moscow

Advances
in
Science
and
Technology
in
the USSR

Physics Series



Quantum Theory of Solids

Edited by
I. M. Lifshits
Mem. USSR Acad. Sc.

MIR Publishers
Moscow

Квантовая теория твёрдого тела
Под редакцией акад. И. М. Лифшица
Издательство «Мир» Москва

TO THE READER

Mir Publishers would be grateful for your comments on the content, translation and design of this book.

We would also be pleased to receive any other suggestions you may wish to make.

Our address is:

Mir Publishers,
2 Pervy Rizhsky Pereulok,
I-110, GSP, Moscow, 129820, USSR.

First published 1982

На английском языке

© Издательство «Мир», 1982

© English translation, Mir Publishers, 1982

Printed in the Union of Soviet Socialist Republics

FOREWORD

Academician I. M. Lifshits

S. I. Vavilov Institute of Physical Problems,
Academy of Sciences of the USSR

The basic problems of solid-state physics are connected with the quantum nature of solids. A number of new remarkable phenomena and properties of matter have been explained and predicted by developing the ideas and methods of the quantum theory of solid state. Although the scope of problems in this field is extremely broad, the inner logic of the development of the theory makes it possible to find unexpected links between what would seem to be rather distant phenomena and build on this basis a new approach to solving a wide spectrum of problems. This refers to most interesting problems concerning new states of matter, to the fluctuation theory of phase transitions, and to the problem of localization of quasiparticles in disordered systems.

The present compilation includes four articles on various topics, each of which contains an exposition of the present state of art in the most interesting and timely problems of solid-state theory. The authors are physicists who have contributed significantly to this field of science.

The paper by A. F. Andreev deals with a new state of matter, quantum crystals. In a certain sense this state stands between classical crystals and quantum liquids: the system possesses translation symmetry (an ordinary crystal) and has zero static shear moduli (a liquid). Mass transport in such systems is due to special quasiparticles, delocalized imperfections (vacancies or impurities), and may be similar to a superfluid motion of an impuriton liquid. The peculiar properties of such systems (mainly solid ^3He and solid ^4He and their solutions) are at present intensely studied both theoretically and experimentally. These properties are the manifestations of quantum laws of motion on the atomic-molecular level instead of the electronic level.

The other three papers are devoted to the study of electronic properties of solids. The work of D. I. Khomskii deals with the connection between electronic phase transitions and the problem of mixed (nonintegral) valence in rare-earth compounds. Electronic phase transitions in such systems possess special properties, since the problem of mixed valence is related to other fundamental problems of the electron theory of solids, namely, the localization of electrons, the metal-insulator transition, or the magnetic-nonmagnetic transitions.

The paper of B. L. Altshuler, A. G. Aronov, D. E. Khmel'nitskii, and A. I. Larkin is devoted to coherent effects in disordered conductors. This problem is one of the most difficult and not yet completely solved problems in the theory of disordered systems, namely, the theory of localization of electrons and the behavior of transport characteristics of electrons near the mobility boundary (the boundary between localized and delocalized states). In a narrower approach, coherent effects are quantum corrections due to the addition of amplitudes of multiply scattered particles in comparison to the classical theory of transport. These corrections grow with λ/l , where λ is the electron wavelength, and l the mean free path. For example, in the electron-electron interaction the transition to the superconducting state constitutes a strongly coherent effect, while production of virtual Cooper pairs constitutes one of the mechanisms of coherent corrections in normal metals. The article analyzes from a unified position the role that coherent effects play in disordered metals. In addition, the same approach is used to examine the problem of electron localization in such systems, for one, localization in magnetic field and in a percolation structure.

The last article, by P. B. Wiegmann, stands apart from the first three. It is devoted not to development of a new field but, rather, contains for the first time a full and exact solution to a problem that was formulated and studied in a great number of works but which did not as yet have any consistent solution. This is the solution of the so-called Kondo problem, which studies the effect of magnetic impurities on the transport and thermodynamic characteristics of nonmagnetic metals. The mathematical beauty of the method which enabled the author to solve a problem that did not yield to the efforts of many theoreticians, and the fact that the problem is interesting in itself explains the reason for including this article.

It goes without saying that the selection of material to illustrate the achievements in solid-state physics must inevitably be subjective. For one, the compilation does not hold works on superconductivity, a problem to which a separate book could be devoted. But we still believe that the articles should be of interest to readers who wish to know what is new in solid-state physics.

Moscow
February, 1982

Academician I. M. Lifshits

CONTENTS

Foreword 5

1	DEFECTS AND SURFACE PHENOMENA IN QUANTUM CRYSTALS BY A. F. ANDREEV (<i>transl. by E. Yankovsky</i>)	11
1.1	Introduction	11
1.2	Quantum Effects in Crystals	11
1.3	Impurity Quasiparticles: Impuritons	14
1.3.1	Diffusion in an Impuriton Gas	14
1.3.2	Diffusion of Strongly Interacting Impuritons	17
1.3.3	Phonon-Impuriton Interaction	20
1.3.4	One- and Two-Dimensional Impuritons	24
1.4	Vacancies	32
1.4.1	Vacancies in ^4He Crystals	32
1.4.2	Zero-Point Vacancies	37
1.4.3	Vacancies in ^3He Crystals	40
1.5	Surface Phenomena	42
1.5.1	The Equilibrium Shape of the Crystal-Liquid Interface	42
1.5.2	Crystallization and Melting	48
1.5.3	Crystallization Waves	51
1.6	Faceting Transitions in Crystals	55
1.6.1	The Role of Fluctuations	55
1.6.2	Thermodynamic Relations	58
1.6.3	A 6-fold Symmetry Axis	60
1.6.4	A 4-fold Symmetry Axis	61
1.7	Delocalization of Dislocations	64
	References	66
2	ELECTRONIC PHASE TRANSITIONS AND THE PROBLEM OF MIXED VALENCE BY D. I. KHOMSKII (<i>transl. by E. Yankovsky</i>)	70
2.1	Introduction	70
2.2	Localization of Electrons and Insulator-Metal Transitions (Mott-Hubbard Transitions)	72
2.3	Electronic Phase Transitions in Rare-Earth Compounds	75
2.3.1	The General Picture of Transitions	75

2.3.2	Theoretical Models for Describing Electronic Phase Transitions and MV States 77
2.4	Valence Transitions in the Falicov-Kimball Model 80
2.4.1	The Mean-Field Approximation 80
2.4.2	Beyond the Mean-Field Approximation. The Role of Local (Excitonic) Correlations 84
2.4.3	The Two-Level Model 87
2.4.4	The Periodic Model 89
2.5	The Electron-Lattice Interaction and Its Role in Transitions 91
2.5.1	Interaction with a Homogeneous Strain 91
2.5.2	The Change in the Width of the f Level and Its Role in Valence Transitions 97
2.5.3	Local (Polaron) Effects in the Electron-Lattice Interaction 99
2.5.4	Interaction via Short-Wavelength Phonons and Formation of Ordered Structures 102
2.6	Mixed-Valence States: The Basic Problems 105
2.6.1	Properties of Mixed-Valence States. The Experimental Situation and Statement of the Problem 106
2.6.2	The Anderson and Kondo Lattices 109
2.6.3	The Valence Transition and the Mott-Hubbard Transition 114
2.6.4	Excitonic Correlations in an MV Phase 117
2.6.5	Spatial Correlations in MV Systems 119
2.6.6	Systems with MV as a Model of Condensed Matter 121
2.7	Conclusion 123
	References 126
3	COHERENT EFFECTS IN DISORDERED CONDUCTORS BY B. L. ALTSHULER, A. G. ARONOV, D. E. KHMELNITSKII AND A. I. LARKIN (transl. by E. Kaminskaya) 130
3.1	Introduction 130
3.2	Quantum Corrections to Conductivity of Noninteracting Electrons 131
3.2.1	Conductivity and Impurity Diagrammatic Technique 131
3.2.2	Cooperon and Quantum Correction to Conductivity 134
3.2.3	Effects of Spin Scattering 137
3.2.4	Properties of Samples of Finite Dimensions. Effective Space Dimensionality 142
3.3	Quantum Effects in High-Frequency Electromagnetic Field 144
3.3.1	Effects of High-Frequency Field on Quantum Corrections to Conductivity 144
3.3.2	Suppression of Coherent Effects by Electromagnetic Fluctuations 146
3.4	Electron-Electron Interaction in Disordered Metallic Systems 151

3.4.1	Electron-Electron Collision Time	151
3.4.2	Effects of Electron-Electron Correlations on the Density of One-Particle States	160
3.4.3	Conductivity of Interacting Electrons	170
3.4.4	Superconducting Fluctuations and Temperature Dependence of Conductivity	176
3.5	Temperature Dependence of Conductivity: Experiment	179
3.6	Hall Effect	187
3.6.1	Introduction	187
3.6.2	Hall Effect for Noninteracting Electrons	188
3.6.3	Hall Effect for Interacting Electrons	189
3.7	Anomalous Magnetoresistance	191
3.7.1	Magnetoresistance of Noninteracting Electrons	191
3.7.2	Magnetoresistance of Thin Films and Wires in Longitudinal Magnetic Field	194
3.7.3	Magnetoresistance and Scattering by Superconducting Fluctuations	196
3.7.4	Magnetoresistance in Many-Valley Semiconductors	197
3.7.5	Effects of Spin-Orbit Scattering on Magnetoconductivity	199
3.7.6	Experiment	202
3.7.7	Aharonov-Bohm Effect in Disordered Metals	206
3.7.8	Effects of Electron-Electron Interaction in Magnetic Field	208
3.8	Electron Localization in Random Potential	213
3.8.1	Analogy Between Electron Properties in Disordered Systems and Statistical Mechanics of Ferromagnets	213
3.8.2	Q-Hamiltonian	214
3.8.3	Renormalization Group Equation	216
3.8.4	Conductivity in Two Dimensions	217
3.8.5	Localization in One and Three Dimensions	219
3.8.6	Localization in Magnetic Field	222
3.8.7	Localization in Percolating Structures	223
3.9	Conclusion	225
3.A	Appendices	226
3.A.1	Cooperon-Current Relation in the Space-Time Representation	226
3.A.2	Cooperon in External Electromagnetic Field	229
3.A.3	Calculation of Path Integrals	230
3.A.4	Expression for Conductivity of Interacting Electrons	232
	References	235

4	AN EXACT SOLUTION OF THE KONDO PROBLEM BY P.B. WIEGMANN (<i>transl. by E. Yankovsky</i>)	238
4.1	Introduction	238
4.2	The Basic Models	244
4.2.1	The Anderson Model	245

4.2.2	The Angular Dependence of Hybridization Amplitudes. A One-Dimensional Hamiltonian	246
4.2.3	Hierarchy of Energies	247
4.2.4	Exchange Hamiltonians	248
4.2.5	The Simple Exchange Hamiltonians	250
4.2.6	Perturbation Theory	254
4.3	Bethe's Method	257
4.3.1	General Survey. The Factorization Equations	257
4.3.2	An Effective Hamiltonian	263
4.3.3	The Bethe Ansatz for the s-d Exchange Model	264
4.3.4	Periodic Boundary Conditions	269
4.3.5	The Set of Commuting Operators	269
4.3.6	Diagonalizing $T(\alpha)$	272
4.3.7	Discussion	275
4.4	The Thermodynamics of the s-d Exchange Model	277
4.4.1	Bethe's Equations for the s-d Exchange Model. Going Over to the Continuous Limit	277
4.4.2	The Equilibrium Distribution	282
4.4.3	The Free Electron Gas ($g \rightarrow 0$ or $S = 0$)	284
4.4.4	Universality	287
4.4.5	The Limits of Strong and Weak Coupling	288
4.4.6	The Thermodynamics of an Impurity	290
4.4.7	Magnetic Susceptibility at $T = 0$ [30, 32, 33]	293
4.4.8	Solution of Equations (4.4.35) and (4.4.36) by an Iterative Method at $T \gg H$ [36, 38] and Perturbation Theory	297
4.4.9	Supplementary Discussion	300
4.5	Solution for the n-fold Degenerate Exchange Model	301
4.5.1	The Bethe Ansatz	301
4.5.2	Magnetic Susceptibility at $T = 0$	303
4.5.3	Thermodynamics	306
4.5.4	Discussion	308
4.6	Conclusion	308
	References	311

Defects and Surface Phenomena in Quantum Crystals

*A. F. Andreev, Corresponding Member
of the USSR Academy of Sciences*

S. I. Vavilov Institute of Physical Problems,
Academy of Sciences of the USSR

1.1. INTRODUCTION

The usual quantum theory of solids is based on the assumption that the crystal lattice is a quasiclassical object. On the one hand, the quantum effects accounted for in this theory play an important role in the behavior of the phonons of the crystal, namely at temperatures below the Debye temperature. On the other hand, the particles that comprise the crystal are considered localized near definite equilibrium positions. The latter property is of a purely classical nature. Indeed, in this case the identical particles comprising the crystal become distinguishable because they belong to different lattice sites. But quantum mechanics states that identical particles must be indistinguishable. Although due to this fact the quasiclassical picture of the crystal is an approximation, its accuracy is high for the majority of crystals and considerably exceeds the possibilities of experimental techniques. A quantitative criterion is the smallness of the ratio of the amplitude of zero-point vibrations in the majority of crystals to the lattice period.

There is a small group of so-called quantum crystals (solid helium being the most striking example) in which the amplitude of the zero-point motion is exceptionally large and, in fact, is only several-fold smaller than the lattice period. The anomalies in the properties of quantum crystals are the consequence of this fact because even at absolute zero the vibrational energy of the particles is of the order of the total energy of the crystal and the vibrations are markedly anharmonic. For the same reason the usual approach to calculating such properties of the quantum crystal as the ground-state energy, compressibility, and phonon spectrum is inapplicable. To describe these properties self-consistent methods of accounting for the zero-point motion were developed (see the review article by Guyer [1]), and the results were in accord with the experimental data, at least qualitatively. However, there is a completely new effect associated with a new aspect in the motion of the constituent particles. Because of the large amplitude of zero-point vibrations in quantum crystals there is a high probability of the tunneling of the particles to neighboring sites. In this way translational motion is imposed on the vibrational motion. As a result there emerges a picture of indistin-

guishable (in the quantum mechanical sense) particles delocalized in the crystal lattice, similar to that in quantum liquids.

The present paper is a review of properties of quantum crystals in which the quantum delocalization of the particles manifests itself. Recent years have seen results achieved by both theoretical and experimental investigations that undoubtedly indicate that here we are dealing with objects very different from ordinary crystals.

1.2 QUANTUM EFFECTS IN CRYSTALS

We will start by reviewing the quantitative role of quantum effects in crystals and establishing the type of crystal in which the deviations from the quasiclassical theory are the greatest. As mentioned above, the relative magnitude of the quantum effects is determined by the dimensionless parameter $\Lambda \sim \bar{u}_0^2/a^2$, with \bar{u}_0^2 the mean-square amplitude of zero-point vibrations, and a the lattice period. We can easily express Λ in terms of the characteristics of the constituent particles if we estimate the amplitude of zero-point motion by the well-known formula $\bar{u}_0^2 \sim \hbar/m\omega$, where m is the particle mass, $\omega \sim (\kappa/m)^{1/2}$ the vibration frequency, and κ the effective stiffness of the "spring" that holds the particle in the equilibrium position. The stiffness κ is determined from the condition that when the particle is displaced from equilibrium by a distance of the order of the lattice period, the change in the potential energy, κa^2 , is of the order of the characteristic interaction energy U of the particles, i.e. $\kappa \sim U/a^2$. This yields $\Lambda \sim (\hbar/a)(mU)^{-1/2}$, which is known as the quantum de Boer parameter [2]. This parameter is maximal for weakly interacting and light particles. The greatest value of Λ is achieved for crystals of ^3He ($\Lambda \approx 0.5$), ^4He ($\Lambda \approx 0.4$), hydrogen ($\Lambda \approx 0.3$), and neon ($\Lambda \approx 0.1$). For all other crystals whose constituent particles are of one type, Λ is very small. However, in some important cases the quantum effects are significant for only a fraction of the constituent particles. This is the case for a solution of hydrogen in lattices of some heavy metals (niobium or zirconium). Because of the small mass of hydrogen and the weakness of its interaction with the matrix atoms, its motion in the lattice is not described by the small parameter Λ , though the matrix atoms behave in a classical manner.

How does Λ depend on pressure? We know that the interaction U between neighboring particles in crystals depends on their separation. As pressure grows, the lattice period a decreases and U increases. The de Boer parameter Λ either increases or decreases depending on the behavior of Ua^2 . Since as a decreases, the interaction energy of electrically neutral particles increases much faster than $1/a^2$, the parameter Λ decreases as the pressure grows. For this reason the quantum effects manifest themselves most strongly at low pressures.

The applicability of the quasiclassical picture of a crystal is restricted by the tunneling of particles to the neighboring lattice sites. A rough estimate of the probability of such processes occurring can be obtained if we note that the probability is that of finding a particle at a distance $u \sim a$ from the equilibrium position. At low temperatures, where zero-point motion plays the main role, the probabilities of various values of u are determined by the squared

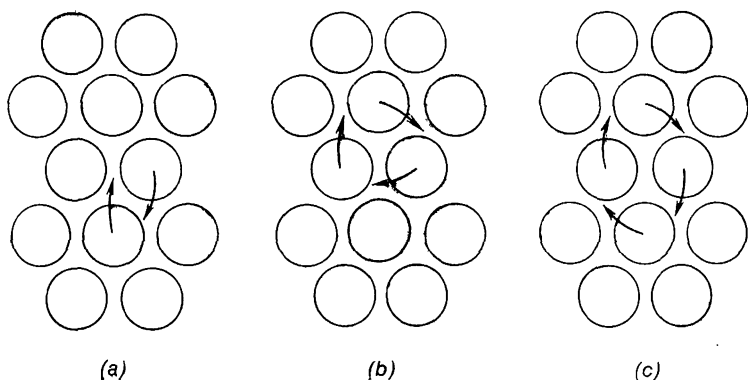


Fig. 1.1. Tunneling permutations of (a) two, (b) three, and (c) four particles in a crystal.

modulus of the wave function of the oscillator ground state and obey the Gaussian law $w(u) \propto \exp(-u^2/2\bar{u}_0^2)$. Therefore, the tunneling probability is proportional to an exponentially small quantity $\exp(-\Lambda^{-1})$. We can say that there are two kinds of quantum effects in crystals. Zero-point vibrations, their contribution to the crystal energy, and the anharmonicity of these vibrations are proportional to some power of the de Boer parameter. These effects do not lead to a delocalization of the particles and do not destroy the quasiclassical picture of the crystal. Delocalization is an exponentially small quantum effect and can therefore be observed only in quantum crystals, in which $\Lambda \sim 1$.

Since the tunneling probability is exponentially low, its actual calculation poses a serious problem [3-9], which as yet has not been solved. In the simplest case we are dealing with a tunneling process in which two neighboring particles change places (Fig. 1.1a). In sufficiently closely packed crystal lattices, such as the hcp and bcc lattices of solid helium, this process is hindered by the lack of sufficient free space. Hence multiparticle tunneling processes are more probable [3, 7, 9-13], since cyclic permutation of three (Fig. 1.1b) or four (Fig. 1.1c) particles requires less free space. An increase in the

number of interacting particles obviously decreases the probability of the process. But in fact there is no increase in the number of particles here since when two particles change places (Fig. 1.1a), the other particles are much disturbed because of the lack of sufficient free space.

If the crystal consists of particles of one type, say solid ^4He , the aforementioned tunneling processes are not observed directly because they reduce to permutations of identical particles. Delocalization of the particles results in new observable phenomena if the tunneling particles differ from each other in some respect. Depending on the nature of this difference there are two types of phenomena associated with particle delocalization in quantum crystals. In the first case, realized in pure ^3He , the constituent particles are of one type but possess nonzero nuclear spin and may differ in the projections of this spin on an axis. Particle delocalization manifests itself here in direct exchange interaction between the nuclear spins, as a result of which crystals of solid ^3He possess nuclear magnetism (see [14-30]). In the second case, which constitutes the topic of this article, delocalization is associated with the behavior of impurities and, in general, any point defects on the surface and in the bulk of the crystal. In pure form this is observed in crystalline ^4He , while in ^3He the situation is more complex because both types of phenomena prove to be closely linked.

1.3 IMPURITY QUASIPARTICLES: IMPURITONS

1.3.1 Diffusion in an Impuriton Gas

A direct method of observing delocalization in a crystal is in the following. Let us consider a crystal of solid ^4He containing a single impurity atom of ^3He . Thanks to the tunneling processes discussed in the previous section, this ^3He atom can move through the lattice and change place with a ^4He atom. Since the crystal of ^4He is absolutely periodic, the states of the impurity atom at absolute zero are described by the values of the quasimomentum \mathbf{p} . The energy $E(\mathbf{p})$ of the system is a periodic function of the quasimomentum. The situation is similar to that for the well-known case of electrons in a metal. The impurity atoms behave like quasiparticles—impuritons [31], or mass fluctuation waves [32]—that move freely through the crystal with a constant velocity. Impuritons are characterized by the width Δ of their energy band or the tunneling frequency Δ/\hbar . Since here the tunneling processes are essentially the same processes that in pure ^3He determine the characteristic frequency $1/\tau_s$ of spin-flip under exchange interaction (see the review [18]), we can obtain a qualitative estimate of the band width by assuming that Δ/\hbar is of the order of the spin-jump frequency. This yields $\Delta \sim \hbar/\tau_s \sim 10^{-4}$ K.

Of course, this estimate was obtained without due regard for the difference between the ^3He matrix and the ^4He matrix; in particular, we ignored the fact that at low pressure solid ^3He has a bcc structure while ^4He has an hcp structure. The characteristic velocity of an impuriton is $v \sim \partial E / \partial p \sim a v_s \sim 10^{-1} \text{ cm} \cdot \text{sec}^{-1}$. It must be noted that the band width Δ and the impuriton velocity v are considerably smaller than all other energies and velocities in the crystal. Below we will see that this fact explains a number of peculiarities in the dynamics of impuritons.

At low concentrations the ^3He impurity atoms constitute a rarefied gas of impuritons. Therefore, the above simple reasoning enables us to draw an important conclusion about the diffusion of impurities in quantum crystals [31]. Namely, there must exist a so-called quantum diffusion similar to the diffusion of particles in gases. To calculate the diffusion coefficient D , we can use the formula of the kinetic theory of gases $D \sim vl$, with l the mean free path of the impuritons. At low temperatures the phonons may be neglected and impuriton-impuriton scattering plays the main role. The mean free path is $l \sim (n\sigma)^{-1} \sim a^3/\sigma x$, where n is the number of impurities per unit volume, $x \sim na^3$ the concentration, and σ the impuriton-impuriton scattering cross section. As a result the diffusion coefficient

$$D \sim \frac{\Delta a^4}{\hbar x \sigma} \quad (1.3.1)$$

is inversely proportional to concentration and does not depend on temperature [33-44].

It is important to note that the scattering cross section in (1.3.1) differs considerably from the square of the atomic separation, or a^2 . This discrepancy can be explained by the special features of the impuriton dynamics, which in turn are caused by the small width of their energy band. Indeed, let us consider the scattering of an impuriton on another impuriton. The total energy of the system is

$$E_{12} = E(\mathbf{p}_1) + E(\mathbf{p}_2) + U(\mathbf{r}_{12}), \quad (1.3.2)$$

where \mathbf{p}_1 and \mathbf{p}_2 are the quasimomenta of the impuritons, $E(\mathbf{p})$ is the energy of an isolated impuriton as a function of the respective quasimomentum, and $U(\mathbf{r}_{12})$ is the interaction energy of the two impuritons ($\mathbf{r}_{12} = \mathbf{r}_1 - \mathbf{r}_2$; \mathbf{r}_1 and \mathbf{r}_2 are the position vectors of the two impuritons). The sum $E(\mathbf{p}_1) + E(\mathbf{p}_2)$ changes as the colliding impuritons move from infinity but cannot differ from its value at $t = -\infty$ by a quantity greater than 2Δ , since Δ is the entire width of the energy band. Since the total energy is conserved, the interaction energy cannot vary by a quantity greater than 2Δ either. Obviously, the colliding impuritons cannot come closer than the interaction radius R_0 determined by the condition that $|U(R_0)| \sim \Delta$. Since Δ is small compared to all other energies and $U(\infty)$ is

zero, the interaction radius R_0 and the scattering cross section $\sigma \sim R_0^2$ are large compared to a and a^2 , respectively.

At great distances the interaction of impurities, and in general of point defects in crystals, is a result of elastic interaction. An impurity generates in the crystal a strain field with which another impurity interacts. Elasticity theory [45] gives the following expression for the interaction energy:

$$U(r_{12}) = V_0(n) \left(\frac{a}{r_{12}} \right)^3, \quad (1.3.3)$$

where V_0 is the characteristic interaction energy, which depends on the relative alignment of the impurities, $n = r_{12}/r_{12}$. Equation (1.3.3) shows that V_0 is the interaction energy of two impurity atoms of ^3He

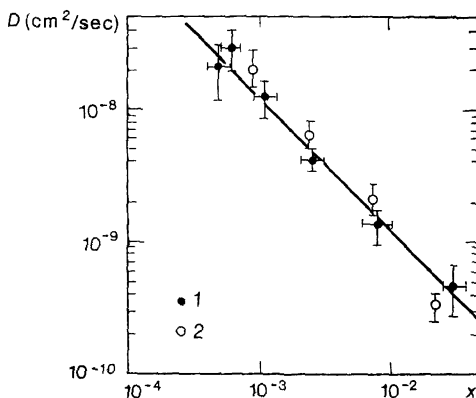


Fig. 1.2. The diffusion coefficient of the ^3He impurities in ^4He crystals with a molar volume of 21 cm^3 as a function of impurity concentration. (1) data cited in [33]; (2) data cited in [35].

in the ^4He lattice at a distance $r_{12} \sim a$. For this reason it must coincide in order of magnitude with the separation temperature of solid ^3He - ^4He solutions, i.e. $V_0 \sim 10^{-1} \text{ K}$ [46], which agrees with direct calculation of the interaction energy for ^3He impurities employing the formulas of elasticity theory (see [18]).

Equation (1.3.3) yields the following expressions for the interaction radius $R_0 \sim a (V_0/\Delta)^{1/3}$ and the impuriton-impuriton scattering cross section:

$$\sigma \sim R_0^2 \sim a^2 (V_0/\Delta)^{2/3}.$$

The diffusion coefficient is [39, 42, 43]

$$D \sim \frac{a^2 \Delta}{\hbar x} \left(\frac{\Delta}{V_0} \right)^{2/3}, \quad (1.3.4)$$

Figure 1.2 gives the experimental data obtained by Richards, Pope, and Widom [33] and Grigor'ev, Esel'son, Mikheev, and Shul'man [35] on the dependence of the diffusion coefficients for ^3He impurities in an hcp crystal of solid ^4He with a molar volume of 21 cm^3 on the concentration of impurities. The data were obtained by the NMR method, so that, strictly speaking, what was measured was the spin diffusion coefficient. However, in our case of low concentrations spin diffusion occurs only because of the diffusion of the impurity atoms proper, so that the two diffusion coefficients coincide. The experimental points in Fig. 1.2 fit fairly well onto the straight line $Dx = 1.2 \times 10^{-11} \text{ cm}^2 \cdot \text{sec}^{-1}$. If we compare this result with Eq. (1.3.4), we find that the band width Δ is about 10^{-4} K , which agrees with the estimate based on NMR data on pure ^3He . Besides, the experiment verifies that the diffusion coefficient does not depend on temperature at $T < 1.2 \text{ K}$. Hence, the entire body of experimental data agrees completely with Eq. (1.3.4), which is based on the assumption that the impurities form an impuriton gas. As $x \rightarrow 0$, the diffusion coefficient grows without limit, which agrees well with the fact that a single impuriton moves like a free particle.

1.3.2 Diffusion of Strongly Interacting Impuritons

The use of the model of an impuriton gas introduced above is restricted to situations in which the mean separation between impurities is much larger than the interaction radius, i.e. $a/x^{1/3} \gg R_0$, or $x \ll \Delta/V_0 \sim 10^{-3}$. But experimental data has proved (see Fig. 1.2) that the diffusion coefficient is approximately inversely proportional to concentration in a much wider range: $10^{-4} < x < 10^{-2}$. The reason for this can be understood if we consider higher concentrations: $10^{-3} < x < 10^{-2}$. Within this range the mean separation of impurities is smaller than R_0 , and the impurities do not constitute a rarefied impuriton gas [38, 44, 47].

To examine the behavior of an impurity atom when it strongly interacts with other impurities, let us consider two impurity atoms separated by a distance that is smaller than the interaction radius: $r_{12} < R_0$. We seek the range of separations within which the impurities can be treated as impuritons with an interaction Hamiltonian defined by (1.3.2). This formula is valid if $U(r_{12})$ is a slowly varying function of impuriton coordinates. Namely, the variation in the interaction energy due to an impurity tunneling to a neighboring site must be small compared to the band width Δ for isolated impuriton, i.e.

$$\delta U(r_{12}) \equiv U(r_{12} + a) - U(r_{12}) \sim a \frac{\partial U}{\partial r_{12}} \ll \Delta \quad (1.3.5)$$

If this is not so, the inhomogeneity in the interaction energy strongly influences the tunneling probability, as a result of which the quasi-

particle energy spectrum $E(\mathbf{p})$ changes considerably. At $r_{12} \sim R_0$ the condition (1.3.5) is satisfied with a large margin. Indeed,

$$\delta U(R_0) \sim V_0 \frac{a^4}{R_0^4} \sim \frac{a}{R_0} \Delta \sim 10^{-1} \Delta.$$

The condition is violated when $r_{12} \lesssim R_1$, where $R_1 \sim a(V_0/\Delta)^{1/4}$. Hence, there is a range of separations, $R_1 < r_{12} < R_0$, in which the interaction of impurities is strong and yet we can still consider them as impuritons with the interaction Hamiltonian given by (1.3.2).

Concentrations for which the above picture of interacting impuritons remains valid are determined by the condition that the mean separation between impurities is smaller than R_0 but greater than R_1 , i.e.

$$\frac{V_0}{\Delta} < x < \left(\frac{V_0}{\Delta} \right)^{3/4}, \quad \text{or} \quad 10^{-3} < x < 10^{-2}.$$

These are the very concentrations that must be examined to explain the experimental data presented in Fig. 1.2.

It is convenient to start the qualitative solution of the problem of strongly interacting impuritons by studying the motion of a single impuriton under a force \mathbf{F} that is constant in time and space.

The equation of motion, $\dot{\mathbf{p}} = \mathbf{F}$, yields the time dependence of the quasimomentum: $\mathbf{p} = \mathbf{p}_0 + \mathbf{F}t$, where \mathbf{p}_0 is the initial quasimomentum. If \mathbf{F} is directed along one of the crystallographic axes, the energy $E(\mathbf{p})$ and velocity $\mathbf{v} = \partial E / \partial \mathbf{p}$, which are periodic in \mathbf{p} with a period of the order of \hbar/a , vary in time with a period of the order of \hbar/aF . The time average of the velocity is obviously zero. Hence, under a constant force an impuriton oscillates in space with a frequency of the order of aF/\hbar and an amplitude of the order of $v/(aF/\hbar) \sim \Delta/F$.

There is, however, an essential difference between this particular case and the general case, when the \mathbf{F} may point in any direction. Since for an arbitrary (irrational) direction the periodicity in momentum space breaks down, all three components of the impuriton velocity change in a random manner. The path of an impuriton then is a random curve like the one in Fig. 1.3. Since the interaction energy $-\mathbf{F} \cdot \mathbf{r}$ cannot change by more than Δ , the trajectory is confined to a vertical layer with a thickness of the order of $L \sim \Delta/F$. The characteristic radius of curvature of the trajectory coincides in order of magnitude with L , and the impuriton moves along this trajectory with a velocity $v \sim a\Delta/\hbar$. Therefore, it undergoes diffusion in a plane perpendicular to the force. The diffusion coefficient is of the order of vL , i.e.

$$D \sim \frac{a\Delta^2}{\hbar F}. \quad (1.3.6)$$

Such behavior is generally well known from the electron theory of metals, but in the case of electrons the diffusion is practically unobservable since L is always considerably greater than the mean free path due to the large width of the energy band.

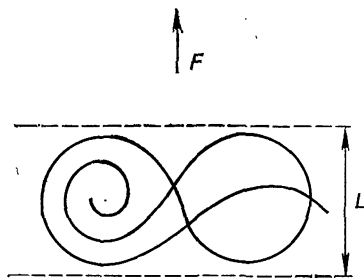


Fig. 1.3. The trajectory of an impuriton under a constant force.

The above reasoning enables us to clarify the nature of motion of strongly interacting impuritons. The force exerted by one impuriton on another is

$$F \sim \frac{\partial U}{\partial r_{12}} \sim V_0 \frac{a^3}{r_{12}^4}. \quad (1.3.7)$$

Under this force the impuritons diffuse, and the diffusion coefficient defined via (1.3.6) and (1.3.7) is

$$D \sim \frac{\Delta^2}{\hbar a^2 V_0} r_{12}^4. \quad (1.3.8)$$

To calculate the diffusion coefficient for a ^3He - ^4He solution with the impurity concentration x from 10^{-3} to 10^{-2} it suffices to substitute the mean distance between impurities $a/x^{1/3}$ for r_{12} in (1.3.8). This yields [38, 47]

$$D \sim \frac{\Delta^2 a^2}{\hbar V_0} x^{-4/3}, \quad (1.3.9)$$

which is in good agreement with the experimental data because when concentration is at its lower limit, i.e. $x \sim \Delta/V_0 \sim 10^{-3}$, formula (1.3.9) gives the same result as (1.3.4). The precision of experiments in the 10^{-3} - 10^{-2} range of concentrations is not high enough to distinguish between the x^{-1} - and the $x^{-4/3}$ -law. Thus, experimental data in the region of not-too-low concentrations is naturally explained by the special mechanism of impuriton diffusion under the interaction forces.

1.3.3 Phonon-Impuriton Interaction

Up till now we have studied the low temperature region, a region where quantum diffusion is determined primarily by impuriton interaction. As temperature grows, the phonon-impuriton interaction starts to play an important role. This, in turn, decreases the mean free path of the impuritons. As a result the diffusion coefficient must decrease as temperature grows. For the same reason, however, at high temperatures the diffusion mechanism that must become more important than the quantum diffusion of impuritons is common

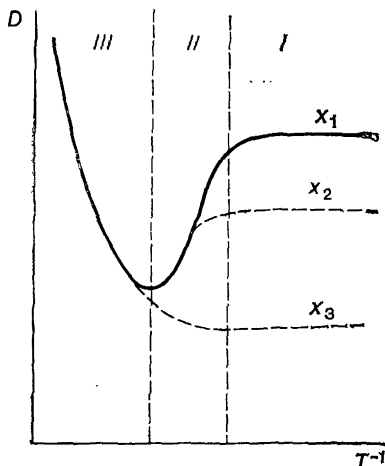


Fig. 1.4. The temperature dependence of the impurity diffusion coefficient for various impurity concentrations: $x_1 < x_2 < x_3$.

thermoactivation diffusion, which grows exponentially with temperature. There are therefore three characteristic temperature regions for this process (Fig. 1.4). In region I (low temperatures) diffusion is restricted to impuriton-impuriton scattering and does not depend on temperature. In region II (medium-range temperatures) diffusion is generally restricted to phonon-impuriton interaction and the diffusion coefficient decreases as the temperature grows. Finally, in region III (high temperatures) the thermoactivation mechanism of diffusion plays the main role. Since diffusion depends on impurity concentration (at low concentrations) obviously only in region I, an increase in concentration leads to region II narrowing and, finally, to its extinction. The two dashed curves in Fig. 1.4 represent the change in the temperature dependence of the diffusion coefficient with concentration (here $x_1 < x_2 < x_3$).

Let us consider the phonon region *II*. The time that elapses between two phonon-impuriton collisions is $\tau \sim (N_{\text{ph}} c \sigma_{\text{ph}})^{-1}$, where $N_{\text{ph}} \sim (T/\Theta a)^3$ is the number of phonons per unit volume, c the speed of sound, and σ_{ph} the phonon-impuriton scattering cross section. At temperatures that are low compared with the Debye temperature Θ , long-wave acoustic phonons play the main role. As known, the cross section of scattering of such phonons on point defects is proportional to the fourth power of the phonon wave vector $q \sim T/\Theta a$. Hence, $\sigma_{\text{ph}} \sim a^2 (qa)^4 \sim a^2 (T/\Theta)^4$ and $\tau \sim (a/c) (\Theta/T)^7 \sim (\hbar/\Theta) (\Theta/T)^7$. The expression for the diffusion coefficient $D \sim v^2 \tau_{\text{tr}}$, however, includes not τ but the transport time τ_{tr} between collisions. This is obviously due to the fact that at all attainable temperatures the band width for impuritons is smaller than the particular temperature. In these conditions the quasimomenta of the impuritons are on the order of \hbar/a , whereas phonon momenta are considerably smaller. Then, according to the theory of low-temperature electrical conductivity in pure metals, the transport time differs from τ by an additional factor of $(\Theta/T)^2$. Thus, in the phonon region,

$$D \sim \frac{a^2 \Delta^2}{\hbar \Theta} \left(\frac{\Theta}{T} \right)^9, \quad (1.3.10)$$

i.e. the diffusion coefficient is proportional to the ninth power of temperature [31].

When can formula (1.3.10) be used? The mean free path for impuritons is $l \sim v \tau \sim a (\Delta/\Theta) (\Theta/T)^7$. At $T \ll T_0$, where $T_0 \sim \Theta (\Delta/\Theta)^7$, the mean free path is large compared with the atomic separation, and the above derivation of formula (1.3.10) is justified. Kagan and Maksimov [41] and Kagan and Klinger [42] have shown that formula (1.3.10) remains valid without any change up to temperatures of the order of the Debye temperature. This is readily seen from the following line of reasoning, which also shows that the concept of impuritons remains valid even when the mean free path of impuritons is much smaller than the atomic separation [47].

To calculate the diffusion coefficient we must resort to the Boltzmann equation for the impuriton distribution function $f(\mathbf{r}, \mathbf{p}, t)$:

$$\frac{\partial f}{\partial t} + \mathbf{v} \cdot \frac{\partial f}{\partial \mathbf{r}} + \mathbf{F} \cdot \frac{\partial f}{\partial \mathbf{p}} = I, \quad (1.3.11)$$

where I is the collision term (phonon-impuriton collisions). The important thing is that the impuriton energy spectrum has the form $E(\mathbf{p}) = E_0 + e(\mathbf{p})$, with E_0 a constant independent of quasimomentum, and $e(\mathbf{p})$ a function of quasimomentum (this function is

of the order of Δ in magnitude and therefore much smaller than T). If $T \ll T_0$, the collision term can obviously be written as

$$I = - \int d^3 p' \int d^3 q \int d^3 q' W(\mathbf{q}, \mathbf{q}') \{ n(\mathbf{q}) [1 + n(\mathbf{q}')] f(\mathbf{p}) - n(\mathbf{q}') [1 + n(\mathbf{q})] f(\mathbf{p}') \} \delta(\mathbf{p} + \mathbf{q} - \mathbf{p}' - \mathbf{q}') \delta[\omega(\mathbf{q}) - \omega(\mathbf{q}')], \quad (1.3.12)$$

where $n(\mathbf{q})$ is the phonon distribution function, $\omega(\mathbf{q})$ the phonon energy spectrum, and W the phonon-impuriton scattering probability. Formula (1.3.12) differs from the usual collision term only in one respect: in the argument of the delta function reflecting energy conservation we have neglected $\epsilon(\mathbf{p})$ and $\epsilon(\mathbf{p}')$ in comparison with phonon energies, since the latter coincide in order of magnitude with the temperature and hence are much larger than Δ .

We can easily see that the Boltzmann equation (1.3.11) with a collision term (1.3.12) is valid if $\hbar/\tau \ll T$. The more stringent condition $\hbar/\tau \ll \Delta$, which is equivalent to the interatomic distance being small compared with the mean free path, is not required here. Indeed, if the distribution function f and the force \mathbf{F} are slowly varying functions of spatial and temporal variables and \mathbf{F} is sufficiently weak, Eq. (1.3.11) holds in the general (quantum) case, too, but I in the general case cannot be expressed only in terms of distribution functions. But if we neglect $\epsilon(\mathbf{p})$ in the formula for the impuriton energy, then condition $\hbar/\tau \ll \omega \sim T$ guarantees that (1.3.12) expresses the collision term, since the quantum uncertainty in the energy, \hbar/τ , is small compared with phonon energies. If this is so, the term $\epsilon(\mathbf{p}) \sim \Delta$ does not appear in our problem at all. The only difference between the case where $\hbar/\tau \ll \Delta$ (or $l \gg a$) and that where $\hbar/\tau \gg \Delta$ (or $l \ll a$) is that in the former the term $\epsilon(\mathbf{p})$ can be included in the argument of the energy-conservation delta function in (1.3.12), whereas in the latter such inclusion would be an overestimate of the accuracy. In both cases it suffices to use (1.3.11) and (1.3.12) to calculate the diffusion coefficient, which yields (1.3.10). The condition that $\hbar/\tau \ll T$ is obviously equivalent to $T \ll \Theta$. However, a remark is in order. The above line of reasoning does not prove the validity of (1.3.10) for the observed diffusion coefficient up to the Debye temperature. In our discussion we have assumed that the contribution of thermoactivation diffusion is negligible, but in fact in ^3He - ^4He solution this mechanism becomes the major one at $T \ll \Theta$.

Figure 1.5 illustrates the experimental data on the temperature dependence of the diffusion coefficient for various concentrations of

^3He impurities in hcp crystals of solid ^4He with a molar volume of 21 cm^3 [48, 49]. Curve 1 corresponds to a very low concentration, $x = 6 \times 10^{-5}$ [48]. The temperature regions I and II can be clearly seen in this figure. In the phonon region II the experimental points are described by a power law T^{-n} , where $n = 9 \pm 1$ [48], which fully agrees with (1.3.10). Curve 2 corresponds to a rather high concentration, $x = 7.5 \times 10^{-3}$ [48]. Here the temperature regions I and III are clearly seen, and the intermediate phonon region is not present,

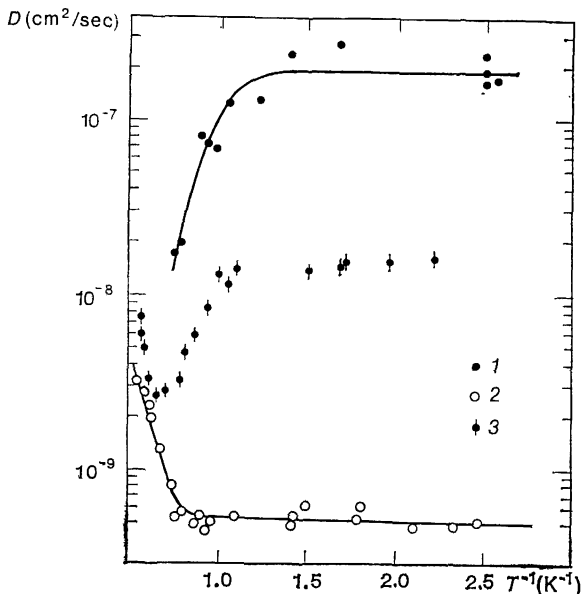


Fig. 1.5. The temperature dependence of the diffusion coefficient for ^3He impurities in ^4He crystals. The impurity concentrations (in %) are: (1) 6×10^{-3} [48]; (2) 0.75 [48]; (3) 5×10^{-2} [49].

as it should be at high concentrations. Curve 3 corresponds to an intermediate concentration, $x = 5 \times 10^{-4}$ [49]. All three temperature regions are clearly seen here.

When comparing formula (1.3.10) quantitatively with the experimental data in region II, we must bear in mind that for the T^{-9} -law the diffusion coefficient strongly depends on the value of the Debye temperature. More precise calculations done by Pushkarov [39] show that in (1.3.10) we must substitute for Θ a quantity that is approximately $\Theta/8$. Mikheev *et al.* [48] compared (1.3.10) with the experimental data and found a value for the impuriton band width Δ that agrees with the above-cited value.

We can therefore assume that it has been firmly established that the ^3He impurities in crystalline ^4He behave like delocalized impurities freely moving through the crystal. The most striking manifestation of this fact is the observed rapid growth in the diffusion coefficient as the temperature decreases (in the phonon region).

In view of the aforesaid we must note that if we are speaking of impuriton diffusion in metals, say hydrogen in niobium or zirconium, a much slower temperature dependence, namely the T^{-1} -law, of the diffusion coefficient is observed instead of the T^{-9} -law [31]; this is due to the interaction between the impurities and conduction electrons. The time between two electron-impuriton collisions is $\tau \sim (n_e v_F \sigma)^{-1}$, where $n_e \sim N_e (T/\varepsilon_F)$ is the number of electrons in the smearing region of the Fermi surface, N_e the total number of electrons per unit volume, ε_F and v_F the energy and velocity on the Fermi surface, and $\sigma \sim a^2$ the electron-impuriton scattering cross section. The diffusion coefficient is, in order of magnitude,

$$D \sim v^2 \tau \sim \frac{\hbar \Delta^2}{p_F^2 T}, \quad (1.3.13)$$

where p_F is the Fermi electron momentum.

1.3.4 One- and Two-Dimensional Impurities

In Sec. 1.3.2 we dealt with the peculiarities of impuriton dynamics caused by the fact that the impuriton band width is small ($\Delta \sim 10^{-4}$ K) compared with the characteristic interaction energy $V_0 \sim 10^{-1}$ K of two impurities separated by the interatomic distance. If the distance r_{12} between two impurities is less than the interaction radius $R_0 \sim a (V_0/\Delta)^{1/3}$ but greater than $R_1 \sim a (V_0/\Delta)^{1/4}$, the impurities diffuse together under the interatomic forces, and the diffusion coefficient is given by (1.3.8). Since at $r_{12} < R_0$ the interaction energy is greater in absolute value than 2Δ , the impurities cannot become widely separated in their motion due to energy conservation. They, therefore, act as particles linked by interaction forces, and the result does not depend on whether the forces are attractive or repulsive. It is interesting to follow the variations in the possible types of motion of two impurities as their separation further decreases. The point is that although in dilute solutions the probability of two closely situated impurities forming pairs is small, there are certain phenomena (for instance, spin-lattice relaxation in ^3He - ^4He solutions) that are caused only by pairs of closely situated impurities in the lattice. We will see below that these pairs of bound impurity atoms with a small separation cause certain quasiparticles to appear in the crystal's energy spectrum; these quasiparticles move in the crystal with a constant velocity only along certain crystallographic axes or in certain planes. They therefore constitute one- and two-

dimensional quasiparticles moving in the bulk of a three-dimensional crystal.

At $r_{12} < R_1$ the tunneling of an impurity atom to a neighboring lattice site is accompanied by a variation δU (see Eq. (1.3.5)) of the interaction energy, a variation much larger than the band width Δ . In these conditions the tunneling probability is proportional to Δ^2 (instead of being proportional to Δ , as is the case with tunneling between states with the same energy) and therefore can generally be ignored. The same can be said about the probability of both impurity atoms tunneling and the energy remaining constant. The atoms, hence, cannot move at all. There are, however, important exceptions to this result. Suppose that the vector \mathbf{r}_{12} connecting two impurities is almost parallel to a high-order crystallographic axis. In an hcp crystal of solid ^4He this may be a hexagonal axis, for one. The function $V_0(\mathbf{n})$, which according to (1.3.3) determines the interaction energy of impurities, attains an extremum for an \mathbf{n} parallel to the hexagonal axis. The tunneling of one of the impurity atoms by a distance ρ in the direction perpendicular to \mathbf{n} leads to a variation of the interaction energy, which in order of magnitude is

$$\delta U(\rho) \sim V_0 \left(\frac{a}{r_{12}} \right)^3 \left(\frac{\rho}{r_{12}} \right)^2. \quad (1.3.14)$$

If $r_{12} > R_2$, where $R_2 \sim a (V_0/\Delta)^{1/5}$, then at $\rho \sim a$ the value of $\delta U(\rho)$ is less than the band width Δ . In these conditions it is practically impossible for the impurities to move along \mathbf{n} , but as for motion in directions perpendicular to \mathbf{n} there emerges a situation that is similar to the one we discussed in Sec. 1.3.2. The impurity atoms move along paths that form random curves lying in planes perpendicular to the hexagonal axis. The radius of curvature of these paths, ρ_0 , is determined from the condition that at $\rho \sim \rho_0$ the variation of the interaction energy is on the order of the band width, i.e. $\rho_0 \sim a (\Delta/V_0)^{1/2} (r_{12}/a)^{5/2}$. The impurity atoms separated by a distance of r_{12} so that $R_1 > r_{12} > R_2$ and lying approximately on \mathbf{n} undergo, therefore, a peculiar two-dimensional diffusion motion in the hexagonal plane of the crystal. The diffusion coefficient is, in order of magnitude,

$$D \sim \nu \rho_0 \sim \left(\frac{\Delta^3 r_{12}^5}{\hbar^2 V_0 a} \right)^{1/2}. \quad (1.3.15)$$

We note that for this motion to materialize it is not sufficient for $V_0(\mathbf{n})$ to have a local extremum in the direction of \mathbf{n} . The crystal must be periodic in a plane perpendicular to \mathbf{n} , which is the case only for selected crystallographic axes.

Finally, let us assume that $r_{12} < R_2$. In this case the tunneling of an impurity atom to a neighboring lattice site changes the interaction energy by a quantity greater than Δ even when the direction is

perpendicular to a hexagonal axis. Here, however, there are also important exceptions. Suppose that an impurity atom lies at a certain point A (Fig. 1.6) of the hexagonal plane P_1 . An hcp crystal of solid ^4He consists of a family of parallel hexagonal planes (P_1 , P_2 , P_3 , etc.). Suppose also that another impurity atom lies at another point B in, generally speaking, another hexagonal plane (plane P_3 in Fig. 1.6), but in such a way that its projection C onto plane P_1 is the closest neighbor of point A. (In Fig. 1.6 plane P_1 with points A and C is shown separately.) The tunneling of the second atom in its hexagonal plane from point B to point B_1 or B_2 , whose projections on

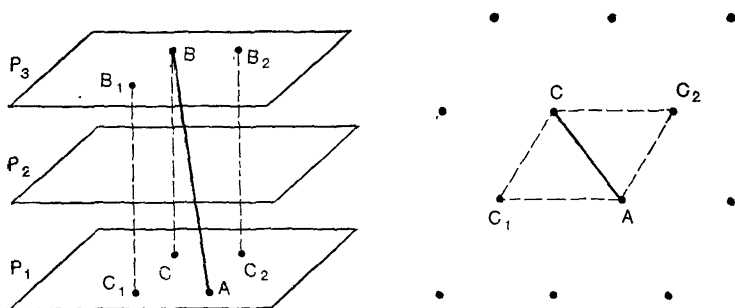


Fig. 1.6. A two-dimensional quasiparticle formed by two impurity atoms.

P_1 are C_1 or C_2 , respectively, does not change the interaction energy because of the symmetry of the crystal lattice. Due to this symmetry the pairs AB, AB_1 , and AB_2 are crystallographically equivalent. The same reasoning holds for the tunneling of the first impurity atom in plane P_1 from point A to point C_1 or C_2 . We can easily see that thanks to the tunneling transitions of the discussed type the system of two impurity atoms can move as a whole over the entire hexagonal plane but cannot move perpendicularly to this plane. Since these transitions occur with the impurity energies exactly constant, the motion is completely coherent. A pair of impurities behaves as a special type of two-dimensional quasiparticle, moving only in a hexagonal plane of the crystal as a free particle [47]. Since for a fixed coordinate of one impurity atom there are six different positions of the second atom in the pair, the energy spectrum of these two-dimensional quasiparticles contains six branches.

Figure 1.7 depicts a configuration of two impurity atoms that can move only in one direction [50]. Point A shows the position of the first atom while point C is the projection of the second atom on the same hexagonal plane. Here the first atom may tunnel from A to A_1 without changing its energy, the second atom may tunnel in its

hexagonal plane from the point whose projection is C to the point with projection C_1 , and the process may be repeated. The pair of impurity atoms behaves here as a one-dimensional quasiparticle that freely moves in the crystal only along one direction parallel to the straight line AA_1 . The energy spectrum of these quasiparticles contains two branches.

Figure 1.8 shows an example of a complex of three impurity atoms that form a one-dimensional quasiparticle [50]. By moving one impur-

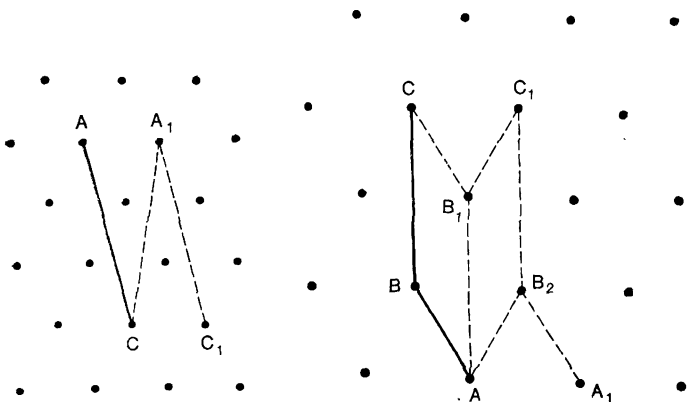


Fig. 1.7. A one-dimensional quasiparticle formed by two impurity atoms.

Fig. 1.8. A one-dimensional quasiparticle formed by three impurity atoms.

ity atom each time to a neighboring lattice site the initial configuration ABC can be transferred step-by-step (through crystallographically equivalent configurations AB_1C , AB_1C_1 , AB_2C_1) to another configuration $A_1B_2C_1$, which differs from the initial configuration by a translation along the straight line AA_1 .

We note that in all the cases considered above the motion of the two- or one-dimensional quasiparticle is achieved by successive coherent tunneling transitions of an impurity to the nearest lattice site. Consequently, the tunneling frequencies and energy band widths (and, hence, velocities) of all quasiparticles coincide, in order of magnitude, with the corresponding quantities for a single impuriton.

That impurity atoms that are the nearest neighbors in the crystal lattice can move coherently has been noted by Richards *et al.* [51] in connection with their study of the dependence of the spin-lattice relaxation time T_1 on the NMR frequency for ^3He impurity atoms in hcp crystals of ^4He . The results of this study are presented in Fig. 1.9. Spin-lattice relaxation depends to a great extent on neighboring

spins being able to move, since relaxation is the result of spin-flip produced by fluctuations of the pair dipole-dipole interaction, which is due to the relative motion of the spins. Since the intensity of dipole-dipole interaction falls off rapidly as separation increases, the pairs of spins in the lattice sites closest to each other play the main role in the relaxation process. The most interesting feature in Fig. 1.9 is

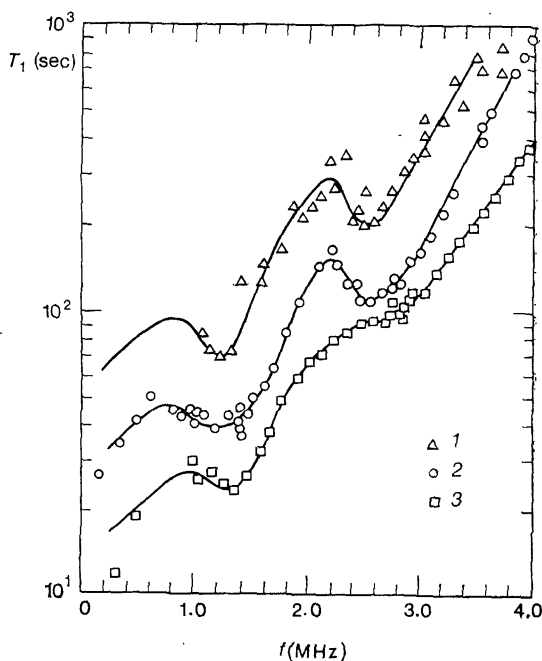


Fig. 1.9. The frequency dependence of sp n -lattice relaxation time for ^3He impurities in ^4He crystals with a molar volume of 21 cm^3 at $T = 0.53 \text{ K}$. The impurity concentrations (in %) are: (1) 0.1; (2) 5×10^{-2} ; (3) 2.5×10^{-2} .

the resonance behavior of the T_1 versus f curves near 1.5 and 3.0 MHz. This behavior clearly points to the presence of motion of pairs of closely spaced impurities with frequencies of the order of 1 MHz, which coincides with the order of the tunneling frequency Δ/\hbar for isolated impurities. Mullin, Guyer, and Goldberg [52] and Sacco and Widom [53] calculated the contribution of the pairs of ^3He impurities that are nearest neighbors in the ^4He lattice to the rate T_1^{-1} of spin-lattice relaxation. They assumed that the main tunneling mechanism was the simplest two-particle process corresponding to that depicted in Fig. 1.1a. (For impurities that are the nearest neighbors the result depends, generally speaking, on the nature of

the tunneling process.) In an hcp structure there are two types of pairs of closest impurities, and both behave like two-dimensional quasiparticles. The first type corresponds to that depicted in Fig. 1.6, in which both impurity atoms lie in the same hexagonal plane (points B and C coincide). The second type is depicted in Fig. 1.10. Here the impurity atoms lie in neighboring hexagonal planes. In Fig. 1.10 the dots correspond to lattice sites in one of the planes and the crosses correspond to the projections of lattice sites from the neighboring plane; point A denotes the position of the first atom, while point C the projection of the second. The first atom may tunnel without

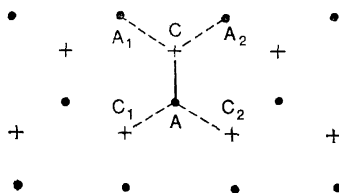


Fig. 1.10. A two-dimensional quasiparticle formed by three impurity atoms that are the closest neighbors.

changing its energy to A_1 and A_2 while the second to sites with projections C_1 and C_2 . The results of these calculations confirm the qualitative picture (Fig. 1.9) but cannot serve as a basis for definite conclusions concerning the two-dimensional motion of the impurities. At present there is no experimental verification of two- and one-dimensional motions of impurities.

In this connection it is interesting to examine the fine structure of the wings of the NMR line due to impurity pairs [54]. It is well known (see, for instance, [19]) that by virtue of dipole-dipole interaction a two-spin system has resonance frequencies ω that are somewhat shifted in relation to γH (γ is the gyromagnetic ratio, H the external magnetic field, and γH the resonance frequency for a single spin):

$$\omega = \gamma H \pm \frac{3}{4} \frac{\hbar \gamma^2}{r_{12}^3} (1 - 3 \cos^2 \theta); \quad (1.3.16)$$

here θ is the angle between the magnetic field vector and the axis connecting the nuclei. This formula shows that the greatest shift is achieved for pairs of spins with $r_{12} \sim a$. There are generally three types of such pairs: fixed pairs, in which tunneling with energy conservation for one of the impurities is impossible and to which formula (1.3.16) can be applied directly, and pairs that are two- and one-dimensional quasiparticles. In the last two cases the state of the system is defined by fixing the (two- or one-dimensional) quasimomen-

tum \mathbf{p} and the number ν of the energy band. The state is a linear combination of all possible localized states of the pair defined by the radius vector \mathbf{R} of one of the atoms and by the label $i = 1, 2, \dots$ that determines the various orientations of the axis connecting the two nuclei. The coefficients in this combination are of the form $A_i^\nu(\mathbf{p}) \exp(i\mathbf{p} \cdot \mathbf{R})$ and play the role of the wave function of state (ν, \mathbf{p}) in the (i, \mathbf{R}) -representation. The resonance frequencies can be obtained from (1.3.16) by averaging over state (ν, \mathbf{p}) . In general, these frequencies depend on ν and \mathbf{p} and are expressed by the following formula:

$$\omega_\nu(\mathbf{p}) = \gamma H \pm \frac{3}{4} \frac{\hbar \gamma^2}{r_{12}^3} (1 - 3 \langle \cos^2 \theta \rangle), \quad (1.3.17)$$

where

$$\langle \cos^2 \theta \rangle = \sum_i |A_i^\nu(\mathbf{p})|^2 \cos^2 \theta_i, \quad (1.3.18)$$

here θ_i is the angle between the magnetic field vector and the axis connecting the nuclei in the localized state with orientation i . The coefficients $A_i^\nu(\mathbf{p})$ satisfy the normalization condition

$$\sum_i |A_i^\nu(\mathbf{p})|^2 = 1. \quad (1.3.19)$$

The greatest shift in frequency is achieved for pairs of impurities closest to each other in the lattice. In the hcp crystal of solid ^4He these pairs act as two-dimensional quasiparticles and may be of two types, as we already know, corresponding to Figs. 1.6 and 1.10. In both cases the label i takes on three values, since the pairs of both types have three different orientations (configurations AC, AC_1 , and AC_2 in Figs. 1.6 and 1.10). Let us suppose that the magnetic field is directed along a hexagonal axis. Then $\cos \theta_i = 0$ for all i 's for pairs of the first type and $\cos \theta_i = \sqrt{2/3}$ for pairs of the second one. The expression in parentheses in (1.3.17) is the same in absolute value but differs in sign for the two types. For this reason the frequency spectrum is discrete and consists only of two lines of the same intensity:

$$\omega_{1,2} = \gamma H \pm \frac{3\hbar\gamma^2}{4r_{12}^3},$$

We would have arrived at the same result for a specific direction of the magnetic field in the case of a rigid lattice, but in our case the quasiparticles can easily move in the hexagonal plane and, hence, respond to the magnetic field gradient, namely to the gradient component parallel to the hexagonal plane. An important aspect of this is that the frequency shift is much larger than the line width. The size of the shift is about $\hbar\gamma^2/a^3 \sim 10^4 \text{ sec}^{-1}$, while the time T_2 observed by Richards, Pope, and Widom [33] and Greenberg, Thom-

lison, and Richardson [55] for dilute ^3He - ^4He solutions are as long as $10^{-1.1}$ sec.

If the magnetic field is at an angle to a hexagonal axis, the resonance frequencies become dependent on the quasimomentum and the spectrum becomes continuous. Its shape, however, can be found exactly, since to calculate the $A_i^{\gamma}(\mathbf{p})$ we can resort to a method that is known in the theory of metals as the strong-binding approximation. As a result, for the A_i^{γ} in the case of two-dimensional quasiparticles we arrive at a simple set of linear algebraic equations (see [47]).

In the case of one-dimensional quasiparticles the frequency spectrum is discrete for any direction of the magnetic field because there are only two orientations and the respective coefficients A_i^{γ} differ only in a phase factor, i.e. $|A_1^{\gamma}(\mathbf{p})| = |A_2^{\gamma}(\mathbf{p})|$. Each one-dimensional quasiparticle produces two lines:

$$\omega_{1,2} = \gamma H \pm \frac{3\hbar\gamma^2}{4r_{12}^3} \left[1 - \frac{3}{2} (\cos \theta_1 + \cos \theta_2) \right].$$

The discrete line structure can be observed, obviously, only in single crystals.

Let us now dwell on the problem of calculating the lifetime of the discussed two- and one-dimensional quasiparticles. The finiteness of the lifetime is due to the tunneling processes that we have not taken into account earlier, processes in which the variation of the interaction energy is much larger than the band width Δ . The simplest process is thermoactivation diffusion, but its probability exponentially decreases with temperature. For this reason at low temperature quantum tunneling must be predominant; this is accompanied by changes in the phonon energy so as to compensate for changes in the interaction energy. Two types of such tunneling are known. In the first the tunneling of the impurity is accompanied by phonon scattering. The probability per unit time of this process occurring, w_1 , can easily be estimated by using the results of Kagan and Maksimov [41] and Kagan and Klinger [42]:

$$w_1 \sim \frac{\Delta^2}{\hbar\Theta} \left(\frac{T}{\Theta} \right)^7.$$

In the second type the tunneling of the impurity is accompanied by spontaneous phonon emission [43]. The phonon energy is equal to the change in the interaction energy:

$$\hbar\omega \sim \delta U \sim V_0 \left(\frac{a}{r_{12}} \right)^4.$$

As usual, the probability of spontaneous emission per unit time, w_2 , is proportional to the third power of the emitted phonon frequency and the second power of the overlap integral for the wave functions

of the tunneling particle, i.e. the square of the band width Δ :

$$w_2 \sim \frac{\Delta^2}{\hbar\Theta} \left(\frac{\hbar\omega}{\Theta} \right)^3 \sim \frac{\Delta^2}{\hbar\Theta} \left(\frac{V_0}{\Delta} \right)^3 \left(\frac{a}{r_{12}} \right)^{12}.$$

Contrary to processes of the first type, which can proceed with both an increase and a decrease in the interaction energy, tunneling with spontaneous emission is possible only if the impurities in the finite state have a lower energy. Therefore, this type of process is forbidden for configurations of impurity pairs corresponding to minimal energy.

In the most interesting case of quasiparticles with $r_{12} \sim a$ the second type of process becomes predominant at $T < V_0 (\Theta/V_0)^{4/7}$ (this case does not include the closest-neighbor impurities since such pairs correspond, probably, to a minimum in the interaction energy). In this low-temperature region the lifetime of the majority of quasiparticles does not depend on temperature.

1.4 VACANCIES

1.4.1 Vacancies in ^4He Crystals

As the temperature grows, the processes responsible for the delocalization of atoms in a crystal become more and more of a thermoactive nature. We were able to see this in the diffusion of ^3He impurity atoms in solid ^4He crystals (region III in Figs. 1.4 and 1.5). Theoretically, a possible mechanism in this case could be the common classical above-the-barrier processes of atomic transitions to neighboring lattice sites, processes in which two neighboring atoms change places or there occurs a cycle permutation of three or four particles (Fig. 1.1). These processes differ from the tunneling discussed above in that they proceed only if the atoms receive energy as a result of thermal fluctuation sufficient to overcome the potential barrier (in the classical sense). Just as tunneling processes are, above-the-barrier transitions in close-packed lattices are considerably inhibited by the lack of sufficient free space. The potential barriers that must be overcome are very high, much higher than the energy ε_0 needed for creating a vacancy in the crystal. For this reason the very presence of thermoactivated vacancies, with a concentration proportional to $\exp(-\varepsilon_0/T)$, and of the tunneling of atoms to vacant lattice sites stipulates the basic mechanism of thermoactivation translational motion of the atoms in crystalline helium. The tunneling of the atom to a neighboring vacant site is usually spoken of as the tunneling of the vacancy to the neighboring site. The delocalization of particles at high temperatures is the result of the tunneling of thermoactivated vacancies in the crystal.

The motion of the atoms in the crystal induced by vacancies is of special interest. The point is that in crystalline ^4He the vacancies become delocalized quasiparticles due to the periodicity of the crystals. The energy band width of these quasiparticles, Δ_v , determined by the vacancy tunneling probability, is much larger than the impuriton energy band width, since in this case we are dealing with the tunneling of one particle only and in conditions where the process is in no way inhibited by the lack of free space. Hetherington [56], who was the first to study this problem, and other researchers (see

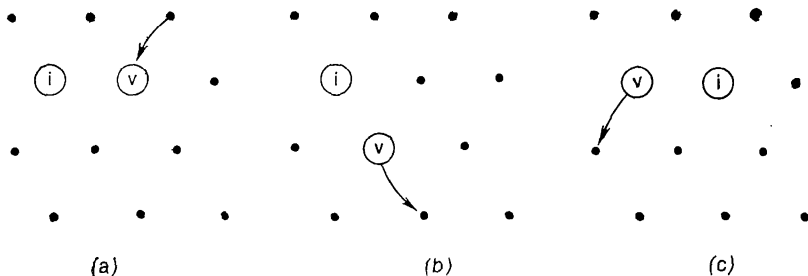


Fig. 1.11. The interaction of a vacancy with an impurity atom.

[18, 39, 57-59]) calculated Δ_v and found it to be 1-10 K. Although at present there is no direct experimental proof that vacancy quasiparticles exist, due to considerable difficulties in observing vacancies, there can be no doubt that they do exist since vacancies are much more mobile than impuritons.

Let us study quantitatively the process of thermoactivation diffusion of impuritons (region *III* in Fig. 1.4) as diffusion induced by vacancies. The impurity moves as a result of the following process (Fig. 1.11). While moving in the crystal, the vacancy may appear at a site that is closest to the impurity atom (see Fig. 1.11a). It may then tunnel to a site that is occupied by a matrix atom (Fig. 1.11b) or an impurity (Fig. 1.11c); after this the vacancy moves far away from the impurity. In the case of Fig. 1.11c the process is accompanied by a shift of the impurity. Since the vacancy band width Δ_v is considerably larger than the impuriton band width, we can neglect the tunneling of the impurity proper and think of the process depicted in Fig. 1.11 as quantum mechanical scattering of a delocalized vacancy quasiparticle on a localized impurity [43]. The process depicted in Fig. 1.11b corresponds to elastic scattering, since the state of the target before and after the collision is the same, while that depicted in Fig. 1.11c corresponds to inelastic scattering accompanied by a shift of the impurity. The impurity diffusion induced by the vacancies is determined by the inelastic scattering probability, and the

diffusion coefficient $D \sim a^2\nu$, where ν is the rate at which the acts of inelastic scattering occur: $\nu \sim N_v\nu\sigma_{in}$ (here σ_{in} is the vacancy-impurity inelastic scattering cross section, N_v the number of vacancies per unit volume, and ν their velocity). When $T \gtrsim \Delta_v$, we have

$$N_v \sim a^{-3}e^{-\varepsilon_0/T}, \quad \nu \sim \frac{a\Delta_v}{\hbar},$$

where ε_0 is the energy of vacancy formation. This yields

$$D \sim \frac{\Delta_v\sigma_{in}}{\hbar} e^{-\varepsilon_0/T}. \quad (1.4.1)$$

If thermoactivation diffusion of impurities is the result of their interaction with vacancies, then from (1.4.1) it follows that the

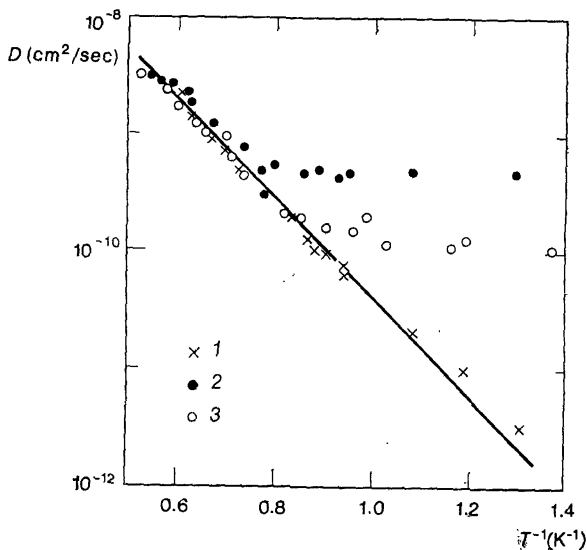


Fig. 1.12. The temperature dependence of impurity diffusion coefficients in ${}^4\text{He}$ crystals with a molar volume of 20.7 cm^3 . The impurity concentrations are: (1) positive ions [64]; (2) 0.75% (${}^3\text{He}$); (3) 2.17% (${}^3\text{He}$) [37].

activation energy does not depend on the type of impurity in one and the same crystal. This result can be directly checked experimentally since aside from isotopic impurities we can in a specified fashion also introduce and then study ions in the ${}^4\text{He}$ crystal. The diffusion coefficient for ions can easily be calculated by measuring the ion mobility in an external electric field. The first to conduct such experiments was Shal'nikov [60], and soon other researchers followed (see [61-64]). Figure 1.12 depicts the experimental data obtained by Keshishev [64] on the temperature dependence of the diffusion

coefficient for positive ions in solid ^4He with a molar volume of 20.7 cm^3 . The same figure shows the data obtained by Grigor'ev, Esel'son, and Mikheev [37] on the diffusion of isotopic impurities. In the temperature region *III*, where diffusion is thermoactivational, not only the activation energies but the absolute values of the diffusion coefficients coincide. Experimental data is described by the equation $D = 6.6 \times 10^{-7} \exp(-9.5/T)$, which in Fig. 1.12 is represented by a solid line. By comparing this formula with (1.4.1), we find the vacancy formation energy to be $\varepsilon_0 = 9.5 \text{ K}$ and if we put $\Delta_v \sim 1 \text{ K}$, the inelastic scattering cross section σ_{in} is about $5 \times 10^{-3} a^2$. The fact that σ_{in} is so small can be explained in the following way (at least qualitatively). The situation is similar to impuriton-impuriton scattering considered in Sec. 1.3.1. The vacancy-impurity interaction has the same form: $U(r) \sim V(a/r)^3$, with V a characteristic interaction energy. If V is greater than Δ_v , the vacancy cannot penetrate the region $r < a(V/\Delta_v)^{1/3}$; more precisely, the probability of the vacancy penetrating the region is very low. In Sec. 1.3.1 we saw that this leads to a large total scattering cross section. But the inelastic process is possible only if the vacancy and impurity are the closest neighbors in the lattice. Whence, at $V > \Delta_v$ the inelastic scattering cross section is much smaller than a^2 while the total cross section is much larger than a^2 . It is essential, however, that the values of the inelastic cross section in these conditions depend largely on the detailed structure of the interaction of the vacancy with ^3He impurities and with ions, so that this coincidence is quite strange. Only refined experimental studies of the diffusion of ^3He impurities and the ion mobility can clarify this problem.

The approach to the problem of vacancy diffusion (or mobility) of ions just outlined, based on the idea of inelastic scattering, enables the researcher to find (at low temperatures) the dependence of mobility on temperature and electric field strength without assuming any knowledge of the structure of the ions [43]. Suppose that $\sigma_n(\mathbf{p})$ is the inelastic scattering cross section of the vacancy with a quasi-momentum \mathbf{p} , where the scattering process is accompanied by a shift of the ion by a vector \mathbf{a}_n that connects the initial lattice site with its n th closest neighbor. The energy of the ion and, hence, of the vacancy changes by $e\mathbf{E} \cdot \mathbf{a}_n$, where e is the ion charge, and \mathbf{E} the applied electric field. We can express the mean drift velocity of the ion in terms of the cross sections in the following manner:

$$\mathbf{u} = \sum_n \mathbf{a}_n \int \frac{d^3 p}{(2\pi\hbar)^3} \sigma_n(\mathbf{p}) v(\mathbf{p}) [n(\varepsilon) - n(\varepsilon + e\mathbf{E} \cdot \mathbf{a}_n)]. \quad (1.4.2)$$

Here $v(\mathbf{p})$ is the velocity of the vacancy, and $n(\varepsilon)$ is the equilibrium distribution function for the vacancies depending only on their energy $\varepsilon = \varepsilon(\mathbf{p})$. The summation in (1.4.2) is over the closest neighbors, for

which $e\mathbf{E} \cdot \mathbf{a}_n > 0$. The translations of the ions by vectors $-\mathbf{a}_n$ are accounted for in (1.4.2) as inverse processes. We can write (1.4.2) thus:

$$\mathbf{u} = \sum_n \mathbf{a}_n \int \frac{d\varepsilon}{(2\pi\hbar)^3} [n(\varepsilon) - n(\varepsilon + e\mathbf{E} \cdot \mathbf{a}_n)] \int \sigma_n(\mathbf{p}) dS, \quad (1.4.3)$$

where the second integral is taken over a constant-energy surface. In the simplest case, where all vectors \mathbf{a}_n are crystallographically equivalent (in a bcc lattice but not in an hcp lattice), this integral does not depend on n because of the lattice symmetry. Let us assume that T is small compared with the vacancy band width Δ_v . In this case practically all the vacancies gather at the bottom of the band, where their spectrum is quadratic and their velocity small. According to quantum mechanics [20], the inelastic scattering cross section for slow particles is inversely proportional to their speed. Hence,

$$\int \sigma_n dS = \alpha \sqrt{\varepsilon - \varepsilon_0},$$

where ε_0 is the energy at the bottom of the band, and α is a constant.

The distribution function $n(\varepsilon)$ can be considered a Boltzmann distribution, since ε_0 is approximately 10 K and, hence, much higher than T . The final expression is

$$\mathbf{u} = \frac{\alpha}{16\pi\hbar^3} \left(\frac{T}{\pi} \right)^{3/2} e^{-\varepsilon_0/T} \sum_n \mathbf{a}_n \left[1 - \exp \left(- \frac{e\mathbf{E} \cdot \mathbf{a}_n}{T} \right) \right]. \quad (1.4.4)$$

In weak fields, $eEa \ll T$ and the drift velocity is proportional to the field strength:

$$u_i = eB_{ik}E_k,$$

where the mobility tensor B_{ik} , according to (1.4.4), is

$$B_{ik} = \frac{\alpha}{16\pi^2\hbar^3} \left(\frac{T}{\pi} \right)^{1/2} e^{-\varepsilon_0/T} \sum_n a_{ni} a_{nk}.$$

In strong fields, $eEa \gg T$ and there emerges a very peculiar situation. Practically for all directions of the field vector the drift velocity achieves saturation and does not depend on $|\mathbf{E}|$:

$$\mathbf{u} = \frac{\alpha}{16\pi\hbar^3} \left(\frac{T}{\pi} \right)^{3/2} e^{-\varepsilon_0/T} \sum_n \mathbf{a}_n. \quad (1.4.5)$$

Since, however, summation in (1.4.5) is over such n 's for which $e\mathbf{E} \cdot \mathbf{a}_n > 0$, velocity \mathbf{u} jumps whenever \mathbf{E} , in varying its direction, passes through a plane that is perpendicular to one of the \mathbf{a}_n 's. The angular width of the transition region is equal to $T/eEa \ll 1$, in order of magnitude, and in this transition region the drift velocity

rapidly changes in both magnitude and direction. Figure 1.13 illustrates this point and shows the dependence of the absolute value and direction of drift velocity on the direction of \mathbf{E} for a two-dimensional

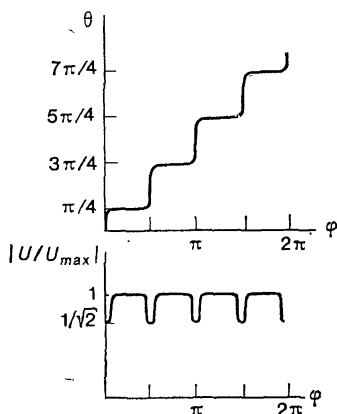


Fig. 1.13. The dependence of the absolute values and direction of ion drift velocity on the direction of electric field; θ is the angle between \mathbf{u} and \mathbf{a}_1 , and φ the angle between \mathbf{E} and \mathbf{a}_1 .

square lattice with a period a . The maximum drift velocity in this case, as is obvious from (1.4.5), is

$$u_{\max} = \frac{\sqrt{2} \alpha a}{16\pi\hbar^3} \left(\frac{T}{\pi} \right)^{3/2} e^{-\varepsilon_0/T}.$$

We see that the angular dependence of the drift velocity directly represents the geometry of the crystal lattice.

1.4.2 Zero-Point Vacancies

In Sec. 1.4.1 we saw that the vacancy formation energy in solid helium and the vacancy band width are quantities of the same order of magnitude. In this connection it is interesting to note that for quantum crystals there is the theoretical possibility of the existence of so-called zero-point vacancies, which in the same way as zero-point vibrations exist in a crystal at absolute zero [31, 65, 66].

To prove this point let us study the behavior of the vacancy energy spectrum as the quantum tunneling probability increases. In the classical limit a vacancy is localized and has a definite energy $E_0 > 0$. The presence of a small but finite tunneling probability for the vacancy to neighboring lattice sites leads to an energy band of a finite width Δ_v . As long as Δ_v is much smaller than E_0 , we can use the method of strong binding to calculate the energy spectrum, and this

method shows that the middle of the energy band coincides with the energy E_0 of the localized vacancy. This implies that as the tunneling probability (and, hence, the band width) increases, the minimal vacancy energy ε_0 corresponding to the bottom of the band decreases. For this reason in very pronounced quantum crystals such as solid helium there can be a situation in which ε_0 becomes negative. This means that the initial ground state of the crystal is in actual fact unstable towards vacancy production. The correct ground state corresponds to a state of the crystal in which there are some vacancies.

If ε_0 is negative but small in absolute value, the vacancies with quasimomenta close to that corresponding to the bottom of the band have negative energies. The energy $E(\mathbf{p})$ of the vacancies in this region near the energy minimum can be written as

$$E(\mathbf{p}) = \varepsilon_0 + \frac{p^2}{2M}, \quad (1.4.6)$$

where M is a certain effective mass, and \mathbf{p} the quasimomentum reckoned from the minimal quasimomentum.

In a Bose crystal of the ^4He type, with which we will start our exposition, the vacancies are obviously bosons. To calculate their contribution (at low density) to the ground state energy of the crystal we can use (see [67]) the well-known formula for the ground state energy of a rarefied Bose gas with spectrum (1.4.6):

$$E = \varepsilon_0 N + \frac{2\pi\hbar^2 f}{M} N^2; \quad (1.4.7)$$

here E and N are the energy of vacancies and their number per unit volume, and f is the vacancy-vacancy scattering length. When f is positive, i.e. the vacancies repel each other, and ε_0 is small and negative, the quantity on the right-hand side of (1.4.7) has a minimum for small N 's, a fact that enables us to calculate the equilibrium density N_0 of zero-point vacancies in a Bose crystal:

$$N_0 = \frac{M |\varepsilon_0|}{4\pi\hbar^2 f}. \quad (1.4.8)$$

A crystal with zero-point vacancies should have many peculiar properties, for one, superfluidity, caused by the possibility of mass transfer via superfluid motion of the "vacancy liquid" through the crystal (see [31, 65, 66, 68]). The experimental data available at present, however, indicates that this possibility, in all likelihood, is not realized in solid ^4He .

The experimental data discussed in Sec. 1.4.1 on the diffusion of ^3He impurity atoms induced by vacancies and on the mobility of charges indicates that the number of vacancies decreases exponentially with temperature, which corresponds to a positive minimal energy of the vacancies. We must note, however, that this result is ob-

tained for conditions with constant pressure. Measurements of the charge-mobility temperature dependence along the crystal-liquid equilibrium curve show that the mobility is approximately constant (see [64]) down to the lowest temperatures studied, of the order of 1 K.

In ^3He crystals the quantum effects are more pronounced than in ^4He thanks to the smaller mass of the atoms. But here too there is experimental data on x-ray scattering [69] that shows that the number of vacancies at temperatures of the order of 1 K decreases with temperature more or less exponentially. But this does not mean that a ^3He crystal has no vacancies at absolute zero. The point is that the vacancies in ^3He crystals behave in a peculiar way because ^3He atoms possess nuclear spins. If all the nuclear spins are parallel, the ^3He crystal, just as the ^4He crystal, is periodic. Then due to the tunneling effect the vacancies become delocalized quasiparticles with a band width of the order of 10 K. Actually, however, down to temperatures of the order of 10^{-3} K the nuclear spins in ^3He are not aligned and for this reason the crystal is not periodic. The vacancies in such a crystal are not quasiparticles with definite quasimomenta. Leaving the discussion of this aspect to the next section, we will nevertheless consider the case of zero-point vacancies in a crystal with all nuclear spins parallel. This state can in fact be achieved by applying a strong magnetic field to the sample.

Since in the case under consideration the crystal has a periodic structure, the vacancy energy spectrum with a small negative energy ε_0 corresponding to the bottom of the band can still be described by formula (1.4.6). In the Fermi crystal of solid ^3He the vacancies are fermions, however, since for vacancy production one fermion, the atom of ^3He , must be annihilated. The ground state for fermions with the spectrum given by (1.4.6) corresponds, obviously, to a complete occupation of all negative-energy states, i.e. states with $p < p_0$, where $p_0 = (2M |\varepsilon_0|)^{1/2}$. The number of zero-point vacancies per unit volume of the crystal is

$$N_0 = (2\pi\hbar)^{-3} \frac{4}{3} \pi p_0^3 = \frac{(2M |\varepsilon_0|)^{3/2}}{6\pi^2 \hbar^3}. \quad (1.4.9)$$

Their contribution to the total energy of the crystal is negative and is

$$E_v = \int_0^{p_0} \left(\varepsilon_0 + \frac{p^2}{2M} \right) \frac{d^3 p}{(2\pi\hbar)^3} = - \frac{(2M |\varepsilon_0|)^{5/2}}{30\pi^2 \hbar^3 M}. \quad (1.4.10)$$

The presence of zero vacancies in a Fermi quantum crystal can, therefore, be described by a Fermi excitation branch in the energy spectrum of the crystal, the excitations lying near the Fermi surface. These excitations cause phenomena commonly associated with Fermi liquids, such as linear temperature dependence of heat capacity at low

temperatures and zero sound [31, 66]. The theory of these phenomena in quantum crystals can be developed (see [66]) without assuming that the quasiparticle concentration or their interaction energy are low.

1.4.3 Vacancies in ^3He Crystals

The behavior of vacancies in ^3He crystals depends greatly on the configuration of the nuclear spins. At temperatures approximately higher than 1 mK and in not very strong magnetic fields the spins are, in fact, distributed at random and the vacancy quasimomentum is not a good quantum number. In this case we can speak only

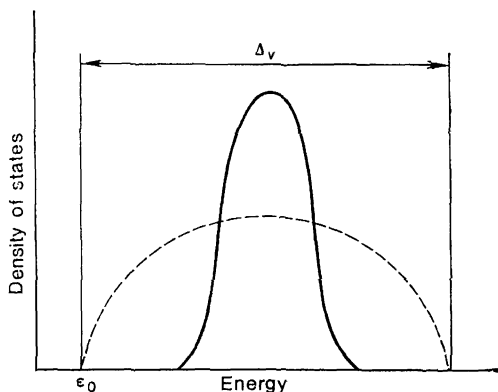


Fig. 1.14. The density of vacancy energy levels: solid line corresponds to a disordered ^3He lattice; dashed line corresponds to a ferromagnetically ordered ^3He lattice.

of the density of the vacancy energy levels, $\nu(E) = \partial N(E)/\partial E$, where $N(E)$ is the number of states with energies lower than E . Mathematically, calculating $\nu(E)$ is equivalent to using the so-called Hubbard model. The results obtained via this model for the bcc lattice by Nagaoka [70] and Brinkman and Rice [71] are illustrated in Fig. 1.14. The solid curve corresponds to a state with disordered spins, and the dotted line to the level density $\nu(E)$ corresponding to the spectrum $E(\mathbf{p})$ in a completely polarized (ferromagnetic) state. It is important to note that the energy of a vacancy in the disordered state is practically always higher than the energy ϵ_0 corresponding to the bottom of the band in the ferromagnetic lattice, and the difference is of the order of the band width $\Delta_v \sim 10$ K. The same picture emerges if instead of a disordered lattice we take an antiferromagnetically ordered lattice. Nagaoka [70] has proved that gener-

ally the bottom of the band, ε_0 , for a ferromagnetic bcc lattice is the absolute energy minimum for the vacancy, and this minimum cannot be attained for any but ferromagnetically ordered spins. Hence, ferromagnetic ordering of nuclear spins in ^3He crystals may be accompanied by a considerable drop in the vacancy energy.

In many respects this situation is similar to the behavior of electrons in liquid helium [72, 73], disordered solids [74, 75], or magnetic semiconductors [76]. It is easily seen that in a ^3He crystal there emerges a macroscopic region around each vacancy in which the nuclear spins are completely polarized [77, 78].

Indeed, suppose that the temperature is such that $J \ll T \ll \Delta_v$, where J is of the order of the exchange interaction energy for two neighboring spins ($J \sim 10^{-4}$ K). In this case the vacancies near the bottom of the band play the dominant role (their energy spectrum is then given by (1.4.6)). Let us assume that inside a sphere of radius R all spins are completely polarized, whereas outside it they are disordered. Then inside the sphere the vacancy's Hamiltonian is $E(\mathbf{p})$ and on its boundary the wave function vanishes since, as noted before, in the disordered state the vacancy has a large excess energy. The ground state energy of the vacancy then is

$$E = \varepsilon_0 + \frac{\pi^2}{2} \frac{\hbar^2}{MR^2}. \quad (1.4.11)$$

The radius R of the ferromagnetic sphere is determined from the condition that the free energy $F = E - TS$ be minimal, where S is the change in the crystal's entropy in the ordering of the spins inside the sphere. (Obviously, $S = -N \ln 2$, with N the total number of ^3He atoms inside the sphere.) The free energy is

$$F = \varepsilon_0 + \frac{\pi^2}{2} \frac{\hbar^2}{MR^2} + Tn \frac{4\pi}{3} R^3 \ln 2, \quad (1.4.12)$$

where n is the number of ^3He atoms per unit crystal volume. The requirement that F be minimal yields the following expression for the equilibrium radius of the sphere:

$$R = \left(\frac{\pi \hbar^2}{2MnT \ln 2} \right)^{1/5}. \quad (1.4.13)$$

The number N of particles inside the sphere is, in order of magnitude, $(\Delta_v/T)^{3/5}$, which is much greater than unity. Each vacancy possesses a large magnetic moment

$$\mathcal{M} = N\mu = \mu n \frac{4\pi}{3} \left(\frac{\pi}{4 \ln 2} \frac{\hbar^2}{MnT} \right)^{3/5}, \quad (1.4.14)$$

where μ is the magnetic moment of the ^3He nucleus.

The temperature dependence of the equilibrium number of vacancies in the crystal, N_v , is determined by the exponential $\exp(-F/T)$,

where F is obtained by substituting (1.4.13) into (1.4.12). We have

$$N_v \propto \exp \left\{ -\frac{\varepsilon_0}{T} - \frac{5}{6} \left(\frac{\pi^2 \hbar^2}{M} \right)^{3/5} (4\pi n \ln 2)^{2/5} T^{-3/5} \right\}. \quad (1.4.15)$$

At high temperatures the second term in the braces is predominant because it is inversely proportional to the temperature raised to a lower power. This term is always negative, i.e. the number of vacancies rapidly decreases with temperature irrespective of the sign of the first term (the sign of the latter is determined by that of the minimal vacancy energy ε_0 in the ferromagnetically polarized state). There is therefore no contradiction with high-temperature data on the temperature dependence of the number of vacancies [69] if we assume that ε_0 is negative. In this case the ferromagnetic state of the crystal is unstable toward zero-point vacancy production, a feature we discussed in Sec. 1.4.2. This instability could in fact be observed in ^3He crystals placed in a strong magnetic field. Therefore on the H - T diagram there should be a region corresponding to a crystal with zero-point vacancies [79]. At present, however, we do not know whether such a phenomenon exists.

In this connection an interesting remark was made by Castaing and Nozieres [80], who studied the crystal-liquid phase equilibrium in ^3He with polarized spins (see also [81]). The experiments discussed by these authors, and also by Lhuillier and Laloe [81], dealt with typical times that were short compared to the spin-lattice relaxation time of both solid and liquid (both time intervals are on the macroscopic scale). If melting does not change the polarization, the Pomeranchuk effect (the increase in the pressure of melting of a crystal as temperature decreases) is not present and, therefore, the solid-state region broadens from the side of small pressures. Since as the pressure drops, the vacancy band width and the probability of tunneling processes increases (see Chap. 1.2), the minimal energy ε_0 decreases, as stated in Sec. 1.4.2, which assists the appearance of a state with zero-point vacancies.

1.5 SURFACE PHENOMENA

1.5.1 The Equilibrium Shape of the Crystal-Liquid Interface

Phenomena occurring at the interface between solid and liquid helium are at present the most vivid manifestations of the quantum nature of solid helium crystals. The fact that a quantum crystal and a superfluid coexist leads to some very peculiar features of the crystallization and melting processes (see [82-85]). These processes can be called supercrystallization and supermelting since at low temperatures they occur in a coherent fashion and without

energy dissipation, i.e. just like any other superphenomenon. Even simple visual observation [83] shows that the interface between solid and liquid ^4He looks more like the interface between two low-viscosity immiscible liquids that constantly vibrates under external perturbations.

Common classical crystals at low temperatures always have a characteristic faceting, and crystallization and melting in such crystals are extremely slow thermoactivation processes (see the review articles by Chernov [86] and Jackson [87]). The reason for this is the different symmetries of the particles' arrangement in the

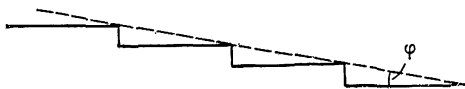


Fig. 1.15. The crystal's surface that is at a small angle to the initial face.

crystal and in the fluid that is in contact with it. A crystal is a periodic structure while a fluid is a homogeneous one. Landau [88] has shown that for this reason the surface energy at the boundary of a crystal is a highly peculiar function of the normal to its surface, a function whose derivative is everywhere discontinuous. The crystal faceting, i.e. the fact that the function that describes the shape of the crystal is not smooth, is a direct consequence of this property of the surface energy.

Following Landau [88], let us study how the surface energy per unit area, α , depends on the direction of the normal to the crystal surface when the normal is close to one of the crystallographic axes. Suppose that α_0 is the energy per unit area of the initial crystal face. A surface slightly inclined to the face must have the shape depicted in Fig. 1.15. For small inclinations φ the number of steps per unit length is small. Therefore we can neglect their interaction and write the surface energy α of the inclined surface as the sum of α_0 and the energy of the steps equal to $\beta\varphi/a$, where a is the lattice period, and β the energy per unit length of an isolated step. If the surface is inclined in the opposite direction, φ is negative but the surface will have steps of the "opposite sign" with the same energy. Whence for small values of $|\varphi|$ the surface energy is

$$\alpha = \alpha_0 + \frac{\beta}{a} |\varphi|. \quad (1.5.1)$$

The derivative $\partial\alpha/\partial\varphi$ of the surface energy with respect to angle φ , therefore, has at $\varphi = 0$ a finite jump $\delta(\partial\alpha/\partial\varphi)$ equal to $2\beta/a$.

In the general case, where the inclination of the surface is defined by two angles instead of one, the steps that appear on the surface

are not straight. The surface may have steps with kinks, as shown in Fig. 1.16.

It is apparent that we can apply the statement that the surface energy has discontinuous angular derivatives to any crystal face and not only to the face with indices (001) depicted in Fig. 1.15. The shape and meaning of steps and kinks on the surface are in each case different and are determined by the condition that the surface

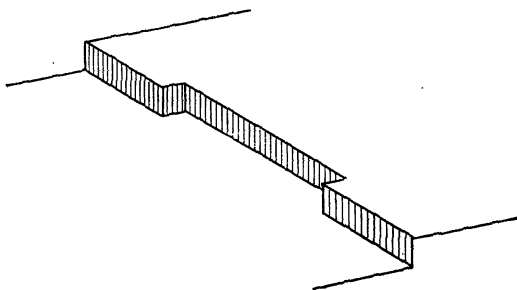


Fig. 1.16. A step with kinks.

energy is minimal. It is important that on the surfaces close to a certain crystal face the steps and kinks can have only one definite shape [88].

Crystal faceting is a direct consequence of the discontinuity of $\partial\alpha/\partial\varphi$. In [88] Landau shows that the fact that the total surface energy is minimal implies that the length of the flat sections with a given value of $\varphi = \varphi_0$ (when the crystal is in its equilibrium shape) is proportional to the jump $\delta(\partial\alpha/\partial\varphi)$ at $\varphi = \varphi_0$, i.e. to the step energy β , as seen from (1.5.1).

At a sufficiently high temperature the crystal faceting usually disappears and the surface energy becomes a smooth function of direction. The surface is then called atomically rough in contrast to the atomically smooth surface of the faceted crystal. The phase transition from an atomically smooth to an atomically rough surface takes place at a definite temperature, which for a given crystal differs from face to face. According to the aforesaid the step energy β must vanish at the transition point. Here we must note that defining β as the step energy is not completely justified. In all the relationships we have discussed so far the energy is actually the free energy (this is always the case if the temperature is not zero), so that β is the free energy per unit step length, which differs from the step energy by $-Ts$, with s the step entropy. At nonzero temperatures, thermoactivation processes produce pairs of kinks of opposite signs in the steps, and the concentration of these kinks grows with temperature and so does their contribution to the entropy of a step. This increase

in entropy s causes the free energy β to vanish at the transition point. A convenient qualitative criterion that defines the transition point in common crystals (see [86, 87]) is the transition entropy ΔS , i.e. the difference between the entropies of the fluid and solid per particle; $\Delta S \geq 1$ corresponds to a smooth surface and $\Delta S \leq 1$ to a rough one. For ordinary classical crystals the transition entropy grows without limit as the temperature drops (at the expense of the increase in the entropy per particle in the gas); whence at a sufficiently low temperature the crystal must have a smooth surface.

The crystals of helium isotopes can be in equilibrium with liquid helium at any low temperature. Since at absolute zero the entropy of both phases vanishes, the transition entropy is small in this case. If we apply the classical criterion, we conclude that solid helium has a rough surface. Although the experimental data [60, 69] in the temperature region above 1 K (crystal faceting is not present and supercooling even at high crystal growth rates is negligible) does confirm this conclusion, the classical criterion is inapplicable here. A rough surface (in the classical sense) at absolute zero cannot be in equilibrium, since its entropy is not zero. The observed phenomena as well as the very fact that there is an interface between a solid crystal and a fluid at absolute zero can be explained only with due regard for quantum effects. Andreev and Parshin [82] have shown that the interface between a quantum crystal and a quantum fluid can exist in a special state, which is the quantum analog of a rough surface.

Since in a quantum crystal the particles are delocalized, we cannot represent the microscopic structure of the interface as literally as in the case of classical crystals. But such notions as a step on the surface and a kink on the step can be introduced for quantum crystals, too. To this end it suffices to use the properties of the interface, which follow from the symmetry of the adjoining phases. For instance, a step on the surface corresponds to a state of the interface in which its position at infinity (to the right and the left in Fig. 1.16) is shifted by a basic vector of the crystal lattice and the system has the lowest possible energy. Due to the periodicity of the crystal and the homogeneity of the liquid this shift transforms the interface into an equivalent position; for this reason a step can be considered as a linear defect on the surface, and essentially only this aspect that will be of interest to us. Obviously, the usual relation remains between the crystal faceting, i.e. the discontinuity of the angular derivatives of the surface energy, and the step energy β . But contrary to classical crystals, where at absolute zero β is always positive, so that at low temperatures they are always faceted, for quantum crystals there are several possibilities. Aside from the usual surfaces, which are characterized by a positive step energy, a quantum crystal may have surfaces whose step energies are exactly zero (we will show this below).

The state of a step on a surface is characterized by the configuration of kinks on it, and the kinks may be of both signs. Each kink can be considered a point defect on the step. If a kink is shifted along the step by a basic vector, the energy of the system will not change since the transfer of an amount of substance from one phase to another as a result of such a shift contributes nothing to the energy because the chemical potentials of the two phases in equilibrium are equal. Therefore, just as in the case of point defects considered in the previous sections (impurities and vacancies), an isolated kink in a quantum crystal behaves like a delocalized quasiparticle, whose state is determined by its quasimomentum. The following fact is basic. Suppose that p_0 is the value of the quasimomentum corresponding to the bottom of the energy band. At absolute zero this state of an isolated kink is stationary and the lowest possible (the ground state), with the velocity of the kink, which is the quasimomentum derivative of the energy, being zero. Stationary states with energies close to the ground-state energy and with $p \rightarrow p_0$ have a nonzero kink velocity. Therefore, an isolated kink on a step can serve as an example of a system whose states are as close to the ground state as desired and in which there is a continuous flow of matter from one phase to another.

If the kink band width Δ is sufficiently large (roughly speaking, $\Delta/2$ must be greater than ε , the energy of a localized kink; cf. similar remarks in Sec. 1.4.2), the energy near the bottom of the band becomes negative. In this case, when kinks with $p = p_0$ form, the total energy of the step starts to drop. Spontaneous production of kinks of both signs will continue until their interaction energy compensates for the negative intrinsic kink energy. This happens for kink concentrations on the order of the atomic. We can write a qualitative expression for the minimal step energy β in the following form:

$$\beta \approx \beta_0 + \left(\varepsilon - \frac{\Delta}{2} \right) / a,$$

where β_0 is the energy of a straight, "bare" step without kinks.

A step in whose ground state there are many kinks is a system, just like an isolated kink on a step, with stationary states close to the ground state in their energy but corresponding to a continuous motion of the step, i.e. states that are characterized by a constant flow of particles from one phase to another. This is clear from the above discussion on the motion of isolated kinks and from a study of the possible processes of kink collisions. When two kinks of either signs collide, they exchange quasimomenta (Fig. 1.17a). If the colliding kinks have the same sign, this is the only elastic process that is possible. But if the signs are opposite, another possible process is the transfer of kinks to an adjacent row, a process in which each kink

conserves its quasimomentum (Fig. 1.17b). It is such processes that make a continuous motion of a step possible.

In ordinary crystals, ε and $a\beta_0$ are on the order of the difference in the energies of the two adjoining phases per interatomic bond [86]. For the solid-liquid helium interface this estimate yields $\varepsilon \sim a\beta \sim 0.1$ K. At the same time the expected value for Δ is about 1 K. For this reason it seems possible that the ground-state energy of an isolated step is negative. In this case an atomically smooth crystal surface is unstable to step production. As a result an equilibrium

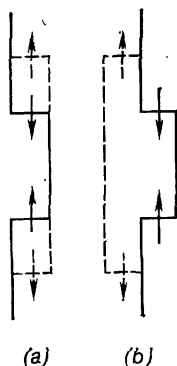


Fig. 1.17. Collision of kinks.

surface must be quantum-rough, i.e. represent a peculiar two-dimensional liquid of delocalized steps of various configurations, including closed steps of finite length. It is important that the number of steps of each kind in such a liquid is not fixed and is determined from the condition that the energy is minimal. Therefore, the step energy β , which is the derivative of the total energy with respect to the number of steps, is zero in equilibrium. This fact implies that the surface energy α is in this case a smooth function of the direction of the normal to the surface.

This discussion shows that the surface of quantum crystal at absolute zero may be either quantum-rough or quantum-smooth. In the latter case it is characterized by a positive step energy β , but there are still two possibilities. A step on a smooth surface may, in turn, be rough or smooth depending on whether there are kinks in the ground state of the step. Naturally, a crystal may have surfaces of both types, depending on their orientation, but in all cases surfaces with large indices are rough. Indeed, from the results of Landau [88] it follows that the discontinuities in the angular derivatives of the surface energy (and, hence, the energy of the effective steps) for faces of the $(1, N_1, N_2)$ type, where N_1 and N_2 are large, are caused by

superstructures produced in the rarefied system of steps and kinks. But this is impossible because of quantum delocalization of kinks and, hence, steps.

1.5.2 Crystallization and Melting

The nature and rate of crystallization and melting depend to a great extent on the type of surface. We will start with a smooth surface. Since the step energy β is positive in this case, a new row of atoms can be created only by overcoming potential barriers. Indeed, let us suppose for the sake of definiteness that the difference $\delta\mu = \mu_l - \mu_s$ of the chemical potentials of the solid, μ_s , and the liq-

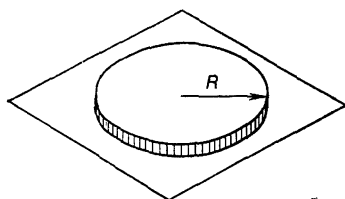


Fig. 1.18. A nucleus of a new atomic row.

uid, μ_l , is positive and small. Then crystal growth is preferable energetically. But creation of the "nucleus" of finite radius R of a new atomic row, depicted in Fig. 1.18 leads to a change in the system energy equal to

$$U(R) = 2\pi R\beta - \pi R^2 \rho_s a \delta\mu, \quad (1.5.2)$$

where ρ_s is the density of the solid phase. At small R 's this change is positive; it becomes negative only for large values of R , such that $R > R_0$, with

$$R_0 = \frac{2\beta}{\rho_s a \delta\mu}. \quad (1.5.3)$$

The situation here is similar to that discussed by Lifshits and Kagan [89] and Iordanskii and Finkel'shtein [90] concerning nucleus production in a first-order phase transition from a metastable state and to that considered by Petukhov and Pokrovskii [91] on moving dislocations. Crystal growth at sufficiently low temperatures is the result of quantum subbarrier production of nuclei with $R = R_0$, which then rapidly grow in size. Let us calculate the probability w of the nucleus of a new atomic row being created. We assume that on the given surface the step is quantum-rough. This case is favorable for crystal growth, since we saw in Sec. 1.5.1 that such steps have stationary states corresponding to a continuous motion of the step and as

close to the ground state as desired. In other words, in this case the step can move freely. But if the step is smooth, its motion is hindered by the fact that it is the result of subbarrier creation of pairs of kinks of opposite signs.

The energy $U(R)$ defined in (1.5.2) plays the role of the nucleus potential energy. To calculate the kinetic energy K associated with the growth of the nucleus at rate \dot{R} we note that the step's movement at rate \dot{R} is accompanied, due to the difference of the densities ρ_s and ρ_l of the solid and liquid, respectively, by a flow of a mass of liquid to the solid (per unit length of step per unit time) equal to $(\rho_s - \rho_l)a\dot{R}$. It is easy to find the speed of liquid flow at distances r from the step, where $a \ll r \ll R$, if we note that at such distances the step can be considered straight and the flow radial. The fact that the liquid is incompressible, i.e.

$$\pi r v(r) \rho_l = (\rho_s - \rho_l) a \dot{R},$$

implies that

$$v(r) = \frac{\rho_s - \rho_l}{\rho_l} \frac{a}{\pi r} \dot{R}. \quad (1.5.4)$$

The kinetic energy per unit step length is given by the integral

$$\int \frac{\rho_l v^2}{2} \pi r dr.$$

which, as can be seen from (1.5.4), is logarithmically divergent and must be cut off at the lower limit at $r \sim a$ and at the upper at $r \sim R$. The total kinetic energy of a nucleus can be found by multiplying the above result by $2\pi R$, which yields

$$K = a^2 \frac{(\rho_s - \rho_l)^2}{\rho_l} R \dot{R}^2 \ln \frac{R}{a}. \quad (1.5.5)$$

If we introduce the momentum

$$P = \frac{\partial K}{\partial \dot{R}} = 2a^2 \frac{(\rho_s - \rho_l)^2}{\rho_l} R \dot{R} \ln \frac{R}{a},$$

which is canonically conjugate to R , we can write the total nucleus energy as

$$E = \frac{P^2}{2M(R)} + U(R), \quad (1.5.6)$$

where

$$M(R) = 2a^2 \frac{(\rho_s - \rho_l)^2}{\rho_l} R \ln \frac{R}{a}$$

is the effective mass.

The probability w of nucleus production is determined via the semiclassical formula [20]

$$w \propto \exp \left\{ -\frac{2}{\hbar} \int_0^{R_0} |P| dR \right\}, \quad (1.5.7)$$

where the integral is evaluated along the classical trajectory from $R = 0$ to $R = R_0$ at a fixed (zero) energy. Equation (1.5.6) then implies that

$$|P(R)| = \{2M(R)U(R)\}^{1/2}.$$

Substituting into (1.5.7) and evaluating the simple integral, we find that

$$w \propto \exp \left\{ -\frac{64}{15\hbar} \frac{\beta^2(\rho_s - \rho_l)}{\rho_s^2 a^2 (\delta\mu)^2} \left(\frac{2\pi\beta}{\rho_l} \ln \frac{\beta}{\rho_s a^2 \delta\mu} \right)^{1/2} \right\}. \quad (1.5.8)$$

Crystal growth rate is usually characterized by a growth coefficient κ , which defines the (linear) dependence of the speed of the crystal boundary, V , on the deviation $\delta\mu$ of the adjacent phases from equilibrium:

$$V = \kappa \delta\mu. \quad (1.5.9)$$

If this dependence is nonlinear, the growth coefficient is defined as

$$\kappa = \lim_{\delta\mu \rightarrow 0} \frac{\partial V}{\partial \delta\mu}. \quad (1.5.10)$$

Formula (1.5.8) shows that for a smooth surface at absolute zero the probability of nucleus production and the rate V of crystal growth diminish as $\delta\mu \rightarrow 0$, roughly speaking, as $\exp(-\text{const}/(\delta\mu)^2)$, i.e. much faster than $\delta\mu$. The growth coefficient determined by (1.5.10) for a smooth surface at absolute zero is, therefore, zero.

A quite different situation emerges for a quantum-rough surface, in the ground state of which there are many steps [82]. The growth of a crystal with such a surface is due both to an increase or decrease in the area of surfaces bounded by closed steps and to the creation of new atomic layers in the collision of two steps (this is similar to the transfer of a kink to an adjacent row in the collision of two kinks; see Fig. 1.17b). It is significant that these and inverse processes are the cause of stationary states of the surface, states as close to the ground state as desired. In these states the crystal constantly grows or melts. The movement of a quantum-rough interphase boundary at absolute zero, therefore, takes place without breakdown of phase equilibrium. In other words, at absolute zero the growth coefficient becomes infinite.

At nonzero temperatures the movement of a quantum-rough boundary is accompanied by energy dissipation caused by interaction with

thermal phonons [82]. The energy dissipated per unit time per unit surface area is of the order of $E_{\text{ph}} (V/c) V$, where c is the sound velocity, $E_{\text{ph}} \sim nT^4/\Theta^3$ the phonon energy, n the number of atoms in a unit volume, and Θ the Debye temperature. On the other hand, this energy is equal to $\delta\mu\dot{M}$, where $\dot{M} \sim mnV$ is the mass of substance flowing each second from one phase to another, and m the mass of one atom. Combining the two formulas, we find that $V \sim mc (\Theta^3/T^4) \delta\mu$, i.e. the growth coefficient for a quantum-rough surface

$$\kappa \sim mc\Theta^3/T^4 \quad (1.5.11)$$

and tends to infinity as $T \rightarrow 0$ as fast as T^{-4} .

Here we must note that the regions where formula (1.5.11) is valid differ considerably for crystals of ^3He and ^4He .

In the case of ^4He crystals phonons must be the main type of thermal excitations in the liquid phase. This condition is satisfied, as is known, for temperatures lower than 0.6 K. For higher temperatures the main dissipation mechanism in the motion of the interphase boundary is the interaction with rotons, and instead of the power law we have an exponential law

$$\kappa \sim \exp (\Delta_r/T), \quad (1.5.12)$$

where Δ_r is the roton gap.

In the case of ^3He crystals formula (1.5.11) is applicable only for very low temperatures, much lower than the temperature of transition of liquid ^3He into the superfluid state. At higher temperatures, where liquid ^3He behaves like a Fermi liquid, the main dissipation mechanism is the interaction with Fermi excitations. Energy dissipation is on the order of $p_F nV^2$ (with p_F the momentum on the Fermi surface), which corresponds to a temperature-independent growth coefficient

$$\kappa \sim v_F^4; \quad (1.5.13)$$

here $v_F \sim p_F/m$ is the speed of the quasiparticles on the Fermi surface.

1.5.3 Crystallization Waves

Along a quantum-rough interface between a crystal and a liquid slowly decaying crystallization and melting waves may propagate [82, 83]. These waves appear similar to common capillary waves in a liquid-vapor interface, but there is an essential difference between the two. Capillary waves correspond to the motion of substance near the interface in the absence of vaporization and condensation. The waves we will now consider are due entirely to periodic melting and crystallization.

Let us assume that a flat crystal-liquid interface $z = 0$ undergoes a displacement

$$\zeta(x_\mu, t) = \zeta(t) e^{ik_\mu x_\mu}$$

in the direction of its normal. Here k_μ and x_μ are the two-dimensional wave vector and radius vector in the plane of the initial interface; $\mu = 1, 2$.

Let us calculate the change ΔU in the potential energy

$$U = \int \alpha(n) dS,$$

where $\alpha(n)$ is the surface energy as a function of unit normal n to the surface, and dS the area element. For small ζ 's we can put $n_z \approx 1$, $n_\mu = \partial\zeta/\partial x_\mu$,

$$dS = dx dy \left\{ 1 + \frac{1}{2} \left(\frac{\partial\zeta}{\partial x_\mu} \right)^2 \right\},$$

and

$$\alpha(n) = \alpha(0) + \alpha_\mu \frac{\partial\zeta}{\partial x_\mu} + \frac{1}{2} \alpha_{\mu\nu} \frac{\partial\zeta}{\partial x_\mu} \frac{\partial\zeta}{\partial x_\nu},$$

where $\alpha_\mu = \partial\alpha/\partial n_\mu$ and $\alpha_{\mu\nu} = \partial^2\alpha/\partial n_\mu \partial n_\nu$.

This yields

$$\Delta U = \frac{S}{4} (\alpha k^2 + \alpha_{\mu\nu} k_\mu k_\nu) |\zeta|^2, \quad (1.5.14)$$

where S is the total surface area.

The nonzero speed of the boundary $\dot{\zeta}$ due to the difference of ρ_s and ρ_l leads to a motion in the liquid (the crystal, naturally, remains at rest). We will see that the speed of the sought-for vibrations is much lower than the speed of sound. In these conditions the liquid can be considered incompressible, i.e. the velocity potential ψ ($\mathbf{v} = \nabla\psi$) satisfies the Laplace equation $\Delta\psi = 0$. At $z = 0$ the law of mass conservation,

$$\rho_l \frac{\partial\psi}{\partial z} \Big|_{z=0} = -\dot{\zeta} (\rho_s - \rho_l),$$

yields

$$\psi = \frac{1}{k} e^{-kz} \frac{\rho_s - \rho_l}{\rho_s} \dot{\zeta}.$$

The total kinetic energy of the surface is

$$K = \int dx dy \int_0^\infty dz \frac{\rho_l}{4} |\nabla\psi|^2 = \frac{S}{4} \frac{(\rho_s - \rho_l)^2}{\rho_l k} |\dot{\zeta}|^2. \quad (1.5.15)$$

Let us also calculate the rate of energy dissipation \dot{E} due to the finiteness of the growth coefficient. The energy that dissipates per

unit surface area, as noted in Sec. 1.5.2, is $\delta\mu\dot{M}$, with \dot{M} the flux of substance across the interface. To determine \dot{M} we need only note that in a reference frame in which the surface is at rest the crystal moves with a speed $-\dot{\xi}$, so that $\dot{M} = \rho_s\dot{\xi}$. As a result we have

$$\dot{E} = \int dx dy \delta\mu \rho_s \dot{\xi} = \frac{S\rho_s}{2\kappa} |\dot{\xi}|^2, \quad (1.5.16)$$

where we have accounted for the fact that according to (1.5.9)

$$\delta\mu = \dot{\xi}/\kappa.$$

Formulas (1.5.14) through (1.5.16) coincide with similar formulas for an oscillator with a natural frequency

$$\omega^2(k) = \frac{\rho_1 k}{(\rho_s - \rho_1)^2} (\alpha k^2 + \alpha_{\mu\nu} k_\mu k_\nu) \quad (1.5.17)$$

and damping coefficient (the imaginary part of the frequency)

$$\gamma = \frac{\rho_s \rho_1 k}{2\kappa (\rho_s - \rho_1)^2}. \quad (1.5.18)$$

Suppose that we want to include gravitational effects. Then in the crystallization wave spectrum, given by (1.5.17), we must include an additional term $\rho_1 g k / (\rho_s - \rho_1)$, where g is the acceleration of free fall. The dependence of the frequency on the length of the wave vector is therefore the same as for capillary-gravitational waves on the liquid-vapor interface. But the frequency dependence of the damping coefficient is quite different.

The use of formulas (1.5.11), (1.5.17), and (1.5.18) for ^4He in the low-temperature phonon range shows that there is a wide range of wave vectors $(T/\Theta)^3 \ll ka \ll 1$ (a is the interatomic distance), where the vibrations are indeed slowly decaying.

On the other hand, in the case of ^3He the substitution of (1.5.13) into (1.5.18) forces us to conclude that in the range where the theory of Fermi liquids works the vibrations decay rapidly at all frequencies.

Crystallization waves in ^4He were discovered by Keshishev, Parshin, and Babkin [83]. This is clearly seen in the photographs made by the authors of [83], where a number of consecutive states of the solid-liquid interface in ^4He are depicted after the surface is suddenly perturbed at time zero. The characteristic decay time for these perturbations was several seconds. The interface responds in the same way as a liquid surface with slowly decaying capillary waves. Such behavior is observed only at low temperatures (below 0.5 K), at higher temperatures the vibrations cease, which qualitatively agrees with the above formulas, according to which the decaying of crystallization waves rapidly increases with temperature. The authors of [83] measured the spectrum of crystallization waves and found that

the data (Fig. 1.19) accords well with the $\omega \propto k^{3/2}$ law, which is represented by the solid line in Fig. 1.19.

The fact that crystallization waves exist proves that quantum-rough surfaces of ^4He crystals do exist. This conclusion is also corroborated by studying the state of surfaces. In most cases the surface has

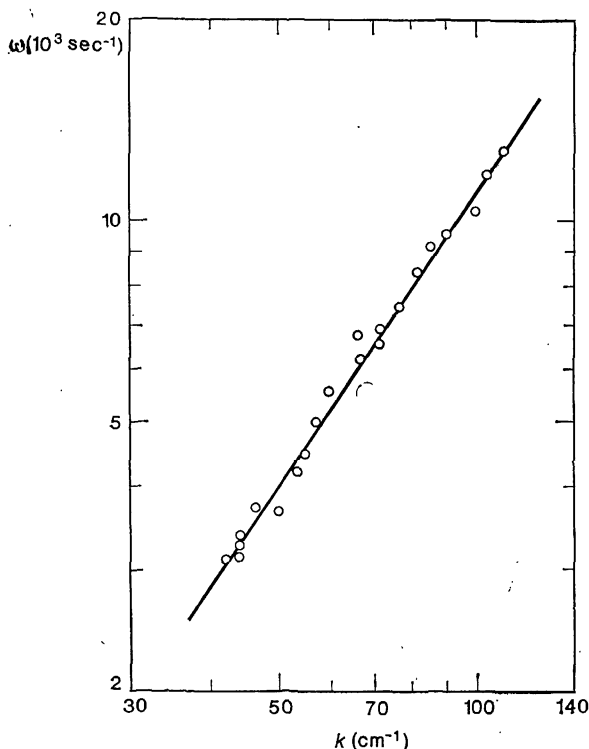


Fig. 1.19. The frequency of crystallization waves as a function of the wave vector [83].

a round shape, which corresponds to the equilibrium state if gravitational and capillary effects are taken into account. But besides quantum-rough faces there are atomically smooth faces. According to observations by Keshishev, Parshin, and Babkin, this is the case with the (0001) symmetry plane. When the orientation of the crystal is such that plane (0001) is almost horizontal, the interphase boundary contains an absolutely smooth section of the face (0001). This situation, obviously, corresponds to a state of thermodynamic equilibrium, which proves that the steps on face (0001) have positive energy. This fact is also corroborated by the data of Castaing *et al.*

[85], who measured the transmission of sound through the interphase boundary. The point is that at low temperatures the transmission coefficient is very sensitive to the crystallization rate. If the rate is sufficiently high, then, as shown by Castaing and Nozieres [84], practically all the sound must be reflected from the interphase boundary. Indeed, in this case the boundary is in a state of phase equilibrium, which at $T \rightarrow 0$ means that the pressure is constant. The pressure must always be equal to solidification pressure. Therefore, at the interphase boundary the varying part of the pressure must vanish, which means that the boundary condition for a sound wave at the interphase boundary coincides with the case of reflection at a medium-vacuum interface. In these conditions, obviously, the reflection coefficient is unity. Indeed, Castaing and others observed only a small transmission of sound through the interphase boundary except when the boundary was along the (0001) direction. This result proves that the growth rate of the crystallographic face (0001) is anomalously low, which according to the results of Sec. 1.5.2 is equivalent to assuming that this face is atomically smooth. Therefore, experiments [83, 85] indicate that in equilibrium conditions and at low temperatures ^4He crystals are partially faceted. Before these experiments crystal faceting in helium was observed by J. Landau *et al.* [92, 93].

As the temperature grows, the face (0001) becomes round. The corresponding transition temperature lies in the interval from 1.0 K to 1.2 K, according to various estimates (see [92-94, 100]).

1.6 FACETING TRANSITIONS IN CRYSTALS

1.6.1 The Role of Fluctuations

The fact that there exists a phase transition associated with the appearance of faceting in quantum crystals of ^4He when the temperature is lowered is of great interest since there is now a way to study such transitions experimentally. The point is that although the notion of faceting transitions was introduced by Burton and Cabrera [95, 96] long ago, the transitions were observed in many classical crystals only qualitatively. The difficulty lies in the enormous transient period in which classical crystals obtain their equilibrium shape. In quantum crystals this difficulty is absent because of the high probability of tunneling processes. At the same time the thermodynamic aspects of such transitions are the same for two types of crystals.

In Chap. 1.5 we saw that each crystal has a set of critical temperatures of crystal faceting. The highest of these is the temperature below which there appears for the first time a flat section, as a result of which the equilibrium shape of the crystal cannot be described

by a smooth function. The other critical temperatures are associated with the appearance of other types of flat sections. We can also say that at critical points of crystal faceting the angular derivatives of the surface energy experience discontinuities or the step energy has a finite value.

The present chapter is devoted to a thermodynamical analysis [97] of the crystal shape and the angular dependence of the surface energy near phase-transition points of crystal faceting. In many cases these transitions are continuous of the common second-order phase transition type. The formulas that describe such transitions are similar to those in Landau's theory of phase transitions, the order parameter being the size of the discontinuities in the angular derivatives of the surface energy. But there are several differences, the main concerning the peculiar role of fluctuations.

Indeed, let us consider the fluctuations of crystal shape at temperatures only somewhat higher than the critical temperature T_{cr} for a given face. Assuming that the fluctuation wavelength is much shorter than the dimensions of the sample, we can think of the equilibrium surface as flat. We select the $z = 0$ plane so that it coincides with this surface. We write the equation for the surface in the presence of fluctuations as $z = z(x_\mu)$ (with $\mu = 1, 2$; $x_1 = x$; and $x_2 = y$) and expand $z(x_\mu)$ in a Fourier series:

$$z(x_\mu) = \sum_{k_\mu} z(k_\mu) e^{ik_\mu x_\mu}, \quad (1.6.1)$$

where k_μ is the two-dimensional wave vector.

The variation of the total free energy of the crystal due to fluctuations can easily be found by applying (1.5.14). We obtain

$$\Delta U = \frac{S}{4} \sum_{k_\mu} (\alpha k^2 + \alpha_{\mu\nu} k_\mu k_\nu) |z(k_\mu)|^2, \quad (1.6.2)$$

whence in the usual way we find the following expression for the mean square of a Fourier transform:

$$\overline{|z(k_\mu)|^2} = \frac{2T}{S \tilde{\alpha}_{\mu\nu} k_\mu k_\nu}, \quad (1.6.3)$$

where $\tilde{\alpha}_{\mu\nu} = \alpha \delta_{\mu\nu} + \alpha_{\mu\nu}$.

The mean square of the fluctuation departure of the points on the surface from the equilibrium position is, in view of (1.6.3),

$$\overline{(\delta z)^2} = \frac{T}{2\pi^2} \int \frac{d^2 k}{\tilde{\alpha}_{\mu\nu} k_\mu k_\nu}. \quad (1.6.4)$$

Let us assume that we are dealing with a face normal to a symmetry axis of an order higher than the second. Then $\tilde{\alpha}_{\mu\nu} = \tilde{\alpha}_{11} \delta_{\mu\nu}$ and

(1.6.4) yields

$$\overline{(\delta z)^2} = \frac{T_{\text{cr}}}{\pi \tilde{\alpha}_{11}} \int \frac{dk}{k} = \frac{T_{\text{cr}}}{\pi \tilde{\alpha}_{11}} \ln \frac{L}{a}. \quad (1.6.5)$$

Here we have taken into account that the logarithmically divergent integral must be cut off at $k \sim L^{-1}$ (L is the size of the sample) at the lower limit and at $k \sim 1/a$ (a is the lattice period) at the upper.

The results obtained in Sec. 1.6.3 will show that $\tilde{\alpha}_{11}$ tends to infinity as $t \equiv T - T_{\text{cr}} \rightarrow 0$ in inverse proportion to t . We put $\tilde{\alpha}_{11} = (U/a^2) (T_{\text{cr}}/t)$, where U is defined as a characteristic interaction energy of the particles in the crystal. From (1.6.5) we obtain

$$\frac{\overline{(\delta z)^2}}{a^2} = \left(\frac{T_{\text{cr}}}{\pi U} \right) \left(\frac{t}{T_{\text{cr}}} \right) \ln \frac{L}{a}. \quad (1.6.6)$$

In the limit $L \rightarrow \infty$ the fluctuation shift of the surface becomes infinite at $t > 0$. But for negative t 's, due to the discontinuities in the angular derivatives of the surface energy or, in other words, due to the finite step energy, the fluctuations remain finite as $L \rightarrow \infty$. However, since the transition is continuous, these fluctuations become infinite as $t \rightarrow -0$. The point $T = T_{\text{cr}}$ is, therefore, characterized by the fact that as it is approached from below in an unlimited system ($L = \infty$) the fluctuations grow in size without limit. The problem of such a "fluctuation" phase transition on a given crystal face has lately been considered (e.g. see [98, 99]) in connection with the general problem of two-dimensional phase transitions (the fact that (1.6.5) contains a logarithm is, obviously, due to the surface being two-dimensional).

It is important, however, to note the following. The parameter T/U is rather small for all crystals, since it determines the degree of anharmonicity of atomic vibrations. Whence at $t \ll T_{\text{cr}}$ formula (1.6.6) yields $\delta z \ll a$ for all values L that are of interest. Let us estimate the extent to which this strong inequality is valid for crystals of helium, the most disadvantageous in this respect. The results of Keshishev, Parshin, and Babkin [100] show that $\tilde{\alpha}_{11} \approx 0.2 \text{ erg/cm}^2$ far from the transition point, so that

$$\frac{\overline{(\delta z)^2}}{a^2} \approx 0.2 \frac{t}{T_{\text{cr}}} \ln \frac{L}{a}. \quad (1.6.7)$$

The dimensions L of the sample for which (1.6.7) is valid are limited from above by the capillary constant $L_m \sim \alpha/g(\rho_s - \rho_l)$, where g is the acceleration of free fall; for helium this constant is about 0.1 cm. (When L is of the order of L_m or greater, we must allow for gravitational effects, as a result of which the integral in (1.6.4) does not diverge for small k_μ 's). For this reason the left-hand side in

(1.6.7) is in fact always small for a small t/T_{cr} , and only at $t/T_{\text{cr}} \approx 0.3$ does it become of the order of unity. Therefore, we arrive at the problem of the faceting transition when δz is much smaller than a , which makes it possible to neglect fluctuation effects [97].

1.6.2 Thermodynamic Relations

The equilibrium shape of a crystal is determined by the condition that the surface energy, more exactly the thermodynamic potential (see [67]) be minimal for a fixed volume of the crystal. If the surface of the crystal is given by an equation $z = z(x_\mu)$, then we have to minimize

$$\int f(h_\mu) d^2x, \quad (1.6.8)$$

where $f = \alpha (1 + h_\mu^2)^{1/2}$ and both α and f can be considered as functions of the angular variables $h_\mu \equiv \partial z / \partial x_\mu$. The condition that the crystal volume must be constant is reduced to the requirement that the integral

$$\int z d^2x \quad (1.6.9)$$

be constant. The variational problem that we have just formulated has the following first integral:

$$f = \lambda \zeta, \quad (1.6.10)$$

where λ is the Lagrange factor, and $\zeta = z - x_\mu h_\mu$.

Since $dz = h_\mu dx_\mu$, we see that $d\zeta = -x_\mu dh_\mu$, so that $x_\mu = -\partial \zeta / \partial h_\mu$. Let us introduce the quantities $\eta_\mu \equiv \partial f / \partial h_\mu$. In view of (1.6.10) we have

$$\eta_\mu = \lambda \frac{\partial \zeta}{\partial h_\mu} = -\lambda x_\mu, \quad (1.6.11)$$

i.e. in the equilibrium state the quantities η_μ differ from the coordinates x_μ in constant factors. Let us introduce a new thermodynamic potential $\tilde{f} = f - h_\mu \eta_\mu$. Since $df = \eta_\mu dh_\mu$, we see that $d\tilde{f} = -h_\mu d\eta_\mu$, so that $h_\mu = -\partial \tilde{f} / \partial \eta_\mu$.

We can write the condition for equilibrium (1.6.10) in the following equivalent form by using (1.6.11):

$$\tilde{f} = \lambda z. \quad (1.6.12)$$

The thermodynamic potential \tilde{f} as a function of the variables η_μ is, therefore, directly linked to the shape of the crystal in an

equilibrium state:

$$z(x_\mu) = \frac{1}{\lambda} \tilde{f}(\eta_\mu) = \frac{1}{\lambda} \tilde{f}(-\lambda x_\mu). \quad (1.6.13)$$

The presence of critical points of crystal faceting can be explained by the appearance of regions of zero curvature on the surface of the crystal. These regions may appear, obviously, as a result of phase transitions of the first kind. But it is more interesting to investigate the possibility of continuous faceting transitions. In such a situation, as a critical temperature is approached from above, a point $x_\mu = x_\mu^{(0)}$ corresponding to the place where the given crystal face emerges at the surface must turn into a flattening, i.e. a point where one or two eigenvalues of matrix $\partial^2 z / \partial x_\mu \partial x_\nu$ vanish. In view of (1.6.13) this means that one or two eigenvalues of matrix $\partial^2 \tilde{f} / \partial \eta_\mu \partial \eta_\nu$ or matrix $\partial h_\mu / \partial \eta_\nu$ vanish on the given face. For the transition to be continuous then it is necessary that at this critical temperature all faces close to the one considered obey the stability criterion (see [86]), which states that the quadratic form

$$\frac{\partial^2 \tilde{f}}{\partial h_\mu \partial h_\nu} \delta h_\mu \delta h_\nu = \frac{\partial \eta_\mu}{\partial h_\nu} \delta h_\mu \delta h_\nu$$

must be positive definite for all δh_μ 's. An equivalent criterion states that

$$\frac{\partial h_\mu}{\partial \eta_\nu} \delta \eta_\mu \delta \eta_\nu \quad (1.6.14)$$

must be positive definite for all $\delta \eta_\mu$'s, or that

$$\frac{\partial h_1}{\partial \eta_1} > 0 \quad \text{and} \quad \frac{\partial h_1}{\partial \eta_1} \frac{\partial h_2}{\partial \eta_2} > \left(\frac{\partial h_1}{\partial \eta_2} \right)^2. \quad (1.6.15)$$

We can easily see that a continuous faceting transition is impossible for faces that are perpendicular to 3-fold symmetry axes. In this case due to the symmetry of the face the eigenvalues of matrix $\partial^2 \tilde{f} / \partial \eta_\mu \partial \eta_\nu$ coincide and therefore both vanish at the critical point. Since the face under consideration corresponds to $\eta_\mu = 0$, the potential \tilde{f} for neighboring faces is determined by a 3rd-order invariant:

$$\tilde{f} = f_0 + a(\eta_1^3 - 3\eta_1\eta_2^2) + b(\eta_2^3 - 3\eta_1^2\eta_2),$$

where a and b are constants. If we use this formula to calculate the derivatives $\partial h_1 / \partial \eta_1$ and $\partial h_2 / \partial \eta_2$, which for small η_μ 's must be positive, we will see that both contain terms linear in η_μ and so have alternating signs. The presence of a symmetry plane passing through the axis does not, obviously help much. In this case a reflection in the plane can be represented by the transformation $\eta_1 \rightarrow -\eta_1$, so

that $a = 0$. But the terms with b still violate the stability criterion.

In most cases, as we will subsequently see, faceting transitions may be second-order phase transitions.

1.6.3 A 6-fold Symmetry Axis

Suppose that the face under consideration is perpendicular to a 6-fold symmetry axis. The potential \tilde{f} for neighbouring faces, i.e. faces with their η_μ 's small, is isotropic in this case with the required degree of accuracy. It can be written as

$$\tilde{f}(t, \eta_\mu) = f_0(t) - \frac{at}{2} \eta_\mu^2 - \frac{b}{4} (\eta_\mu^2)^2, \quad (1.6.16)$$

where $t = T - T_{cr}$ (T_{cr} is the critical temperature of crystal faceting), and a and b are constants and must be positive for the stability criterion (1.6.15) to be met at $t \geq 0$ for all η_μ 's.

We find the derivative of (1.6.16) with respect to η_μ . This yields

$$h_\mu = at\eta_\mu + b\eta_\mu^3. \quad (1.6.17)$$

From (1.6.16) and (1.6.17) it follows that at $t > 0$ and sufficiently small h_μ 's the surface energy is

$$f(t, h_\mu) = f_0 + \frac{1}{2} \frac{h_\mu^2}{at}, \quad (1.6.18)$$

i.e. its second derivatives with respect to the angular variables h_μ on the given face ($h_\mu = 0$) tend to infinity in inverse proportion to $T - T_{cr}$.

At the critical point we have

$$\eta_\mu = (bh^2)^{-1/3} h_\mu,$$

which corresponds to a nonanalytical dependence of the surface energy on the angles of the following type:

$$f = f_0 + \frac{3}{4} \left(\frac{h^4}{b} \right)^{1/3}. \quad (1.6.19)$$

In view of the general relationships (1.6.11) and (1.6.13), the shape of the crystal at $t \geq 0$ is determined directly by (1.6.16).

At $t < 0$ the dependence of η_μ on h_μ given by (1.6.17) is not one-to-one (the same is true for $f(h_\mu)$). This fact is demonstrated by Fig. 1.20, where $f - f_0$ is plotted against h_1 at $h_2 = 0$. To separate a branch of this function we note the following. First, Eq. (1.6.17) for η_μ is satisfied for values of η_μ that are realized for given values of h_μ , but generally not all solutions of this equation correspond to a real state of the surface. The same is true for various values of f for fixed values of h_μ . Second, if there are two or more values of f

for given values of h_μ that refer to actual states, then the equilibrium state corresponds to the minimal of the values of f . Third, the equilibrium surface energy f must, obviously, be a continuous function of the angular variables h_μ . The aforesaid implies that in Fig. 1.20 the f versus h_μ dependence is represented by the solid line. The dashed curve lying below the singularity O and, hence, the solutions to Eq. (1.6.17) with $\eta^2 < a|t|/b$, have no physical meaning. As a result the η_μ 's tend to a finite value $\eta_\mu = \eta_0 (h_\mu/h)$ as $h_\mu \rightarrow 0$, where $\eta_0 = (a|t|/b)^{1/2}$. In view of (1.6.11) this means that on the surface of the crystal there appears a flat section of circular shape with a

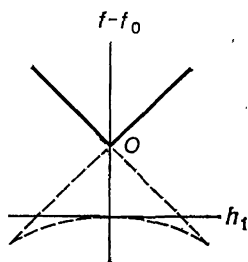


Fig. 1.20. The angular dependence of the surface energy below the transition point.

radius proportional to η_0 , i.e. to the square root of $T_{cr} - T$. The difference in the shape of this flat section from circular can be accounted for only if we include higher-order terms in $T_{cr} - T$. The dependence of the surface energy on angles and the temperature at $t < 0$ and $h \rightarrow 0$ is given by the following formula:

$$f(t, h_\mu) = f_0 + \frac{a^2}{4b} t^2 + \eta_0 h. \quad (1.6.20)$$

The size of the discontinuity in the angular derivatives at $h = 0$ is $2\eta_0$.

Therefore, in the simple case we have just studied the faceting transition is described by formulas that are similar to those in Landau's theory of phase transitions, provided we take η_μ as the order parameter and the angular variables h_μ as the external field. Note, however, the negative signs in (1.6.16).

1.6.4 A 4-fold Symmetry Axis

Suppose that the face under consideration is perpendicular to a 4-fold symmetry axis and in addition has two symmetry planes that are perpendicular to each other and contain the symmetry axis.

Among faces with a 4-fold symmetry axis this case is the most interesting experimentally. The point is that, as noted above, the most suitable objects for studying faceting transitions are crystals of helium isotopes. On the melting curve at low temperatures the isotope ^4He forms a hcp structure whose basic planes undergo a faceting transition, described in Sec. 1.6.3. In the same conditions the ^3He crystals form a bcc structure, and the basic planes have symmetry planes.

In the case we are studying the η_μ 's can form two independent fourth-order invariants. If we send the coordinate axes x_1 and x_2 along the intersection lines of the symmetry planes with the face, then we can take $\eta_1^4 + \eta_2^4$ and $\eta_1^2\eta_2^2$ as these invariants. The potential \tilde{f} has the following form:

$$\tilde{f} = f_0 - \frac{at}{2} (\eta_1^2 + \eta_2^2) - \frac{b}{4} (\eta_1^4 + \eta_2^4) - \frac{c}{2} \eta_1^2 \eta_2^2, \quad (1.6.21)$$

where a , b , and c are constants. The stability criterion at $t \geq 0$ yields the following inequalities:

$$a > 0, \quad 0 < c/3 < b.$$

By finding the derivatives of \tilde{f} with respect to the η_μ 's we arrive at the following expressions for the angular variables:

$$h_1 = \eta_1 (at + b\eta_1^2 + c\eta_2^2), \quad h_2 = \eta_2 (at + b\eta_2^2 + c\eta_1^2). \quad (1.6.22)$$

To find the specific structure of the crystal faceting at $t < 0$ we note the following. For a fixed direction of vector η_μ the potential \tilde{f} is an increasing function of η for small η 's and a decreasing function for large values. As to the dependence of \tilde{f} on the direction of η_μ , it is different for $b > c$ and $b < c$. Suppose that $b > c$. Then \tilde{f} as a function of the direction of η_μ at fixed η has minima along the coordinate axes $\eta_1 = 0$ and $\eta_2 = 0$. Since sections with zero curvature must appear where the initial potential \tilde{f} (and coordinate z in view of (1.6.13)) is minimal, such sections at $b > c$ must lie along the coordinate axes. The first formula in (1.6.22) shows that for a fixed value of η_2 ($\eta_2^2 < a|t|/c$) h_1 vanishes at two values of η_1 (differing only in sign):

$$\eta_1^{(1,2)} = \pm \left(\frac{a|t| - c\eta_2^2}{b} \right)^{1/2}.$$

At these points the potential \tilde{f} (and, hence, coordinate z), which depends only on η_1^2 , assumes the same value. Whence it is clear that the entire segment $\eta_1^{(2)} < \eta_1 < \eta_1^{(1)}$ corresponds, in fact, to a constant (zero) value of the angular variable h_1 . Similarly, for a fixed value of η_1 ($\eta_1^2 < a|t|/c$) h_2 vanishes in the segment $\eta_2^{(2)} < \eta_2 <$

$< \eta_2^{(1)}$, where

$$\eta_2^{(1,2)} = \pm \left(\frac{a|t| - c\eta_1^2}{b} \right)^{1/2}$$

Therefore, the crystal facets must have the structure depicted in Fig. 1.21. Inside the ellipse

$$b\eta_1^2 + c\eta_2^2 = a |t|$$

the crystal's surface has zero curvature along the η_1 axis. Accordingly, inside the ellipse

$$c\eta_1^2 + b\eta_2^2 = a |t|$$

it has zero curvature along the η_2 axis. In the region that is the intersection of the two ellipses there is, therefore, square flat section

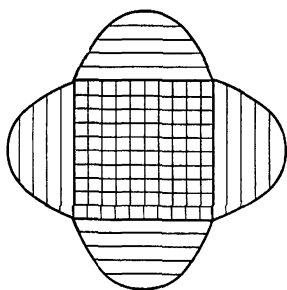


Fig. 1.21. The facet structure for a face perpendicular to a 4-fold symmetry axis.

of the surface; to this section there adjoin four sections of zero curvature in only one direction.

In the case where $b < c$ the potential \tilde{f} as a function of the direction of η_μ has minima along the bisectors $\eta_1 = \pm \eta_2$. The sections with zero curvature must lie along the two bisectors. The structure that emerges must be similar to the previous one but rotated as a whole through an angle of $\pi/4$. Indeed, if we perform a rotation through $\pi/4$, i.e. instead of η_1 and η_2 introduce the new variables

$$\eta'_1 = (\eta_1 + \eta_2)/\sqrt{2}, \quad \eta'_2 = (\eta_1 - \eta_2)/\sqrt{2},$$

then in terms of the new variables the potential \tilde{f} has the previous form but with coefficients $a' = a$, $b' = (b + c)/2$, and $c' = b' - (c - b)$. The inequality $b' > c'$ remains valid.

All linear dimensions of the facets structures vary in inverse proportion to the square root of $T_{cr} - T$, just as they did in Sec. 1.6.3.

We can easily see that if on the crystal's surface there are sections with only one axis along which the curvature is zero, then at $t < 0$ the surface energy $f(h_\mu)$ as a function of angles has singularities not only at $h_1 = h_2 = 0$ but on segments of the coordinate axes in the (h_1, h_2) plane defined by the conditions: $h_1 = 0$, $|h_2| < h_0$ and $h_2 = 0$, $|h_1| < h_0$, where

$$h_0 = \left(\frac{a^3 |t|^3}{c} \right)^{1/2} \left(\frac{b}{c} - 1 \right).$$

The surface $f = f(h_1, h_2)$ is cone-shaped with kinks of finite length situated in the region near the vertex along four generators.

Finally, we note that faceting transitions may also be continuous for faces of lower symmetry perpendicular to 2-fold symmetry axes or symmetry planes or even faces of a general type (for more details see [97]). A special feature of these cases is that the transition is accompanied by the vanishing of only one of the eigenvalues of matrix $\partial h_\mu / \partial \eta_\nu$, instead of both as in the cases just studied. As a result below the transition point there appear cylindrical sections with only one zero-curvature surface instead of flat sections. Flat sections appear only as a result of a second faceting transition on an initially cylindrical surface. Such transitions may also be of the second-order type.

1.7 DELOCALIZATION OF DISLOCATIONS

We can obtain another example of quasiparticles characteristic of quantum crystals if we consider a linear dislocation in its slip plane that is at an angle to the crystallographic directions [47]. The dislocation line in this case, as we know, is not straight.

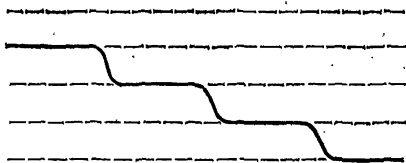


Fig. 1.22. Dislocation with kinks.

It consists of straight segments lying in the direction along which the energy of the dislocation line is minimal (this direction coincides with one of the major crystallographic axes) and a number of kinks in whose neighbourhoods the dislocation moves from one "valley" to another (Fig. 1.22). Each kink can be considered as a point defect on the dislocation. Since a crystal is periodic along a major crystallographic axis, a point defect of this kind in a quantum crystal

transforms, due to tunneling, into a delocalized quasiparticle whose states are given by the values of a one-dimensional quasimomentum.

Suppose that a dislocation has a kink with a definite value of quasimomentum. In this state the kink is completely delocalized on the dislocation, i.e. the probability of finding it is the same at any point of the dislocation. The dislocation then is found to be uniformly distributed between two neighbor valleys. If a dislocation has many kinks, it is distributed over a large number of valleys. Hence, the quantum mechanical delocalization of kinks on a dislocation leads to the dislocation being delocalized in the slip plane.

At sufficiently low concentrations, kinks can be considered as a rarefied gas of quasiparticles. For this the mean distance n^{-1} between kinks (n is the number of kinks per unit length of dislocation) must be large compared with the kink-kink interaction radius r_0 . The interaction radius is defined in the same way as in the case of impuriton-impuriton interactions. Namely, at $r = r_0$ the potential energy $U(r)$ of interaction of two kinks must coincide, in order of magnitude, with the energy band width Δ_k of a single kink. For kinks the potential energy is proportional to r^{-1} (see [101]), i.e. $U(r) \sim \delta/r$, with $\delta \sim \mu a^4$ in order of magnitude (μ is the shear modulus). As a result we have $r_0 \sim \mu a^4 / \Delta_k$.

The characteristic of a kink gas observed in experiments is its diffusion coefficient D . In the high- T region it is determined by phonon-kink collisions and dislocation vibrations. As the temperature decreases, the number of phonons and vibrations decreases, and D attains its maximal value determined by kink-kink collisions. When estimating this limiting value we must bear in mind the specific feature of the one-dimensional case. The fact is that the momenta acquired by the quasiparticles as a result of pair collisions are uniquely determined by conservation laws. There are two unknown momenta and two conditions that determine them (energy and momentum conservation laws). It is obvious that the only solution is the trivial one, corresponding to the case where the particles exchange their momenta. The momentum distribution function of the quasiparticles does not change in the process. In other words, the collision term in pair collisions vanishes and all kinetic phenomena are determined by triple collisions. The mean free path l_3 for triple collisions differs from the mean free path $l_2 \sim n^{-1}$ for pair collisions by a large factor $(nr_0)^{-1}$. For this reason the kink diffusion coefficient is, in order of magnitude,

$$D \sim v l_3 \sim \frac{a \Delta_k}{\hbar} l_3 \sim \frac{\Delta_k^2}{\hbar \mu a^3 n^2}.$$

Hence, instead of the $D \propto n^{-1}$ law, we see that D is inversely proportional to the square of quasiparticle density.

The motion of the kinks on the dislocation cannot ensure con-

tinuous motion of the dislocation under external forces. Such motion must certainly be accompanied by production of pairs of kinks of opposite signs, as a result of which part of the dislocation line transfer to a neighboring valley. In common crystals this is a thermo-activation above-the-barrier process, whence the rate of advance of a dislocation under a given force falls off exponentially with temperature. Petukhov and Pokrovskii [91] have shown that in quantum crystals the production of kink pairs is a quantum tunneling process, with a probability that is temperature-independent.

The most suitable experimental method of observing the discussed behavior of dislocations is to measure the internal friction. This method enables the researcher to study the diffusion of defects not accessible to observation by other methods. For quantum crystals there are additional possibilities [102]. Aside from the relaxation of inhomogeneities in the spatial distribution of defects (a mechanism common to ordinary crystals), there is a special relaxation of the nonequilibrium (spatially homogeneous) distribution of defects over the quasimomenta. Although at present there is a large body of data on internal-friction measurements in quantum crystals of solid helium and in solutions of hydrogen in niobium [103-107] no clearly interpretable quantum peculiarities have as yet been discovered.

References

1. R.A. Guyer, in: *Solid State Physics: Advances in Research and Applications* [eds. H. Ehrenreich, F. Seits, and D. Turnbull], Vol. 23, Academic Press, New York (1969), p. 412.
2. J. de Boer, *Physica*, **14**, 139 (1948).
3. D.J. Thouless, *Proc. Roy. Soc. (London)* **86**, 893 (1965).
4. J.H. Hetherington, W.J. Mullin, and L.H. Nosanow, *Phys. Rev.* **154**, 175 (1967).
5. L.H. Nosanow and C.M. Varma, *Phys. Rev.* **187**, 660 (1969).
6. A.K. McMahan, *J. Low Temp. Phys.* **8**, 115 (1972).
7. A.K. McMahan and R.A. Guyer, *Phys. Rev.* **A7**, 1105 (1973).
8. V.V. Avilov and S.V. Iordanskii, *Sov. Phys. JETP* **42**, 683 (1976).
9. J.M. Delrieu and M. Roger, *J. de Phys. Colloq.* **39**, C6-123 (1978).
10. L.I. Zane, *J. Low Temp. Phys.* **9**, 219 (1972).
11. R.A. Guyer, *Phys. Rev.* **A10**, 1785 (1974).
12. A.K. McMahan and J.M. Wilkins, *Phys. Rev. Lett.* **35**, 376 (1975).
13. J.H. Hetherington and F.D.C. Willard, *Phys. Rev. Lett.* **35**, 1442 (1975).
14. H.A. Reich and W.N. Yu, *Phys. Rev.* **129**, 630 (1963).
15. R.L. Garwin and A. Landesman, *Phys. Rev.* **133**, A1503 (1964).
16. M.G. Richards, J. Hutton, and R. Giffard, *Phys. Rev.* **139**, A1991 (1965).
17. R.C. Richardson, E. Hunt, and H. Meyer, *Phys. Rev.* **138**, A1326 (1965).
18. R.A. Guyer, R.C. Richardson, and L.I. Zane, *Rev. Mod. Phys.* **43**, 532 (1971).
19. A. Abragam, *The Principles of Nuclear Magnetism*, Oxford U.P., Oxford (1961).
20. L.D. Landau and E.M. Lifshitz, *Quantum Mechanics*, Pergamon Press, Oxford (1965).
21. W.P. Kirk, E.B. Osgood, and M.C. Garber, *Phys. Rev. Lett.* **23**, 833 (1969).

22. D.M. Bakalyar, E.D. Adams, Y.C. Hwaug, and C.V. Britton, in: *Proc. Int. Quantum Crystal Conf.*, Fort Collins, Colo., Aug. 1977.
23. T.C. Prewitt and J.M. Goodkind, *Phys. Rev. Lett.* **39**, 1283 (1977).
24. W.P. Halperin, F.B. Rasmussen, C.N. Archie, and R.C. Richardson, *Phys. Rev. Lett.* **32**, 927 (1974); *J. Low Temp. Phys.* **31**, 617 (1978).
25. R.B. Kummer, R.M. Mueller, and E.D. Adams, *J. Low Temp. Phys.* **27**, 319 (1977).
26. D.D. Osheroff, M.C. Gross, and D.S. Fisher, *Phys. Rev. Lett.* **44**, 792 (1980).
27. L.D. Landau and E.M. Lifshitz, *Statistical Physics*, Addison-Wesley, Reading, Mass. (1969).
28. M. Roger, J.M. Delrieu, and J.H. Hetherington, *Phys. Rev. Lett.* **45**, 137 (1980).
29. H. Godfrin, G. Frossati, D. Thouloure, M. Chapellier, and W.G. Clark, *J. de Phys.* **C6**, 283 (1978); K. Yosida, *Prog. Theor. Phys. Suppl.* **69**, 475 (1980).
30. A. Landesman, *J. de Phys. Colloq.* **39**, C6-1305 (1978).
31. A.F. Andreev and I.M. Lifshits, *Sov. Phys. JETP* **29**, 1107 (1969).
32. R.A. Guyer and L.I. Zane, *Phys. Rev. Lett.* **24**, 660 (1970).
33. M.G. Richards, J. Pope, and A. Widom, *Phys. Rev. Lett.* **29**, 708 (1970).
34. A. Widom and M.G. Richards, *Phys. Rev.* **A6**, 1196 (1972).
35. V.N. Grigor'ev, B.N. Esel'son, V.A. Mikheev, and Y.E. Shul'man, *JETP Lett.* **17**, 16 (1973).
36. V.N. Grigor'ev, B.N. Esel'son, V.A. Mikheev, V.A. Slyusarev, M.S. Strzheimchyn, and Y.E. Shul'man, *J. Low Temp. Phys.* **13**, 65 (1973).
37. V.N. Grigor'ev, B.N. Esel'son, and V.A. Mikheev, *Sov. Phys. JETP* **39**, 153 (1974).
38. A. Landesman and J.M. Winter, in: *Proc. of the 13th Int. Conf. on Low Temp. Phys. (LT-13)* [eds. W.J. O'Sullivan and K.D. Timmerhaus], Vol. 2, *Quantum Crystals and Magnetism*, Plenum Press, New York (1974), p. 73.
39. D.I. Pushkarov, *Sov. Phys. JETP* **32**, 954 (1971); *JETP Lett.* **17**, 386 (1974).
40. Y. Yamashita, *J. Phys. Soc. Japan* **37**, 1210 (1974).
41. Yu. Kagan and L.A. Maksimov, *Sov. Phys. JETP* **38**, 307 (1974).
42. Yu. Kagan and M.I. Klinger, *J. Phys.* **C7**, 2791 (1974).
43. A.F. Andreev and A.E. Meierovich, *Sov. Phys. JETP* **40**, 776 (1975).
44. W. Huang, H.A. Goldberg, and R.A. Guyer, *Phys. Rev.* **B11**, 3374 (1975).
45. J. Eshelby, in: *Solid State Physics: Advances in Research and Applications* [eds. H. Ehrenreich, F. Seits, and D. Turnbull], Vol. 3, Academic Press, New York (1956), p. 79.
46. J. Wilks, *The Properties of Liquid and Solid Helium*, Clarendon Press, Oxford (1967).
47. A.F. Andreev, *Sov. Phys. JETP* **41**, 1170 (1975).
48. V.A. Mikheev, B.N. Esel'son, V.N. Grigor'ev, and N.P. Mikhin, *Fiz. Nizk. Temp.* **3**, 385 (1977).
49. A.R. Allen and M.G. Richards, in: *Proc. Int. Quantum Crystal Conf.*, Fort Collins, Colo., Aug. 1977, p. C-83.
50. A.E. Meierovich, *Sov. Phys. JETP* **42**, 676 (1975).
51. M.G. Richards, J.H. Smith, P.S. Tofts, and W.J. Mullin, *Phys. Rev. Lett.* **34**, 1545 (1975).
52. W.J. Mullin, R.A. Guyer, and H.A. Goldberg, *Phys. Rev. Lett.* **35**, 1007 (1975).
53. J.E. Sacco and A. Widom, *J. Low Temp. Phys.* **24**, 241 (1975); *Phys. Rev.* **B17**, 204 (1978).
54. A.F. Andreev, *Sov. Phys.-Uspekhi* **19**, 137 (1976).
55. A.S. Greenberg, W.C. Thomlinson, and R.C. Richardson, *J. Low Temp. Phys.* **8**, 3 (1972).

56. J.H. Hetherington, *Phys. Rev.* **176**, 231 (1968).
57. R.A. Guyer, *J. Low Temp. Phys.* **8**, 427 (1972).
58. V.P. Mineev, *Sov. Phys. JETP* **36**, 964 (1973).
59. N. Sullivan, G. Deville, and A. Landesman, *Phys. Rev.* **B11**, 1858 (1975).
60. A.I. Shal'nikov, *Sov. Phys. JETP* **20**, 1161 (1965).
61. K.O. Keshishev, L.P. Mezhev-Deglin, and A.I. Shal'nikov, *JETP Lett.* **12**, 160 (1970).
62. G.A. Sai-Halasz and A.J. Dahm, *Phys. Rev. Lett.* **28**, 124 (1972).
63. D. Marty and F.I.B. Williams, *J. de Phys.* **34**, 989 (1973).
64. K.O. Keshishev, *Sov. Phys. JETP* **45**, 273 (1977).
65. G.V. Chester, *Phys. Rev.* **A2**, 256 (1970).
66. I.E. Dzyaloshinskii, P.S. Kondratenko, and V.S. Levchenkov, *Sov. Phys. JETP* **35**, 823, 1213 (1972).
67. L.D. Landau and E.M. Lifshitz, *Statistical Physics*, Addison-Wesley, Reading, Mass. (1969).
68. A.J. Leggett, *Phys. Rev. Lett.* **25**, 1543 (1970).
69. B.A. Fraass, S.M. Heald, and R.O. Simmons, in: *Proc. Int. Quantum Crystal Conf.*, Fort Collins, Colo., Aug. 1977.
70. A. Nagaoka, *Phys. Rev.* **147**, 392 (1966).
71. Wm. Brinkman and M. Rice, *Phys. Rev.* **B1**, 1324 (1970).
72. R.A. Ferrell, *Phys. Rev.* **108**, 167 (1957).
73. C.G. Kuper, *Phys. Rev.* **122**, 1007 (1961).
74. I.M. Lifshits and S.A. Gredeskul, *Sov. Phys. JETP* **30**, 1197 (1970).
75. M.A. Krivoglaz, *Sov. Phys.-Uspekhi* **16**, 856 (1974).
76. E.L. Nagaev, *Sov. Phys. JETP* **27**, 122 (1968).
77. A.F. Andreev, *JETP Lett.* **24**, 564 (1976).
78. H. Heritier and P. Lederer, *J. de Phys. Lett.* **38**, L-209 (1977).
79. A.F. Andreev, V.I. Marchenko, and A.E. Meierovich, *JETP Lett.* **26**, 36 (1977).
80. B. Castaing and P. Nozieres, *J. de Phys.* **40**, 257 (1979).
81. C. Lhuillier and F. Laloe, *J. de Phys.* **40**, 239 (1979).
82. A.F. Andreev and A.Ya. Parshin, *Sov. Phys. JETP* **48**, 763 (1978).
83. K.O. Keshishev, A.Ya. Parshin, and A. Babkin, *JETP Lett.* **30**, 56 (1979).
84. B. Castaing and P. Nozieres, *J. de Phys.* **41**, 701 (1980).
85. B. Castaing, S. Balibar, and C. Laroche, *J. de Phys. Lett.* **41**, L-897 (1980).
86. A.A. Chernov, *Sov. Phys.-Uspekhi* **4**, 116 (1961).
87. K.A. Jackson, in: *Crystal Growth and Characterization* [eds. R. Veda and J.B. Mullin], North-Holland, Amsterdam (1975), p. 21.
88. L.D. Landau, in: *Collected Works* [in Russian], Vol. 2, Nauka, Moscow (1969), p. 119 [English transl.: *Collected Papers of L.D. Landau*, Pergamon Press, Oxford (1965-70)].
89. I.M. Lifshits and Yu. Kagan, *Sov. Phys. JETP* **35**, 206 (1972).
90. S.V. Iordanskii and A.M. Finkel'shtein, *Sov. Phys. JETP* **35**, 215 (1972).
91. B.V. Petukhov and V.L. Pokrovskii, *Sov. Phys. JETP* **36**, 336 (1973).
92. J. Landau, S.G. Lipson, L.M. Maattanen, L.S. Balfour, and D.O. Edwards, *Phys. Rev. Lett.* **45**, 31 (1980).
93. J.E. Avron, L.S. Balfour, C.G. Kuper, J. Landau, S.G. Lipson, L.S. Schulman, *Phys. Rev. Lett.* **45**, 814 (1980).
94. S. Balibar and B. Castaing, *J. de Phys. Lett.* **41**, L-320 (1980).
95. W.K. Burton and N. Cabrera, *Disc. Faraday Soc.* No. 5, 33 (1949).
96. W.K. Burton, N. Cabrera, and F.C. Frank, *Phil. Trans. Roy. Soc. (London)* **243A**, 299 (1951).
97. A.F. Andreev, *Zh. Éksp. Teor. Fiz.* **80**, 2042 (1981).
98. J.D. Weeks, in: *Ordering in Strongly Fluctuating Condensed Matter Systems* [ed. T. Riste], Plenum Press, New York (1980), p. 293.

99. H. Müller-Krumbhaar, in: *Crystal Growth and Materials* [eds. E. Kaldis and H. Scheel], Vol. 2, North-Holland, Amsterdam (1977), p. 115.
100. K.O. Keshishev, A.Ya. Parshin, and A.V. Babkin, *Zh. Éksp. Teor. Fiz.* **80**, 716 (1981).
101. J.P. Hirth and J. Loethe, *Theory of Dislocations*, McGraw-Hill, New York (1968).
102. A.E. Meierovich, *Sov. Phys. JETP* **44**, 617 (1976), *ibid.*, **40**, 368 (1974).
103. H. Suzuki, *J. Phys. Soc. Japan* **35**, 1472 (1973), *ibid.*, **42**, 1865 (1977).
104. É.L. Andronikashvili, I.A. Gachechiladze, and V.A. Melik-Shakhnazarov, *J. Low Temp. Phys.* **23**, 5 (1976).
105. É.L. Andronikashvili, V.A. Melik-Shakhnazarov, and I.A. Naskidashvili, *Sov. J. Low Temp. Phys.* **1**, 290 (1975).
106. V.L. Tsymbalenko, *Sov. Phys. JETP* **45**, 989 (1977).
107. F. Tsuruoka and Y. Hiki, *Phys. Rev.* **B20**, 2702 (1979).

Electronic Phase Transitions and the Problem of Mixed Valence

D. I. Khonskii, Cand. Sc. (Physics and Mathematics)

P. N. Lebedev Institute of Physics,
Academy of Sciences of the USSR

2.1 INTRODUCTION

Electronic phase transitions (EPT) are usually understood to be the phase transitions in a solid that basically involve the electron subsystem. Such, for instance, are the Mott metal-insulator transitions [1-3] and valence-change transitions in rare-earth metals and compounds [4-8]. Another example is the transition from localized to delocalized electrons (the Anderson transition) [9, 10]. It is natural that the change in the state of the outermost (valence) electrons affects other properties of solids, namely, those associated with the crystal lattice. We can also say that the interaction of electrons with the lattice influences the parameters of EPT. From this viewpoint singling out EPT is a somewhat artificial procedure, since in the final analysis all phase transitions in solids (e.g. structural transitions) are "electronic" in origin because the types of chemical bond and lattice structure depend on the configuration of the valence electrons. However, this basic fact often remains concealed, and many transitions are described without such analysis. For instance, the usual way of interpreting ferroelectric phase transitions is to resort to the anharmonicity of lattice vibrations as the basic mechanism [11]. At the same time, the main features of phenomena like the Mott transition or a transition with valence change can be interpreted mainly by using the language of valence electrons, which justifies our singling out such phenomena and employing the term EPT.

The present review focuses on transitions in rare-earth compounds associated with a change in the electron configuration of the rare-earth ions but not with a change in lattice symmetry (so-called isostructural phase transitions). It also describes the electronic states that occur in such transitions, mixed valence (MV) states. Only recently have such phenomena been thoroughly studied (e.g. see [4-8]), although the first experimental works appeared in the early sixties [12, 13].

The class of substances is fairly large in which, in contrast to typical rare-earth compounds, the 4f shell loses its stability while in many ways retaining its atomlike character. At present more than a hundred such compounds have been discovered. In such substances states having different numbers of f-electrons per site

(e.g. states $4f^n$ and $(4f^{n-1} + \text{one electron in the conduction band})$) prove to lie close in energy. Due to this resonance transitions may occur between these configurations, the f-electrons acquire a partially band nature, the mean number of f-electrons per center (the ion's valence) becomes nonintegral, etc. Such compounds have come to be known as mixed-valence compounds.

States with mixed valence have a number of unique properties, which are of interest in themselves but can also contribute to our understanding of the behaviour of electrons in a solid. Under variation of external conditions (temperature, pressure, composition) compounds of this type often undergo phase transitions involving variation in the filling of electron levels. In some cases these transitions are of the insulator-metal type. Also there is often a change in magnetic properties (localized magnetic moments vanish), i.e. these transitions are of the magnetic-nonmagnetic state type.

Systems with mixed-valence states show marked anomalies in practically all experimentally measured characteristics: in lattice properties (anomalously high compressibility), in specific heat (anomalously high linear specific heat at low temperatures), in magnetic susceptibility, and transport characteristics (especially in electric conductivity).

The fundamental problem that we can hope to solve by studying such substances is the relationship between the pictures of localized and collective states in describing the behavior of the electrons in solids, i.e. when does one or the other language fit, how do transitions between these states occur, and what peculiar features in the behavior of the electron (and lattice) system accompany such transitions? Since the f-electrons do to a great extent retain their atom-like character, there is the hope that at least in certain respects the corresponding substances may be simpler than compounds of d metals and actinides, for which all characteristic parameters are of the order of unity. We may assume, therefore, that an understanding of the situation with mixed valence will also help clarify the properties of transition metals and their compounds.

The physics of mixed valence is, in fact, closely related to a number of problems and phenomena in solids. These include the question of the nature of magnetism, the Kondo effect, insulator-metal transitions, spatial ordering and Wigner crystallization; one can also add superconductivity [95]. We must also note that EPT in such compounds resemble phenomena occurring in superdense matter, a topic that is important for astrophysics [96]. To a certain extent systems with mixed valence may serve as a general model of condensed matter (see Chap. 2.6). All this together with the intrinsic importance of such compounds explains the growing interest in this class of physical objects, which in many respects are unique.

This review is concerned mainly with the theoretical aspects of

the MV problem. Experimental results are brought in largely to illustrate and justify the theoretical discussion. Although solid-state theoreticians in many countries are working in this field and our aim is to give a comprehensive picture of the present state of this field, we will dwell chiefly on the works of Soviet authors.

2.2 LOCALIZATION OF ELECTRONS AND INSULATOR-METAL TRANSITIONS (MOTT-HUBBARD TRANSITIONS)

We will start with a brief survey of a problem that is important not only to the physics of rare-earth compounds and the MV problem but has general significance. This problem is the relationship between the localized and collective states of electrons in a solid. As is known, there are two limiting pictures of the behavior of electrons in a solid. The usual band scheme, which works well for normal metals and semiconductors, deals with almost free electrons moving in the periodic lattice potential. The corresponding states (Bloch waves) prove to be delocalized; the electron-electron interaction is usually taken into account by the Hartree-Fock approximation and does not violate the one-electron picture.

On the other hand, in some cases a more appropriate way to describe the behavior of electrons is to use the language of localized states (in the theory of molecules this is the Heitler-London approximation). This approach is justified for strong interelectronic correlation; in reality it is valid for the electrons of inner shells. For filled shells both approaches are completely equivalent, but for partially filled shells this is not so. These are the partially filled *d* and *f* states in transition and rare-earth metals and actinides and their compounds. Since the electrons are localized, such substances are magnetic, as a rule. It is this localization that explains the fact that, in contrast to the predictions of the band theory, many such substances are insulators (Mott insulators).

The criterion that enables us to choose between the two types of states involves the mean Coulomb interaction energy between two electrons, $\bar{U} \sim e^2/\bar{r}$, and the characteristic kinetic energy, $E_{\text{kin}} \sim \hbar^2/m\bar{r}^2$: at $E_{\text{kin}} > \bar{U}$ the electrons are delocalized, while the opposite inequality enables us to use the picture of localized electrons. We see that the second case is realized in a rarefied system:

$$\bar{r} \gg \frac{\hbar^2}{me^2} = a_0, \quad (2.2.1)$$

i.e. when the mean distance between electrons *r* is greater than the Bohr radius a_0 . In other words, the overlap of the wave functions of

neighboring centers must be small, a situation realized for d- and especially f-electrons.

The fact that in a system with low density the electrons are localized and because of this lose their "metallic" nature was first pointed out for an electron gas by Wigner [14] (the jellium model) and for real solids by Landau and Zel'dovich [1]. The latter work, which unfortunately remained largely unnoticed, contains practically all the ideology of insulator-metal transitions and the argument (related to R. Peierls) showing that such transitions must be of the first order [1]:

A dielectric differs from a metal in that it has an energy gap in its electronic spectrum. But does this gap tend to zero when we approach the point of transition from dielectric to metal? If this was the case, we should have a transition without latent heat, without jumps in volume, and other properties. Peierls has shown that a transition continuous in this sense is impossible. Suppose we are studying an excited state of a dielectric, a state in which it conducts electricity. An electron leaves its place and is moving in the lattice, leaving a positive charge in another place in the lattice. When the electron has traveled far from the positive charge, it is attracted by a Coulomb force that tends to return the electron to its site. In an attractive Coulomb field there are always discrete levels of negative energy, corresponding to an electron binding. Therefore, the excited and conducting states of a dielectric are always separated from the ground state, in which the electrons are bound, by a gap of finite width.

Later Mott [16] expounded these ideas independently. By estimating the screening of the Coulomb potential as the number of excited electrons grows and using the condition for a bound electron state to disappear, he found the criterion for an insulator-metal transition:

$$\bar{r} \sim n^{-1/3} \leq 4a_0 \quad (2.2.2)$$

(n is the electron concentration). The phenomenon associated with this transition is often called a Mott transition.

The simplest model employed in studying Mott transitions was proposed by Hubbard [17]. In this model the electrons in a non-degenerate band interact via a repulsive force at one site:

$$H = \sum_{ij, \sigma} t_{ij} a_{i\sigma}^\dagger a_{j\sigma} + \frac{U}{2} \sum_{i\sigma} a_{i\sigma}^\dagger a_{i\sigma} a_{i, -\sigma}^\dagger a_{i, -\sigma}. \quad (2.2.3)$$

The tunneling integral t is the measure of kinetic energy, and criterion (2.2.1) here has the form $t < U$. When there is one electron per site and t is greater than U , the system is a metal (if we

ignore special cases of so-called nesting); at $t < U$ the electrons in the ground state are localized at the centers and the substance is an insulator.

Although there are many works devoted to the Hubbard model (e.g. see [2] and a rather old review [3]) and qualitatively the picture is clear, there is as yet no consistent treatment of Mott transitions (which occurs at $t/U \sim 1$). One reason, aside from the absence of a small parameter, is apparently the fact that for such transitions it is impossible to introduce an order parameter [3] in the usual sense, i.e. defined as an average of some operator over the ground state. This is because an insulator differs from a metal not so much in the properties of the ground state as in the characteristics of the excited states (the presence or absence of a gap in the single-particle spectrum of current-carrying excitations).^{*} Moreover, a Mott transition is accompanied by the disappearance of localized magnetic moments at a site (the ground state in the dielectric phase proves to be magnetically ordered). It is not known at present whether the insulator-metal transition in the Hubbard model occurs simultaneously with the disappearance of magnetic ordering or there exists an antiferromagnetic metal phase [2, 18]. The close interrelationship of charge excitations and spin excitations also has a marked influence on the spectrum of elementary excitations (see [3, 19]); this problem, however, is also not solved completely.

In essence the difficulty in building the theory of Mott transitions is due to the fact that to describe the transition we must change the mode of description: from electrons localized at the centers with a "single" filling of each level we must switch to the usual band "double" filling. When this is done even the statistics of the electrons changes [89, 90]: the "atomic" statistics becomes the usual Fermi statistics.

In reality the systems closest to the Hubbard model appear to be the transition metals and their compounds [of course many important details are ignored in the Hamiltonian (2.2.1)]. In such substances the width of the d band, t , is of the order of the Coulomb interaction, U , and, therefore, these substances constitute, as Varma noticed in [5], a "theorist's nightmare". With this fact are associated the well-known difficulties in describing magnetism in substances of the type of iron [22, 23] and insulator-metal transitions often observed in such compounds as vanadium oxides [2, 24].

* Because of this the insulator-metal transition in the "pure" Hubbard model may not be a real phase transition in the usual sense and becomes one only after an extra degree of freedom has been added (a change in the lattice constant, for one).

2.3 ELECTRONIC PHASE TRANSITIONS IN RARE-EARTH COMPOUNDS

2.3.1 The General Picture of Transitions

At first glance the situation with rare-earth compounds seems simpler than with transition metals. In typical rare-earth compounds there are two groups of electrons: the outer valence electrons, which form chemical bonds or form the metallic band (they are described by usual Bloch waves), and the electrons of the inner partially filled 4f shells.* Since the radius of the 4f wave function is exceptionally small (~ 0.5 Å), we can neglect the overlap of the wave functions of neighboring centers. At the same time the Coulomb interaction of f-electrons at the center is strong ($U_{ff} \sim 5-7$ eV), and we can assume that the f-electrons are far on the dielectric "side" of the Mott-Hubbard transition ($t_{ff} \ll U_{ff}$). This is usually the case for most rare-earth metals and compounds; on the f shells there is an integral number of f-electrons, which behave like atomic electrons—they possess the same properties and are characterized by the same quantum numbers L , S , and J as the states of the corresponding isolated ion. The only degree of freedom of these electrons is the magnetic moment: 4f-electrons determine the magnetic properties of the corresponding substances but do not directly participate in forming chemical bonds or in the electric conductivity. They act on the conduction electrons via the exchange interaction

$$H = -J \sum_{\mathbf{k}\mathbf{k}'\sigma\sigma'} \mathbf{S} \cdot \mathbf{a}_{\mathbf{k}\sigma}^+ \sigma \mathbf{a}_{\mathbf{k}'\sigma'}. \quad (2.3.1)$$

For isolated impurities this interaction results in the Kondo effect (see [29]), while in condensed systems it results in the RKKY interaction between localized moments.

However, systems exist in which the f level (we mean the upper filled f level where the Coulomb interaction with the other f-electrons of the ion has been taken into account) lies near the Fermi surface of the metal. In this case the nature of the interaction of the f-electrons with the conduction electrons and the very state of the f-electrons change considerably. The electrons may leave the f level for the conduction band and become collectivized there; in addition to spin fluctuations there appear charge fluctuations; the mean occupation number of the f level (i.e. the average valence of the rare-earth ion) becomes nonintegral; etc. Besides, under external factors

* In real rare-earth compounds the conduction band has partially a d-character and the electrons in this band may be correlated to some degree. In some models these electrons are even considered localized [25, 26]. This, however, is hardly the case (see band calculations in [27, 28]), and in what follows such models will be considered only briefly.

(pressure, temperature, variation in composition) both the position of the f level E_f relative to the Fermi level ϵ_F and its width Γ may change, and as a result the electron configuration of the ions changes (for one, if the f level rises above the Fermi level, the electrons from it "spill over" into the conduction band (Fig. 2.1); the broadening

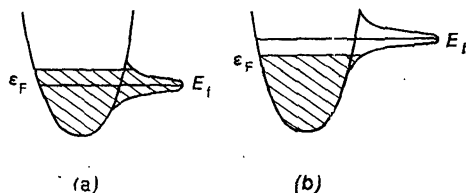


Fig. 2.1. A schematic view of changes in the energy spectrum when the f level shifts. Occupied states are cross-hatched.

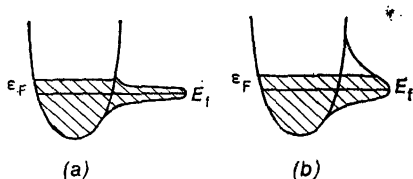


Fig. 2.2. The change in spectrum and the occupation of the f level under its broadening.

of the f level also leads to a change in the number of occupied f states (Fig. 2.2). In condensed systems such rearrangements are cooperative and lead to phase transitions (often to first-order phase transitions). Here the main change occurs in the electronic subsystem while the lattice symmetry does not usually change (the one thing that changes is the specific volume).

The basic feature of these transitions is that usually the occupation number of the f level does not change by an integer but becomes nonintegral after the transition, as though there were ions in the system with different electron configurations (different valencies) in equivalent positions in the lattice simultaneously, say the configurations $4f^n$ and $(4f^{n-1}$ plus a conduction electron). It is clear that this is the case if the f level has risen insufficiently above ϵ_F : if the number of unoccupied states below this level where the f -electrons can go is less than unity, there occurs a partial electronic transfer and the valence remains intermediate. In the process the position of the f level automatically coincides with that of the (new) Fermi level. Thus, in the mixed-valence phase there is a narrow resonance (when we allow for the f - s transitions, the f level acquires a finite width), and the number of such resonances is about 10^{22} cm^{-3} . Since the majority of the properties of solids (at least at low temperatures)

is determined by the electrons at the Fermi surface, this leads to extremely strong anomalies in all characteristics of a substance in the mixed-valence phase (e.g. see [7] and Sec. 2.6.1).

2.3.2 Theoretical Models for Describing Electronic Phase Transitions and MV States

In describing systems with the f level lying near the Fermi level ε_F two types of questions arise. First, we are concerned with the structure and properties of a mixed-valence state, i.e. the type of ground state and its physical properties. Second, we are interested in the nature of the valence transition: its type (discontinuous or continuous) and the mechanism underlying this transition. Of course, these questions are basic to any transitions in a solid, but we would also like to know how the MV phase remains stable in such transitions.

A theoretical model that claims a correct description of EPT and properties of MV states must include f -electrons with a strong Coulomb f - f interaction (the direct overlap of the wave functions of these electrons can be ignored), conduction electrons, and the various types of interaction of the f - and s -electrons with each other and also, if necessary, their interaction with the lattice. Accordingly, EPT theories fall into two categories: theories in which the Coulomb interaction of the f - and s -electrons determines the characteristics of the EPT's (the Falicov-Kimball model [30]) and those in which these transitions are due to electron-lattice interaction. We will consider both later (see Chaps. 2.4 and 2.5); here we will proceed with what may seem to be a simpler model but which contains all the physics (and basic difficulties) of the phenomena considered.

For one center the simplest model describing the behavior of an f -electron in the "sea" of conduction electrons is the Anderson model [31] of magnetic impurities in a metal:

$$H = E_f \sum_{\sigma} f^{\dagger}_{f\sigma} f_{f\sigma} + \sum_{k\sigma} \varepsilon_k a^{\dagger}_{k\sigma} a_{k\sigma} + \sum_{k\sigma} (V_k f^{\dagger}_{f\sigma} a_{k\sigma} + \text{h.c.}) + U n_{f\uparrow} n_{f\downarrow}. \quad (2.3.2)$$

For a "deep" impurity ($E_f \ll \varepsilon_F$ and $\varepsilon_F - E_f \gg \Gamma = \rho\pi V^2$) the model (2.3.2) is equivalent to the s - f exchange model (the Kondo model) (2.3.1), where the exchange integral is given by the following formula [32]:

$$J = \frac{2V^2 U}{(E_f - \varepsilon_F)(E_f - \varepsilon_F + U)} = \frac{2V^2}{(E_f - \varepsilon_F)} \Big|_{U \rightarrow \infty}. \quad [(2.3.3)]$$

Many results, including exact results (see [29]), are known for this model. We will be interested chiefly in the asymmetric Anderson model, where $E_f \sim \varepsilon_F$; besides, unlike the case of impurities, we will consider a condensed system, in which there is an f level at each

lattice site. The respective generalization of the Anderson model of a magnetic impurity is quite obvious; it is known as the Anderson lattice:

$$H = \sum_{i\sigma} E_f f_{i\sigma}^\dagger f_{i\sigma} + \sum_{k\sigma} \varepsilon_k a_{k\sigma}^\dagger a_{k\sigma} + \sum_{ik\sigma} (V_{ik} f_{i\sigma}^\dagger a_{k\sigma} + \text{h.c.}) \\ + U \sum_i f_{i\uparrow}^\dagger f_{i\uparrow} f_{i\downarrow}^\dagger f_{i\downarrow}. \quad (2.3.4)$$

Even for one site (see (2.3.2)) the problem is essentially many-particle. Besides, because of the scattering of s-electrons by the f centers there appears an effective interaction of f-electrons with each other (for "deep" centers this is a magnetic interaction of the RKKY type, while for the asymmetric case it includes also the density-density interaction).

We are interested primarily in the variation in the state of the system as the f level moves (i.e. as E_f changes) and, perhaps, as the level broadens (i.e. as V changes). We know, for instance, that if pressure is applied to the system, the f level indeed moves up and away from ε_F and broadens. In the Anderson model both factors lead to the disappearance of a localized magnetic moment [31]. It follows from (2.3.3) that at first the effective s-f exchange increases (as does the Kondo temperature). Then as the f level crosses ε_F and depopulates, the localized magnetic moment disappears. Thus, a transition in which the valence changes is at the same time a magnetic-nonmagnetic transition (similar to a Mott-Hubbard transition; see Chap. 2.2). We see that at first this transition proceeds via an increase of the Kondo spin compensation. In this sense a phase with MV is one on the boundary of the magnetic and nonmagnetic states.

The Anderson lattice model (2.3.4) describes many basic properties of MV states. As to an electronic phase transition, in this model it seems to be continuous [33] because the Hamiltonian (2.3.4) has no terms that could speed up the transition as the f level depopulates (the effective interaction of the f-electrons via conduction electrons is oscillating [34] and does not lead to the transition becoming a first-order one). In real experiments the majority of such transitions are discontinuous. To explain this discrepancy Falicov and Kimball [30] allowed for the Coulomb interaction of f- and s-electrons:

$$H_{fs} = \sum_{ikh'\sigma\sigma'} G_{ikh'} f_{i\sigma}^\dagger f_{i\sigma} a_{k\sigma'}^\dagger a_{k'\sigma'}. \quad (2.3.5)$$

This interaction is important since in an electronic phase transition the number of f- and s-electrons changes or, in other words, the charge state of an ion changes (there appear positively charged ions, f-holes). This means that the interaction Hamiltonian (2.3.5) contributes considerably to the energy of the transition and may, in principle, be the predominant factor (see Chap. 2.4).

Another important physical effect is that when the electronic state of the ion core varies, the radius of the corresponding ion changes considerably (about 15 to 20 per cent). Therefore, the interaction with lattice strain (more generally, with phonons) may play an important role. Yet another factor is the increase with pressure of the f-s (more exactly, f-d) hybridization. In rare-earth systems it is due primarily to the overlap of f and (sd) orbitals at neighboring sites, which increases under compression.

In the simplest form the electron-lattice interaction can be taken into account by the dependence of the parameters of the Hamiltonian (2.3.4), E_f and V , on the specific volume v . If we consider these parameters as the same for all centers, then we would account for the interaction with the bulk strain (dilatation), which can be treated in the mean-field approximation. In the general case we can represent the electron-lattice interaction in the following form:

$$H_{\text{el-ph}} = \sum_{iq\sigma} g_{1iq} f_{i\sigma}^\dagger f_{i\sigma} (b_q^\dagger + b_{-q}) + \sum_{iq\sigma} (g_{2iqh} f_{i\sigma}^\dagger a_{h\sigma} + \text{h.c.}) (b_q^\dagger + b_{-q}), \quad (2.3.6)$$

where the first term describes the change in position of the f level under pressure (due to the change in the ion radius) and the second the change in hybridization.

The Hamiltonian (2.3.4) with, if necessary, the interaction Hamiltonians (2.3.5) and (2.3.6) usually serves as the basis for a theoretical treatment of EPT and of MV states.

Often a number of simplifications are introduced. Since the system is periodic, we can write the constants in (2.3.4)-(2.3.6) as

$$V_{ik} = V_k e^{i\mathbf{k} \cdot \mathbf{R}_i}, \quad G_{ikhk'} = G_{khk'} e^{i(\mathbf{k} - \mathbf{k}') \cdot \mathbf{R}_i}, \quad \dots \quad (2.3.7)$$

Often, however, a rare-earth compound is considered as a collection of rare-earth "impurities". Then the Hamiltonian is as (2.3.2) but the impurity concentration is taken to be high, $c \simeq 1$. This formally results in the coherent factors $\exp(i\mathbf{k} \cdot \mathbf{R}_i)$ in (2.3.7) being neglected and V_{ik} being equal to V_k (further simplification usually consists in neglecting the momentum dependence of the matrix elements and considers the parameters in the Hamiltonians (2.3.4)-(2.3.6) as constants, i.e. $V_{ik} = V$ and $G_{ikhk'} = G$, etc.). The physics of such an approximation lies in the fact that at a narrow f resonance and high temperatures $T \gg \Gamma$ (a more exact criterion may be different) the scattering of the conduction electrons by the f-electrons is incoherent, so that the impurity model indeed works. At low temperatures (for the ground state, for one) the processes become coherent and the approximation may not work. Nevertheless, the impurity, or local, model gives a good description of both the qualitative features of EPT's [7, 35] and many properties of MV states, including properties at low temperatures [36]. There are also some theoretical arguments

in favor of the description via incoherent rare-earth impurities; we may assume that a sufficiently strong f-f interaction [37, 38] and, possibly, an f-s interaction [39] effectively lead to a localization of the f-electrons and in this way to a great extent disrupt the coherence (for this reason the temperature criterion $T \gg \Gamma$ may prove to be too stringent and therefore incorrect). But in general form this question remains unsolved, as does the question of the nature of the ground state of systems with mixed valence and of the degree of localization of the f-electrons in this state; see below.

Another simplification that is often assumed in the model with the Hamiltonians (2.3.4)-(2.3.6) is to neglect the electron spin. The use of the spinless model is usually justified by the fact that the Coulomb repulsion U_{ff} is great (in real systems of this type $U_{ff} \sim 7-10$ eV, i.e. is considerably higher than the effective kinetic energy of the f-electrons, measured by the width of the f level, $\Gamma = \pi \rho V^2 \simeq 10^{-2}$ eV) and hence the f-electrons prove to be strictly localized in the Mott-Hubbard sense, so that only one electron can be placed on each f level. As $U_{ff} \rightarrow \infty$ the situation becomes similar to the case of spinless fermions. The spinless version of the model (we note that the Hamiltonian (2.3.4) formally becomes quadratic) describes sufficiently well a number of features of EPT's and properties of such systems. We will often resort to this version, but we must bear in mind the severe restrictions of this model; these are discussed below.

2.4 VALENCE TRANSITIONS IN THE FALICOV-KIMBALL MODEL

2.4.1 The Mean-Field Approximation

One of the first attempts to describe electronic phase transitions was made by Falicov and Kimball [30] and Ramirez and Falicov [40]; in these works the authors took into account the Coulomb interaction between the f- and s-electrons and used the so-called mean-field approximation (MFA); hybridization of f-electrons with conduction electrons was not accounted for. Let us consider the simplest version of this model, in which at the start the f level lies at a distance E_f below the bottom of the empty conduction band (Fig. 2.3). For the sake of simplicity we will take the density of states in the conduction band as constant, $\rho(\varepsilon) = \rho = \text{const.}^*$ Treating the f-s interaction (2.3.5) in the mean-field approximation,

$$G f^\dagger f a^\dagger a \rightarrow G (\langle f^\dagger f \rangle a^\dagger a + f^\dagger f \langle a^\dagger a \rangle - \langle f^\dagger f \rangle \langle a^\dagger a \rangle) \quad (2.4.1)$$

* Accounting for the dependence of the density of the states on the energy, say of the type $\rho(\varepsilon) \sim \varepsilon^{1/2}$ on the band edge, does not change the situation considerably (e.g., see the review article [7]).

(the angle brackets stand for the average over the ground state or for the thermodynamic average), we can easily write the energy of the system as a function of the number of electrons

$$n_s = \frac{1}{N} \sum_{k\sigma} \langle a_{k\sigma}^\dagger a_{k\sigma} \rangle$$

promoted from the f level to the conduction band (here $n_s + n_f = 1$):

$$\mathcal{E}(n_s) = E_g n_s + \frac{1}{2\rho} n_s^2 - G n_s^2,$$

$$E_g = G - E_f. \quad (2.4.2)$$

We see that if in (2.4.2) $G > 1/2\rho$, then as the f level moves up the number of f-electrons changes suddenly from $n_f = 1$ to $n_f = 0$

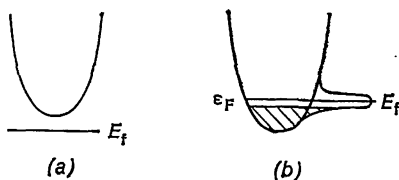


Fig. 2.3. The energy diagram for a system undergoing an insulator-metal transition.

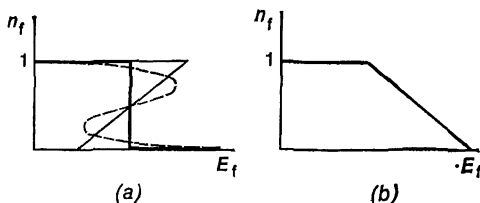


Fig. 2.4. The change in the occupation of the f level in the Falicov-Kimball model in the mean-field approximation: (a) $G > 1/2\rho$, and (b) $G < 1/2\rho$. Solid lines represent the behavior without f-s hybridization, and the dashed line with hybridization.

(while n_s changes from 0 to 1); if $G < 1/2\rho$, the transition is smooth (see Fig. 2.4). Qualitatively, the sudden nature of the transition can be associated with the fact that the attraction of the electrons that went over to the conduction band and the f-holes that remained behind lowers the bottom of the conduction band and hence promotes further excitation of the electrons to the s band; at $G > 1/2\rho$ this process becomes avalanche-like and leads to collapse. Thus, even this simple model would seem to lead to first-order transitions (see,

however, Sec. 2.4.2). The valence (the number of f-electrons, n_f), to be sure, proves to be an integer and does not attain intermediate values.

To correct this deficiency at least partially one could introduce f-s hybridization. This was first done in [41, 42]; similar results were obtained later in [43, 44]. In the simplest case of the spinless impurity model (or in accounting for the Coulomb f-f interaction in the Hartree-Fock approximation) a corresponding treatment [42] is completely analogous to Anderson's discussion [31]. The equation of motion in terms of the Green function is

$$\begin{aligned}\omega \langle\langle f_m | f_m^+ \rangle\rangle &= \frac{1}{2\pi} + (E_f + Gn_s) \langle\langle f_m | f_m^+ \rangle\rangle + \sum_k V_k \langle\langle a_k | f_m^+ \rangle\rangle, \\ \omega \langle\langle a_k | f_m^+ \rangle\rangle &= (\varepsilon_k + Gn_f) \langle\langle a_k | f_m^+ \rangle\rangle + V_k \langle\langle f_m | f_m^+ \rangle\rangle,\end{aligned}\quad (2.4.3)$$

whence

$$G_{ff}(\omega) = \langle\langle f_m | f_m^+ \rangle\rangle = \frac{1}{2\pi} \frac{1}{\omega - E_f - Gn_s - \Sigma(\omega)}, \quad (2.4.4)$$

with

$$\Sigma(\omega) = \sum_k \frac{V_k^2}{\omega - \varepsilon_k - Gn_f}. \quad (2.4.5)$$

The difference from Anderson's work [31] lies only in the appearance of level shifts, Gn_s and Gn_f ; the renormalized position of the f level will from now on be denoted by \tilde{E}_f , i.e. $\tilde{E}_f(n_s) = E_f + Gn_s$.

If we neglect the real part of $\Sigma(\omega)$ (this is correct for the case of cerium, shown in Fig. 2.1, but is generally incorrect for systems of the SmS type, where the f level lies near the bottom of the conduction band), we find from (2.4.4) and (2.4.5) the density of the states of f-electrons:

$$\rho_f(\omega) = \frac{1}{\pi} \frac{\Gamma}{(\omega - E_f - Gn_s)^2 + \Gamma^2}, \quad (2.4.6)$$

$$\Gamma = \text{Im } \Sigma(\omega) = \pi \rho V^2. \quad (2.4.7)$$

Hence, we have arrived at a virtual f level of width Γ , and the position of this level can be determined in a self-consistent manner in terms of the occupation numbers of the f and s levels via the equation

$$\begin{aligned}n_f &= \int_{-\infty}^{\varepsilon_F(n_f)} \rho_f(\omega) d\omega \\ &= \frac{1}{\pi} \left\{ \text{arccot} \frac{E_f + Gn_s - \varepsilon_F(n_f)}{\Gamma} - \text{arccot} \frac{E_f + Gn_s}{\Gamma} \right\}\end{aligned}\quad (2.4.8)$$

(provided the density of states ρ and, hence, Γ are constant).

If we note that $\varepsilon_F(n_f) = \varepsilon_f(1) + n_s/\rho - Gn_s$ and $n_f + n_s = 1$, we can easily analyze Eq. (2.4.8) and see that as E_f grows, the electronic phase transition retains its discontinuous character if hybridization is weak:

$$\pi\Gamma < 2G - 1/\rho, \quad (2.4.9)$$

but becomes smooth for large values of width Γ of the f level; the behavior of $n_f(E_f)$ for $\Gamma=0$ is shown in Fig. 2.4 by a dashed curve. Hence, just as it follows from qualitative arguments (see, for instance, Fig. 2.1), the f - s hybridization blurs the electronic phase transition: near the transition point n_f is neither zero nor unity, i.e. mixed valence is present.

If we take into account the periodicity in the positions of the centers, this somewhat changes the form of the energy spectrum, but in the mean-field approximation all qualitative conclusions concerning the transition remain valid (see Sec. 2.4.3).

The full model with the Hamiltonians (2.3.4) and (2.3.5) and with the spin taken into account has been considered in the mean-field approximation for both f - s and f - f interactions in [42]. Instead of one equation (2.4.8) for the number of f -electrons there is a system of coupled equations for $n_{f\uparrow}$ and $n_{f\downarrow}$. An analysis of this system shows that first-order transitions become possible from the magnetic state with $n_{f\uparrow} \neq n_{f\downarrow}$ and $n_f \simeq 1$ (this phase corresponds to a state with localized magnetic moments in the Anderson model [31]) to the nonmagnetic state with $n_{f\uparrow} = n_{f\downarrow} \ll 1$. Similar results were obtained by Haldane [45], who reduced the f - s interaction (2.3.5) to the interaction of the f -electrons with the boson field that describes the fluctuations in the density of the s -electrons.

In [41] the f - f interaction in (2.3.4) was accounted for not in the Hartree-Fock approximation but in the Hubbard approximation. Qualitatively this introduces no significant changes and leads only to a slight asymmetry in the n_f versus E_f dependence. We note, however, that in the full picture (i.e. if the spins and f - f interactions are taken into account together with the periodicity of the system) the properties of the system and the features of the electronic phase transition are not yet fully understood. The results cited in this section represent only the first step towards a complete solution of the problem. We will leave the discussion of the situation that has emerged at present in this field and the unsolved problems to Chap. 2.6. Here we will show that even in the simple (at first glance) case of the spinless variant of the model the situation is not as trivial as could be expected from the above discussion; even here if we go beyond the mean-field approximation, the character of the EPT may change considerably, and the tendency towards jumplike transitions may be eliminated or, at least, considerably suppressed.

2.4.2 Beyond the Mean-Field Approximation. The Role of Local (Excitonic) Correlations

We have just seen that if we allow for the f-s interaction in the mean-field approximation, we arrive at first-order phase transitions between states whose valencies are integers. But the tendency to a jump is perhaps somewhat exaggerated. If we go beyond the approximation, there are factors in the f-s interaction that smear the transition and stabilize the states with mixed valence. The physics of these factors lies in the importance of the role of local correlations of f- and s-electrons or of s-electrons and f-holes, i.e. excitonic effects.

Indeed, the strong tendency to a first-order transition is connected with the term $-Gn_s^2$ in (2.4.2), which is quadratic in n_s and is typical of the mean-field approximation (*all* f-electrons interact with *all* conduction electrons). But if we allow for the local correlations of a given s-electron with an f-hole (these correlations are important at least for low hole concentration), the accelerating effect produced by this term will be weakened and the tendency toward pinning the f level near the Fermi level will increase.

This idea was first expounded by Khomskii and Kocharyan [46]. They used a generalized Hartree-Fock approximation, which allowed for excitonic correlations and is similar to the approximation used by Keldysh and Kopayev [47] in the study of excitonic insulators. Namely, in the term responsible for the f-s interaction the most general decoupling scheme was made:

$$Gf^{\dagger}fa^{\dagger}a \rightarrow G(\langle f^{\dagger}f \rangle a^{\dagger}a + f^{\dagger}f \langle a^{\dagger}a \rangle) + G(\Delta f^{\dagger}a + \text{h.c.}) - G\langle f^{\dagger}f \rangle \langle a^{\dagger}a \rangle + G\Delta^2, \quad (2.4.10)$$

$$\text{with } \Delta = \sum_k \langle fa_k^{\dagger} \rangle.$$

The anomalous average Δ describes the electron-hole correlation and must be determined self-consistently. We can easily see that after such a decoupling the problem is reduced to that considered in Sec. 2.4.1, where we have only to substitute $\tilde{V} = V + G\Delta$ for V .

If we use approximation (2.4.10), the equation of motion for the Green function and the self-consistency equation for n_f take the same form as Eqs. (2.4.3)-(2.4.8), where \tilde{V} is substituted for V . However, in the process the quantity Δ in \tilde{V} must be determined self-consistently. It can be found via the Green function $G_{fs}(k, \omega) = \langle \langle a_k | f_m^{\dagger} \rangle \rangle \omega$, which according to (2.4.3) and (2.4.4) takes on in this case the following form:

$$G_{fs}(k, \omega) = \frac{\tilde{V}}{\omega - \varepsilon_k} G_{ff}(\omega) = \frac{1}{2\pi} \frac{V + G\Delta}{(\omega - \varepsilon_k)(\omega - E_f - Gn_s - i\pi\Gamma)} \quad (2.4.11)$$

[here $\Gamma = \pi\rho\tilde{V}^2 = \pi\rho(V + G\Delta)^2$]. The self-consistency equation for the anomalous average can then be obtained in the usual way:

$$\begin{aligned}\Delta &= \sum_k \langle fa_k^\dagger \rangle = - (V + G\Delta) \int d\omega \operatorname{Im} \sum_k G_{fs}(k, \omega) \\ &= - \frac{\rho(V + G\Delta)}{2} \ln \frac{(E_f + Gn_s - \varepsilon_F)^2 + \Gamma^2}{(E_f + Gn_s)^2 + \Gamma^2}.\end{aligned}\quad (2.4.12)$$

We can arrive at the same equations (2.4.8) and (2.4.12), which enable finding n_f and Δ , by writing the free energy of the system in terms of these parameters. Namely [35],

$$\begin{aligned}\mathcal{E} &= \frac{E_f + Gn_s - \varepsilon_F}{\pi} \operatorname{arccot} \frac{E_f + Gn_s - \varepsilon_F}{\Gamma} - \frac{E_f + Gn_s}{\pi} \operatorname{arccot} \frac{E_f + Gn_s}{\Gamma} \\ &+ \rho G \varepsilon_F n_f - \frac{\Gamma}{2} \ln \frac{(E_f + Gn_s - \varepsilon_F)^2 + \Gamma^2}{(E_f + Gn_s)^2 + \Gamma^2} \\ &- Gn_s n_f + G\Delta^2 - \frac{1}{2} \rho \varepsilon_F^2 - \frac{1}{2} \rho G^2 n_f^2.\end{aligned}\quad (2.4.13)$$

We will also need this formula in Chap. 2.5.

The analysis of Eqs. (2.4.8) and (2.4.12) is especially straightforward in the case of weak coupling, $\rho G < 1$, if the external hybridization, V , is zero. Equation (2.4.12) then yields

$$\Gamma = [\xi_0^2 \exp(-2/\rho G) - (E_f + Gn_s - \varepsilon_F)^2]^{1/2}, \quad (2.4.14)$$

where ξ_0 is the cut-off energy (of the order of the Fermi energy ε_F or the conduction band width). Substituting into Eq. (2.4.8), we transform the latter into

$$\xi_0 \exp(-1/\rho G) \cos \pi n_f = E_f - \varepsilon_F - 2G' n_f, \quad (2.4.15)$$

where we have introduced the notation

$$G' = G - 1/2\rho.$$

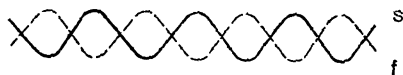
An analysis of Eq. (2.4.15) shows that for small G 's ($\rho G < 1$) it yields a smooth transition, in accordance with the results of Sec. 2.4.1. But if G is large, Eq. (2.4.15) would yield formally two successive first-order transitions with a mixed-valence phase between [46]. However, Eq. (2.4.15) was derived only for weak coupling and, hence, is inapplicable at $\rho G \gg 1$. With this approach we can arrive at two jumplike transitions only if the effective constant G' on the right-hand side of (2.4.15) differs from the purely Coulomb constant due to, for instance, the electron-lattice interaction [7, 35]; this fact was tacitly assumed in [46]. But we cannot apply this conclusion about two jumplike transitions to the original model of Falicov and Kimball.

It is difficult to study analytically the case of an arbitrary coupling. We can do this, however, for the other limiting case of strong coupling.

ing: $\rho G \gg 1$. Here we can neglect the width $W \sim \rho^{-1}$ of the conduction band, which means that we can effectively reduce the problem to a two-level one (a two-level model, however, corresponds to a periodic system rather than to an impurity system). We can easily see (see Secs. 2.4.3 and 2.4.4) that in this model the electronic phase transition proves to be smooth even when $\rho G \gg 1$ (where a simple mean-field approximation (2.4.1) leads to a first-order transition) provided that we have allowed for excitonic correlations. Evidently, the same is true in the approximation given by (2.4.10) for all values of G .

The above facts can be explained as follows. When the decoupling scheme (2.4.10) is used, by allowing for the anomalous averages $\langle af^+ \rangle$ we arrive at an effective renormalization of the hybridization: $V \rightarrow V + G \langle af^+ \rangle$. As a result, in this approximation the width of the f level, Γ , grows with the strength of the f - s interaction in direct proportion to G , so that the condition (2.4.9) for a first-order phase transition to occur is not met. In other words, we may say that, due to local correlations of an s -electron and an f -hole, the system transforms from the metallic phase (itinerant s -electrons with a concentration n_s on the background of f -holes with a concentration $n_f = 1 - n_s$, a fact that was postulated in the mean-field approximation and produced the term $-Gn_s^2$ in (2.4.2)) into the "excitonic" phase, in which each s -electron is localized near its f -hole, at least when strong coupling $\rho G > 1$ is present. Because of this the quadratic term of the type $-Gn_s^2$ in the energy is drastically weakened (this term is now due only to the exciton-exciton interaction, provided that the excitonic wave functions do not considerably overlap); the transition is then strongly leveled off.

We see, therefore, that if we go beyond the mean-field approximation, the nature of valence transitions changes. We cannot, however, consider the generalized mean-field approximation fully justified in the strict sense of the word. It allows for important processes that are not included in the simple mean-field approximation; in terms of diagrams they correspond to summing logarithmically divergent diagrams of the type



These are the diagrams usually taken into consideration in the theory of excitonic insulators [47]. But in our case of heavy f -electrons there are also other types of diagrams [50] equally important. In essence the problem is close to that of the X-ray absorption and emission threshold [50, 51] and also (even in its spin-zero version) of the Kondo model (see Chap. 2.6). Recently Schlottmann [39]

applied a method developed by Nozieres and de Dominicis [51] to electronic phase transitions in the Falicov-Kimball model. He showed that the characteristic exponential behavior (2.4.14) changes to a power law*:

$$V^* = V \left(\frac{W}{V} \right)^{\rho G / (1 + \rho G)}.$$

Hence, we see that, on the one hand, a nonzero "bare" hybridization is essential, but, on the other hand, in the process of renormalization the initially small V rapidly increases and at $\rho G \gg 1$ tends to $V^* \simeq W \sim \rho^{-1}$. The line $V = 0$ is a special one; namely, the model is nonanalytic and has an essential singularity as $V \rightarrow 0$, so that the solution for small V 's is not linked to the solution at $V = 0$. In this sense the exact solution for the case with $V = 0$ obtained by Hewson and Riseborough [59] is unrelated to the EPT problem.

The fact that the effective hybridization and the level width Γ tend at $\rho G \gg 1$ to a finite limit $\sim W$ and do not increase in proportion to G , as is the case of the decoupling (2.4.10), again leads to the possibility of a first-order transition (condition (2.4.9) can be met). Since the level width Γ becomes energy-dependent in the process [39], there is a possibility for two transitions to occur at $E_f \neq \epsilon_F - Gn_s$, as was first obtained (in not a rigorous fashion) in [46]. This aspect has not yet been analyzed in the approach of Schlottmann [39].

Thus, the above reasoning leads us to the conclusion that excitonic correlations essentially blur EPT's. If the simple mean-field approximation (2.4.1) overemphasizes the tendency towards a first-order transition, the generalized mean-field approximation (2.4.10), while embracing the tendency of leveling off the transition due to excitonic correlations, may even somewhat overestimate this tendency, and the truth may lie somewhere in between. We also note that in the periodic model, in contrast to the impurity model, both the decoupling of the type (2.4.10) (see [48, 49] and Sec. 2.4.4) and the approach of Schlottmann [39] produce only a smooth transition in the Falicov-Kimball model.

2.4.3 The Two-Level Model

On the whole we must say that the final situation in the Falicov-Kimball model is not clear even in the spinless case. We have seen that different approximations lead to contradictory conclusions concerning electronic phase transition. It is therefore interest-

* This is true for the impurity model. In the coherent case the result (2.4.14) remains valid [39]. However, as stated by Schlottmann, the coherent regime is not realized for a strong f-s interaction.

ing to verify these conclusions on a simpler model that can be solved exactly, a model in which the dispersion of the s-electrons is neglected and a narrow s level with an energy ε_s is substituted for the conduction band [35, 54].*

In the spinless case the model Hamiltonian is

$$H = \sum_i \{ \varepsilon_s a_i^\dagger a_i + E_f f_i^\dagger f_i + V (f_i^\dagger a_i + \text{h.c.}) + G f_i^\dagger f_i a_i^\dagger a_i \}. \quad (2.4.16)$$

We see that in this approximation the model is reduced to a single-site one. Its solution is simple, and the energy is

$$\mathcal{E} = \frac{E_f}{2} - \frac{1}{2} V \sqrt{E_f^2 + 4V^2} \quad (2.4.17)$$

(here and below we assume that $\varepsilon_s = 0$). As the position of the f level changes, the E_f state of the system varies continuously (as expected in a single-site case). We note that the Coulomb interaction (constant G) is not included in the final solution. From the standpoint of physics this result is clear: there is exactly one electron at each site and only the electronic wave function changes (it has an f-nature or an s-nature or is a superposition of the f and s states); naturally, the electron cannot interact with itself.

We can verify that the generalized mean-field approximation (2.4.10) that allows for excitonic correlations yields a solution coinciding with the exact solution. In this approximation the system's energy is

$$\begin{aligned} \mathcal{E} = & \frac{E_f + Gn_s + Gn_f}{2} - \frac{1}{2} [(E_f + Gn_s - Gn_f)^2 \\ & + 4(V + G\Delta)^2]^{1/2} - Gn_s n_f + G\Delta^2. \end{aligned} \quad (2.4.18)$$

We see that on the extrema of (2.4.17), given by the equations $\partial\mathcal{E}/\partial n_f = 0$ and $\partial\mathcal{E}/\partial\Delta = 0$, there is no dependence on G :

$$\frac{d\mathcal{E}}{dG} = \frac{\partial\mathcal{E}}{\partial n_f} \frac{dn_f}{dG} + \frac{\partial\mathcal{E}}{\partial\Delta} \frac{d\Delta}{dG} + \frac{\partial\mathcal{E}}{\partial G} = \frac{\partial\mathcal{E}}{\partial G} = 0. \quad (2.4.19)$$

For this reason we can set $G = 0$ in (2.4.18). We then arrive at a result that coincides with the exact solution (2.4.17). Therefore, we see that if we allow for the averages n_f and $\Delta \neq 0$ in the two-level model, we arrive at a complete compensation of the interaction. But if we use the usual mean-field approximation for the f-s interaction and do not include the excitonic averages $\langle fa^+ \rangle$ [i.e. if in

* Apart from the model nature, there exists experimental evidence (see [68, 69]) that sd states of rare-earth compounds with MV are to a great extent local.

(2.4.18) we set $\Delta = 0$], then for n_f we have the following equation:

$$n_f = \frac{1}{2} \left\{ 1 - \frac{E_f + Gn_s - Gn_f}{\sqrt{(E_f + Gn_s - Gn_f)^2 + 4V^2}} \right\}, \quad (2.4.20)$$

which implies that for small V 's the electronic phase transition is discontinuous when E_f varies, in contrast to the exact solution.

We see once again that even the simple two-level model shows that local (excitonic) correlations play an important role, in our case completely blurring the transition. The above discussion may also serve as justification for the use of the generalized approximation (2.4.10) in the more realistic case of a broad conduction band.

2.4.4 The Periodic Model

Inclusion of coherence effects caused by the periodicity in the position of the centers and accounted for by choosing the hybridization (and interaction) matrix elements in the form (2.3.7) leads to a number of special features. First, the character of the

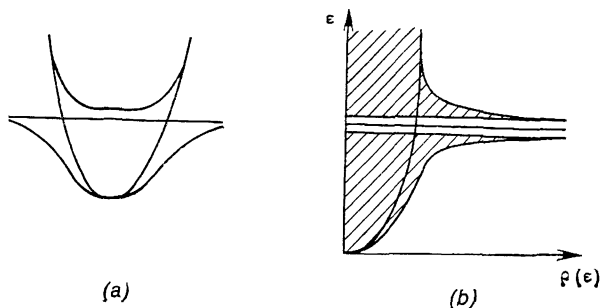


Fig. 2.5. The energy spectrum and density of states in the model with periodic f-s hybridization. The density of states in (b) is similar to the case of an "impurity" model (cf. Fig. 2.1), the only difference being that there is a narrow gap "cut" in the peak in the ρ versus ϵ dependence.

spectrum changes: instead of virtual states a gap may appear in the spectrum. In the simple spinless case this becomes apparent from Fig. 2.5: due to f-s hybridization there appears the usual repulsion of levels. In the full model of an Anderson lattice, when we allow for the spins and Coulomb f-f interaction U_{ff} , the situation grows much more complex (we will discuss this aspect in Chap. 2.6). Nevertheless, in respect to the nature of the EPT the periodic model does not differ radically from the impurity model. In this case the equation of motion for the Green function in the spinless model has a form similar to (2.4.3)-(2.4.5), the difference being that instead of summing over momenta k we have only terms with one value of k . For

instance,

$$G_{ff}(k, \omega) = \frac{1}{2\pi} \left[\omega - E_f - Gn_s - \frac{V_k^2}{\omega - \varepsilon_k - Gn_f} \right]^{-1}. \quad (2.4.21)$$

Knowing the spectrum of the system, we can easily find the electron energy:

$$\begin{aligned} \mathcal{E} = \frac{1}{2} \int_{-\infty}^{\varepsilon_F} \{E_f + G(n_s + n_f) + \varepsilon \\ - [(E_f + Gn_s - \varepsilon - Gn_f)^2 + 4(V + G\Delta)^2]^{1/2}\} \rho(\varepsilon) d\varepsilon - Gn_s n_f + G\Delta^2. \end{aligned} \quad (2.4.22)$$

When density of states is constant, namely, $\rho(\varepsilon) = W^{-1} \theta(2\varepsilon - W) \theta(W - 2\varepsilon)$ (with W the width of the conduction band), the problem of the phase transition can be solved analytically for any value of G . Minimizing (2.4.22) with respect to n_f and Δ , we arrive at the self-consistency equations [which can also be obtained directly from the Green function of the type (2.4.21)]:

$$\begin{aligned} W(1 - 2n_f) = [(\bar{E}_f + W/2)^2 + 4(V + G\Delta)^2]^{1/2} \\ - [(\bar{E}_f - W/2)^2 + 4(V + G\Delta)^2]^{1/2}, \end{aligned} \quad (2.4.23)$$

$$\Delta = \frac{V + G\Delta}{W} \ln \frac{\bar{E}_f + W/2 + [(\bar{E}_f + W/2)^2 + 4(V + G\Delta)^2]^{1/2}}{\bar{E}_f - W/2 + [(\bar{E}_f - W/2)^2 + 4(V + G\Delta)^2]^{1/2}}, \quad (2.4.24)$$

where $\bar{E}_f = E_f + G(1 - 2n_f)$. Solving (2.4.23) and (2.4.24) for Δ , we arrive at an equation for n_f , which at $V = 0$ is

$$E_f = (1 - 2n_f) \left(\frac{W}{2} \coth \frac{W}{2G} - G \right) \quad (2.4.25)$$

(provided that $0 < n_f < 1$). We see that in this case the EPT is continuous for any value of G (nonzero hybridization will only blur the transition still further). Hence, in contrast to the impurity model, all calculations can be carried out for any strength of the f-s interaction. Via numerical calculations Leder [48] has also established that there are no first-order transitions in the periodic model with excitonic averages. Jumplike transitions in this case become possible when we add the electron-lattice interaction (see Chap. 2.5).

Note that in this model the spectrum of the system given by (2.4.21) has the form shown in Fig. 2.5 and the chemical potential always lies in the gap when there is one electron per center. Therefore, the electronic phase transition is, in fact, an insulator-insulator transition (presumably, this is the case with SmS; e.g. see [7]). The main factors that determine the nature of the transition probably act in the general case as well, with the spins taken into account. Here, however, the researcher is confronted with the difficult question as

to the type of the emerging ground state, in particular whether the gap will remain. The electron spin may also contribute to the nature of the transition, as shown by Druzhinin [56]. These aspects will be discussed more thoroughly in Chap. 2.6.

2.5 THE ELECTRON-LATTICE INTERACTION AND ITS ROLE IN TRANSITIONS

2.5.1 Interaction with a Homogeneous Strain

The most widely used method of inducing transitions with MV in rare-earth compounds is to apply pressure to the sample. This very fact indicates that the states of such a substance greatly depend on the specific volume and, therefore, that the electron-lattice interaction plays an important role in EPT [35, 57, 58]. As noted before, the explanation is that when the system is compressed, first, the relative position of the f level and the Fermi level (the conduction band) changes and, second, the f-s hybridization increases. In the simplest version of the model we can allow for these effects by taking the parameters of the Hamiltonian (2.3.4), E_f and V , to be functions of the specific volume v or introducing the electron-phonon interaction (2.3.6). The two approaches are equivalent if for the interaction Hamiltonian (2.3.6) we use the mean-field approximation $\langle b_i \rangle = b = \text{const}$ and assume that strains near every site are the same. We can obtain the first term in (2.3.6) from the first term in (2.3.4) by expanding $E_f(v)$ in the small deviations $v - v_0$, while the second term can be obtained by expanding the term that describes the f-s hybridization. If we keep to the mean-field approximation, it is apparently expedient to work with $E_f(v)$ and $V(v)$; this enables us to easily account for the electron-lattice and Coulomb f-s interactions simultaneously [35].

If we allow for the electron-lattice interaction, we must add the energy of the lattice

$$E_{\text{latt}} = \frac{B(v - v_0)^2}{2} \quad (2.5.1)$$

to the energy of the system. We confine ourselves to small deviations $\bar{v} = v - v_0$ and assume that

$$\begin{aligned} E_f(v) &= E_0 - \bar{\gamma}\bar{v}, \\ V(v) &= V_0 - \alpha\bar{v} \end{aligned} \quad (2.5.2)$$

(with α and γ positive).* Let us first take the simplest phenomenological scheme [of the type of (2.4.2)], which enables us to illustrate

*

Nonlinear effects can easily be included in this scheme (see [57, 58]).

the effect of the electron-lattice interaction on the EPT. We neglect the direct and excitonic f-s hybridizations and allow only for the shift of the f level with volume, given by (2.5.2). We can then easily write the energy of the system and include the E_f versus v dependence and the lattice energy:

$$\mathcal{E} = [G - E_f(v)] n_s + \frac{1}{2\rho} n_s^2 - G n_s^2 + \frac{B(v-v_0)^2}{2}. \quad (2.5.3)$$

Minimizing the energy [more exactly, the enthalpy $\mathcal{H} = \mathcal{E} + P(v - v_0)$, with P being the external pressure] with respect to v we find that

$$v - v_0 = -\frac{P + \gamma n_s}{B}, \quad (2.5.4)$$

which after substituting into (2.5.3) yields

$$\mathcal{H} = -\left(E_0 + \frac{\gamma}{B}P - G\right) n_s + \frac{1}{2\rho} n_s^2 - \left(G + \frac{\gamma^2}{2B}\right) n_s^2 + \text{const.} \quad (2.5.5)$$

We see that, first, the f level moves upward as the pressure increases and, second, the inclusion of the interaction of the electrons with the homogeneous strain leads to the term $-\gamma^2 n_s^2/2B$ in the energy, a term that in structure and effect is similar to the term $-G n_s^2$ in (2.4.2). Accordingly, all conclusions about the nature of the phase transition induced by applying pressure, discussed in Chap. 2.4, remain valid in this model.

Let us now consider the general case, in which we allow for both effects associated with the Coulomb f-s interaction and hybridization and the electron-lattice interaction.

The impurity model. In the spinless impurity model we can express the free energy via (2.4.13), add to it the lattice energy (2.5.1), and allow for (2.5.2). In addition to varying this energy with respect to n_f and Δ we must minimize it with respect to v . The condition $\partial\mathcal{E}/\partial v = -P$ yields the following equation of state:

$$P = -B\bar{v} + \frac{\gamma}{\pi} \left(\operatorname{arccot} \frac{E_f + G n_s - \varepsilon_F}{\Gamma} - \operatorname{arccot} \frac{E_f + G n_s}{\Gamma} \right) + \rho V \alpha \ln \frac{(E_f + G n_s - \varepsilon_F)^2 + \Gamma^2}{(E_f + G n_s)^2 + \Gamma^2}. \quad (2.5.6)$$

When the Coulomb interaction is absent ($G = 0$), Eq. (2.5.6) suffices to describe the behavior of the system as P varies, while Eq. (2.4.8) shows how the valence n_f changes. But if $G \neq 0$, we must solve a simultaneous set of equations (2.4.8), (2.4.12), and (2.5.6). By using Eqs. (2.4.8) and (2.4.12) we can write the equation of state in a convenient (although implicit) form

$$\bar{v} = B^{-1} (\gamma n_f - 2\alpha \Delta - P). \quad (2.5.7)$$

Let us study the behavior of the EPT with respect to various factors. A first-order phase transition accompanied by a sudden change in ν and the occupation number of the f level, n_f , occurs if

$$\frac{dP}{d\nu} = -B + \gamma \frac{dn_f}{d\nu} - 2\alpha \frac{d\Delta}{d\nu} \geq 0. \quad (2.5.8)$$

This condition is written for the case where the renormalized f level coincides with the Fermi level: $E_f + Gn_s = \varepsilon_F$.

We start with the case of constant hybridization, $\alpha = 0$ (we will discuss the case of an f level with a varying width in Sec. 2.5.2). Combining (2.4.8) and (2.4.12) with (2.5.8), we transform the lattice to

$$\gamma^2 B^{-1} \geq \pi\Gamma + \rho^{-1} - 2G. \quad (2.5.9)$$

This condition is sufficient for a first-order transition to occur; it generalizes criterion (2.4.9) to the case of a compressible lattice. We see that if we allow for the electron-lattice interaction, the EPT may become jumplike even in the absence of the Coulomb f-s interaction. We also note that contrary to the results of Entel, Leder, and Grewe [65] a first-order transition is possible at nonzero hybridization.

Condition (2.5.9) for a first-order transition at $\tilde{E}_f = E_f + Gn_s = \varepsilon_F$ is sufficient but not necessary; namely, jumplike transitions may take place for other positions of the f level. The explanation is as follows. As we see from criteria (2.4.9) and (2.5.8), the fact that the f level possesses a finite width Γ blurs the transition. If Γ is constant, $dP/d\nu$ changes its sign for the first time at $\tilde{E}_f = \varepsilon_F$. But if Γ changes when pressure is applied [at the expense of the variation of $V(\nu)$ or of the electronic contribution to hybridization, $G\Delta$; see Eqs. (2.4.10) and (2.4.14)], the system may become unstable at other values of E_f (values for which Γ is smaller). For one, the excitonic contribution to the level width (2.4.14) is the greatest exactly at $\tilde{E}_f = \varepsilon_F$, a fact that may hinder the criterion (2.5.9) at this point and stabilize the phase with the f level pinned at ε_F . For other values of E_f the width Γ is smaller and condition (2.5.9) can be met.

The situation can be analyzed in greater detail when the external hybridization V is zero and the entire broadening has an excitonic nature and is given by (2.4.14). (Strictly speaking, a small bare hybridization is always needed; see Sec. 2.4.2.) But at $V = 0$ the problem becomes essentially nonanalytic in V , and because of the f-s interaction the initially small hybridization is renormalized and attains values given by (2.4.14) or a modification of this formula (see [39]). In this case the self-consistency equation for n_f takes the form (2.4.15), with the constant on the right-hand side $G' = G -$

$-1/2\rho + \gamma^2/2B$. An analysis of this equation leads to the following results:

(A) The EPT proves to be continuous at $G' < 0$.

(B) At

$$0 < G' < (\pi/2) \xi_0 \exp(-1/\rho G)$$

there are two consecutive jumps in the n_f versus P and v versus P functions at $\tilde{E}_f < \varepsilon_F$ and $\tilde{E}_f > \varepsilon_F$, with a MV state in between.

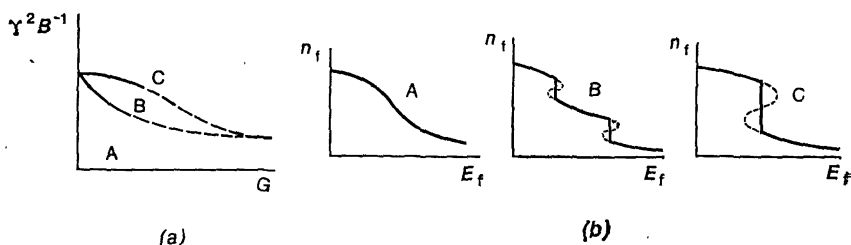


Fig. 2.6. The "phase diagram" (a) and the behavior of the occupation number of the f level (b) in the impurity model with electron-phonon interaction. The letter A denotes the region of a continuous transition, B the region of two successive jumplike transitions, and C the region of one first-order transition.

(C) For still greater values of G there is one jumplike first-order phase transition. The condition for such a transition to occur coincides with the above-discussed criterion (2.5.9), as we can easily see.

The phase diagram, in which all three regions are shown, is depicted in Fig. 2.6. We note once more that when the electron-lattice interaction is taken into account, first-order transitions may be realized for a weak f - s interaction, $\rho G < 1$, where the method employed is justified.

The periodic model. We can consider the periodic model in a similar way (see [35, 49]). Employing the energy in the form (2.4.22) and adding to it the lattice energy given by (2.5.1), we can find the equation of state and formulate the condition for a discontinuous transition. At $\alpha = 0$ and $V = 0$ the behavior of the n_f versus P function is given by the following relationship [cf. (2.4.25)]:

$$\begin{aligned} E_f + \frac{\gamma P}{B} - \frac{\gamma^2}{2B} \\ = (1 - 2n_f) \left(\frac{W}{2} \coth \frac{W}{2G} - G - \frac{\gamma^2}{2B} \right). \end{aligned} \quad (2.5.10)$$

We see that as P grows the effective f level moves upward with a constant speed, and the criterion for a first-order phase transition

to occur in this case is

$$\gamma^2 B^{-1} > W \coth \frac{W}{2G} - 2G. \quad (2.5.11)$$

Hence, in the periodic model a jumplike transition is realized only because of the interaction with the lattice; we came to the same conclusion in Sec. 2.4.4. Here, unlike the incoherent case (the impurity model), we do not have two phase transitions in this approximation, and the phase diagram has the form depicted in Fig. 2.7. Nevertheless, qualitatively the conclusion is the same, i.e. the f

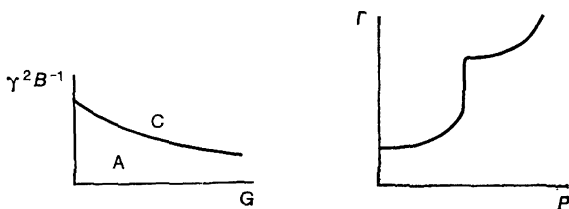


Fig. 2.7. The "phase diagram" similar to that in Fig. 2.6a in the periodic model.

Fig. 2.8. A rough sketch of the pressure dependence of the width Γ of the f level.

level moves as the pressure (which is characterized by the parameter γ or the electron-lattice interaction constant g_1 in (2.3.6)) varies, and this motion assists the discontinuous transition.

What is the physics of the discontinuous transition? Suppose that initially the f level lies below the bottom of the conduction band (or the Fermi level) and some f-electrons are excited out of this level to the s band. Accordingly, there appears in the system n_s ions with large valence but smaller radius. In the mean-field approximation this is equivalent to a decrease in the average lattice parameter, or the atomic volume v , which according to (2.5.2) make the f level move upward, i.e. decreases the activation energy needed for promoting other f-electrons to the conduction band. In some cases this "feedback" becomes quite strong and causes an avalanche-type process with a large number of f-electrons going over to the s band and the respective lattice parameter decreasing. (The mechanism resembles the mechanism of first-order transitions in the Falicov-Kimball model; cf. Sec. 2.4.1.)

Variation of physical quantities under pressure. Now we are prepared to analyze the behavior of various physical quantities, such as the width of the f level and the compressibility, when we apply pressure to the system.

The change in the width Γ of the f level is determined by two factors: on the one hand, Γ grows with pressure due to (2.5.2) (possibly discontinuously if the EPT is of the first order); on the other, the excitonic contribution to Γ is not monotonic. At $\tilde{E}_f < \varepsilon_F$ both mechanisms act in one direction, while at $\tilde{E}_f > \varepsilon_F$ (after the transition) the second counteracts the first. As a result the behavior of Γ as a function of P depends on the concrete values of the parameters; a typical curve of the Γ versus P dependence is shown schematically in Fig. 2.8. A considerable (more than threefold) increase in the characteristic energy of spin fluctuations (which is apparently proportional to Γ) in a phase with MV was found in the experiment of Shapiro *et al.* [60] (also see [61, 62]).

We can find the compressibility of the system by using the equation of state (2.5.7):

$$\kappa = \frac{dv}{dP} = \kappa_0 \left(1 + 2\alpha \frac{d\Delta}{dP} - \gamma \frac{dn_f}{dP} \right), \quad \kappa_0 = B^{-1}. \quad (2.5.12)$$

The next step is to substitute the functions $\Delta(P)$ and $n_f(P)$ determined from the simultaneous self-consistency equations. Naturally, the behavior of κ with P may be quite complex, but we can get a general idea from the following considerations. At $\tilde{E}_f < \varepsilon_F$ and an increase in pressure, n_f drops, i.e. $dn_f/dP < 0$, while the width of the f level increases (due to the growth in the bare hybridization V and the electronic contribution $G \langle fa^+ \rangle$). Equation (2.5.12) shows that both factors soften the lattice. On the other hand, at $\tilde{E}_f > \varepsilon_F$ the f level moves away from the Fermi level, and because of this n_f continues to decrease but the effective width of the f level (the electronic contribution to it) begins to diminish. The net change in κ depends on the model parameters, but generally we can say that in a phase with MV near the transition point the compressibility is exceptionally high, and the softening of the lattice increases faster *before* the transition, a fact that has been established in experiments with SmS (see [4, 8]).

Qualitatively such behavior is due to the fact that in the region with MV compression is facilitated by the decrease in the ionic radius because a number of the f -electrons goes over to the conduction band and, as a result, the lattice parameter decreases. The upward shift of the f level assists such transitions, while the broadening of the level initially (at $\tilde{E}_f < \varepsilon_F$) also leads to a decrease in n_f and in this way increases the compressibility, but later (at $\tilde{E}_f > \varepsilon_F$) acts in the reverse.

2.5.2 The Change in the Width of the f Level and Its Role in Valence Transitions

In the previous section we dealt mainly with the motion of the f level with pressure. At the same time other parameters of a system also change when the sample is compressed. For example, both the hybridization V and the width Γ of the virtual f level increase. Recently there have been experimental indications that at least in compounds of Ce this factor plays a no less important role in EPT's than a shift of the f level. Here we will consider the effect of the f level broadening on the EPT and demonstrate [64] that in certain conditions such broadening causes an abrupt transition with a valence change and the final state has mixed valence.

The reasoning up till now leads us to the conclusion that the f - s hybridization, in broadening the f level, blurs the transition and makes it smoother [see Eqs. (2.4.9) and (2.5.9)]. But we assumed all along that hybridization was constant. However, if we take into account that under pressure it grows (α in (2.5.2) is nonzero), the situation changes.

Qualitatively the picture is as follows. Let us assume that in the initial state, with $P = 0$ and specific volume $v = v_0$, the f level lies below the Fermi level, $E_0 < \varepsilon_F$, and has a width $\Gamma_0 = \pi \rho V_0^2$. We also assume that when pressure grows, the f level moves upward and broadens. As it broadens, the number of occupied f states decreases (see Fig. 2.2), and since ions without an f -electron are smaller, this leads to a smaller average lattice parameter. As a result we are again dealing with the situation described in the previous section, namely, due to such additional compression the width of the f level grows still greater and n_f diminishes still further; we again have a feedback that leads to the transition becoming a first-order one. We must note, however, that in contrast to the shift of the f level this mechanism of accelerating the transition acts only as long as E_f is smaller than ε_F or $n_f > 1/2$. In the opposite case this mechanism hinders the transition. As a result, in the final state the effective f level may be fixed near ε_F and we have a phase with MV ($n_f \simeq 1/2$). This mechanism (the broadening of the f level under pressure) may, therefore, be highly effective in stabilizing the MV phase after the transition has been completed [7].

The easiest way to illustrate the above arguments is to use the two-level model considered in Sec. 2.4.3 (similar results are obtained for models with a wide s band). The energy of the system in this case is given by (2.4.17) to which we must add the lattice energy (2.5.1). From the resulting formula we can find the equation of state

$$P = -\frac{\partial \mathcal{G}}{\partial v} = -B\bar{v} + \frac{1}{2} \left(\gamma + \frac{\gamma E_f + 4\alpha V}{\sqrt{E_f^2 + 4V^2}} \right), \quad (2.5.13)$$

where we have used (2.5.2) and introduced the notation $\bar{v} = v - v_0$.

The instability condition for the system (the condition for a first-order phase transition) has the form

$$\frac{dP}{dv} = -B + \frac{2(V_0\gamma - E_0\alpha)^2}{(E_f^2 + 4V^2)^{3/2}} \geq 0. \quad (2.5.14)$$

This condition is fulfilled most easily at

$$\bar{v}_{cr} = \frac{E_0\alpha + 4V_0\gamma}{\gamma^2 + 4\alpha^2}; \quad (2.5.15)$$

Eq. (2.5.14) then takes the form

$$(\gamma^2 + 4\alpha^2)^{3/2} > 4B |V_0\gamma - E_0\alpha|, \quad (2.5.16)$$

which is a necessary and sufficient condition for a first-order transition in our model.

We can easily see that the small increase in hybridization with pressure (small α 's) hinders the abrupt transition; but for large values of α this criterion is met more easily and the increase in hybridization assists the jump. For the transition to occur under positive pressure ($\bar{v}_{cr} < 0$) we must require that

$$\alpha < \alpha_{max} = \frac{|E_0|\gamma}{4V_0}. \quad (2.5.17)$$

We can verify that the criteria (2.5.16) and (2.5.17) do not contradict each other. From (2.5.17) we see that for a jump to occur a shift of the f level ($\gamma \neq 0$) is necessary in addition to the broadening. Actually, criterion (2.5.16) can be met at $\gamma = 0$, too. But in this case the transition would occur in the nonphysical region $P < 0$, at a point where hybridization $V(v)$ passes through zero and changes its sign, which is completely unphysical (such a false transition was obtained in [65]).*

Thus, our simple model corroborates the above qualitative reasoning and shows that the increase in the f - s hybridization or the width of the f level under pressure in certain conditions assists a discontinuous valence transition. Such a transition starts at a state with a rather low lying f level, i.e. from a phase with $n_f \simeq 1$ (the increase in hybridization with pressure hinders the upward motion of the f level, and the abrupt transition takes place at large values of $|E_f|$). The final state is one with mixed valence, $n_f \simeq 1/2$ (the f level moves upward to the Fermi level and broadens considerably). These results are in good qualitative agreement with the main features of valence transitions, for one, with the results of [61, 62].

* We can verify that this mechanism of transition due to f level broadening acts also for the nonlinear V versus v dependence. Both the high growth rate $V(dV/dv \gg 1)$ and the nonlinearity ($d^2V/dv^2 > 0$) contribute to the jump.

2.5.3 Local (Polaron) Effects in the Electron-Lattice Interaction

When studying the Falicov-Kimball model in Chap. 2.4, we saw how important the local (excitonic) effects are; namely, the mean-field approximation overestimates the tendency to a jumplike transition, while if we allow for excitonic correlations, the transition becomes smoother (local correlations are also important when one considers the properties of the MV state proper; we will touch on these questions in Chap. 2.6). Similarly, local effects may play an important role in the electron-lattice interaction. Up till now we considered the electron-lattice system in the mean-field approximation, i.e. it was assumed that the deformations at every center are the same and are determined by the average occupation number n_f of the f levels. A real lattice, however, reacts near a given center to the electronic state of that center mainly; correspondingly, the local correlations have in essence a polaron nature (the deformations near a particular center may differ depending on whether there is an f -electron at that center).

Intuitively it is clear that when we allow for local effects in the electron-lattice interaction, just as in the Coulomb f - s interaction, the coupling between the various centers becomes weaker and, hence, the tendency to a first-order phase transition is suppressed. However, there is another nontrivial effect here; namely, if there are local deformations of the polaron type, there emerges an effect known from polaron theory resulting in the reduction of off-diagonal matrix elements (polaron band narrowing). But f - s hybridization is just such an off-diagonal quantity. It acquires an exponential factor [66]:

$$V \rightarrow V \exp(-g_1^2/\omega^2), \quad (2.5.18)$$

with g_1 the electron-phonon interaction constant (2.3.6), and ω the characteristic phonon frequency. In turn, such a decrease in hybridization and in the corresponding width of the f level facilitates a first-order transition. Therefore, a priori the final result is not clear.

To clarify this question let us take the two-level model [67]. We take the Hamiltonian in the form

$$H = \sum_i \{ \epsilon_s a_i^\dagger a_i + E_f f_i^\dagger f_i + V (a_i^\dagger f_i + \text{h.c.}) + \omega b_i^\dagger b_i - g f_i^\dagger f_i (b_i^\dagger + b_i) \}. \quad (2.5.19)$$

Here we consider the phonons to be local. Strictly speaking, we must take into account phonon dispersion or the k -dependence of electron-phonon interaction (see Sec. 2.5.4), but in the variational approach we will now use this is unimportant. In this way the model

Hamiltonian (2.5.19) enables us to illustrate the main features of polaron effects in EPT's and in phases with MV.

There are two limiting cases here: strict localization [66] (lattice deformation instantly follows the electronic state of the center, i.e. acquires two values corresponding to $n_f = 0$ and $n_f = 1$) and the case where due to rapid f-s transitions the deformation corresponds to the average occupation of the f levels, which is equivalent to the mean-field approximation. To study the general case and establish the conditions for the limiting cases we use a variational method and seek the wave function at each site i in the form

$$|\psi_i\rangle = ua_i^\dagger |0\rangle \parallel \beta_s\rangle + v f_i^\dagger |0\rangle \parallel \beta_f\rangle, \quad u^2 + v^2 = 1. \quad (2.5.20)$$

Here $\parallel \beta\rangle$ is the coherent state of phonons with the eigenvalue $\beta = \langle b \rangle$, which describes the deformation of the lattice near the i th site; these functions have the following properties:

$$b \parallel \beta\rangle = \beta \parallel \beta\rangle, \quad \langle \beta \parallel \beta'\rangle = \exp \left\{ -\frac{|\beta|^2}{2} - \frac{|\beta'|^2}{2} + \beta\beta' \right\}. \quad (2.5.21)$$

The meaning of the wave function (2.5.20) is that different electronic states of a center have corresponding to them different lattice deformations. The response of the lattice, however, is not instantaneous and the lattice does not manage to completely follow the fast f-s transitions caused by hybridization; therefore, the quantities β_s , β_f , and n_f must be determined in a self-consistent manner.

The average value of the energy (2.5.19) over the wave function (2.5.20) is a functional of three variational parameters, β_s , β_f , and $n_f = v^2$ ($n_s = u^2 = 1 - n_f$). (In what follows we will assume that all centers are equivalent and hence drop the site index i .) Bearing (2.5.21) in mind, we can write this functional as

$$\begin{aligned} \mathcal{E} = & (1 - n_f)(\varepsilon_s + \omega\beta_s^2) + n_f(E_f + \omega\beta_f^2 - 2g\beta_f) \\ & - 2V \exp \left\{ -\frac{(\beta_s - \beta_f)^2}{2} \right\} \sqrt{n_f(1 - n_f)}. \end{aligned} \quad (2.5.22)$$

The mean-field approximation, which on qualitative assumptions is justified for strong hybridization (fast f-s transitions), corresponds to $\beta_s = \beta_f = \beta$. Minimization of (2.5.22) then yields $\beta_{\text{MFA}} = g n_f / \omega$, and the energy $\mathcal{E}(n_f)$ is

$$\mathcal{E}_{\text{MFA}} = (E_f - \varepsilon_s) n_f - \frac{g^2}{\omega} n_f^2 - 2V \sqrt{n_f(1 - n_f)}, \quad (2.5.23)$$

which corresponds to (2.5.5). This implies that there exists a first-order phase transition for sufficiently weak hybridization, $V < g^2/2\omega$. (This condition is equivalent to (2.5.16) with $\alpha = 0$, obtained earlier.)

The other limiting case of slow f-s transitions ($V \ll \omega$) would correspond to the deformation at a center being local: from (2.5.22)

with $V \rightarrow 0$ we find that $\beta_s = 0$ and $\beta_f = g/\omega$, i.e. the deformation is zero at a center with $n_f = 0$ and is the maximum possible at a center with $n_f = 1$. The energy of the system in this case proves to be a linear function of n_f , and we have returned, so to say, to the case of free (noninteracting) electrons, the only difference being that the energies of occupied and empty levels are renormalized differently. Naturally, there is no first-order transition here.

Minimization of the entire expression (2.5.22) yields three equations for β_s , β_f , and n_f . Analytical and numerical studies of these equations lead to the following results:

(1) $\beta_s \simeq \beta_f$ for an f level that is far from the Fermi level (in the given model from the s level ε_s); at $E_f \ll \varepsilon_s$ we have $n_f \simeq 1$ and $\beta_s \simeq \beta_f \simeq g/\omega$, while at $E_f \gg \varepsilon_s$ we have $n_f \simeq 0$ and $\beta_s \simeq \beta_f \simeq 0$. But, strictly speaking, the mean-field approximation ($\beta_s = \beta_f$) is realized for large V 's only asymptotically, as $V \rightarrow \infty$.

(2) As E_f approaches ε_s , the difference $\beta_f - \beta_s$ increases and, accordingly, the effective hybridization $\tilde{V} = V \exp \{-(\beta_s - \beta_f)^2/2\}$ falls off faster and faster [in accordance with (2.5.18)]. This reduction of hybridization is maximal at $E_f = \varepsilon_s$.

(3) Notwithstanding the suppression of hybridization, which would seem to increase the tendency to a jumplike transition, the EPT actually becomes smoother than predicted by the mean-field approximation. For instance, at $g/2\omega < 1$ the transition proves to be smooth at any value of V , however small. This means that the tendency of the various centers to "uncouple" [which in effect results in reduction of the quadratic term of the type $-Cn_f^2$ in (2.5.23)] prevails over the tendency to accelerate the transitions due the decrease in hybridization and the polaron narrowing of the f level.

We note also that the degree to which the f level is narrowed depends not only on the relation between the model constants g , ω , and V but on the position of the f level in relation to the Fermi level. The authors of [66, 70] did not allow for this effect.

Newson and Newns [71], using a variational method [67] and the Green-function technique for the case of a broads band, also came to the conclusion that the decrease in correlations between different sites due to polaron effects is more important than the single-site effect, the narrowing of the f level. We see, therefore, that both in the model with electron-electron interaction and in that with electron-lattice interaction, allowing for local correlations greatly weakens the coupling between the centers, i.e. suppresses the cooperative effects and brings the system nearer in its properties to that of independent "impurities". This can serve as partial justification for the impurity model, which we have used extensively in our review. We see that these effects also modify valence transitions acting contrary to the first-order phase transition and stabilizing the MV phase.

2.5.4 Interaction via Short-Wavelength Phonons and Formation of Ordered Structures

Above we discussed largely the interaction with a homogeneous strain or, which is the same, with long-wave phonons. But electrons interact with other phonon modes as well, and such interaction may have quite different consequences for the entire problem of EPT. Indeed, the interaction of electrons with dilatation results in the electrons being attracted to each other, a fact that is reflected by terms of type $-\gamma^2 n_s^2/2B$ in (2.5.5) or $-g^2 n_f^2/\omega$ in (2.5.23) and leads to a first-order transition. But the interaction via short-wavelength phonons may lead to repulsive forces, in this way slowing down the transition and stabilizing the MV phase. Because of such interaction there may also appear spatial correlations within the system. We will study this aspect [7] using the model Hamiltonian

$$H = \sum_{\mathbf{k}} \varepsilon_{\mathbf{k}} a_{\mathbf{k}}^{\dagger} a_{\mathbf{k}} + E_f \sum_i f_i^{\dagger} f_i + \sum_{\mathbf{q}} \omega_{\mathbf{q}} b_{\mathbf{q}}^{\dagger} b_{\mathbf{q}} + \sum_{i\mathbf{q}} g_{i\mathbf{q}} f_i^{\dagger} f_i (b_{\mathbf{q}}^{\dagger} + b_{-\mathbf{q}}), \quad (2.5.24)$$

where $g_{i\mathbf{q}} = g_{\mathbf{q}} \exp(i\mathbf{q} \cdot \mathbf{R}_i)$.

We exclude the electron-phonon interaction by introducing the "polaron" canonical transformation

$$H \rightarrow \tilde{H} = e^{iR} H e^{-iR}, \quad R = i \sum_{i\mathbf{q}} \frac{g_{i\mathbf{q}}}{\omega_{\mathbf{q}}} f_i^{\dagger} f_i (b_{\mathbf{q}}^{\dagger} - b_{-\mathbf{q}}), \quad (2.5.25)$$

or the equivalent shift

$$b_{\mathbf{q}} \rightarrow \tilde{b}_{\mathbf{q}} = b_{\mathbf{q}} + \sum_i \frac{g_{i\mathbf{q}}}{\omega_{\mathbf{q}}} f_i^{\dagger} f_i.$$

This yields

$$\begin{aligned} \tilde{H} = & \sum_{\mathbf{k}} \varepsilon_{\mathbf{k}} a_{\mathbf{k}}^{\dagger} a_{\mathbf{k}} + \sum_i \left(E_f - \sum_{\mathbf{q}} \frac{g_{\mathbf{q}}^2}{\omega_{\mathbf{q}}} \right) f_i^{\dagger} f_i \\ & + \sum_{\mathbf{q}} \omega_{\mathbf{q}} \tilde{b}_{\mathbf{q}}^{\dagger} \tilde{b}_{\mathbf{q}} - \sum_{i \neq i'} J_{ii'} f_i^{\dagger} f_i f_{i'}^{\dagger} f_{i'}, \end{aligned} \quad (2.5.26)$$

where

$$J_{ii'} = \sum_{\mathbf{q}} \frac{g_{\mathbf{q}}^2}{\omega_{\mathbf{q}}} \exp\{i\mathbf{q} \cdot (\mathbf{R}_i - \mathbf{R}_{i'})\}. \quad (2.5.27)$$

Equations (2.5.26) and (2.5.27) show that, first, there is a constant shift of the f level (the polaron shift) and, second, the f -electrons at different centers interact. Depending on the dispersion of $\omega_{\mathbf{q}}$ and $g_{\mathbf{q}}$, the interaction may have different signs. If the interaction

$$J(\mathbf{q}) = \frac{g_{\mathbf{q}}^2}{\omega_{\mathbf{q}}} - \frac{1}{N} \sum_{\mathbf{q}} \frac{g_{\mathbf{q}}^2}{\omega_{\mathbf{q}}}$$

is of maximal strength when $q = 0$ (the net interaction of the f-electrons is attractive, the strain is homogeneous, and all centers are occupied equally), we find that in the mean-field approximation for (2.5.26) the total energy is given by an expression of the type (2.5.5):

$$\mathcal{E} = \left(E_f - \sum_q \frac{g_q^2}{\omega_q} \right) n_f - J(0) n_f^2 + \frac{1}{2\rho} (1 - n_f)^2 \quad (2.5.28)$$

(we assume the constant density of states $\rho(\epsilon)$ in the s-band). We note that (2.5.28) differs somewhat from what we may have obtained if we applied the mean-field approximation directly to (2.5.24); in (2.5.28) the effect of self-action has been excluded correctly. For one, for purely local phonons (in the absence of dispersion in ω_q and g_q , i.e. $\omega_q = \omega$ and $g_q = g$) Eq. (2.5.5) would give a jumplike phase transition; on the other hand, in this case $J_{i \neq i'} = 0$ and, according to Eqs. (2.5.26) and (2.5.28), the transition can only be smooth. Indeed, local phonons do not lead to an interaction between the centers, and there is no question of a cooperative transition. Hence, we again see that allowing for local effects (the exclusion of self-energy) smooths the transition and makes the term $-Cn_f^2$ in the energy decrease (in Sec. 2.5.3 this effect was considered in a model without dispersion, where, strictly speaking, a transition is always smooth; however, the method used there imitates the general situation).

If the strongest interaction is that with short-wavelength phonons (e.g., in SmS, the interaction with phonons at the L -point of the Brillouin zone, $\mathbf{q}_0 \approx \frac{\pi}{a} (1, 1, 1)$), there may appear in the system a density wave of the f-electrons with a wave vector \mathbf{q}_0 and $n_{fi} = n_f [1 + \cos(\mathbf{q}_0 \cdot \mathbf{R}_i)]$. This phase corresponds to one with MV of a periodic structure (a density wave of f-electrons or, more exactly, a valence density wave, VDW). As E_f grows, the system goes through the following phases: the homogeneous phase with $n_f \approx 1 \rightarrow$ the MV phase with spatial correlations and $\bar{n}_f \approx 1/2 \rightarrow$ the phase with $n_f \approx 0$.

This becomes especially evident if we assume that the s-electrons are localized (the two-level model) and $n_{fi} + n_{si} = 1$. If we introduce the pseudospin operators $\sigma_i = 1/2$ ($\sigma_i^z = -1/2$ for $n_{fi} = 1$ and $\sigma_i^z = 1/2$ for $n_{fi} = 0$ and $n_{si} = 1$), we can write the effective Hamiltonian (2.5.26) in the form

$$\tilde{H} = - \sum_{i \neq i'} J_{ii'} \sigma_i^z \sigma_{i'}^z - h \sum_i \sigma_i^z, \quad h = E_f + \sum_q \frac{g_q^2}{\omega_q} - \bar{\epsilon}_s. \quad (2.5.29)$$

If the interaction with the mode $q = \pi/a$ is strong, we arrive at the Ising model of an antiferromagnet in a parallel field, and the sequence of transitions as h (or E_f) grows corresponds to that described above

(the phase with $\sigma_i^z = -1/2$, i.e. $n_{fi} = 1 \rightarrow$ the "antiferromagnetic" phase with MV, $n_{fi} = 0; 1; 0; 1; \dots$, and $\bar{n}_f = 1/2 \rightarrow$ the phase with $\sigma_i^z = +1/2$, i.e. $n_{fi} = 0$).

In terms of pseudospin, hybridization of f- and s-electrons is equivalent to the presence of a transverse field $V\sigma_i^x$; it smooths out

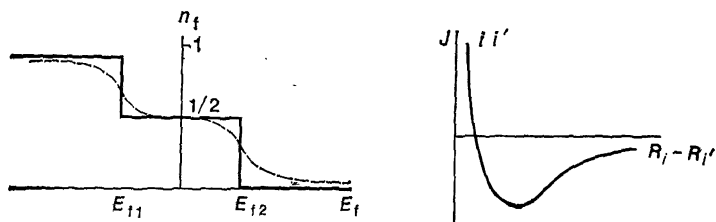


Fig. 2.9. The change in the occupation of the f level for the interaction via short-wave phonons. The solid line represents the case with $T = 0$ and $V = 0$, while the dashed line the case with $T \neq 0$ or $V \neq 0$.

Fig. 2.10. The qualitative behavior of the electron-electron interaction via phonons with distance.

the transition and destroys long-range order. Since this term does not commute with the canonical transformation operator R defined in (2.5.25), we cannot completely separate out the phonons. It is this that leads to polaron reduction of hybridization (2.5.18) and results in the additional complications studied in Sec. 2.5.3. Transition with the field (with increasing E_f) in the model with an interaction Hamiltonian (2.5.29) of an antiferromagnetic type becomes also continuous at any nonzero temperature (Fig. 2.9).

The total interaction of the f-electrons via the lattice, $J_{ii'}$, which includes the exchange of both long-wave and short-wave phonons, may be much more complicated since the interaction with a homogeneous strain results in long-range attraction while interaction via short-wavelength phonons results in short-range repulsion (such is interaction of impurities of the interstitial atoms in a solid, e.g. hydrogen atoms in a metal [72], where the effect is known as the nearest-neighbor-blocking effect). The resulting interaction shown in Fig. 2.10 resembles the standard interaction of atoms and molecules. The resulting spin model (2.5.29) with short-range antiferromagnetic interaction and long-range ferromagnetic interaction also behaves in the fashion depicted in Fig. 2.9, only in this case the transitions at points E_{f1} and E_{f2} are real first-order transitions [73]. As the temperature increases, there appear tricritical points on the lines of phase transition. The resulting phase diagram (Fig. 2.11) resembles the real phase diagram of cerium (Fig. 2.12).

Hence, by allowing for the electron-phonon interaction we are able to reproduce the basic features of valence transitions, e.g. the presence in a number of systems (see [7]) of two phase transitions,

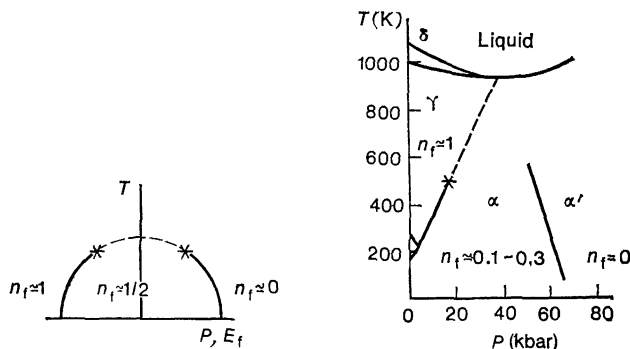


Fig. 2.11. The phase diagram of a system with the interaction depicted in Fig. 2.10.

Fig. 2.12. The phase diagram of cerium [20].

the stabilization of MV phase in the intermediate region, the existence of critical points on the lines of phase equilibrium, and the anomalous behavior of the compressibility and phonon frequencies.

2.6 MIXED-VALENCE STATES: THE BASIC PROBLEMS

Up till now we have mainly discussed the results obtained in the theory of EPT's and mentioned the various difficulties only in passing. But the situation is not as good as it might seem. More than that, there are many more questions than answers in the MV problem. In this chapter we will try to describe the situation as it stands and reveal the relationship between the MV problem and other fashionable, so to say, and difficult problems and phenomena in solid-state physics. We will also try to indicate, at least qualitatively, possible ways of solving the problems emerging.

The main difficulties emerge when we try to describe the structure and properties of the MV phase proper and the type of ground state.

This is the range of questions to be considered in this chapter. The two previous chapters were devoted largely to EPT's. Now we turn to the problem of mixed valence. This is still a formidable problem; there is yet no real solution.

2.6.1 Properties of Mixed-Valence States. The Experimental Situation and Statement of the Problem

We will start with a brief review of the properties of mixed-valence states. This will help us to correctly formulate the various problems and suggest several possible ways of solving them.

States with MV are characterized by the fact that the f level lies close to the Fermi level or, in other words, there is a resonance between the electron configurations $4f^n$ and $(4f^{n-1} + \text{an } (sd)\text{-electron})$. Mathematically, the criterion for this is

$$|E^n - E^{n-1, sd}| = |E_f - \varepsilon_F| \lesssim \Gamma = \pi \rho V^2. \quad (2.6.1)$$

If the f level lies much deeper than the Fermi level ε_F , we are dealing with the Kondo effect (for a concentrated system one speaks of the Kondo lattice [74]); in the opposite case, when $E_f \gg \varepsilon_F$, we simply have a partially filled conduction band, i.e. a normal Fermi liquid.

A phase with MV is characterized by the presence of a narrow resonance or a peak in the density of states near ε_F . This affects the majority of properties of such compounds—practically all of their physical features behave in an anomalous way. Thermodynamically, these substances are usually characterized by a very large linear electronic specific heat $c = \gamma T$ (the factor γ is proportional to the density of states, $\rho_{\text{tot}}(\varepsilon_F)$, and in cases typical of such compounds is higher by 2 to 3 orders of magnitude than for normal metals of the Na and Al type). At high temperatures their magnetic susceptibility obeys the Curie-Weiss law, but as $T \rightarrow 0$ it tends to a constant $\chi(0)$, often passing through a maximum. The magnitude of $\chi(0)$ is also very high and, in general, corresponds to a high value of γ . The properties of the lattice have characteristic features, too. Namely, in a phase with MV the compressibility is usually anomalously high while the frequency of the longitudinal phonons is anomalously low (to an extent that in $\text{Sm}_{1-x}\text{Y}_x\text{S}$ the frequencies of the longitudinal optical phonons lie below those of the transverse phonons over the entire Brillouin zone [75], despite the fact that this compound is similar to ionic crystals of the NaCl type). Of special interest are the transport properties of compounds with MV, on which we will dwell later.

Qualitatively, the above-mentioned features can be explained by the simple idea of a narrow ($\Gamma \simeq 10^{-2}$ eV) peak in the density of states at ε_F . If we assume that the usual notion of a Fermi liquid is applicable here, the only difference being the large effective mass, then we can explain the high value of the electronic specific heat ($\gamma \sim \rho_{\text{tot}}(\varepsilon_F) \sim \hbar/\Gamma$) and the constant (and high) value of the magnetic susceptibility at absolute zero, $\chi(0)$, which is also pro-

portional to $\rho_{\text{tot}}(\epsilon_F)$. The high density of states at ϵ_F also explains the high compressibility of the system. (Another explanation of the high compressibility and the softness of the longitudinal phonons, which we gave in Sec. 2.5.1, is in essence closely related to the current one.)

This simple interpretation gives a qualitatively satisfactory explanation of many properties of states with MV but runs into a

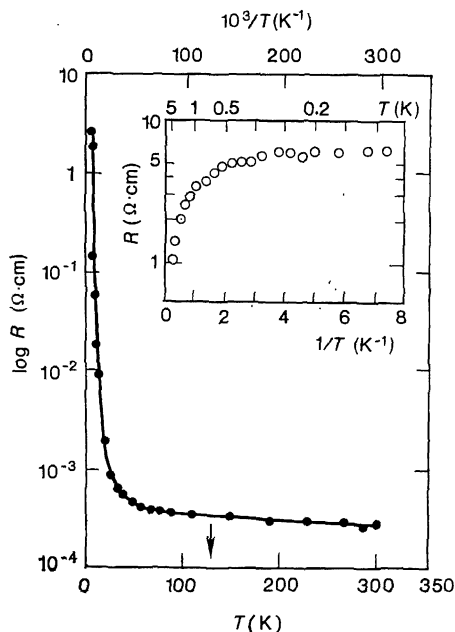


Fig. 2.13. The temperature dependence of the resistivity in SmB_6 [77, 80].

number of difficulties, both theoretical difficulties and difficulties in explaining various peculiarities observed in experiments.

Theoretically it is difficult to understand how there can exist a Fermi liquid with an effective mass so high and degeneracy temperatures so low (the latter are about 10^2 K in such substances). It would seem that any interactions, both those discussed in Chaps. 2.4 and 2.5 and those not mentioned (e.g. the Coulomb interaction of the f-electrons or f-holes at different centers), make such a model inapplicable [76]. First, the electrons in such narrow bands must be localized according to Mott and Hubbard. Next, they could form a Wigner-like crystal (this possibility was discussed in Sec. 2.5.4). Another factor that could drastically change the properties of such a Fermi liquid is the interaction between the f- and s-electrons, which

would lead to a state of the excitonic insulator type [47]. In general, as a result of any of these factors, both separately and jointly, we could expect the Fermi-liquid behavior to break down; for one, we could expect the system to transfer to the dielectric state.

Interestingly, it was recently established that for some compounds with MV the situation is apparently just what we have described. It has been discovered, primarily in studying transport properties, that in some such substances (SmB_6 , SmS , TmTe , and others) there is probably a small gap in the ground state. The most representative in this sense is SmB_6 [77]. The temperature dependence of the resistivity of the compound is shown in Fig. 2.13 (for comparison

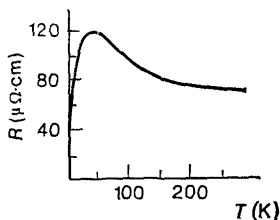


Fig. 2.14. The temperature dependence of the resistivity in CeAl_3 [79].

we have depicted the temperature dependence of the resistivity of the CeAl_3 compound in Fig. 2.14 [79]; although the resistivity of this compound does behave in a peculiar fashion, at low temperatures the compound closely resembles a Fermi liquid, $R \sim BT^2$, the only difference being the low degeneracy temperature, $T_F \simeq 20$ K). We see that in SmB_6 , in contrast to CeAl_3 , the resistivity rises as the temperature drops, and the compound shows no tendency to become a Fermi liquid down to very low temperatures. Correspondingly, the study of the optical properties of SmB_6 in the far-infrared region has shown that its dielectric constant $\epsilon(\omega)$ does not behave like that of a metal; namely, in the very-low-frequency range $\text{Re } \epsilon$ becomes positive. Hall effect studies have revealed that at low temperatures the concentration of conduction electrons in SmB_6 is about $5 \times 10^{17} \text{ cm}^{-3}$ [77].

The entire body of experimental results would seem to point to the presence of a small semiconductor gap, $E_g \sim 20$ K, in the MV phase of SmB_6 . Although this assumption is not free from flaws either (for one, it is difficult to explain why as $T \rightarrow 0$ the resistivity does not become infinite but reaches a plateau at a residual value of $R_0 \sim 2.6 \Omega\cdot\text{cm}$, which is four orders of magnitude greater than the typical maximum metallic resistivity [80]), it does give a better explanation of the entire body of experimental data on SmB_6 than the idea of a Fermi liquid.

But what is the nature of this gap? Is it due simply to a single-particle effect, i.e. has a purely hybridization nature (see Fig. 2.5), or is it a reflection of some collective effect that we have already discussed? If the second assumption is true, it would be desirable to determine exactly what mechanism is responsible for the presence of a gap and whether the properties of the system will be similar to those of an ordinary semiconductor. Another interesting question is how the state of the system and its properties change when external conditions change (e.g. when pressure is applied). This question is closely related to the EPT problem; namely, is the gap preserved in transitions or does the EPT change, say, an insulator to a metal (i.e. bring about a transition from the case with a gap to the Fermi-liquid picture)? Moreover, many compounds with MV (e.g. the α phase of Ce and the majority of intermetallic compounds) have no gap; for them the picture of a Fermi liquid is quite applicable. Correspondingly, it would be desirable to know the reason for this and why substances with MV apparently divide into two classes: metals that behave like Fermi liquids and insulators with a narrow gap.

All these questions are at the center of attention of researchers studying the MV problem, but no final answers have yet been found. For this reason our exposition is largely hypothetical and qualitative. We will elucidate the situation that exists at present and will express a viewpoint that to us seems most convincing.

2.6.2 The Anderson and Kondo Lattices

Theoretically almost all the above-mentioned questions spring from and may be analyzed within the framework of the model of an Anderson lattice, which we discussed in Chap. 2.3. For this reason we will start with this case and only then discuss the possible role of other factors and interactions not included in the model (2.3.4).

The properties of a single impurity, described by the Anderson model (2.3.2), are now well known. There exist several approximate studies (see [81]), such as the approach developed by Haldane [82] using renormalization-group methods and the detailed numerical calculations of Krishna-Murthi *et al.* [83]. Moreover, there is an exact solution [29], although this is brought up only to a set of integral equations. (Quite recently these equations have been solved [21].) All these approaches lead us to the following picture: for a deep-lying level the problem is equivalent to the Kondo model, while for $E_f \rightarrow \varepsilon_F$ (the MV case) the Kondo temperature T_K grows, tending to Γ , and the strong-coupling regime is achieved directly from a threefold degenerate state (i.e. the states $|n_f = 0\rangle$, $|\uparrow\rangle$, and $|\downarrow\rangle$ are occupied); see Fig. 2.15. Here at low temperatures

($T \ll \Gamma$) the elementary excitations have a Fermi-liquid nature, but unlike the case of a Kondo impurity there is no universality in the MV case. For instance, the ratio of the magnetic susceptibility to the heat capacity as $T \rightarrow 0$, namely $\zeta = (4\pi^2/3) T\chi(T)/c(T)$, is

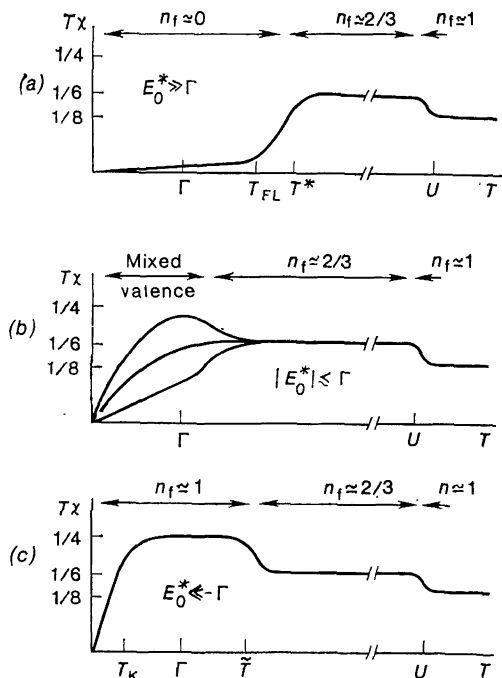


Fig. 2.15. A rough sketch of the behavior of the susceptibility in the Anderson model [82]. We can see a transition between states of fourfold degeneracy ($T\chi = 1/8$ and equally probable occupation of the f-level states $|0\rangle$, $|\uparrow\rangle$, and $|\downarrow\rangle$), threefold degeneracy ($T\chi = 1/6$ and occupied states $|0\rangle$, $|\uparrow\rangle$, and $|\downarrow\rangle$), twofold degeneracy ($T\chi \approx 1/4$, occupied states $|\uparrow\rangle$ and $|\downarrow\rangle$), and localized magnetic moments in the system), and the singlet state ($T\chi \approx 0$ and the Fermi-liquid regime). The regime with localized magnetic moments is not realized in the MV case (b).

not a universal quantity and depends on the position of the f level relative to the Fermi level; it changes (for spin 1/2) from the value of 2, characteristic of a Kondo impurity, to the value of 1 at $E_f \gg \varepsilon_F$, the value for a Fermi gas without interaction [83].

In accordance with qualitative reasoning we can expect this ratio to take the following form:

$$\zeta = \frac{4\pi^2}{3} \frac{T\chi}{c} \simeq 1 + n_f. \quad (2.6.2)$$

Indeed, n_f gives the probability of finding on the f level a localized electron with a magnetic moment, i.e. on the average the impurity ensemble has n_f impurities with a localized spin, which produce a ratio $\xi = 2$, and $(1 - n_f)$ impurities without spin, for which $\xi = 1$. The exact solution of the single-impurity case [21] shows that (2.6.2) indeed is roughly correct in an MV phase ($E_f \gtrsim \varepsilon_F$) but does not hold in the Kondo regime ($E_f \ll \varepsilon_F$).

In concentrated systems (the Anderson lattice) the situation is not so clear. For deep-lying levels ($E_f \ll \varepsilon_F$) we obtain an equivalent lattice of Kondo impurities, the so-called Kondo lattice [74], with

$$H_{KL} = -J \sum_i \{2(a_{i\uparrow}^\dagger a_{i\downarrow} S_i^- + a_{i\downarrow}^\dagger a_{i\uparrow} S_i^+) + (a_{i\uparrow}^\dagger a_{i\uparrow} - a_{i\downarrow}^\dagger a_{i\downarrow}) S_i^z\} \\ + \sum_{ij} W_{ij} (a_{i\uparrow}^\dagger a_{j\uparrow} + a_{i\downarrow}^\dagger a_{j\downarrow}). \quad (2.6.3)$$

This model was studied for the one-dimensional case numerically using the renormalization-group technique [84] and for the three-dimensional case using the method of functional integration [85]. And an interesting result was obtained when the number of electrons N_e in the conduction band differs from the number of spins N_s , the system is a metal, while when $N_e = N_s$, a gap develops at the Fermi level and the system is an insulator. The ground state in the latter case is a singlet and can be thought of as a state produced as a result of singlet pairing (the Kondo compensation of the moment) of *each* of the s -electrons with a corresponding localized spin (although this effect has, of course, a cooperative nature).

We note an analogy between this situation and that of an excitonic insulator [47], where there is pairing (usually singlet pairing) of electrons with holes, which takes place when the concentrations of both are the same and leads to a gap in the spectrum.

We can fill this analogy with more details if we use the equivalence of the Kondo model and the model of a spinless impurity with an f - s interaction [52, 53]. Namely, in the case of a single Kondo impurity the authors of [52, 53] proved the equivalence of the initial Kondo model (with different constants of the longitudinal and transverse exchange interactions, J_{\parallel} and J_{\perp}) and the Falicov-Kimball model

$$H = \sum_k \varepsilon_k c_k^\dagger c_k + E_f f^\dagger f + \sum_k V (c_k^\dagger f + \text{h.c.}) + G f^\dagger f \sum_{kk'} c_k^\dagger c_{k'}, \quad (2.6.4)$$

where c_k^\dagger and c_k are new fermions that do not coincide with the initial fermions $a_{k\sigma}^\dagger$ and $a_{k\sigma}$; ε_k gives the (linear in k) dispersion law at ε_F ; E_f is zero for the Kondo model without a magnetic field (i.e. the resonance level lies exactly at the Fermi level), and

$$2V = J_{\perp}, \quad \sqrt{2} (G\rho + \sqrt{2} - 1) = J_{\parallel} \rho. \quad (2.6.5)$$

Apparently, we can connect the appropriate models in the case of concentrated systems in a similar fashion, i.e. the model of the Kondo lattice should be equivalent to the spinless periodic model of Falicov and Kimball. The latter differs from the standard case of an excitonic insulator (see [47]) only in one respect: the effective mass of the holes is much greater than the electron mass. Correspondingly, the gap for a Kondo lattice [84, 85] is similar to the gap in an excitonic insulator.

A comparison of these two models clarifies the difference mentioned in Chap. 2.4 between the MV problem and the excitonic-insulator problem; namely, strong coupling is always the case for heavy f-electrons (f-holes) and the usual approach to this problem [47] is inapplicable—even one such center is equivalent to the Kondo model and brings in all the difficulties inherent in this model (the model (2.6.4) for a single impurity has been solved exactly in [20]).

Another model that, apparently, is connected with the Kondo-lattice model is the Hubbard model (2.2.3). We know that the ground state in the Kondo problem is equivalent to a Fermi-liquid state in which, however, there appears an interaction of the Hubbard type between the fermions (the s-electrons), $U a_{i\uparrow}^\dagger a_{i\uparrow} a_{i\downarrow}^\dagger a_{i\downarrow}$ [87]. The same terms appear when the Kondo lattice is analyzed by the renormalization-group technique [84], so that, in accordance with Nozières's ideology, we can expect that at low temperatures the Kondo lattice is equivalent to fermions with such an interaction, i.e. the Hubbard model. In this case we can relate the gap in the Kondo lattice (which in one dimension exists for all values of the parameters of the Hamiltonian (2.6.4)) to the respective gap in the Hubbard model (see [86]). That all three models, the Kondo-lattice model, excitonic-insulator model, and Hubbard model, are similar is proved by the fact that for all of them the gap in the one-dimensional case depends on the coupling constant (J , G , or U) in a similar manner (see [47, 84, 86]):

$$E_g \simeq F(\rho J) \exp(-1/\rho J).$$

On the basis of this analogy we can conclude that singlet pairing and the gap in the spectrum of the Kondo lattice in the three-dimensional case exist not for any value of the coupling constant but only for a strong f-s exchange interaction. Indeed, calculations show that for weak coupling in three dimensions the regime is not a singlet one (i.e. not a Kondo type) but a magnetically ordered (apparently, the latter state has no gap except in the case of nesting).

The possibility of a magnetic regime instead of a Kondo regime for small J 's is (at least qualitatively) due to the fact that while the characteristic energy of singlet pairing $E_K \simeq W \exp(1/\rho J)$ (we note that here J is negative), the energy of magnetic ordering (the Ruderman-Kittel exchange) $E_{\text{RKKY}} \simeq \rho J^2$. We see that for small J 's

$E_{\text{RKKY}} > E_{\text{K}}$, i.e. the magnetic state proves preferable. The possibility of a magnetic solution in the Kondo lattice at $J \lesssim 0.3W$ was first obtained for the one-dimensional model [74]; further calculations (see [84]) have not corroborated the existence of two different regimes in one dimension, but in three dimensions the situation is, apparently, what we have described. The deep f levels, in agreement with (2.3.3), give a small exchange interaction J , and for these centers the magnetic regime is realized; in fact such are the typical magnetic compounds of rare-earth metals. On the other hand, as $E_f \rightarrow \varepsilon_F$ (when we approach a state with MV), $|J|$ grows and a transition is possible to the Kondo regime, in which at $N_e = N_s$ a gap appears at the Fermi level.

We note that from what has been said a change from one regime to the other will take place at $|J| \simeq 0.3W = 0.3\rho^{-1}$, i.e., in accordance with (2.3.3), at $\varepsilon_F - E_f \simeq 3\rho V^2 \simeq \Gamma$, which is exactly in an MV phase. In this case, however, the transition via Schrieffer-Wolff transformation from the Anderson lattice (2.3.4) to the Kondo lattice (2.5.3) cannot be achieved, and one must resort to the original model (2.3.4). Therefore, we see that the singlet regime with a gap realized in a three-dimensional Kondo lattice for strong coupling, $\rho J \simeq 1$, apparently can serve only as an indication that a similar situation is present in the mixed-valence case in the realistic model of the Anderson lattice as well.

Although the studies of the Kondo lattice are far from complete, the situation appears to be such as discussed above; possibly, the appropriate one-dimensional model can even be solved exactly (in a way similar to the solution of the Kondo problem [29] or the one-dimensional Hubbard model [86]). However, as yet there is no reliable data on the Anderson lattice. Among the exact results we can recall only the interesting work of Jullien and Martin [88], who made a numerical calculation for a one-dimensional model with a finite number of centers and, by applying an extrapolation technique, established that the gap at $N_e = N_s$ for deep-lying levels (the Kondo lattice) is present here for any position of the f level (including the mixed-valence case) and the chemical potential lies inside the gap. The authors study the case where there are two electrons per site and in the initial state, at $E_f \ll \varepsilon_F$, one electron localized on the f level produces a localized spin while the rest $N_e = N$ electrons lie in the conduction band and fill it up to the middle (in [88] the conduction band is taken nondegenerate in the tight-binding approximation, $\varepsilon_k \sim \cos k$). In this case at one limit (deep-lying levels and a Kondo lattice) the gap lies at the Fermi level and appears due to the singlet pairing discussed above. At the other limit, when the f level lies quite high (above the top of the conduction band), the s band proves to be completely filled and we again have an insulator. It was found that the dielectric nature of the system is preserved for all interme-

diate values of E_f . This conclusion agrees with Luttinger's theorem on the constancy of the volume of the Fermi sphere. (This theorem, however, is not applicable in the insulator-metal transition of the Mott-Hubbard type; see Sec. 2.6.3.)

Qualitatively, the reason for the preservation of the gap at all positions of the f level can be pictured in the following manner (U_f is large). As the f level moves upward at $E_f \gtrsim \varepsilon_{F0}$, some of the f -electrons go over to the conduction band, but the number of remaining f -electrons will nevertheless always remain equal to the number of holes in the conduction band; apparently, their pairing produces the gap in the spectrum.

Thus, we again arrive at the case of an excitonic insulator. We note that, in contrast to this case, in the initial Hamiltonian (2.3.4) [or (2.6.3)] there is no direct interaction between the f - and s -electrons of the type $Gn_{\uparrow}n_s$, which is usually responsible for excitonic pairing. Obviously, the respective interaction appears due to the renormalization process or in a way similar to the way it emerges in the transition from model (2.6.3) to (2.6.4); here we can clearly see the importance of the strong f - f interaction, $Un_{\uparrow\uparrow}n_{\uparrow\downarrow}$. This problem has not yet been studied in detail.

The situation just discussed (the dielectric state for all E_f 's with two electrons per site) must also occur in the opposite case, where starting from the initial state the f level moves downward instead of upward, so that the upper Hubbard level $E_f + U$ drops below the bottom of the conduction band. After this both electrons are on the f level with opposite spins and the system will again be in the singlet insulator state (this state resembles the semiconductor phase of SmS). It is clear that there will be a gap for any value of E_f .

2.6.3 The Valence Transition and the Mott-Hubbard Transition

A totally different situation may arise if there is one electron per site instead of two. In this case we obviously encounter a transition of the Mott-Hubbard type.

At $n = 2$, the state of the system is, apparently, always dielectric, and an electronic phase transition is a transition of the insulator-insulator type, even if it is a first-order transition by one of the mechanisms discussed in Chaps. 2.4 and 2.5. Now let us suppose that $n = 1$ and in the initial phase the f level lies far below the bottom of the conduction band. Then this level contains one electron and a localized spin, $n_{\uparrow} = 1$, while the conduction band is empty; obviously, the substance in this phase is an insulator. On the other hand, when the f level lies far above ε_F , we are dealing with a case where the f level is unoccupied and can be ignored while the conduction band is partially filled with free electrons of concentration $n_s = 1$. Hence,

the system is now a metal, and the transition accompanied by a change in valency is that of the insulator-metal type, in which the regime of localized electrons transforms into the Fermi-liquid regime (in other words, we can say that the statistics has changed from atomic at $E_f \ll \varepsilon_F$ (or $\ll 0$) to Fermi-Dirac at $E_f \gg \varepsilon_F$ (or $\gg W$); see [89, 90]). How such a transition takes place remains completely unknown. In some approximate approaches [91-93] the authors used the Hubbard approximation [17] to study the properties of this system (and also the case with $n = 2$). In these approaches hybridization of localized ("single occupied") f states with free ("doubly occupied") states of the conduction band was introduced. As a result

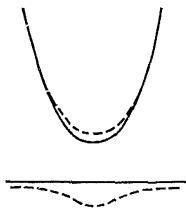


Fig. 2.16. The change in spectrum (dashed lines) in the semiconductor case under f - s hybridization.

the spectrum had the form shown in Fig. 2.16; even at $E_f < 0$ the fraction of occupied f states, n_f , is less than unity. But the total number of states in the lower subband immediately becomes greater than unity. As a result this band becomes only partially filled, the chemical potential lies not in the gap but inside this band (near its upper edge), and, irrespective of the gap, the system in the formal sense, is a metal, no matter how deep the f level lies or how weak the f - s hybridization is*. In this case there is no EPT at all, since from the very beginning the hybridization makes the system a metal, while as the f level moves upward the lower band gradually broadens and the Fermi level in it moves toward its center. This result, however, from the physical standpoint is totally unrealistic, since it is clear that just as in the Hubbard model with $t \ll U$, for a deep-lying f level ($|E_f| \gg V$) the system must be dielectric and, irrespective of the character of the wave function (determined by the admixture of s states to it), the total number of states per site in the lower band must in this case be equal to unity.

To correct this deficiency Kikoin and Flerov [89] suggested first introducing a canonical transformation that would diagonalize the

* This resembles the situation with the Hubbard model, when under an incorrect approximation scheme (the Hartree-Fock approximation, say) the system proves to be metallic, no matter how narrow the band is, $t \ll U$.

quadratic part of the Hamiltonian (2.3.4):

$$\alpha_k^\dagger = u_k f_k^\dagger + v_k a_k^\dagger, \quad \beta_k^\dagger = v_k f_k^\dagger - u_k a_k^\dagger, \quad u_k^2 + v_k^2 = 1. \quad (2.6.6)$$

The next step is to express the interaction in terms of these new wave functions. Clearly, if the width of the lower band \tilde{t} (at $V \ll |E_f| < 0$ it is of the order of $V^2/|E_f|$) is less than the new effective interaction

$$\tilde{U}^\alpha = \langle \alpha\alpha | U n_{f\uparrow} n_{f\downarrow} | \alpha\alpha \rangle \simeq u^4 U, \quad (2.6.7)$$

where $u^2 \simeq n_f \simeq 1 - (V/E_f)^2$ for $V \ll |E_f|$, in the already hybridized lower band α all electrons will be in the Hubbard regime, i.e. this system, even when hybridization is taken into account, will remain a Mott-Hubbard dielectric.

One difficulty arises however, when we try to describe the transition; namely, there must be a point where the regime changes, so that the lower subband lies on the metallic "side" of the Mott-Hubbard transition. It is highly probable that this happens simultaneously with a valence transition, especially if this is a first-order transition. But it is also probable that these two transitions are "uncoupled" and, say, the insulator-insulator transition with an abrupt valence change takes place first and only after this, in the phase with MV, the insulator-metal transition occurs (cf. a similar discussion by Landau and Zel'dovich [1]). The problem remains unsolved as yet.

In this connection it would be interesting to see what really are the electrons in typical systems with MV. Do they lie on the "localized" or "delocalized" side of the Mott-Hubbard transition? We can make a qualitative estimate (see [7, 90]) if we make more precise the reasoning discussed above [see (2.6.7)] and compare the electron kinetic energy on the Fermi level, $E_{\text{kin}} \sim 1/\rho_{\text{tot}}(\epsilon_F)$, with the mean potential energy (2.6.7) at $k = k_F$. This yields

$$\tilde{U}_{(k_F)}^\alpha = U u_{k_F}^4, \quad \rho_{\text{tot}}^\alpha(\epsilon_F) = \frac{\rho}{v_{k_F}^2} = \frac{\rho}{1 - u_{k_F}^2},$$

i.e. $E_{\text{kin}}^\alpha = W(1 - u_{k_F}^2)$ (2.6.8)

From this it readily follows that at $U \simeq W$ the electrons on the Fermi level remain in the strong correlation regime ($\tilde{U} > E_{\text{kin}}$) down to $u_{k_F}^2 \simeq 1/2$, and at $U > W$ down to even smaller values. Bearing in mind that for the lower hybridized band [band α ; see (2.6.6)]

$$u_k^2 = \frac{1}{2} \left(1 + \frac{\epsilon_k - E_f}{\sqrt{(\epsilon_k - E_f)^2 + 4V^2}} \right),$$

we see that strong correlation is preserved until the f level rises above practically the middle of the conduction band. We can easily

verify that the total number of f-electrons is then

$$n_f = \frac{1}{N} \sum_{|k| < k_F \approx \pi/2} u_k^2 \simeq \frac{V}{W},$$

i.e. in typical cases ($W \simeq 3$ eV, $V \simeq 0.3$ eV, and $\Gamma = \rho\pi V^2 = \pi V^2/W \simeq 10^{-2}$ eV) the electrons on the Fermi level remain strongly correlated down to $n_f \simeq 0.1$ and only at smaller value of n_f transform to a real delocalized state *. From this viewpoint, MV compounds, which have the characteristic value $n_f \simeq 0.3$, are still on the dielectric "side" or at the most on the threshold of the Mott-Hubbard transition. Of course, this estimate is qualitative; effects that we have not allowed for (electron screening, for one) may change the picture. The transition to a Fermi-liquid regime at small values of n_f may be facilitated by the weakening of the effective interelectronic interaction due to multiple scattering [90], just as in a low density gas. We also note that the relationship between the localization discussed above and the Fermi-liquid behaviour may be more complex. For instance, in the case of a Kondo impurity the f-electron is strictly localized, and nevertheless elementary excitations near ε_F at $T < T_K$ are well described by the Fermi-liquid picture. The estimates we have just made prove rather that the role of interelectronic correlations, e.g. the one-site correlations, in a phase with MV may be quite large.

2.6.4 Excitonic Correlations in an MV Phase

In discussing the nature of the gap in the Kondo and Anderson lattices we mentioned the fact that this problem is related to that of an excitonic insulator. Effects of this type manifest themselves even more strongly if we include the Coulomb f-s interaction (2.3.5) directly in the Hamiltonian (we mentioned this in passing in Chap. 2.4).

The excitonic insulator phase usually occurs when a wide valence band and a wide conduction band with the same Fermi surfaces cross and the number of electrons n_e and of holes n_h coincide. If we now "unbend" the valence band and make it flatter, preserving the equality $n_e = n_h$, we arrive at the Anderson-Falicov model, which makes us think that the gap already existing in an excitonic insulator for small masses of f-holes is preserved and even broadens as $m_f \rightarrow \infty$. Thus, in this approach we also arrive at the conclusion that in systems of the SmS and SmB₆ type, where all conduction electrons are electrons that have left the f levels ($n_s = n_f$ hole), the gap will remain in the phase with MV as well; in this case it is

*

A similar estimate can be obtained for the impurity model.

of an excitonic nature*. It is not important for our reasoning whether the f-holes are localized (i.e. of the Hubbard type) or delocalized. In both cases f-s pairing is possible and each s-electron finds a partner. Here the conclusion that in this situation ($n_s = n_{\text{f hole}}$) there is a gap on the Fermi surface in the MV phase appears to be even more natural than in the Anderson-lattice model discussed in Sec. 2.6.2. Obviously, we may again conclude that these two versions are simply different limiting cases, or two modes of description, of a single picture.

With this approach we can also easily understand why, when the number of s-electrons is not equal to the number of f-holes, i.e. when the substance is initially a metal, allowing for excitonic effects is unlikely to lead to a gap at the Fermi level: either there will be no excitonic pairing or a gap may appear, but not at ε_F , so that the system will behave like a heavily doped semiconductor [94]. The first situation is present, apparently, in intermetallic MV compounds (such as CePd_3 and YbAl_3), while the second might describe the properties of SmB_6 : the low concentration of electrons (most probably due to the nonstoichiometry of the samples) may explain the fact that at low temperatures the resistivity has a plateau [80] (see Sec. 2.6.1). However, there remains the question of why below 1 K the carriers are not frozen out and are not bound by the corresponding defects or impurities.

Incidentally, the fact that the majority of compounds with MV are nevertheless metals (see [7]) can serve as additional proof that the gap, which, apparently, exists in SmB_6 or SmS , has a collective nature, since the usual hybridization gap would always lead to a dielectric state when the f level lies near the Fermi level, irrespective of the concentration of conduction electrons and f-holes. The strong Coulomb correlations between f-electrons and, possibly, between f- and s-electrons, apparently, extinguish the common hybridization gap near E_f but in certain conditions produce a gap directly at ε_F . Indeed, a summing of the diagrams [37] or a specific decoupling of the equations of motion [38] leads to the following result: if we allow for multiple scattering of s-electrons on one f center, instead of a gap at E_f there appears a pseudogap

$$G_{\text{ff}\sigma}(k, \omega) = \frac{1}{2\pi} \frac{1 - n_{\text{f}-\sigma}}{\omega - E_f - \Sigma_{\sigma}(k, \omega)}, \quad (2.6.9)$$

$$\Sigma_{\sigma}(k, \omega) = n_{\text{f}-\sigma} \sum_k \frac{V_k^2}{\omega - \varepsilon_k} + (1 - n_{\text{f}-\sigma}) \frac{V_k^2}{\omega - \varepsilon_k}, \quad (2.6.10)$$

* There is also the opposite statement that sufficiently strong Coulomb f-f and f-s interactions destroy the coherence and eliminate the gap in the spectrum, so that we can apply the idea of local virtual f states [39].

i.e. near E_f the levels appear to be pushed apart [the second term on the right-hand side of (2.6.10)]; they also decay. At the same time, as we have just seen, collective effects may produce a gap at ϵ_F even when the f level does not coincide with the Fermi level.

On the basis of the excitonic-correlation model we may give an alternative description of the insulator-metal transition, which we mentioned in Sec. 2.6.3. Namely, we can imagine that as the f level enters the conduction band (starting at the semiconductor phase), s -electrons and f -holes gradually appear, but at the beginning (at low concentrations) they are bound into excitons. As their concentrations grow, their wave functions overlap more and more, and in the exciton system (just as in the impurity system in a heavily doped semiconductor) there will occur a Mott transition with an excitonic band created as a result. This transition is not the Mott transition discussed in Sec. 2.6.3 and connected with the delocalization of the f -electrons. Here the f -electrons and f -holes may remain in the strong-correlation regime. It remains unknown what picture of the transition is closer to reality.

In contrast to the problem of a doped semiconductor the concentrations of s -electrons and f -holes are not fixed and can change during the transition. This can make the transition a first-order one. Druzhinin [56] pointed to the important role of spins and exchange interaction for these transitions.

Another aspect in which this problem differs from the impurity case is that even if initially the f -electrons were infinitely heavy (the bare width of the f band is zero), due to f - s transitions they acquire an effective kinetic energy proportional to Γ . For this reason the corresponding "excitons" must be mobile. Such motion, apparently, will facilitate the transition into the metallic state and effectively increase the overlap. Besides, this factor is important by itself, for one, in many respects it determines the character of spatial correlations in a phase with MV.

2.6.5 Spatial Correlations in MV Systems

In any system consisting of heavy f -holes (or f -electrons) there is the possibility that a spatial structure will form. This was demonstrated in Sec. 2.5.4, where we showed that a periodic structure may form as a result of the electron-lattice interaction. A similar effect can be achieved by introducing the direct Coulomb interaction of f -electrons at different centers, an interaction we did not include in the Hamiltonians (2.3.4)-(2.3.6), or the interaction of f -electrons via conduction electrons, an interaction of the Ruderman-Kittel type [34].

The appearance of such a spatial superstructure of heavy f -holes on the neutralizing background of s -electrons is, in fact, similar to

Wigner crystallization or formation of charge density waves. For systems considered here this would mean the creation of an inhomogeneous MV system; the various centers would cease to be equivalent, and the valency (the number of f-electrons) on these centers would differ. A theoretical possibility for such ordering has been discussed in [5, 7, 34]; in relation to SmB_6 a similar hypothesis was put forward in [80]. We must note, however, that as yet there is no reliable experimental data on such superstructures in MV systems (we do not mention the compounds of the Sm_3S_4 type, where the valence of the rare-earth ion is mixed due to the chemical composition of the compound). The arguments given in [80] are highly indirect, and a different interpretation of the properties of SmB_6 is more probable (see [77] and the text above).

If there really was a superstructure of the Wigner-crystal type, the properties of the corresponding phase would, apparently, follow the tendency we have mentioned many times, i.e. if the number of s-electrons is equal to the number of f-holes, such a crystal is most likely an insulator, if the opposite is true, then a metal. However, if there is a gap in the spectrum, long-range order is not necessarily the case; short-range order would be sufficient for such a gap to appear. In other words, even a dielectric system may be more like a liquid than a crystal consisting of heavy f-holes or excitons. Here is a simple estimate showing whether the ground state of an MV system possesses long-range order (at reasonable values of parameters) or is characterized only by short-range spatial correlations. We estimate the amplitude of zero-point vibrations of the f-holes, δ . If the interaction potential between the holes is U_{int} and their mass is m_h , the characteristic frequency of their vibrations

$$\omega \simeq \left(\frac{d^2 U_{\text{int}}/dx^2}{m_h} \right)^{1/2} \simeq \left(\frac{U_{\text{int}}}{m_h a^2} \right)^{1/2}$$

(a being the average distance between the f-holes, i.e. the period of the "crystal"), while the amplitude of zero-point vibrations

$$\delta \simeq \left(\frac{\hbar}{m_h \omega} \right)^{1/2}.$$

Then

$$\frac{\delta}{a} \simeq \left(\frac{\hbar^2}{m_h U_{\text{int}} a^2} \right)^{1/4} \simeq \left(\frac{\Gamma}{U_{\text{int}}} \right)^{1/4}, \quad (2.6.11)$$

where $\Gamma \simeq \hbar^2/m_h a^2 \simeq \hbar^2 k_F/m_h$ is the effective width of the f band corresponding to a particle of mass m_h , and k_F is the Fermi momentum. Using the Lindemann criterion of melting, $\delta/a \simeq 0.1$, we see that there may be a crystalline phase only if $\Gamma/U_{\text{int}} \lesssim 10^{-4}$, or, put differently, since the characteristic interaction energy U_{int} is no more than 1-10 eV, for long-range order to occur Γ must be less

or of the order of 10^{-4} - 10^{-3} eV. But in real MV compounds Γ is about 10^{-3} - 10^{-2} eV, which means that the corresponding phases resemble liquids rather than crystals.

We can arrive at the same conclusion from the usual reasoning involving a Wigner crystal; according to recent results, crystallization sets in not at $r_s \simeq U_{\text{int}}/E_{\text{kin}} \simeq 1$ but at $r_s \gtrsim 10^2$, which once more makes us to conclude that MV compounds must resemble liquids. Presumably, it is due to this that superstructures in phases with MV have not yet been observed. Nevertheless, since the criterion for melting is met at the limit, it is possible that at low temperatures some compounds with MV will indeed display spatial ordering. Besides, even in common compounds it would be interesting to experimentally study short-range ordering (correlations of valence fluctuations between different centers), which obviously must be present to a certain extent.

2.6.6 Systems with MV as a Model of Condensed Matter

In discussing the various aspects and properties of MV compounds we have repeatedly used such terms as "metal", "insulator", "binding of an s-electron and an f-hole", and "crystal" or "liquid" consisting of heavy f-holes. We could do so because the states with MV in rare-earth compounds largely resemble the general condensed state of matter. Indeed, if we can speak of the usual condensed matter as made of heavy positively charged ions and light electrons, then the situation remains similar if we substitute heavy and positively charged f-holes for the ions. Hence, in this sense we can speak of MV compounds and all phenomena in them, including EPT's, as modelling the general case of condensed matter. This analogy may help us understand and systematize the possible types of behavior of such compounds.

The initial phase with integer valence and $n_f \simeq 1$ resembles a gas or plasma (a low-density phase consisting of electrons and ions). This system is not bound and tends to expand ($n_e = n_{\text{ion}} \rightarrow 0$, or in our case $n_s = n_{f \text{ hole}} \rightarrow 0$ and $n_f \rightarrow 1$). When compressed, the gas condenses, i.e. there forms a condensed phase characterized by an equilibrium density n_0 . An EPT into a state with MV is an analogy of this phenomenon. In Sec. 2.5.4 we saw that the interaction of f-electrons via the lattice greatly resembles interatomic interaction (see Fig. 2.10). An electron system acts in a similar way if we include exchange and correlation effects (see [55]). Here the equilibrium concentration of f-electrons may well correspond to an intermediate value $0 < n_f < 1$.

When the gas (or plasma) condenses, the substance that forms may, depending on the conditions, be either a liquid or a solid

This is similar to the structure of the Wigner-crystal type discussed in Sec. 2.6.5 or the valence density waves. Theoretically, if we use this analogy, in MV systems both "liquid" and "crystalline" phases are possible (including, perhaps, transitions between these phases within the substance). At the same time, judging by the estimates of the previous section, it is more probable that, just as in He, MV systems remain "liquid" under all conditions. In this case, according to the Nernst heat theorem, additional ordering must appear in the system as the temperature drops. In liquid He this is the Bose-Einstein condensation, while in a MV system its place is taken either by a Fermi liquid at low temperatures (apparently, a single Fermi liquid consisting of f- and s-electrons) or by a gap in the spectrum.

In turn, these two last situations also have analogies in usual condensed matter: when the condensed phase is formed of ions and electrons, it is either a metal or an insulator. Apparently, the division of substances with MV into two classes, which we have mentioned before, is similar to the same division for common substances.

We note that apart from similarity between MV systems and condensed matter, there is an important difference between the two. In contrast to ions, the f- and s-electrons are identical particles. This means that transitions are possible between them. In view of this, in compounds with MV there may appear a state resembling a single Fermi liquid. We must bear this in mind when comparing the properties of the two types of systems. Nevertheless, however, the analogy is justified and may be fruitful. For instance, it enables us to study in general form some of the features of EPT's and parameters of systems with MV.

Without restricting ourselves to a definite type of interaction, we can write the energy of a system in terms of the number of f- or s-electrons for the general case (see [15, 55]) in the form (cf. (2.4.2))

$$\mathcal{E} = E_g n_s - E_{\text{ex}} n_s^{4/3} + E_{\text{kin}} n_s^{5/3} - E_{\text{int}} n_s^2. \quad (2.6.12)$$

Here the second term on the right-hand side constitutes the exchange energy, the third term the kinetic energy of the electrons in the conduction band with a density of states $\rho(\epsilon) \sim \epsilon^{1/2}$, and the last term the interaction or correlation energy. The signs in (2.6.12) are chosen so that all constants E_i are positive. It is important that (2.6.12) is valid in the excitonic (i.e. dielectric) phase as well. Here the last term in (2.6.12) represents the exciton-exciton interaction; because of excitonic correlations it is numerically much smaller than the corresponding term in (2.4.2).

Even without a detailed calculation of the E_i 's we can conclude from (2.6.12) that

- (1) At low temperatures the EPT from state $n_s = 0$, $n_f = 1$, a transition that occurs as E_f grows, must be a first-order transi-

tion [the function $\mathcal{E}(n_s)$ given by (2.6.12) has a negative curvature as $n_s \rightarrow 0$].

(2) Depending on the interplay between the E_i 's in (2.6.12), there are three possibilities: (a) a direct transition from the phase with $n_f = 1$ to that with $n_f = 0$; (b) a first-order transition from $n_f = 1$ to the phase with MV, $0 < n_f < 1$, after which there is one more jumplike transition to the phase with $n_f = 0$; or (c) a first-order transition from $n_f = 1$ to an MV state followed by a smooth transition with n_f diminishing. It is rather difficult to find the value of the various factors in (2.6.12) especially in the low-concentration limit. It is especially difficult to obtain the contribution provided by the "heavy" f component and the f-s hybridization (i.e. f-s exchange and correlation effects, together with contributions provided by f-f and f-s interactions). But this approach seems to be very promising both for the study of EPT's and for investigating the nature of the ground state and properties of MV phases.

2.7 CONCLUSION

In summarizing the results of our investigation, let us try to sum up the situation that has emerged at present in the theory of electronic phase transitions and mixed-valence states. The problem itself is quite clear. We know fairly well what factors must be taken into account and what consequences, qualitatively, they may lead to. In the EPT problem the research has moved quite far ahead. We know the mechanisms that accelerate a transition and make it jumplike and other mechanisms that hinder and blur it. The tendency toward a first-order transition is caused by the Coulomb f-s interaction and the interaction with a homogeneous strain of the lattice. The local effects (excitonic and polaron) act contrary to the jump and weaken the effective attraction of the f-electrons at different centers, and so does the interaction with short-wavelength phonons, for one.

An important question, in addition to the character of an EPT, is the reasons for the stabilization of an MV phase. Here are some factors that facilitate stabilization:

(1) The f level is pinned at ε_F if the kinetic energy needed for arranging the electrons in the conduction band is greater than the gain in energy. In other words, the large additional density of states introduced by the f levels and concentrated at E_f pins the Fermi level (a similar situation is encountered in a number of other systems, say, compounds with the A15 structure, such as Nb_3Sn and V_3Si).

(2) A phase with MV may be stabilized due to the increase in the width of the f level, $\Gamma = \pi\rho V^2$, in the course of a transition (see Sec. 2.5.2); this leads to an asymmetry in the EPT, with the valency after transition differing greatly from an integer.

(3) Similarly, an MV phase and an f level pinned at ϵ_F is stabilized by local (excitonic and polaron) correlations.

(4) A certain role is played by the direct interaction of the f -electrons at different centers and the interaction via short-wavelength phonons. The result is repulsion between the f -electrons that opposes a complete valence transition and prohibits two f -holes to be close; the resulting energy may have a minimum at an intermediate value of the valence, $0 < n_f < 1$. Simultaneously, spatial correlations may appear in the system, preferably of the liquid type.

(5) Among the factors that stabilize MV phases and that we have not discussed we note the possible important role of nonlinear effects. For instance, the growth of the compression bulk modulus B with pressure may check the transition half-way, so to say, in a phase with MV [57, 58]. As a whole we may say that a certain clarity has been achieved in the question of the causes and nature of EPT's. The situation is much worse when it comes to understanding the properties of MV phases.

In the first stage the properties of MV states were studied primarily using the model of an isolated impurity. This approach was often used in our review, and at present the situation is sufficiently clear on this level. At least qualitatively we can say that even a single impurity can have properties typical of compounds with MV: when the f level E_f is close to the Fermi level, the occupation of the f level is nonintegral, there arises a high density of states at the Fermi surface, at low temperatures the system goes over to a nonmagnetic state, a narrow resonance at the Fermi surface may give rise to a strong scattering mechanism, etc. This situation is described by the asymmetric Anderson model (where, possibly, other interactions may have to be included) and possesses many properties typical of the Kondo effect (slow spin fluctuations and strong coupling). In addition to spin fluctuation, slow charge fluctuations occur in this case, too, with respect to which the system also behaves as a Kondo system.

Thus, the fundamental properties of a single impurity are now known. The center of the stage in the MV problem has now been occupied by studies of the interaction of sites in MV system. All of the collective effects, the properties of the ground state and the conditions for a phase with MV to emerge rest on this problem. The main problem here is the type of ground state realized in MV system, the uniqueness of this state, the possibility of describing it by a Fermi liquid, and the possibility of a gap in the spectrum and the origin of this gap. There is no theory answering all these questions, and the discussion in Chap. 2.6 necessarily had a qualitative nature. Nevertheless, general considerations and the existing results in this field enable us to arrive at certain conclusions. For one, we can say that MV substances are divided by the type of ground state into two

categories. To one belong compounds that are metals in both phases, with integral and mixed valencies; the Fermi-liquid picture can be used here with success. The other category includes compounds that are semiconductors in the initial phase with integral valence. Apparently, the gap in the spectrum of these substances is preserved in a significant part of the range where an MV phase exists, if not in the entire range. The gap here has most likely a collective nature and is caused by effects of the excitonic type and, to some extent, by spatial ordering. These conclusions, however, require both theoretical and experimental verification.

In this review we have concentrated on description of the transition in the course of which valence changes and on the major questions concerning the nature of a MV state. We did not touch upon many interesting aspects, important from the standpoint of practice and widely discussed in the literature, such as the magnetic properties of MV substances, their response to various external probes, and a detailed analysis of the anomalies in phonon spectra. The discussion of these and other related aspects can be found in the above-cited reviews [4-8].

Two more remarks are in order. First, we note the analogy of the properties of MV states and the states "inside" a phase transition [7]; namely, MV states can be considered a result of an electronic phase transition that has not finished and is spread over a finite range of pressures, temperatures, etc. Many peculiar features of MV states (anomalously high compressibility and specific heat, the important role of slow valence fluctuations, and strong scattering on these fluctuations) can be interpreted in this manner. It is not clear how far this analogy can be extended nor whether it can be realized in a more specific way.

Second, it is interesting that in rare-earth compounds with MV the characteristic times τ of valence fluctuations are usually $\hbar/\Gamma \simeq \simeq 10^{-12}$ - 10^{-13} sec, which is of the order of characteristic phonon times. Apparently there is a reason for this [7]. If the τ 's were much longer than the phonon times, $\tau \gg \tau_{ph} \simeq 10^{-12}$ - 10^{-13} sec, the lattice would be able to relax differently at centers with different valencies. This, in turn, would still further suppress transition between the configurations. As a result a static distribution of ions of different valencies is more likely to be realized, i.e. the case of inhomogeneous MV will occur. On the other hand, the case $\tau \ll 10^{-13}$ - 10^{-14} sec would correspond to an ordinary metal with a broad band and rapid charge fluctuations. It is when the fluctuation times are of the order of the phonon times that all the features of MV states we have mentioned above manifest themselves.

Usually in treating the MV problem it is stressed that mixed-valence states are observed when $|E_f - \epsilon_F| \lesssim \Gamma$, i.e. in the intermediate case between the situation with a deep-lying level, $E_f \ll \epsilon_F$,

and that with an empty level, $E_f \gg \epsilon_F$. It appears, however, that as regards the electron-phonon interaction MV compounds also lie at the boundary between phases with averaged and with local deformations, and that the very existence of MV states is closely related to this circumstance.

In conclusion we can say that as yet it is not always clear in what cases in the transition to a concentrated system the properties of an isolated impurity "survive" or how they change; what type of a coherent ground state is realized and whether it is the same for different compounds; whether the ground state will be spatially homogeneous or whether a periodic structure will arise in it of the Wigner-crystal type or a valency density wave; whether the energy spectrum will contain a gap (or pseudogap); when the magnetic behavior will be similar to the Kondo behavior and when magnetic ordering will arise; and, finally, what role excitonic and lattice effects will play in MV states. Theoretically, the problems that emerge in this respect are extremely complicated (Anderson [76] even compares them to the confinement problem); here we are confronted by the case of strong coupling, where even for a single center the problem is quite nontrivial. But it is this difficulty together with the richness of physical effects and phenomena and the relationship of the MV problem to other important questions in solid state physics that make this problem extremely attractive for further studies.

References

1. L.D. Landau and Ya.B. Zel'dovich, *Zh. Eksp. Teor. Fiz.* **14**, 32 (1944); *Acta Phys.-Chem. USSR* **18**, 194 (1943); L.D. Landau, *Sobranie trudov*, Vol. 1, Nauka, Moscow (1969), p. 439 [English transl.: *Collected Papers*, Vol. 1, Pergamon Press, Oxford (1965)].
2. N.F. Mott, *Metal-Insulator Transitions*, Taylor and Francis, London (1974).
3. D.I. Khomskii, *Fiz. Metallov i Metalloved.* **29**, 31 (1970).
4. *Valence Instabilities and Related Narrow Band Phenomena* [ed. R.D. Parks], Plenum Press, New York (1977).
5. C.M. Varma, *Rev. Mod. Phys.* **48**, 219 (1976).
6. J.M. Robinson, *Phys. Reports* **51**, 1 (1979).
7. D.I. Khomskii, *Usp. Fiz. Nauk* **129**, 443 (1979) [English transl.: *Sov. Phys.-Uspekhi* **22**, 879 (1979)].
8. J.M. Lawrence, P.S. Riseborough, and R.D. Parks, *Rep. Progr. Phys.* **44**, 1 (1981).
9. M.V. Sadovskii, *Usp. Fiz. Nauk* **133**, 223 (1981).
10. B.L. Al'tshuler, A.G. Aronov, A.I. Larkin, and D.I. Khmel'nitskii, this issue, p. 130.
11. V.G. Vaks, *Introduction to the Microscopic Theory of Ferroelectrics* [in Russian], Nauka, Moscow (1973).
12. K.A. Gschneidner, Jr. and R. Smoluchowski, *J. Less-Common Metals*, **374** (1963).

13. E.E. Vainstein, S.M. Blokhin, and Yu.B. Paderno, *Sov. Phys.-Solid State* **6**, 2318 (1965).
14. E. Wigner, *Trans. Farad. Soc.* **34**, 678 (1938).
15. P.W. Anderson and S.T. Chui, *Phys. Rev.* **B9**, 3229 (1974).
16. N.F. Mott, *Proc. Phys. Soc. (London)* **A62**, 416 (1949); *Can. J. Phys.* **34**, 1356 (1956).
17. J. Hubbard, *Proc. Roy. Soc. (London)* **A276**, 238 (1963); *ibid.* **A277**, 237 (1964); *ibid.* **A281**, 401 (1968).
18. P.O. Zaitsev, *Zh. Éksp. Teor. Fiz.* **75**, 2632 (1978).
19. W.F. Brinkman and T.M. Rice, *Phys. Rev.* **B2**, 1324 (1970).
20. V.M. Filyov and P.B. Wiegmann, *Phys. Lett.* **A76**, 283 (1980).
21. P.B. Wiegmann, V.M. Filyov, and A.M. Tsvelik, *Pis'ma Zh. Éksp. Teor. Fiz.* **35**, 77 (1982); P.B. Wiegmann and A.M. Tsvelik, *ibid.* **35**, 100 (1982).
22. C. Herring, *Exchange Interaction Among Itinerant Electrons* (Volume 4 of *Magnetism: A Treatise on Modern Theory and Materials* [eds. G.T. Rado and H. Suhl]), Academic Press, New York (1966).
23. S.V. Vonsovskii, *Magnetism*, 2 Vols., Wiley, New York (1974).
24. A.A. Bugaev, B.P. Zakharchenya, and F.A. Chudnovskii, *The Metal-Semiconductor Phase Transition and Its Application* [in Russian], Nauka, Leningrad (1979).
25. T.A. Kaplan and S.D. Mahanti, *Phys. Lett.* **A51**, 265 (1975); *J. Phys.* **C12**, L23 (1979).
26. A.A. Druzhinin, *Pis'ma Zh. Éksp. Teor. Fiz.* **32**, 596 (1980).
27. O.B. Farberovich, *Fiz. Tverdogo Tela* **21**, 3434 (1979); *ibid.* **22**, 669 (1980).
28. W.E. Pickett, A.J. Freeman, and D.D. Koelling, *Phys. Rev.* **B23**, 1266 (1981).
29. P.B. Wiegmann, this issue, p. 238.
30. L.M. Falicov and J.C. Kimball, *Phys. Rev. Lett.* **22**, 997 (1969).
31. P.W. Anderson, *Phys. Rev.* **124**, 41 (1961).
32. J.R. Schrieffer and P.A. Wolff, *Phys. Rev.* **149**, 491 (1966).
33. H.J. Leder and B. Mühlischlegel, *Z. Physik* **B29**, 241 (1978).
34. A. Sakurai and P. Schlottmann, *Solid State Commun.* **27**, 991 (1978).
35. D.I. Khomskii, A.N. Kocharyan, and P.S. Ovnanyan, *Preprint FIAN*, No. 190 (1980).
36. D.M. Newns and A.C. Hewson, *J. Phys.* **F10**, 2429 (1980).
37. A.F. Barabanov, K.A. Kikoin, and L.A. Maksimov, *Teor. Mat. Fiz.* **25**, 87 (1975).
38. A.I. Kocharyan, dissertation, P.N. Lebedev Institute of Physics, Academy of Sciences of the USSR (1976).
39. P. Schlottmann, *Phys. Rev.* **B22**, 613, 622 (1980).
40. R. Ramirez and L.M. Falicov, *Phys. Rev.* **B3**, 2425 (1971).
41. B. Alascio, A. Lopez, and C.F.E. Olmedo, *J. Phys.* **F3**, 1324 (1973).
42. A.I. Kocharyan and D.I. Khomskii, *Kr. Soobshch. Fiz. (Sbornik FIAN)*, No. 8, 3 (1974) [English transl.: *Sov. Phys.-Lebedev Inst. Reports* No. 8, 1 (1974)].
43. M. Avignone and S.K. Ghatak, *Solid. State Commun.* **16**, 1243 (1975).
44. C.E.T. Gonsalves Da Silva and L.M. Falicov, *Solid State Commun.* **16**, 1521 (1975).
45. F.D.M. Haldane, *Phys. Rev.* **B15**, 281, 2477 (1976).
46. D.I. Khomskii and A.N. Kocharyan, *Solid State Commun.* **18**, 985 (1976); *Zh. Éxp. Teor. Fiz.* **71**, 767 (1976) [English transl.: *Sov. Phys. JETP* **44**, 404 (1976)].
47. L.V. Keldysh and Yu.V. Kopaev, *Fiz. Tverdogo Tela* **18**, 1686 (1964).
48. H.J. Leder, *Solid State Commun.* **27**, 579 (1978).
49. N.Sh. Izmailyan, A.N. Kocharyan, P.S. Ovnanyan, and D.I. Khomskii, *Fiz. Tverdogo Tela* **23**, 2977 (1981).

50. G.D. Mahan, *Phys. Rev.* **163**, 612 (1967).
51. P. Nozieres and C.T. de Dominicis, *Phys. Rev.* **178**, 1097 (1969).
52. P.B. Wiegmann and A.M. Finkel'shtein, *Zh. Éksp. Teor. Fiz.* **75**, 204 (1978).
53. P. Schlottmann, *J. de Phys. Colloq.* **39**, C6-1486 (1978).
54. B.R. Alascio, R. Allub, and A. Aligia, *J. Phys.* **C13**, 2869 (1980).
55. A.A. Druzhinin, thesis, Moscow State Univ. (1974).
56. A.A. Druzhinin, *Solid State Commun.* **42**, 313 (1982).
57. L.L. Hirst, *J. Phys. Chem. Solids* **35**, 1285 (1974).
58. C.M. Varma and V. Heine, *Phys. Rev.* **B11**, 4763 (1975).
59. A.C. Hewson and P.S. Riseborough, *Solid State Commun.* **22**, 379 (1977).
60. S.M. Shapiro, J.D. Axe, R.J. Birgenau, J.M. Lawrence, and R.D. Parks, *Phys. Rev.* **B16**, 2225 (1977).
61. J.W. Allen S.-J. Oh, J. Landau, J.M. Lawrence, L.I. Johansson, and S.B. Hagström, *Phys. Rev. Lett.* **46**, 1100 (1981).
62. M. Croft, J.H. Weaver, D.J. Peterman, and A. Franciosi, *Phys. Rev. Lett.* **46**, 1104 (1981).
63. G. Güntherodt, R. Merlin, A. Frey, and M. Cardona, *Solid State Commun.* **27**, 551 (1978).
64. A.N. Kocharyan, P.S. Ovnanyan, and D.I. Khomskii, *Pis'ma Zh. Éksp. Teor. Fiz.* **34**, 25 (1981). English transl. *Sov. Phys.-JETP Lett.*, **34**, 23 (1981).
65. P. Entel, H.J. Leder, and N. Grewe, *Z. Physik* **B30**, 277 (1978).
66. D. Sherrington and S. von Molnar, *Solid State Commun.* **16**, 1347 (1975).
67. D.I. Khomskii, *Solid State Commun.* **27**, 775 (1978).
68. J.M. Lawrence and R.D. Parks, *Phys. Rev.* **B16**, 2225 (1977).
69. J.M.D. Coey, S. Ghatak, A. Avignone, and F. Holtzberg, *Phys. Rev.* **14**, 3744 (1977).
70. D. Sherrington and P. Riseborough, *J. de Phys. Colloq.* **37**, C4-225 (1976).
71. A.C. Newson and D.M. Newns, *J. Phys.* **C13**, 4477 (1980).
72. V.A. Somenkov and A.A. Shil'shtein, "Phase transitions of hydrogen in metals", *Preprint IAE* (1978).
73. K. Motizuki, *J. Phys. Soc. Japan* **14**, 759 (1959).
74. S. Doniach, *Physica* **B91**, 231 (1977); R. Jullien, J.N. Fields, and S. Doniach, *Phys. Rev.* **B16**, 4889 (1977).
75. H.A. Mook, R.M. Nicklow, T. Penney, F. Holtzberg, and M.W. Shafer, *Phys. Rev.* **B18**, 2925 (1978).
76. P.W. Anderson, in: *Valence Instabilities and Related Narrow Band Phenomena* [ed. R.D. Parks], Plenum Press, New York (1977), p. 389.
77. J.W. Allen and R.M. Martin, *J. de Phys. Colloq.* **41**, C5-171 (1979).
78. E. King, J.A. Lee, I.R. Harris, and T.F. Smith, *Phys. Rev.* **B1**, 1380 (1970).
79. K.W.H. Buschow and H.J. van Daal, *Solid State Commun.* **8**, 363 (1970).
80. T. Kasuya, K. Takegahara, T. Fujita, T. Tanaka, and E. Bannai, *J. de Phys. Colloq.* **40**, C5-308 (1979).
81. G. Grüner and A. Zawadowski, *Rep. Progr. Phys.* **37**, 1497 (1974); *Progress in Low Temperature Physics* [ed. D.F. Brewer], Vol. 7B, North-Holland, Amsterdam (1978).
82. F.D.M. Haldane, *Phys. Rev. Lett.* **40**, 416 (1978).
83. H.R. Krishna-Murthi, J.W. Wilkins, and K.G. Wilson, *Phys. Rev.* **B21**, 1003, 1044 (1980).
84. R. Jullien and P. Pfeuty, *J. Phys.* **F11**, 353 (1981).
85. C. Lacroix and M. Cyrot, *Phys. Rev.* **B20**, 1969 (1979).
86. E. Lieb and F.Y. Wu, *Phys. Rev. Lett.* **20**, 1445 (1968).
87. P. Nozieres, *J. Low Temp. Phys.* **17**, 31 (1974).
88. R. Jullien and R.M. Martin, *Preprint*, Orsay (1981).
89. K.A. Kikoin and V.N. Flerov, *Zh. Éksp. Teor. Fiz.* **77**, 1032 (1979).
90. K.A. Kikoin, *Solid State Commun.* **33**, 323 (1980).
91. A.F. Barabanov and A.M. Tsvelik, *Zh. Éksp. Teor. Fiz.* **76**, 558 (1979).

- 92. B.H. Brandow, *Int. J. Quantum Chem.: Quantum Chem. Symposium B*, p. 423 (1979).
- 93. M. Roberts and K.W.H. Stewens, *J. Phys.* **C13**, 5941 (1980).
- 94. Yu.V. Kopaev, *Trudy FIAN* **86**, 3 (1975).
- 95. F. Steglich, J. Aarts, C.D. Bredl, W. Lieke, W. Franz, H. Schafer, and D. Meschede, *Phys. Rev. Lett.* **43**, 1892 (1979).
- 96. D.A. Kirzhnits, *Usp. Fiz. Nauk* **104**, 489 (1971).

Coherent Effects in Disordered Conductors

B. L. Altshuler, A. G. Aronov,

Leningrad Nuclear Physics Institute,
Academy of Sciences of the USSR

D. E. Khmel'nitskii, A. I. Larkin

L. D. Landau Institute for Theoretical Physics,
Academy of Sciences of the USSR

3.1 INTRODUCTION

The usual theory of transport phenomena in conductors is based upon the classical kinetic equation for conduction electrons. It is assumed that in the time interval between two collisions an electron moves along classical trajectories. This approach is valid, when the interference of two waves scattered by different centres is negligible, i.e. when the electron wavelength $\lambda = \frac{h}{p_F}$ is much smaller than the mean free path l (the Yoffe-Regel-Mott principle [1, 2]). If this condition is not satisfied, then, as has been shown by Anderson [3], electron states become localized and conductivity vanishes at zero temperatures.

In conductors with strong disorder electron momentum relaxation is determined by elastic collisions. In this case, even if $\lambda/l \ll 1$, quantum corrections to conductivity σ are of great interest, since they lead to nontrivial dependence of σ on temperature, sample dimensions and external fields. This is true even for free electrons interacting only with impurities. Electron-electron interaction also involves quantum corrections of order λ/l , these corrections appearing not only in kinetic, but also in thermodynamic quantities. The situation is quite different for ordered systems, where electron-electron interaction at low temperature manifests itself only in the Fermi-liquid renormalization of electron spectrum parameters.

We shall consider the properties of conductors with a small mean free path l , i.e. impure metals and semiconductors. Quantum effects are the strongest in one- and two-dimensional systems, e.g. MOS-structures and relatively thick films and wires. We shall dwell upon effects leading to anomalous temperature and frequency dependence of conductivity and Hall effect, to anomalous magnetoresistance and to energy dependence of the density of states, showing itself in zero-bias anomalies of tunnelling junctions.

3.2 QUANTUM CORRECTIONS TO CONDUCTIVITY OF NONINTERACTING ELECTRONS

3.2.1 Conductivity and Impurity Diagrammatic Technique

Residual resistance in conductors is determined by the electron-impurity interaction. In good conductors the mean free path is much greater than the electron wavelength, $l \gg \lambda = \hbar/p$, where p is the electron momentum. Between two collisions an electron may be described quasi-classically to yield the well-known Drude formula

$$\sigma = \frac{ne^2\tau}{m}, \quad (3.2.1)$$

where n is the carrier concentration, m is the carrier mass, and τ the time between collisions. In this section we shall find quantum corrections to σ , given by (3.2.1).

A general expression for conductivity at frequency ω is obtained by calculating the energy absorption of an AC electric field \mathcal{E}_ω :

$$\mathcal{E}_\omega \mathcal{E}_{-\omega} \operatorname{Re} \sigma_{ij}(\omega) = 2\pi\omega \sum_{\mathbf{k}, l} \frac{e^2}{c^2} |\langle \mathbf{k} | \mathbf{A}_\omega \cdot \hat{\mathbf{v}} | l \rangle|^2 \times \delta(\varepsilon_l - \varepsilon_{\mathbf{k}} - \omega) \{n(\varepsilon_{\mathbf{k}}) [1 - n(\varepsilon_l)] - n(\varepsilon_l) [1 - n(\varepsilon_{\mathbf{k}})]\}, \quad (3.2.2)$$

where $n(\varepsilon_{\mathbf{k}})$ are the occupation numbers of exact electron states with energy $\varepsilon_{\mathbf{k}}$ and the matrix element of the velocity operator $\hat{\mathbf{v}}$ is taken between such states. Substituting $\mathbf{A} = i \frac{c}{\omega} \mathcal{E}_\omega$ in (3.2.2) and using analytical properties of $\sigma(\omega)$, we obtain*

$$\sigma_{ij}(\omega) = \frac{1}{\omega} (K_{ij}(\omega) - K_{ij}(0)), \quad (3.2.3)$$

$$K_{ij}(\omega) = +2ie^2 \sum_{\mathbf{k}, l} \frac{[n(\varepsilon_{\mathbf{k}}) - n(\varepsilon_l)] \langle \mathbf{k} | \hat{v}_i | l \rangle \langle l | \hat{v}_j | \mathbf{k} \rangle}{\varepsilon_l - \varepsilon_{\mathbf{k}} - \omega + i\delta}. \quad (3.2.3a)$$

It is convenient to express matrix elements in (3.2.3a) in terms of the one-particle Green functions

$$G_{\varepsilon}^{R(A)}(\mathbf{r}, \mathbf{r}') = \sum_i \frac{\psi_i^*(\mathbf{r}) \psi_i(\mathbf{r}')}{\varepsilon - \varepsilon_i \pm i\delta}. \quad (3.2.4)$$

Then

$$K_{ij}(\omega) = \frac{e^2}{m^2} \int d\mathbf{r} \int \frac{d\varepsilon d\varepsilon'}{(2\pi)^2} [n(\varepsilon') - n(\varepsilon)] \hat{p}_i [G_{\varepsilon}^R(0, \mathbf{r}) - G_{\varepsilon}^A(0, \mathbf{r})] \times \hat{p}_j [G_{\varepsilon'}^R(\mathbf{r}, 0) - G_{\varepsilon'}^A(\mathbf{r}, 0)] \frac{1}{\varepsilon - \varepsilon' - \omega + i\delta}, \quad (3.2.5)$$

where $\hat{\mathbf{p}} = m\hat{\mathbf{v}} = -i\nabla$ is the electron momentum operator. Since $G^R(\varepsilon)$ and $G^A(\varepsilon)$ are analytical in the upper and lower half-planes of the complex variable ε respectively, we can integrate over ε or ε' and reduce (3.2.5) to

$$K_{ij}(\omega) = \frac{e^2}{m^2} \int d\mathbf{r} \int \frac{d\varepsilon}{2\pi} \{ [n(\varepsilon + \omega) - n(\varepsilon)] \hat{p}_i G_{\varepsilon+\omega}^R(0, \mathbf{r}) \hat{p}_j G_{\varepsilon}^A(\mathbf{r}, 0) + n(\varepsilon) [\hat{p}_i G_{\varepsilon}^A(0, \mathbf{r}) \hat{p}_j G_{\varepsilon-\omega}^A(\mathbf{r}, 0) - \hat{p}_i G_{\varepsilon+\omega}^R(0, \mathbf{r}) \hat{p}_j G_{\varepsilon}^R(\mathbf{r}, 0)] \}. \quad (3.2.6)$$

Equations (3.2.3) through (3.2.6) are exact relations defining conductivity at arbitrary $p_F l$. As shown below, at $p_F l \gg 1$ they reduce to the Drude formula with small corrections of order $(p_F l)^{-1}$. We are specially interested in those corrections, which have non-analytical dependence on ω . Omitting regular corrections, we may rewrite (3.2.6) as

$$K_{ij}(\omega) = \int d\varepsilon [n(\varepsilon + \omega) - n(\varepsilon)] \mathcal{K}_{ij}(\varepsilon, \omega), \quad (3.2.7)$$

where

$$\mathcal{K}_{ij}(\varepsilon, \omega) = \frac{e^2}{2\pi m^2} \int d\mathbf{r} \hat{p}_i G_{\varepsilon+\omega}^R(0, \mathbf{r}) \hat{p}_j G_{\varepsilon}^A(\mathbf{r}, 0).$$

Equations (3.2.3) and (3.2.6) show that in the absence of inelastic scattering the total conductivity σ is the sum of contributions from different energy levels taken with the weight depending on the distribution function. In the case of a degenerate gas σ is defined by the conductivity of the electrons on the Fermi surface. In what follows we shall consider only this case.

For samples with a sufficient amount of impurities, σ_{ij} and \mathcal{K}_{ij} coincide with their averages over impurity configurations. The equation for $G_{\varepsilon}(\mathbf{r}, \mathbf{r}')$ may be written as

$$(\varepsilon - U(\mathbf{r}) - \hat{H}) G_{\varepsilon}(\mathbf{r}, \mathbf{r}') = \delta(\mathbf{r} - \mathbf{r}'). \quad (3.2.8)$$

If we solve this equation using the perturbation theory for the impurity potential $U(\mathbf{r})$ and average the solution, then the average product of two Green functions can be represented as a series, each term of which is associated with a graph drawn according to the rules of the impurity diagrammatic technique [4] (see Fig. 3.1). In this technique solid lines correspond to bare Green functions and dashed lines, to random potential correlators. We assume that the random potential is distributed according to the Gauss δ -correlated law. Then all the correlators can be represented as the products of pair correlators

$$\langle U(\mathbf{r}) \rangle = 0, \quad \langle U(\mathbf{r}) U(\mathbf{r}') \rangle = \langle U^2 \rangle \delta(\mathbf{r} - \mathbf{r}'), \quad (3.2.9)$$

where the angle brackets denote averaging over the impurity configuration. Equation (3.2.9) corresponds to the Born approxima-

tion for the interaction with short range impurities, and $\langle U^2 \rangle = c_{\text{im}} \left(\int V(\mathbf{r}) d\mathbf{r} \right)^2$, where c_{im} is the impurity concentration and $V(\mathbf{r})$ is the potential of a single impurity. The sum of diagrams with non-intersecting dashed lines defines the Green function and

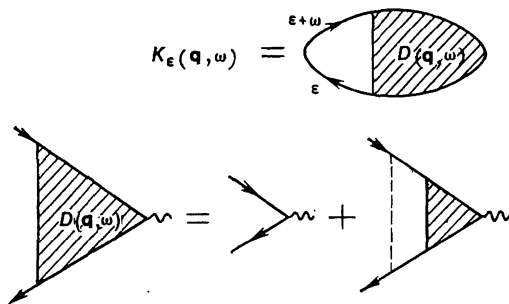


Fig. 3.1.

conductivity to the leading approximation in $(p_F l)^{-1}$. In this approximation the averaged Green function is given by the formula [4]

$$\langle G_{\varepsilon}(\mathbf{r}, \mathbf{r}') \rangle = \int (dp) \exp\{i\mathbf{p} \cdot (\mathbf{r} - \mathbf{r}')\} G_{\varepsilon}(\mathbf{p}),$$

where $(dp) = dp/(2\pi)^d$, d is the space dimensionality and

$$G_{\varepsilon}^{\text{R(A)}}(\mathbf{p}) = \left(\varepsilon - \frac{\mathbf{p}^2}{2m} + \mu \pm \frac{i}{2\tau} \right)^{-1}. \quad (3.2.10)$$

Here energy ε is counted from the chemical potential μ , $1/\tau = \pi v \langle U^2 \rangle$ is the frequency of elastic collisions and v is the electronic density of states. If scattering is isotropic, then in calculating the conductivity to the leading approximation in $1/\mu\tau$ we can ignore the graphs with vertical dashed lines. These graphs give zero contribution after integration over angles of p due to the vectorial character of the current vertex. The first term in (3.2.6) gives

$$\begin{aligned} K_{ij}(\varepsilon, \omega) &= \frac{e^2 v_F^2 \delta_{ij}}{2\pi d} \int_{-\infty}^{+\infty} \frac{d\xi}{\left(-\xi + \frac{i}{2\tau} + \varepsilon\right) \left(-\xi + \omega + \varepsilon - \frac{i}{2\tau}\right)} \\ &= \frac{v_F^2 v e^2 \tau}{d} \frac{1}{1 + i\omega\tau}, \end{aligned} \quad (3.2.11)$$

where an energy variable $\xi = \frac{p^2}{2m} - \mu$ is introduced. It is seen from (3.2.11) that $K(\varepsilon, \omega)$ does not depend on ε , so we can set ε to zero. In the integral over ξ the main contribution comes from

a narrow range $\xi \lesssim 1/\tau$. Therefore we can integrate between infinite limits.

In each of the last two terms in Eq. (3.2.6) the poles of the Green functions lie in the same half-plane of the complex variable ξ , hence the integrals over ξ between infinite limits are equal to zero, and the contribution of these terms is small in the parameter $(\mu\tau)^{-1}$ and independent of ω . Neglecting this contribution, we obtain Eq. (3.2.7). Substituting (3.2.11) into (3.2.7) and (3.2.4), we obtain the Drude formula (3.2.1).

The density correlator

$$\mathcal{K}(\omega, \mathbf{q}) = \int d\varepsilon [n(\varepsilon + \omega) - n(\varepsilon)] \mathcal{K}_\varepsilon(\omega, \mathbf{q})$$

can also be calculated by means of the impurity technique:

$$\mathcal{K}_\varepsilon(\omega, \mathbf{q}) = \left\langle \int G_{\varepsilon+\omega}^R(\mathbf{p} + \mathbf{q}) G_\varepsilon^A(\mathbf{p}) (d\mathbf{p}) \right\rangle. \quad (3.2.12)$$

In the leading approximation \mathcal{K}_ε is given by the sum of ladder-type diagrams (Fig. 3.1):

$$\mathcal{K}_\varepsilon(\omega, \mathbf{q}) = \pi v \tau \zeta(\mathbf{q}, \omega) D(\mathbf{q}, \omega), \quad (3.2.13)$$

where

$$\zeta(\mathbf{q}, \omega) = \frac{1}{\pi v \tau} \int (d\mathbf{p}) G^R(\varepsilon + \omega, \mathbf{p} + \mathbf{q}) G^A(\varepsilon, \mathbf{p}). \quad (3.2.14)$$

In the limit $ql \ll 1$, $\omega\tau \ll 1$, we have

$$\zeta(\mathbf{q}, \omega) = 1 + i\omega\tau - D\mathbf{q}^2\tau. \quad (3.2.14a)$$

Here $D = v_F^2 \tau / d$ is the diffusion coefficient, related to σ by the Einstein relation

$$\sigma = e^2 v D.$$

Solving the equation for $D(\mathbf{q}, \omega)$ shown in Fig. 3.1, we find

$$D(\mathbf{q}, \omega) = \frac{1}{1 - \zeta(\mathbf{q}, \omega)} = \frac{1}{\tau(-i\omega + D\mathbf{q}^2)}. \quad (3.2.15)$$

Substituting (3.2.14a) and (3.2.15) into (3.2.13), we obtain

$$\mathcal{K}_\varepsilon(\mathbf{q}, \omega) = \frac{\pi v}{-i\omega + D\mathbf{q}^2}. \quad (3.2.16)$$

3.2.2 Cooperon and Quantum Correction to Conductivity

The Drude formula corresponds to the classical motion of an electron scattered by impurities. However, travelling along classical trajectories, an electron is, at the same time, a wave packet of dimensions of order $\lambda = h/mv$ and $v\tau_\varphi$ in transverse and longitu-

dinal directions, respectively. Here τ_ϕ is the electron phase breaking time. Different sequences of the scattering acts give different classical trajectories. Quantum corrections arise due to the interference of wave packets moving along different trajectories. However, phase difference for these trajectories is random and the interference of the wave packets moving along two arbitrary paths gives, on the average, zero contribution to the conductivity. The only exception is the case of a self-intersecting trajectory. A wave packet can traverse such loop in two opposite directions, the phase acquired in each direction being the same. Thus, the interference is strong for self-intersecting trajectories, i.e. the trajectories, the distance between which is of order λ . The density of probability that a trajectory, beginning at a point \mathbf{r} , t , passes through a point \mathbf{r}' , t' , is determined via the diffusion equation and equals

$$W(|\mathbf{r} - \mathbf{r}'|, t' - t) = \frac{1}{[2\pi D(t' - t)]^{d/2}} \exp\left\{-\frac{(\mathbf{r}' - \mathbf{r})^2}{2D(t' - t)}\right\}. \quad (3.2.17)$$

The magnitude of the expected effect, $\delta\sigma/\sigma$, is determined by the probability that the trajectory returns to the region of dimensions λ about r in a time which does not exceed the phase breaking time τ_ϕ :

$$\frac{\delta\sigma}{\sigma} = \int_{\tau}^{\tau_\phi} \frac{v dt}{(Dt)^{d/2}} \lambda^{d-1}. \quad (3.2.18)$$

The time τ_ϕ is temperature-dependent and can be very large. If $\omega\tau_\phi \gg 1$, where ω is the frequency of an external field, then in (3.2.18) we must replace τ_ϕ by $1/\omega$.

Separating the contribution of large t , we obtain

$$\frac{\delta\sigma}{\sigma} \sim \begin{cases} -\frac{\hbar}{mD} \sqrt{\frac{D}{\lambda^2\omega}} & \text{at } d=1, \\ -\frac{\hbar}{mD} \ln \frac{1}{\omega\tau} & \text{at } d=2, \\ \text{const} + \frac{\hbar}{mD} \sqrt{\frac{\lambda^2\omega}{D}} & \text{at } d=3. \end{cases} \quad (3.2.19)$$

In three dimensions the integral in (3.2.18) is determined by small time intervals $t \sim \tau$; the contribution of large t gives non-analytical dependence of the conductivity on frequency or temperature. In one and two dimensions quantum corrections can be large even if the quasi-classical parameter $\hbar/mD \sim \frac{\hbar}{\mu\tau}$ is small. This is due to the fact that in one and two dimensions a diffusing particle will, in a sufficiently large time interval, pass as near the initial point as desired.

For a trajectory beginning and ending at the same point the amplitudes of the probability of traversing it in opposite directions obey the relation $A_1 = A_2^*$. The interference term is proportional to $A_1 \cdot A_2^* = A_1^2$. Since \hat{A} is bilinear in the Heisenberg electronic operators $\hat{\psi}_e(\mathbf{r}, t)$, to describe the interference it is natural to examine the correlator

$$C_\omega(\mathbf{Q}) = \frac{1}{\pi\nu\tau} \langle \hat{\psi}_{e+\omega}(0, 0) \hat{\psi}_e(0, 0) \hat{\psi}_{e+\omega}^+(\mathbf{r}, t) \hat{\psi}_e^+(\mathbf{r}, t) \rangle_Q \quad (3.2.20)$$

Diagrams for $C_\omega(\mathbf{Q})$ are shown in Fig. 3.2.

$$c_\omega(\mathbf{Q}) = \frac{1}{\pi\nu\tau} \left\{ \text{bubble}(p+Q, -p) + \text{bubble}(p+Q, -p, \text{dashed}) + \text{bubble}(p+Q, -p, \text{dashed}, \text{dashed}) + \dots \right\}$$

Fig. 3.2.

These diagrams are similar to diagrams for $\mathcal{K}_e(\omega, \mathbf{q})$; the factor $(\pi\nu\tau)^{-1}$ cancels the empty loop contribution. Therefore

$$C_\omega(\mathbf{Q}) = \frac{1}{\tau(-i\omega + DQ^2)}. \quad (3.2.21)$$

By contrast with the density correlator, $C_\omega(\mathbf{Q})$ is described by a two-particle Green function in the particle-particle channel (the Cooper channel) and has a singularity at a small total momentum \mathbf{Q} . In what follows we shall call $C_\omega(\mathbf{Q})$ the "cooperon".

Similarity between Eqs. (3.2.15) and (3.2.21) is not accidental. The fact is that we can obtain $C_\omega(\mathbf{Q})$ from $\mathcal{K}(\omega, \mathbf{q})$ by the substitution $\psi_p \rightarrow \psi_{-p}^*$, corresponding to the change in direction of one of the solid lines in the Feynman graphs.

Thus, to calculate quantum corrections having singularities at small ω 's, it is necessary to find the Feynman diagrams for the conductivity, containing as an internal block the graphs, the sum of which is equal to $\int C_\omega(\mathbf{Q}) (dQ)$. Such diagrams [5] are shown in Fig. 3.3.

To evaluate the total contribution of these diagrams, we should find the integrals

$$\int (dp) |G_e(\mathbf{p})|^2 |G_{e-\omega}(-\mathbf{p} + \mathbf{Q})|^2 \mathbf{p} \cdot (-\mathbf{p} + \mathbf{Q})$$

and

$$\int C_\omega(\mathbf{Q}) (dQ).$$

In the first integral we can set Q to zero, as characteristic $p \sim 1/L$ and characteristic $Q \sim (\omega/D)^{1/2} \sim (\omega\tau/l^2)^{1/2} \ll \frac{1}{L}$. As a result we obtain the following expression for the quantum correction to the conductivity:

$$\delta\sigma^{(d)} = -\frac{2De^2}{\pi} \int (dQ) \frac{1}{-i\omega + DQ^2}. \quad (3.2.22)$$

Here $\sigma^{(d)}$ is the conductivity at $d = 3$, conductance per unit area at $d = 2$, and conductance per unit wire length at $d = 1$. As has been noted above, the external frequency determines quantum

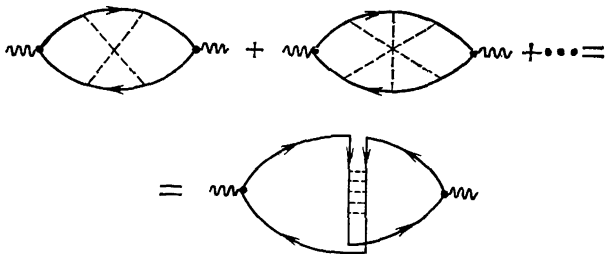


Fig. 3.3.

corrections, if $\omega\tau_\varphi \gg 1$. If $\omega\tau_\varphi \ll 1$, instead of ω in (3.2.22) we should write $1/\tau_\varphi$. Therefore quantum corrections to the DC conductivity have the form

$$\delta\sigma^{(d)} = \begin{cases} -\frac{e^2}{\pi\hbar} \sqrt{D\tau_\varphi} & \text{at } d=1 \\ -\frac{e^2}{2\pi^2\hbar} \ln \frac{\tau_\varphi}{\tau} & \text{at } d=2 \\ \text{const} + \frac{e^2}{2\pi^2\hbar} \frac{1}{\sqrt{D\tau_\varphi}} & \text{at } d=3. \end{cases} \quad (3.2.23)$$

In the absence of spin relaxation the electron phase breaking occurs as a result of inelastic processes. We shall consider this phenomenon in detail in Secs. 3.3 and 3.4. Now we only note that all characteristic times of inelastic processes increase with decreasing temperature, and we can adopt the following expression for τ_φ : $1/\tau_\varphi = AT^p$. Thus, (3.2.23) gives the temperature dependence of the anomalous negative correction to the conductivity [7].

3.2.3 Effects of Spin Scattering

Up to now we have not considered effects connected with electron spin-flop. Spin-flop occurs due to the exchange interaction with magnetic impurities or spin-orbit coupling. The electron-impu-

rity interaction can be written in the form

$$\int \psi_{\alpha}^*(\mathbf{p}) U_{\alpha\beta}(\mathbf{p}, \mathbf{p}') \psi_{\beta}(\mathbf{p}') (d\mathbf{p}) (d\mathbf{p}'),$$

where

$$U_{\alpha\beta}(\mathbf{p}, \mathbf{p}') = \delta_{\alpha\beta} U + U_s \mathbf{S} \cdot \boldsymbol{\sigma}_{\alpha\beta} + U_{so} [\mathbf{p} \times \mathbf{p}'] \boldsymbol{\sigma}_{\alpha\beta}. \quad (3.2.24)$$

The Green function has the form $G_{\alpha\beta} = G \delta_{\alpha\beta}$, where G is given by (3.2.10) and

$$1/\tau = 1/\tau_p + 1/\tau_s + 1/\tau_{so}, \quad (3.2.25a)$$

$$1/\tau_p = \pi v U^2,$$

$$\left. \begin{aligned} \frac{1}{\tau_s} &= \pi v S (S+1) U_s^2, \\ \frac{1}{\tau_{so}} &= \pi v \overline{U_{so}^2 [\mathbf{p} \times \mathbf{p}']^2}. \end{aligned} \right\} \quad (3.2.25b)$$

Here the bar means averaging over directions of \mathbf{p} and \mathbf{p}' . For the two-particle Green function in the particle-particle channel we

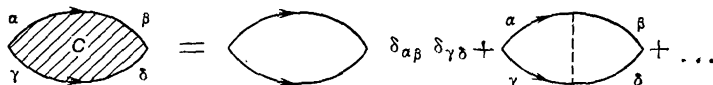


Fig. 3.4.

have in the ladder approximation the equation shown in Fig. 3.4. At an arbitrary relation between τ_p and τ_{so} this equation is a complicated integral equation with a kernel $U_{\alpha\mu}(\mathbf{p}, \mathbf{p}') \cdot U_{\delta\nu}(-\mathbf{p}, -\mathbf{p}')$. If $\tau_{so} \gg \tau_p \simeq \tau$, then the electron momentum changes many times during the time of spin-flop. Hence the solutions are determined by the kernel averaged over the directions of momenta. In this case the equation for the cooperon acquires the form

$$C_{\alpha\beta\gamma\delta} = \delta_{\alpha\beta} \delta_{\gamma\delta} \zeta + \overline{U_{\alpha\mu}(\mathbf{p}, \mathbf{p}') U_{\delta\nu}(-\mathbf{p}, -\mathbf{p}')} \zeta C_{\mu\beta\gamma\nu}, \quad (3.2.26)$$

where ζ is given by (3.2.14).

It is convenient to look for the solution of (3.2.26) in the form

$$C_{\alpha\beta\gamma\delta} = A \delta_{\alpha\beta} \delta_{\gamma\delta} + B \boldsymbol{\sigma}_{\alpha\beta} \cdot \boldsymbol{\sigma}_{\gamma\delta}. \quad (3.2.27)$$

Substituting (3.2.27) into (3.2.26), we obtain

$$A = \frac{1}{2\tau} \left\{ \frac{1}{2} \frac{1}{-i\omega + DQ^2 + 2/\tau_s} + \frac{3}{2} \frac{1}{-i\omega + DQ^2 + 2/3\tau_{so} + 1/\tau_s} \right\}, \quad (3.2.28)$$

$$B = \frac{1}{2/3\tau} \left\{ \frac{1}{-i\omega + DQ^2 + 2/3\tau_s + 4/3\tau_{so}} - \frac{1}{-i\omega + DQ^2 + 2/\tau_s} \right\}.$$

Equation (3.2.22) for the conductivity contains

$$C_{\alpha\beta\beta\alpha}(\omega, \mathbf{Q}) = 2(A + 3B) = \left\{ -\frac{1}{2} \frac{1}{-i\omega + DQ^2 + 2/\tau_s} + \frac{3}{2} \frac{1}{-i\omega + DQ^2 + 2/3\tau_s + 4/3\tau_{so}} \right\} \cdot \frac{2}{\tau}. \quad (3.2.29)$$

It is easily seen that the frequency enters (3.2.29) in the combination $\omega + i/\tau_s$. This means that at $\omega\tau_s \ll 1$ the quantum correction has a weak dependence on the frequency and is determined by the time τ_s of spin-flop due to the exchange scattering [8]. This is because in the time interval τ_s a random change of the spin state occurs and the wave function ceases to be coherent with the wave function of the initial state. If $1/\tau_s \neq 0$, the cooperon $C_\omega(\mathbf{Q})$ does not coincide with the density correlator, which has a pole according to the particle conservation law. We must account for the spin-flop scattering, calculating the phase breaking time

$$\frac{1}{\tau_\varphi} = AT^p + \frac{2}{\tau_s}, \quad (3.2.30)$$

where the first term on the right-hand side corresponds to various inelastic processes and vanishes at $T \rightarrow 0$, and the second term is connected with the spin-flop elastic scattering.

The spin-orbit coupling has somewhat different effects. As is seen from (3.2.29), if $1/\tau_s = 0$, $\tau_{so} \gg \tau$, then at $1/\tau_{so} < \omega + 1/\tau_\varphi < 1/\tau$ the conductivity decreases with decreasing frequency or temperature and at $\omega < 1/\tau_{so}$ it increases [9]. This is due to the fact [10] that the correlator $C_{\alpha\beta\gamma\delta}$ can be represented as a sum of correlators with angular momenta I equal to zero and unity:

$$\mathbf{C} = -\frac{1}{2} C^{(0)} + \frac{3}{2} C^{(1)}. \quad (3.2.31)$$

The contribution of each correlator is proportional to the angular momentum degeneracy, and the signs are chosen in such a way that in the absence of the spin-orbit coupling, when $C^{(0)} = C^{(1)}$, the total factor should equal unity. The spin-orbit coupling leads to the spin relaxation in the time interval τ_{so} , therefore $C^{(1)}$ cannot become larger than τ_{so} . Thus, at low frequencies \mathbf{C} is determined by $C^{(0)}$, which enters (3.2.31) with a negative factor.

Note that the spin-orbit coupling does not suppress the growth of the quantum corrections with decreasing frequency or temperature, but changes their sign and magnitude. Note also that the factors 3 and -1 are connected with the properties of the group of three-dimensional rotations. Therefore in two dimensions, when the momenta \mathbf{p} and \mathbf{p}' can lie only in the xy -plane, the situation changes. To make sure of that, let us write (3.2.25a) in the form [9]

$$\frac{1}{\tau} = \frac{1}{\tau_p} + \frac{2}{\tau_s} + \frac{1}{\tau_s^z} + \frac{2}{\tau_{so}^x} + \frac{1}{\tau_{so}^z}, \quad (3.2.32a)$$

where

$$\begin{aligned}\frac{1}{\tau_s^x} &= \pi v U_s^2 \langle S_x^2 \rangle = \pi v U_s^2 \langle S_y^2 \rangle, \\ \frac{1}{\tau_s^z} &= \pi v U_s^2 \langle S_z^2 \rangle, \\ \frac{1}{\tau_{so}^x} &= \pi v U_{so}^2 \langle [\mathbf{p} \times \mathbf{p}']_x^2 \rangle = \pi v U_{so}^2 \langle [\mathbf{p} \times \mathbf{p}']_y^2 \rangle, \\ \frac{1}{\tau_{so}^z} &= \pi v U_{so}^2 \langle [\mathbf{p} \times \mathbf{p}']_z^2 \rangle.\end{aligned}\quad (3.2.32b)$$

The transition to two dimensions corresponds to $1/\tau_{so}^x \rightarrow 0$. We should look for the solution of Eq. (3.2.26) in the form

$$C_{\alpha\beta\gamma\delta} = A\delta_{\alpha\beta}\delta_{\gamma\delta} + B_x(\sigma_{\alpha\beta}^x\sigma_{\gamma\delta}^x + \sigma_{\alpha\beta}^y\sigma_{\gamma\delta}^y) + B_z\sigma_{\alpha\beta}^z\sigma_{\gamma\delta}^z. \quad (3.2.33)$$

Substituting (3.2.33) into (3.2.26), we obtain

$$\begin{aligned}A &= \frac{1}{\tau} \left(-\frac{t_1}{2} + \frac{t_3}{4} + \frac{t_2}{4} \right), \\ B_x &= \frac{1}{\tau} \left(\frac{t_3}{4} - \frac{t_2}{4} \right), \\ B_z &= \frac{1}{\tau} \left(-\frac{t_1}{2} - \frac{t_2}{4} - \frac{t_3}{4} \right),\end{aligned}\quad (3.2.34)$$

where

$$\begin{aligned}t_1 &= \left(-i\omega + DQ^2 + \frac{2}{\tau_{so}^z} + \frac{2}{\tau_{so}^x} + \frac{2}{\tau_s^x} \right)^{-1}, \\ t_2 &= \left(-i\omega + DQ^2 + \frac{2}{\tau_s^z} + \frac{4}{\tau_s^x} \right)^{-1}, \\ t_3 &= \left(-i\omega + DQ^2 + \frac{2}{\tau_s^z} + \frac{4}{\tau_{so}^x} \right)^{-1}.\end{aligned}$$

The expression for the correlator $C_{\alpha\beta\beta\alpha}$, which determines the quantum correction, acquires the form

$$\begin{aligned}C_{\alpha\beta\beta\alpha} &= 2(A + B_z + 2B_x) = \frac{2}{\tau} \left\{ \frac{1}{-i\omega + DQ^2 + \frac{2}{\tau_{so}^z} + \frac{2}{\tau_s^x} + \frac{2}{\tau_{so}^x}} \right. \\ &\quad \left. - \frac{1}{2} \frac{1}{-i\omega + DQ^2 + \frac{2}{\tau_s^z} + \frac{4}{\tau_s^x}} + \frac{1}{2} \frac{1}{-i\omega + DQ^2 + \frac{2}{\tau_s^z} + \frac{4}{\tau_{so}^x}} \right\}. \quad (3.2.35)\end{aligned}$$

It is seen that at $1/\tau_s = 0$ and $1/\tau_{so}^x = 0$, the second and third terms cancel and $1/\tau_{so}^z$ enters the first term in the same way as $1/\tau_s$, restrict-

ing thus the growth of the quantum corrections to conductivity with decreasing temperature. This is what we have in two dimensions.

The spin-orbit coupling can also lead to splitting of the electron spectrum into two branches, corresponding to two spin directions. In combination with the potential scattering, this brings about effects analogous to the spin-orbit scattering [10, 13]. For example, in cubic crystals without the inversion centre (GaAs, InSb, etc.) the electronic Hamiltonian has the form [12]

$$\hat{\mathcal{E}}_{\alpha\beta}(\mathbf{p}) = \delta_{\alpha\beta} \frac{\mathbf{p}^2}{2m} + \hbar \boldsymbol{\Omega}(\mathbf{p}) \cdot \boldsymbol{\sigma}_{\alpha\beta}, \quad (3.2.36)$$

where

$$\Omega_x = \delta p_x (p_y^2 - p_z^2). \quad (3.2.37)$$

If the momentum relaxation is sufficiently fast ($\Omega\tau \ll 1$), then during the time

$$\frac{1}{\tau_{so}} = \tau \int \frac{dO_{\mathbf{p}}}{4\pi} \sum_{i=1}^3 \Omega_i^2(\mathbf{p}) \quad (3.2.38)$$

spin relaxes [11] and $\tau_{so} \gg \tau$. If $\Omega\tau \geq 1$, $\tau_{so} \sim \tau$. Thus, in semiconductors of GaAs type τ_{so} decreases drastically with increasing chemical potential until it becomes of the order of the momentum relaxation time. If $\tau_{so} \sim \tau$, then $\partial\sigma/\partial T < 0$ at all temperatures, provided that $\tau_{\varphi} \gg \tau$. Therefore, if in a doped semiconductor $\partial\sigma/\partial T > 0$ at $\tau_{so} \gg \tau_{\varphi}$, then $\partial\sigma/\partial T$ changes its sign with increasing concentration. In two dimensions in crystals of GaAs type $1/\tau_{so}^z = 0$ and $1/\tau_{so}^x \neq 0$. Consequently [see (3.2.35)], the conductivity increases logarithmically as $T \rightarrow 0$.

We can verify our theory, investigating the hole conductivity in semiconductors with the cubic lattice (Ge, Si, etc.) [13]. Near the top of the valence band, anisotropy being ignored, the hole Hamiltonian may be written as [12]

$$H = \frac{\mathbf{p}^2}{4} \left(\frac{3}{m_l} - \frac{1}{m_l} \right) + (\mathbf{p} \cdot \mathbf{J})^2 \left(\frac{1}{m_l} - \frac{1}{m_h} \right), \quad (3.2.39)$$

where m_l and m_h are the masses of light and heavy holes respectively and \mathbf{J} is the matrix of the angular momentum of 3/2. As has been already done [see (3.2.29)], the cooperon can be represented as a sum of cooperons corresponding to angular momenta of 0, 1, 2 and 3:

$$\mathbf{C} = -\frac{1}{4} C^{(0)} + \frac{3}{4} C^{(1)} - \frac{5}{4} C^{(2)} + \frac{7}{4} C^{(3)}. \quad (3.2.40)$$

If the masses of light and heavy holes coincided, we would have $C^{(0)} = C^{(1)} = C^{(2)} = C^{(3)}$. The spectrum splitting at $m_l \neq m_h$ leads to the relaxation of higher multipoles in any elastic scattering.

Hence $\mathbf{C} = -\frac{1}{4} C^{(0)}$ and $\partial\delta\sigma/\partial T < 0$. It is important to note that the correlator $C^{(0)}$ corresponds to the scalar part of the wave function. Therefore the obtained result will be left unchanged, even if we account for anisotropy.

If a cubic crystal is deformed along one axis, the hole spectrum degeneracy at $\mathbf{p} = 0$ is removed and in a highly deformed sample we can consider only one energy spectrum branch. In this case the momentum relaxation does not lead to the spin relaxation and $\partial\delta\sigma/\partial T > 0$. Thus, investigating piezoresistance of p -type semiconductors, we can verify the validity of our qualitative predictions.

In a ferromagnet, even in the absence of an external field, there is induction $\mathbf{B} = 4\pi\mathbf{M}$. The suppression of the quantum corrections in a magnetic field is considered in detail in Chap. 3.7. If the field of spontaneous magnetization is not strong enough to suppress the interference, we should bear in mind that due to the exchange interaction the Fermi momenta p_{\uparrow} and p_{\downarrow} for opposite spin directions do not coincide. Therefore, spin-flop processes being ignored, only those components of $C_{\alpha\beta\gamma\delta}$ have poles, for which $\alpha = \beta = \gamma = \delta$. These components correspond to the states with nonzero angular momentum. Hence the spin relaxation due to the spin-orbit coupling in ferromagnetic metals leads to the suppression of interference. A similar argument gives an analogous result for antiferromagnetic metals.

3.2.4 Properties of Samples of Finite Dimensions. Effective Space Dimensionality

The aim of this section is to explain in what cases, as far as the quantum corrections to the conductivity are concerned, a sample may be considered one-, two- or three-dimensional. Consider, for example, a rectangular sample of dimensions $L_x \geq L_y \geq L_z$. Let the faces perpendicular to the x axis be connected to massive conductors, the dimensions of which may be considered infinite. The cooperon $C_{\omega}(\mathbf{r}, \mathbf{r}')$ which enters the expression for the quantum correction to the conductivity obeys the diffusion equation. The boundary conditions at the sample-vacuum boundary consist in the flux being equal to zero. At the boundary with massive conductors $C_{\omega} = 0$ just as in the case of diffusion an excessive part of density vanishes at the boundary with a massive body. The solution of the diffusion equation with such boundary conditions may be expanded in eigenfunctions of the form $\sin(Q_x x) \sin(Q_y y) \sin(Q_z z)$, where

$$Q_x = \frac{2n+1}{L_x} \pi,$$

$$Q_y = \frac{2\pi m}{L_y},$$

$$Q_z = \frac{2\pi k}{L_z},$$

(3.2.41)

and n, m, k are integers. For a sample of finite dimensions the integral $\int (dQ) C_\omega(\mathbf{Q})$ should be replaced by the sum over eigenstates:

$$\frac{\delta\sigma}{\sigma} = -\frac{1}{L_x L_y L_z} \sum_{Q_x Q_y Q_z} \left[-i\omega + D(Q_x^2 + Q_y^2 + Q_z^2) + \frac{1}{\tau_\varphi} \right]^{-1}, \quad (3.2.42)$$

where $Q_{x,y,z}$ are defined by (3.2.41). In the case when $L_z \ll L_x, L_y$, we should separate the term with $Q_z = 0$

$$-\frac{\delta\sigma}{\sigma} = \frac{1}{L_z} \left\{ \frac{1}{L_x L_y} \sum_{Q_x Q_y} \left[-i\omega + D(Q_x^2 + Q_y^2) + \frac{1}{\tau_\varphi} \right]^{-1} + \frac{1}{L_x L_y L_z} \sum'_{Q_z} \sum_{Q_x Q_y} \left[-i\omega + D(Q_x^2 + Q_y^2 + Q_z^2) + \frac{1}{\tau_\varphi} \right]^{-1} \right\}. \quad (3.2.43)$$

The first term on the right-hand side of Eq. (3.2.43) corresponds to $C_\omega(\mathbf{r}, \mathbf{r}')$, which is independent of z (two-dimensional fluctuations), and the second term describes three-dimensional fluctuations. If

$$L_z \ll \min \left\{ \sqrt{\frac{D}{\omega}}, \sqrt{D\tau_\varphi} \right\}, \quad (3.2.44)$$

then the first term in (3.2.43) is larger than the second one.

Thus, a film can be considered two-dimensional if its thickness is so small that during the phase breaking time τ_φ an electron diffuses from one boundary to another, the anomalous correction to resistance being dependent only on the resistance itself [5, 7]:

$$\Delta R_\square = \frac{e^2}{2\pi^2\hbar} R_\square^2 \ln \frac{\tau_\varphi}{\tau} = \text{const} + \frac{e^2 p}{2\pi^2\hbar} R_\square^2 \ln \frac{1}{T}. \quad (3.2.45)$$

Here we have accounted for $\tau_\varphi = T^{-p}$.

Similar arguments show that if L_z and L_y satisfy the condition (3.2.44), a wire can be considered one-dimensional. As a result, the anomalous correction to the resistance is defined by [5]

$$\Delta R = \frac{e^2}{\pi\hbar} R^2 \frac{\sqrt{D\tau_\varphi}}{L_x}. \quad (3.2.46)$$

If the sample length L_x also satisfies the condition (3.2.44), τ_φ disappears from the formulae for the quantum corrections:

$$\Delta R = \frac{e^2}{4\pi\hbar} R^2. \quad (3.2.47)$$

We see that for a sufficiently long wire, when $R \sim \pi\hbar/e^2 \sim 10 \text{ kohm}$, $\Delta R/R \sim 1$. This means that in long wires we observe localization, their resistance increasing exponentially with increasing length [6].

The characteristic localization length may be estimated from the fact that the resistance of a wire of length L is of order \hbar/e^2 , i.e.

$$L_c \sim l \frac{Sp_F^2}{\hbar^2}. \quad (3.2.48)$$

In one dimension, when $Sp_F^2/\hbar^2 \sim 1$, the localization length is of the order of a mean free path. Therefore the theory valid in the case when $l \ll L_x \ll L_c$, applies only to the wires of cross section $S \gg \gg \lambda^2 \sim \hbar^2/p_F^2$.

In films of finite dimensions $L_x \sim L_y \sim L \ll \sqrt{D\tau_\varphi}$, we have

$$\Delta R_\square = \frac{e^2}{\pi^2 \hbar} R_\square^2 \ln \frac{L}{l}. \quad (3.2.49)$$

3.3 QUANTUM EFFECTS IN HIGH-FREQUENCY ELECTROMAGNETIC FIELD

3.3.1 Effects of High-Frequency Field on Quantum Corrections to Conductivity

The effects considered in Sec. 3.2 are due to the interference of probability amplitudes, corresponding to two electron paths. Moving along these paths, differing only in direction, an electron returns to the starting point. For purely elastic collisions the electron wave functions corresponding to both paths are in phase.

It has been found out that an alternating electromagnetic field destroys this phase coherence [14, 15]. If both paths begin at a given point at a time $-t$ and end at the same point at time t , then the phase difference for these two paths is

$$\begin{aligned} \Delta\varphi &= \int_{-t}^t [\delta\varepsilon_1(t_1) - \delta\varepsilon_2(t_1)] dt_1 \\ &= e \int_{-t}^t dt_1 \int_{-t}^{t_1} dt' \{ \mathbf{E}(t') \cdot \mathbf{v}_1(t') - \mathbf{E}(t') \cdot \mathbf{v}_2(t') \} \end{aligned} \quad (3.3.1)$$

where $\delta\varepsilon_{1,2}(t_1)$ is the energy gained by the electron in an external field by the time t_1 and $\mathbf{v}_{1,2}(t_1)$ is its velocity at that time [$\mathbf{v}_1(t_1) = \mathbf{v}_2(-t_1)$]. Due to scattering by impurities this phase difference is random. Averaging (3.3.1) over different paths and taking into account that at $\Omega t \ll 1$ (Ω is the external field frequency), $\mathbf{E}(t) - \mathbf{E}(0) \cong t\dot{\mathbf{E}}$ and $\langle \mathbf{r}^2 \rangle \sim Dt$, we obtain

$$\langle (\Delta\varphi)^2 \rangle \sim e^2 \dot{\mathbf{E}}^2 D t^5. \quad (3.3.2)$$

It is evident that in a constant field $\langle (\Delta\varphi)^2 \rangle = 0$, and the phase coherence is not destroyed.

In an alternating field the characteristic time t_0 , during which the phase breaking becomes essential, is defined by the condition $\langle(\Delta\varphi)^2\rangle \sim 1$ or

$$t_0 \sim (e^2 E^2 \Omega^2 D)^{-1/5}. \quad (3.3.3)$$

Therefore if $t_0 < \tau_\varphi$, quantum corrections to static conductivity in an external alternating field are determined by the amplitude of this field.

The Fourier transform of the current j_ω in a constant measuring field E_0 and a high-frequency field E_Ω is expressed through the coöperon by means of Eq. (3.A.10). Taking an integral over ε , this equation acquires the form

$$j_\omega = \frac{2}{\pi} e^2 D E_0 \tau \int_{-\infty}^{+\infty} dt \int_{-\infty}^{+\infty} e^{-i\omega(t-\eta)} C_{\eta, -\eta}^t(\mathbf{r}, \mathbf{r}) d\eta, \quad (3.3.4)$$

and the coöperon is defined by Eq. (3.A.18):

$$\left\{ \frac{\partial}{\partial \eta} + D \left[-i\nabla - \frac{e}{c} \mathbf{A} \left(\mathbf{r}, t - \frac{\eta}{2} \right) - \frac{e}{c} \mathbf{A} \left(\mathbf{r}, t + \frac{\eta}{2} \right) \right]^2 + \frac{1}{\tau_\varphi} \right\} C_{\eta\eta'}^t(\mathbf{r}, \mathbf{r}') = \frac{1}{\tau} \delta(\eta - \eta') \delta(\mathbf{r} - \mathbf{r}').$$

The solution of this equation in a uniform high-frequency field has the form

$$C_{\eta\eta'}^t(\mathbf{r}, \mathbf{r}) = \int (d\mathbf{Q}) \frac{\theta(\eta - \eta')}{\tau} \exp \left\{ -D \int_{\eta'}^{\eta} d\eta_1 \times \left[Q - \frac{2e}{c} \mathbf{A}(t) \cos \frac{\Omega \eta_1}{2} \right]^2 - \frac{\eta - \eta'}{\tau_\varphi} \right\}. \quad (3.3.5)$$

Substituting this expression into Eq. (3.3.4), integrating over \mathbf{Q} and t and subtracting from (3.3.4) the value of the current in the absence of a high-frequency field, we find that the static conductivity in a high-frequency field changes by the magnitude

$$\Delta\sigma^{(d)} = - \frac{8}{2d\pi (4\pi)^{d/2}} \frac{e^2 \Omega^{d/2-1}}{D d^{2-1}} \int_0^\infty \frac{dx}{x^{d/2}} e^{-\frac{4x}{\Omega \tau_\varphi}} \{ e^{-\alpha f(x)} I_0[\alpha f(x)] - 1 \}, \quad (3.3.6)$$

where

$$f(x) = x \left[1 + \frac{\sin 2x}{2x} - 2 \frac{\sin^2 x}{x^2} \right],$$

$$f(x) = \begin{cases} \frac{2x^5}{45} & \text{for } x \ll 1 \\ x & \text{for } x \gg 1, \end{cases} \quad (3.3.7)$$

$\alpha = \frac{4e^2 D E_0^2}{\Omega^3}$, and $I_0(y)$ is the imaginary-argument Bessel function.

We see from the expression in braces in Eq. (3.3.6) that it changes over the scale

$$x_0 = \Omega t_0 = \begin{cases} \left(\frac{45}{2\alpha}\right)^{1/5} & \text{at } \alpha \gg 1 \\ \frac{1}{\alpha} & \text{at } \alpha \ll 1. \end{cases} \quad (3.3.8)$$

Therefore the conductivity variation in a high-frequency field is defined by the relation between t_0 and τ_φ . In a weak high-frequency field, when $t_0 \gg \tau_\varphi$, it is possible to expand the expression in braces in (3.3.6) into a power series in α . As a result we obtain

$$\Delta\sigma^{(d)} = \frac{e^2 (eFL_\varphi^2)}{(2\pi)^{d/2} \hbar L_\varphi^{d-2}} \begin{cases} \frac{\Gamma\left(6 - \frac{d}{2}\right)}{180} \left(\frac{\Omega\tau_\varphi^2}{\hbar}\right)^2 & \text{at } \Omega\tau_\varphi \ll 1 \\ \frac{2\Gamma\left(2 - \frac{d}{2}\right)}{(\hbar\Omega)^2} & \text{at } \Omega\tau_\varphi \gg 1. \end{cases} \quad (3.3.9)$$

In a strong high-frequency field, when $t_0 \ll \tau_\varphi$, we have in two dimensions

$$\Delta\sigma^{(2)} = -\frac{e^2}{2\pi^2\hbar} \ln \frac{t_0}{\tau_\varphi}, \quad (3.3.10)$$

and in quasi-one dimension

$$\Delta\sigma^{(1)} = -\frac{e^2}{h} L_\varphi \times \begin{cases} \frac{\hbar\Omega}{\sqrt{\pi} eEL_\varphi} \ln \frac{eEL_\varphi}{\hbar\Omega} & \text{at } \alpha \ll 1, \\ \frac{2.65}{\sqrt{\Omega\tau_\varphi}} \left(\frac{\hbar^2\Omega^2}{e^2E^2D}\right)^{1/10} & \text{at } \alpha \gg 1. \end{cases} \quad (3.3.11)$$

In three dimensions

$$\Delta\sigma^{(3)} = -\frac{e^2}{2\pi^{3/2}\hbar \sqrt{Dt_0}} \times \begin{cases} 2.27 & \text{at } \alpha \ll 1 \\ 1.93 & \text{at } \alpha \gg 1. \end{cases} \quad (3.3.12)$$

Usually nonlinear effects are due to electron heating. It is important to note that the effect of a high-frequency field we are considering is not connected with heating and manifests itself when $t_0 \ll \tau_\varphi [T_{\text{eff}}(E)]$.

3.3.2 Suppression of Coherent Effects by Electromagnetic Fluctuations

It has been shown in Sec. 3.3.1 that an external electromagnetic field leads to the electron phase breaking, while the distribution function does not change. In any sample of finite resistance there are fluctuating thermal electric fields which also lead to the electron phase breaking [14, 15].

Let us estimate this effect. The phase variation during time t is determined by the total effect of fields with different frequencies (3.3.6):

$$\langle (\Delta\varphi(t)^2) \sim \left\langle \int d\Omega \alpha_{\Omega} f(\Omega t) \right\rangle. \quad (3.3.13)$$

The fluctuation spectrum does not depend on frequency. Therefore the characteristic frequencies, typical of the phase breaking, are of order $\Omega \sim 1/t$, as is seen from (3.3.13). Fluctuating fields are nonuniform, but to suppress the coherence we need only the fields, uniform over the length $L(t) \sim \sqrt{Dt}$. For such fields

$$\langle E_{\Omega}^2 \rangle \sim \frac{T}{\sigma [L(t)]^d}.$$

Hence the phase breaking time τ_N is defined by the relation

$$\langle \alpha_{\Omega} \rangle \Omega f(1) \sim \frac{T e^2}{\sigma} D^{1-\frac{d}{2}} \tau_N^{2-\frac{d}{2}} = \frac{T \tau_N^{\frac{4-d}{2}}}{D d^{d/2} \nu a^{3-d}} \sim 1. \quad (3.3.14)$$

In a sample of transverse dimensions $a \ll L_N$ the conductivity is equal to $\sigma^{(d)} = e^2 D \nu a^{3-d}$. It follows from (3.3.14) that

$$\tau_N \sim \left(\frac{D d^{d/2} \nu a^{3-d}}{T} \right)^{\frac{2}{4-d}}, \quad (3.3.15)$$

and the characteristic length is

$$L_N \sim \left(\frac{D^2 \nu a^{3-d}}{T} \right)^{\frac{1}{4-d}}. \quad (3.3.16)$$

If the time τ_N is shorter than the phase breaking time due to other mechanisms of inelastic scattering, then the temperature dependence of the conductivity is determined precisely by τ_N . Thus, in two dimensions $\tau_N \sim 1/T$, and therefore

$$\sigma(T) - \sigma(T_0) = \frac{e^2}{2\pi^2 \hbar} \ln \frac{T}{T_0}. \quad (3.3.17)$$

In quasi-one dimension

$$\frac{\hbar}{\tau_N} \sim \left(\frac{e^2 T^2}{\hbar \sigma^{(1)} \nu_1} \right)^{1/3}, \quad (3.3.18)$$

$$\Delta \sigma^{(1)} \sim - \frac{e^2}{\hbar} L_N \sim - \left[\frac{e^2}{\hbar} \frac{\sigma^{(1)2}}{\nu_1 T} \right]^{1/3}. \quad (3.3.19)$$

Here $\nu_1 = \nu a^2$. The transition from one effective dimensionality to the other occurs when $L_N \sim a$. The characteristic scale of this transition is

$$a_c \sim \frac{\hbar^2 D^2 \nu}{T}. \quad (3.3.20)$$

Let us compare the time τ_N , say, with the time of electron-electron collisions in the case of a strong impurity scattering (3.4.6):

$$\frac{\tau_N}{\tau_{ee}} \sim (T\tau_{ee})^{\frac{d-2}{4-d}}. \quad (3.3.24)$$

Evidently, if quasiparticle description of a metal is valid ($T\tau_{ee} \gg 1$), then for $d \leq 2$ the phase relaxation is determined by electromagnetic fluctuations, and for $d = 3$ the main role is played by strongly inelastic Coulomb collisions.

If the investigated sample has a resistance R and is connected into an external circuit of a resistance R_0 , having a temperature T_0 , then a fluctuating voltage U_Ω appears in the sample, this voltage being defined by the relation

$$\langle |U_\Omega|^2 \rangle = \frac{2T_0 R^2 R_0}{(R + R_0)^2}.$$

Therefore the phase breaking time due to the external circuit noise is

$$\tau_N \sim \sqrt{\left(1 + \frac{R_0}{R}\right)^2 \frac{VvR^2}{T_0 R_0}}, \quad (3.3.22)$$

where V is the sample volume.

Now we shall derive relations (3.3.15)-(3.3.22). First we have to solve Eq. (3.A.18) in an arbitrary nonuniform random field $A(\mathbf{r}, t)$. The solution can be written as a path integral

$$C_{\eta_1 \eta_2}^t(\mathbf{r}_1, \mathbf{r}_2) = \int_{\mathbf{r}(\eta_1)=\mathbf{r}_1}^{\mathbf{r}(\eta_2)=\mathbf{r}_2} D\mathbf{r}(t_1) \exp \left\{ - \int_{\eta_1}^{\eta_2} dt_1 \left[\frac{\dot{\mathbf{r}}^2(t_1)}{4D} + i\mathbf{r}(t_1) \cdot \frac{e}{c} \mathbf{A}_t(\mathbf{r}(t_1), t_1) \right] \right\}. \quad (3.3.23)$$

The conductivity is related to the cooperon averaged over random electromagnetic fields by Eq. (3.A.10). Averaging (3.3.23), we obtain

$$C_{-\eta, \eta}^t(\mathbf{r}, \mathbf{r}) = \int_{\mathbf{r}(-\eta)=\mathbf{r}}^{\mathbf{r}(\eta)=\mathbf{r}} D\mathbf{r}(t_1) \exp \left\{ - \int_{-\eta}^{\eta} dt_1 \frac{\dot{\mathbf{r}}^2(t_1)}{4D} - \frac{e^2}{2c^2} \int_{-\eta}^{\eta} dt_1 \int_{-\eta}^{\eta} dt_2 \dot{\mathbf{r}}_i(t_1) \dot{\mathbf{r}}_j(t_2) \langle A_i^t(\mathbf{r}(t_1), t_1) A_j^t(\mathbf{r}(t_2), t_2) \rangle \right\}. \quad (3.3.24)$$

The potential correlator $\langle A_i^t(\mathbf{r}_1, t_1) A_j^t(\mathbf{r}_2, t_2) \rangle$ is

$$\langle A_i^t(\mathbf{r}_1, t_1) A_j^t(\mathbf{r}_2, t_2) \rangle = 2 \int (dk) \int \frac{d\omega}{2\pi} \left\{ \cos \frac{\omega}{2} (t_1 + t_2) + \cos \frac{\omega}{2} (t_1 - t_2) \right\} \exp [ik \cdot (\mathbf{r}_1 - \mathbf{r}_2)] \langle A^t(\mathbf{k}, \omega) A^j(-\mathbf{k}, -\omega) \rangle, \quad (3.3.25)$$

where the correlator $\langle A^i(\mathbf{k}, \omega) A^j(-\mathbf{k}, -\omega) \rangle$ is defined in the classical limit by the fluctuation-dissipation theorem [16]:

$$\langle A^i(\mathbf{k}, \omega) A^j(-\mathbf{k}, -\omega) \rangle = -8\pi c^2 \frac{T}{\omega} \operatorname{Im} \left\{ \left(\delta_{ij} - \frac{k_i k_j}{k^2} \right) \frac{1}{\omega^2 \varepsilon_2^t(\mathbf{k}, \omega) - k^2 c^2} + \frac{k_i k_j}{k^2 \omega^2 \varepsilon_1(\mathbf{k}, \omega)} \right\}. \quad (3.3.26)$$

At small ω and \mathbf{k} it is possible to use the following expressions for $\varepsilon_t(\omega, \mathbf{k})$ and $\varepsilon_1(\omega, \mathbf{k})$:

$$\begin{aligned} \varepsilon_t(\omega, \mathbf{k}) &= 1 + \frac{4\pi i \sigma}{\omega}, \\ \varepsilon_1(\omega, \mathbf{k}) &= 1 + \frac{D\kappa^2}{-i\omega + Dk^2}, \end{aligned} \quad (3.3.27)$$

where κ is the inverse length of the Debye screening. Two different limiting cases are possible: if $c^2 k^2 \ll 4\pi\sigma\omega$, i.e. if the characteristic length L_ω is greater than the skin length, $\delta_\omega = \sqrt{c^2/2\pi\sigma\omega}$, we can omit the term $c^2 k^2$ in the denominator. If, on the contrary, $L_\omega \ll \delta_\omega$, we can neglect the transverse field fluctuations in comparison with longitudinal field fluctuations. Using the relation $D\kappa^2 = 4\pi\sigma$, we obtain

$$\langle A^i(\mathbf{k}, \omega) A^j(-\mathbf{k}, -\omega) \rangle = \frac{2T}{\sigma} \frac{c^2}{\omega^2} \begin{cases} \delta_{ij}, & k\delta_\omega \ll 1, \\ \frac{k_i k_j}{k^2}, & k\delta_\omega \gg 1. \end{cases} \quad (3.3.28)$$

As $L_\omega^2 = D/\omega$, the condition $L_\omega \gg \delta_\omega$ can be written as

$$\frac{c}{v_F} \ll l\kappa.$$

Consider first the case $k\delta_\omega \ll 1$. Substituting (3.3.28) into (3.3.25) and (3.3.24), the cooperon can be written in the form

$$\begin{aligned} C_{-\eta, \eta}^t(\mathbf{r}, \mathbf{r}) &= \int_{\mathbf{r}(-\eta)=\mathbf{r}}^{\mathbf{r}(\eta)=\mathbf{r}} D\mathbf{r}(t_1) \exp \left\{ - \int_{-\eta}^{\eta} dt_1 \frac{\dot{\mathbf{r}}^2(t_1)}{4D} \right. \\ &\quad \left. - \frac{e^2 T}{2\sigma} \int_{-\eta}^{\eta} dt_1 \int_{-\eta}^{\eta} dt_2 \delta[\mathbf{r}(t_1) - \mathbf{r}(t_2)] \dot{\mathbf{r}}(t_1) \cdot \dot{\mathbf{r}}(t_2) (|t_1 + t_2| + |t_1 - t_2|) \right\}. \end{aligned} \quad (3.3.29)$$

Thus, the cooperon averaged over thermal fluctuation of the electromagnetic field describes diffusion of a particle interacting with itself at the points of trajectory self-intersection. Here the characteristic length is $L(t) \sim \sqrt{Dt}$. Therefore, if the sample transverse dimensions $a \ll L(t)$ for essential t 's then δ -function can be estimated

as $\delta^{(3)}(\mathbf{r}_1 - \mathbf{r}_2) = \frac{1}{V_d} \delta^{(d)}(\mathbf{r}_1 - \mathbf{r}_2)$ (here $V_d \sim a^{3-d}$, i.e. V_0 is the sample volume, V_1 the wire cross-section area, V_2 the film thickness, and $V_3 = 1$).

Let us introduce now dimensionless variables x and y such that $t = \tau_N y$, $r = L_N x$, where

$$\tau_N = \left[\frac{2\sigma^{(d)}}{e^2 T} (2D)^{\frac{d-2}{2}} \right]^{\frac{2}{4-d}},$$

$$L_N = \sqrt[4]{2D\tau_N} = \left[\frac{4\sigma^{(d)}D}{e^2 T} \right]^{\frac{1}{4-d}}. \quad (3.3.30)$$

N.B.: the scales of τ_N and L_N differ from the estimates (3.3.15) and (3.3.16) only in numerical factors.

Using these variables, it is possible to express the conductivity correction through a dimensionless path integral:

$$\Delta\sigma^{(d)} = -\frac{e^2}{2\pi^2} (2D\tau_N)^{1-d/2} \int_{\tau/\tau_N}^{\infty} dy \int_{x(-y)=0}^{x(y)=0} Dx(y_1)$$

$$\times \exp \left\{ -\frac{1}{2} \int_{-y}^y dy_1 \dot{x}^2(y_1) - \int_{-y}^y dy_1 \int_{-y}^y dy_2 \dot{x}(y_1) \dot{x}(y_2) \delta[x(y_1) - x(y_2)] \right.$$

$$\left. \times (|y_1 + y_2| + |y_1 - y_2|) \right\}. \quad (3.3.34)$$

In quasi-two dimensions the integral diverges logarithmically at the lower limit which is equal to τ/τ_N . Integrating to a logarithmic accuracy, we obtain (3.3.17). In one dimension the path integral can be calculated exactly, yielding a numerical factor in (3.3.19):

$$\Delta\sigma^{(1)} = -C_1 \left[\frac{e^2}{\hbar} \frac{\sigma^{(1)2}}{v_1 T} \right]^{1/3},$$

$$C_1 = \frac{2\sqrt{2}}{3^{5/6} 2^{1/6} \Gamma^2\left(\frac{2}{3}\right)} \simeq 0.55. \quad (3.3.32)$$

In quasi-one dimension Eq. (3.3.32) holds for any relation between L_N and δ_ω , because $k_i k_j / k^2 = \delta_{ij} = 1$. In quasi-two dimensions, accounting for the difference in the tensor structure of the fluctuation correlator from the case $k\delta_\omega \ll 1$ considered above, we obtain only a new numerical factor in the argument of the logarithm.

In the case of a spatially uniform noise caused by voltage fluctuations in the external circuit, the path integral can also be calculated exactly. If the phase relaxation is determined by this very noise,

then

$$\Delta\sigma^{(d)} = -\frac{e^2}{\hbar} \left[\frac{4\pi D^2 v V}{T} \left(1 + \frac{R_0}{R} \right)^2 \frac{R}{R_0} \right]^{\frac{2-d}{4}} C^{(d)}. \quad (3.3.33)$$

$$C^{(1)} = 6.57; \quad C^{(2)} = 1; \quad C^{(3)} = -0.7.$$

Note that the considered mechanism of the phase relaxation due to the electron interaction with electromagnetic field fluctuations is quite general and can be taken into account, for instance, in the theory of superconductivity. The effect of electromagnetic fluctuations on the critical temperature T_c has been considered in [17, 18]. The T_c shift is small and can be calculated by the perturbation theory. On the contrary, the noise effects on superconducting fluctuations at $T > T_c$ and the Maki-Thompson correction to the conductivity are not small and must be calculated by the method considered above.

3.4 ELECTRON-ELECTRON INTERACTION IN DISORDERED METALLIC SYSTEMS

3.4.1 Electron-Electron Collision Time

The quasiparticle description of electrons in metals and semiconductors is based on the decay of electronic excitations being small compared with their energy. For degenerate Fermi-systems the inverse decay time connected with electron-electron collisions is of order ε^2/μ and evidently small compared with the excitation energy ε above the Fermi level. As a consequence the electronic distribution function in pure metals always has a sharp discontinuity at the Fermi level. These assertions do not depend on the details of electron-electron interactions and are based on the fact that in quasiparticle scattering only large and, what is more important, energy-independent momentum transfers are essential. Therefore the decay is determined only by the phase volume of finite states. By analogy with the Fermi-liquid description of ordered systems, it has been assumed that in the case of weak disorder, $p_F l \gg 1$, the excitation decay is also proportional to ε^2 . It appears, however, that in a disordered system excitations decay more rapidly, and even the validity of the quasiparticle description of low-dimensional disordered systems becomes questionable. The decay time of one-electron excitations is important not only for the construction of the theory, but it also determines the magnitude and temperature dependence of the quantum corrections to the conductivity. In this section we examine the time of electron-electron collisions in disordered conductors [18, 20, 21]. Before giving a rigorous derivation of basic relations, we shall consider qualitatively what changes occur in disordered Fermi-systems in comparison with pure metals.

The inverse electron-electron collision time $1/\tau_{ee}(\varepsilon)$ for an electron of energy ε (the Fermi level set to zero) can be represented as

$$\frac{1}{\tau_{ee}(\varepsilon)} \sim \int_0^\varepsilon d\omega \int_0^\omega d\varepsilon' \int_0^\infty q^2 dq W_q \int_{-1}^1 dx \delta(\omega - qv_F x) \int_{-1}^1 dx' \delta(\omega - qv_F x'), \quad (3.4.1)$$

where ω is the energy transfer in a single collision event, ε' the energy of the second quasiparticle, taking part in collision with an electron of energy ε , W_q the square of the matrix element of interaction, q the momentum transfer, $x = \cos(\mathbf{p}, \mathbf{q})$, $x' = \cos(\mathbf{p}', \mathbf{q})$ (\mathbf{p} and \mathbf{p}' are the quasiparticle momenta before collision).

Integrating over x and x' and taking into account that the integral over \mathbf{q} converges at large and ε -independent \bar{q} 's so that $\bar{q}v_F \gg \varepsilon$, we obtain

$$\frac{1}{\tau_{ee}(\varepsilon)} \sim \int_0^\varepsilon d\omega \int_0^\omega d\varepsilon' \int_0^\infty q^2 dq W_q \frac{1}{(qv_F)^2}. \quad (3.4.2)$$

It follows immediately from (3.4.2) that $1/\tau_{ee}(\varepsilon) \sim \varepsilon^2$. Note that each integration over x in (3.4.1) yields a factor $(qv_F)^{-1}$, having a meaning of interaction time t_{int} . In fact, particles traverse the interaction region of dimensions $1/q$ with velocity v_F , hence their interaction time is $(qv_F)^{-1}$. In a disordered system particles diffuse through this region, so that the interaction time is determined either by the inverse transferred energy, or by the diffusion time $1/Dq^2$. This means that we should replace $(qv_F)^{-1}$ in (3.4.2) by the diffusion pole $(-i\omega + Dq^2)^{-1}$ [as will be shown later, the correct expression is $\text{Re}(i\omega + Dq^2)^{-1}$]. Thus, we have

$$\frac{1}{\tau_{ee}(\varepsilon)} \sim \int_0^\varepsilon d\omega \int_0^\omega d\varepsilon' \int_0^\infty q^2 dq W_q \left[\text{Re} \frac{1}{i\omega + Dq^2} \right]^2. \quad (3.4.3)$$

In this formula essential q 's are of order $\sqrt{\omega/D} \sim \sqrt{\varepsilon/D} = L_\varepsilon^{-1}$. If $q \ll \kappa$ (κ is the inverse Debye screening length, $\kappa^2 = 4\pi e^2 \nu$), then W_q can be considered constant. Equation (3.4.3) yields

$$\frac{1}{\tau_{ee}(\varepsilon)} \sim \varepsilon^{3/2}. \quad (3.4.4)$$

The value of $1/\tau_{ee}(\varepsilon)$ decreases with energy slower than in a pure case. The exact expression, found below, has the form [19]

$$\frac{1}{\tau_{ee}(\varepsilon)} = \frac{1}{6\sqrt{2}\pi^2} \frac{\varepsilon^{3/2}}{\nu D^{3/2}}, \quad (3.4.5)$$

where ν is the density of states at the Fermi level. The effective dimensionality of a sample changes with its transverse dimensions.

The transition from one dimensionality to another occurs, when one of the sample dimensions becomes smaller than L_ε . The situation reminds of that considered in Section 3.2 where the transition occurs, when sample dimensions become of order L_φ . At $\varepsilon\tau_\varphi \gg 1$, $L_\varepsilon \ll L_\varphi$. In general,

$$\frac{1}{\tau_{ee}(\varepsilon)} = C \frac{1}{v L_\varepsilon^d a^{3-d}} \sim \varepsilon^{d/2}, \quad (3.4.6)$$

where C is of order unity. It is readily seen that in two dimensions $1/\tau_{ee}\varepsilon \sim 1/p_F^2 l a \ll 1$, and in one dimension $1/\varepsilon\tau_{ee} \sim 1/\sqrt{\tau\varepsilon}(p_F a)^2$; at sufficiently small ε this value may exceed unity. This means that at $\varepsilon < 1/\tau(p_F a)^4$ the quasiparticle description breaks down.

Now we shall derive the expressions describing electron-electron collisions. The decay time of excitations of energy ε due to electron-electron interactions at $T = 0$ has the following form in three dimensions:

$$\frac{1}{\tau_{ee}(\varepsilon)} = \frac{(2\pi)^3}{vv} \int_0^\varepsilon \frac{d\omega}{2\pi} \int_{-\omega}^0 \frac{d\varepsilon'}{2\pi} \sum_{\alpha\beta\gamma\delta} |V_{\gamma\delta}^{\alpha\beta}|^2 \delta(\varepsilon - \varepsilon_\alpha) \delta(\varepsilon - \omega - \varepsilon_\beta) \delta(\varepsilon' - \varepsilon_\gamma) \delta(\varepsilon' + \omega - \varepsilon_\delta). \quad (3.4.7)$$

This expression is written in the representation of exact electron wave functions in random potential. Indices $\alpha, \beta, \gamma, \delta$ label these exact one-particle states, $V_{\gamma\delta}^{\alpha\beta}$ is the matrix element of the electron-electron interaction, v is the volume of the system. Equation (3.4.7) can be rewritten in terms of imaginary parts of the exact Green functions:

$$\frac{1}{\tau_{ee}(\varepsilon)} = -\frac{4}{\pi^3 v v} \int_0^\varepsilon d\omega \int_{-\omega}^0 d\varepsilon' \int d\mathbf{r}_1 d\mathbf{r}_2 d\mathbf{r}'_1 d\mathbf{r}'_2 V_\omega(\mathbf{r}_1 - \mathbf{r}_2) V_\omega(\mathbf{r}'_2 - \mathbf{r}'_1) \times \text{Im } G_\varepsilon(\mathbf{r}'_1, \mathbf{r}_1) \text{Im } G_{\varepsilon-\omega}(\mathbf{r}_1, \mathbf{r}'_1) \text{Im } G_{\varepsilon'}(\mathbf{r}'_2, \mathbf{r}_2) \text{Im } G_{\varepsilon'+\omega}(\mathbf{r}_2, \mathbf{r}'_1). \quad (3.4.8)$$

Let us rewrite (3.4.8) once more:

$$\frac{1}{\tau_{ee}(\varepsilon)} = \frac{4}{\pi^3 v v} \int_0^\varepsilon d\omega \int_{-\omega}^0 d\varepsilon' \int (dq) (dq_1) \times V(\omega, \mathbf{q}) V^*(\omega, \mathbf{q}_1) \Pi_{\varepsilon, \varepsilon-\omega}(\mathbf{q}, \mathbf{q}_1) \Pi_{\varepsilon', \varepsilon'+\omega}(\mathbf{q}_1, \mathbf{q}). \quad (3.4.9)$$

Here

$$\Pi_{\varepsilon, \varepsilon-\omega}(\mathbf{q}, \mathbf{q}_1) = \int d\mathbf{r}_1 d\mathbf{r}'_1 \text{Im } G_\varepsilon(\mathbf{r}'_1, \mathbf{r}_1) \text{Im } G_{\varepsilon-\omega}(\mathbf{r}_1, \mathbf{r}'_1) \exp[i(\mathbf{q} \cdot \mathbf{r}_1 - \mathbf{q}_1 \cdot \mathbf{r}'_1)]$$

and $V(\omega, \mathbf{q})$ is the retarded electron-electron interaction potential.

Averaging over impurity configuration, it is necessary to separate the contribution to τ_{ee}^{-1} , which includes diffusion poles, corresponding to the changes in the interaction time due to diffusion. To perform this, we should average over the impurity potential as shown in Fig. 3.5. After that the expression for $\Pi_{\varepsilon, \varepsilon-\omega}(\mathbf{q}, \mathbf{q}_1)$ acquires the form

$$\begin{aligned} & \Pi_{\varepsilon, \varepsilon-\omega}(\mathbf{q}, \mathbf{q}_1) \\ &= \frac{\pi\nu\tau}{2} (2\pi)^3 \delta(\mathbf{q}-\mathbf{q}_1) \operatorname{Re} [\zeta_{\varepsilon}(\mathbf{q}, \omega) D_{\varepsilon}(\mathbf{q}, \omega) - \zeta'_{\varepsilon}(\mathbf{q}, \omega) D'_{\varepsilon}(\mathbf{q}, \omega)], \end{aligned} \quad (3.4.10)$$

where

$$\begin{aligned} \zeta_{\varepsilon}(\mathbf{q}, \omega) &= \frac{1}{\pi\nu\tau} \int (dp) G_{\varepsilon}(\mathbf{p}) G_{\varepsilon-\omega}(\mathbf{p}-\mathbf{q}), \\ \zeta'_{\varepsilon}(\mathbf{q}, \omega) &= \frac{1}{\pi\nu\tau} \int (dp) G_{\varepsilon}(\mathbf{p}) G_{\varepsilon-\omega}^*(\mathbf{p}-\mathbf{q}). \end{aligned}$$

Here $G_{\varepsilon}(\mathbf{p})$ is the electron Green function averaged over impurity configuration, $D_{\varepsilon}(\mathbf{q}, \omega)$ is the sum of ladder diagrams, the equation for which is shown in Fig. 3.1. The quantity $D'_{\varepsilon}(\mathbf{q}, \omega)$ differs

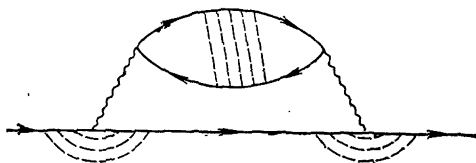


Fig. 3.5.

from $D_{\varepsilon}(\mathbf{q}, \omega)$ in complex conjugation of all the Green functions with energy $\varepsilon - \omega$. Solving the equation depicted in Fig. 3.1 we obtain

$$\begin{aligned} D_{\varepsilon}(\mathbf{q}, \omega) &= \frac{1}{1 - \zeta_{\varepsilon}(\mathbf{q}, \omega)}, \\ D'_{\varepsilon}(\mathbf{q}, \omega) &= \frac{1}{1 - \zeta'_{\varepsilon}(\mathbf{q}, \omega)}. \end{aligned} \quad (3.4.11)$$

Due to analytical properties of $G_{\varepsilon}(\mathbf{p})$, ζ_{ε} is small in the parameter $(\mu\tau)^{-1}$, if ε and $\varepsilon - \omega$ have the same signs. Therefore

$$\begin{aligned} \zeta_{\varepsilon}(\mathbf{q}, \omega) &= \zeta(\mathbf{q}, \omega) [\theta(\varepsilon) \theta(\omega - \varepsilon) + \theta(-\varepsilon) \theta(\varepsilon - \omega)], \\ \zeta'_{\varepsilon}(\mathbf{q}, \omega) &= \zeta(\mathbf{q}, \omega) [\theta(\varepsilon) \theta(\varepsilon - \omega) + \theta(-\varepsilon) \theta(\omega - \varepsilon)]. \end{aligned}$$

Thus, at $\omega < \varepsilon$, $\Pi_{\varepsilon, \varepsilon-\omega}(\mathbf{q}, \mathbf{q}_1)$ can be written as

$$\Pi_{\varepsilon, \varepsilon-\omega}(\mathbf{q}, \mathbf{q}_1) = \frac{\pi\nu\tau}{2} (2\pi)^3 \delta(\mathbf{q}-\mathbf{q}_1) \operatorname{Re} \frac{\zeta(\mathbf{q}, \omega)}{1 - \zeta(\mathbf{q}, \omega)}. \quad (3.4.12)$$

As a result we obtain

$$\frac{1}{\tau_{ee}(\varepsilon)} = \frac{1}{v} \int_0^{\varepsilon} d\omega \int_0^{\omega} \frac{d\varepsilon'}{\pi} \int (dq) |V(\mathbf{q}, \omega)|^2 \left[\operatorname{Re} \frac{v\tau\zeta(\mathbf{q}, \omega)}{1-\zeta(\mathbf{q}, \omega)} \right]^2. \quad (3.4.13)$$

To generalize Eq. (3.4.13) to the case of an arbitrary dimensionality, it is sufficient to replace v by v_d , where v_d is the density of states in a sample, effective dimensionality of which equals d :

$$v_3 = v, \quad v_d = va^{3-d}.$$

In two dimensions $v_2 = m/\pi$.

The quantity $\zeta(\mathbf{q}, \omega)$ also depends on dimensionality. In quasi-one, quasi-two and three dimensions

$$\zeta(\mathbf{q}, \omega) = \frac{i}{2ql} \ln \frac{1-i(|\omega|\tau+ql)}{1-i(|\omega|\tau-ql)},$$

and in two dimensions

$$\zeta(\mathbf{q}, \omega) = \frac{1}{V(1-i|\omega|\tau)^2 + (ql)^2},$$

At $\omega\tau \ll 1$ and $ql \ll 1$, $\zeta(\mathbf{q}, \omega)$ has the form

$$\zeta(\mathbf{q}, \omega) = 1 + i|\omega|\tau - D\mathbf{q}^2\tau,$$

where

$$D(\mathbf{q}, \omega) = \frac{1}{[-i|\omega| + D\mathbf{q}^2]\tau}. \quad (3.4.11a)$$

In quasi-one, quasi-two and three dimensions the diffusion coefficient $D = \frac{1}{3}v_F^2\tau$ and in two dimensions $D = v_F^2\tau/2$.

The potential $V(\mathbf{q}, \omega)$ can be represented as

$$V(\mathbf{q}, \omega) = \frac{V_0(\mathbf{q})}{1 + V_0(\mathbf{q})\Pi(\mathbf{q}, \omega)}, \quad (3.4.14)$$

where $\Pi(\mathbf{q}, \omega)$ is the polarization operator. In the limit of small ω and \mathbf{q} it has a usual form

$$\Pi(\mathbf{q}, \omega) = v_d \frac{D\mathbf{q}^2}{-i\omega + D\mathbf{q}^2}. \quad (3.4.15)$$

In three dimensions $V_0(\mathbf{q}) = 4\pi e^2/q^2$. In low dimensions $V_0(\mathbf{q})$ is the Fourier transform of the Coulomb potential e^2/r , corresponding to the interaction of particles either in a plane (two-dimensional case), or on a line (one-dimensional case). Therefore at $d = 2$

$$V_0(q) = \int \frac{dq_x}{2\pi} \frac{4\pi e^2}{q^2 + q_x^2} = \frac{2\pi e^2}{|\mathbf{q}|}, \quad (3.4.16)$$

and at $d = 1$

$$V_0(q) = \int \frac{dq_x dq_y}{(2\pi)^2} \frac{4\pi e^2}{q^2 + q_x^2 + q_y^2} = e^2 \ln \frac{1}{q^2 a^2}. \quad (3.4.17)$$

Equations (3.4.16) and (3.4.17) are also valid in quasi-two and quasi-one dimensions, as we are interested in interactions at distances of order L_e much larger than a , where a is the sample transverse dimension. Therefore the logarithmically divergent integral in (3.4.17) can be cut off at the upper limit at $q \sim 1/a$. Using (3.4.14)-(3.4.17), we obtain the following expressions for the potential:

$$d=3, \quad V(q, \omega) = \frac{4\pi e^2}{q^2 + \frac{Dq^2}{-i\omega + Dq^2} \kappa_3^2}, \quad (3.4.18)$$

$$d=2, \quad V(q, \omega) = \frac{2\pi e^2}{|q| + \kappa_2 \frac{Dq^2}{-i\omega + Dq^2}}, \quad (3.4.19)$$

$$d=1, \quad V(q, \omega) = \frac{e^2}{e^2 v_1 \frac{Dq^2}{-i\omega + Dq^2} - \ln^{-1} q^2 a^2}, \quad (3.4.20)$$

where $\kappa_3^2 = \kappa^2 = 4\pi e^2 v_3$ and $\kappa_2 = 2\pi e^2 v_2$.

In three dimensions, substituting (3.4.12) and (3.4.18) into (3.4.13), we find

$$\frac{1}{\tau_{ee}^{(3)}(\varepsilon)} = \frac{\kappa^4}{2\pi^3 v} \int_0^{\varepsilon} \omega d\omega \int_0^{\infty} \frac{q^2 dq}{|-i\omega + D(q^2 + \kappa^2)|^2} \frac{D^2}{\omega^2 + D^2 q^4}. \quad (3.4.21)$$

In (3.4.21) essential q 's are of order $\sqrt{\omega/D}$, hence at $\omega \ll D\kappa^2 = \omega_p^2$ we can ignore Dq^2 and ω in comparison with $D\kappa^2$. Finally

$$\frac{1}{\tau_{ee}^{(3)}} = \frac{1}{6\sqrt{2}\pi^2 v L_e^3} \sim \varepsilon^{3/2}. \quad (3.4.22)$$

In quasi-two dimensions

$$\frac{1}{\tau_{ee}^{(2)}} = \frac{1}{8\pi^2 v_2 L_e^2} \sim \frac{\varepsilon}{a}, \quad (3.4.23)$$

and in quasi-one dimension

$$\frac{1}{\tau_{ee}^{(1)}} = \frac{1}{4\sqrt{2}\pi^3 v_1 L_e} \sim \frac{\sqrt{\varepsilon}}{a^2}. \quad (3.4.24)$$

Note that in the expression (3.4.13) for $\tau_{ee}^{-1}(\varepsilon)$, besides the considered contribution from the range of small transferred momenta, there is a contribution from large transferred momenta. This contribu-

tion has a usual form [4]

$$\frac{1}{\tau_{ee}} = \frac{\pi^2}{64} \frac{\kappa}{p_F} \frac{\varepsilon^2}{\mu}. \quad (3.4.25)$$

Comparing (3.4.22) and (3.4.25), we see that in three dimensions the relation $\tau_{ee}^{-1} \sim \varepsilon^{-3/2}$ is valid at

$$\varepsilon \ll \frac{1}{\tau} \frac{p_F}{\kappa} \frac{1}{(p_F l)^2}.$$

As seen from the expressions for $1/\tau_{ee}$ in different dimensions, they do not contain the Debye screening length and, consequently, the electron charge, since $4\pi e^2 v / \kappa^2 = 1$. This follows from the approximation of weakly non-ideal gas with the Coulomb interaction,

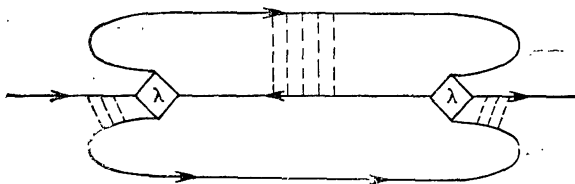


Fig. 3.6.

when $\kappa \ll p_F$. If this approximation is not valid, then the higher-order perturbation theory in electron-electron interaction gives only renormalization of the effective dimensionless scattering amplitude λ . As a result, the right-hand sides of Eqs. (3.4.22)-(3.4.24) will contain λ^2 (Fig. 3.6). The fact is that the scattering amplitude renormalization, which is necessary to perform when the weakly non-ideal gas approximation does not work, is determined by large transferred momenta, while diffusion poles and, consequently, the energy dependence of $1/\tau_{ee}$ are connected with small transferred momenta. Taking this into account, Eqs. (3.4.22)-(3.4.24) hold also in the case, typical of real metals, when κ and p_F are of the same order.

However, besides the singularity in the particle-hole channel, leading to diffusion poles in the expression for the energy relaxation time, there is a singularity in the particle-particle channel, leading to the cooperon.

By the method [20] analogous to that used above to separate the contributions connected with diffusion poles, it is possible to obtain the following expression for the electron-electron relaxation rate connected with the Cooper poles (Fig. 3.7):

$$\frac{1}{\tau_{ee}^c(\varepsilon)} = \frac{4\pi}{v_d} \tau^2 \int_{\varepsilon}^{2\varepsilon} \frac{d\omega}{2\pi} \int_{\omega-2\varepsilon}^{2\varepsilon} \frac{d\omega'}{2\pi} \int (dQ) |\lambda_Q^c(2\varepsilon - \omega)|^2 \times \text{Re } C_\omega(Q) \text{Re } C_{\omega'}(Q), \quad (3.4.26)$$

where $\lambda_Q^c(2\varepsilon - \omega)$ is the electron-electron scattering constant at a small total momentum. The quantity $\lambda_Q^c(2\varepsilon - \omega)$ is defined by the equation shown in Fig. 3.8, the solution of which at $T = 0$ has the form

$$\lambda_Q^c(2\varepsilon - \omega) = \frac{1}{\lambda_0^{-1} - \ln \frac{DQ^2 - i|2\varepsilon - \omega|}{\varepsilon_0}}, \quad (3.4.27)$$

where ε_0 is a cut-off parameter. If the interaction between electrons is the Coulomb repulsion, then $\varepsilon_0 \cong \mu$ and $\lambda_0 > 0$. If, however, the interaction at a small total momentum is determined by the phonon exchange, then $\varepsilon_0 = 2\omega_D$ (see, for example, [4]), and the bare dimen-

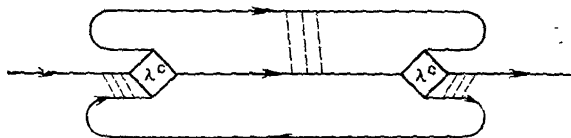


Fig. 3.7.

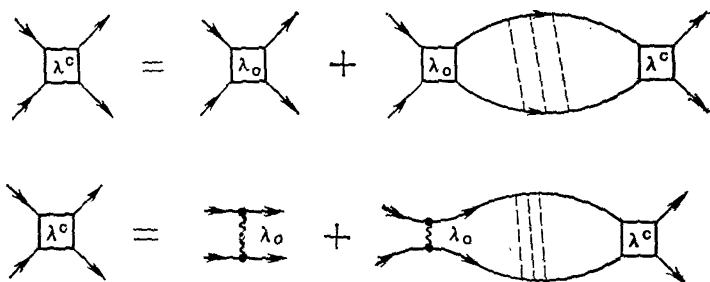


Fig. 3.8.

sionless interaction constant $\lambda_0 < 0$. In this case Eq. (3.4.27) has a pole corresponding to instability towards the transition into superconducting state. We restrict ourselves to the case $T \gg T_c$. It is seen from Eq. (3.4.27) that at $\lambda_0 > 0$, $Q = 0$, and $(2\varepsilon - \omega) \rightarrow 0$, $\lambda^c \rightarrow 0$ [22]

$$C_\omega(Q) = \frac{1}{(-i\omega + DQ^2)\tau}. \quad (3.4.28)$$

Substituting the expression for $C_\omega(Q)$ and the interaction constants into (3.4.26), and integrating over Q , ω and ω' , we find that at $\varepsilon \gg T$

$$\frac{1}{\tau_{ee}^c} \simeq \frac{|\lambda_0|^2}{\left|1 + \lambda_0 \ln \frac{\varepsilon_0}{\varepsilon}\right|^2} \frac{1}{\tau_{ee}(\varepsilon)} \quad (3.4.29)$$

to a logarithmic accuracy. The total decay time of one-particle states is the sum of two contributions, related to the interaction in the diffusion and Cooper channels. If we take into account only the Coulomb interaction, then λ_0^c is small in the non-ideality parameter of the electron gas. Therefore $1/\tau_{ee}^c$ is much smaller than $1/\tau_{ee}$.

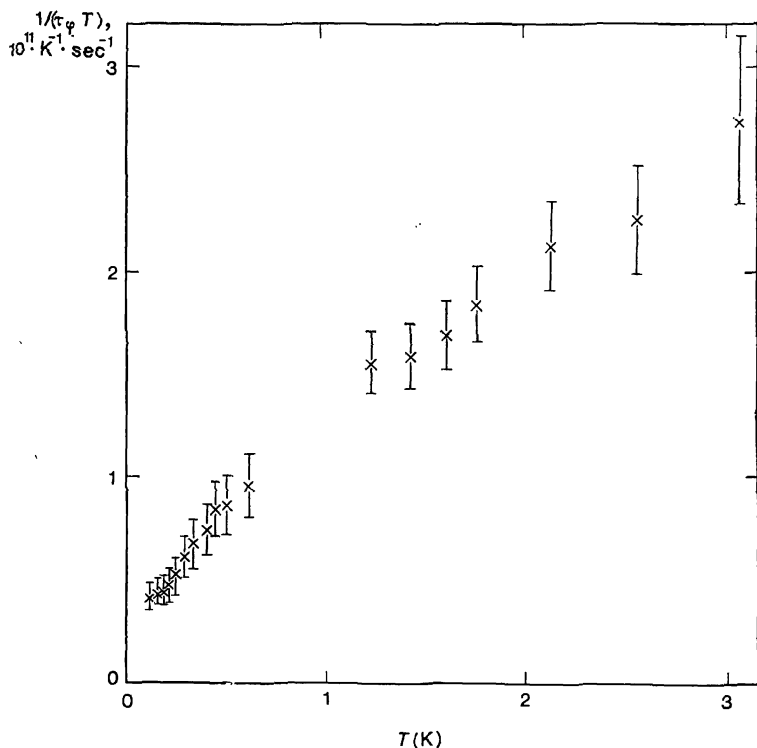


Fig. 3.9. $1/T\tau_\phi$ versus T . Solid line shows the validity of Eq. (3.4.30) [23].

In real metals, however, they are of the same order. Moreover, the contribution connected with the cooperon strongly depends on magnetic field (see Sec.3.7). The electron-electron collision time in strongly inelastic scattering coincides with the phase relaxation time τ_ϕ , which determines the temperature dependence of the quantum localization corrections to the conductivity considered in Sec. 3.2. This very time determines also the magnitude and temperature dependence of anomalous negative magnetoresistance (Sec. 3.7). Hence, investigating the temperature dependence of negative magnetoresistance, we can obtain the temperature dependence of the phase breaking time τ_ϕ . Such an investigation has been carried out in the temperature

range from 0.1 to 3 K [23] and it has been shown that at $d = 2$, τ_ϕ is described by the expression (Fig. 3.9)

$$\frac{1}{\tau_\phi} = A_1 T + A_2 T^2, \quad (3.4.30)$$

where $A_1 = (3.6 \pm 0.6) \times 10^{10} \text{ K}^{-1} \text{ sec}^{-1}$ and $A_2 = (8.6 \pm 1.3) \times 10^{10} \text{ K}^{-2} \text{ sec}^{-1}$. The second term in (3.4.30) is the usual electron-electron relaxation time, and the first term is evidently connected with the mechanism of the electron-electron relaxation in strongly inelastic electron scattering by impurities, described above. However, comparing the theory with experiment, we must remember that the time of phase breaking due to the Nyquist noise has the same temperature dependence and even the same (to an accuracy of a factor) magnitude [see Eq. (3.3.30)]. Therefore the first term in (3.4.30) seems to be the total phase breaking time $1/\tau_{ee} + 1/\tau_N$. According to Uren *et al.* [23], in these experiments $p_{Fl} \simeq 4$, which gives together with (3.4.23) and (3.3.30) $A_1 \simeq 10^{10} \text{ K}^{-1} \text{ sec}^{-1}$. This value is in good agreement with experiment.

3.4.2 Effects of Electron-Electron Correlations on the Density of One-Particle States

The account for electron-electron correlations in the Fermi-liquid theory, although leading to strong renormalization of the density of states, leaves it a smooth function of energy at the Fermi level.

As noted above, in disordered metallic systems the properties of excitations with energies small in comparison with the inverse mean free time differ from those predicted by the Fermi-liquid theory, the validity of which is based upon the spatial homogeneity of a system. If a system is not homogeneous, the energy dependence of the density of states near the Fermi level also changes.

It has been shown by Shklovskii and Efros [24] that the account for the long range Coulomb repulsion, when all electrons are localized, leads to the density of excitation states vanishing at the Fermi level, i.e. to a so-called Coulomb gap. We shall show that the density of delocalized electron states also has a singularity at the Fermi level, electron-electron interactions taken into account.

One-electron density of states may be written as

$$\begin{aligned} \nu_d(\varepsilon) &= -\frac{2}{\pi} \int (dp) \text{Im} \tilde{G}^{(R)}(\mathbf{p}, \varepsilon) \\ &= -\frac{2}{\pi} \int (dp) \text{Im} \tilde{G}(\mathbf{p}, i\varepsilon_n \rightarrow \varepsilon), \end{aligned} \quad (3.4.31)$$

where $\tilde{G}^{(R)}$ and \tilde{G} are retarded and the Matsubara electron Green functions respectively [4] averaged over the impurity potential; a

wavy line means that electron-electron correlations are accounted for.

$$\begin{aligned}\tilde{G}(\mathbf{p}, i\varepsilon_n) &= \left[-i\varepsilon_n - \xi_{\mathbf{p}} - \frac{i}{2\tau} \operatorname{sgn} \varepsilon_n - \Sigma_{ee}(\mathbf{p}, i\varepsilon_n) \right]^{-1} \\ &= [G^{-1}(\mathbf{p}, i\varepsilon_n) - \Sigma_{ee}(\mathbf{p}, i\varepsilon_n)]^{-1}.\end{aligned}\quad (3.4.32)$$

Here $\Sigma_{ee}(\mathbf{p}, i\varepsilon_n)$ is the proper energy part associated with the electron-electron interaction. The energy dependence of the density of states arises due to the interference of the electron-electron interaction and multiple impurity scattering. It means that even if the

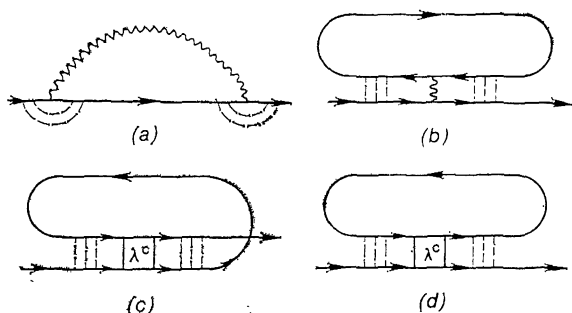


Fig. 3.10.

electron-electron interaction is considered to a first order of perturbation theory, it is necessary to account for all singularities in two-particle Green functions (diffusion and Cooper poles).

The diagrams for the calculation of Σ_{ee} by the lowest order perturbation theory in the electron-electron interaction are shown in Fig. 3.10. If the non-ideality parameter of the electron gas is small, $\kappa^2/p_F^2 \ll 1$, the contribution of the graph shown in Fig. 3.10a is much larger than the contribution of the graphs b, c, and d, since only in this graph the electron interaction at distances up to the Debye radius is essential. In other graphs essential distances are much smaller, being of the order of the electron wavelength.

The expression for $\Sigma_{ee}(\mathbf{p}, i\varepsilon_n)$ shown in Fig. 3.10a at $ql \ll 1$ and $\omega_m \tau \ll 1$ has the form

$$\begin{aligned}\Sigma_{ee}(\mathbf{p}, i\varepsilon_n) &= T \sum_{\omega_m} \int (dq) G(\mathbf{p}, i\varepsilon_n - i\omega_m) \frac{V(\mathbf{q}, i\omega_m)}{(|\omega_m| + D\mathbf{q}^2)^2 \tau^2} \\ &\times [\theta(\varepsilon_n) \theta(\omega_m - \varepsilon_n) + \theta(-\varepsilon_n) \theta(\varepsilon_n - \omega_m)],\end{aligned}\quad (3.4.33)$$

where $\omega_m = 2\pi mT$, $\varepsilon_n = \pi T(2n + 1)$ are the Matsubara energies. The first-order perturbation theory in the electron-electron interaction gives the following expression for the density of states:

$$\nu_d(\varepsilon) = \nu_d - \frac{2}{\pi} \int (dp) \operatorname{Im} [G^2(\mathbf{p}, i\varepsilon_n \rightarrow \varepsilon) \Sigma_{ee}(\mathbf{p}, i\varepsilon_n \rightarrow \varepsilon)], \quad (3.4.34)$$

where

$$v_d = -\frac{2}{\pi} \int (dp) \frac{1}{\varepsilon - \xi_p - \frac{i}{2\tau}} \quad (3.4.35)$$

is the density of states of noninteracting electrons.

Substituting (3.4.34) into (3.4.35), we continue analytically the obtained expression to real values of ε . Integration over p yields

$$\begin{aligned} \delta v(\varepsilon, T) &= v(\varepsilon, T) - v(0, 0) = \text{Im} \int_0^\infty \frac{d\omega}{2\pi} \int \frac{d^3q}{(2\pi)^3} V(\mathbf{q}, \omega) v \\ &\times \frac{2 - \tanh \frac{\varepsilon + \omega}{2T} - \tanh \frac{\omega - \varepsilon}{2T}}{(-i\omega + Dq^2)^2}. \end{aligned} \quad (3.4.36)$$

For $d = 1, 2$

$$\begin{aligned} \delta v_d &= v_d(\varepsilon, T) - v_d = -\text{Im} \int_0^\infty \frac{d\omega}{2\pi} \int (dq) V(\mathbf{q}, \omega) \\ &\times v_d \frac{\tanh \frac{\omega + \varepsilon}{2T} + \tanh \frac{\omega - \varepsilon}{2T}}{(-i\omega + Dq^2)^2}. \end{aligned} \quad (3.4.36a)$$

Here $v(0, 0)$ is the density of states at the Fermi level at $T = 0$, the interactions taken into account. We have performed subtraction in (3.4.36), as the correction to the density of states related to the interaction diverges at the upper limit of the integral over ω . If $d = 1, 2$, this subtraction is superfluous.

In Eqs. (3.4.36) and (3.4.36a) essential ω 's and q 's are of order $\max(\varepsilon, T) \ll \tau^{-1}$ and $\sqrt{\omega/D} \ll l^{-1}$, respectively. Therefore for $\xi(\mathbf{q}, \omega)$ we have used the expression (3.4.12) in the limit of small ω and \mathbf{q} . For the screened Coulomb potential $V(\mathbf{q}, \omega)$ we must use Eqs. (3.4.18)-(3.4.20) valid in this limit.

In three dimensions integration over q in (3.4.36) gives

$$\begin{aligned} \delta v(\varepsilon, T) &= \frac{4\pi e^2 v_0}{\kappa^2} \cdot \frac{1}{8\sqrt{2}\pi^2 D^{3/2}} \int_0^\infty \frac{d\omega}{V\omega} \\ &\times \left[2 - \tanh \frac{\varepsilon + \omega}{2T} - \tanh \frac{\omega - \varepsilon}{2T} \right]. \end{aligned} \quad (3.4.37)$$

Since $4\pi e^2 v_0 / \kappa^2 = 1$, we obtain from (3.4.37) at $T = 0$

$$\delta v(\varepsilon) = \frac{\sqrt{|\varepsilon|}}{2\sqrt{2}\pi^2 D^{3/2}} = \frac{1}{2\sqrt{2}\pi^2 |\varepsilon| L_E^3}. \quad (3.4.38)$$

At finite temperatures the singularity at $\varepsilon \rightarrow 0$ is smoothed out:

$$\delta v(\varepsilon, T) = \frac{1}{2\sqrt{2}\pi^2} \frac{\sqrt{T}}{D^{3/2}} f\left(\frac{\varepsilon}{T}\right), \quad (3.4.39)$$

$$f(x) = \int_0^\infty \frac{dy}{4\sqrt{y}} \left[2 - \tanh \frac{x+y}{2} - \tanh \frac{y-x}{2} \right].$$

At $|x| \gg 1$ the function $f(x)$ equals $\sqrt{|x|}$, and at $x \rightarrow 0$ $f(x) = c + O(x^2)$,

$$c = \sqrt{\pi} (1 - \sqrt{2}) \zeta\left(\frac{1}{2}\right) \cong 1.07, \quad (3.4.40)$$

where $\zeta(y)$ is the Riemann ζ function.

Note that the law $\delta v(\varepsilon) \sim \sqrt{\varepsilon}/D^{3/2}$ does not depend on the details of the interaction. The same relation between the correction to the density of states and energy is obtained also in the case when the electron-electron interaction is short-range. Moreover, the relation $\delta v(\varepsilon) \sim \sqrt{\varepsilon}/D^{3/2}$ always holds in three dimensions, if electrons are localized ($D \neq 0$).

As seen from (3.4.38), in the weakly non-ideal electron gas approximation this correction does not even depend on the electron charge. Thus, in disordered metallic systems the density of states has a minimum at the Fermi level.

In two dimensions the density of states also has a minimum, but of a logarithmic character. Inserting the expression (3.4.19) for $V(\mathbf{q}, \omega)$ into Eq. (3.4.36) and taking into account that $q \ll \kappa_2$, we obtain at $T = 0$

$$\delta v_2(\varepsilon) = \text{Im} \int_{\varepsilon}^{\infty} \frac{d\omega}{\pi} \int (dq) \frac{\kappa_2}{|q|(-i\omega + D|q|\kappa_2)(-i\omega + Dq^2)}. \quad (3.4.41)$$

Integration over \mathbf{q} yields

$$\delta v_2(\varepsilon) = -\frac{1}{4\pi^2 D} \int_{\varepsilon}^{\infty} \frac{d\omega}{\omega} \ln \frac{\omega}{D\kappa_2^2}. \quad (3.4.42)$$

The upper limit in (3.4.42) is $1/\tau$, as the diffusion approximation used in (3.4.41) is valid only at $\omega\tau \ll 1$. Finally [27],

$$\delta v_2(\varepsilon) = \frac{1}{8\pi^2 D} \ln \frac{\varepsilon}{D^2 \kappa_2^2 \tau} \ln \varepsilon \tau. \quad (3.4.43)$$

The first logarithm in (3.4.43) is connected with the long range character of the Coulomb interaction. The fact is that, screening taken into account, at fixed ω and $q \rightarrow 0$, $V(\mathbf{q}, \omega) \rightarrow \infty$ [see Eq. (3.4.19)]. At $q \ll \omega/D\kappa_2$, $V(\mathbf{q}, \omega) \sim q^{-1}$ and at $\omega/D\kappa_2 \ll q \ll \sqrt{\omega/D}$, $V \sim 1/q^2$, therefore integration over this region in (3.4.41) gives the

first logarithm. By analogy with three-dimensional case, the second logarithm in (3.4.43) does not depend on the character of the electron-electron interaction and is again connected only with the fact that electrons are delocalized.

If the interaction potential λ has short range,

$$\delta v_d = \begin{cases} C_d \frac{\lambda}{\varepsilon L_e^d}, & d=1, 3, \\ \frac{\lambda}{4\pi^2 D} \ln \varepsilon \tau, & d=2, \end{cases} \quad (3.4.44)$$

where $C_3 = 1/4\sqrt{2}\pi^2$ and $C_1 = -1/\pi\sqrt{2}$.

The fact that nonvanishing corrections to the density of states exist even for a short-range interaction potential means that corresponding corrections should also arise from the Hartree term shown in Fig. 3.10b. In the absence of impurities the Hartree term is cancelled with the positive background. However, in the presence of impurities the electronic density $n(\mathbf{r})$ is inhomogeneous, so that an additional particle with a wave function $\psi_\alpha(\mathbf{r})$ leads to the interaction of the density-density type, $\psi_\alpha^*(\mathbf{r})\psi_\alpha(\mathbf{r})[n(\mathbf{r}) - \overline{n(\mathbf{r})}]$, where $\overline{n(\mathbf{r})}$ is the mean electronic density. In averaging over random impurity configuration this quantity does not factorize. As a result, the graph in Fig. 3.10b for the proper energy appears. In contrast with the exchange graph (Fig. 3.10a), the Hartree term contains the interaction potential with the momentum transfer of order p_F . Hence, as shown above, this term is small in the parameter κ^2/p_F^2 . Indeed, the Hartree term contains the potential $\bar{V}(\mathbf{k}, 0)$. Due to the fact that $k \sim p_F$, the interaction potential is effectively short-range, but depends on the angle between the incident and scattered particle momenta \mathbf{p} and \mathbf{p}' . Therefore the Hartree term contribution to the density of states is described by the expression (3.4.44) with $\lambda = -2F$, where

$$F = \frac{\overline{V(\mathbf{p}-\mathbf{p}', 0)}}{\overline{V(0, 0)}} \quad (3.4.45)$$

Here the bar means averaging over the Fermi surface and a factor 2 arises due to electrons with both spin directions, contributing to the Hartree energy. As usual, the Hartree and exchange terms have opposite signs (Fig. 3.10a). In two dimensions [27]

$$F = \int_0^{2\pi} \frac{d\theta}{2\pi} \frac{1}{1 + \frac{2p_F}{\kappa_2} \sin \frac{\theta}{2}} = \frac{1}{\pi} \frac{1}{\sqrt{\frac{4p_F^2}{\kappa_2^2} - 1}} \ln \frac{\frac{2p_F}{\kappa_2} + \sqrt{\frac{4p_F^2}{\kappa_2^2} - 1}}{\frac{2p_F}{\kappa_2} - \sqrt{\frac{4p_F^2}{\kappa_2^2} - 1}}, \quad (3.4.46)$$

and in three dimensions [28]

$$F = \frac{\kappa^2}{4p_F^2} \ln \left(1 + \frac{4p_F^2}{\kappa^2} \right). \quad (3.4.47)$$

Note that in quasi-one and quasi-two dimensions, when the film thickness is large in comparison with the Debye length, F is given by (3.4.47).

When $\kappa/2p_F$ is of order unity, we must allow for next orders of the perturbation theory in the Coulomb interaction. Then, for example, the contribution of the graph shown in Fig. 3.11 is small in comparison with the Hartree term only in the parameter κ/p_F . For the

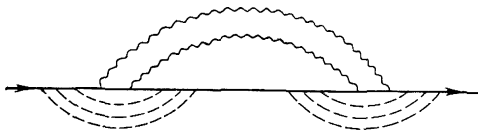


Fig. 3.11.

majority of metals this condition is not satisfied. Moreover, the matrix element of the interaction potential at small distances can strongly differ from that calculated between the states described by plane waves. As a result, the state density corrections are given by (3.4.44) with the effective electron-electron coupling constant λ . The expressions obtained for F have sense only for degenerate semiconductors and good metals.

In the case of a short-range potential (when the potential radius is shorter than the wavelength), the Hartree corrections to the density of states are two times larger than the exchange corrections, arising due to spin degeneracy, and have opposite sign. Therefore the total correction to the density of states in this case differs from (3.4.44) in sign.

The changes brought about by high orders of the perturbation theory in the electron-electron interaction are small not in the electron-electron coupling constant λ , but in the parameter

$$\alpha_d = \frac{\delta v_d}{v_d} = \begin{cases} \frac{\lambda}{(p_F l)^{d/2}} \frac{1}{(p_F a)^{3-d}} \left(\frac{\varepsilon}{\mu} \right)^{(d-2)/2} & \text{at } d \neq 2, \\ \frac{\lambda}{p_F^2 l a} \ln \frac{1}{\varepsilon \tau} & \text{at } d = 2. \end{cases} \quad (3.4.48)$$

Note that in three dimensions the theory is valid even when $p_F l \lesssim 1$ (at sufficiently small ε , if electrons are delocalized).

As in quasi-one dimension the localization length $L_c^{(1)} \sim l (p_F a)^2$, the perturbation theory parameter has the form

$$\alpha_1 = \lambda \frac{L_e}{L_c^{(1)}} \ll 1. \quad (3.4.49)$$

In quasi-two dimensions

$$L_c^{(2)} \sim l \exp(p_F^2 a l),$$

and

$$\alpha_2 = \lambda \frac{\ln L_e / l}{\ln L_c^{(2)} / l} \ll 1. \quad (3.4.50)$$

As seen from (3.4.49) and (3.4.50), at $\lambda \sim 1$ the perturbation theory is valid when an electron in the time $1/\varepsilon$ covers a distance less than the localization length ($L_e \ll L_{loc}$).

The contribution of interactions in the Cooper channel (Fig. 3.10c,d) to the density of states needs a special consideration. In the Cooper channel the lowest-order perturbation theory does not work, and we have to sum up ladder graphs (Fig. 3.8). As a result, instead of $V(q, \omega)$ in the expression (3.4.36) for the density of states, we obtain $\lambda^c (2\varepsilon - \omega)$, given at $T = 0$ by (3.4.27). Integrating over ω and Q in (3.4.36) ($d = 3$) and in (3.4.36a) ($d = 1$) to a logarithmic accuracy, we can factor out λ^c , assuming that

$$\lambda^c = \frac{\lambda_0}{1 + \lambda_0 \ln \frac{\varepsilon_0}{\max(\varepsilon, T)}}. \quad (3.4.51)$$

Therefore the corrections to the density of states in three and one dimensions, arising from the interaction in the Cooper channel, are given by Eq. (3.4.44), where λ is replaced by λ^c .

In two dimensions we should not ignore the ω and Q dependence of λ^c , since at $d = 2$ the integral over ω in (3.4.36a) is logarithmic and the main contribution comes from the region $\omega \gg \varepsilon, T$. As a result, the correction to the density of states, arising due to the interaction in the Cooper channel, is

$$\delta v_2^c = \frac{1}{8\pi D} \ln \frac{1 + \lambda_0 \ln \varepsilon_0 \tau}{1 + \lambda_0 \ln \frac{\varepsilon_0}{\max(\varepsilon, T)}}.$$

It is well known that current-voltage characteristics of tunnelling junctions have so-called zero-bias anomalies [29]. These anomalies exist as minima and maxima of the tunnelling conductivity. The conductivity maximum can be explained by tunnelling followed by the electron scattering by magnetic impurities [30], but this mechanism cannot account for the conductivity minimum. The theory exposed above gives a general explanation of the tunnelling anom-

alies arising due to singularities in the density of states at the Fermi surface associated with interactions in impure metals [25].

Consider for simplicity a symmetric tunnelling junction, comprising two similar metals or degenerate semiconductors with a potential barrier U between them. If a voltage V is applied to the junction, the tunnelling current has the form

$$I = -\pi^2 e \int W(\varepsilon) v\left(\varepsilon - \frac{eV}{2}\right) v\left(\varepsilon + \frac{eV}{2}\right) \left[n_F\left(\varepsilon + \frac{eV}{2}\right) - n_F\left(\varepsilon - \frac{eV}{2}\right) \right] \frac{d\varepsilon}{2\pi}, \quad (3.4.52)$$

where $W(\varepsilon)$ is the probability of tunnelling of an electron of energy ε . If $v(\varepsilon)$ and $W(\varepsilon)$ are smooth functions at $\varepsilon = 0$, the tunnelling junction conductivity takes on the form

$$\sigma = \frac{dI}{dV} = \sigma_0 (1 + \alpha V^2), \quad (3.4.53)$$

where

$$\sigma_0 = \frac{\pi e^2}{2} W(0) v^2(0), \quad \alpha \sim \max\{U^{-2}, \mu^{-2}\}.$$

The correction to the tunnelling current, arising due to the changes in the density of states, is given by

$$\delta I = -e\pi^2 W(0) v \int \frac{d\varepsilon}{2\pi} \delta v(\varepsilon, T) \left[\tanh \frac{2\varepsilon - eV}{4T} - \tanh \frac{2\varepsilon + eV}{4T} \right]. \quad (3.4.54)$$

Substituting the expression (3.4.44) for $\delta v(\varepsilon, T)$ in three dimensions into (3.4.54), we obtain

$$\frac{\delta\sigma}{\sigma_0} = \frac{\lambda}{2\sqrt{2}\pi^2} \frac{\sqrt{T}}{vD^{3/2}} f_1\left(\frac{eV}{2T}\right), \quad (3.4.55)$$

where

$$f_1(x) = \int_0^\infty dy f(y) \left[\cosh^{-2} \frac{x-y}{2} + \cosh^{-2} \frac{x+y}{2} \right], \quad (3.4.56)$$

and $f(y)$ is defined by (3.4.39). In the limit as $x \rightarrow \infty$, $f_1(x) = \sqrt{x}$ and at $x \ll 1$

$$f_1(x) = c_1 + O(x^2), \quad c_1 = -4\sqrt{\pi}\zeta\left(\frac{1}{2}\right) \approx 10.35.$$

As has already been mentioned, there is a large amount of experimental data on the tunnelling anomalies.

The theory set forth in this review has been used by Altshuler and Aronov [25] to explain voltage dependence of tunnelling resistance, observed in the junctions Al-I-Au [31]. In [32, 33] the tunnelling

anomalies versus resistivity of the film forming the junction have been investigated. Dynes and Garno [32] have examined the tunnelling anomalies in the Al-I-granular Al film junctions versus the resistance of Al films. The \sqrt{V} dependence of the tunnelling conductivity is plotted in Fig. 3.12. It is seen that at large voltages the tunnelling conductivity versus applied voltage relation fits the \sqrt{V}

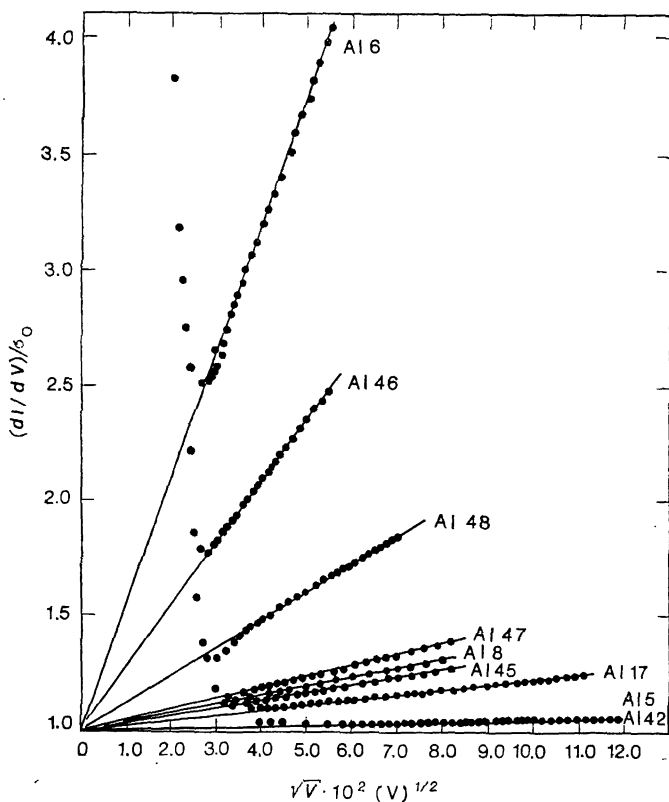


Fig. 3.12. Normalized tunnelling conductivity versus \sqrt{V} for granular aluminium films. At low voltages there is a singularity connected with the superconducting gap [32].

dependence in accordance with (3.4.55). (At small voltages there is a singularity related to the superconducting gap; this singularity is not connected with the problem in question.) The slope of these curves increases with resistance, which corresponds to deepening of the minimum in the density of states. As seen from Fig. 3.12, the root singularity in the density of states exists also at $p_F l < 1$ (the

point $p_F l \sim 1$ corresponds to the Al47, Al8 samples). If the expression (3.4.55) is represented in the form

$$\frac{\delta\sigma}{\sigma_0} = \sqrt{\frac{\bar{V}}{\Delta}}$$

at $T = 0$, then, according to (3.4.55), $\Delta \sim D^3 \sim \rho^3$. The Δ versus film resistivity ρ relation is plotted in Fig. 3.13. According to [32],

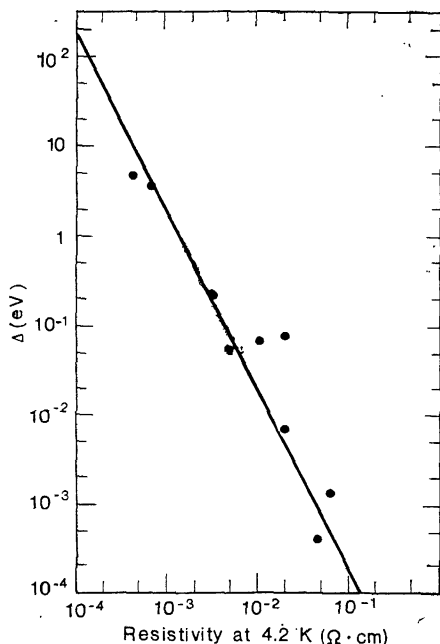


Fig. 3.13. Δ versus resistivity for Al films. The slope of a straight line equals -2 [32].

experimental data fit rather the curve $\Delta \sim \rho^{-2}$, than the curve $\Delta \sim \rho^{-3}$.

McMillan and Mochel [33] have examined the tunnelling anomalies in the Al-I-amorphous $\text{Ge}_{1-x}\text{Au}_x$ junctions. They have observed the anomalies of the tunnelling conductivity in samples with different Au concentration ($x = 0.08$ to 0.2). At $x \simeq 0.12$ the metal-insulator transition has been found. Figure 3.14 shows the relation between the tunnelling conductivity and the junction voltage at different x . In the metallic region the minimum in the density of states deepens in the vicinity of the transition point, and at the transition point the density of states at the Fermi level vanishes, having a linear dependence on energy above the Fermi level. The authors suppose

this to be a critical behavior of the density of states at the transition point. In the insulator phase an energy gap (or pseudo-gap) appears.

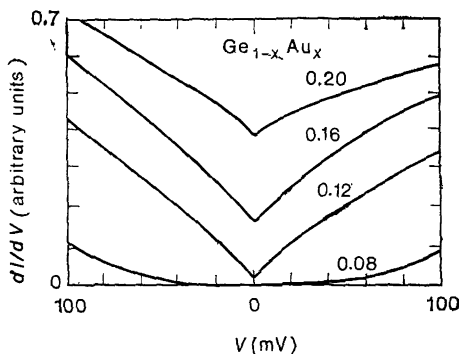


Fig. 3.14. Conductivity of a tunnelling junction with a $\text{Ge}_{1-x}\text{Au}_x$ electrode as a function of voltage for different Au concentrations [33].

In the metallic phase at $x = 0.2$ experimental data fit the relation $\delta v/v \sim \varepsilon^{0.6}$. We see that the exponent value is close to 0.5—the value predicted by the theory [see (3.4.44)] [25].

3.4.3 Conductivity of Interacting Electrons

It has been shown in Sec. 3.4.2 that the electron-electron correlations lead to energy and temperature dependence of the density of one-particle states near the Fermi level. The conductivity is related to the density of states by the Einstein relation $\sigma = e^2 v D$. We therefore may expect that these correlations lead also to non-trivial conductivity versus temperature and frequency relations [25, 26].

At a small ratio κ/p_F the main contribution to the state density correction comes, as shown above, from the exchange interaction between electrons (see Fig. 3.15). Consider first the temperature dependence of the conductivity, arising due to the exchange interaction given by Eq. (3.A.36):

$$\delta\sigma(T) = -\frac{\sigma}{\pi d} \int_{-\infty}^{\infty} d\omega \frac{\partial}{\partial\omega} \left(\omega \coth \frac{\omega}{2T} \right) \int (dq) \frac{V(\mathbf{q}, \omega) D\mathbf{q}^2}{(-i\omega + D\mathbf{q}^2)^3}.$$

The integral over q in this expression differs from the corresponding integral, which enters Eq. (3.4.36) in a factor $D\mathbf{q}^2/(-i\omega + D\mathbf{q}^2)$.

According to Eqs. (3.4.18)-(3.4.20), at $q \ll \kappa$ and $q \sim \sqrt{\frac{\omega}{D}}$

$$\frac{Dq^2}{-i\omega + Dq^2} V(\mathbf{q}, \omega) = \frac{1}{v_d}, \quad (3.4.57)$$

and at $q \ll \sqrt{\omega/D}$ this product vanishes as $\mathbf{q} \rightarrow 0$. Hence the conductivity correction in one and two dimensions does not contain additional logarithm arising due to the singularity in the screened

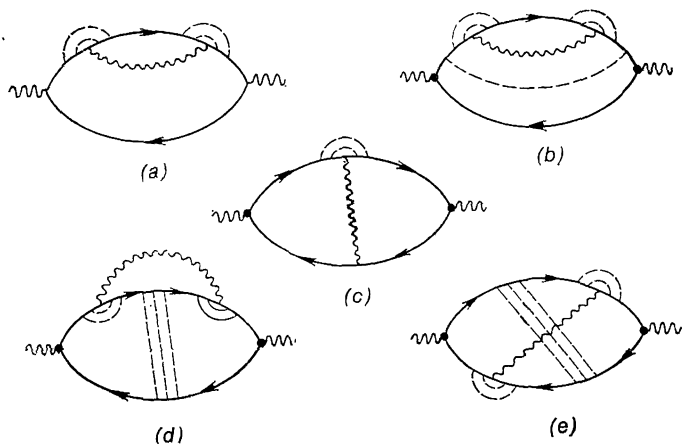


Fig. 3.15.

Coulomb potential $V(\mathbf{q}, \omega)$ at finite ω and $q \rightarrow 0$ [see Eqs. (3.4.18)-(3.4.20)]. As a result, the electron charge does not enter the expression for $V(0, \omega)$ in the leading approximation in the parameter κ/p_F at any space dimensionality.

Substituting (3.4.57) into (3.A.36), we find that, given the Coulomb interaction between electrons, the conductivity correction takes on the form

$$\delta\sigma(T) = -4 \frac{e^2 D}{\pi d a^{3-d}} \text{Im} \int_0^\infty d\omega \frac{\partial}{\partial \omega} \left[\omega \coth \frac{\omega}{2T} \right] \int \frac{(dq)}{(-i\omega + Dq^2)^2}. \quad (3.4.58)$$

Integration over \mathbf{q} gives

$$\delta\sigma(T) = -\text{Im} \frac{C_d e^2}{2D^{d/2-1} \pi d a^{3-d}} \int_0^\infty d\omega \omega^{\frac{d-4}{2}} \frac{\partial}{\partial \omega} \left[\omega \coth \frac{\omega}{2T} \right], \quad (3.4.59)$$

where

$$C_d = \begin{cases} \frac{1+i}{\sqrt{2}\pi} & \text{at } d=3, \\ \frac{2i}{\pi} & \text{at } d=2, \\ (1-i)\sqrt{2} & \text{at } d=1. \end{cases} \quad (3.4.60)$$

In three dimensions the integral (3.4.59) diverges at the upper limit. This divergency, however, can be removed by subtraction of a temperature-independent constant. As a result, at $d=3$ [25]

$$\delta\sigma(T) = \frac{\sqrt{2}}{6\pi^2} e^2 \sqrt{\frac{T}{D}} B_3, \quad (3.4.61)$$

where

$$B_3 = \int_0^\infty \frac{dx}{\sqrt{x}} \frac{d}{dx} \left[\frac{x}{1-e^x} \right] \cong 2.5.$$

In two dimensions the integral (3.4.59) diverges logarithmically. As an upper limit one should take τ^{-1} —the maximum value of ω up to which the diffusion approximation is valid. Therefore at $d=2$ [27]

$$\delta\sigma(T) = \frac{e^2}{2\pi^2 a} \ln T\tau. \quad (3.4.62)$$

At $d=1$ the conductivity correction has the form [27]

$$\delta\sigma(T) = \frac{\sqrt{2}}{2\pi^2 d^2} \sqrt{\frac{D}{T}} B_1, \quad (3.4.63)$$

$$B_1 = - \int_0^\infty \frac{dx}{x^{3/2}} \frac{\partial}{\partial x} \left(x \coth \frac{x}{2} \right).$$

It is seen from Eqs. (3.4.61) and (3.4.62) that the conductivity correction increases with temperature, i.e. resistance declines. This means that the considered effect leads to a minimum in the temperature dependence of the resistance.

Consider now the conductivity versus frequency relation at $\Omega \gg T$. At $T \rightarrow 0$

$$\omega \coth \frac{\omega}{2T} = \omega - 2\omega\theta(-\omega).$$

Substituting this expression into (3.A.34), we see that the integral over ω of the first term vanishes due to analytical properties of F : all singularities of $F(\omega)$ lie in the lower half-plane. There-

fore

$$\delta\sigma(\Omega) = -\frac{\sigma}{2\pi i\Omega} \int_{-\infty}^0 \omega d\omega [F(-i\Omega, -i\omega - i\Omega) - F(-i\Omega, -i\omega)]. \quad (3.4.64)$$

Integrating over \mathbf{q} in (3.A.30) and substituting the obtained expressions into (3.4.64), we obtain

$$\delta\sigma(\Omega) = -\frac{e^2 C_d}{D^{\frac{d-2}{2}} \pi i d a^{3-d}} \int_{-\infty}^0 \frac{\omega d\omega}{\Omega^2} \left\{ 2(\omega + \Omega)^{\frac{d-2}{2}} - \omega^{\frac{d-2}{2}} - (\omega + 2\Omega)^{\frac{d-2}{2}} \right\}, \quad (3.4.65)$$

where C_d is given by (3.4.60). In two dimensions corresponding frequency powers are replaced by $\ln \omega$. Integration over ω in (3.4.65) yields [25-27]

$$\begin{aligned} \delta\sigma(\Omega) &= -\frac{4e^2 C_d}{\pi d a^{3-d}} \frac{2^{d/2}-1}{d(d+2)} \left(\frac{\Omega}{D} \right)^{\frac{d-2}{2}} \quad \text{at } d=1, 3, \\ \delta\sigma(\Omega) &= \frac{e^2}{2\pi^2 a} \ln \Omega \tau \quad \text{at } d=2. \end{aligned} \quad (3.4.66)$$

These formulae describe complex high-frequency conductivity at $\Omega \gg T$. Note that in two dimensions, at $\Omega \gg T$, $\text{Im } \delta\sigma$ does not contain a large logarithmic factor and does not depend on Ω .

Up to now we have taken into account only effects of the electron exchange interaction. However, to each graph with the exchange interaction shown in Fig. 3.15, there corresponds a graph with direct interaction, a Hartree-type graph. The graph in Fig. 3.16c corresponds to the graph in Fig. 3.15c and the graphs in Fig. 3.16d,e to the graphs in Fig. 3.15d,e.

As in the case of the density of states, the Hartree-type graphs differ from the "exchange" graphs in that the former contain the potential with momentum of order p_F . Therefore the sum of all Hartree-type graphs is given by (3.4.59), where C_d is replaced by $=2FC'_d$. Here

$$\begin{aligned} C'_1 &= \frac{1}{2\sqrt{2}} (1-i), \\ C'_2 &= \frac{i}{\pi}, \\ C'_3 &= \frac{3(1+i)}{4\sqrt{2}\pi}. \end{aligned} \quad (3.4.67)$$

The difference between C_d and C'_d is connected with the fact that at large momenta the factor $D\mathbf{q}^2/(-i\omega + D\mathbf{q}^2)$ in (3.4.57) equals unity.

All corrections to the DC conductivity associated with the Hartree-type graphs are in fact determined only by the changes in the density of states due to the Hartree interaction:

$$\delta\sigma(T) = -e^2 D \int_{-\infty}^{\infty} d\varepsilon \delta v(\varepsilon, T) \frac{\partial n_F(\varepsilon)}{\partial \varepsilon}, \quad (3.4.68)$$

where

$$n_F(\varepsilon) = \left[\exp\left(\frac{\varepsilon}{T}\right) + 1 \right]^{-1}.$$

Given the long-range exchange interaction, Eq. (3.4.68) is not valid, so it is possible to say that the interaction alters the density of states as well as the diffusion coefficient.

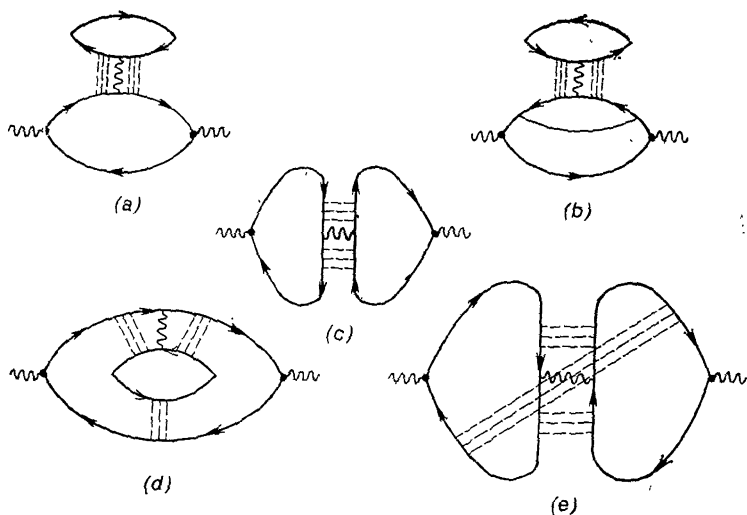


Fig. 3.16.

The expression (3.4.68) can be obtained, allowing only for the graphs in Fig. 3.16a,b. The contribution of the graph in Fig. 3.16a is two times larger than that of the graph in Fig. 3.16b and has a reversed sign. The diagrams in Fig. 3.16c,d,e cancel out. This can be shown by the method used in [13].

As in quasi-one, quasi-two and three dimensions, at $\kappa/2p_F \gg 1$, the value of F can be larger than unity, the sum of the exchange and Hartree contributions to the conductivity can change its sign with electron concentration [28]. However, as discussed in Sec. 3.4.2, the expression (3.4.38) for F is valid only at $\kappa/2p_F \ll 1$.

Consider now the effect of the interaction in the Cooper channel on the conductivity. To account for this effect, it is sufficient to consider only the diagrams in Fig. 3.17 [13]. The contributions of other graphs cancel out. Diagrams in Fig. 3.17*c,f*—the so-called Maki-Thompson diagrams [34]—describe the effect of superconducting fluctuations on the conductivity near the normal metal-superconductor transition point. These diagrams will be dwelt upon in the next section.

As far as the graphs in Fig. 3.17*a,b,d,e* are concerned, their contribution to the conductivity is related to the state density correc-

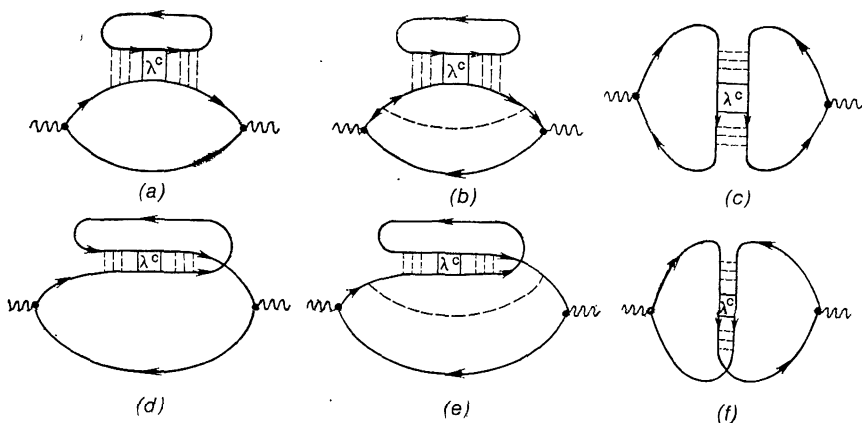


Fig. 3.17.

tion due to the Cooper channel interaction by the relation (3.4.68). As a result, we have

$$\delta\sigma_c^{(d)}(T) = \frac{e^2}{2\pi d} \operatorname{Im} C_d' B_d \lambda^c(T) \left(\frac{T}{D}\right)^{\frac{d}{2}-1} \quad \text{at } d=1, 3, \quad (3.4.69)$$

where $\lambda^c(T)$ is defined by Eq. (3.4.51) at $T \gg \varepsilon$.

In two dimensions, accounting for the ω and \mathbf{q} dependence of the coupling constant (3.4.27), as in the case of the state density correction we obtain

$$\delta\sigma_c^{(2)}(T) = \frac{e^2}{4\pi^2} \ln \frac{1 + \lambda_0 \ln \varepsilon_0 \tau}{1 + \lambda_0 \ln \frac{\varepsilon_0}{T}}. \quad (3.4.70)$$

The conductivity corrections, arising due to the Cooper channel interaction, have a temperature dependence somewhat different from that given by Eqs. (3.4.61)-(3.4.63) (due to the T -dependence

of λ^c). Moreover, they strongly depend on magnetic field in the range of classically weak magnetic fields. Arising magnetoresistance will be discussed in Sec. 3.7.

3.4.4 Superconducting Fluctuations and Temperature Dependence of Conductivity

Superconductivity is the most strong quantum coherent effect in metals. At temperatures above the critical point there are superconducting fluctuations, the contribution of which to the conductivity is, to a large degree, analogous to the quantum corrections discussed above. It is possible either to consider these corrections to the conductivity as the contribution of superconducting fluctuations in the limit of weak electron-electron interactions, or to consider the contribution of superconducting fluctuations as quantum corrections.

In general superconducting fluctuations are described by the correlation function

$$\langle \Delta(0, 0) \Delta^*(\mathbf{r}, t) \rangle = \lambda_0^2 \langle \psi^2(0, 0) \psi^{+2}(\mathbf{r}, t) \rangle.$$

In the ladder approximation the correlation function takes on the form

$$\langle \Delta \Delta^* \rangle_{\mathbf{q}, \omega} = \frac{\lambda_0^2 \Pi_c}{1 + \lambda_0^2 \Pi_c}, \quad (3.4.71)$$

where Π_c is the correlation function of noninteracting electrons, which is found by summation of the Cooper propagator over Matsubara frequencies:

$$\Pi_c(\mathbf{Q}, \omega) = 4\pi T \sum_{n>0} \tau C_Q[|\omega| + 2\pi T(2n+1)]. \quad (3.4.72)$$

Here C_Q is given by (3.2.21).

Superconducting fluctuations give two contributions to the conductivity, having different physical origin. The first one (the Aslamazov-Larkin correction [35]) arises due to the fact that fluctuating pairs have a charge and can carry electric current. The second one (the Maki-Thompson correction [34]) is connected with the electron scattering by fluctuations and has a singularity at small frequencies $\omega \sim \tau_\phi^{-1}$. We therefore consider only the second contribution, bearing in mind the case $\tau_\phi^{-1} \ll T - T_c$. This contribution is shown in Fig. 3.17c,f. The square in this figure is associated with the amplitude λ^c in the Cooper channel (with a small total momentum):

$$\lambda_Q^c(\Omega) = \lambda_0 + \langle \Delta \Delta^* \rangle = \frac{\lambda_0}{1 + \lambda_0 \Pi_c(\Omega)}. \quad (3.4.73)$$

It is convenient to express $\lambda_Q^c(\Omega)$ in terms of the temperature-dependent constant $\lambda(T)$:

$$\lambda_Q^c(\Omega) = - \frac{1}{\psi\left(\frac{1}{2} + \frac{\Omega + DQ^2}{2\pi T}\right) - \psi\left(\frac{1}{2}\right) + \lambda^{-1}(T)}, \quad (3.4.74)$$

where

$$\lambda(T) = \lambda_0^c(0) = \left(\lambda_0^{-1} + \ln \frac{\omega_D}{T}\right)^{-1} = - \frac{1}{\ln \frac{T}{T_c}}, \quad (3.4.75)$$

and T_c is the temperature of the superconducting transition:

$$T_c = \omega_D e^{1/\lambda_0}.$$

If in the electron-electron interaction repulsion prevails, $\lambda_0 > 0$, the superconducting transition is absent and the parameter T_c has only a formal meaning. In this case the interaction $\lambda^c(T)$ is positive at all temperatures and vanishes logarithmically at low temperatures. The constant λ_0 is equal to the effective interaction at $T \sim \Theta_D$. It is expressed in terms of the Coulomb coupling constant λ_{Coul} and the phonon exchange constant λ_{ph} [36]:

$$\lambda_0 = \lambda_{\text{ph}} + \frac{\lambda_{\text{Coul}}}{1 + \lambda_{\text{Coul}} \ln \frac{\varepsilon_F}{\omega_D}}. \quad (3.4.76)$$

The set of ladder diagrams, consisting of solid and dashed lines, vanishes as a result of integration over (dp) , when energy variables ε and ε_1 , corresponding to one-particle Green functions, have the same signs. For opposite signs this set is equal to $C_Q(|\varepsilon - \varepsilon_1|)$. As a result, the contribution to the conductivity given by the diagrams in Fig. 3.17c,f at Matsubara frequencies $\omega = 2\pi nT > 0$ is equal to

$$\begin{aligned} \delta\sigma_{M-T}^{(d)} &= \frac{e^2 D}{\omega \tau} \cdot 4T^2 \sum_{\substack{0 < \varepsilon < \omega \\ -\omega < \varepsilon_1 < 0}} \int \frac{(dp)}{v} G(\varepsilon) G(\varepsilon_1) G(\varepsilon - \omega) G(\varepsilon_1 + \omega) \\ &\times \int (dq) C_Q(\varepsilon - \varepsilon_1) C_Q(2\omega + \varepsilon_1 - \varepsilon) \lambda_Q^c(|\varepsilon + \varepsilon_1|). \end{aligned} \quad (3.4.77)$$

Here $\varepsilon = \pi T(2n + 1)$. The product of two cooperons is convenient to represent as a sum

$$\begin{aligned} C_Q(\varepsilon - \varepsilon_1) C_Q(2\omega - \varepsilon + \varepsilon_1) &= \frac{1}{2} C_Q(\omega) [C_Q(\varepsilon - \varepsilon_1) \\ &+ C_Q(2\omega - \varepsilon + \varepsilon_1)]. \end{aligned} \quad (3.4.78)$$

The second term is reduced to the first by the substitution $\omega - \varepsilon \rightarrow \varepsilon$, $\omega + \varepsilon_1 \rightarrow -\varepsilon_1$, because other terms in Eq. (3.4.77) do not change upon this substitution. Integrating in this formula over

(dp) and substituting $\Omega - \varepsilon$ for ε_1 , we obtain

$$\delta\sigma_{M-T}^{(d)}(\omega) = \frac{2e^2}{\pi} D\tau \int (dQ) C_Q(\omega) \beta(T), \quad (3.4.79)$$

$$\begin{aligned} \omega\beta(T) = & 2\pi T \cdot \frac{2}{\tau} \left\{ \frac{1}{2} \lambda_Q^c(0) [C_Q(2\varepsilon) - C_Q(2\varepsilon + 2\omega)] \right. \\ & \left. + \sum_{\substack{\omega > \Omega > 0 \\ \varepsilon > 0}} \lambda_Q^c(\Omega) [C_Q(2\varepsilon + \Omega) - C_Q(2\varepsilon + 2\omega - \Omega)] \right\}. \end{aligned} \quad (3.4.80)$$

Near the superconducting transition point the first term in braces in (3.4.80) is greater than other terms, since $\lambda_Q^c(0)$ increases as $T \rightarrow T_c$. This term is seen to be analytical in the region $\text{Re } \omega > 0$, as the function $C_Q(\omega)$ is analytical in this region. To continue (3.4.80) analytically in ω , we rewrite the expression under \sum as a sum of terms analytical at $\Omega > 0$ and $\Omega < 0$:

$$\begin{aligned} & \lambda_Q^c(\Omega) C(2\varepsilon + \Omega) - [\lambda_Q^c(\Omega) - \lambda_Q^c(2\varepsilon + 2\omega + DQ^2)] \\ & \times C(2\varepsilon + 2\omega - \Omega) - \lambda_Q^c(2\varepsilon + 2\omega + DQ^2) C(2\varepsilon + 2\omega - \Omega). \end{aligned} \quad (3.4.81)$$

The function $C(\Omega)$ has a simple pole dependence on its argument, and the function $\lambda_Q^c(\Omega)$ is analytical at $\text{Re } \Omega > 0$, therefore the first two terms are analytical at $\text{Re } \Omega > 0$. To sum each of these terms, we replace $\sum_{0 < \Omega < \omega}$ by $\sum_{0 < \Omega} - \sum_{\omega \leq \Omega}$. The last term in (3.4.81)

is analytical at $\text{Re } \Omega < 0$, hence the corresponding substitution is

$$\sum_{0 < \Omega < \omega} \rightarrow \sum_{\Omega < \omega} - \sum_{\Omega \leq 0}.$$

Performing this shift in the sums over Ω , we obtain the expression for β , analytical at $\text{Re } \omega > 0$:

$$\begin{aligned} \beta(T) = & \frac{2\pi T\tau}{\omega} \sum_{\varepsilon > 0} \sum_{\Omega} \{ \lambda_Q^c(|\Omega|) [C(2\varepsilon + |\Omega|) \\ & - C(2\varepsilon - |\Omega| + 2\omega) + 2 \text{sgn } \Omega \lambda_Q^c(|\Omega| + \omega) C(2\varepsilon + \Omega + \omega) \\ & + 2\lambda_Q^c(2\varepsilon + 2\omega + DQ^2) [C(2\varepsilon - \Omega + 2\omega) - C(2\varepsilon - \Omega + \omega)] \}. \end{aligned} \quad (3.4.82)$$

In the limit of small ω and Q we find

$$\beta(T) = \frac{\pi^2}{4} \sum_{\Omega} \cos \frac{\Omega}{2} \lambda_Q^c(|\Omega|) - \sum_{\varepsilon > 0} \lambda_Q^{\varepsilon''}(2\varepsilon) (2\pi T)^2. \quad (3.4.83)$$

Substituting (3.4.74) into this expression, we obtain $\beta(T)$ as a function of the effective electron-electron interaction constant $\lambda(T) = - \left(\ln \frac{T}{T_c} \right)^{-1}$. This function is tabulated for different temperatures in [37]. In the limit $T \rightarrow T_c$, $-\lambda(T) \gg 1$ and only the term with $\Omega = 0$ in (3.4.82) is important, β being equal to $-\lambda(T) \frac{\pi^2}{4}$,

and the expression for the conductivity transforming into the Thompson result [34]. In the opposite case of high temperatures, $T \gg T_c$, $|\lambda(T)| \ll 1$, the parameter $\beta(T)$ is inversely proportional to the square of temperature logarithm. The same dependence, but with a different factor, has been obtained in [38].

Note that the function $\beta(T)$ and, consequently, the conductivity correction connected with this interaction, are positive independently of the sign of the interaction λ_0 :

$$\delta\sigma_{M-T}^{(d)} = \frac{e^2}{2\pi^2\hbar} \beta(T) \begin{cases} 2\pi\sqrt{D\tau_\varphi} & \text{at } d=1, \\ \ln T\tau_\varphi & \text{at } d=2, \\ (D\tau_\varphi)^{-1/2} & \text{at } d=3. \end{cases} \quad (3.4.84)$$

In two dimensions at temperatures near T_c it is necessary to replace T by $T - T_c$ under the sign of logarithm.

Thus, the Maki-Thompson fluctuation correction together with the localization correction lead to expressions (3.2.23) times $1 - \beta(T)$. In the case of attraction $\beta(T)$ increases with decreasing temperature; at $T < 2.7T_c$ the effect of the interaction exceeds the localization effect in the ideal gas, and the total quantum correction to the conductivity becomes positive. In the case of repulsion $\lambda(T)$ and, consequently, $\beta(T)$ vanish logarithmically with decreasing temperature.

3.5 TEMPERATURE DEPENDENCE OF CONDUCTIVITY: EXPERIMENT

At present there is a large amount of experimental data, concerning the temperature dependence of the conductivity in various disordered conductors: amorphous metals, disordered alloys, metallic glasses, degenerate semiconductors and semi-metals with high defect concentration.

As in other sections of this review, we do not aim at discussing all available data, but restrict ourselves to those experimental works in which comparison with the theory has been performed.

Table 3.5.1 contains the quantum corrections to the conductivity due to localization effects (Chapter 3.2) and to the electron-electron interaction (Chapter 3.4). It is seen that in three dimensions the quantum corrections due to the interaction are larger than corresponding localization corrections in a parameter $\sqrt{T\tau_\varphi} \gg 1$. In two dimensions both types of corrections are practically the same and in quasi-one dimension the localization corrections are larger than the corrections, arising due to the interaction, just in the same parameter. In all metallic glasses the temperature dependence of resistivity has a minimum, probably, of a non-Kondo origin [39, 40]. This minimum can be naturally explained in terms of the electron-

Table 3.5.1. Temperature Dependence of Resistance and the Hall Coefficient

	Interaction	Localization
$d=1, 3$		
$\frac{\delta R^{(d)}(T)}{R}$	$\lambda_{\text{eff}} \frac{e^2}{\hbar} \cdot \frac{1}{V_d} \cdot \frac{L_T^{2-d}}{\sigma} \sim \frac{T^{\frac{d}{2}-1}}{V_d}$	$\frac{e^2}{\hbar} \cdot \frac{L_\Phi^{2-d}}{V_d(\sigma)} \sim \frac{T^p \left(\frac{d}{2}-1\right)}{V_d}$
$d=2$		
$\frac{\delta R_{\square}(T)}{R_{\square}}$	$-\lambda_{\text{eff}} \frac{e^2}{\pi^2 \hbar} R_{\square} \ln \frac{L_T}{l}$	$-\frac{e^2 R_{\square}}{\pi^2 \hbar} \ln \frac{L_\Phi}{l}$
$\frac{\delta R_H}{R_H}$	$2 \frac{\delta R(T)}{R}$	0
Dimensionality crossover	$a < L_T = \sqrt{\frac{\hbar D}{T}}$	$a < L_\Phi = \sqrt{D \tau_\Phi}$

$V_2 = A$ is the cross-sectional area, $V_3 = 1$.
 Given only the exchange and Hartree interactions,

$$\lambda_{\text{eff}}^{(d)} = \left(1 - \frac{d}{2} F\right).$$

electron interaction in disordered metals. Estimations show that the temperature-dependent correction to resistivity has a right order of magnitude and changes with residual resistivity as predicted by Eq. (3.4.61).

The temperature and frequency dependence of the conductivity was measured in phosphorus doped silicon [28]. The conductivity was found to increase with decreasing temperature according to the law (Fig. 3.18)

$$\sigma(T) = \sigma_0 + mT^\beta,$$

where β ranges from 0.3 to 0.7. The σ versus T curves for β equal to 1/3 and 1/2 are plotted for comparison in Fig. 3.18. Note that the sign of the temperature-dependent correction to the conductivity is opposite to that given by exchange effects: the conductivity increases with decreasing temperature. Figure 3.19 shows the coefficient m as a function of electronic concentration. In the whole range of investigated concentrations $m < 0$ except for the immediate vicinity of the metal-insulator transition point n_c , where m becomes positive.

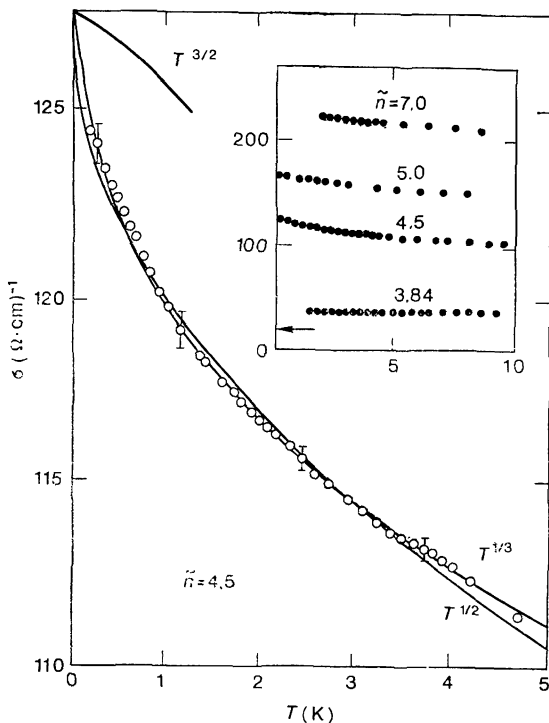


Fig. 3.18. σ versus T for Si:P; $n = 4.5 \times 10^{18} \text{ cm}^{-3}$. Temperature dependences for various impurity concentrations are shown in another scale in the insert [28].

As shown in Sec. 3.4.3, allowing both for the exchange and Hartree terms, the conductivity correction takes on the form*

$$\begin{aligned} \delta\sigma(T) &= \left[1 - \frac{3}{2x} \ln(1+x) \right] \cdot \frac{2.5 \sqrt{2}}{6\pi^2} e^2 \sqrt{\frac{T}{D}} \\ &= f(x) \cdot \frac{2.5 \sqrt{2}}{6\pi^2} e^2 \sqrt{\frac{T}{D}}, \end{aligned} \quad (3.4.61a)$$

where

$$x = \left(\frac{2p_F}{\kappa} \right)^2.$$

At $x \gg 1$, $f(x) \rightarrow 1$; at $x \simeq 1.2$, $f(x)$ changes its sign. The negative sign of the temperature correction to the resistivity was explained in [28] by the fact that in these experiments $x < 1.2$.

* Note that the numerical factor in (3.4.61a) is equal to 2.16, i.e. it is three times larger than the factor $A = 0.72$ [28]. Experiment gives $A = 1.7 \pm 0.5$.

The theoretical curve for the coefficient m given by (3.4.61a) is plotted in Fig. 3.19. The curve is seen to fit well the experimental data. In the vicinity of the metal-insulator transition point screening

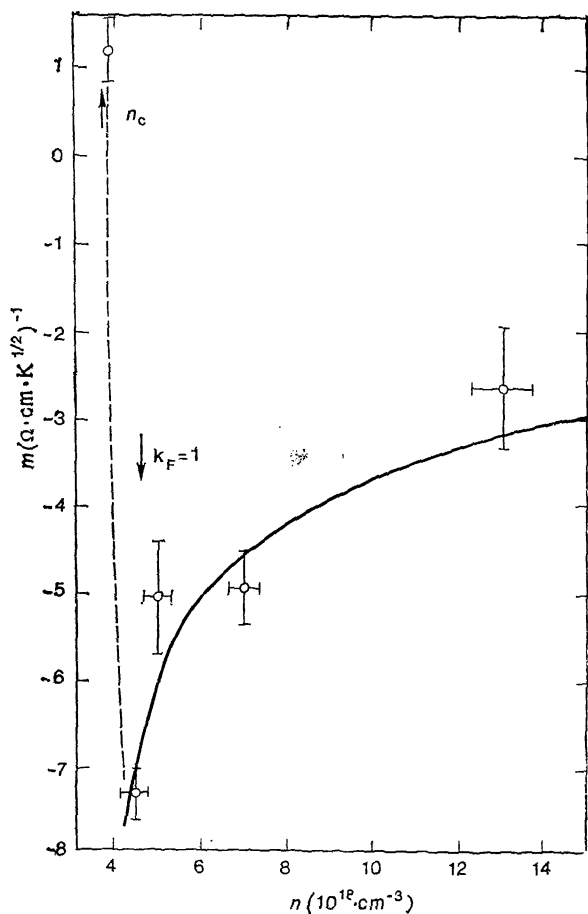


Fig. 3.19. m versus concentration. Solid line is calculated from Eq. (3.4.61). Dashed line shows qualitatively the approach to the metal-insulator transition [28].

becomes less effective and $\kappa \rightarrow 0$. Therefore $f(x)$ again changes its sign.

As shown in Sec. 3.4.3, when the nonideality parameter of the electron gas, κ/p_F , is large, there are, besides Hartree corrections, many other contributions, which, though not altering completely the

temperature dependence, must change the expression for $f(x)$. Hence the fact that the theory accounting only for the exchange and Hartree corrections is in good agreement with experimental data implies merely that higher-order corrections in κ/p_F are numerically small.

In the low-frequency range, at $\hbar\omega \gg T$, $\sigma(\omega)$ increases with

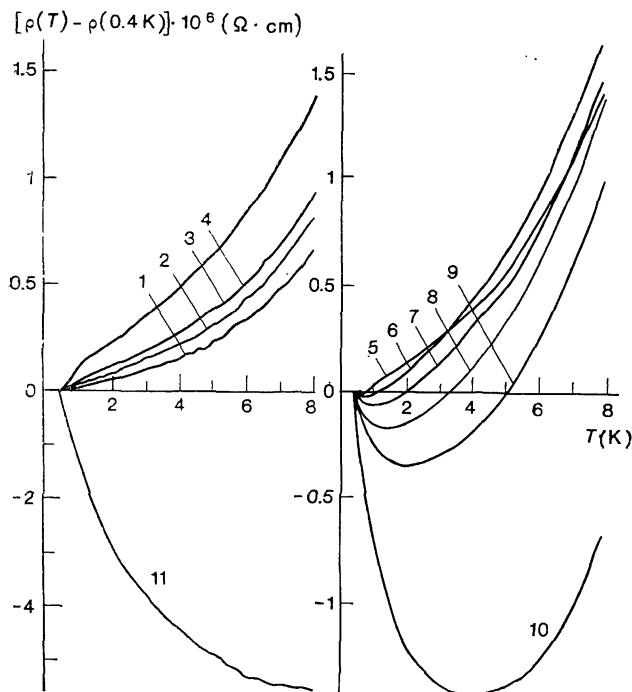


Fig. 3.20. Resistivity versus temperature for plastically deformed bismuth. Residual resistivity increases with increasing number. The curve 11 is given in a reduced scale [41].

frequency when $n = 3.84 \times 10^{18} \text{ cm}^{-3}$, i.e. in the vicinity of the metal-insulator transition point [28]. This contradicts the simple Drude theory, which asserts that $\sigma(\omega)$ declines with increasing frequency. Near the transition point the theory exposed in Sec. 3.4.3 is not valid. However, it can be used qualitatively, since the criterion of its validity consists in smallness of the parameter $\lambda_{\text{eff}} \frac{V\omega\tau}{(p_F l)^2} \ll 1$ rather than of the coupling constant. Hence we can compare the scales of the conductivity variations with frequency and temperature. In the temperature range from zero to 40 K the conductivity appears to change by a factor of 2, as well as in the

frequency range from zero to 40 cm^{-1} at $T = 2 \text{ K}$, and at $\hbar\omega \gg T \simeq 2 \text{ K}$ it is temperature-independent [28]. The resistivity versus temperature relation in a bismuth sample with plastic strains has been obtained in [41]. The sample resistivity increased with strain, its temperature dependence changing simultaneously. In

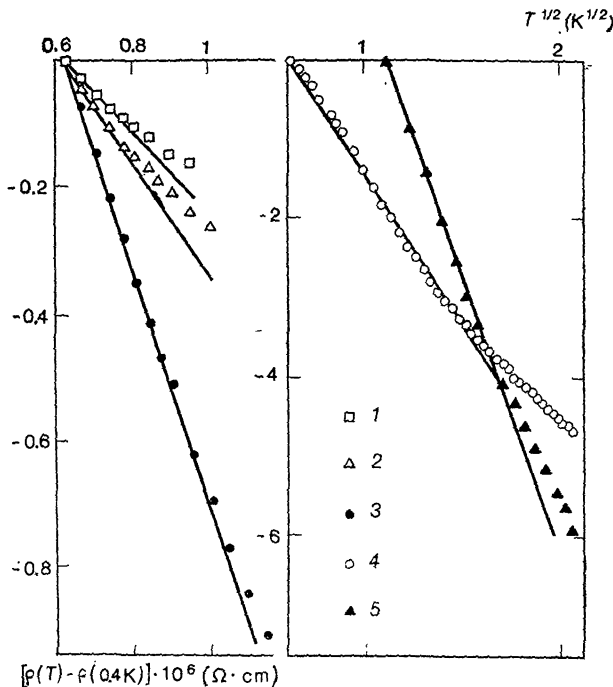


Fig. 3.21. ρ versus \sqrt{T} [41]. $\rho(0.4 \text{ K})$ is given in ohm · cm: 1— 7.36×10^{-5} ; 2— 1.13×10^{-4} ; 3— 2.47×10^{-4} ; 4— 6.22×10^{-5} ; $\rho(1.3 \text{ K}) = 1.9 \times 10^{-3} \text{ ohm} \cdot \text{cm}$ (5).

strongly deformed samples the resistivity as a function of temperature has a minimum (Fig. 3.20). At $T < T_{\min}$ the experimental curve fits the \sqrt{T} law (Fig. 3.21), which is an evidence of the electron-electron interaction effect. According to the theory, $\delta\rho(T)$ should be proportional to $\rho^{5/2}(0)$. Experimental points, however, fit rather the curve $\delta\rho(T) \sim \rho(0)$. Note that the correction to the density of states in experiments with granular aluminium films [32] appears to be proportional to ρ and not to $\rho^{3/2}$, as the theory predicts.

Experimental investigations of the temperature-dependent corrections to the conductivity have been carried out on a series of systems, e.g. inversion layers in silicon [42, 43], thin Au-Pd [44, 45]

and Cu [46] films. In all these experiments the resistivity increases logarithmically with decreasing temperature.

As we have shown, both types of corrections (due to the localization and to the interaction) lead to logarithmic growth of the resistivity with decreasing temperature, but numerical factors in front of logarithm are different. If $\tau_{\varphi} \sim T^{-p}$, the localization corrections take on the form (see Table 3.5.1)

$$\delta\sigma^{(2)}(T) = -\frac{pe^2}{2\pi^2\hbar} \ln T\tau = -\alpha_T^l \frac{e^2}{2\pi^2\hbar} \ln T\tau. \quad (3.5.1)$$

Interaction effects give the same expression, but, instead of p , in the lowest order in the nonideality parameter of the electron gas we have in this case $\alpha_T^{\text{int}} = 1 - F$, or, in general, $\alpha_T^{\text{int}} = \lambda_{\text{eff}}$. Therefore, to compare the theory with experiment, it is necessary to obtain experimentally the temperature dependence of the conductivity and to determine the prelogarithmic factor.

As shown in Chapter 3.3, a constant electric field does not affect the localization in the absence of heating. If the heating of the electron gas is allowed for, then all expressions with or without the interaction should contain the electronic temperature, which depends on electric field [7]. The electronic temperature is defined by the relation

$$eEL_{e\text{-ph}} \simeq T_e, \quad (3.5.2)$$

where $L_{e\text{-ph}} = \sqrt{D\tau_{e\text{-ph}}}$, $\tau_{e\text{-ph}}$ is the time of the electron energy relaxation due to the electron-phonon scattering. Therefore, if $\tau_{e\text{-ph}}^{-1} \sim T^{p'}$, the prelogarithmic factors in the expressions describing the field dependence of the conductivity at $T_e \gg T$, where T is the thermostat temperature, are equal to

$$\alpha_E^l = \frac{2p}{2+p'} \quad (3.5.3)$$

for the localization correction and to

$$\alpha_E^{\text{int}} = \frac{2}{2+p'} (1 - F) \quad (3.5.4)$$

for the correction due to the interaction. Thus, the temperature dependence of the electron energy relaxation time can be obtained from the ratio $\frac{\alpha_E}{\alpha_T} = \frac{2+p'}{2}$. In fact, the logarithmic growth of the conductivity with the field with $p' = 3$ has been observed in [40, 47].

In many experiments on the temperature dependence of the conductivity it has been found that $\alpha_T^l + \alpha_T^{\text{int}} = \alpha_T = 1$ [42-45, 47, 48]. Only in pure copper films α_T changes with increasing resistance from 3 to 2 [46]. According to (3.4.47), the corrections arising due to the electron-electron interaction are proportional to a factor $(1 - F)$,

which, in the case of copper, equals 0.4 [46]; therefore the interaction effects are numerically small and the observed growth of resistance may be accounted for by the localization corrections. This means that in these experiments α_T changes from 3 to 2 with increasing resistance. In the limit of low impurity concentration $p = 3$ for the electron-phonon scattering.

Given a large film resistance, the value $p = 2$ can be accounted for by two effects: (a) with decreasing film thickness phonons become two-dimensional and the electron-phonon scattering by these phonons gives $p = 2$ [6]; and (b) the elastic electron scattering taken into consideration, the electron-phonon scattering also gives $p = 2$ [49]. The last explanation seems to be more correct. The situation becomes much more complicated when we try to allow for the data obtained in [42-45, 47]. Perhaps, the localization effects are suppressed by a temperature-independent phase breaking mechanism (e.g. by a sufficiently strong spin scattering). This is confirmed by the measurements of the Hall effect in silicon MOS-structures [43]. It has been shown that at a sufficiently small resistance the relation

$$\frac{\delta R_H}{R_H} = 2 \frac{\delta R(T)}{R}, \quad (3.5.5)$$

where $\delta R(T)$ is the temperature-dependent correction to resistance, is valid. According to the theory [27, 50] (Sec. 3.6.3), this relation holds only if the localization corrections to $\delta R(T)$ are small and $\delta R(T) = \delta R_{\text{int}}$. According to [43], Eq. (3.5.5) is valid unless hopping conductivity appears, when the ratio $\delta R_H R / \delta R(T) R_H$ changes from 2 to 1.

The temperature dependence of the conductivity has been investigated in thin wires [45, 48, 51]. Careful experiments on AuPd wires with triangular cross section [45, 48] have shown that the resistance correction obeys the relation

$$\frac{\delta R(T)}{R} \sim \frac{1}{A \sqrt{T}}, \quad (3.5.6)$$

where A is the wire cross-sectional area, and does not depend on the wire length. The experimental relation (3.5.8) is in agreement with the interaction theory (Table 3.5.1). On the other hand, according to (3.4.24), the electron-electron relaxation time τ_{ee} in quasi-one dimension is proportional to A/\sqrt{T} . As a result, $\delta R(T)/R \sim T^{-1/4} A^{-1/2}$, which does not agree with the experiment. Our assumption concerning a strong effect of the Nyquist noise, leading to the relation $\delta R(T)/R \sim T^{-1/3} A^{-2/3}$, also disagrees with the experiment. We therefore may think that in the experiments [45, 48] the temperature dependence of the resistance arises due to the electron-electron interaction. Analogous results have been obtained with thin narrow amorphous W-Re films [51]. However, in these

experiments the Maki-Thompson correction, subtracted from experimental curves, is quite evident.

Thus, the whole set of experimental data shows that in the temperature dependence of the resistance the interaction effects prevail, except for copper [46], where the interaction and localization effects give the same contribution.

3.6 HALL EFFECT

3.6.1 Introduction

Here we shall calculate the Hall coefficient in impure metals, taking into account both the effects of quantum interference and the electron-electron interaction*.

In the presence of an external field \mathbf{H} and a measuring electric field \mathbf{E} the electron kinetic energy may be written as

$$\mathcal{H} = \frac{1}{2m} \left[\mathbf{p} + \frac{e}{c} (\mathbf{A}_1 + \mathbf{A}_2) \right]^2 = \frac{\mathbf{p}^2}{2m} + \frac{e}{mc} \mathbf{p} (\mathbf{A}_1 + \mathbf{A}_2) + \frac{e^2}{2mc^2} (\mathbf{A}_1 + \mathbf{A}_2)^2, \quad (3.6.1)$$

where $i\Omega\mathbf{A}_1/c = \mathbf{E}$ and $i[\mathbf{k} \times \mathbf{A}_2] = \mathbf{H}$. We choose the following gauge: $\mathbf{k} \cdot \mathbf{A}_2 = 0$. The Hall current is proportional to

$$[\mathbf{E} \times \mathbf{H}] = \frac{\Omega}{c} \{ \mathbf{A}_2 (\mathbf{k} \cdot \mathbf{A}_1) - \mathbf{k} (\mathbf{A}_1 \cdot \mathbf{A}_2) \}. \quad (3.6.2)$$

Calculating the Hall conductivity, we shall pay attention only to the terms proportional to $\mathbf{A}_2 (\mathbf{k} \cdot \mathbf{A}_1)$. It is evident that the third term on the right-hand side of Eq. (3.6.1) does not lead to such terms. Therefore the Hall conductivity can be evaluated by inserting into the graphs for the conductivity an additional vertex $\frac{e}{mc} \mathbf{A}_2 \cdot \mathbf{p}$ arising from the second term on the right-hand side of (3.6.1). Thus the graph in Fig. 3.22a is associated with the following contribution to the current:

$$\mathbf{j}_a = \frac{e^3 \Omega}{2\pi m^3 c^2} \int (dp) G^R(\mathbf{p}) G^R(\mathbf{p} + \mathbf{k}) G^A(\mathbf{p}) (\mathbf{A}_1 \cdot \mathbf{p}) (\mathbf{A}_2 \cdot \mathbf{p}) \left(\mathbf{p} + \frac{\mathbf{k}}{2} \right). \quad (3.6.3)$$

To obtain the term, proportional to $\mathbf{A}_2 (\mathbf{k} \cdot \mathbf{A}_1)$, we must expand the Green function $G^R(\mathbf{p} + \mathbf{k})$ in powers of \mathbf{k} . As a result, \mathbf{j}_a appears t

* This chapter is close to paper [50].

be proportional to an integral over the angles of \mathbf{p}

$$\int dO_p (\mathbf{A}_1 \cdot \mathbf{p}) (\mathbf{A}_2 \cdot \mathbf{p}) (\mathbf{p} \cdot \mathbf{k}) \cdot \mathbf{p} \sim \frac{p^4}{d(d+2)} \times [(\mathbf{k} \cdot \mathbf{A}_1) \mathbf{A}_2 + \mathbf{k} (\mathbf{A}_1 \cdot \mathbf{A}_2) + (\mathbf{k} \cdot \mathbf{A}_2) \mathbf{A}_1]. \quad (3.6.4)$$

The contribution to the electric current, proportional to the combi-

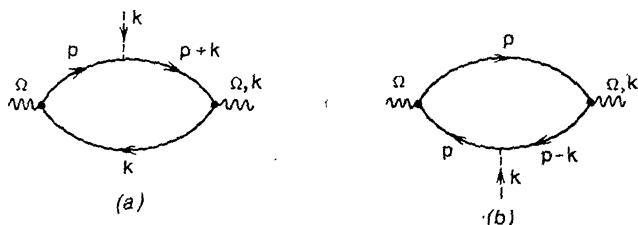


Fig. 3.22.

nation of vector potentials of interest, is

$$\mathbf{j}_a = \frac{e^3 \Omega n \tau^2}{2m^2 c^2} (\mathbf{A}_1 \cdot \mathbf{k}) \mathbf{A}_2. \quad (3.6.5)$$

As $\mathbf{j}_a = \mathbf{j}_b^*$, the Hall conductivity takes on the usual Drude form

$$\sigma_{xy} = \frac{e^3 \tau^2 n}{m^2 c}; \quad R_H = \frac{\sigma_{xy}}{\sigma_0^2} = \frac{1}{nec}. \quad (3.6.6)$$

3.6.2 Hall Effect for Noninteracting Electrons

Feynman graphs for the quantum corrections and Hall conductivity are shown in Fig. 3.23. The correction to the Hall current has the form

$$\delta \mathbf{j}_H = \frac{2e^3 \Omega}{2\pi m^3 c^2} C(\mathbf{r}, \mathbf{r}) \mathbf{P}, \quad (3.6.7)$$

where $C(\mathbf{r}, \mathbf{r})$ is the cooperon with coinciding coordinates and

$$\mathbf{P} = \frac{2}{m} \int (d\mathbf{p}) [(G^R(\mathbf{p}))^3 (G^A(\mathbf{p}))^2 - (G^R(\mathbf{p}))^2 (G^A(\mathbf{p}))^3] \times (\mathbf{A}_1 \cdot \mathbf{p}) (\mathbf{A}_2 \cdot \mathbf{p}) (\mathbf{k} \cdot \mathbf{p}) (-\mathbf{p}). \quad (3.6.8)$$

Finally, the Hall conductivity correction appears to be twice as large as the conductivity correction:

$$\frac{\delta \sigma_{xy}}{\sigma_{xy}} = 2 \frac{\delta \sigma_0}{\sigma_0}. \quad (3.6.9)$$

As for the experimentally measured Hall coefficient, we obtain [50, 52]

$$\delta R_H = 0. \quad (3.6.10)$$

This result could be expected, since in the absence of the interaction the interference leads only to renormalization of the scattering

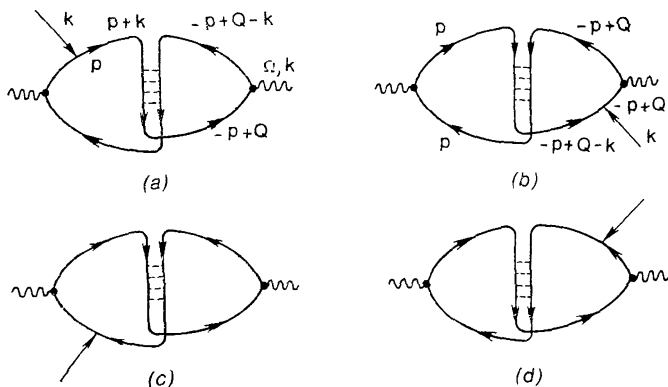


Fig. 3.23.

time τ rather than the density of states ν . As τ does not enter Eq. (3.6.6) for the Hall coefficient, in the absence of the interaction the correction to R_H should also equal zero.

3.6.3 Hall Effect for Interacting Electrons

To evaluate the correction to the Hall conductivity arising due to the electron-electron interaction, we must insert the magnetic vertex $e\mathbf{A}_2 \cdot \mathbf{p}/mc$ into the conductivity graphs shown in Fig. 3.15.

As shown in Chapter 3.4, the contributions of the graphs in Fig. 3.15a-c to the conductivity cancel. The same happens when we calculate the Hall conductivity. The contribution to the Hall conductivity of the graphs, obtained from the diagrams shown in Fig. 3.15d,e can be found, having calculated the element M equal to the sum of the diagrams shown in Fig. 3.24. Note that M is proportional to \mathbf{q} . Therefore, separating the terms linear in \mathbf{q} and \mathbf{k} , we obtain the following expression for the contribution of the graph

in Fig. 3.24a:

$$\begin{aligned} \mathbf{M}_a &= \int (dp) (\mathbf{A}_2 \cdot \mathbf{p}) (\mathbf{p} - \mathbf{q}) G^A(\mathbf{p} - \mathbf{k}) G^A(\mathbf{p}) [G^R(\mathbf{p} - \mathbf{q})]^2 \\ &= \int (dp) \left\{ (\mathbf{A}_2 \cdot \mathbf{p}) \mathbf{q} \left(\mathbf{k} \cdot \frac{\mathbf{p}}{m} \right) [G^R(\mathbf{p})]^2 [G^A(\mathbf{p})]^3 \right. \\ &\quad \left. + 2 (\mathbf{A}_2 \cdot \mathbf{p}) \mathbf{p} \left(\mathbf{k} \cdot \frac{\mathbf{p}}{m} \right) \left(\mathbf{q} \cdot \frac{\mathbf{p}}{m} \right) [G^R(\mathbf{p})]^3 [G^A(\mathbf{p})]^3 \right\}. \end{aligned} \quad (3.6.11)$$

After integrating over the angles of \mathbf{p} the first term on the left-hand

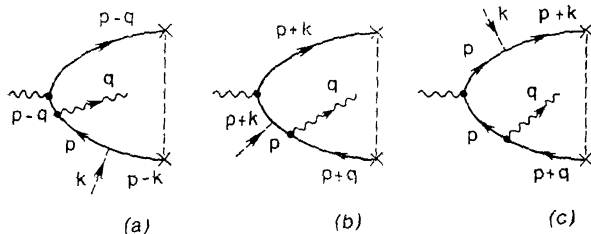


Fig. 3.24.

side of (3.6.11) will be proportional to $(\mathbf{A}_2 \cdot \mathbf{k}) \mathbf{q} = 0$,

$$\begin{aligned} \mathbf{M}_b &= \int (dp) (\mathbf{A}_2 \cdot \mathbf{p}) (\mathbf{p} + \mathbf{k}) G^A(\mathbf{p} + \mathbf{q}) G^R(\mathbf{p}) [G^R(\mathbf{p} + \mathbf{k})]^2 \\ &= \int (dp) (\mathbf{A}_2 \cdot \mathbf{p}) \left\{ \mathbf{k} \left(\mathbf{q} \cdot \frac{\mathbf{p}}{m} \right) [G^A(\mathbf{p})]^2 [G^R(\mathbf{p})]^3 \right. \\ &\quad \left. + 2 \mathbf{p} \left(\mathbf{q} \cdot \frac{\mathbf{p}}{m} \right) \left(\mathbf{k} \cdot \frac{\mathbf{p}}{m} \right) [G^A(\mathbf{p})]^2 [G^R(\mathbf{p})]^4 \right\}, \end{aligned} \quad (3.6.12)$$

$$\begin{aligned} \mathbf{M}_c &= \int (dp) (\mathbf{A}_2 \cdot \mathbf{p}) \mathbf{p} G^A(\mathbf{p} + \mathbf{q}) [G^R(\mathbf{p})]^2 G^R(\mathbf{p} + \mathbf{k}) \\ &= \int (dp) (\mathbf{A}_2 \cdot \mathbf{p}) \mathbf{p} \frac{(\mathbf{k} \cdot \mathbf{p})}{m} \frac{(\mathbf{q} \cdot \mathbf{p})}{m} [G^R(\mathbf{p})]^4 [G^A(\mathbf{p})]^2. \end{aligned} \quad (3.6.13)$$

Finally, allowing for $\text{div } \mathbf{A}_2 = 0$, we find

$$\begin{aligned} \mathbf{M}_a + \mathbf{M}_b + \mathbf{M}_c &= \int (dp) \left\{ (\mathbf{A}_2 \cdot \mathbf{p}) \mathbf{p} \frac{(\mathbf{k} \cdot \mathbf{p})}{m} \frac{(\mathbf{q} \cdot \mathbf{p})}{m} 2 [G^R(\mathbf{p})]^3 [G^A(\mathbf{p})]^3 \right. \\ &\quad \left. + 3 [G^A(\mathbf{p})]^2 [G^R(\mathbf{p})]^4 + (\mathbf{A}_2 \cdot \mathbf{p}) \mathbf{k} \frac{(\mathbf{q} \cdot \mathbf{p})}{m} [G^A(\mathbf{p})]^2 [G^R(\mathbf{p})]^3 \right\}. \end{aligned} \quad (3.6.14)$$

Integration over the angles of \mathbf{p} yields combinations $\mathbf{A}_2 (\mathbf{q} \cdot \mathbf{k})$, $\mathbf{q} (\mathbf{A}_2 \cdot \mathbf{k})$ and $\mathbf{k} (\mathbf{q} \cdot \mathbf{A}_2)$, which should be multiplied by $\mathbf{q} \cdot \mathbf{A}_1$ and integrated over \mathbf{q} . The expression $(\mathbf{A}_1 \cdot \mathbf{k}) \mathbf{A}_2$ arises only from the combination $\mathbf{A}_2 (\mathbf{q} \cdot \mathbf{k})$, given by the first term on the right-hand side of Eq. (3.6.14). Note now that the integral over \mathbf{p} of the expression in square brackets equals zero. Thus,

$$\delta \sigma_H = 0. \quad (3.6.15)$$

The Hartree and Cooper terms taken into account, this result does not change.

From (3.6.15) we obtain the expression for the correction to the Hall coefficient (a rule of two)

$$\frac{\delta R_H}{R_H} = 2 \frac{\delta R}{R}. \quad (3.6.16)$$

3.7 ANOMALOUS MAGNETORESISTANCE

3.7.1 Magnetoresistance of Noninteracting Electrons

The problem of anomalous magnetoresistance (AMR) is one of the still unsolved problems of the semiconductor kinetics. The AMR can be either positive (e.g. in *p*-Ge [53, 54]), or negative (*n*-Ge, GaAs, Te, etc.). Peculiar features of the AMR consist in that (a) the AMR does not depend on the direction of magnetic field with respect to the current direction and can be either longitudinal or transverse; (b) the AMR arises in magnetic fields weak in classical sense (i.e. $\omega_c \tau \ll 1$, where $\omega_c = \frac{eH}{mc}$ is the cyclotron frequency).

The latter fact is very difficult to account for, because it shows that there is a new characteristic scale of magnetic fields. This scale should be small in comparison with the scales both of a classical field, defined by the relation $\omega_c \tau \sim 1$, and a quantum magnetic field ($\hbar \omega_c \sim \bar{\varepsilon}$, where $\bar{\varepsilon}$ is a characteristic electron energy). Another peculiar feature of the AMR phenomenon is that the scale in question is temperature dependent.

The quantum corrections connected with the localization are very sensitive to magnetic fields [50]. Switching on a weak magnetic field depresses localization effects and increases the sample conductivity, leading thus to a negative magnetoresistance. This effect could be understood in the following way. The localization takes place, when the probability that an electron returns to a given point increases, because the probability amplitudes corresponding to two trajectories, which differ only in the direction of electron movement (clockwise and counterclockwise), interfere. In the absence of magnetic field the phases of these amplitudes are the same. In magnetic field each amplitude acquires a phase factor

$$\varphi = \frac{e}{c} \oint_C \mathbf{A}(\mathbf{r}) d\mathbf{r} = \frac{e\Phi}{c}, \quad (3.7.1)$$

where the integral is taken along the electron trajectory, \mathbf{A} is the vector potential of the magnetic field, and Φ is the magnetic flux through the contour C . As the two considered trajectories differ only in direction, the corresponding phases will differ only in their signs.

Therefore in the magnetic field a phase difference

$$\Delta\varphi = \frac{2e}{c\hbar} \oint \mathbf{A}(\mathbf{r}) d\mathbf{r} = \frac{2e\Phi}{c\hbar} \quad (3.7.2)$$

arises. As a result, the waves propagating along two trajectories differing only in directions acquire a random phase difference, depending on the trajectory form. Hence, on the average, the probability of return decreases, leading to increasing conductivity. The characteristic magnetic field scale can be estimated, taking into account that the interference breaks down, if the phase difference becomes of order unity. As the distance L_φ over which coherence is conserved is of order $\sqrt{D\tau_\varphi}$, the flux through this contour is of order $HL_\varphi^2 = DH\tau_\varphi$. Therefore characteristic magnetic fields are defined by the relation

$$\frac{eH}{c} D\tau_\varphi \sim 1,$$

whence it follows that the quantum corrections begin to depend upon the magnetic field at

$$H \sim \frac{c}{e} D\tau_\varphi.$$

This condition can be written as

$$\omega_c \tau \sim \frac{1}{\mu\tau_\varphi}. \quad (3.7.3)$$

It is seen that characteristic magnetic fields are much weaker in the parameter than the fields strong in a classical sense, $\mu\tau_\varphi \ll 1$.

As shown in Chapter 3.2, the main quantum correction to the conductivity of noninteracting particles arises when we account for the Cooper diagrams describing the interference arising in multiple backward scattering. The amplitude of this interference, $C(\mathbf{r}, \mathbf{r})$, precisely determines the AMR.

The conductivity correction at frequency ω is related to $C_\omega(\mathbf{r}, \mathbf{r})$ by the relation (3.A.1):

$$\delta\sigma(\omega) = -\frac{2e^2}{\pi} D\tau C_\omega(\mathbf{r}, \mathbf{r}). \quad (3.7.4)$$

and $C_\omega(\mathbf{r}, \mathbf{r})$ in the magnetic field obeys the equation

$$\left\{ -i\omega + D \left(-i\nabla - \frac{2e}{c} \mathbf{A} \right)^2 + \frac{1}{\tau_\varphi} \right\} C_\omega(\mathbf{r}, \mathbf{r}') = \frac{\delta(\mathbf{r} - \mathbf{r}')}{\tau}. \quad (3.7.5)$$

Eq. (3.7.5) formally coincides with the Green function equation for a particle of the charge $2e$ and mass $(2D)^{-1}$, moving in the magnetic field. It is the small mass of this imaginary particle that is the

cause of a strong field effect, since the corresponding cyclotron frequency obeys the inequality $DeH/c \sim \mu\tau\omega_c \gg \omega_c$.

If $\psi_{n,Q_y}(\mathbf{r})$ is a normalized wave function of this particle in the magnetic field, the expression for $C_\omega(\mathbf{r}, \mathbf{r}')$ takes on the form

$$C_\omega(\mathbf{x}, \mathbf{x}', Q_z) = \frac{1}{\tau} \sum_{n, Q_y} \frac{\psi_{n, Q_y}(\mathbf{x}) \psi_{n, Q_y}^*(\mathbf{x}')}{-i\omega + DQ_z^2 + \frac{4DeH}{c} \left(n + \frac{1}{2}\right) + \tau_\varphi^{-1}}. \quad (3.7.6)$$

As mentioned in Chapter 3.2, a sample is two-dimensional if its thickness $a < \sqrt{D\tau_\varphi}$. If the magnetic field is perpendicular to the film surface, we should ignore the term DQ_z^2 in (3.7.6). Substituting (3.7.6) into (3.7.4), integrating over Q_y and summing over n , we obtain [50]

$$\sigma^{(2)}(H) - \sigma^{(2)}(0) = \frac{e^2}{2\pi^2} f_2 \left(\frac{4DeH}{c} \tau_\varphi \right), \quad (3.7.7)$$

where

$$f_2(x) = \ln x + \psi \left(\frac{1}{2} + \frac{1}{x} \right) = \begin{cases} \frac{x^2}{24} & \text{at } x \ll 1, \\ \ln x & \text{at } x \gg 1. \end{cases} \quad (3.7.8)$$

Here $\psi(y)$ is the logarithmic derivative of the Γ -function. As seen from Eq. (3.7.7), characteristic magnetic fields are really defined by the condition (3.7.3), hence the classical positive magnetoresistance in this range is still very small.

In three dimensions [55]

$$\delta\sigma^{(3)}(H) = \frac{e^2}{2\pi^2} \sqrt{\frac{eH}{c}} f_3 \left(\frac{4DeH}{c} \tau_\varphi \right), \quad (3.7.9)$$

where

$$f_3(x) = \sum_{n=0}^{\infty} \left\{ 2 \left(\sqrt{n+1+x} - \sqrt{n+x} \right) - \frac{1}{\sqrt{n+x+1/2}} \right\}, \quad (3.7.10)$$

$$f_3(x) = \begin{cases} \frac{x^{3/2}}{48} & \text{at } x \ll 1, \\ 0.605 & \text{at } x \gg 1. \end{cases} \quad (3.7.11)$$

We can see from Eqs. (3.7.9) and (3.7.10) that in a strong magnetic field ($H \gg \frac{c}{4De\tau_\varphi}$) the absolute value of the magnetoconductivity is universal and independent of scattering mechanisms as well as other sample parameters.

Therefore in handling the experimental data it is more natural to study the magnetic field dependence of the conductivity, $\delta\sigma(H)$, and not relative resistivity $\delta\rho(H)/\rho$, as is usually done.

The AMR arising from the quantum coherence being destroyed by the magnetic field is evidently independent of the mutual-orient-

tation of the magnetic field and current. Therefore it can be both longitudinal and transverse, which is precisely observed in experiments.

3.7.2 Magnetoresistance of Thin Films and Wires in Longitudinal Magnetic Field

If a thin wire is placed in a magnetic field, the AMR builds up. However, the preceding argument is not applicable in this case, since the diffusion in the plane perpendicular to the wire axis is limited by transverse dimensions. This is also true for a thin film in a magnetic field lying in the film plane [56].

Let the sample transverse dimensions a be less than $L_\varphi = \sqrt{D\tau_\varphi}$. This means that during the time τ_φ an electron would visit all the points in the transverse plane of the sample. To estimate the effect, we use de Gennes's method of calculating the phase relaxation time in small superconductor samples in the presence of magnetic fields [57]. The phase gain at different sections of the trajectory is random, therefore

$$\langle e^{i\varphi(t)} \rangle = e^{-\frac{1}{2} \langle \varphi^2(t) \rangle},$$

where

$$\varphi(t) = \int_0^t \frac{2e}{c} (\mathbf{A} \cdot \mathbf{v}) dt'. \quad (3.7.12)$$

In the time intervals large in comparison with the time between collisions, we have

$$\begin{aligned} \langle \varphi^2 \rangle &= 2t \int_0^\infty \frac{4e^2}{c^2} A_\alpha(\mathbf{r}) A_\beta(\mathbf{r}') \langle v_\alpha(0) v_\beta(t') \rangle dt' \\ &= 2t \frac{4e^2}{c^2} A^2(\mathbf{r}) \frac{v_F^2}{3} \int_0^\infty dt' e^{-t'/\tau}, \end{aligned}$$

since during the time of order τ a particle covers a distance small ($\sim l$) compared with the characteristic scale of $\mathbf{A}(\mathbf{r})$. As a result, we have

$$\langle e^{i\varphi(t)} \rangle = e^{-t/\tau_H}, \quad t \gg \tau,$$

where

$$\frac{1}{\tau_H} = \frac{4e^2}{c^2} D \langle A^2(\mathbf{r}) \rangle. \quad (3.7.13)$$

In the gauge $A_y = A_z = 0$, $A_x = Hy$ ($\mathbf{H} \parallel z$) for a film of thickness a , $\langle A^2(\mathbf{r}) \rangle = H^2 a^2 / 12$.

The influence of a longitudinal magnetic field becomes considerable when τ_H is comparable to τ_φ , or, according to (3.7.13), when the relation

$$L_\varphi^2 a^2 \sim \frac{4e^2 H^2}{c^2} = L_H^4 \quad (3.7.14)$$

holds.

When the film thickness a is of the order of the magnetic length or L_φ , in the magnetic field the film behaves as a three-dimensional system. Note that in the longitudinal field the magnetoresistance effect is weaker than in the transverse field, as characteristic fields in a longitudinal configuration are $L_\varphi/a \gg 1$ times larger. Though the expression (3.7.13) is not gauge invariant, a consistent derivation excludes, of course, such an ambiguity.

To calculate the magnetoresistance, we solve Eq. (3.7.5) for $C_\omega(\mathbf{r}, \mathbf{r}')$ in the magnetic field in a sample of finite dimensions with the boundary condition

$$\left\{ \frac{\partial}{\partial \mathbf{n}} + \frac{2ie}{c} (\mathbf{A} \cdot \mathbf{n}) \right\} C_\omega(\mathbf{r}, \mathbf{r}') \Big|_S = 0. \quad (3.7.15)$$

The condition (3.7.15) implies that the particle flux through the sample boundary equals zero. Equation (3.7.5) with the boundary condition (3.7.15) can be solved by the perturbation theory in the magnetic field.

Consider first a thin film in a longitudinal magnetic field. The solution of Eq. (3.7.5) with the gauge $A_y = A_z = 0$, $A_x = Hy$ can be represented as

$$C(y, y') = \frac{1}{\tau} \int \frac{dQ_x dQ_z}{(2\pi)^2} \sum_n \frac{\varphi_{n, Q_x}(y) \varphi_{n, Q_x}^*(y')}{DQ_z^2 + \varepsilon_{n, Q_x} + \frac{1}{\tau_\varphi}}, \quad (3.7.16)$$

where $\varphi_{n, Q_x}(y)$ and ε_{n, Q_x} are eigenfunctions and eigenvalues of the equation

$$-D \left[\frac{\partial^2}{\partial y^2} - \left(Q_x - \frac{2eHy}{c} \right)^2 \right] \varphi_{n, Q_x} = \varepsilon_{n, Q_x} \varphi_{n, Q_x}(y) \quad (3.7.17)$$

with a boundary condition

$$\frac{\partial}{\partial y} \varphi_{n, Q_x}(y) \Big|_{y=\pm \frac{a}{2}} = 0. \quad (3.7.18)$$

If $a \ll L_\varphi$, then in (3.7.16) we can keep only the ground state with $n = 0$.

In the second-order perturbation theory in the magnetic field, ε_{0, Q_x} has the form

$$\varepsilon_{0, Q_x} = DQ_x^2 + \frac{a^2 D}{12 L_H^4} = DQ_x^2 + \frac{1}{\tau_H}. \quad (3.7.19)$$

Then the variation of the film conductivity in the field can be written as

$$\sigma^{(2)}(H) - \sigma^{(2)}(0) = -\frac{2e^2}{\pi} \int \frac{dQ_x dQ_z}{(2\pi)^2} \cdot \frac{1}{Q_x^2 + Q_z^2 + \frac{1}{D\tau_H} + \frac{1}{D\tau_\varphi}}. \quad (3.7.20)$$

Integrating over Q_x and Q_z , we obtain

$$\sigma^{(2)}(H) - \sigma^{(2)}(0) = -\frac{e^2}{2\pi^2} \ln \left(1 + \frac{\tau_\varphi}{\tau_H} \right). \quad (3.7.21)$$

As seen from Eqs. (3.7.19)-(3.7.21), τ_H really coincides with the decay time of the phase of the wave function (3.7.13). Note that the perturbation theory and, consequently, Eq. (3.7.21) holds when $a \ll L_H$. According to (3.7.14), the field becomes strong when $L_H \simeq \simeq \sqrt{aL_\varphi} \gg a$, i.e. when the perturbation theory is valid. For a thin wire the conductance per unit length has the form

$$\sigma^{(1)} = \frac{e^2}{\pi^2} \cdot \frac{1}{\sqrt{L_\varphi^2 + (D\tau_H)^{-1}}}, \quad (3.7.22)$$

the time τ_H being dependent of the orientation of the field and the form of the wire cross section. For a wire of a circular cross section of a radius R in the longitudinal magnetic field we have

$$\tau_H = \frac{L_H^4}{DR^2}. \quad (3.7.23)$$

For a wire of a rectangular cross section in the field parallel to one of the rectangle sides,

$$\tau_H = \frac{12L_H^4}{Da^2}, \quad (3.7.24)$$

where a is the wire transverse dimension in the direction, perpendicular to the field [cf. (3.7.19)].

3.7.3 Magnetoresistance and Scattering by Superconducting Fluctuations

The electron scattering by superconducting fluctuations leads to the temperature-dependent correction to the conductivity even far from the transition point (see Chapter 3.4). Furthermore, these fluctuations exist even in the case of electronic repulsion, when the superconducting transition is absent.

Magnetic field depresses these fluctuations and the arising effect partially compensates the effect of the AMR considered in Sec. 3.7.1 [37]. As shown in Chapter 3.4, the correction to the conductivity, arising due to the scattering by superconducting fluctuations, is

related to the cooperon by the relation

$$\delta\sigma_{M-T} = \frac{2e^2 D}{\pi} \tau C(\mathbf{r}, \mathbf{r}) \beta(T). \quad (3.7.25)$$

The properties of $\beta(T)$ have already been discussed in Sec. 3.4.4. Here we only note that the sign of $\beta(T)$ does not depend on the sign of the coupling constant, $\beta(T)$ being always positive. In calculating $\beta(T)$, it is possible to neglect the magnetic field influence on the effective coupling constant λ^c , because λ^c changes essentially only in the fields $H \sim \frac{Tc}{4eD}$, which are much larger than the fields characteristic of the magnetoresistance, $H \sim \frac{c}{4eD\tau_\phi}$.

The magnetic field dependence of the Maki-Thompson correction (3.7.25) is precisely the same as for noninteracting electrons, because the Maki-Thompson term is related to the cooperon by a linear relation, just as the correction to the conductivity of noninteracting electrons. However, these two effects have opposite signs, hence the magnetoresistance partially decreases due to the scattering by superconducting fluctuations, and the magnetoconductivity is described by expressions (3.7.7) and (3.7.9) with a factor $1 - \beta(T)$.

As mentioned above, the asymptotics of the magnetoconductivity have a universal form (3.7.8) and (3.7.11), independent of sample parameters. The scattering by superconducting fluctuations accounted for, the slope of the $\delta\sigma(H)$ versus $\ln H$ curve in two dimensions and the $\delta\sigma(H)$ versus \sqrt{H} curve in three dimensions allows to find the value and the temperature dependence of $\beta(T)$. Thus, we extract information concerning the effective interaction between electrons at large momentum and energy transfers.

3.7.4 Magnetoresistance in Many-Valley Semiconductors

The theory exposed above is easily generalized to the case of anisotropic diffusion [13]. The magnetoconductivity is now a tensor related to the diffusion coefficient tensor D_{ik} by the formulae:

$$\delta\sigma_{ik}^{(2)} = \frac{D_{ik}}{D_a} \frac{e^2}{2\pi^2} f_2 \left(\frac{4eD_c H}{c} \tau_\psi \right) \quad (3.7.26)$$

in two dimensions, the field being perpendicular to the film plane, and

$$\delta\sigma_{ik}^{(3)} = \frac{D_{ik}}{D_a} \frac{e^2}{2\pi^2} f_3 \left(\frac{4eD_c H}{c} \tau_\psi \right) \sqrt{\frac{eH}{c} \frac{D_c}{D_a}} \quad (3.7.27)$$

in three dimensions. Here

$$D_c^2 = D_\perp (D_\perp \cos^2 \theta + D_\parallel \sin^2 \theta), \quad (3.7.28)$$

θ is the angle between the ellipsoid axis and the magnetic field direction, $D_a = (D_{\parallel} D_{\perp}^2)^{1/3}$. The Maki-Thompson correction leads, as in the isotropic case, to a factor $1 - \beta(T)$ on the right-hand sides of Eqs. (3.7.26) and (3.7.27).

In some semiconductors, such as Ge, Si, and Te, the conduction band consists of several valleys, the diffusion coefficient being anisotropic in each valley. If U-processes can be ignored, the contributions of different valleys are additive. The number of particles in each valley is conserved and density fluctuations for charge carriers are described by the diffusion equation. If U-processes cannot be neglected, only the total number of particles is conserved and the diffusion equation describes only total density fluctuations. Asymmetric fluctuations of the occupation numbers in different valleys relax during the time of intervalley transitions τ_v , which can be much longer than the intravalley energy relaxation time τ .

An analogous situation is also realized for phase fluctuations described by the cooperon. Only the cooperon symmetric in valley indices and off-diagonal in each pair of equivalent (having the same orientation) valleys (if there is any) conserves the pole $(-i\omega + DQ^2)^{-1}$; all other components decay during the time τ_v , i.e. at $\tau_v \gg \tau$ they have the form $(-i\omega + DQ^2 + \tau_v^{-1})^{-1}$.

The fact that the non-decaying cooperon is off-diagonal in the indices of equivalent valleys is connected with the total momentum $\mathbf{Q} = \mathbf{p}_1 + \mathbf{p}_2$ being equal to zero. As a result, for time intervals much larger than the intervalley transition time, instead of n independent cooperons we have only one. It contains the diffusion coefficient D related to the total sample conductivity by the Einstein relation. Therefore at $\tau_v \ll \tau_{\varphi}$ and $4D_{\perp, \parallel} eH\tau_v/c \ll 1$ the magnetoconductivity has the form (3.7.7) in two dimensions and the form (3.7.9) in three dimensions for crystals with cubic symmetry [13].

If, however, $4D_{\perp, \parallel} eH\tau_v/c \gg 1$ or $\tau_v \gg \tau_{\varphi}$, then

$$\delta\sigma_{ih}^{(d)}(H) = \sum_{\alpha} \delta\sigma_{ih}^{(d)}(H, \alpha), \quad (3.7.29)$$

where $\delta\sigma_{ih}^{(d)}(H, \alpha)$ is the magnetoconductivity of a valley with index α , defined by Eqs. (3.7.26) and (3.7.27). Note that the angles between the magnetic field and ellipsoid axis are different for different valleys. As seen from Eqs. (3.7.26) and (3.7.27), the magnetoconductivity anisotropy is related only to the anisotropy of the diffusion coefficient and not to the anisotropy of the effective mass tensor (cf. [55]).

Thus, the magnetoconductivity in the anisotropic case also does not depend on the mutual orientation of the field and current flowing through the sample. In weak fields ($4eD_{\perp, \parallel} H\tau_v/c \ll 1$) the magnetoconductivity is independent of the magnetic field orientation with respect to crystal axes. In strong fields (or if $\tau_v \gg \tau_{\varphi}$) a noticeable

anisotropy of the magnetoconductivity must exist. If the anisotropy of the diffusion coefficient in one valley is large, there is an interval of intermediate magnetic fields,

$$\frac{c}{4eD_{\max}\tau_v} \ll H \ll \frac{c}{4eD_{\min}\tau_v},$$

in which the magnetoconductivity is anisotropic, but the degree of the anisotropy depends on the magnetic field.

As in the case of a simple band structure, for many-valley semiconductors it is necessary to account for the electron scattering by superconducting fluctuations. In weak magnetic fields (or at small τ_v) this leads to a factor $1 - \beta(T)$ in Eqs. (3.7.26), (3.7.27), (3.7.7) and (3.7.9), independent of the number of valleys. In strong fields, or at $\tau_v \gg \tau_\varphi$ the Maki-Thompson correction leads to a factor $1 - \beta(T)(2n_1 - 1)$ in Eq. (3.7.29), where n_1 is the number of equivalent valleys [13]. (In Ge $n_1 = 1$, in Si $n_1 = 2$.)

3.7.5 Effect of Spin-Orbit Scattering on Magnetoconductivity

As shown in Chapter 3.2, spin-orbit scattering influences both the magnitude and the sign of the localization corrections to the conductivity. This scattering accounted for in a simple band, each cooperon is splitted into two cooperons: one of them describes the propagation of a singlet and the other, of a triplet two-particle wave function [9, 10]. Spin-orbit scattering leads to decay of the triplet part, leaving unchanged the singlet part of the cooperon. Hence in the fields satisfying the condition

$$\frac{4DeH}{c} \tau_{so} \ll 1, \quad (3.7.30)$$

and at $\tau_\varphi \gg \tau_{so}$ the contribution of the triplet part to the magnetoconductivity can be neglected. The singlet part, according to (3.2.29), is two times smaller than the unsplitted cooperon and has a reversed sign. This means that the spin-orbit scattering changes simultaneously the sign of the temperature-dependent localization correction to the conductivity and the sign of the magnetoconductivity [9], diminishing their values by a factor of two. Thus, the AMR becomes positive.

The magnetic field increasing, the condition (3.7.30) ceases to be valid and the sign of the magnetoconductivity changes (the magnetoresistance becomes negative). The absolute value of the magnetoconductivity is the same as without the spin-orbit interaction. If $\tau_\varphi \ll \tau_{so}$, spin-orbit effects can be ignored.

Contrary to the localization corrections to the conductivity, the Maki-Thompson corrections contain two cooperons. There are

two terms: one is of Hartree type (Fig. 3.17c) and the other is of exchange type (Fig. 3.17d) These terms are proportional to

$$\sum_{\alpha\beta\gamma\delta} C_{\alpha\beta\gamma\delta} C_{\beta\alpha\delta\gamma} = 4(A^2 + B_z^2 + 2B_x^2) \quad (3.7.31)$$

and

$$-\sum_{\alpha\beta\gamma\delta} C_{\alpha\beta\gamma\delta} C_{\beta\gamma\delta\alpha} = -2[(A + 2B_x + B_z)^2 - 4B_x(B_x + 2B_z)]$$

respectively. As a result, the total Maki-Thompson correction is proportional to [see (3.2.35)]

$$2(A - B_z - 2B_x)^2 = \frac{2}{\tau^2} t_2 = \frac{2}{\tau^2} \left(-i\omega + DQ^2 + \frac{2}{\tau_s^2} + \frac{4}{\tau_s^2} \right)^{-1} \quad (3.7.32)$$

and does not depend on the spin-orbit scattering. Such a result is related to the Pauli principle due to which the contact interaction between electrons is possible only if they are in the singlet state which is not sensitive to the spin-orbit interaction. Thus, the account for the spin-orbit coupling leads to the magnetoconductivity given in the case of a simple anisotropic band by the expression (3.7.27) with a factor $\left[-\frac{1}{2} - \beta(T) \right]$.

As mentioned in Chapter 3.2, two types of spin relaxation due to the spin-orbit coupling can take place: (a) relaxation arising due to the electron spin interaction with impurity potential, the corresponding relaxation time being described by (3.2.32b), and (b) relaxation due to the spin-orbit splitting of the conduction band in crystals without the inversion centre.

In two dimensions, when a film is thick, i.e. size quantization is absent (quasi-two-dimensional case), all effects of the spin-orbit coupling are analogous to three-dimensional case. However in truly two-dimensional case (e.g. in MOS-structures) they manifest themselves in a different way (Chapter 3.2). As shown in this chapter, at $T \rightarrow 0$ the quantum corrections to the conductivity, the spin-orbit scattering by impurities accounted for, are limited [see Eq. (3.2.35)]. This means that if $\tau_\phi \gg \tau_{so}^2$ and $DeH/c \ll 1/\tau_{so}^2$, the magnetoresistance is small. At the same time the spin-orbit splitting of the carrier spectrum influences the magnetoconductivity in two dimensions in the same way as in three dimensions, as in this case $(\tau_{so}^2)^{-1} \neq 0$ (see Chapter 3.2).

As noted in Chapter 3.2, in cubic semiconductors of *p*-type the spin relaxation is realized in the elastic electron scattering due to complicated structure of the valence band. The magnetoresistance of noninteracting electrons should be positive and two times smaller than the magnetoresistance in a simple band. If uniaxial stresses are applied, the four-fold degenerate band splits up into two two-fold degenerate bands. When the deformational band splitting is larger

than the Fermi energy, the magnetoresistance becomes negative, its magnitude increasing by a factor of four. Accounting for a complicated structure of the valence band results in that $\delta\sigma_{M-T}(H)$ becomes 16 times smaller than in the case of a simple band, without changing its sign. Therefore in a deformed crystal the Maki-Thompson correction $\delta\sigma_{M-T}(H)$ increases drastically and in the limit of strong deformations it is 16 times larger than in an undeformed crystal.

In inversion p -type layers the magnetoresistance logarithmically depends on H [see Eqs. (3.7.7) and (3.7.8)] and, as far as the prelogarithmic factor is concerned, two situations are possible. If the band splitting due to size quantization in an inversion layer is larger than the Fermi energy, then the magnitude and sign of the factor are the same as in the case of a simple band or deformed three-dimensional semiconductors of p -type. If, however, the "size splitting" is small, the situation is similar to that in three-dimensional samples of p -type, when deformation is small.

Theoretical results for different band structures and mechanisms of intervalley and spin relaxation are listed in Table 3.7.1.

Table 3.7.1

Semiconductors	Three dimensions	Two dimensions
	k_3	k_2
A simple band without spin-orbit effects	1	1
Spin-orbit scattering by impurities	$-\frac{1}{2}$	Quasi-two-dimensional case $-\frac{1}{2}$ Two-dimensional case 0
n -GaAs, n -InSb	$-\frac{1}{2}$	$-\frac{1}{2}$
p -Ge	$-\frac{1}{4}$	$-\frac{1}{4}$
p -Ge (deformed)	1	1

3.7.6 Experiment

The negative magnetoresistance has been observed in various materials by many authors. However, only in some cases experimental results have been compared with the theory exposed above. Two-dimensional experiments were carried out in (100)-plane [58-60]. In [58, 59] transverse magnetoresistance was investigated.

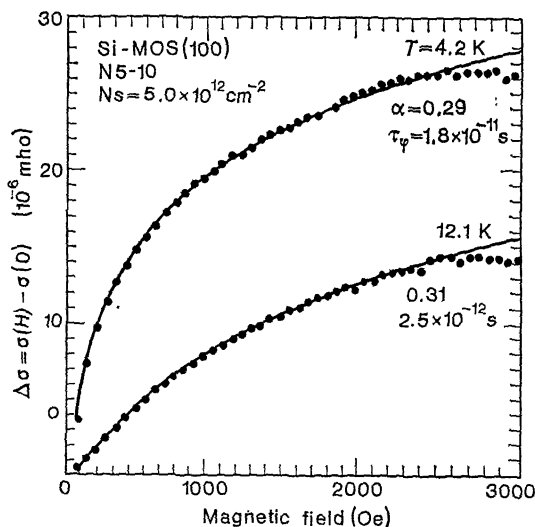


Fig. 3.25. $\Delta\sigma(H)$ versus H for Si-MOS structure at two temperatures [58].

The negative magnetoresistance was shown to depend only on the normal component of magnetic field [60], consequently, it cannot be accounted for by field-dependent spin effects.

Figure 3.25 shows experimental data [58] compared with the theoretical expression (3.7.7) times 2α . It is seen that experimental points fit the theoretical curve at $\alpha \simeq 0.3$. In an inversion layer electrons fill two equivalent valleys in which the motion in the (100)-plane is isotropic. If intervalley transitions are frequent enough, the magnetoconductivity must be described by the expression (3.7.7) with a factor $[1 - \beta(T)] = 2\alpha$ independent of the number of valleys. In this case $\beta(T) \simeq 0.4$, indicating a strong interaction between electrons. If, however, $\tau_\phi \ll \tau_v$, then $2\alpha \approx 2[1 - 3\beta(T)]$, as in Si $n_1 = 2$, and $\beta(T) = 0.23^*$. Comparing the theory with

* Note that in [58] the expression (3.7.7) times the number of valleys, n_v , was used. As shown in Sec. 3.7.4, this expression is valid in the absence of intervalley transitions.

experimental results in the temperature range from 4 to 20 K, the temperature dependence of τ_φ has been found to fit the T^{-2} curve (Fig. 3.26), apparently indicating that the phase relaxation is determined mainly by the electron-electron collisions. Analogous results have been obtained in [59], but the estimate of τ_φ is in good agreement with that obtained from the expression (3.4.23) for the electron-electron collisions in the case of strong disorder.

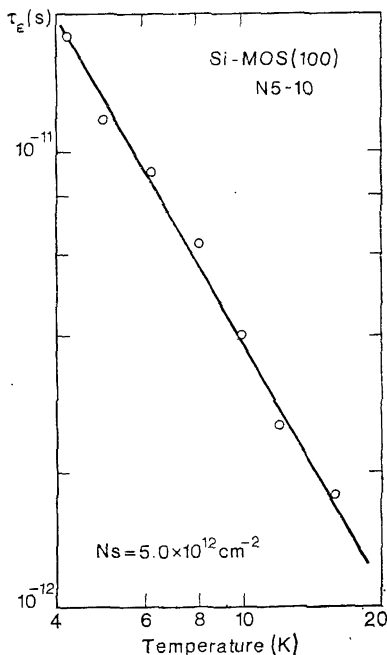


Fig. 3.26. τ_φ versus T for Si-MOS structure [58].

The magnetoresistance was investigated in the low temperature range 0.1-4 K [23] and analogous result was found: $\alpha \approx 0.28$. However, the magnetoresistance vanished at 4 K. Estimations show that in these experiments, at $T = 4$ K, τ and τ_φ become equal. In this temperature range the temperature dependence of τ_ψ (see Sec. 3.4.3) was found.

Kawabata[55] compared the theory of the AMR with experimental data for GaAs [61] and Ge [62-65].

Table 3.7.2. lists the data for GaAs [61]. The theoretical value of $\delta\sigma(H)$ has been found by Kawabata [55]. The value found by Eqs. (3.7.9)-(3.7.11) in the strong field limit is seen to be two times larger than the experimental value. The Maki-Thompson correction was not

Table 3.7.2

Sample	$(10^{18} \cdot \text{cm}^{-3})$	$(\text{ohm}^{-1} \cdot \text{cm}^{-1})$	$\frac{\Delta\rho}{\rho} \%$	$\delta\sigma$ $(\text{ohm}^{-1} \cdot \text{cm}^{-1})$	$\delta\sigma_{\text{theor}}$ $(\text{ohm}^{-1} \cdot \text{cm}^{-1})$
No.2	0.5	156	-0.5	0.78	1.45
No.3	0.75	298	-0.25	0.74	1.45
No.4	3.1	690	-0.09	0.62	1.45
Conditions				4.2 K;	2.5 kOe

taken into account in [55]. This correction accounted for, $\beta(T) \simeq 0.5$. As in Si inversion layers, this means that the electron-electron interaction in GaAs is also sufficiently strong.

Let us estimate the spin relaxation time τ_{so} due to the spin-orbit coupling. According to [66], the constant δ in Eq. (3.2.37) is expressed through the material parameters:

$$\delta = \frac{\alpha}{2 \sqrt{2} m_c^{3/2} E_g^{1/2}}, \quad (3.7.33)$$

where m_c is the electronic mass in the conduction band, E_g is the width of the forbidden band. In GaAs, $\alpha = 2.2 \times 10^{-2}$ [66]. From Eq. (3.2.38), at $m_c = 6 \times 10^{-29}$ g and $E_g = 1.5$ eV, we obtain $\tau_{\text{so}} \sim 2 \times 10^{-9} - 2 \times 10^{-10}$ sec. Note that $\tau_\varphi \sim 10^{-11}$ sec $\ll \tau_{\text{so}}$, and therefore spin-orbit effects are not observed. Apparently, to observe them in the AMR, narrow-band semiconductors of the InSb type are to be taken.

Sasaki [62] examined the angular dependence of the negative magnetoresistance in n -Ge. When the current flows in the $[1\bar{1}0]$ direction and a field points in the $[111]$ direction, $\delta\rho/\rho \simeq -2.6\%$ at $\rho = 5.8 \times 10^{-3}$ ohm·cm in the field $H = 5$ kOe. This corresponds to $\delta\sigma \simeq 4.5$ ohm $^{-1}$ ·cm $^{-1}$. If an anisotropy parameter of the diffusion coefficient in one valley, $k = D_{||}/D_{\perp}$, is introduced, then for these directions of the current and magnetic field at $\tau_\varphi \ll \tau_v$ the magnetoconductivity, according to (3.7.29) and (3.7.27), can be written in the form

$$\delta\sigma(H) = \frac{0.918}{\sqrt{k}} \left[1 - \beta(T) \right] \left[k^{1/4} + \frac{(5+4k)(8+k)^{1/4}}{3\sqrt{3}} \right] \sqrt{H \text{ (kOe)}}. \quad (3.7.34)$$

If we assume, as in [55], that the anisotropy of the diffusion coefficient k coincides with the anisotropy of the inverse effective mass tensor and equals 0.05, and if we ignore the Maki-Thompson corrections, then the theoretical value of $\delta\sigma$ equals 19.9 ohm $^{-1}$ ·cm $^{-1}$, being 4.4 times greater than the experimental value. In reality, the

anisotropy of the diffusion coefficient is less than the anisotropy of the effective masses. According to [67], $k \simeq 0.1-0.25$. Using $k = 0.2$, we find that a good fitting is obtained when $\beta(T) \simeq 0.6$. In fact, $\beta(T)$ may be smaller if we take into account that the asymptotics (3.7.34) is possibly achieved in higher fields.

Rotar et al. [65], examining the magnetoresistance in Ge, have shown that their data can be well approximated by the relation

$$\frac{\Delta\rho}{\rho} \simeq aH^c + bH^2, \quad (3.7.35)$$

where a , b and c are fitting parameters. The second term in this expression gives the normal classical magnetoresistance. The exponent c declines with increasing concentration and decreasing temperature and approaches $1/2$ [65]. This behavior is in qualitative agreement with the theory, if we take into account that the length $L_\varphi = \sqrt{D\tau_\varphi}$ increases with increasing concentration and decreasing temperature, and therefore the strong field condition holds for weaker magnetic fields [55].

A negative magnetoresistance was observed in thin copper films [46]. Along with the logarithmic temperature dependence of the conductivity, this apparently indicates that the authors observed the localization corrections to the conductivity and their suppression by the magnetic field.

In a strongly doped p -Ge in the range of helium temperatures an "anomalous" positive magnetoresistance is observed, which has the same concentration and temperature dependence as the negative magnetoresistance in n -Ge [65, 68].

If a uniaxial stress is applied, the positive anomalous magnetoresistance turns into negative [53, 54]. Simultaneously the temperature correction to the conductivity changes its sign [53].

The theory exposed above correctly predicts the sign of the magnetoresistance: positive in undeformed samples and negative in strongly deformed ones. The theory also predicts a correlation of the signs of the magnetoresistance and localization corrections to the conductivity. Note that the sign of the temperature corrections to the conductivity due to localization effects is opposite to that observed in experiment. However, as shown in Sec. 3.4.3, in three dimensions the temperature dependence of the conductivity is determined by the electron interaction effects, the increase or decrease in the conductivity being dependent of the sign of the effective electron-electron interaction constant. This sign, in its turn, depends on the Fermi energy (or the nonideality parameter of the electron gas). As shown in experiments on n -Si [28], the interaction constant may change its sign with carrier concentration. If a uniaxial stress is applied to

p -Ge, bands split and the Fermi energy of the holes increases, which may result in the electron-electron interaction constant changing its sign. However, this question requires an additional detailed consideration.

3.7.7 Aharonov-Bohm Effect in Disordered Metals

As has been already shown, the quantum corrections to the conductivity are related to the electronic interference. This follows directly from Eq. (3.7.4), relating the conductivity to the cooperon $C_\omega(\mathbf{r}, \mathbf{r}')$. However, the relation between the conductivity and wave interference is most striking in the Aharonov-Bohm effect [69] in disordered conductors.

It is well known that the electronic wave functions and energy spectrum depend on the vector potential \mathbf{A} of magnetic field. This effect (the Aharonov-Bohm effect) manifests itself, for example, in the quantization of magnetic flux in a superconducting ring, in oscillations of the superconducting transition temperature with the magnitude of magnetic flux [70]. These phenomena can also take place in normal metals. Thus, Dingle [71] has shown that thermodynamic quantities should oscillate with the flux piercing a metallic cylinder. Analogous oscillations of kinetic quantities have been considered by Bogachek and Gogadze [72]. However, when scattering is switched on and the mean free path becomes of the order of sample dimensions, all these effects disappear, since elastic scattering broadens quantum levels connected with size quantization. Interference effects of the Aharonov-Bohm type occur also in impure metals, the relative magnitude of the effect growing with decreasing mean free path. The period of oscillations, $\Phi_0 = hc/2e$, appears to be two times shorter than in the ordinary Aharonov-Bohm effect ($\Phi'_0 = hc/e$).

Consider a hollow metallic cylinder with thin walls, in which a long solenoid is placed so that the magnetic field outside the solenoid equals zero (Fig. 3.27). However, in the sample itself the vector potential \mathbf{A} is not zero and has only a tangential component constant over the sample width. As the circumference of the cylinder is much larger than the mean free path, the size-quantized electron levels are smeared by elastic scattering. The equation for the cooperon $C_\omega(\mathbf{r}, \mathbf{r}')$ in the field of the vector potential \mathbf{A} has the form

$$\left\{ D \left(-i\nabla - \frac{2e}{c} \mathbf{A} \right)^2 - i\omega + \tau_\varphi^{-1} \right\} C_\omega(\mathbf{r}, \mathbf{r}') = \frac{\delta(\mathbf{r} - \mathbf{r}')}{\tau}. \quad (3.7.35)$$

This equation must be solved with periodic boundary conditions along the y -axis (Fig. 3.27) (i.e. along the cylinder circumfer-

ence). As a result, the solution of Eq. (3.7.5) has the form

$$C_{\omega}(\mathbf{r}, \mathbf{r}') = \frac{1}{L_y} \int \frac{d\mathbf{Q}_{\perp}}{(2\pi)^2} \sum_{l=-\infty}^{\infty} \frac{e^{i\mathbf{Q} \cdot (\mathbf{r} - \mathbf{r}')}}{-i\omega + \tau_{\Phi}^{-1} + D\mathbf{Q}_{\perp}^2 + D \left(Q_y^l - \frac{2e}{c} A \right)^2}, \quad (3.7.36)$$

where $\mathbf{Q}_{\perp} = (Q_x, Q_z)$, $Q_y^l = 2\pi l/L_y$, and $L_y = 2\pi R$ is the cylinder circumference. Inserting (3.7.36) into (3.7.4), we obtain at $\omega = 0$

$$\delta\sigma = -\frac{2e^2}{\pi} \cdot \frac{1}{L_y} \int \frac{d\mathbf{Q}_{\perp}}{(2\pi)^2} \sum_{l=-\infty}^{\infty} \frac{1}{Q_{\perp}^2 + \left(\frac{2\pi}{L_y} \right)^2 \left(l - \frac{\Phi}{\Phi_0} \right)^2 + L_{\Phi}^{-2}}. \quad (3.7.37)$$

Consider first quasi-one-dimensional case, when both the width, L_x , and the height, L_z , of the ring are much smaller than L_{Φ} . In this

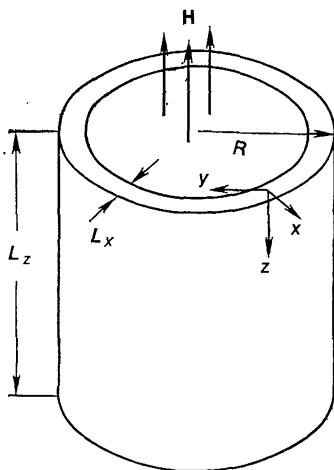


Fig. 3.27.

case the integrals over Q_x and Q_z should be replaced by the sum in which only the term with $Q_x = Q_z = 0$ should be retained. Hence the conductance per unit length, $\delta\sigma^{(1)} = \delta\sigma L_x L_z$, is given by the formula

$$\delta\sigma^{(1)} = \delta\sigma L_x L_z = -\frac{e^2}{2\pi^3} L_y \sum_{l=-\infty}^{\infty} \frac{1}{\left(l - \frac{\Phi}{\Phi_0} \right)^2 + \left(\frac{L_y}{2\pi L_{\Phi}} \right)^2}. \quad (3.7.38)$$

The sum in (3.7.38) is easily calculated, and we obtain

$$\delta\sigma^{(1)} = -\frac{e^2}{\pi} L_\varphi \frac{\sinh\left(\frac{L_y}{L_\varphi}\right)}{\cosh(L_y/L_\varphi) - \cos(2\pi\Phi/\Phi_0)}. \quad (3.7.39)$$

It is seen that the conductance of the ring oscillates with the flux with a period $\Phi_0 = hc/2e$, and the modulation amplitude declines exponentially with increasing length of the ring at $L_y \gg L_\varphi$. Let $L_z \gg L_\varphi$, i.e. the sample is a film rolled up into a cylinder. If the film is square in shape, then its conductance, $\sigma^{(2)} = \sigma L_x$, is

$$\delta\sigma^{(2)} = \frac{e^2}{\pi^2} \left\{ \ln \frac{L_\varphi}{l} + 2 \sum_{n=1}^{\infty} K_0\left(n \frac{L_y}{L_\varphi}\right) \cos \frac{2\pi n \Phi}{\Phi_0} \right\}. \quad (3.7.40)$$

Thus, as in the case of a thin ring, the conductance oscillates with a period Φ_0 . The oscillation amplitude equals $K_0(L_y/L_\varphi)$, where $K_0(x)$ is McDonald's function, and decreases exponentially at $L_y \gg L_\varphi$. As $T \rightarrow 0$, $L_\varphi \rightarrow \infty$ and the oscillation amplitude is seen to tend to infinity and ceases to depend on the degree of disorder.

Let us discuss the conditions under which this effect is observed. In [46] the temperature dependence of conductance of thin copper films was investigated. The electronic mean free path l was determined by the scattering at the film boundaries and equaled approximately 10^{-6} cm. The phase relaxation time τ_φ was determined by inelastic electron-phonon processes. If it is assumed that $\tau_\varphi^{-1} \sim \tau_e^{-1} \simeq \simeq \frac{T^3}{\theta^3}$, then for $\theta \simeq 300$ K and $T \simeq 1$ K, $\tau_\varphi \simeq 10^{-6}$ sec, and $L_\varphi = l \sqrt{\tau_\varphi/3\tau} \simeq 10^{-2}$ cm. Hence for a cylinder of diameter $d \simeq 10 \mu\text{m}$, $L_\varphi \gg 2\pi R$ and the Aharonov-Bohm effect should be observed.

3.7.8 Effects of Electron-Electron Interaction in Magnetic Field

It has been shown in Chapter 3.4 that there are two types of contributions from the electron-electron interaction:

1. Contributions arising when the interaction in the diffusion channel is taken into account. Magnetic field changes not the diffusion character of propagation of density fluctuations, but only the diffusion coefficient. As a result, all expressions conserve their form, the field dependence of the diffusion coefficient and arising anisotropy accounted for [26]. This field effect is observed only in classically strong fields, when $\omega_c \tau \gg 1$.

2. Contributions arising when interactions in the Cooper channel are considered. These contributions essentially depend on magnetic

field already in the range of classically weak fields, i.e. at

$$\omega_c \tau \sim \frac{T}{\mu} \ll 1. \quad (3.7.41)$$

For such fields the magnetic field dependence of all quantities is determined entirely by the interactions in the Cooper channel.

Consider first the density of states. The field dependence of the state density correction is connected with the graphs shown in Fig. 3.10c,d. Using Eq. (3.7.6) for the cooperon in a magnetic field, we obtain that the correction we are considering has the form

$$\begin{aligned} \delta v(\varepsilon, T) = & \frac{2eH}{c} \ln \int_0^\infty \frac{d\omega}{2\pi} \int \frac{dQ_z}{2\pi} \sum_{n=0}^{(L_H/l)^2} \lambda_n^c(2\varepsilon - \omega, H, Q_z) \\ & \times \frac{\tanh \frac{\varepsilon + \omega}{2T} + \tanh \frac{\omega - \varepsilon}{2T}}{\left[-i\omega + DQ_z^2 + \frac{D}{L_H^2}(2n+1) \right]^2}. \end{aligned} \quad (3.7.42)$$

The interaction constant λ^c depends on the field, n and Q . First we shall ignore these dependences, as well as the dependence on ε and ω . Using the relation

$$\sum_{n=0}^{\infty} \frac{1}{x + ny} = \int_0^\infty \frac{e^{-xt} dt}{1 - e^{-yt}},$$

Equation (3.7.41) can be written in the form

$$\begin{aligned} \delta v_d(\varepsilon, T, H) = & v_d(\varepsilon, T, H) - v_d(\varepsilon, T, 0) \\ = & \frac{\lambda^c}{2(4\pi D)^{d/2}} \int_0^\infty d\omega \left[\tanh \frac{\varepsilon + \omega}{2T} + \tanh \frac{\omega - \varepsilon}{2T} \right] \\ & \times \int_0^\infty t^{1-d/2} dt \sin \omega t \left[1 - \frac{\Omega_H t}{2 \sinh \frac{\Omega_H t}{2}} \right], \end{aligned} \quad (3.7.43)$$

where $\Omega_H = 4DeH/c$.

This expression is valid for $d = 2, 3$. To derive it in the case $d = 2$, the integral over Q_z should be replaced by the sum in which only the term with $Q_z = 0$ should be left. Asymptotic behavior of $\delta v_d(\varepsilon, T, H)$ for different relations between ε , T and Ω_H (or between L_ε , L_T and L_H) is represented in Table 3.7.3.

Table 3.7.3

	$d=2$	$d=3$
$\varepsilon \gg T$ $\Omega_H \ll \varepsilon$ $(L_H \gg L_\varepsilon)$	$\delta v(H) = -6.63 \times 10^{-3} \frac{\lambda^c L_\varepsilon^2}{\varepsilon a L_H^4}$ $\sim -\lambda^c \frac{H^2}{\varepsilon^2 a}$	$\delta v(H) = -4.69 \times 10^{-3} \frac{\lambda^c L_\varepsilon^{5/2}}{\varepsilon L_H^4}$ $\sim -\lambda^c \frac{H^2}{\varepsilon^{3/2}}$
$\varepsilon \ll T$ $\Omega_H \ll T$ $(L_H \gg L_T)$	$\delta v(H) = -2.83 \times 10^{-2} \frac{\lambda^c L_T^2}{T a L_H^4}$ $\sim -\lambda^c \frac{H^2}{T^2 a}$	$\delta v(H) = -9.86 \times 10^{-4} \frac{\lambda^c L_T^{5/2}}{T L_H^4}$ $\sim -\lambda^c \frac{H^2}{T^{3/2}}$
$\Omega_H \gg \varepsilon, T$ $(L_H \gg L_\varepsilon, L_T)$	$\delta v(H) = -\frac{\lambda^c}{2\pi a} \frac{1}{\Omega_H L_H^3} \ln \frac{L_\varepsilon}{L_H}$ $= -\frac{\lambda^c}{2\pi \hbar} \frac{\ln H}{Da}$	$\delta v(H) = -6.81 \times 10^{-2} \frac{\lambda^c}{\omega_H L_H^3}$ $\sim -\lambda^c \sqrt{H}$

Generally speaking, the interaction constant λ^c depends on the energy and magnetic field, so that (3.4.27) takes on the form

$$\lambda_n^c(2\varepsilon - \omega, H, Q_z)$$

$$= \left[\lambda_0^{-1} - \ln \frac{-i |2\varepsilon - \omega| + DQ_z^2 + \Omega_H \left(n + \frac{1}{2}\right)}{\varepsilon_0} \right]^{-1}. \quad (3.7.44)$$

If in the sum over n in Eq. (3.7.41) only small n are important, then, to a logarithmic accuracy, we can substitute into (3.7.42) the following expression for λ^c in three dimensions:

$$\lambda^c = \frac{\lambda_0}{1 - \lambda_0 \ln \frac{\max\{\varepsilon, T, \Omega_H\}}{\varepsilon_0}}. \quad (3.7.45)$$

In two dimensions and at $\Omega_H \gg \varepsilon, T$, the n dependence of the interaction constant accounted for, we obtain

$$\begin{aligned} \delta v_2(H) &= \frac{\Omega_H}{8\pi D} \sum_{n=0}^{\infty} \frac{1}{\Omega_H \left(n + \frac{1}{2}\right)} \frac{\lambda_0}{1 - \lambda_0 \ln \frac{\Omega_H \left(n + \frac{1}{2}\right)}{\varepsilon_0}} \\ &= -\frac{1}{8\pi D} \ln \frac{1 + \lambda_0 \ln \varepsilon_0 \tau}{1 + \lambda_0 \ln \varepsilon_0 / \Omega_H}. \end{aligned} \quad (3.7.46)$$

In the range of classically weak magnetic fields the electron-electron interaction in the Cooper channel gives a large contribution to the decay of one-electron excitations, leading to field dependence of τ_{ee} .

In the magnetic field Eq. (3.4.26) has the form

$$\frac{1}{\tau_{ee}^c} = \frac{4\pi}{v} \int_{\varepsilon}^{2\varepsilon} \frac{d\omega}{2\pi} \int_{\omega-2\varepsilon}^{2\varepsilon-\omega} \frac{d\varepsilon'}{2\pi} \int \frac{dQ_z}{2\pi} L_H^{-2} \sum_{n=0}^{(L_H/l)^2} |\lambda_n^c(2\varepsilon - \omega, Q_z, H)|^2 \times \operatorname{Re} \left[\frac{1}{-i\omega + DQ_z^2 + \Omega_H \left(n + \frac{1}{2} \right)} \right] \operatorname{Re} \left[\frac{1}{-i\omega' + DQ_z^2 + \Omega_H \left(n + \frac{1}{2} \right)} \right]. \quad (3.7.47)$$

If $\Omega_H \gg \varepsilon$, we can neglect ω and ω' in denominators and, taking into account that in Eq. (3.7.47) small n are essential, find

$$\frac{1}{\tau_{ee}^c} \simeq |\lambda^c|^2 \frac{(V/2L_H)^{4-d}}{\pi v_d (2L_e)^4} \zeta \left(3 - \frac{d}{z}, \frac{1}{2} \right) \sim \frac{e^2 a^{d-3}}{H^{\frac{2-d}{2}} \ln^2 \frac{\Omega_H}{\varepsilon_0}}. \quad (3.7.48)$$

Here $\zeta(x, \alpha)$ is the generalized Riemann ζ -function:

$$\zeta(x, \alpha) = \sum_{n=0}^{\infty} (n + \alpha)^{-x},$$

$$\zeta\left(\frac{3}{2}, \frac{1}{2}\right) \simeq 4.78, \quad \zeta\left(2, \frac{1}{2}\right) \simeq 4.94.$$

In weak fields $\Omega_H \ll \varepsilon$ the field-dependent correction to the decay is proportional to the square of the field.

The conductivity corrections, arising due to the electron-electron interaction in the Cooper channel, depend strongly on the magnetic field [13]. Characteristic fields are defined by (3.7.41), and, if $T\tau_\phi \gg \gg 1$, they are much larger than the fields which depress localization effects. To find the magnetoconductivity related to the Cooper channel interaction let us use the relation (3.4.68) between corrections to the conductivity and to the density of states, valid in this case. If the bare interaction constant λ_0 is small, its renormalization is unimportant. Substituting (3.7.43) into (3.4.68), we obtain in three dimensions

$$\delta\sigma_{\text{int}}^{(3)}(H) = -\frac{e^2}{4\pi^3} \lambda_0 \sqrt{\frac{eH}{c}} \Phi_3 \left(\frac{2eHD}{\pi T} \right), \quad (3.7.49)$$

where

$$\Phi_3(x) = \sqrt{\frac{\pi}{2x}} \int_0^{\infty} \frac{V\tilde{t} dt}{\sinh^2 t} \left[1 - \frac{xt}{\sinh xt} \right]. \quad (3.7.50)$$

At $x \gg 1$, $\varphi_3(x) \simeq 1.5$, and at $x \ll 1$, $\varphi_3(x) = \frac{5\pi}{64} \zeta\left(\frac{5}{2}\right) x^{3/2}$, where $\zeta(y)$ is the Riemann ζ -function. We see from (3.7.49) that in strong fields ($2eHD/c\pi T \gg 1$) the magnetoconductivity depends only on the interaction constant and its sign is determined by the sign of λ_0 .

If $\lambda_0 > 0$, $\delta\sigma_{\text{int}}^{(3)} < 0$ and the AMR is positive; if $\lambda_0 < 0$, it is negative. Note once more that in this case the range of strong fields also coincides with the range of classically weak fields ($\omega_c\tau \ll 1$). In two dimensions

$$\delta\sigma_{\text{int}}^{(2)}(H) = -\frac{e^2}{2\pi^2} \lambda_0 \varphi_2\left(\frac{2eHD}{c\pi T}\right), \quad (3.7.51)$$

where

$$\varphi_2(x) = \int_0^\infty \frac{t dt}{\sinh^2 t} \left[1 - \frac{xt}{\sinh xt}\right]. \quad (3.7.52)$$

At $x \gg 1$, $\varphi_2(x) = \ln x$ and at $x \ll 1$, $\varphi_2(x) = \zeta(3) x^2/4 \simeq 0.3x^2$. If the interaction constant λ_0 is large enough, its renormalization and, consequently, its field and temperature dependence become important. Unfortunately, in this case only asymptotic expressions for the magnetoconductivity can be obtained. In three dimensions these expressions can be found from (3.7.49), replacing λ_0 by λ^c given by (3.7.44).

At $d = 2$ and $\Omega_H \ll T$ the expression for $\delta\sigma_{\text{int}}^{(2)}$ is related to (3.7.51) in a similar way. If, however, $\Omega_H \gg T$, then

$$\delta\sigma^{(2)}(H) = \frac{e^2}{4\pi^2\hbar} \ln \frac{1 + \lambda_0 \ln \varepsilon_0 \tau}{1 + \lambda_0 \ln \varepsilon_0 / \Omega_H}. \quad (3.7.53)$$

In the case of an anisotropic simple band Eqs. (3.7.49) and (3.7.50) acquire the form

$$\begin{aligned} \delta\sigma_{ik}^{(2)} &= \frac{D_{ik}}{D_a} \frac{e^2 \lambda_0}{2\pi^2 \hbar} \varphi_2\left(\frac{2eD_c H}{\pi c T}\right), \\ \delta\sigma_{ik}^{(3)} &= \frac{D_{ik}}{D_a} \frac{e^2 \lambda_0}{4\pi^2 \hbar} \varphi_3\left(\frac{2eD_c H}{\pi c T}\right) \sqrt{\frac{eH}{c} \frac{D_c}{D_a}}. \end{aligned} \quad (3.7.54)$$

In a many-valley semiconductor U-processes can be ignored if

$$\frac{1}{\tau_v} \ll \max\left\{T, \frac{D_{\perp, \parallel} eH}{c}\right\}. \quad (3.7.55)$$

The contribution of each valley to the magnetoconductivity has the form (3.7.54), these contributions being additive.

Frequent intervalley transitions influence the magnetoconductivity related to the electron-electron interaction in the same way as they influence the Maki-Thompson corrections, i.e. an additional factor

$(2n_1 - 1)$ appears compared with Eqs. (3.7.49) and (3.7.51) for a simple band.

The spin-orbit scattering influences $\delta\sigma_{\text{int}}^{(d)}(H)$ in the same way as the Maki-Thompson corrections with the difference that this scattering becomes strong only when the time τ_{so} is smaller than the inverse temperature. Thus, the total AMR in the case of a simple band can be written in the form

$$\sigma^{(d)}(H) - \sigma^{(d)}(0) = [k_d - \beta(T)] \delta\sigma^{(d)}(H) + \delta\sigma_{\text{int}}^{(d)}(H), \quad (3.7.56)$$

where $\delta\sigma^{(d)}(H)$ is defined by Eqs. (3.7.9) and (3.7.20) and $\delta\sigma_{\text{int}}^{(d)}(H)$, by Eqs. (3.7.50), (3.7.51) and (3.7.53). The values of the coefficients k_d for different cases are listed in Table 3.7.3.

3.8 ELECTRON LOCALIZATION IN RANDOM POTENTIAL

The temperature and field dependence of the conductivity has been treated in Chapters 3.2 and 3.7 to a first order in the parameter $(p_F l)^{-1} \ll 1$. Here we formulate general notions allowing one to describe the properties of disordered conductors also at $(p_F l)^{-1} \gg 1$. Thus, it will be possible to span the gap between weak effects of quantum interference in metals and the Anderson localization.

3.8.1 Analogy Between Electron Properties in Disordered Systems and Statistical Mechanics of Ferromagnets

The treatment of interference effects, when the latter are not small, is to a considerable degree based upon an analogy with the theory of phase transitions in magnetic systems. The electron diffusion is analogous to the propagation of spin waves. The quantum corrections to the diffusion coefficient are analogous to thermal corrections to the spectrum of spin waves [73]. In two dimensions these corrections were found by Polyakov [74], who showed that they diverged logarithmically at large distances or small frequencies. An external magnetic field and anisotropy of the "easy plane" type remove this divergence, but in different ways. In a magnetic field a gap in the spectrum of spin waves arises, and the spin correlator has no singularities at small \mathbf{k} . The "easy plane"-type anisotropy does not lead to any gap, but results in that long wavelength spin waves cease to interact with each other. Hence an external magnetic field in a ferromagnet corresponds to the external field frequency when the electron diffusion is considered, and the "easy plane"-type anisotropy to the magnetic field or magnetic impurities.

Temperature increasing, a ferromagnet transits into the paramagnetic phase, where spin waves are absent. The region near the tran-

sition point is described by the scaling theory. In particular, the frequency of spin waves vanishes as $(T - T_c)^{\nu}$. We may expect that in the framework of the diffusion theory at some critical value of disorder a transition to a new phase, where diffusion is absent (a phase of localized states), will occur. The region near the localization threshold can also be described by the scaling theory. In one- and two-dimensional ferromagnets spin waves are absent at all finite temperatures. Hence we may think in one- and two-dimensional conductors the localization should exist also at a weak disorder. The analogy between statistical mechanics of ferromagnets and kinetic properties of disordered conductors is shown in Table 3.8.1.

Table 3.8.1

Kinetic properties of metals	Statistical mechanics of ferromagnets
Degree of disorder, $\hbar/E_F\tau$	Temperature, T
Diffusion coefficient, D	Spin wave stiffness, ρ_s
External field frequency, ω	External magnetic field, H
External magnetic field, H	Magnetic anisotropy energy, β
Mobility edge, F	Curie point, T_c
Diffusion mode	Spin waves

3.8.2 Q-Hamiltonian

The analogy between the diffusion and spin waves can be expressed analytically if we compare the effective Hamiltonians describing these phenomena. The Hamiltonian of a ferromagnet is

$$\mathcal{H} = \int \left[\frac{1}{2} \rho_s \left(\frac{\partial \mathbf{M}}{\partial x_\alpha} \right)^2 - \beta M_z^2 - \mathbf{H} \cdot \mathbf{M} \right] dx, \quad (3.8.1)$$

$$M^2 = 1,$$

where ρ_s is the stiffness of spin waves, β is the energy of anisotropy and H is the magnetic field.

For electrons in a random potential it is possible to average the conductivity over impurity configurations and to write the effective Hamiltonian of interacting diffusion modes [10, 75-77]. Following [10], we introduce as an order parameter a matrix \mathbf{Q} of $2N \times 2N$ dimensions, where N is an arbitrary integer. We introduce also a diagonal matrix Λ , first N elements of which are equal to unity and other N elements to -1 . Each element of the matrix \mathbf{Q} is a quaternion and can be represented in the form

$$Q_{ij} = \begin{pmatrix} D_{ij}, & \Delta_{ij} \\ -\Delta_{ij}^*, & D_{ij}^* \end{pmatrix}, \quad (3.8.2)$$

where D_{ij} are elements of a Hermitian matrix, and Δ_{ij} are elements of an antisymmetric matrix. The expression (3.8.2) means that \mathbf{Q} is a quaternionic real matrix, i.e. $Q_{ij} = Q_{ij}^{(k)} \tau_k$, where $Q_{ij}^{(k)}$ have real values, and

$$\begin{aligned} \tau_1 &= \begin{pmatrix} 0 & -i \\ -i & 0 \end{pmatrix}, & \tau_2 &= \begin{pmatrix} 0 & -1 \\ 1 & 0 \end{pmatrix}, \\ \tau_3 &= \begin{pmatrix} -i & 0 \\ 0 & i \end{pmatrix}, & \tau_0 &= \begin{pmatrix} 1 & 0 \\ 0 & 1 \end{pmatrix}. \end{aligned} \quad (3.8.3)$$

The correlator of \mathbf{D} -elements corresponds to the diffuson, and the correlator of Δ -elements, to the cooperon. By analogy with statistical mechanics of ferromagnets,

$$\mathbf{Q}^2 = 1, \quad \text{Tr } \mathbf{Q} = 0. \quad (3.8.4)$$

The effective Hamiltonian of diffusion modes [10] is similar to the Hamiltonian (3.8.1) of a ferromagnet. It contains $(\nabla \mathbf{Q})^2$ in the gauge-invariant form, as well as "anisotropy" connected with magnetic impurities and spin-orbit coupling:

$$\begin{aligned} \mathcal{H} &= D_0 \text{Tr} \left(-i \nabla \cdot \mathbf{Q} - \frac{e}{c} \mathbf{A} [\mathbf{Q} \tau_3] \right)^2 - i\omega \text{Tr } \mathbf{A} \cdot \mathbf{Q} \\ &+ \frac{1}{\tau_s} \text{Tr} [\tau_3 \boldsymbol{\sigma} \times \mathbf{Q}]^2 + \frac{1}{\tau_{so}} \text{Tr} [\boldsymbol{\sigma} \times \mathbf{Q}]^2. \end{aligned} \quad (3.8.5)$$

Any observable quantity, e.g. the density correlator $K_\varepsilon(\omega, \mathbf{r})$, can be written in the form of a statistical average [10]

$$\begin{aligned} K_\varepsilon(0, \mathbf{r}) &= \left\{ \int D\mathbf{Q} \exp \left[\int \mathcal{H} d\mathbf{r} \right] \right. \\ &\times \left. \frac{\text{Tr} \left[\frac{1}{16} (1 + \Lambda) (1 + i\tau_3) \mathbf{Q}(0) (1 - \Lambda) (1 - i\tau_3) \mathbf{Q}(\mathbf{r}) \right]}{\int D\mathbf{Q} \exp \left(\int \mathcal{H} d\mathbf{r} \right)} \right\}_{N=0}. \end{aligned} \quad (3.8.6)$$

The expression in braces should be calculated at an arbitrary even rank $2N$ of the matrix \mathbf{Q} ; after that N should be set to zero.

Equations (3.8.5) and (3.8.6) reflect the analogy we are speaking about. More exactly, they are analogous to the formula (3.8.1), the frequency ω corresponding to the magnetic field. The anisotropy energy is described by several terms of different symmetry. This is connected with a high symmetry of the matrix \mathbf{Q} . The anisotropy depresses long wavelength fluctuations of some components of \mathbf{Q} . As a result, in the long wavelength fluctuation range the symmetry of \mathbf{Q} differs from that in the short wavelength range given by Eqs. (3.8.3) and (3.8.4). Thus, if \mathbf{D} and Δ are written as $\mathbf{D} = \mathbf{D}_0 + \mathbf{D} \cdot \boldsymbol{\sigma}$, $\Delta = \Delta_0 + \Delta \cdot \boldsymbol{\sigma}$, then it follows from (3.8.5) that the field depresses

the fluctuations of Δ_0 and Δ , while the magnetic impurities and spin-orbit coupling depress the fluctuations of \mathbf{Q} , Δ_0 and Δ , and of \mathbf{D} and Δ respectively.

3.8.3 Renormalization Group Equation

The Hamiltonian (3.8.5) contains a bare diffusion coefficient D_0 determined by scattering at the distances of the order of the mean free path. Rescattering gives rise to spatial and time dispersion of D . Usually experiments determine D ($\mathbf{k} = 0$), i.e. the mobility in a uniform field. To find the equation connecting the values of D (\mathbf{k} , ω) for different \mathbf{k} , we shall use the renormalization method. This method consists in that we integrate over diffusion modes with wavelengths shorter than a certain wavelength. If the effective Hamiltonian obtained by this procedure has the same form as the initial one, the theory is said to be renormalizable. An equation can be found for renormalizable theories, which describes the parameter variation with changing scales (the so-called Gell-Mann-Low equation). To prove renormalizability and to derive this equation, let us represent the matrix \mathbf{Q} in the form

$$\mathbf{Q} = \mathbf{U}^+ \wedge \mathbf{U}, \quad (3.8.7)$$

where \mathbf{U} is a unitary quaternionic real matrix. The renormalization procedure begins with the representation

$$\mathbf{U} = \mathbf{U}_0 \tilde{\mathbf{U}} \quad (3.8.8)$$

where \mathbf{U}_0 and \mathbf{U} are unitary matrices, and $\mathbf{U}_0(\mathbf{k}) \neq 1$ at $k_0 > k > k_1$ while $\tilde{\mathbf{U}}(\mathbf{k}) \neq 1$ at $k_1 > k$. The functional integral over \mathbf{U}_0 calculated, the remaining integral depends on $\tilde{\mathbf{U}}$. In the long wavelength limit it can be represented as an integral over $\tilde{\mathbf{Q}} = \tilde{\mathbf{U}}^+ \wedge \tilde{\mathbf{U}}$, and

$$\mathcal{H} = D \operatorname{Tr} (\nabla \tilde{\mathbf{Q}})^2 + i\omega \xi_0 \operatorname{Tr} (\wedge \tilde{\mathbf{Q}}). \quad (3.8.9)$$

This means that the theory is renormalizable, and D and ξ satisfy the Gell-Mann-Low equations

$$\frac{d}{d \ln k_1} \ln D = \beta(D), \quad (3.8.10)$$

$$\frac{d}{d \ln k_1} \xi = \Phi(D). \quad (3.8.11)$$

In [10, 75] the renormalizability of the Hamiltonian (3.8.5) was proved in two dimensions, and the functions $\beta(D)$ and $\Phi(D)$ were calculated as an expansion in $1/D$. The function Φ vanishes at $N = 0$. It is quite natural, since in the one-particle approach loga-

rithmic corrections to the density of states are absent at $p_F l \gg 1$:

$$\beta(D) = -\frac{\alpha}{D} + O\left(\frac{1}{D^2}\right), \quad D \gg 1, \quad (3.8.12)$$

where

$$\alpha = \begin{cases} 1 & \text{for potential scattering,} \\ 0 & \text{in the presence of the magnetic field and} \\ & \text{magnetic impurities,} \\ -1 & \text{for spin-orbit coupling.} \end{cases}$$

Thus, the conductivity in two dimensions depends on the size of a sample not arbitrarily, but obeying Eq. (3.8.10), i.e. if we take two samples of different dimensions but having equal conductivities then, their dimensions doubled, the conductivities change by the same magnitude. The idea that quantum effects in scattering processes are determined only by conductivities [6] led Abrahams et al. [78] to Eq. (3.8.10), the formulation of the basic principle of the theory. This equation should be solved on condition that at distances of the order of the mean free path the diffusion coefficient is equal to its bare value D_0 . As a result,

$$\int_{D_0}^{D(L)} \frac{dD}{D\beta(D)} = \ln \frac{L}{l}. \quad (3.8.13)$$

At $D \ll 1$ the dependence of D on sample dimensions L is [78]

$$D \sim \exp\left(-\frac{L}{L_c}\right), \quad (3.8.14)$$

where L_c is the localization length, i.e. at $D \ll 1$

$$\beta(D) = \ln D. \quad (3.8.15)$$

At $D \gg 1$ the function $\beta(D)$ is given by (3.8.12).

The results of Chapter 3.2 obtained by the perturbation theory can also be obtained by the renormalization group method, if the expression (3.8.12) for $\beta(D)$ is substituted into (3.8.13).

3.8.4 Conductivity in Two Dimensions

Equation (3.8.10) and the form of the function $\beta(D)$ allow one to judge the properties of diffusion in the case of a strong disorder. These properties are essentially different for the cases of potential scattering, magnetic scattering and magnetic impurities, and spin-orbit coupling. In the case of potential scattering it is natural to assume that the function β is negative not only at small and large D , but at all D (Fig. 3.30). It means that for arbitrary weak disorder the localization regime will set in at large distances $L \sim l \exp(p_F l)$.

In the case of magnetic scattering $\beta(D) = 0$ to a first order in $1/D$. It is shown in [75] that $\beta(D) = -1/D^2$, and therefore the local-

ization length $L_c \sim l \exp [(p_F l)^2]$. A very interesting situation is realized in the case of a strong spin-orbit interaction. It is seen from Fig. 3.28 that there is a point $D = D_2 \sim 1/m$ where the function $\beta(D)$ vanishes.

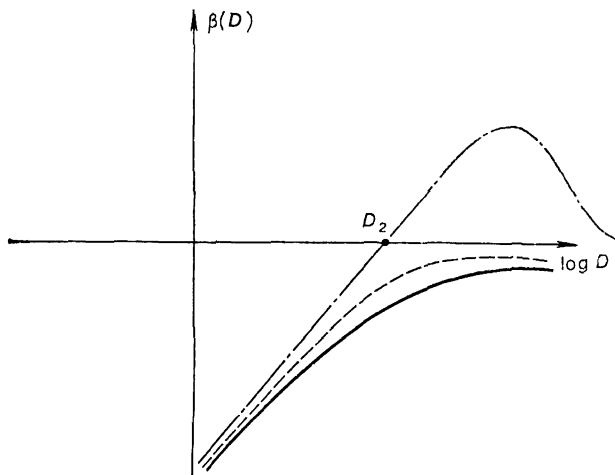


Fig. 3.28.

If disorder is weak, i.e. $D > D_2$, the Gell-Mann-Low function is positive, and the effective diffusion coefficient increases with increasing sample dimensions. In the range of large D the function $\beta(D)$ is given by (3.8.12) with $\alpha = -1$, and solving Eq. (3.8.10) we obtain

$$\sigma^{(2)} = \frac{e^2}{\pi^2 \hbar} \ln \frac{\tau}{\tau_c}. \quad (3.8.16)$$

Usually a logarithmic growth of the conductivity is limited not by the film dimensions, but by thermal processes of phase breaking (or by the magnetic field). The formula (3.8.16) takes on the form

$$\sigma^{(2)} = \frac{e^2}{2\pi^2 \hbar} \ln \frac{\tau}{\tau_c}. \quad (3.8.17)$$

Thus, in the presence of the spin-orbit interaction the interference depresses the scattering, and residual resistivity is absent.

Note that the factor in (3.8.17) does not depend on the impurity concentration (or on the mean free path). It is only the factor τ_c under the sign of logarithm that is concentration-dependent. In the case $p_F l \gg 1$, τ_c in Eq. (3.8.17) can be estimated as

$$\tau_c \sim \tau e^{p_F l}. \quad (3.8.18)$$

Near the localization threshold, when $D_0 \sim D_2$, the integral on the left-hand side of Eq. (3.8.13) is determined, besides large D , by the region $|D - D_2| \ll 1$. If at the point D_2

$$D \frac{\partial \beta(D)}{\partial D} \Big|_{D=D_2} = \frac{1}{\nu}, \quad \text{then} \quad \tau_c \sim \tau (D_0 - D_2)^{-2\nu}. \quad (3.8.19)$$

If the bare diffusion coefficient D_0 is less than D_2 , then the diffusion coefficient D declines exponentially with increasing sample dimensions. Calculating (3.8.13) at $D_0 \sim D_2$, we obtain the relation (3.8.14) for $D(L)$, and the localization length L_c in the vicinity of the mobility edge in the form

$$L_c \sim (D_2 - D_0)^{-\nu}. \quad (3.8.20)$$

In the case of a strong spin-orbit coupling the mobility edge corresponds to $mD_2 \sim 1$ ($l \sim \lambda$). In many cases this coupling is weak ($\tau_{so} \gg \tau$). Hence we can ignore it at small distances and substitute into Eq. (3.8.12) the function $\beta(D)$ corresponding to $\alpha = 1$ (the lower curve in Fig. 3.28). At distances $L \sim L_{so} = \sqrt{D\tau_{so}}$ the regime changes, and at larger distances we have to use the upper curve of Fig. 3.28. If the regime changes at $D < D_2$, then D continues to decrease, and the spin-orbit interaction does not affect the localization. If the spin-orbit interaction is switched on when $D > D_2$, D begins to grow, and its asymptotic behavior is given by Eqs. (3.8.6) and (3.8.7). The temperature dependence of the conductivity in this case has a maximum when $\tau_\varphi(T) \sim \tau_{so}$ (!). The mobility edge for a weak spin-orbit coupling is given by the relation $D(L_{so}) = D_2$ and equals

$$D_c \simeq \frac{1}{\nu(\mu)} \ln \frac{\tau_{so}}{\tau}, \quad \sigma_c^{(2)} \simeq \frac{e^2}{h} \ln \frac{\tau_{so}}{\tau}. \quad (3.8.24)$$

At high temperatures or at small sample dimensions $\sigma^{(2)} < \sigma_c^{(2)}$ while at low temperatures the localization sets in; if, however, $\sigma^{(2)} > \sigma_c^{(2)}$, we obtain a regime with a zero residual resistance.

3.8.5 Localization in One and Three Dimensions

In two dimensions the interference corrections diverge logarithmically and the renormalization group method gives new quantitative results in the region where it is equivalent to the method of summation of leading logarithms. In one and three dimensions the corrections have power singularities, and we use the renormalization group method only to obtain qualitative results.

In these cases the conductivity cannot be used as an effective charge, since it is a dimensional quantity. It is natural to choose as a dimensionless charge the conductance G (inverse resistance) of a cube of dimensions L or wire of length L , measured in the units

of e^2/\hbar . In two dimensions the conductance coincides with the conductivity of a square film, is related to the diffusion coefficient by the Einstein relation and satisfies therefore Eq. (3.8.10). In other dimensions the conductance satisfies the same equation, therefore

$$\frac{d \ln G}{d \ln L} = \beta_d(G). \quad (3.8.22)$$

For each dimensionality d the function $\beta_d(G)$ has its own form. In the localization region ($G \ll 1$) the conductance declines exponentially

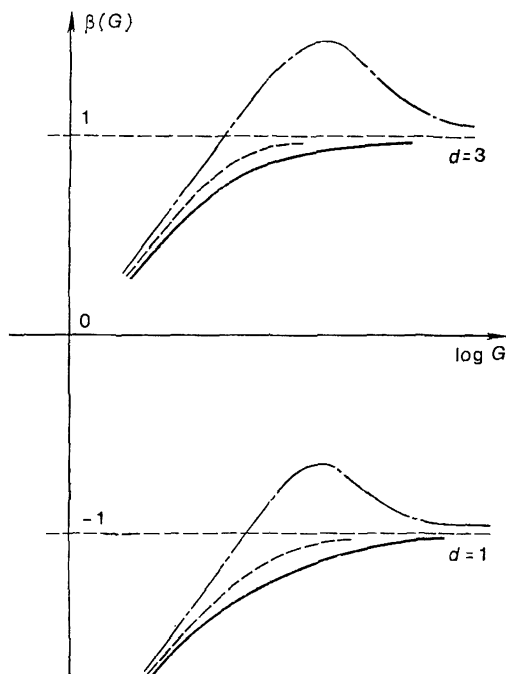


Fig. 3.29.

with increasing L for all d . In the metallic region the conductance obeys the law $G = \sigma^{(d)} L^{d-2}$. Hence for large G the function $\beta_d(G)$ is constant and equals $d-2$. For one and three dimensions $\beta_d(G)$ is plotted in Fig. 3.29. We see that in one dimension $\beta_1(G)$ is negative irrespective of the magnetic and spin-orbit interactions. This means that in one dimension at any impurity concentration electronic states are localized.

In three dimensions, also irrespective of the strength of the magnetic and spin-orbit interactions, the curve $\beta_3(G)$ intersects the G -axis.

Consequently, at $G_c \sim 1$ the localization threshold should exist. At $G = G_c$ the sample conductance does not depend on sample dimensions. Since $G = \sigma L$, this means that at $G \rightarrow G_c$ the conductivity vanishes [78]. Thus, the renormalization group theory contradicts Mott's concept of a minimal metallic conductivity.

If at small distances the conductance $G_0 > G_c$, then calculating the integral (3.8.13) at $L \rightarrow \infty$ we obtain

$$G = \sigma^{(d)} L^{d-2}, \quad (3.8.23)$$

where

$$\sigma^{(d)} \sim (G_0 - G_c)^{\nu}, \quad \frac{1}{\nu} = G \left. \frac{\partial \beta_d}{\partial G} \right|_{G=G_c}. \quad (3.8.24)$$

If $G_0 < G_c$, we obtain in a similar way

$$G \sim \exp(-L/L_c), \quad L_c = (G_c - G_0)^{-\nu}. \quad (3.8.25)$$

The exponent ν is universal for each type of scattering (potential, magnetic, or spin-orbit). In the case of the potential scattering this exponent can be calculated by means of the $2 + \varepsilon$ expansion [79]. For space dimensionality $d = 2 + \varepsilon$ we have

$$\beta_d(G) = \varepsilon - \frac{1}{G} + O\left(\frac{1}{G^3}\right). \quad (3.8.26)$$

Therefore

$$G_c = \frac{1}{\varepsilon} + O(\varepsilon), \quad \nu = 1 + O(\varepsilon^2). \quad (3.8.27)$$

In statistical mechanics, along with the $2 + \varepsilon$ expansion, a successful method of expansion in $\varepsilon = d_u - d$ [79] is used. Here d is the space dimensionality and d_u is the upper critical dimensionality (in statistical mechanics $d_u = 4$). As a zero approximation the mean field theory of phase transition is used, which is exact at $d > d_u$. At $d = d_u$ fluctuations lead to logarithmic corrections to mean field results. The summation of leading logarithms and expansion in $\varepsilon = d_u - d$ give the expressions for critical indices in the form of a power series in ε .

This approach to the localization problem was realized by Harris and Lubensky [80]. As a mean field Hamiltonian the expression

$$\mathcal{H} = \int d\mathbf{r} \operatorname{Tr} \left\{ \frac{1}{2} a \mathbf{Q}^2 + \frac{1}{2} (\nabla \mathbf{Q})^2 + \mathbf{Q}^3 + \dots \right\} \quad (3.8.28)$$

was used. It was found out that $d_u = 8$, and that the density of states in the mean field theory vanishes at the mobility edge. This effect is apparently absent at $d \leq 4$. Therefore the theory of Harris and Lubensky is most likely valid for high dimensionalities $4 < d < 8$, but fails to describe the properties of quantum states near the mobility edge in three dimensions.

The qualitative conclusion about the absence of a minimal metallic conductivity was experimentally verified for $\text{Ge}_{1-x}\text{Au}_x$ and $\text{Si}_{1-x}\text{P}_x$ [81, 82]. It was shown that the conductivity value extrapolated to zero temperature decreases slowly with impurity concentration according to the law (3.8.24), and $\nu \simeq 2/3$. The decrease in σ ($T = 0$) down to the values by a few orders smaller than Mott's minimal metallic conductivity [1, 2] was also observed. Such a behavior does not contradict the theory we are discussing. However, to describe quantitatively these effects in real solids, we have to generalize the theory to interacting electrons in random potential.

3.8.6 Localization in Magnetic Field

There are two mechanisms of magnetic field effects on the conductivity of metals with impurities. A simple classical mechanism is connected with the fact that electrons rotate in the field at frequency $\omega_c = eH/mc$, leading to $\omega_c\tau$ dependence of D . Therefore, if $\omega_c \geq E_g$, the field favours the localization and shifts the mobility edge, E_g , to higher energies. The second, essentially quantum, mechanism has been discussed in Chapter 3.7. A negative magnetoresistance arising due to this mechanism in the range of weak fields exceeds the classical value. Hence we shall ignore the field dependence of D_0 . In the region of localized states the magnetic field can influence the conductivity, decreasing the probability of tunnelling. However, the contribution of this mechanism in the range of weak fields is proportional to H^2 and can be neglected in comparison with the contribution of the quantum interference which, as shown below, shifts the mobility edge:

$$E_g(H) - E_g(0) = AH \frac{1}{2\nu}. \quad (3.8.29)$$

In three dimensions and, given the spin-orbit coupling, also in two dimensions there is a mobility edge at $G = G_c$. At a given disorder this mobility edge is associated with an energy E_g .

From general scaling concept the conductivity in a magnetic field near the mobility edge E_g (G_c) can be represented as

$$\sigma = (E - E_g)^\nu f\left(\frac{H}{(E - E_g)^\nu}\right). \quad (3.8.30)$$

The magnetic field enters the Hamiltonian through a vector potential which is not gauge-invariant. It is the flux Φ_c of the field H through the region of dimensions L_c ($\Phi_c = HL_c^2$) that is gauge-invariant. As shown above [Eqs. (3.8.20) and (3.8.25)], $L_c \sim (E - E_g)^{-\nu}$. Only Φ_c or its powers can be the argument of the function f

in (3.8.30), hence $\alpha = 2\nu$. The asymptotics

$$f(z) = \begin{cases} A_1 \sqrt{z}, & z \gg 1, \\ 1 + A_2 \sqrt{z}, & z \ll 1 \end{cases} \quad (3.8.31)$$

determine the magnetoconductivity in the range of strong and weak fields. The signs of A_1 and A_2 cannot be found from general notions, but it is quite natural to suppose that in the vicinity of the mobility edge the magnetoresistance has the same sign as in the metallic region.

The mobility edge shift in the magnetic field is determined by the singularity of the expression (3.8.30). This singularity arises when the argument of f is of order unity. Therefore the shift is given by (3.8.29), and its sign coincides with the sign of the magnetoresistance, i.e. in the case of the potential scattering the mobility edge is shifted to lower energies, and in the case of the spin-orbit interaction to higher energies.

3.8.7 Localization in Percolating Structures

To apply the ideas developed in this section, let us discuss an interesting example of localization occurring in conductors with a large number of macroscopic ruptures [83]. Consider a powder comprising a random distribution of macroscopic metallic particles of

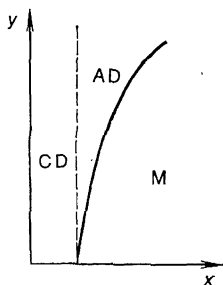


Fig. 3.30.

size a in a dielectric matrix. Let x be the volume fraction occupied by the metal, any y the resistance of the contact of two particles in units of \hbar/e^2 . We can plot a phase diagram of this system (Fig. 3.30). If x is small, the metallic particles do not form macroscopic conducting paths, and therefore at $x < x_c$ and arbitrary y the powder behaves as a classical dielectric (CD). At $x > x_c$ macroscopic conducting paths arise forming a spatial network of dimensions $L_c \sim a(x - x_c)^{-s}$ ($s = 1.8$ is the correlation length critical exponent). In a classical metal of such a configuration and unit resistance of each contact the conductivity would be equal to $\Sigma \sim (x - x_c)^t$ (here $t = 1.6$). At

sufficiently large disorder y quantum effects lead to the localization. The mobility edge is defined by the relation $y = y_c(x)$ (a solid line in Fig. 3.30). The region $y < y_c$ corresponds to the metallic conductivity (M) and the region $y > y_c$ to the Anderson dielectric (AD).

Let us calculate now the quantum correction to the conductivity given by (3.2.22), taking into account a strong spatial dispersion of the diffusion coefficient D :

$$D(q) \sim \frac{\Sigma}{y} f(qL_c), \quad (3.8.32)$$

$$f(z) = \begin{cases} 1, & z \ll 1, \\ z^\gamma, & z \gg 1, \end{cases} \quad \gamma = t/s.* \quad (3.8.33)$$

It follows from the expression for the quantum correction to the conductivity

$$\frac{\delta\sigma}{\sigma} \sim - \int \frac{(dQ)}{D(q)q^2 + \tau_\varphi^{-1}} \quad (3.8.34)$$

that at zero temperature, when $\tau_\varphi^{-1} = 0$, the quantum correction is given by $q \sim L_c^{-1}(x)$ and $\delta\sigma/\sigma \sim y/\Sigma L_c$. At the mobility edge the quantum correction equals by the order of magnitude the Drude conductivity. From this we obtain the estimate for the mobility edge:

$$y_c(x) \sim (x_c - x)^{t-s}. \quad (3.8.35)$$

At $y > y_c(x)$ electronic states are localized. The localization length L_{loc} can be found from the condition that the resistance of a sample of dimensions L_{loc} is of order \hbar/e^2 :

$$1 \sim \frac{\Sigma(L_{loc})L_{loc}}{ya} \sim \frac{(L_{loc}/a)^{-t/s}L_{loc}}{ya} \sim \frac{1}{y} \left(\frac{L_{loc}}{a} \right)^{-\frac{t-s}{s}},$$

whence

$$L_{loc} \sim ay^{\frac{s}{t-s}}. \quad (3.8.36)$$

At sufficiently high temperatures, when $\sqrt{D\tau_\varphi} \ll L_{loc}, L_c$, the quantum corrections which determine the anomalous temperature dependence of the conductivity are small, and to find them we can use again Eq. (3.8.34). Thus,

$$\delta\sigma(T) \sim - \left(\frac{\Sigma L_c^{t/s}}{y} \right)^{-\frac{3s}{t+2s}} \tau_\varphi^{\frac{t-s}{t+2s}} \sim - \left[\left(\frac{y^s}{at} \right)^3 T^{s-t} \right]^{\frac{1}{t+2s}}, \quad (3.8.37)$$

where it is taken into account that $\tau_\varphi \sim T^{-1}$.

* The equality $\gamma = t/s$ follows from the condition that at $qL_c \gg 1$, $D(q)$ does not depend on $(x_c - x)$.

3.9 CONCLUSION

The theory described in this review is mostly a theory of small corrections arising in disordered conductors due to the quantum interference of scattered waves and to the electron-electron interaction. Although these corrections are small in the region where the theory is applicable, their dependence on frequency, temperature and magnetic field determines the conductivity and the density of states. This dependence accounted for, many experimentally known but quite mysterious phenomena, such as the AMR, the zero-bias tunnelling anomaly, the minimum in the temperature dependence of the resistance in disordered conductors, were explained. The experiments carried out to verify the theory on the whole confirm it. In the nearest future the effects due to which the localization is not always observable will evidently be accounted for. The verification of other predictions of the theory, i.e. the Aharonov-Bohm effect*, the localization suppression by an external high-frequency field, the logarithmic growth of the conductivity with decreasing temperature in two-dimensional conductors with the spin-orbit interaction, is also in store. The examination of small corrections leads to the renormalization group theory for conductivity. In the region near the mobility edge predictions of this theory are not unambiguous; however, the second-order transitions between the conducting and dielectric phases, so that the metallic conductivity tends to zero according to a power law with a definite exponent seems to be most natural. The experimental investigation of the conductivity behavior in the vicinity of the mobility edge is very important and can stimulate new theoretical efforts. The theory predicts also a series of other qualitative effects, such as the shift of the mobility edge in the magnetic field.

The fact that the electron-electron interaction, whatever weak it may be, increases when the Fermi level approaches the mobility edge is very important and quite unexpected. It means that the theory of the metal-dielectric transition cannot be constructed as a one-electron localization theory. The interaction can change both the transition and the nature of localized states.

* This review had already been written, when the Aharonov-Bohm oscillations of the resistance were observed [86].

3.A.1 Cooperon-Current Relation in the Space-Time Representation

Deriving the cooperon-current relation in the space-time representation in a high-frequency field, it is convenient to use the Keldysh diagrammatic technique [84]. The electron Green function in this technique is a matrix

$$\mathbf{G} = \begin{pmatrix} 0 & G^A \\ G^R & F \end{pmatrix}, \quad (3.A.1)$$

and the current is related to the function F by the equation

$$\mathbf{j} = e \int \mathbf{v} F(\mathbf{p}, \varepsilon) \frac{d\varepsilon}{2\pi i} (dp). \quad (3.A.2)$$

In equilibrium the Green function F is expressed through the retarded and advanced Green functions (G^R and G^A):

$$F(\varepsilon) = [2n_F(\varepsilon) - 1] [G^A(\varepsilon) - G^R(\varepsilon)], \quad (3.A.3)$$

where $n_F(\varepsilon)$ is the Fermi distribution function.

To derive the expression for the current, it is sufficient to calculate F in the first-order perturbation theory in electric field (Fig. 3.A.1a) and substitute it into Eq. (3.A.2). The field vertex is also a matrix and has the form

$$\hat{\gamma} = \frac{e}{c} \mathbf{v} \cdot \mathbf{A} \hat{\sigma}_x \quad \hat{\sigma}_x = \begin{pmatrix} 0 & 1 \\ 1 & 0 \end{pmatrix}. \quad (3.A.4)$$

It is assumed that in the electron propagators shown in Fig. 3.A.1a the impurity potential is already taken into account, therefore these propagators should be considered as equilibrium, i.e. we can use Eq. (3.A.3). In order to account for the Cooper pole effect on the conductivity, in averaging over the impurity potential, it is sufficient to consider only the graphs shown in Fig. 3.A.1b. Since impurity vertices are also proportional to the matrix $\hat{\sigma}_x$, the contribution of any graph in Fig. 3.A.1b to the current before integration over momenta is proportional to the expression

$$\sum_j \prod_{i=1}^j G^R(\mathbf{p}_i) F(\mathbf{p}_j) \prod_{k=j+1}^s G^A(\mathbf{p}_k).$$

(Here electron propagator momenta are labelled according to their order in the graph.) For the Cooper pole to appear, one of the electron Green functions in each cell of the ladder should be retarded and the other should be advanced, or one of them should be a function of F . The function F can stand only at the points denoted by a circle in Fig. 3.A.1b. As a result, we obtain the cooperon—the sum of the graphs shown in Fig. 3.A.2, one of the electronic lines being retarded and the other advanced. This result is also valid in the case when the

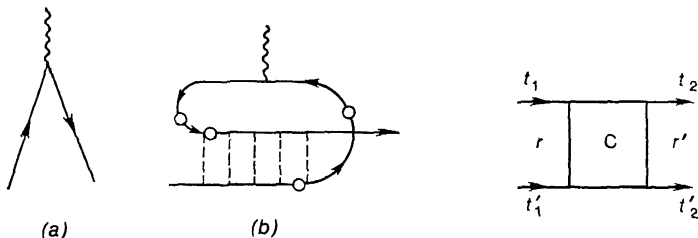


Fig. 3.A.1.

Fig. 3.A.2.

sample is placed into a strong external electromagnetic field. Consequently the Fourier transform of the current at frequency ω_2 in the presence of a measuring field at frequency ω_1 has the following form (heating effects are ignored):

$$\delta \mathbf{j}_{\omega_2} = \frac{4i\tau}{cv} \sigma_0 \mathbf{A}(\omega_1) \int \frac{d\varepsilon_1 d\varepsilon_2}{(2\pi)^2} (dQ)(dQ') [n_F(\varepsilon_1^+) - n_F(\varepsilon_1^-)] \\ \times C_{QQ'}(\varepsilon_2^-, \varepsilon_1^+; \varepsilon_1^-, \varepsilon_2^+), \quad (3.A.5)$$

where

$$\varepsilon_i^\pm = \varepsilon_i \pm \frac{\hbar\omega_i}{2}.$$

If the influence of the external field on the cooperon $C_{QQ'}(\varepsilon_2^-, \varepsilon_1^+; \varepsilon_1^-, \varepsilon_2^+)$ is neglected, the latter is

$$C_{QQ'}(\varepsilon_2^-, \varepsilon_1^+, \varepsilon_1^-, \varepsilon_2^+) = (2\pi)^2 \delta(\varepsilon_1 - \varepsilon_2) \delta(\omega_1 - \omega_2) \\ \times (2\pi)^d \delta(Q - Q') C(Q, \omega_1), \\ C(Q, \omega_1) = \frac{1}{\tau(-i\omega_1 + DQ^2)}. \quad (3.A.6)$$

Substituting (3.A.6) into (3.A.5), we find the conductivity corrections obtained in Chapter 3.2 by means of the Matsubara diagrammatic technique.

The equation for the cooperon in an external field has the simplest form in the space-time representation (see 3.A.2). We shall now obtain the expression for the Fourier transform of the current in this representation. From (3.A.5) it follows that

$$\delta \mathbf{j}_{\omega_2} = \frac{4\tau}{icv} \sigma_0 \mathbf{A}(\omega_1) \int \frac{d\epsilon}{(2\pi)} [n_F(\epsilon_1^-) - n_F(\epsilon_1^+)] \int dt_1 dt_2 dt_1' dt_2' \delta(t_1 - t_2') \times \exp\{i(\epsilon_1^+ t_1' - \epsilon_1^- t_2 - \omega_2 t_1)\} C_{\mathbf{r}, \mathbf{r}'}(t_1 t_1', t_2 t_2'). \quad (3.A.7)$$

The notations for times and coordinates are shown in Fig. 3.A.2. It is convenient to use the following variables:

$$t = \frac{t_1 + t_1'}{2}, \quad t' = \frac{t_2 + t_2'}{2}, \\ \eta = t_1 - t_1', \quad \eta' = t_2' - t_2, \\ C_{\mathbf{r}\mathbf{r}'}(t_1 t_1', t_2 t_2') = C_{\eta\eta'}^{tt'}(\mathbf{r}, \mathbf{r}'). \quad (3.A.8)$$

As shown in 3.A.2, $C_{\eta\eta'}^{tt'}$, can be written as

$$C_{\eta\eta'}^{tt'}(\mathbf{r}, \mathbf{r}') = C_{\eta\eta'}^t(\mathbf{r}, \mathbf{r}') \delta(t - t'). \quad (3.A.9)$$

Using (3.A.9), we obtain

$$\delta \mathbf{j}_{\omega_2} = \frac{8\tau\sigma_0}{\pi icv} \mathbf{A}(\omega_1) \int d\epsilon_1 [n_F(\epsilon_1^-) - n_F(\epsilon_1^+)] \int dt d\eta \\ \times \exp\left\{i\left[t(\omega_1 - \omega_2) + \eta \frac{\omega_1 + \omega_2}{2}\right]\right\} C_{\eta, -\eta}^t(\mathbf{r}, \mathbf{r}'). \quad (3.A.10)$$

In the case of a constant magnetic field the cooperon does not depend on t and therefore

$$\delta \mathbf{j}_{\omega_2} = \frac{2\tau\sigma_0}{\pi icv} \mathbf{A}(\omega_1) \int d\epsilon_1 [n_F(\epsilon_1^-) - n_F(\epsilon_1^+)] \\ \times C_{\omega}(\mathbf{r}, \mathbf{r}') 2\pi \delta(\omega_1 - \omega_2), \quad (3.A.11)$$

where

$$C_{\omega}(\mathbf{r}, \mathbf{r}') = \int_{-\infty}^{+\infty} d\eta C_{\eta, -\eta}(\mathbf{r}, \mathbf{r}') e^{i\omega\eta}.$$

Equations (3.A.10) and (3.A.11) hold for arbitrary distribution functions $n_F(\epsilon)$. In the degenerate case, integrating over ϵ , we find

$$\delta \sigma(\omega_1, \omega_2) = -\frac{4e^2}{\pi} D\tau \int dt d\eta \exp\left\{i\left[t(\omega_1 - \omega_2) + \eta \frac{\omega_1 + \omega_2}{2}\right]\right\} \\ \times C_{\eta, -\eta}^t(\mathbf{r}, \mathbf{r}'), \quad (3.A.10a)$$

where

$$\delta \sigma(\omega_1, \omega_2) = \frac{\mathbf{j}_{\omega_2}}{E(\omega_1)}.$$

In a constant magnetic field

$$\delta\sigma(\omega_1, \omega_2) = 2\pi\delta(\omega_1 - \omega_2) \delta\sigma(\omega_1) = -\frac{2e^2 D\tau}{\pi} C_{\omega_1}(\mathbf{r}, \mathbf{r}') 2\pi\delta(\omega_1 - \omega_2). \quad (3.A.11a)$$

3.A.2 Cooperon in External Electromagnetic Field

Let a sample be placed in a field given by a vector potential $\mathbf{A}(\mathbf{r}, t) = \mathbf{A} \exp \{i(\Omega t + \mathbf{k} \cdot \mathbf{r})\}$. As a function of the momentum and energy initial values, the cooperon satisfies the equation

$$\mathbf{C}_Q(\varepsilon^+, \varepsilon^-) = \mathbf{C}_Q^{(0)}(\varepsilon^+ - \varepsilon^-) [1 + \hat{\xi}(\mathbf{Q}, \varepsilon^+, \varepsilon^-)] \mathbf{C}_Q(\varepsilon^+, \varepsilon^-), \quad (3.A.12)$$

where $\mathbf{C}_Q^{(0)}(\varepsilon^+ - \varepsilon^-)$ is the sum of ladder graphs in the absence of the external field,

$$\mathbf{C}_Q^{(0)}(\varepsilon^+ - \varepsilon^-) = \frac{1}{[-i(\varepsilon^+ - \varepsilon^-) + DQ^2]}, \quad (3.A.13)$$

and $\hat{\xi}$ is an operator, since the external field changes both the cooperon momentum and energy. Calculating $\hat{\xi}$, it is necessary to account for the external field both to the first and second orders of the perturbation theory. Then the expression for $\hat{\xi}$ is written as

$$\hat{\xi}(\mathbf{Q}, \varepsilon^+, \varepsilon^-) = \sum_{\alpha=1,2} \sum_{\beta=0}^{\alpha} \zeta_{\alpha\beta} \exp \left\{ \alpha \mathbf{k} \frac{\partial}{\partial \mathbf{Q}} + \beta \Omega \frac{\partial}{\partial \varepsilon^+} + (\alpha - \beta) \Omega \frac{\partial}{\partial \varepsilon^-} \right\}. \quad (3.A.14)$$

Note that calculating $\zeta_{\alpha\beta}$ we can set \mathbf{k} and Ω to zero. In fact, as shown in 3.A.1, one of the electronic lines (with the initial energy ε^+) is retarded and the other is advanced. Therefore we should compare k with l^{-1} and Ω with τ^{-1} . At $\mathbf{k} = 0$, $\Omega = 0$ the field vertex corresponds to differentiation of the electron Green function with respect to its momentum. As a result,

$$\begin{aligned} \zeta_{1\beta} &= \frac{eA_i}{c} \frac{\partial \zeta_{00}}{\partial Q_i} = -2\tau DQ_i A_i \frac{e}{c}, \\ \zeta_{20} &= \zeta_{22} = \frac{1}{2} \zeta_{21} = \frac{e^2}{2c^2} A_i A_j \frac{\partial^2 \zeta_{00}}{\partial Q_i \partial Q_j} = -\frac{e^2}{c^2} \tau D A^2. \end{aligned} \quad (3.A.15)$$

Here

$$\zeta_{00} = \frac{1}{\pi v \tau} \int (dp) G^R(\varepsilon^+, \mathbf{p}) G^A(\varepsilon^-, -\mathbf{p} + \mathbf{Q}) = 1 + i(\varepsilon^+ - \varepsilon^-) \tau - DQ^2 \tau.$$

Eq. (3.A.12) can be represented as

$$[\mathbf{C}_Q^{(0)-1} - \hat{\xi}] \mathbf{C}_Q(\varepsilon^+, \varepsilon^-) = 1. \quad (3.A.16)$$

Substituting (3.A.14) and (3.A.15) into (3.A.16), we obtain

$$\left\{ -i(\varepsilon^+ - \varepsilon^-) + D \left[Q - \frac{e}{c} \mathbf{A} \left(e^{\Omega \frac{\partial}{\partial \varepsilon^+}} + e^{\Omega \frac{\partial}{\partial \varepsilon^-}} \right) e^{k_i \frac{\partial}{\partial Q_i}} \right]^2 \right\} \\ \times \mathbf{C}_Q(\varepsilon^+, \varepsilon^-) = \frac{1}{\tau}. \quad (3.A.17)$$

In the space-time representation and in the notations of Sec. 3.A.1 the cooperon equation has the form

$$\left\{ \frac{\partial}{\partial \eta} + D \left[-i \frac{\partial}{\partial \mathbf{r}} - \frac{e}{c} \left(\mathbf{A} \left(\mathbf{r}, t - \frac{\eta}{2} \right) + \mathbf{A} \left(\mathbf{r}, t + \frac{\eta}{2} \right) \right) \right]^2 \right\} \\ \times \mathbf{C}_{\eta, \eta'}^t(\mathbf{r}, \mathbf{r}') = \frac{\delta(\eta - \eta') \delta(\mathbf{r} - \mathbf{r}')}{\tau}. \quad (3.A.18)$$

This equation is valid for arbitrary dependence of the external field on coordinates and time.

If the field vector potential is time-independent (i.e. magnetic field is constant), then Eq. (3.A.18) can be written as

$$\left\{ -i\omega + D \left[-i \frac{\partial}{\partial \mathbf{r}} - \frac{2e}{c} \mathbf{A}(\mathbf{r}) \right]^2 \right\} \mathbf{C}_\omega(\mathbf{r}, \mathbf{r}') = \frac{\delta(\mathbf{r} - \mathbf{r}')}{\tau}. \quad (3.A.19)$$

3.A.3 Calculation of Path Integrals

In a spacially uniform case the path integral (3.3.31) does not contain δ -function. Therefore the double integral over y can be reduced to one-dimensional. Then the path integral can be written as

$$\langle \mathbf{C}(0, 0, -y, y) \rangle = \int_{x(-y)=0}^{x(y)=0} D\mathbf{x}(y) \exp \left\{ -\frac{1}{2} \int_{-y}^y dy_1 [\dot{\mathbf{x}}(y_1)]^2 \right. \\ \left. - \int_{-y}^y [x(y_1) - x(-y_1)]^2 dy_1 \right\}. \quad (3.A.20)$$

The vector sign in the exponential in the second integral is absent, since the direction of vector potential \mathbf{A} of fluctuations due to noise in the external circuit coincides with the current direction. Separating the motion along the current direction from the transverse motion and calculating the integral over transverse coordinates, we obtain the cooperon in the form of an integral over longitudinal coordinates:

$$\langle \mathbf{C}(0, 0, -y, y) \rangle = \frac{1}{(4y) \frac{d-1}{2}} \int_{x(-y)=0}^{x(y)=0} D\mathbf{x}(y) \exp \left\{ -\frac{1}{2} \int_{-y}^y dy_1 \dot{x}^2(y_1) \right. \\ \left. - \int_{-y}^y dy_1 [x(y_1) - x(-y_1)]^2 \right\}. \quad (3.A.21)$$

We are interested in the paths that return to the initial point. Therefore, if we write $x(y)$ as the sum of the even and odd parts, $x(y) = x_+(y) + x_-(y)$, we find the following integration limits: $x_-(0) = x_-(y) = 0$, $x_+(y) = 0$, $x_+(0) = x$.

The integral (3.A.21) can be written as

$$\begin{aligned} \langle C(0, 0, -y, y) \rangle &= (4y)^{\frac{1-d}{2}} \int_{x_+(0)=x}^{x_+(y)=0} dx \int_{x_-(0)=0}^{x_-(y)=0} Dx_+(y) \\ &\times \exp \left\{ -\frac{1}{2} \int_0^y dy_1 \dot{x}_+^2(y_1) \right\} \int_{x_-(0)=0}^{x_-(y)=0} Dx_-(y) \\ &\times \exp \left\{ -\int_0^y dy_1 \left[\frac{1}{2} \dot{x}_-^2(y_1) + 8x_-^2(y_1) \right] \right\}. \end{aligned} \quad (3.A.22)$$

The integral over $x_+(y)$ is equal to the probability of reaching in the process of diffusion a point x in a time y . By the probability normalization the integral over x equals unity. Therefore C is the Green function at coinciding points for the diffusion equation with oscillating potential.

For the Schrödinger equation this function can be found in [85]. Hence

$$\langle C(0, 0, -y, y) \rangle = \frac{1}{4} (4y)^{\frac{1-d}{2}} \sqrt{\frac{2}{\pi \sinh y}}. \quad (3.A.23)$$

The integral over y of $\langle C(0, 0, -y, y) \rangle$ converges for $d = 1, 2$. In the case $d = 3$ it is necessary to perform subtraction to avoid divergence at small y :

$$\int_{y_0}^{\infty} \langle C(0, 0, -y, y) \rangle dy = \begin{cases} \frac{\Gamma^2(1/4)}{4\pi \sqrt{2}} \simeq 0.08 & \text{at } d=1, \\ \frac{1}{4\sqrt{2\pi}} \ln y_0 & \text{at } d=2, \\ -0.06 & \text{at } d=3. \end{cases} \quad (3.A.24)$$

Using Eq. (3.A.24), we obtain the coefficient $C^{(d)}$ given in the text.

In one dimension let us use the equality

$$\dot{x}(y_1) \dot{x}(y_2) \delta[x(y_1) - x(y_2)] = -\frac{1}{2} \frac{\partial^2}{\partial y_1 \partial y_2} |x(y_1) - x(y_2)|$$

and integrate the double integral in (3.3.31) by parts. As a result the double integral in the exponential will become one-dimensional

$$\begin{aligned} \langle C(0, 0, -y, y) \rangle &= \int_{x(-y)=0}^{x(y)=0} Dx(y) \exp \left\{ -\int_{-y}^y dy_1 \left[\frac{\dot{x}^2(y_1)}{2} \right. \right. \\ &\left. \left. + |x(y_1) - x(-y_1)| \right] \right\}. \end{aligned} \quad (3.A.25)$$

Representing the path $x(y_1)$ in the form $x(y_1) = x_+ + x_-$ and integrating over x_+ , we find that the cooperon is equal to the Green function of the diffusion equation in the potential $|x|$. The integral over y is expressed through the Green function in the frequency representation at frequency equal to zero:

$$\int_0^\infty \langle C(0, 0, -y, y) \rangle dy = G(0, 0),$$

$$\left\{ -\frac{\partial^2}{\partial x^2} + 4|x| \right\} G(x, x') = \delta(x - x'). \quad (3.A.26)$$

The Green function $G(x, x')$ can be written as

$$G(x, x') = -\frac{1}{W(g_1, g_2)} \begin{cases} g_1(x) g_2(x'), & x < x', \\ g_1(x') g_2(x), & x > x', \end{cases} \quad (3.A.27)$$

where

$$g_1(x) = Ai(4|x|), \quad g_2(x) = Bi(4|x|)$$

are linearly independent solutions of the uniform equation (3.A.26) and $W(g_1, g_2)$ is the Wronski determinant. We have

$$W(g_1, g_2) = Ai(0) Bi'(0) - A'i(0) Bi(0) = \frac{1}{\pi},$$

$$G(0, 0) = -\pi Ai(0) Bi(0) = \frac{\pi}{3^{5/6} \Gamma^2\left(\frac{2}{3}\right)} = 0.17.$$

The last relation allows to obtain the coefficient C_1 given in the text.

3.A.4 Expression for Conductivity of Interacting Electrons

The corrections to the conductivity, arising due to the exchange interaction of electrons, are given by the graphs in Fig. 3.15 and also by the graphs differing from those shown in Fig. 3.15a, b, d, e only in direction of the electronic line.

Calculating the corrections to the conductivity, it is necessary to remember that the main contribution is given by the terms containing maximal number of diffusion poles. In these terms imaginary parts of the Green functions in each vertex should have opposite signs. This condition restricts the summation region over ϵ_n and ω_m in each expression.

Note that the total contribution of the graphs in Fig. 3.15a-c at $T_{\tau} \ll 1$, $\Omega_k \tau \ll 1$ ($\Omega_k = 2\pi kT$ is the Matsubara frequency of external field) is small compared with the contribution of all other graphs.

We can say that the sum of the graphs in Fig. 3.15a-c corresponds to renormalization of the density of states and transport relaxation time. Since this time is inversely proportional to the density of states, these renormalizations cancel.

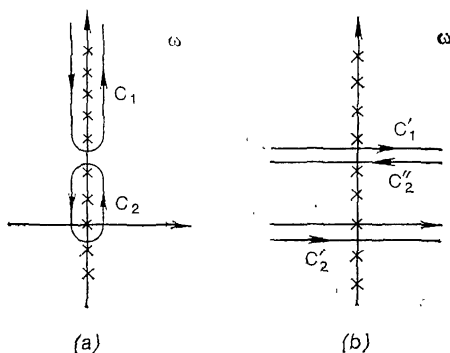


Fig. 3.A.3.

To calculate the sum of the graphs shown in Fig. 3.15d, e we first evaluate T , the graphical equation for which in ladder approximation is shown in Fig. 3.A.3. The solution of this equation has the form:

$$T(\mathbf{p}, \mathbf{p}_1 | \mathbf{p} + \mathbf{q}, \mathbf{p}_1 + \mathbf{q}) = \frac{1}{\pi v \tau} \left\{ \frac{\theta(\varepsilon_n) \theta(\omega_m - \varepsilon_n) + \theta(-\varepsilon_n) \theta(\varepsilon_n - \omega_m)}{|\omega_m| + Dq^2} + \theta(\varepsilon_n) \theta(\varepsilon_n - \omega_m) + \theta(-\varepsilon_n) \theta(\omega_m - \varepsilon_n) \right\}. \quad (3.A.28)$$

As current vertices are vectorial, the graphs in Fig. 3.15d, e give zero contribution if the Green functions standing to the left and to the right from T are taken to zeroth order in \mathbf{q} . The next terms in the expansion of the Green functions in $\mathbf{q} \cdot \mathbf{v}$ accounted for, we obtain a factor Dq^2 in the numerator. This factor cancels one of the diffusion poles so that each graph contains effectively two such poles. As a result, in the expression for the current correction arising due to interference effects only the graphs in Fig. 3.15d, e are important. Tedious but quite simple calculations lead to the following expression for δj_α (we assume that $\Omega_k > 0$):

$$\delta j_\alpha(i\Omega_k) = \sigma_0 A_\beta \left\{ T \sum_{\omega_m=0}^{\Omega_k} \omega_m F(\Omega_k, \omega_m) + T \sum_{\omega_m=\Omega_k}^{\infty} \Omega_k F(\Omega_k, \omega_m) \right\}, \quad (3.A.29)$$

where A_β is the vector potential of external electric field, and σ_0 is the classical conductivity of noninteracting electrons. The function

$F(\Omega_k, \omega_m)$ has the form

$$F(\Omega_k, \omega_m) = 8 \int (dq) \frac{Dq_{\alpha} q_{\beta} V(\mathbf{q}, \omega_m)}{(\omega_m + Dq^2)^2 (\omega_m + \Omega_k + Dq^2)}. \quad (3.A.30)$$

It is seen that at $\Omega_k \rightarrow 0$ the contribution to the current, proportional to the vector potential, vanishes.

To obtain the frequency and temperature dependences of the conductivity, it is necessary to continue analytically the expression for the current (3.A.29) to real values of the argument.

The expression in braces in (3.A.29) can be represented as

$$\begin{aligned} \Lambda &= T \sum_{\omega_m=0}^{\Omega_k} \omega_m F(\Omega_k, \omega_m) + T \sum_{\omega_m=\Omega_k}^{\infty} \Omega_k F(\Omega_k, \omega_m) \\ &= \frac{1}{4\pi i} \left[\int_{C_1} d\omega \Omega_k F(\Omega_k, -i\omega) \coth \frac{\omega}{2T} \right. \\ &\quad \left. + \int_{C_2} d\omega (-i\omega) F(\Omega_k, -i\omega) \coth \frac{\omega}{2T} \right], \end{aligned} \quad (3.A.31)$$

where contours C_1 and C_2 are shown in Fig. 3.A.3a.

Since the function $F(\Omega_k, -i\omega)$ has no singularities in ω in the upper half-plane, the integration contours C_1 and C_2 can be deformed into contours C'_1 , C'_2 and C''_2 , as shown in Fig. 3.A.3b. As a result,

$$\begin{aligned} \Lambda &= \frac{1}{4\pi i} \left\{ \int_{-\infty+i\Omega_k}^{+\infty+i\Omega_k} d\omega \Omega_k F(\Omega_k, -i\omega) \coth \frac{\omega}{2T} \right. \\ &\quad + \int_{-\infty}^{+\infty} d\omega (-i\omega) F(\Omega_k, -i\omega) \coth \frac{\omega}{2T} \\ &\quad \left. - \int_{-\infty+i\Omega_k}^{+\infty+i\Omega_k} d\omega (-i\omega) F(\Omega_k, -i\omega) \coth \frac{\omega}{2T} \right\}. \end{aligned} \quad (3.A.32)$$

Replacing ω by $\omega + i\Omega_k$ in the first and third integrals, and using the relation $\coth \frac{\omega + i\Omega_k}{2T} = \coth \frac{\omega}{2T}$, we find

$$\Lambda = \frac{1}{4\pi} \int_{-\infty}^{+\infty} \omega d\omega \coth \frac{\omega}{2T} [F(\Omega_k, -i\omega + \Omega_k) - F(\Omega_k, -i\omega)]. \quad (3.A.33)$$

To continue (3.A.33) analytically, it is sufficient to replace Ω_k by $-i\Omega$.

The expression for the conductivity correction takes on the form

$$\delta\sigma(\Omega, T) = \frac{\sigma_0}{4\pi i\Omega} \int_{-\infty}^{+\infty} \omega d\omega \coth \frac{\omega}{2T} [F(-i\Omega, -i\omega - i\Omega) - F(-i\Omega, -i\omega)]. \quad (3.A.34)$$

When calculating the temperature dependence of the conductivity, it is necessary to proceed to the limit as $\Omega \rightarrow 0$ in (3.A.34):

$$\delta\sigma(\Omega, T) = -\frac{\sigma_0}{4\pi} \int_{-\infty}^{+\infty} d\omega F(0, -i\omega) \frac{\partial}{\partial \omega} \left(\omega \coth \frac{\omega}{2T} \right). \quad (3.A.35)$$

Substituting (3.A.30) into (3.A.35) and integrating over directions of vector \mathbf{q} , we obtain

$$\delta\sigma^{(d)}(T) = -\frac{4\sigma_0}{\pi d} \int_{-\infty}^{+\infty} d\omega \frac{\partial}{\partial \omega} \left(\omega \coth \frac{\omega}{2T} \right) \int \frac{V(\mathbf{q}, \omega) Dq^2 (dq)}{(-i\omega + Dq^2)^3}. \quad (3.A.36)$$

References

1. N.F. Mott, *Adv. Phys.*, **16**, 49 (1961).
2. N.F. Mott and E.A. Davis, *Electronic Processes in Non-crystalline Materials*, Clarendon Press, Oxford (1971).
3. P.W. Anderson, *Phys. Rev.*, **102**, 1008 (1958).
4. A.A. Abrikosov, L.P. Gorkov, and I.E. Dzyaloshinskii, *Methods of Quantum Field Theory in Statistical Physics* [in Russian], Fizmatgiz, Moscow (1962).
5. L.P. Gorkov, A.I. Larkin, and D.E. Khmel'nitskii, *Pis'ma Zh. Éksp. Teor. Fiz.*, **30**, 248 (1979).
6. D.J. Thouless, *Phys. Rev. Lett.*, **39**, 1167 (1977).
7. P.W. Anderson, E. Abrahams, and R. Ramakrishnan, *Phys. Rev. Lett.*, **43**, 718 (1979).
8. P.A. Lee, *J. Noncrystall. Solids*, **35**, 21 (1980).
9. S. Hikami, A.I. Larkin, and N. Nagaoka, *Progr. Theor. Phys.*, **63**, 707 (1980).
10. K.B. Yefetov, A.I. Larkin, and D.E. Khmel'nitskii, *Zh. Éksp. Teor. Fiz.*, **79**, 1920 (1980).
11. M.I. Dyakonov and V.I. Perel, *Zh. Éksp. Teor. Fiz.*, **60**, 1954 (1971); *Solid State Phys.*, **13**, 3581 (1971).
12. G.L. Birr and G.E. Pikus, *Symmetry and Deformational Effects in Semiconductors* [in Russian], Nauka, Moscow (1972).
13. B.L. Altshuler, A.G. Aronov, A.I. Larkin, and D.E. Khmel'nitskii, *Zh. Éksp. Teor. Fiz.*, **81**, 8 (1981).
14. B.L. Altshuler, A.G. Aronov, and D.E. Khmel'nitskii, *Solid State Commun.* (1981), to be published.
15. B.L. Altshuler, A.G. Aronov, and D.E. Khmel'nitskii, *Zh. Éksp. Teor. Fiz.* (1981), to be published.
16. V.P. Silin and A.A. Rukhadze, *Electromagnetic Properties of Plasma and Plasma-like Media* [in Russian], Atomizdat, Moscow (1962).
17. I.O. Kulik, *Pis'ma Zh. Éksp. Teor. Fiz.*, **14**, 341 (1971).
18. Yu.N. Ovchinnikov, *Zh. Éksp. Teor. Fiz.*, **64**, 719 (1973).

19. B.L. Altshuler and A.G. Aronov, *Pis'ma Zh. Éksp. Teor. Fiz.*, **30**, 514 (1979).
20. B.L. Altshuler and A.G. Aronov, *Solid State Commun.*, **38**, 1031 (1981).
21. A. Schmid, *Z. Physik*, **271**, 251 (1974).
22. E.M. Lifshits and L.P. Pitaevsky, *Statistical Physics* [in Russian], Nauka, Moscow (1978).
23. M.J. Uren, R.A. Davies, M. Kaveh, and M. Pepper, *J. Phys. C*, (1981), to be published.
24. B.I. Shklovsky and A.L. Efros, *Electronic Properties of Doped Semiconductors* [in Russian], Nauka, Moscow (1979).
25. B.L. Altshuler and A.G. Aronov, *Solid State Commun.*, **30**, 115 (1979).
26. B.L. Altshuler and A.G. Aronov, *Zh. Éksp. Teor. Fiz.*, **77**, 2028 (1979).
27. B.L. Altshuler, A.G. Aronov, and P.A. Lee, *Phys. Rev. Lett.*, **46**, 1288 (1980).
28. T.F. Rosenbaum, K. Andres, G.A. Thomas, and P.A. Lee, *Phys. Rev. Lett.*, **46**, 568 (1981).
29. J.M. Rowel, in: *Tunneling Phenomena in Solids* [ed. E. Burstein and S. Lundqvist], Plenum Press, New York (1969).
30. J. Appelbaum, *Phys. Rev. Lett.*, **17**, 91 (1966).
31. S. Bermon and C.K. So, *Solid State Commun.*, **27**, 727 (1978).
32. R.C. Dynes and J.P. Garno, *Phys. Rev. Lett.*, **4**, 137 (1981).
33. W.L. McMillan and J. Mochel, *Phys. Rev. Lett.*, **46**, 556 (1981).
34. R. Thompson, *Phys. Rev.*, **B1**, 327 (1970).
35. L.G. Aslamazov and A.I. Larkin, *Solid. State Phys.*, **10**, 1106 (1968); *Phys. Lett.*, **26**, 238 (1968).
36. N.N. Bogoliubov, D.V. Shirokov, and V.V. Tolmachev, *New Method in the Theory of Superconductivity* [in Russian], Izd-vo AN SSSR, Moscow (1958).
37. A.I. Larkin, *Pis'ma Zh. Éksp. Teor. Fiz.*, **31**, 239 (1980).
38. L.G. Aslamazov and A.A. Varlamov, *J. Low Temp. Physics*, **18**, 223 (1980).
39. R.W. Cochran, R. Harris, J.O. Strom-Olsen, and M.J. Zuckermann, *Phys. Rev. Lett.*, **35**, 110 (1975).
40. B.L. Altshuler and A.G. Aronov, *Lectures in LNPI School*, (1979), p. 45.
41. I.L. Bronevoy, *Zh. Éksp. Teor. Fiz.*, **79**, 1936 (1980).
42. D.J. Bishop, D.C. Tsui, and R.C. Dynes, *Phys. Rev. Lett.*, **44**, 1153 (1980).
43. M.J. Uren, R.A. Davies, and M. Pepper, *J. Phys.*, **C13**, L958 (1980).
44. G.J. Dolan and D.D. Osheroff, *Phys. Rev. Lett.*, **43**, 721 (1979).
45. N. Giordano, W. Gilson, and D.E. Prober, *Phys. Rev. Lett.*, **43**, 725 (1979).
46. L. Van den Dries, G. Van Haesendouck, Y. Bruysenraede, and G. Deutscher, *Phys. Rev. Lett.*, **46**, 565 (1981).
47. G.J. Dolan, Preprint (1980).
48. N. Giordano, Preprint (1980).
49. B.L. Altshuler, *Zh. Éksp. Teor. Fiz.*, **75**, 1330 (1978).
50. B.L. Altshuler, D.E. Khmel'nitsky, A.I. Larkin, and P.A. Lee, *Phys. Rev.*, **B22**, 5142 (1980).
51. P. Chaudhari and H.U. Habermeier, *Solid State Commun.*, **34**, 687 (1980).
52. H. Fukuyama, *J. Phys. Soc. Japan*, **49**, 644 (1980).
53. A.N. Ionov, *Pis'ma Zh. Éksp. Teor. Fiz.*, **29**, 76 (1979).
54. K. Sugiyama, *J. Phys. Soc. Japan*, **19**, 1745 (1964).
55. A. Kawabata, *Solid State Commun.*, **34**, 431 (1980); *J. Phys. Soc. Japan*, **49**, 628 (1980).
56. B.L. Altshuler and A.G. Aronov, *Pis'ma Zh. Éksp. Teor. Fiz.* (1981) to be published.
57. P.G. De Gennes, *Superconductivity of Metals and Alloys*, W.L. Benjamin, Inc., New York-Amsterdam (1966).
58. Y. Kawaguchi and S. Kawaji, *J. Phys. Soc. Japan*, **42**, 699 (1980).

59. Yu.S. Zinchik, S.V. Kozyrev, and G.A. Polyanskaya, *Pis'ma Zh. Éksp. Teor. Fiz.*, **33**, 278 (1981).
60. Y. Kawaguchi, H. Kitahara, and S. Kawaji, *Solid. State Commun.*, **26**, 701 (1978).
61. O.V. Yemelyanenko and D.N. Nasledov, *Zh. Teor. Fiz.*, **28**, 117 (1958).
62. W. Sasaki, *J. Phys. Soc. Japan*, **20**, 825 (1965).
63. W. Sasaki, in: *Proc. Int. Conf. Phys. Semicond.*, Kyoto [*J. Phys. Soc. Japan, Suppl.*], **21**, 543 (1966).
64. C. Yamanouchi, K. Mizuquchi, and W. Sasaki, *J. Phys. Soc. Japan*, **22**, 859 (1967).
65. H. Roth, W.D. Straub, W. Bernard, and J.E. Mulhern, *Phys. Rev. Lett.*, **11**, 328 (1963).
66. A.V. Andrianov, E.L. Ivchenko, G.E. Pikus, R.Ya. Rasulov, and I.D. Yaroshetskii, *Zh. Éksp. Teor. Fiz.*, (1982), to be published.
67. M.J. Katz, *Phys. Rev.* **140A**, 1323 (1966).
68. H. Fukurawa, *J. Phys. Soc. Japan*, **18**, 737 (1963).
69. B.L. Altshuler, A.G. Aronov, and B.Z. Spivak, *Pis'ma Zh. Éksp. Teor. Fiz.*, **33**, 101, (1981).
70. R.D. Parks, W.A. Little, *Phys. Rev.*, **A133**, 97 (1964).
71. R.B. Dingle, *Proc. Roy. Soc.*, **A212**, 47 (1952).
72. E.N. Bogachek and G.A. Gogadze, *Zh. Éksp. Teor. Fiz.*, **63**, 1839 (1972).
73. F. Dyson, *Phys. Rev.*, **102**, 1217 (1956).
74. A.M. Polyakov, *Phys. Lett.*, **B59**, 79 (1975).
75. F. Wegner, *Z. Physik*, **35**, 203 (1979).
76. L. Schäfer and F. Wegner, *Z. Physik*, **338**, 113 (1980).
77. A. Houghten, A. Jevicki, R.D. Kenway, A.M.M. Pruisken, *Phys. Rev. Lett.*, **45**, 394 (1980).
78. E. Abrahams, P.W. Anderson, D.C. Liccardello, T.V. Ramakrishnan, *Phys. Rev. Lett.*, **42**, 673 (1979).
79. M.E. Fisher, K. Wilson, *Phys. Rev. Lett.*, **28**, 548 (1972).
80. A.B. Harris, T. Lubensky, *Phys. Rev.*, **B23**, 2640 (1981).
81. B.W. Dodson, W.L. McMillan, J.M. Mochel, and R.C. Dynes, *Phys. Rev. Lett.*, **46**, 46 (1981).
82. T.F., Rosenbaum, K. Andres, G.A. Thomas, and R.N. Bhatt, *Phys. Rev. Lett.*, **45**, 1723 (1980).
83. D.E. Khmel'nitskii, *Pis'ma Zh. Éksp. Teor. Fiz.*, **32**, 248 (1980).
84. L.V. Keldysh, *Zh. Éksp. Teor. Fiz.*, **47**, 1515 (1964).
85. R.P. Feynman and A.R. Hibbs, *Quantum Mechanics and Path Integrals*, McGraw Hill, New York (1965).
86. D.Yu. Sharvin and Yu.V. Sharvin. *Pis'ma Zh. Éksp. Teor. Fiz.* (1982), to be published.

An Exact Solution of the Kondo Problem

P.B. Wiegmann, Cand. Sc. (Physics and Mathematics)

L.D. Landau Institute for Theoretical Physics,
Academy of Sciences of the USSR

4.1 INTRODUCTION

It is now a well-known fact that a small amount of magnetic impurity drastically changes the properties of simple metals. The first experiments in this field date from the 1930s, when researchers observed a minimum in the temperature dependence of the resistivity of some, as it was thought, pure metals. Later it was established that this effect is due to a small admixture of impurity atoms of transition metals.

The subject called "magnetic impurities in metals" is extremely broad and encompasses a large variety of physical phenomena. This article deals with alloys in which the impurity atoms with unfilled d- or f-shells have well-defined valencies. This means that at high temperatures the impurities have a magnetic moment corresponding to their valence, and the magnetic susceptibility obeys the Curie law.

In the sixties the magnetic properties of such alloys were thoroughly studied experimentally. It was found that as the temperature drops below a certain temperature characteristic of the alloy and known as the Kondo temperature T_K , the impurity part of the magnetic susceptibility ceases to grow and at absolute zero remains constant (Fig. 4.1). In other words, with a decrease in temperature the impurity paramagnetism vanishes. This smooth transition to the nonmagnetic state is associated with certain anomalies in the thermal and transport properties of the alloys. Figures 4.1-4.4 give the temperature dependencies established in experiments of the magnetic susceptibility, resistivity, thermoelectric power, and heat capacity (the experimental data available at the end of 1974 is given in the reviews [1-4]).

Two obvious conclusions can be drawn from the results of experiments with an enormous number of dilute alloys with atoms of transition and some rare-earth elements.

(1) The Kondo temperature T_K is the only common scale, from the energy standpoint, that determines the dependence of various physical quantities on temperature, magnetic field strength, and frequency. For various matrix atoms of the metal T_K varies greatly. For instance for Mn alloys the Kondo temperature changes from 1 K (for ZnMn) to 500 K (for AlMn) [1], while for Ce and Yb alloys it changes from 1 μ K (for AuYb) [24i] to 40 K (for AlCe) [1].

(2) The physical quantities behave quite differently in the regions where $T \gg T_K$ and $T \ll T_K$. At high temperatures ($T \gg T_K$) this behavior can fairly well be approximated by an inverse-power logarithmic law. The most widely known law is the logarithmic growth of resistivity as temperature decreases (Fig. 4.2):

$$R_{\text{imp}} \sim \frac{1}{\ln^2(T/T_K)}. \quad (4.1.1)$$

At $T \ll T_K$ the temperature dependence is quite different. It is now proved that the temperature dependences for various quantities

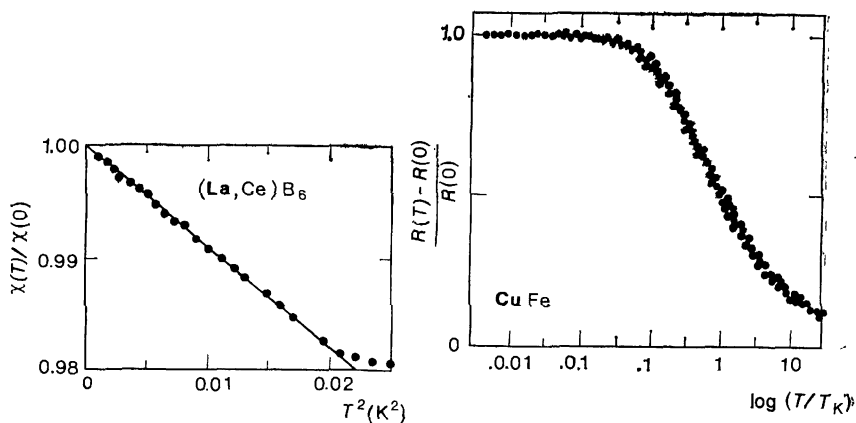


Fig. 4.1. Normalized impurity magnetic susceptibility $\chi(T)/\chi(0)$ in $(\text{La, Ce})\text{B}_6$ versus T at low temperatures [61].

Fig. 4.2. The temperature dependence of impurity resistivity in CuFe on the logarithmic scale [24g].

are described at low energies by integral-power laws (e.g. see [6]):

$$\begin{aligned} R_{\text{imp}} &= R(0) (1 - \kappa_R (T/T_K)^2 + \dots), \\ C_{\text{imp}} &= \gamma T/T_K (1 - \kappa_C (T/T_K)^2 + \dots), \\ \chi_{\text{imp}} &= \chi_0 (1 - \kappa_\chi (T/T_K)^2 + \dots). \end{aligned} \quad (4.1.2)$$

Here the factors κ_R , κ_C , and κ_χ are constants of the order of unity. The dependence of physical quantities on the magnetic field strength (at $k_B T \ll \mu_B H \ll k_B T_K$) is quite similar.

The properties of dilute magnetic alloys are determined, in general by the exchange interaction between the conduction electrons and the magnetic moment of the impurity. The common way to study this interaction is to employ the s-d exchange model. This is the simplest idealized model, in which the impurity is considered as

a localized moment S . Exploring this model by a perturbation-theory technique, J. Kondo in 1964 gave an explanation [7] for the minimum in the temperature dependence of resistivity. His work laid the ground for theoretical work in this field that continued until the midseventies.

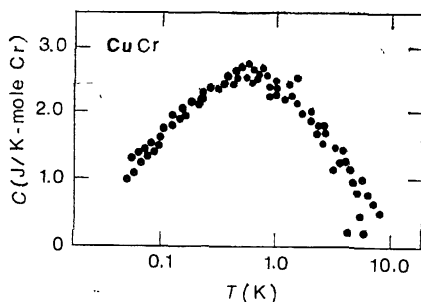
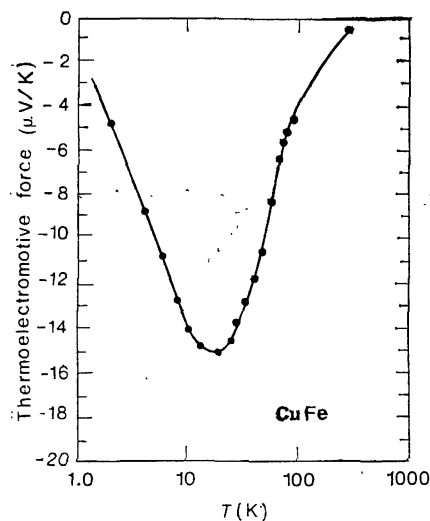


Fig. 4.3. The temperature dependence of the thermoelectric power in CuFe.

Fig. 4.4. The temperature dependence of heat capacity in CuCr. The Kondo anomaly manifests itself at $T = 22$ K [5].

The Hamiltonian for the s-d exchange model is

$$\mathcal{H} = \mathcal{H}_0 + JS \cdot \sigma(0), \quad (4.1.3)$$

where

$$\mathcal{H} = \sum_{\mathbf{k}, \sigma=\uparrow, \downarrow} \epsilon_{\mathbf{k}} c_{\mathbf{k}\sigma}^\dagger c_{\mathbf{k}\sigma},$$

$$\sigma(0) = \sum_{\mathbf{k}, \mathbf{k}'} c_{\mathbf{k}\sigma}^\dagger \sigma_{\sigma\sigma'} c_{\mathbf{k}'\sigma'}.$$

Here $\epsilon_{\mathbf{k}}$ is the kinetic energy, $c_{\mathbf{k}\sigma}^\dagger$ and $c_{\mathbf{k}\sigma}$ are the creation and annihilation operators for the conduction electrons with momentum \mathbf{k} and spin component $\sigma = \uparrow, \downarrow$ (the conduction electrons are assumed free), $S = (S_x, S_y, S_z)$ is the impurity spin operator, $\sigma(0)$ is the electron spin density operator at the point $x=0$ of the impurity, and $\sigma = (\sigma_x, \sigma_y, \sigma_z)$ are the Pauli matrices.

We will be interested in effects that are linear in the impurity concentration. Hence we may assume that the conduction electrons interact with only one impurity, say, at $x = 0$, which is the case with the Hamiltonian (4.1.3).

In real alloys the exchange interaction is always antiferromagnetic and the dimensionless quantity $J\rho$ ($\in \mathbf{F}$) small:

$$0 < J\rho (\in \mathbf{F}) \ll 1,$$

where ρ ($\in \mathbf{F}$) is the density of states at the Fermi surface.

Kondo discovered that the effective scattering amplitude of conduction electrons on an impurity accompanied by spin flip, when calculated within the s-d model in the second-order perturbation theory, grows when the energy or temperature drops:

$$J(T) = J + J^2\rho(\in \mathbf{F}) \ln(\in \mathbf{F}/T) + \dots \quad (4.1.4)$$

The resistivity connected with magnetic impurities at $J(T) \ll 1$ is proportional to the square of the scattering amplitude:

$$R_{\text{imp}} \propto J^2(T). \quad (4.1.5)$$

Therefore, when the temperature decreases and the interaction is antiferromagnetic, the impurity part of resistivity, R_{imp} , increases, in contrast with the phonon part. This explains the old puzzle with the minimum in the resistivity.

At a temperature of the order of the Kondo temperature, i.e.

$$T_K \sim \in \mathbf{F} \exp(-1/J\rho(\in \mathbf{F})), \quad (4.1.6)$$

all terms in the series (4.1.2) are of the same order and, notwithstanding the fact that the coupling constant is small, perturbation theory ceases to work.

Soon, however, the most divergent terms in the perturbation theory series, corresponding to the so-called parquet diagrams, were summed. In 1965 Abrikosov [8] and Suhl [9, 10] showed that in the principal logarithmic approximation,

$$J(T) = \frac{J}{1 - J\rho(\in \mathbf{F}) \ln(\in \mathbf{F}/T)} + \dots \quad (4.1.7)$$

When the exchange interaction is ferromagnetic ($J < 0$), Eq. (4.1.7) determines the behavior of the magnetic impurity, since in the entire temperature range the effective scattering amplitude is small and higher-order terms need not be taken into account. For instance, the temperature dependence of the impurity part of the magnetic susceptibility at any T differs from the Curie law by a logarithmic term, which remains small at all temperatures and vanishes as $T \rightarrow 0$:

$$\chi_{\text{ferro}}(T) = \frac{S(S+1)}{3T} \left(1 + \frac{1}{\ln(T/\in \mathbf{F})} \right). \quad (4.1.8)$$

A totally different situation arises when the exchange is antiferromagnetic ($J > 0$). Here the effective interaction amplitude grows as T decreases and has a pole at T_K :

$$J(T) \approx \frac{1}{\ln(T/T_K)} \frac{1}{\rho(\epsilon_F)}. \quad (4.1.9)$$

Allowing for the next logarithmic approximation changes nothing. For instance, the magnetic susceptibility, which in this approximation is a linear function of the scattering amplitude, has the form [11, 12]

$$\begin{aligned} \chi(T) &\simeq \frac{J(T)}{T} (g\mu_B)^2 \frac{S(S+1)}{3} \\ &\simeq \frac{1}{T} (g\mu_B)^2 \frac{S(S+1)}{3} \left(\frac{1}{\ln(T/T_K)} + \frac{1}{2} \frac{\ln \ln(T/T_K)}{\ln^2(T/T_K)} + \dots \right). \end{aligned} \quad (4.1.10)$$

It is quite clear that this divergence is a consequence of the chosen approximation. Perturbation theory, for which the natural smallness parameter is $1/\ln(T/T_K)$, becomes invalid at $T \sim T_K$, and the question of how a magnetic impurity behaves in a nonmagnetic metal at low energies remains open. This is what is called the Kondo problem. The remarkable simplicity of the Hamiltonian of the s - d model and convincing experiments led to the great popularity of this problem. But the simplicity turned out to be illusory. Great efforts were made to surpass perturbation-theory schemes. The majority of theories that emerged in the midsixties represent a failure in building an approximate approach for studying the ground state of the impurity. The fact that at $T \ll T_K$ there is no parameter made the different approximation schemes uncontrolled, which often led to incorrect results. No consistent theoretical investigation of low-temperature properties of magnetic alloys existed, although the correct assumption that the ground state of an impurity with spin $S = 1/2$ is singlet was put forward by Nagaoka [13] in 1965.

In 1967 Mattis [20] cited qualitative arguments in favor of the fact that the ground state of a magnetic impurity with spin S is $2S$ -fold degenerate. In this case the impurity remains magnetic event at $T = 0$, but the spin is $S - 1/2$.

A qualitative understanding of the impurity-moment compensation phenomenon that emerged in the 1970s is connected with the works of Anderson, Yuval, Hamann [14-16], Wilson [17], and Nozieres [18].

In 1970, Anderson, Yuval, and Hamann discovered that for a certain (not really small) value of the spin-conserving scattering amplitude, the problem becomes equivalent to a model that is easily diagonalized. This solution yielded a finite value for the magnetic susceptibility at $T = 0$. Using qualitative arguments, the authors

showed that

$$\chi_{\text{imp}} \sim 1/T_K, \quad (4.1.11)$$

provided the exchange interaction is weak. This result was confirmed by Wilson [17] in 1973. He developed a numerical renormalization procedure and showed without doubt that as the energy scale decreases and $J \ll 1$, the distribution of the energy levels in the system tends to what exists for the nonrenormalized energy, but that $J = \infty$. For this reason, as the energy decreases and $T \rightarrow 0$, even for a small "bare" value of J the system goes into the strong-coupling regime. The point $J = \infty$ is the fixed point for the Hamiltonian (4.1.3). Apart from calculating the impurity part of the magnetic susceptibility at $T \rightarrow 0$,* Wilson showed (also numerically) that the impurity heat capacity is a linear function of T as $T \rightarrow 0$:

$$C_{\text{imp}} \sim T/T_K, \quad (4.1.12)$$

and that the universal ratio

$$W = \lim_{T \rightarrow 0} \frac{C_{\text{imp}}}{T\chi_{\text{imp}}} \frac{3}{4\pi^2} (g\mu_B)^2 = 0.5 \quad (4.1.13)$$

is half the value obtained in the theory of Fermi liquids.

Using these results as a basis, Nozieres [18] in 1974 proposed an effective phenomenological theory along the same lines as Landau's theory of Fermi liquids. For one, he found that Eq. (4.1.13), which Wilson obtained numerically, is exact. Also, he determined the first term in the series expansion of the resistivity in powers of $(T/T_K)^2$:

$$\frac{R_{\text{imp}}(0) - R_{\text{imp}}}{R_{\text{imp}}(0)} = \frac{9}{4} C_{\text{imp}}^2, \quad T \rightarrow 0. \quad (4.1.14)$$

Equation (4.1.13) was later obtained by many investigators using various approaches (see [21-23]). We note the interesting works of Yamada and Yosida [23], who arrived at Eqs. (4.1.13) and (4.1.14) by analyzing the perturbation-theory series in the Anderson model.

At present there is a vast literature—more than 20 review papers encompassing more than 2×10^3 works that appeared between 1961 and 1975 and devoted to theoretical and experimental studies of dilute magnetic alloys. Some review articles are listed in the literature cited in [24].

* * *

A possible explanation for such a great interest in the Kondo problem, which in reality is a limited problem, may be the fact that many of the methods developed in connection with this problem have

* The fact that the magnetic susceptibility has a finite value at $T = 0$ was convincingly established earlier by Schotte and Schotte [19], who used a different numerical procedure.

proved to be universal and been very productive in other fields of theoretical physics. Sufficient to note that the recursive procedure, which forms the basis for the modern renormalization-group technique, was first effectively employed by Anderson, Yuval, and Hamann [16]. The method of boson representation of fermion operators, which has proved so fruitful in the physics of one-dimensional quantum systems [25, 26] and two dimensional classical systems (e.g. see the review article [27]), was developed in the remarkable work of Schotte [28]. More examples of this process could be cited.

We note that historically the exchange Hamiltonian (4.1.3) was one of the first and, apparently, one of the simplest examples in quantum field theory in which the strength of the interaction grows as the energy scale diminishes (i.e. as the time scale increases).

In 1980 in [29-38] it was shown that the traditional s-d exchange model is completely integrable, and the Hamiltonian (4.1.3) was diagonalized exactly. The method employed in these works goes back to Hans Bethe and has been known since 1931 [39]. This enabled completely solving the problem of the ground state of a magnetic impurity in a nonmagnetic metal and the problem of the dependence of thermodynamic functions on temperature and magnetic field strength [36-38].

The present paper is basically concerned with this method as applied to the Kondo problem and the results obtained along these lines. Not only the s-d model but also the Anderson model, which describes magnetic moment formation in metals, is fully integrable (see [34]).

The method used by Bethe (called the Bethe Ansatz) to build the solution for the one-dimensional Heisenberg chain drew no interest for more than 30 years (if one disregards the works of Hulthen [40], Orbach [41], and Walker [42]). The first revival of interest in the Bethe Ansatz took place in the midsixties and almost coincided with a period of active investigation into the Kondo problem. Recent years have seen a new interest in this field of mathematical physics (see [43-49]).

4.2 THE BASIC MODELS

The majority of works on the Kondo effect are devoted to many-particle effects proper and are, therefore, based on the simplest, idealized s-d exchange model (4.1.3). It is assumed that the impurity is pointlike, the only degrees of freedom being associated with spin. The orbital degeneracy of the impurities, which are usually atoms of transition or rare-earth elements, is completely ignored. This simplifies the theory considerably and still preserves its main features and difficulties. However, such simplification restricts a direct comparison with experimental data.

Although attempts have long been made to build exchange Hamiltonians that describe real impurities in real metals, this process cannot be considered finished. The literature is scant. The fullest and best works are those of Schrieffer [50], Cogblin and Schrieffer [51], and Nozieres and Blandin [52], which we follow here. Although detailed study of specific alloys is in the future, we can still cite several exchange Hamiltonians that can serve as the first approximation in relation to real substances. Here we dwell on the derivation of exchange Hamiltonians based on the Anderson model.

4.2.1 The Anderson Model

Writing the exchange Hamiltonian, we assume that there is a localized magnetic moment in the metal but do not ask how such a moment was formed. The electronic mechanism of localized moment formation and the origin of the exchange interaction with the conduction electrons are commonly studied using the so-called Anderson model. In this model the metallic matrix of a normal metal is represented, as usual, by a band of conduction electrons with the spectrum $\epsilon_{\mathbf{k}}$. The interaction of the electrons on the unfilled d (or f) shell is given by the atomic Hamiltonian $\mathcal{H}_{\text{atom}}$; the interaction between an impurity atom and conduction electrons is described phenomenologically by the amplitude of mixing of the band and orbital electronic states. The Anderson Hamiltonian is [53]

$$\mathcal{H}_A = \sum_{\mathbf{k}, \sigma} \epsilon_{\mathbf{k}} a_{\mathbf{k}\sigma}^\dagger a_{\mathbf{k}\sigma} + \sum_{\mathbf{k}, m, \sigma} V_{\mathbf{k}m} (a_{\mathbf{k}\sigma}^\dagger d_{m\sigma} + \text{h.c.}) + \mathcal{H}_{\text{atom}} + \text{Crystal field.} \quad (4.2.1)$$

Here $a_{\mathbf{k}\sigma}^\dagger$ is the creation operator for a conduction electron with momentum \mathbf{k} and spin $\sigma = \downarrow, \uparrow$, and $d_{m\sigma}^\dagger$ is the creation operator for an electron with spin σ and orbital angular-momentum component m in the unfilled shell of the impurity atom.

In writing the Hamiltonian (4.2.1), we introduced certain simplifications. We assumed that the Fermi surface is a sphere and neglected the interaction between the conduction electrons. The crystal-field term in (4.2.1) is responsible for the fact that the crystalline surroundings of the impurity are nonspherical; it leads to an orbital splitting of the atomic levels.

The atomic Hamiltonian contains terms invariant under independent rotation in the spin and coordinate spaces and a spin-orbit coupling term:

$$\mathcal{H}_{\text{atom}} = \mathcal{H}_{\text{sph}} - A \mathbf{L}_d \cdot \mathbf{S}_d. \quad (4.2.2)$$

The rotational-invariant part was usually written (e.g. see [2]) as

$$\mathcal{H}_{\text{sph}} = \sum_{\sigma} \epsilon_d n_{d\sigma} + \frac{U}{2} (n_d^2 - n_d) - \frac{J}{2} \left(2S_d^2 + \frac{1}{2} n_d^2 - 2n_d \right), \quad (4.2.3)$$

with

$$n_d = \sum_{m, \sigma} d_{m\sigma}^+ d_{m\sigma}, \quad S_d = \sum_{m, \sigma, \sigma'} d_{m\sigma}^+ \sigma_{\sigma\sigma'} d_{m\sigma'},$$

$$L_d = \sum_{m, m', \sigma} d_{m\sigma}^+ L_{mm'} d_{m'\sigma}$$

being the number of electrons on the d shell and their spin and orbital angular momentum. The quantity U describes the Coulomb repulsion between orbital electrons and J the Hund interaction.

Only recently did Nozieres and Blandin [52] and Mihaly and Zawadowski [54] note that there is no reason to write $\mathcal{H}_{\text{atom}}$ in the form (4.2.3). Indeed, the nonrelativistic two-particle interaction of orbital electrons is described by $l + 1$ Slater coefficients:

$$\mathcal{H}_{\text{sph}} = \sum_{m\sigma} \Gamma_{m_1\sigma_1; m_2\sigma_2}^{m_3\sigma_3; m_4\sigma_4} d_{m_1\sigma_1}^+ d_{m_2\sigma_2}^+ d_{m_3\sigma_3} d_{m_4\sigma_4}; \quad (4.2.4)$$

the magnitudes of these coefficients are restricted only by invariance under rotations in the spin and coordinate spaces:

$$m_1 + m_2 = m_3 + m_4, \quad \sigma_1 + \sigma_2 = \sigma_3 + \sigma_4.$$

4.2.2 The Angular Dependence of Hybridization Amplitudes. A One-Dimensional Hamiltonian

The mixing (or hybridization) amplitude $Y_{\mathbf{k}m}$ in (4.2.1) is the matrix element of the Hamiltonian of an electron in the potential field $V_{\text{imp}}(\mathbf{r})$ of the impurity ion, the matrix element taken between the band and orbital states:

$$V_{\mathbf{k}} = \int \psi_e(\mathbf{k} \cdot \mathbf{r}) \left(-\frac{1}{2m} \nabla^2 + V_{\text{imp}}(\mathbf{r}) \right) \psi_d(\mathbf{r}) r^2 dr d\Omega, \quad (4.2.5)$$

where $\psi_e = 1/\sqrt{\mathcal{V}} \exp(i\mathbf{k} \cdot \mathbf{r})$ and $\psi_d(\mathbf{r})$ are the band and orbital electronic wave functions, with \mathcal{V} the volume of the system. The wave function of an orbital electron with an angular momentum component $m = -l, \dots, l$, is

$$\psi_m^d(\mathbf{r}) = R_d(r) Y_l^m(r/r). \quad (4.2.6)$$

If we assume the ion potential $V_{\text{imp}}(\mathbf{r})$ to be spherically symmetric and integrate in (4.2.5) over the solid angle Ω_r , we find the angular dependence of $V_{\mathbf{k}m}$:

$$V_{\mathbf{k}m} = Y_l^m(\mathbf{k}/k) (-1)^l \frac{\sqrt{6\pi}}{k\mathcal{H}} v_{kl}, \quad (4.2.7)$$

where

$$v_{kl} = \sqrt{\frac{2}{\mathcal{H}}} k \int j_l(kr) V_{\text{imp}}(r) \mathcal{R}_d(r) r^2 dr, \quad (4.2.8)$$

with $J_l(kr)$ a spherical Bessel function, and \mathcal{R} the radius of a spherical crystal centered at the impurity site.

We expand the plane wave of the conduction electrons in eigenfunctions of the orbital angular momentum by introducing the partial-wave creation operator *

$$a_{|\mathbf{k}| l m \sigma}^{\dagger} = (-1)^l \frac{k \mathcal{H}}{\sqrt{6\pi}} \int d\Omega_{\mathbf{k}} Y_l^m(\Omega_{\mathbf{k}}) a_{\mathbf{k}\sigma}^{\dagger}. \quad (4.2.9)$$

In this basis the hybridization amplitude and the kinetic energy of the conduction electrons are diagonal in m . The Anderson Hamiltonian, therefore, is [50]

$$\begin{aligned} \mathcal{H}_{\text{A}} = \mathcal{H}_{\text{atom}} + \sum_{|\mathbf{k}|, m, \sigma} \epsilon_{|\mathbf{k}|} a_{|\mathbf{k}| m \sigma}^{\dagger} a_{|\mathbf{k}| m \sigma} \\ + \sum_{|\mathbf{k}|, m, \sigma} v_{|\mathbf{k}| m} (a_{|\mathbf{k}| m \sigma}^{\dagger} d_{m \sigma} + \text{h.c.}). \end{aligned} \quad (4.2.10)$$

In other words, an impurity interacts only with the partial wave with orbital angular momentum l , and the interaction of the band and orbital electronic states is diagonal in m and σ . An important fact here is that the Hamiltonian (4.2.10) is, in essence, one-dimensional. All the quantities in this Hamiltonian depend only on $|\mathbf{k}|$. This is a consequence of the assumption that the Fermi surface and the impurity ion potential are spherical. The angular dependence of $V_{\mathbf{k}}$ leads to $(2l+1)$ -fold degeneracy of the one-dimensional conduction band. Of course, this is true only when the impurities may be considered independent, i.e. in an approximation linear in their concentration.

4.2.3 Hierarchy of Energies

The Anderson Hamiltonian (4.2.5) contains many parameters that have the dimensions of energy, but in many cases of interest to the researcher the magnitudes of these quantities are different. This fact greatly simplifies the problem.

The subject of this article, as mentioned before, is Kondo alloys. In these alloys the valence of the impurity atoms, i.e. the number of orbital electrons n_d , changes in the scattering process only virtually. The energies E_{\pm} associated with the change of n_d by ± 1 are very large (on the order of 5-10 eV).**

For a fixed valence the atomic terms split according to the Hund rule. The basic state corresponds to the maximal value of total spin, and for fixed spin to the maximal value of total orbital angular

* More exactly, allowing for the crystal field, we must use states that transform under the irreducible representations of the crystal's point group of symmetry in relation to the impurity.

** Note that E_+ and E_- may differ considerably. E.g., for cerium atoms, $E_+ \sim 6$ eV while $E_- \sim 2$ eV.

momentum. The characteristic splitting energies are on the order of 1 eV.

The next energy scale for transition impurities is the crystal field, on the order of 0.5 eV. Orbital states split according to the irreducible representations of the symmetry group of the crystal.

The situation gets considerably simpler if according to the Hund rule the ground state is an orbital singlet. This is the case for Mn ($n_d = 5$) and Eu ($n_f = 7$). Here the crystal field has practically no influence on the impurity. However, in some cases it is the crystal field that leads to an orbital singlet. If the ground state of the atom is an orbital multiplet, it is split by spin-orbit coupling into states with different total angular momentum J . For transition metals the LS is of the order of 0.1 eV.

Quite a different situation is present for atoms of rare-earth elements. In this case the spin-orbit coupling considerably exceeds the magnitude of the crystal field. E.g., for Ce [55], the crystal field is roughly 50-100 K, while LS is about 0.3 eV.

The discussed atomic energy scales must be compared with the resonance level width $\Delta \sim \pi \rho (\epsilon_F)^2$. In transition metals this quantity is about 0.1 eV, while in rare earths it is much smaller, of the order of 10^3 K. If Δ is much smaller than the ionization energy E_{\pm} we can speak of a constant valence of the impurity and of a localized magnetic moment. In this case the interaction of the conduction electrons with the impurity is described by an exchange Hamiltonian.

The size of the orbital splitting of a state with fixed valence must be compared, in what follows, only with the possible temperature interval or the Kondo temperature. For transition impurities the latter is always the smaller. For this reason $\mathcal{H}_{\text{atom}}$ projects the Anderson Hamiltonian onto the ground state of the atom. In rare-earth alloys the situation is just the opposite: the splittings associated with the crystal field are often comparable with the Kondo temperature.

4.2.4 Exchange Hamiltonians

Here we will consider the strongest inequality in the energy hierarchy; namely, the energies that are connected with variations in valence, E_{\pm} , are high compared with the resonance level width. This is the condition for the formation of localized magnetic moments. When we study processes in which the variation of n_d is virtual, an exchange Hamiltonian emerges as a result of projecting the Anderson Hamiltonian onto a sector with a fixed number of the localized particles n_d [56, 57].

In second-order perturbation theory in $v_{|k|}$ the effective exchange Hamiltonian in the most general form can be written as

$$\mathcal{H}_{\text{ex}} = \mathcal{H}_{\text{atom}}^0 + \sum_{\mathbf{k}, \mathbf{k}'} T_{m\sigma, m'\sigma'}(\mathbf{k}, \mathbf{k}') a_{\mathbf{k}m\sigma}^+ a_{\mathbf{k}'m'\sigma'}. \quad (4.2.11)$$

Here $\mathcal{H}_{\text{atom}}^0$ is the projection of $\mathcal{H}_{\text{atom}}$ onto the subspace with a given n_d , and matrix \mathbf{T} in the same subspace is written as

$$T_{m\sigma, m'\sigma'} = v_{\mathbf{k}} v_{\mathbf{k}'} \left(d_{m\sigma} \frac{1}{\varepsilon_{\mathbf{k}} - \mathcal{H}_{\text{atom}}} d_{m'\sigma'}^+ - d_{m\sigma}^+ \frac{1}{\varepsilon_{\mathbf{k}'} - \mathcal{H}_{\text{atom}}} d_{m'\sigma'} \right). \quad (4.2.12)$$

These formulas express virtual transitions from a sector with a given n_d to a sector with $n_d \pm 1$, and vice versa. In the process of such transition the momentum, projection of angular momentum, and spin of the electronic partial wave (\mathbf{k}, m, σ) change to $(\mathbf{k}', m', \sigma')$.

The next energy in this hierarchy, the Hund interaction energy, is also very great, and $\mathcal{H}_{\text{atom}}^0$ should be considered as the projection operator on the ground state of the impurity atom, a state characterized by orbital angular momentum L and spin S . Apart from some special cases, the exchange operator \mathbf{T} projected onto the subspace L, S has a rather complex structure. In general its form is restricted only by invariance under rotations in the spin and coordinate spaces and may be written thus:

$$\mathcal{H}_{\text{ex}} = \sum_{p, q=0}^{1, 2 \min(L, S)} (\mathbf{S} \cdot \boldsymbol{\sigma})_{\sigma\sigma'}^p (\mathbf{L} \cdot \mathbf{l})_{mm'}^q J_{pq}(\mathbf{k}, \mathbf{k}') a_{\mathbf{k}m\sigma}^+ a_{\mathbf{k}'m'\sigma'}, \quad (4.2.13)$$

where $\boldsymbol{\sigma}$ are the Pauli matrices, and \mathbf{l} is the operator of orbital angular momentum of the electronic partial wave that interacts with the impurity.

To this Hamiltonian we must add the spin-orbit coupling and the crystal field. For impurities of transition elements, as said before, the state of the atomic shell is split first by the crystal field. If after this the ground state is still a multiplet, we must allow for spin-orbit coupling.

For rare-earth impurities the large spin-orbit coupling immediately projects the Hamiltonian (4.2.13) onto the state of the shell with total angular momentum J , which is $L + S$ for $n_f > 7$ and $|L - S|$ for $n_f < 7$. In this case the general form of the exchange Hamiltonian is

$$\mathcal{H}_{\text{ex}} = \sum_{q, p=0}^{2 \min(L, J), 1} (\mathbf{J} \cdot \boldsymbol{\sigma})_{\sigma\sigma'}^p (\mathbf{J} \cdot \mathbf{l})_{mm'}^q J_{pq} a_{\mathbf{k}m\sigma}^+ a_{\mathbf{k}'m'\sigma'}. \quad (4.2.14)$$

Further splitting of the multiplet is caused by the crystal field.

The quantities J_{pq} in Eqs. (4.2.13) and (4.2.14) are the amplitudes of the exchange interaction. To estimate their values we neglect

the energy splitting within one valence in comparison with the energies E_{\pm} . Then the energy denominators (propagators) in (4.2.12) do not depend on m, σ and m', σ' , and matrix T contains only one parameter:

$$T_{m\sigma, m'\sigma'} = \left(\frac{v_k v_{k'}}{\varepsilon_k - E_+} \delta_{mm'} \delta_{\sigma\sigma'} - J_{kk'} \right) d_{m\sigma}^+ d_{m'\sigma'}, \quad (4.2.15)$$

where

$$J_{kk'} = v_k v_{k'} \left(\frac{1}{E_+ - \varepsilon_k} + \frac{1}{E_- - \varepsilon_{k'}} \right).$$

This formula provides for the upper estimate of J_{pq} . It is important that J never changes its sign and corresponds to antiferromagnetic interaction. Although $\rho (\epsilon_F) J \ll 1$, in view of the resonance nature of the superexchange it considerably exceeds the direct exchange, which is caused by the Coulomb interaction of orbital and band electrons and is usually ferromagnetic interaction.

The Hamiltonians (4.2.13) and (4.2.14) may be assumed to be the first terms in a series expansion in v^2 , which can be obtained from (4.2.1) as a result of a canonical Schrieffer-Wolf transformation [57]. Higher-order terms are small:

$$v^2 \rho (\epsilon_F) \left(\frac{n_d}{E_-} + \frac{2(2l+1) - n_d}{E_+} \right) \ll 1. \quad (4.2.16)$$

4.2.5 Two Simple Exchange Hamiltonians

Below we will consider two simple cases important from the practical standpoint.

4.2.5a. An orbital singlet. If the atomic shell of the impurity atom is half-filled, the Hund rule states that the ion ground state is an orbital singlet with spin $S = l + 1/2$. This is the case with Mn, which has $n_d = 5$ and whose d shell has the configuration ${}^6S_{5/2}$. Here scattering involves only exchange of spins, while the projection of the orbital angular momentum of the electronic partial wave remains unchanged. As a result the exchange Hamiltonian simplifies considerably. If in the general formula (4.2.13) we put $L = 0$ [50], we have

$$\mathcal{H}_{\text{ex}} = (V \delta_{\sigma\sigma'} + JS \cdot \sigma_{\sigma\sigma'}) \sum_{\substack{m=1 \\ k, k'}}^n a_{km\sigma}^+ a_{k'm'\sigma'}, \quad (4.2.17)$$

with

$$n \equiv 2l + 1 = 2S. \quad (4.2.18)$$

Since the ground state of the ion is spherically symmetric, the influence of the crystal field is negligible. It manifests itself in the exchange

Hamiltonian only in virtual states with $n_d = n_{d_0} \pm 1$, which leads to a weak dependence of J on m .

An orbital singlet may also appear as the result of the combined action of the Hund rule and the crystal field. This is the case with impurities of vanadium ($n_d = 3$) and cobalt ($n_d = 8$) in a cubic crystal field [52]. In this field the five orbital states split into a doublet (E) and a triplet (T), with the triplet lying below the doublet on the energy scale. Then at $n_d = 3$ the triplet is half-filled and, according to the Hund rule, there forms an orbital singlet state with spin $S = 3/2$. The situation is similar for $n_d = 8$ —the triplet is filled completely but the doublet is half-filled; for this reason $L = 0$ again, but $S = 1$. In these cases the exchange Hamiltonian again has the form (4.2.17). The plane wave corresponding to the conduction electrons must be expanded in the irreducible representations of cubic symmetry. The splitting of atomic levels leads to a situation in which the electrons that belong to the doublet and triplet are scattered by the impurity with markedly different amplitudes. E.g. for $n_d = 3$ we have $J_T \gg J_E$, and the difference is the greater the higher the strength of the crystal field.

In studying the equations for the renormalization group for such a doubly charged model, Nozieres and Blandin [52] demonstrated that the amplitude J_E , being bare and small, vanishes completely as the energy decreases. Hence, if we ignore J_E , we return to the Hamiltonian (4.2.17) but with spin 3/2 and three values of m ($n = 3$). The case $n_d = 8$ is described by the same Hamiltonian but with $S = 1$ and $n = 2$.

Here we must note an important aspect. In (4.2.17) n is always equal to $2S$. This, apparently, is the general case for all real alloys. Below we will illustrate this fact with another important example.

The multiplicity of an impurity is always equal to the effective multiplicity of the scattered electrons. This property results in the total compensation of the impurity magnetic moment at low temperatures, so that the ground state of an impurity in a metal is an orbital and spin singlet [20].

Theoretically it would be interesting to consider a Hamiltonian (4.2.17) with arbitrary n and S .

The case $n < 2S$ will be studied below (Chap. 4.3) using as an example the s-d exchange model with an arbitrary impurity spin ($n = 1$). Just as with $n = 2S$, the strength of the effective interaction grows indefinitely as the energy decreases; however, even at absolute zero the impurity retains its magnetic properties and has an effective magnetic moment $S - n/2$.

The opposite case, when $n > 2S$, is also interesting. According to the view of Nozieres and Blandin [52] and numerical calculations by Cragg, Lloyd, and Nozieres [58], the scaling trajectory has a fixed point at finite value $J^* \sim 1/n$. This means that at low temperatures

all physical quantities are related to the temperature by a power law and the critical exponents can be calculated in the $1/n$ approximation [11, 12]. *

4.2.5b. An n -fold degenerate exchange model. Another important Hamiltonian comes into play when there is either an electron or hole in the d or f shell. The Hund rule does not work any more, whence the exchange operator coincides with (4.2.15) and acts in the subspace with $\sum_{m, \sigma} d_{m\sigma}^\dagger d_{m\sigma} = 1$ or $\sum_{m, \sigma} d_{m\sigma} d_{m\sigma}^\dagger = 1$. In this subspace the operator $d_{m\sigma}^\dagger d_{m'\sigma'}$ is a permutation operator $P_{m\sigma, m'\sigma'}$:

$$P_{m\sigma, m'\sigma'} | m'\sigma' \rangle = | m\sigma \rangle.$$

The exchange Hamiltonian is then [59]

$$\mathcal{H}_{\text{ex}} = \sum_{k, m, \sigma} \varepsilon_k a_{km\sigma}^\dagger a_{km\sigma} + J \sum_{k, k', m, \sigma} a_{km\sigma}^\dagger a_{k'm'\sigma'} P_{m'\sigma', m\sigma}. \quad (4.2.19)$$

In the presence of a strong crystal field the dimension of the space in which \mathbf{P} operates decreases, just as in the previous case. But in the process the exchange amplitude becomes dependent on m in a way such that the impurity interacts with electrons from the multiplet to which the impurity belongs. The scattering amplitude for the electrons of another multiplet is negligible. As in the previous case, the number of operators $a_{m\sigma}^\dagger$ coincides with the number of degrees of freedom of the impurity.

Among the transition impurities only Ni ($n_d = 9$) could be described by the Hamiltonian (4.2.19). But for alloys with Ni, apparently, the condition $v^2\rho (\epsilon_F)/E_\pm \ll 1$ for the formation of a localized moment [4] is not met, and an exchange Hamiltonian cannot be employed.

With rare-earth impurities the situation is just the opposite. Among these a Kondo effect is observed only in alloys with Ce ($n_f = 1$) and Yb ($n_f = 13$), two elements of the lanthanide series. For other elements the inequality (4.2.16) is so strong that the Kondo temperature is very small, so that the impurity is free practically at all temperatures. The level of the f -electron (or hole) in Ce (or Yb) is close to the Fermi surface, $E_- \sim 0.1$ eV, and its energy is much lower than that of spin-orbit coupling or the Coulomb interaction: $LS \sim 0.3$ eV and $E_+ \sim 4$ eV. This enables us to consider transitions only between states whose projection of total angular momentum is $J = l - 1/2 = 5/2$ and an empty shell for Ce or between the state with $J = l + 1/2 = 7/2$ and a completely filled shell for Yb.

* The case where the multiplicity of band electrons is higher than that of the orbital electrons was studied by Fateev and Wiegmann [94] using another model. In this model, which proved to be integrable for an arbitrary S , the interaction Hamiltonian is $\mathcal{H} = (c\sigma^\dagger S_{\sigma\sigma'} c\sigma') \cdot \sigma$. The exact solution for this model corroborates the scaling predicted in [52].

For this reason the hybridization amplitude is diagonal only in the basis of the eigenfunctions of the total angular momentum operator. This is the basis in which one must expand the plane electronic wave [51]. The creation operator $a_{|\mathbf{k}|Jj}^\dagger$ for the partial wave with projection j of total angular momentum \mathbf{J} is linked to the creation operator $a_{|\mathbf{k}|lm\sigma}^\dagger$ for the partial wave with projection m of orbital angular momentum \mathbf{l} and projection of spin equal to $1/2$ by Clebsch-Gordan coefficients:

$$a_{|\mathbf{k}|Jj}^\dagger = (-1)^{l+J-1/2} \sqrt{2J+1} \left\{ \begin{pmatrix} l & (1/2)J \\ j+1/2 & -1/2-j \end{pmatrix} \right. \\ \left. \times a_{kl, j+1/2, -1/2}^\dagger + \begin{pmatrix} l & (1/2)J \\ j-1/2 & 1/2-j \end{pmatrix} a_{kl, j-1/2, 1/2}^\dagger \right\}. \quad (4.2.20)$$

The Anderson Hamiltonian in this basis is

$$\mathcal{H}_A = \mathcal{H}_{\text{atom}} + \sum_{\mathbf{k}} \epsilon_{|\mathbf{k}|} (a_{|\mathbf{k}|J}^\dagger a_{|\mathbf{k}|J} + v_{|\mathbf{k}|} (a_{|\mathbf{k}|J}^\dagger d_J + \text{h.c.})) \quad (4.2.21)$$

(here and in what follows we drop the subscript J).

Next, after the Schrieffer-Wolf transformation we arrive at the Hamiltonian (4.2.19), in which one subscript $j = -J, \dots, J$ is substituted for the pair $m\sigma$:

$$\mathcal{H} = \sum_{j=-J, \mathbf{k}, \mathbf{k}'}^J J_{jj'} a_{|\mathbf{k}|J}^\dagger a_{|\mathbf{k}'|J} P_{jj'} + E_j P_{jj} + \sum_{\mathbf{k}} \epsilon_{|\mathbf{k}|} a_{|\mathbf{k}|J}^\dagger a_{|\mathbf{k}|J}. \quad (4.2.22)$$

Here E_j is the level splitting introduced by the crystal field which as noted in the case of rare-earth impurities is small if compared with spin-orbit coupling. The exchange interaction amplitude in this case is

$$J_{jj'} = v^2 \left(\frac{1}{E_+ + E_j} + \frac{1}{E_- + E_{j'}} \right). \quad (4.2.23)$$

At $E_j = 0$ the Hamiltonian (4.2.22) is invariant under transformations of the $\text{SU}(n)$ group, where $n = 2J + 1$. In these conditions we will speak of an n -fold degenerate model.

The Kondo temperature in such a model depends strongly on the value of n [51]:

$$T_K = \epsilon_F \exp(-1/Jn). \quad (4.2.24)$$

Often even in the presence of a crystal field we can assume that $J_{jj'}$ is isotropic since, as a rule, $E_- \gg \max(E_j - E_{j'})$. Then the last term in (4.2.22) describes the effect of the crystal field.

In alloys with rare-earth impurities the crystal field, which splits the J -multiplet, is commensurable with the possible temperature interval. Whence, as the temperature rises, more and more degrees of freedom may take part in the scattering process. On the other hand,

an increase in J leads, according to (4.2.24), to an increase in T_K , and we may once more have the Kondo effect. The possibility of such a "sequence" of Kondo effects was pointed out by Cornut and Cogblin [60]. Indeed, suppose that the crystal field splits the J -multiplet into n_0, n_1, \dots -multiplets with energies $0, E_1, \dots$. At $T \ll E_1$ the particular alloy is described by the n_0 -fold degenerate model (4.2.22) with a Kondo temperature $T_K(n_0)$ given by (4.2.24). Let us assume that $T_K(n_0) \ll E_1$. Then the system, after reaching the weak-coupling regime at $T \gg T_K(n_0)$, with a further increase in temperature reaches the region where $T \gg E_1$ and is again in the strong-coupling regime; but now its effective multiplicity is $n_0 + n_1$. As a result $T_K(n_0 + n_1)$ may prove to be higher than E_1 . This process repeats as the temperature increases. If $n_1 = 2$, then the traditional s-d exchange model with spin 1/2 (4.1.3) is realized at $T \ll E_1$. The author knows only two such alloys: (La, Ce)B₆ and (La, Ce)Al₂ [61, 62].

4.2.6 Perturbation Theory

Just as in the case of the nondegenerate s-d exchange model (4.1.3), at low energies perturbation-theory series in the strength of the exchange interaction lead to logarithmic singularities. The Kondo temperature is the characteristic that divides the regions of weak and strong coupling. If the physically possible temperature interval is commensurable with the size of the level splitting in the d (or f) shell (since the latter cannot be considered infinite and, therefore, it is impossible to take only the ground state of the atom), there will be other characteristic parameters in the system besides T_K . Practically this is the case only for rare-earth impurities. Now we will assume, although this is not always true, that there is a temperature region between two energy levels of the ion, $E_\alpha \ll T \ll E_{\alpha+1}$, so that inside this region we can ignore all transitions to levels higher than $E_{\alpha+1}$ and assume all levels below E_α degenerate. Then in the system there is only one energy scale, $E_\alpha \ll T_K \ll E_{\alpha+1}$, and scaling can be employed.*

The condition for renormalization implies that as the ultraviolet limit D , equal in this case to ϵ_F , changes accompanied by a respective variation in the coupling constants J_{pq} , physical quantities are multiplied by a constant that is not a function of the energy variable ϵ (external frequency, temperature, or magnetic field). This means that any physical quantity, as a function of, say, temperature, is expressed as

$$Q = Q_0(D, J) \zeta(T/T_K). \quad (4.2.25)$$

* The renormalization-group technique as applied to the Kondo problem is discussed in [11, 12, 17].

If we assume, for simplicity, that there is only one interaction amplitude J in the system, then mathematically the renormalization condition (4.2.25) can be expressed in the following manner.

Suppose that z is a function of J , D , and ε that is invariant under transformations of the renormalization group and chosen by convenience. Then another invariant quantity, $\zeta(\varepsilon/T_K)$, is a function of the invariant charge z :

$$\frac{d \ln \zeta}{d \ln (D/\varepsilon)} = \frac{d \ln Q}{d \ln (D/\varepsilon)} = \varphi(z). \quad (4.2.26)$$

As for z , it can be defined as the solution to

$$\frac{dz}{d \ln (D/\varepsilon)} = \beta(z). \quad (4.2.27)$$

To build a perturbation theory it is expedient to select z in such a way that at $\varepsilon = D$ it coincides with the bare interaction amplitude at $J \ll 1$:

$$z_0 = z(\varepsilon = D) = J + O(J^2). \quad (4.2.28)$$

Then, knowing the terms in the perturbation-theory series for $z(\varepsilon)$ and $Q(\varepsilon)$, we can easily find the expansions of $\beta(z)$ and $\varphi(z)$ in powers of z . Suppose that

$$z(\varepsilon) = J + J^2 + \dots + J^2 \ln(\varepsilon/D) + J^3 \ln^2(\varepsilon/D) + \dots + bJ^3 \ln(\varepsilon/D) + \dots \quad (4.2.29)$$

Then, if we find the derivative of (4.2.29) with respect to $\ln(\varepsilon/D)$ and put $\varepsilon = D$, according to (4.2.28), we have

$$\beta(z) = z - bz^2 + O(z^3). \quad (4.2.30)$$

Equation (4.2.27), which defines the invariant charge z , can be written thus:

$$\varphi(z) = \ln(\varepsilon/T_K), \quad (4.2.31)$$

with

$$\varphi(z) = \int \frac{dz}{\beta(z)} = \frac{1}{z} - b \ln|z| + O(1) \quad (4.2.32)$$

and the Kondo temperature defined as

$$T_K = D \exp\{\varphi(z)\} = \text{const } D \exp(-1/J - J^b(1 + O(j))). \quad (4.2.33)$$

It is understood that the choice of the invariant charge is not unique. More than that, if we do choose z , the functions $\varphi(z)$ and $\beta(z)$ may still change in the process of regularization of the theory at small distances and times and, therefore, are not universal. The pre-exponential dependence of T_K on the constant J is also not univer-

sal. But the simultaneous solution of Eqs. (4.2.26) and (4.2.27) leads to a universal dependence of all physical quantities on the ratios ε/T_K , T/T_K , and H/T_K :

$$Q = Q_0 \exp \int_z^{z(\varepsilon/T_K)} \frac{\varphi(z')}{\beta(z')} dz', \quad (4.2.34)$$

where Q_0 is the value of Q at $\varepsilon = D$.

If for the sake of simplicity we put $O(1) = 0$ in (4.2.32), we will find the function $\varphi(z)$ and the invariant charge z :

$$1/z - b \ln |z| = \ln(\varepsilon/T_K). \quad (4.2.35)$$

(We retained the term $\ln |z|$ in the definition of $\varphi(z)$ so that all physical quantities at $0 < z \ll 1$, i.e. $\varepsilon \gg T_K$, could be expanded in a power series in z .) We note that Eq. (4.2.25) is valid only if the cut-off D can be considered infinite when compared with T_K , while the separation between the atomic levels α and $\alpha + 1$ is infinite as compared with D :

$$E_\alpha \ll T_K, \quad T \ll D \ll E_{\alpha+1}.$$

In what follows we give the results obtained via perturbation theory for the impurity parts of thermodynamic functions in the s-d exchange model discussed in detail in Chaps. 4.2 and 4.3.

The Gell-Mann—Low equation (4.2.35) in this case takes the form

$$\frac{1}{z(x)} - \frac{1}{2} \ln |z| = \ln \left(\frac{x}{T_K} \right) \quad (4.2.36)$$

and does not depend on the impurity spin S .

At $H = 0$ the magnetic susceptibility as a function of temperature $T \gg T_K$ is expressed [11, 12] thus:

$$\chi(T) = (g\mu_B)^2 \frac{S(S+1)}{3T} (1 - z(T/T_K) + O(z^2)), \quad (4.2.37)$$

or, if we do not employ (4.2.35),

$$\chi(T) = (g\mu_B)^2 \frac{S(S+1)}{3T} \left(1 - \frac{1}{\ln(T/T_K)} + \frac{\ln \ln(T/T_K)}{\ln^2(T/T_K)} + \dots \right). \quad (4.2.38)$$

The impurity magnetic moment at $T = 0$ and $H \gg T_K$ is [11]

$$M(H) = S - \frac{S}{2} z(H/T_K) + O(z^2). \quad (4.2.39)$$

Finally, the heat capacity at $H = 0$ and $T \gg T_K$ is [24c]

$$C(T) = S(S+1)\pi^2 z^4 (T/T_K) + \dots \quad (4.2.40)$$

Here we also give the Gell-Mann—Low equations for the Hamiltonians (4.2.17) and (4.2.19). In the first instance

$$\ln(\varepsilon/T_K) = 1/z - n \ln |z|, \quad (4.2.41)$$

while in the second

$$\ln (\varepsilon/T_K) = 1/Mz - \ln |z|. \quad (4.2.42)$$

We note that the perturbation-theory series (4.2.37)-(4.2.40) are asymptotic. Therefore, even a large number of terms can hardly help in studying the low-energy properties of a system (as $z \rightarrow -0$).

In the chapters that follow we will build exact solutions for the s-d exchange model with arbitrary impurity spin (the Hamiltonian (4.2.17) with $n = 1$) and for the n -fold degenerate exchange model (4.2.19). On the basis of these solutions we will establish the general nature of the ground state of the impurity and find the thermodynamic functions at finite temperatures and magnetic field strengths. At present there is no solution for the interesting and widely used problem (4.2.17) for arbitrary n and S .

4.3 BETHE'S METHOD

4.3.1 General Survey. The Factorization Equations

In 1931 Bethe [39] built a solution for an isotropic chain of $1/2$ -spins in the nearest-neighbor interaction. After 30 years this work started to draw attention and at present forms the basis of a broad and rapidly developing field of mathematical physics. In 1963, Lieb and Liniger [63] revived the interest in the Bethe method by building a solution for a one-dimensional system of interacting bosons. An important step in developing this method was taken when the Lieb-Liniger solution was generalized to the case of interacting fermions. Solution of this problem required considerable effort [64, 65] and was first done in 1967 almost simultaneously by Gaudin [66, 67] * and Yang [68]. In the process certain relationships, which proved to be of a general nature, were found for two-particle scattering amplitudes. These are the necessary and sufficient conditions for the Bethe Ansatz to be valid. These conditions are known as factorization equations, or triangle equations [44, 45].** In the general case of a one-dimensional quantum theory of n -color particles these conditions take the form (see also Fig. 4.5)

$$\begin{aligned} S_{a_2 a_2}^{a_1 a_1'}(k_1 k_2) S_{a_3 a_3}^{a_1' a_1''}(k_1 k_3) S_{a_3 a_3}^{a_2' a_2''}(k_2 k_3) \\ = S_{a_3 a_3}^{a_2 a_2'}(k_2 k_3) S_{a_3 a_3}^{a_1 a_1'}(k_1 k_3) S_{a_2 a_2}^{a_1' a_1''}(k_1 k_2), \end{aligned} \quad (4.3.1)$$

* Unfortunately, Gaudin published only the results of his work. In full his study has not been published and exists only in the form of his thesis [67].

** Note that as applied to the problem of interacting fermions the factorization equations first appeared in the work by McGuire [65].

where $|S_{a_2 a'_2}^{a_1 a'_1}(k_1 k_2)|$ is the two-particle S-matrix (Fig. 4.6). The labels $(a_1 a_2)$ and $(a'_1 a'_2)$ stand for the types of particles in the $|in\rangle$ and $|out\rangle$ states with momenta k_1 and k_2 . Any index that appears twice is to be summed over.

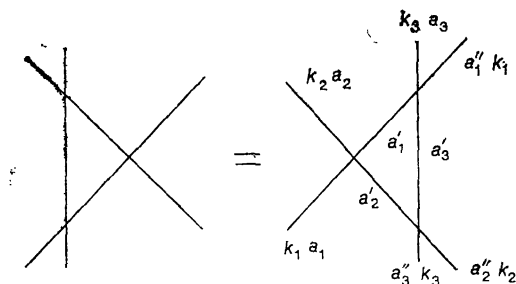


Fig. 4.5. A graphic representation of factorization conditions (the triangle equations).

The factorization conditions mean that the scattering matrix for N particles is two-particle factorized, i.e. is the product of $N(N-1)/2$ scattering matrices of two particles, as if the N -particle

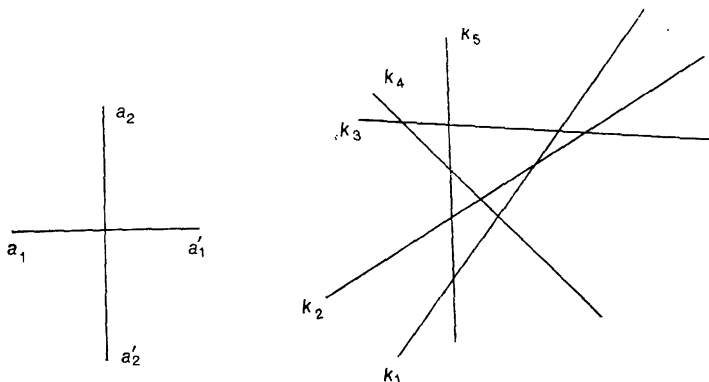


Fig. 4.6. A graphic representation of the two-particle scattering matrix $S_{a_2 a'_2}^{a_1 a'_1}$.

Fig. 4.7. A factorized two-particle S-matrix for five particles.

scattering matrix were a sequence of pair collisions. Take three particles, for example. Obviously, the three-particle scattering matrix can be represented by a product of two-particle scattering matrices in two ways, generally speaking. The right- and left-hand sides of

Eq. (4.3.1) and Fig. 4.5 reflect these two possibilities. If as a result we arrive at the same answer, as required by (4.3.1), the three-particle S-matrix (and, hence, the N -particle scattering matrix, see Fig. 4.7) is two-particle factorized.

The factorization conditions impose very stringent restrictions on the one-dimensional scattering kinematics. Besides requiring that the number of particles be conserved, they require that the energies of individual particles be conserved, too. In other words, if the incoming particles have energies $(\varepsilon_1, \dots, \varepsilon_N)$, after collision the energies of the outgoing particles are also $(\varepsilon_1, \dots, \varepsilon_N)$. Therefore, in theories with a factorized S-matrix the energies are only redistributed, in the collision process, between different colors of the particles. These selection rules are the result of an infinite set of conservation laws, whose existence can be considered necessary for the S-matrix to be factorizable.

To clarify the aforesaid let us consider the case of a system of different one-dimensional particles interacting via a pair delta-like potential. The hyperplanes $x_i = x_j$ separate the configuration space of the system into regions $X_Q = \{x_{q_1} < \dots < x_{q_N}\}_Q$ where the particles move independently and are described by the wave function

$$\Psi(X_Q) = \sum_P \mathcal{A}_{i_1 \dots i_N}(P, Q) \exp\{ik_{p_j} x_j\}. \quad (4.3.2)$$

Here $P = \{p_1, \dots, p_N\}$ and $Q = \{q_1, \dots, q_N\}$ are permutations of integers $\{1, \dots, N\}$, x_j are the coordinates of the particles, and i_1, \dots, i_N their colors; all possible permutations P are summed over, while the factors $\mathcal{A}(P, Q)$ do not depend on coordinates inside X_Q . Conservation of momenta of individual particles in collision requires that the set of momenta $\{k_j\}$ remain the same in a transition from one region to another, i.e. be independent of Q . The wave function (4.3.2) is customarily called the Bethe Ansatz.

To find the coefficients $\mathcal{A}(P, Q)$ we must establish how the wave function changes in the process of crossing the boundaries of the regions; it is on these boundaries that the particles interact. We take two neighboring regions X_Q and $X_{Q\langle ij \rangle}$ differing only in the transposition of x_i and x_j . At the boundary between the two regions only two particles, i and j , collide, whereby continuation of the wave function from region X_Q to region $X_{Q\langle ij \rangle}$ constitutes a two-body problem. The energy and momentum conservation laws in one-dimensional space lead, in this case, to conservation of k_i and k_j separately, so that the set of momenta remains the same and the factors \mathcal{A} are related through the two-particle S-matrix:

$$\mathcal{A}_{\dots kl \dots}(P, Q) = S_{ij}^{ki} \mathcal{A}_{\dots ij \dots}(P, Q_{\langle ij \rangle}). \quad (4.3.3)$$

Knowing the two-particle S-matrix enables us to express all the $\mathcal{A}(P, Q)$ in terms of, say, $\mathcal{A}(P, I)$, with $I = \{1, \dots, N\}$ and obtain the N -particle scattering matrix in the form of a product of $N(N-1)/2$ two-particle scattering matrices (Fig. 4.7).

This situation is possible provided that the wave function in each region X_Q is a linear combination of a finite number of waves. This constitutes the essence of Bethe's hypothesis. For the hypothesis to be self-consistent it is necessary that the different ways of

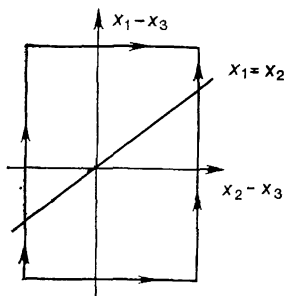


Fig. 4.8. Two ways of going over from region $x_1 < x_2 < x_3$ to region $x_3 < x_2 < x_1$.

combining the transpositions connecting regions X_Q and $X_{Q'}$ into products of transpositions of pairs lead to the same result when the wave function is continued from one region to the other. It suffices to verify the hypothesis for three particles. Namely, suppose that as a result of collision the particles from region $(x_1 < x_2 < x_3)$ go over to region $(x_3 < x_2 < x_1)$. Pair collisions may occur in two different ways (Fig. 4.8):

$$x_1 < x_2 < x_3 \rightarrow x_1 < x_3 < x_2 \rightarrow x_3 < x_1 < x_2 \rightarrow x_3 < x_2 < x_1 \quad (4.3.4)$$

and

$$\begin{aligned} x_1 < x_2 < x_3 &\rightarrow x_2 < x_1 < x_3 \rightarrow x_2 < x_3 < x_1 \\ &\rightarrow x_3 < x_2 < x_1. \end{aligned} \quad (4.3.5)$$

The fact these two paths are equivalent expresses the factorization condition (4.3.1).

We can consider (4.3.1) as functional equations for $S(k_1, k_2)$, whose solution combined with the unitarity condition

$$\{S_{a_2 a_2}^{a_1 a_1'}(k_1, k_2) S_{a_2 a_2}^{a_1' a_1''}(k_2, k_1) = \delta^{a_1 a_1''} \delta_{a_2 a_2''}\}$$

leads to systems of equations that are fully integrable (see [44, 45]). Writing (4.3.1) in components, we can easily see that the number of

equations considerably exceeds the number of unknowns. Nevertheless, at present there are many nontrivial solutions to the factorization equations corresponding to rich models of one-dimensional quantum field theory and two-dimensional classical statistics (for a review see, e.g., [69]).

All known cases of integrable systems possess the property that we can express the particle momentum in terms of a parameter α such that the two-particle scattering amplitude depends only on the difference arguments:

$$S(k_1, k_2) \rightarrow S(\alpha_1 - \alpha_2). \quad (4.3.6)$$

The variable α is called rapidity.

The parameters k_j in the scattering wave function (4.3.2) are arbitrary. To find the eigenvalue spectrum we must first introduce certain boundary conditions for the system. As usual, the specific type of boundary conditions is not important in the case of a large number of particles. The most convenient way to introduce them is to place the system in a box of length L and impose the conditions of periodicity:

$$\Psi(x_1, \dots, x_N)|_{x_j=L/2} = \Psi(x_1, \dots, x_N)|_{x_j=-L/2}$$

$$\text{with } j = 1, \dots, N. \quad (4.3.7)$$

These conditions lead to a relationship between $\mathcal{A}(Q, P)$ and $\mathcal{A}(I, P)$:

$$e^{ik_j L} \mathcal{A} = \mathbf{T}_j \mathcal{A}, \quad (4.3.8)$$

where

$$\mathbf{T}_j = S_{jj+1} \dots S_{jN} S_{j1} \dots S_{jj-1} \quad (4.3.9)$$

and S_{jh} stands for the matrix-operator $S_{p_j p_h}(\alpha_j - \alpha_h)$.

Equations (4.3.8) imply that \mathcal{A} is an eigenvector of N operators simultaneously. However, using the factorization equations, we can show that the operators \mathbf{T}_j commute with each other and can be diagonalized simultaneously [68]. The diagonalization problem for the \mathbf{T}_j was first solved by Yang [68] for one-dimensional fermions interacting via a pair delta-like potential. The solution required using the Bethe hypothesis a second time.

In a series of papers Baxter [43, 70, 71] built a solution for an eight-vertex model of classical statistics. He developed a method which served as a basis for a modern formulation of Bethe's method in a new way. Baxter's method enabled him to approach the diagonalization problem for the \mathbf{T}_j in a new way.*

* For the relation between fully integrable one-dimensional quantum systems, the factorized scattering theory, and the two-dimensional lattice statistical systems see the review paper [45].

Baxter [43, 70] demonstrated that the operators

$$\mathbf{T}_{j_1 \dots j_N}^{i_1 \dots i_N}(\alpha; \alpha_1, \dots, \alpha_N) = \sum_{\substack{p_1=p_{N+1} \\ \{p_k\}}} \prod_{k=1}^N S_{p_k p_{k+1}}^{i_k j_k}(\alpha - \alpha_k) \quad (4.3.10)$$

form a parametric family of commuting operators:

$$[\mathbf{T}(\alpha), \mathbf{T}(\alpha')] = 0. \quad (4.3.11)$$

The above important relation is a direct consequence of the triangle condition (4.3.1) [45, 46, 70]. To verify this we consider the

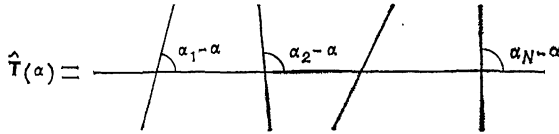


Fig. 4.9. A graphic representation of the operator $\mathbf{T}(\alpha; \alpha_1, \dots, \alpha_N)$.

matrix-operator in indices (p, q) (Fig. 4.9):

$$\begin{aligned} \hat{\mathbf{T}} &\equiv \mathbf{T}_q^p \{j_N\}(\alpha; \alpha_1, \dots, \alpha_N) \\ &= \sum_{\{p_k\}} S_{p p_1}^{i_1 j_1}(\alpha - \alpha_1) S_{p_2 p_3}^{i_2 j_2}(\alpha - \alpha_2) \dots S_{p_N q}^{i_N j_N}(\alpha - \alpha_N). \end{aligned} \quad (4.3.12)$$

Let us consider the product $\mathbf{S}(\alpha - \alpha') \hat{\mathbf{T}}(\alpha') \hat{\mathbf{T}}(\alpha)$ depicted on

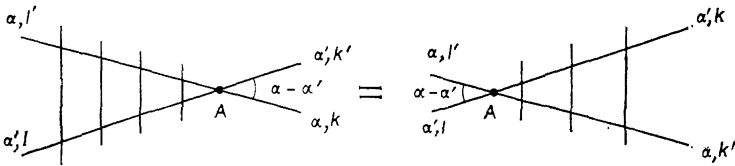


Fig. 4.10. Commutation relations for $\hat{\mathbf{T}}(\alpha)$ and $\hat{\mathbf{T}}(\alpha')$.

the left-hand side of Fig. 4.10. Using (4.3.1) and Fig. 4.5, we successively take the "tie" across point A. Hence, we have

$$S_{q'k'}^{qk}(\alpha - \alpha') \mathbf{T}_q^l(\alpha') \mathbf{T}_{q'}^{l'}(\alpha) = \mathbf{T}_{k'}^{q'}(\alpha) \mathbf{T}_k^q(\alpha') S_{l'q'}^{lq}(\alpha - \alpha').$$

Multiplying (4.3.13) into \mathbf{S}^{-1} and taking the trace of the two $\hat{\mathbf{T}}$ operators, we arrive at (4.3.11). Equations (4.3.11) and (4.3.13) play a central role in diagonalizing the matrix \mathbf{T} .

The operators \mathbf{T}_j in (4.3.9), which emerge as a result of imposing the boundary conditions (4.3.7) in Bethe's method, and the $\mathbf{T}(\alpha;$

$\alpha_1, \dots, \alpha_N$) matrix are related. To establish this relation we note that from the triangle condition (4.3.1) it follows that at $k_1 = k_2$, or $\alpha_1 = \alpha_2$, the two-particle scattering matrix, or the vertex-weight matrix, is proportional to the permutation operator. Indeed, if we put $\alpha = 0$ in (4.3.1), we have

$$S_{12}(0) M(\alpha') = M(\alpha') S_{12}(0), \quad (4.3.14)$$

with

$$M = S_{13}(\alpha') S_{23}(\alpha'). \quad (4.3.15)$$

This yields, to within a factor,

$$S_{\beta\beta'}^{\gamma\gamma'}(k, k) \equiv S(0) = P = \delta_{\beta}^{\gamma} \delta_{\beta'}^{\gamma'}. \quad (4.3.16)$$

Let us now turn to the operator (4.3.10). Assuming that $\alpha = \alpha_j$ and bearing in mind that $k_j = f(\alpha_j)$, we have [72]

$$\begin{aligned} & \mathbf{T}_{\{i_k'\}}^{\{i_k\}}(\alpha_j; \alpha_1, \dots, \alpha_j, \dots, \alpha_N) \\ &= \sum_{\{p_m\}} \prod_{k=1}^{j-1} S_{p_k p_{k+1}}^{i_k i_{k+1}'}(\alpha_j - \alpha_k) \delta_{p_j}^{i_j'} \delta_{p_{j+1}}^{i_{j+1}'} \\ & \times \prod_{l=j+1}^N S_{p_l p_{l+1}}^{i_l i_{l+1}'}(\alpha_j - \alpha_l) = \mathbf{T}_j. \end{aligned} \quad (4.3.17)$$

This implies, for one, that the \mathbf{T}_j commute and the eigenvalue problem for (4.3.6) has a solution.

Recently it was established that there is a profound relation between Bethe's method and the method of the inverse problem in scattering theory, the latter being used for solving some nonlinear classical equations. The remarkable method of the quantum inverse scattering problem developed in a number of works (e.g. see [46-48, 73-75]), enabled finding all the formulas of Bethe's method within a unique algebraic scheme (for an overall review see [48, 49, 76, 77]). In particular, the diagonalization of $\mathbf{T}(\alpha_j; \alpha_1, \dots, \alpha_N)$ is achieved by this method in a simple and graphic way.

4.3.2 An Effective Hamiltonian

As we saw in Sec. 4.2.2., the problem of scattering by a single impurity is, in essence, one-dimensional. Here we will show this once more by starting directly from the s-d exchange model (4.1.3).

We expand the plane electronic wave in spherical waves at the impurity:

$$a_{\mathbf{k}\sigma}^\dagger = \sum_{l, m} Y_l^m \left(\frac{\mathbf{k}}{|\mathbf{k}|} \right) a_{|\mathbf{k}| m l \sigma}^\dagger. \quad (4.3.18)$$

Writing the Hamiltonian (4.1.3) in terms of $a_{|\mathbf{k}|m\sigma}^\dagger$, we have

$$\begin{aligned} \mathcal{H}_{s-d} = & \sum_{l,m} \sum_{|\mathbf{k}|} \epsilon(|\mathbf{k}|) a_{|\mathbf{k}|lm\sigma}^\dagger a_{|\mathbf{k}|lm\sigma} \\ & + J \sum_{|\mathbf{k}|, |\mathbf{k}'|} S a_{|\mathbf{k}|00\sigma}^\dagger a_{|\mathbf{k}'|00\sigma} \sigma_{\sigma\sigma'}; \end{aligned} \quad (4.3.19)$$

whence only the s wave interacts with the impurity.

Next, we assume that the interaction amplitude is small, so that $T_K \ll \epsilon_F$. Whence, at $H, T \ll \epsilon_F$ we can ignore the electronic states that lie far from the Fermi surface and consider a linear section of the spectrum near $|\mathbf{k}| = k_F$:

$$\epsilon(|\mathbf{k}|) = \epsilon_F + v_F(|\mathbf{k}| - k_F). \quad (4.3.20)$$

In what follows we take v_F equal to unity. Reckoning momentum from k_F , we arrive at an effective Hamiltonian for the s-d model*

$$\mathcal{H}_{s-d} = \sum_p p c_{p\sigma}^\dagger c_{p\sigma} + J \sum_{p, p', \sigma, \sigma'} S c_{p\sigma}^\dagger \sigma_{\sigma\sigma'} c_{p'\sigma'}. \quad (4.3.21)$$

Here $c_{p\sigma}^\dagger$ and $c_{p\sigma}$ are the creation and annihilation operators for an electron in an s state with momentum $k_F + |\mathbf{p}|$.

The condition that (4.3.1) be integrable poses stringent restrictions on the two-particle scattering amplitudes and, therefore, on the Hamiltonian. For this reason even small variations in the Hamiltonian at small distances, which practically do not change the properties of the system, almost always destroy the integrability. Below we will show that the Hamiltonian (4.3.21) is completely integrable.

4.3.3 The Bethe Ansatz for the s-d Exchange Model

Here we formulate and prove Bethe's hypothesis for the s-d exchange model. First we shift the Hamiltonian (4.3.21) to the coordinate representation. Suppose that x is a coordinate on a straight line passing through the impurity and

$$c_\sigma(x) = \int e^{ipx} c_\sigma(p) \frac{dp}{2\pi}.$$

Then the Hamiltonian (4.3.21) for the s-d model is

$$\mathcal{H}_{s-d} = \int dx \left(-i c_\sigma^\dagger(x) \frac{d}{dx} c_\sigma(x) + J \delta(x) S c_\sigma(x) \sigma_{\sigma\sigma'} c_{\sigma'}(x) \right). \quad (4.3.22)$$

We consider the eigenstate of (4.3.21) in which there are N electrons with spin components $\{\sigma_1, \dots, \sigma_N\}$ and a localized moment

* The emerging problem could be called one-half-dimensional, since the particles have only one Fermi point instead of two as is customary.

with component $s = -S, \dots, +S$:

$$|\Psi\rangle = \int \Psi_{\sigma_1 \dots \sigma_N; s}(x_1, \dots, x_N) c_{\sigma_1}^+(x_1) \dots c_{\sigma_N}^+(x_N) \\ \times (S^+)_{dx_1 \dots dx_N}^{s+S} |0\rangle \quad (4.3.23)$$

where $|0\rangle$ is the state without particles and with a component of the impurity moment equal to $-S$.

The wave function $\Psi_{\sigma_1 \dots \sigma_N; s}$ satisfies Schrödinger's equation

$$\left(-i \sum_{j=1}^N \frac{\partial}{\partial x_j} - E \right) \Psi_{\sigma_1 \dots \sigma_N; s}(x_1, \dots, x_N) \\ + J \sum_{j=1}^N \delta(x_j) S_{ss'} \sigma_j \sigma_j' \Psi_{\sigma_1 \dots \sigma_j' \dots \sigma_N; s'}(x_1, \dots, x_j, \dots, x_N) = 0. \quad (4.3.24)$$

Bethe's method provides the means for finding every solution of this equation for an arbitrary number of particles.

Suppose that $Q = \{q_0, \dots, q_N\}$ is a permutation of the numbers $\{0, 1, \dots, N\}$ while $Q' = \{q'_1, \dots, q'_N\}$ and $P = \{p_1, \dots, p_N\}$ are permutations of the numbers $\{1, \dots, N\}$ with Q' coinciding with Q from which $q_i = 0$ is excluded. Then in the region $X_Q = \{x_{q_0} < \dots < x_{q_N}\}$ the wave function is

The Bethe Ansatz:

$$\Psi_{\sigma_1 \dots \sigma_N; s}(x_1, \dots, x_N) \\ = \sum_P \mathcal{A}_{\sigma_1 \dots \sigma_N; s}(Q, Q'; P) \exp\left(i \sum_{j=1}^N k_{p_j} x_j\right). \quad (4.3.25)$$

Here the first sum is over all permutations P , $\{k_j\}$ is a sequence of different values of k_j , and $x_0 = 0$. The state (4.3.23) is the eigenstate of the Hamiltonian (4.3.22) with the energy

$$E = \sum_{j=1}^N k_j. \quad (4.3.26)$$

The factors $\mathcal{A}_{\sigma_1 \dots \sigma_N; s}$ are, obviously, not fully independent. First we must require that Ψ be antisymmetric under permutations in the pairs (x_i, σ_i) . As a result

$$\mathcal{A}_{\sigma_1 \dots \sigma_N; s}(Q; Q'; P) = \mathcal{A}_{\sigma_1' \dots \sigma_N'; s}(Q; Q' \cdot P) (-1)^P, \quad (4.3.27)$$

where $Q' \cdot P$ is the product of permutations, and the factor $(-1)^P$ determines whether permutation P is even or odd.

The factors \mathcal{A} for different regions are linked through the Schrödinger equation (4.3.24). As mentioned above, the hypothesis that the wave function consists of a finite number of waves implies that the S-matrix is two-particle factorized. In other words, the interrelation between the \mathcal{A} 's in two neighboring regions is determined by the characteristics of only two particles or a particle and an impurity on the boundary. Suppose that the boundary between regions X_Q and $X_{\bar{Q}}$ is the plane $x_j = 0$, i.e. Q and \bar{Q} differ in a permutation of the j th particle and impurity. Then

$$\mathcal{A} \dots \sigma'_j \dots; s' (\bar{Q}) = R_{\sigma'_j s'}^{\sigma_j s} \mathcal{A} \dots \sigma_j \dots; s (Q), \quad (4.3.28)$$

where the matrix

$$R_{\sigma'_j s'}^{\sigma_j s} \equiv R_{j0} = \exp(iJ\sigma_j \cdot S), \quad (4.3.29)$$

Indeed, let us take the case of one particle scattered by an impurity. Then

$$-i \frac{d}{dx} \Psi_{\sigma; s}(x) + J\delta(x) \sigma \cdot S \Psi_{\sigma'; s'} = E \Psi_{\sigma; s}. \quad (4.3.30)$$

This equation is poorly defined. To redefine it, for the delta-function in (4.3.29) we substitute a smooth potential $V_\varepsilon(x)$ such that $\lim_{\varepsilon \rightarrow 0} V_\varepsilon(x) = J\delta(x)$. Then the solution to Eq. (4.3.30) has the form

$$\Psi_{\sigma; s}(x) = e^{ikx} \mathcal{A}_{\sigma; s}(x), \quad (4.3.31)$$

where the dependence of matrix \mathcal{A} on coordinate x is determined thus:

$$\mathcal{A}(x) = \exp\left(i\sigma \cdot S \int_x^0 V_\varepsilon(x') dx'\right) \mathcal{A}(y), \quad (4.3.32)$$

Sending ε to zero, we find that

$$\mathcal{A}_{\sigma', s'}(x < 0) = R_{\sigma s}^{\sigma' s'} \mathcal{A}_{\sigma; s}(x > 0), \quad (4.3.33)$$

where matrix R is given by (4.3.29).

Now let us assume that plane $x_i = x_j$ is the boundary between X_Q and $X_{\bar{Q}}$. In this case the factors $\mathcal{A}(Q)$ and $\mathcal{A}(\bar{Q})$ are connected via the permutation operator:

$$\mathcal{A} \dots \sigma_i \dots \sigma_j \dots (\bar{Q}) = P_{\sigma'_i \sigma'_j}^{\sigma_i \sigma_j} \mathcal{A} \dots \sigma'_i \dots \sigma'_j \dots (Q) = \mathcal{A} \dots \sigma_j \dots \sigma_i (Q), \quad (4.3.34)$$

where

$$P_{\sigma'_i \sigma'_j}^{\sigma_i \sigma_j} = 2 \left(\frac{1}{2} \cdot \frac{1}{2} + \sigma_{\sigma_i \sigma_j} \cdot \sigma_{\sigma'_i \sigma'_j} \right) = \delta_{\sigma_i \sigma'_j} \delta_{\sigma_j \sigma'_i}$$

is the permutation operator. This fact requires some explaining.

Let us take two particles far from the impurity, say $x_1, x_2 < 0$. The particles are free:

$$-i(\delta_1 + \delta_2)\psi = E\psi. \quad (4.3.35)$$

The usual solution to this equation, which provides the first perturbation-theory approximation, is

$$\psi_{\sigma_1\sigma_2} = \exp(ip_1x_1 + ip_2x_2) \mathcal{A}_{\sigma_1\sigma_2} - \exp(ip_2x_1 + ip_1x_2) \mathcal{A}_{\sigma_2\sigma_1}, \quad (4.3.36)$$

where the factors $\mathcal{A}_{\sigma_1\sigma_2}$ do not depend on the positions of the particles. What will happen with the wave (4.3.36) after the particles scatter by the impurity? We can readily see that in the region $x_1, x_2 > 0$ the wave function is not given by (4.3.36). Indeed, in transferring from the region $x_1, x_2 < 0$ first to region $x_1 < 0 < x_2$ and then to region $0 < x_1, x_2$ the factor $\mathcal{A}_{\sigma_1\sigma_2}$, according to (4.3.33), becomes $\mathbf{R}_{10}\mathbf{R}_{20}\mathcal{A}$ (see Fig. 4.7). Another sequence of events (say, the first particle is scattered by the impurity and then the second) leads to quite a different state. Suppose that the electrons, the first having spin "up" and the second spin "down", are scattered with spin flip by the impurity, which has spin "up". The first electron cannot change the direction of impurity spin, but the second flips this spin over. But if the sequence is reverse, then the impurity spin flips twice and its direction as a result does not change. In other words, matrices \mathbf{R}_{10} and \mathbf{R}_{20} do not commute:

$$\mathbf{R}_{10}\mathbf{R}_{20} \neq \mathbf{R}_{20}\mathbf{R}_{10}. \quad (4.3.37)$$

These arguments vividly demonstrate that particles cannot be considered individually in the presence of an impurity. The fact that the impurity has a degree of freedom is sufficient for the problem to become a many-body problem.

To build the scattering wave function in the region $x_1, x_2 > 0$, we note once more the peculiar feature of the Hamiltonian (4.3.22). All particles move in one direction with the same speed. Therefore, if $\psi(x_1, x_2)$ is a solution to Eq. (4.3.35), then $\psi(x_1, x_2)f(x_1 - x_2)$ is also a solution (here $f(x)$ is an arbitrary function that may have, for example, a discontinuity at $x_1 = x_2$). This property enables easily finding the wave function in the region $x_1, x_2 > 0$. The wave function is again given by (4.3.36), but the factors have a discontinuity on the line $x_1 = x_2$:

$$\begin{aligned} \psi(x_1, x_2) &= [\mathbf{R}_{20}\mathbf{R}_{10}\theta(x_1 - x_2) + \mathbf{R}_{10}\mathbf{R}_{20}\theta(x_2 - x_1)] \\ &\times (e^{ik_1x_2 + ik_2x_1} - \mathbf{P}_{12}e^{ik_1x_1 + ik_2x_2}) \mathcal{A}. \end{aligned} \quad (4.3.38)$$

Obviously, in this case the discontinuity in the wave function at $x_1 = x_2$ does not mean there is interaction far from the impurity. However, the scattering wave function does depend on the order of events in the scattering of particles, and the "memory" of this does not decrease as the particles move away from the impurity.

The line of attack we have just studied is not very well suited for building a wave function of a system of N particles that satisfies the given boundary conditions. The correct way to do this is to "order" the spins of the incoming particles in the region $x_1, x_2 < 0$, so that the impurity "knows" which particle it will encounter first. This is another solution to Schrödinger's equation (4.3.35) with a linear spectrum:

$$\psi(x_1, x_2) = (e^{ik_1x_1 + ik_2x_2} - e^{ik_1x_2 + ik_2x_1}) [\theta(x_1 - x_2) + P_{12}\theta(x_2 - x_1)] \mathcal{A}. \quad (4.3.39)$$

Unlike solution (4.3.36), this function changes when both the spins of the particles and their momenta k_1 and k_2 are interchanged and corresponds to the particles being "ordered" on the straight line that passes through the impurity. Strictly speaking, k_1 and k_2 are not the momenta of free particles. Indeed, $\psi_{\sigma_1\sigma_2}(x_1, x_2)$ is not an eigenfunction of the operators $i(\partial/\partial x_1)$ and $i(\partial/\partial x_2)$ separately. Rather, k_1 and k_2 are the momenta of charge density waves, whose generation does not lead to a local change in spin. They resemble momenta of spinless fermions: the wave function (4.3.39) vanishes at $k_1 = k_2$ irrespective of the total spin of the system. We see, therefore, that free particles with a linear spectrum are described equally well by functions (4.3.36) and (4.3.39). The first function has corresponding to it a unit scattering matrix: $S_{\sigma_2\sigma_2'}^{\sigma_1\sigma_1'} = \delta_{\sigma_1\sigma_1'}\delta_{\sigma_2\sigma_2'}$, while the second corresponds to an S-matrix that is the permutation operator:

$$S_{\sigma_2\sigma_2'}^{\sigma_1\sigma_1'} = P_{\sigma_2\sigma_2'}^{\sigma_1\sigma_1'}. \quad (4.3.40)$$

We return to the case of two particles scattered by an impurity. As usual, there are two ways in which we can go from the region $x_1 < x_2 < 0$ to, say, the region $x_1 > x_2 > 0$ (see Fig. 4.8 with $x_3 = 0$). The first path, i.e.

$$x_1 < x_2 < 0 \rightarrow x_1 < 0 < x_2 \rightarrow 0 < x_1 < x_2 \rightarrow 0 < x_2 < x_1,$$

transforms \mathcal{A} into $P_{12}R_{10}R_{20}\mathcal{A}$. The other path, namely

$$x_1 < x_2 < 0 \rightarrow x_2 < x_1 < 0 \rightarrow x_2 < 0 < x_1 \rightarrow 0 < x_2 < x_1,$$

brings us to another transformation matrix:

$$\mathcal{A} \rightarrow R_{20}R_{10}P_{12}\mathcal{A}.$$

But now the result in both cases must be the same, since*

$$R_{10}R_{20}P_{12} = P_{12}R_{20}R_{10}. \quad (4.3.41)$$

* We note that since the scattering matrices do not depend on the particle velocities, the factorization condition (4.3.40) is always met, irrespective of the form of matrix R (compare with (4.3.16)).

We have, therefore, proved Bethe's hypothesis. The general solution to Schrödinger's equation (4.3.24) is given by (4.3.25) together with conditions (4.3.27), (4.3.28), and (4.3.34) [30-32].

Applying these conditions, we can express $\mathcal{A}(Q; Q'; P)$ in terms of $\mathcal{A}(I; I'; P)$, with $I = \{1, \dots, N\}$ a unit permutation. To this end we must take Q as one of the possible products of pair transpositions and to each cofactor assign either operator P_{ij} or operator R_{j_0} , depending on whether this transposition changes the position of particles i and j or of particle j and the impurity. Condition (4.3.41) together with the unitarity conditions

$$P_{ij}P_{ji} = 1 \text{ and } R_{j_0}R_{j_0} = 1 \quad (4.3.42)$$

guarantee that all ways of factoring Q into products of pair transpositions lead to the same results.

4.3.4 Periodic Boundary Conditions

Let us place our system inside a sphere of radius $L/2$ centered at the impurity site and require that the Ψ -function satisfy the periodic boundary conditions (4.3.5). If $\Omega_0 = \mathcal{A}_{\sigma_1 \dots \sigma_N; s}(I; I')$, the periodicity conditions bring us to the problem of simultaneously diagonalizing the operators

$$\mathbf{T}_j = P_{jj+1}P_{jj+2} \dots P_{jN}R_{j_0}P_{j1} \dots P_{jj-1}; \quad (4.3.43)$$

namely,

$$e^{ikh_j L} \Omega_0 = \mathbf{T}_j \Omega_0. \quad (4.3.44)$$

We readily see that here the \mathbf{T}_j not only commute but are equal:

$$\mathbf{T}_{j_{\sigma_1} \dots \sigma_N; s}^{\sigma'_1 \dots \sigma'_N; s'} = \delta_{\sigma'_1 \sigma_1} \delta_{\sigma'_2 \sigma_2} \dots \delta_{\sigma'_{N-1} \sigma_{N-1}} R_{\sigma_{N-1} \sigma_N}^{\sigma'_N s'}. \quad (4.3.45)$$

This does not, however, make the problem of diagonalization simpler. For this reason we will follow the general scheme discussed in Sec. 4.3.1. Namely, we start by building a parametric set of commuting operators $\mathbf{T}(\alpha)$, the \mathbf{T}_j being members of this set. Next, employing the commutation relations (4.3.13), we solve the eigenvalue problem for $\mathbf{T}(\alpha)$.

4.3.5 The Set of Commuting Operators

To build a set of commuting operators that includes the \mathbf{T}_j , it suffices to solve the factorization equations (4.3.1), which describe the scattering of two particles by an impurity, and add the condition that for an $\alpha = \alpha_0$ the matrix $\mathbf{S}(\alpha_0)$ coincides with \mathbf{R} . Then, according to (4.3.16), the two-particle scattering matrices (4.3.29) and (4.3.34) will lie on the curve $\mathbf{S}(\alpha)$.

For an arbitrary impurity spin the factorization equations include matrices of different rank. For this reason it is expedient to separate the matrices that refer only to the particles $r(\alpha)_{\sigma_1\sigma'_1}^{\sigma_2\sigma'_2}$ ($\sigma = 1, 2$) (the solid line in Fig. 4.11), from those that refer to a particle and impurity, $R_{ss'}^{\sigma_1\sigma'_1}$ ($s = -S, \dots, +S$) (the dashed line in Fig. 4.11). Equations (4.3.1) in these notations are

$$r_{ij}(\alpha) R_{i0}(\alpha + \alpha') R_{j0}(\alpha') = [R_{j0}(\alpha') R_{i0}(\alpha + \alpha') r_{ij}(\alpha)] \quad (4.3.46)$$

with the condition that

$$r_{ij}(0) = P_{ij}, \quad R_{ij}(\alpha_0) = \exp(iJ\sigma \cdot S). \quad (4.3.47)$$

For the case of $S = 1/2$, Eqs. (4.3.46) were cited by Yang [68]. In the general anisotropic case they were solved by Baxter [70]

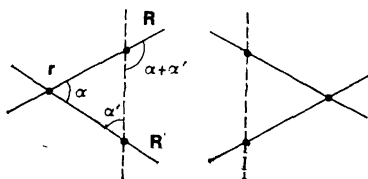


Fig. 4.11. The factorization condition for the s-d exchange model. The dashed line corresponds to the impurity and solid lines to electrons.

(see also [78]). Below we will show that their solution does not depend on the magnitude of S [33, 69]. The most general case, which includes various representations of the $O(3)$ group, is studied in [79].

First, we write $R(\alpha_0)$ in the form

$$\exp(iJ\sigma \cdot S) = w_0 + 4w\sigma \cdot S, \quad (4.3.48)$$

where w_0 and w are functions of J (we recall that $\sigma^2 = 3/4$). The simplest way to find these functions is as follows. The total spin $\sigma + S$ can assume the values $S \pm 1/2$, and either $\sigma \cdot S = S/2$ or $\sigma \cdot S = -(S + 1)/2$. Therefore,

$$e^{iJS/2} = w_0 + wS, \quad e^{-iJ(S+1)/2} = w_0 - w(S + 1). \quad (4.3.49)$$

Now we turn to Eqs. (4.3.46) and (4.3.47). In view of the fact that conditions (4.3.47) are invariant under the transformations of the $O(3)$ group, the matrices r and R must be sought for in the form

$$\begin{aligned} R_{ss'}^{\sigma\sigma'}(\alpha) &= w_0(\alpha) \delta_{\sigma\sigma'} \delta_{ss'} + 4w(\alpha) \sigma_{\sigma\sigma'} \cdot S_{ss'}, \\ r_{\mu\mu'}^{\sigma\sigma'}(\alpha) &= w'_0(\alpha) \delta_{\sigma\sigma'} \delta_{\mu\mu'} + 4w'(\alpha) \sigma_{\sigma\sigma'} \cdot \sigma_{\mu\mu'}. \end{aligned} \quad (4.3.50)$$

It is expedient to introduce the following notations:

$$a = w_0 + w, \quad b = w_0 - w, \quad c = 2w. \quad (4.3.51)$$

Substituting (4.3.48) into Eq. (4.3.46), we find that

$$h(\alpha) \equiv \frac{b(\alpha)}{c(\alpha)} = \frac{b'(\alpha)}{c'(\alpha)} \quad (4.3.52)$$

and

$$b(\alpha)c(\alpha + \alpha')c'(\alpha') + c(\alpha)c(\alpha + \alpha')b'(\alpha') \\ = c(\alpha)b'(\alpha + \alpha')c'(\alpha'). \quad (4.3.53)$$

In terms of $h(\alpha)$ the above equation assumes the form

$$h(\alpha) + h(\alpha') = h(\alpha + \alpha'). \quad (4.3.54)$$

Whence, without loss of generality, we can assume that

$$h(\alpha) = \alpha. \quad (4.3.55)$$

Equations (4.3.52) and (4.3.54) define $b(\alpha)$ and $c(\alpha)$ to within an arbitrary factor. Conditions (4.3.49) determine the value of this factor at points $\alpha = 0$ and $\alpha = \alpha_0$. In all other respects the factor is arbitrary. It is convenient to select it in such a way that the unitarity condition (4.3.42) be valid for any α :

$$b'(\alpha) = b(\alpha) = \frac{\alpha}{\alpha + i} a(\alpha), \\ c'(\alpha) = c(\alpha) = \frac{i}{\alpha + i} a(\alpha), \quad (4.3.56)$$

and

$$a(\alpha)a(-\alpha) = 1.$$

Here $\alpha_0 = 1/g$, where

$$g = \tan \frac{J}{4} (2S + 1) \quad (4.3.57)$$

and

$$a(0) = 1, \quad a(\alpha_0) = \frac{2e^{iJS/2} - e^{-iJ/4} (2S - 1) \sin J(2S + 1)/4}{2S + 1}.$$

The characteristic feature of the factorized matrices (4.3.50) and (4.3.56) is that the functions w and w_0 do not depend on the impurity spin S . This is because Eqs. (4.3.46) are bilinear in the impurity spin operator S and contain only commutators of the type $[S^a, S^b] = i\varepsilon_{abc}S^c$, whose form does not depend on the group representation.

Knowing the solution to the factorization equations, we can, in accord with Sec. 4.3.1, build a set of commuting operators

$$\mathbf{T}(\alpha; \alpha_1, \dots, \alpha_{N+1}) = \text{Sp } \hat{\mathbf{T}}(\alpha; \alpha_1, \dots, \alpha_N), \quad (4.3.58)$$

where

$$\hat{\mathbf{T}}(\alpha; \alpha_1, \dots, \alpha_N) = \mathbf{r}_{*1}(\alpha - \alpha_1) \mathbf{r}_{*2}(\alpha - \alpha_2) \dots \mathbf{r}_{*N}(\alpha - \alpha_N) \mathbf{R}_{*0}(\alpha - \alpha_0). \quad (4.3.59)$$

Formula (4.3.59) means that we must form the product of matrix-operators (Fig. 4.12)

$$\mathbf{r}_{*0}(\alpha) = \begin{pmatrix} w'_0(\alpha) + 2w'(\alpha) \sigma_n^z & 2w'(\alpha) \sigma_n^- \\ 2w'(\alpha) \sigma_n^+ & w'_0(\alpha) - 2w'(\alpha) \sigma_n^z \end{pmatrix} \quad (4.3.60)$$

$$\mathbf{R}_{*0}(\alpha) = \begin{pmatrix} w_0(\alpha) + 2S_z w(\alpha) & 2w(\alpha) S^- \\ 2w(\alpha) S^+ & w_0(\alpha) - 2S_z w(\alpha) \end{pmatrix}. \quad (4.3.61)$$

In Sec. 4.3.1 we showed that the operators $\mathbf{T}(\alpha; \alpha_1, \dots, \alpha_N)$



Fig. 4.12. The operator $\hat{\mathbf{T}}$ for the s-d exchange model. The dashed line corresponds to the impurity and solid lines to fermions.

commute for arbitrary α and α' and, according to (4.3.21),

$$\mathbf{T}_j = \mathbf{T}(\alpha; \alpha_1, \dots, \alpha_N, \alpha_{N+1}) |_{\alpha=\alpha_j, \alpha_1=\dots=\alpha_{N+1}=0}, \quad (4.3.62)$$

where \mathbf{T}_j are the operators that enter the periodic boundary conditions (4.3.43).

4.3.6 Diagonalizing $\mathbf{T}(\alpha)$

The best way to diagonalize $\mathbf{T}(\alpha)$ is to employ the method developed in [46-48, 73, 74], the quantum method of the inverse scattering problem. We show below how to apply this method to operator (4.3.58).

The method is based on the consistent use of commutation relations (4.3.13), which in our case take the form

$$r_{kk'}^{qq'}(\alpha - \alpha') \mathbf{T}_q^l(\alpha') \mathbf{T}_{q'}^{l'}(\alpha) = \mathbf{T}_{k'}^{q'}(\alpha) \mathbf{T}_k^q(\alpha') r_{qq'}^{ll'}(\alpha - \alpha'), \quad (4.3.63)$$

where $\mathbf{T}_g^l(\alpha)$ is the matrix-operator (4.3.59).

It is customary to write the commutation relations (4.3.63) using tensor products of matrices. We introduce the matrix element of the

matrix-operator (4.3.59) as follows:

$$\hat{\mathbf{T}} = \begin{pmatrix} \mathbf{A} & \mathbf{B} \\ \mathbf{C} & \mathbf{D} \end{pmatrix}. \quad (4.3.64)$$

Then the tensor product is a four-by-four matrix:

$$\hat{\mathbf{T}} \otimes \hat{\mathbf{T}} = \begin{pmatrix} \mathbf{A}\hat{\mathbf{T}} & \mathbf{B}\hat{\mathbf{T}} \\ \mathbf{C}\hat{\mathbf{T}} & \mathbf{D}\hat{\mathbf{T}} \end{pmatrix}. \quad (4.3.65)$$

The relations (4.3.63) can then be written thus:

$$\mathbf{r}(\alpha - \alpha') (\hat{\mathbf{T}}(\alpha) \otimes \hat{\mathbf{T}}(\alpha')) = (\hat{\mathbf{T}}(\alpha') \otimes \hat{\mathbf{T}}(\alpha)) \mathbf{r}(\alpha - \alpha'), \quad (4.3.66)$$

where $\mathbf{r}(\alpha)$ is a four-by-four number matrix, which in this case is

$$\mathbf{r}(\alpha) = w'_0(\alpha) + 4w'(\alpha) \sigma \otimes \sigma. \quad (4.3.67)$$

If we write (4.3.66) in components, we arrive at commutation relations for the matrix elements of $\hat{\mathbf{T}}$, of which we will need the following:

$$\begin{aligned} [\mathbf{A}(\alpha), \mathbf{A}(\beta)] &= [\mathbf{B}(\alpha), \mathbf{B}(\beta)] = [\mathbf{D}(\alpha), \mathbf{D}(\beta)] = 0, \\ a(\alpha - \beta) \mathbf{B}(\alpha) \mathbf{A}(\beta) &= b(\alpha - \beta) \mathbf{B}(\beta) \mathbf{A}(\alpha) \\ &+ c(\alpha - \beta) \mathbf{A}(\beta) \mathbf{B}(\alpha), \\ a(\alpha - \beta) \mathbf{B}(\beta) \mathbf{D}(\alpha) &= b(\alpha - \beta) \mathbf{B}(\alpha) \mathbf{D}(\beta) \\ &+ c(\alpha - \beta) \mathbf{D}(\alpha) \mathbf{B}(\beta). \end{aligned} \quad (4.3.68)$$

The fact that the traces of the $\hat{\mathbf{T}}$ -matrices commute (see (4.3.11)), i.e.

$$[\mathbf{A}(\alpha) + \mathbf{D}(\alpha), \mathbf{A}(\beta) + \mathbf{D}(\beta)] = 0, \quad (4.3.69)$$

is a corollary of (4.3.68).

Let us consider state Ω_0 in which the spins of all particles are "up", while the projection of the impurity spin is $+S$. In this state the lower left matrix element of the matrix-operators \mathbf{r} and \mathbf{R} (4.3.60) and (4.3.61) vanishes and the state is an eigenstate of the diagonal elements:

$$\begin{aligned} \mathbf{r}^{11} \Omega_0 &= a(\alpha) \Omega_0, & \mathbf{R}^{11} \Omega_0 &= (w_0 + wS) \Omega_0, \\ \mathbf{r}^{22} \Omega_0 &= b(\alpha) \Omega_0, & \mathbf{R}^{22} \Omega_0 &= (w_0 - wS) \Omega_0, \\ \mathbf{r}^{21} \Omega_0 &= \mathbf{R}^{21} \Omega_0 = 0. \end{aligned} \quad (4.3.70)$$

This means that the same is true for the elements of $\hat{\mathbf{T}}$:

$$\mathbf{C}(\alpha) \Omega_0 = 0, \quad \mathbf{A}(\alpha) \Omega_0 = \Lambda_A(\alpha) \Omega_0, \quad \mathbf{D}(\alpha) \Omega_0 = \Lambda_D(\alpha) \Omega_0. \quad (4.3.71)$$

If we use the rule for multiplying triangular matrices, we can easily find the eigenvalues of **A** and **D**:

$$\Lambda_A = \prod_{n=1}^N a(\alpha - \alpha_n) [(S + 1/2) a(\alpha - \alpha_0) - (S - 1/2) b(\alpha - \alpha_0)],$$

$$\Lambda_D = \prod_{n=1}^N b(\alpha - \alpha_n) [b(\alpha - \alpha_0) (S + 1/2) - (S - 1/2) a(\alpha - \alpha_0)]. \quad (4.3.72)$$

The eigenvectors of **T**(α) with other spin components can be built by successively applying operator **B**(α'_n) as a creation operator:

$$\Omega(\alpha'_1, \dots, \alpha'_M) = \prod_{\beta=1}^M \mathbf{B}(\alpha'_\beta) \Omega_0. \quad (4.3.73)$$

The vectors $\Omega(\alpha'_1, \dots, \alpha'_M)$ are eigenvectors of **T**(α) not at all values from $\{\alpha'_\beta\}$. Indeed, if we use the commutation relations (4.3.68), we find that

$$(\mathbf{A}(\alpha) + \mathbf{D}(\alpha)) \prod_{\beta=1}^M \mathbf{B}(\alpha'_\beta) \Omega_0 = \Lambda(\alpha; \{\alpha'\}) \prod_{\beta=1}^M \mathbf{B}(\alpha'_\beta) \Omega_0 + \sum_{\gamma} \Lambda_{\gamma}(\alpha; \{\alpha'\}) \prod_{\beta \neq \gamma} \mathbf{B}(\alpha'_\beta) \mathbf{B}(\alpha) \Omega_0. \quad (4.3.74)$$

The term with $\Lambda(\alpha; \{\alpha'\})$ in this formula is obtained if in commutators we use only the first term in (4.3.68):

$$\Lambda(\alpha; \{\alpha'\}) = \prod_{\beta=1}^M \frac{a(\alpha - \alpha'_\beta)}{b(\alpha - \alpha'_\beta)} \Lambda_D + \prod_{\beta=1}^M \frac{a(\alpha'_\beta - \alpha)}{b(\alpha'_\beta - \alpha)} \Lambda_A. \quad (4.3.75)$$

Here using the second term leads to "undesirable" terms Λ_{γ} in (4.3.74). To calculate Λ_{γ} we note that the left-hand side of (4.3.74) is symmetric in the permutation of α'_β . Whence it suffices to calculate Λ_1 , since all the other Λ_{γ} can be obtained by a proper permutation of α' . And Λ_1 is found if we use the second terms on the right-hand sides of (4.3.68) only once in the commutators of **A** and **D** with **B**(α'_1). We have

$$\Lambda_{\gamma} = -\frac{b(\alpha'_\gamma - \alpha)}{c(\alpha'_\gamma - \alpha)} \prod_{\beta=1}^M \frac{a(\alpha'_\beta - \alpha'_\gamma)}{c(\alpha'_\beta - \alpha'_\gamma)} \Lambda_A(\alpha'_\gamma) - \frac{b(\alpha - \alpha'_\gamma)}{c(\alpha - \alpha'_\gamma)} \prod_{\beta=1}^M \frac{a(\alpha'_\gamma - \alpha'_\beta)}{c(\alpha'_\gamma - \alpha'_\beta)} \Lambda_D(\alpha'_\gamma). \quad (4.3.76)$$

If all the undesirable terms $\Lambda_j = 0$, then Ω is an eigenvector of **T**(α) with a z-component of spin

$$S^z = N/2 + S - M, \quad (4.3.77)$$

since each operator $\mathbf{B}(\alpha'_\beta)$ in (4.3.73) increases the z -component of spin by unity. The α'_i satisfy the equations

$$\prod_{n=1}^{N-1} \frac{a(\alpha'_\beta - \alpha_n)}{b(\alpha'_\beta - \alpha_n)} \frac{a(\alpha'_\beta - \alpha_0)(S+1/2) - b(\alpha'_\beta - \alpha_0)(S-1/2)}{-a(\alpha'_\beta - \alpha_0)(S-1/2) + b(\alpha'_\beta - \alpha_0)(S+1/2)} \\ = \prod_{\gamma=1}^M \frac{a(\alpha'_\beta - \alpha'_\gamma)}{a(\alpha'_\gamma - \alpha'_\beta)} \frac{b(\alpha'_\beta - \alpha'_\gamma)}{b(\alpha'_\gamma - \alpha'_\beta)}, \quad \beta = 1, \dots, M. \quad (4.3.78)$$

Assuming that $\alpha'_\beta = J(-\lambda_\beta + i/2)$ and $\alpha_n = 0$, using (4.3.62), and allowing for $b(0) = 0$, we find that

$$e^{ik_j L} = \prod_{\alpha=1}^M \frac{\lambda_\alpha + i}{\lambda_\alpha - i} e^{iJS}, \quad (4.3.79)$$

with λ_α satisfying the equations

$$\left(\frac{\lambda_\alpha + i}{\lambda_\alpha - i} \right)^N \frac{\lambda_\alpha + i2S - 1/g}{\lambda_\alpha - i2S - 1/g} = \prod_{\beta \neq \alpha}^M \frac{\lambda_\alpha - \lambda_\beta + 2i}{\lambda_\alpha - \lambda_\beta - 2i}. \quad (4.3.80)$$

Equations (4.3.79) and (4.3.80), which we will call Bethe's equations, solve the problem of diagonalizing the Hamiltonian of the s - d exchange model and completely determine its spectrum. We note that the energy of a state characterized by the momenta of charge density waves, $\{k_j\}$, and the rates of spin density waves, $\{\lambda_\alpha\}$, is

$$E = \sum_{j=1}^N k_j, \quad (4.3.81)$$

while the z -component of spin is given by (4.3.77). Equations (4.3.79) and (4.3.80) were obtained in [30-32] for $S = 1/2$, and for arbitrary S in [33].

4.3.7 Discussion

In Chap. 4.4 we will study the physical properties of a system consisting of a large number of particles N , $L \rightarrow \infty$, on the basis of Eqs. (4.3.77), (4.3.79)-(4.3.81). But let us first examine some properties of the above equations.

First, it is clear that at $g = 0$ or $S = 0$ the equations describe a gas of free electrons. A full proof of this statement will be given in Sec. 4.4.3; here we simply show that all energy levels can be described by the formula

$$E = 2\pi K/L,$$

with K an arbitrary integer. Indeed, if we multiply Eqs. (4.3.79) and (4.3.80) over all j and α , we have (at $g = 0$)

$$e^{iEL} = 1.$$

Hence, to account for the interaction with the impurity we had to part with the traditional division of the system of free spin-1/2 particles into two independent systems, one with particles with spin "up" and the other with particles with spin "down" (the scattering matrix is a unit matrix). However, an equally consistent way to represent the system is to divide it into a charge and a spin subsystems.* In this case the permutation operator is the scattering matrix.

Each subsystem has a Fermi spectrum. Indeed, the wave function, $\Psi(x_1, \dots, x_N)$, vanishes only when there is a pair of equal numbers from $\{k_j\}$ and $\{\lambda_\alpha\}$. The number of particles in the spin subsystem is equal to the number of flipped spins, M . It is natural to define the spin excitation momentum as

$$p(\lambda) = 2 \arctan \lambda \quad (-\pi < p(\lambda) < \pi).$$

Taking the logs of Eqs. (4.3.79) and (4.3.80), we have

$$k_j L = 2\pi I_j + JS + \sum_{\alpha=1}^M p(\lambda_\alpha), \quad (4.3.82)$$

$$Np(\lambda_\alpha) = 2\pi J_\alpha + \sum_{\beta=1}^M \Phi(\lambda_\alpha - \lambda_\beta) - \delta(\lambda_\alpha), \quad (4.3.83)$$

where $\Phi(\lambda) = 2 \arctan(\lambda/2)$ is the two-particle scattering phase for spin density waves, and $\delta(\lambda) = 2 \arctan \frac{\lambda - 1/g}{2S}$ is the one-particle phase for the scattering of spin waves by the impurity. The integers I_j and J_α are quantum numbers of the system.

We note also that at $\delta(\lambda) = 0$, Eq. (4.3.83) is exactly Bethe's equation for a one-dimensional Heisenberg model. We have repeatedly stated that the s-d model with an impurity spin $S = 1/2$ is formally close to the problem of a gas of interacting fermions. It is easy to see the relationship if we consider the relativistic statement of the problem, with the Hamiltonian

$$\mathcal{H} = \int \left[i \left(\psi_{1\sigma}^\dagger \frac{d}{dx} \psi_{1\sigma} - \psi_{2\sigma}^\dagger \frac{d}{dx} \psi_{2\sigma} \right) + g \psi_{1\sigma}^\dagger \psi_{1\sigma} \psi_{2\sigma}^\dagger \psi_{2\sigma} \right] dx. \quad (4.3.84)$$

Here $\psi_{1\sigma}$ and $\psi_{2\sigma}$ are the operators of right- and left-handed ($\sigma = \pm 1$) fermions.

The number of right- and left-handed particles, $N_\pm = i \times \int \psi_{1(2)\sigma}^\dagger \psi_{1(2)\sigma} dx$, is conserved in scattering; whence, if

* We note that charge and spin variables arise very naturally in the boson representation of fermion operators [28, 80].

we set $N_+ = N$ and $N_- = 1$, we arrive at the s-d model Hamiltonian (4.3.22). This becomes clear if we use the pseudofermions introduced by Abrikosov [8] and change the operator of the impurity spin ($S = 1/2$) to an equivalent representation $\mathbf{S} = \psi_{2\sigma}^\dagger \boldsymbol{\sigma}_{\sigma\sigma'} \psi_{2\sigma'}$.

Bethe's Ansatz for the Hamiltonian (4.3.84) has been built by Belavin [72] and Andrei and Lowenstein [81]. In this case the operators \mathbf{T}_j can be obtained from $\mathbf{T}(\alpha)$ with $\alpha_n = \gamma_n$, where $\gamma_n = \pm 1$ is the particle's helicity.

4.4 THE THERMODYNAMICS OF THE S-D EXCHANGE MODEL

Here we will investigate Bethe's equations (4.3.79) and (4.3.80) and then calculate the thermodynamic functions for the system using these equations as a basis. Methods of studying sets of algebraic equations of this type were developed by Leib and Liniger [63] and Yang and Yang [82], who used the simplest integrable system, a one-dimensional gas of bosons.

Equation (4.3.80) at $g = 0$ coincides with Bethe's equation for a one-dimensional Heisenberg chain, whose detailed investigation was undertaken by Gaudin, Johnson, McGoy, Takahashi, and Suzuki [83-87]. We will use some techniques developed in these works.

4.4.1 Bethe's Equations for the s-d Exchange Model. Going Over to the Continuous Limit

The solutions to Eq. (4.3.80), generally speaking, lie in the complex λ -plane. Bethe [39] discovered that for equations whose structure is similar to that of Eq. (4.3.80) all solutions at $N \rightarrow \infty$ are grouped into so-called strings, or spin complexes:

$$\lambda_{\alpha}^{n,j} = \lambda_{\alpha}^n + i(n+1-2j) + \delta_{n,j} \quad (j = 1, \dots, n). \quad (4.4.1)$$

Solutions belonging to one complex of size n have a common real part λ_{α}^n . Their imaginary parts are equidistant and lie symmetric to the real axis. The correction term $\delta_{n,j}$ is exponentially small as $N \rightarrow \infty$:

$$\delta_{n,j} = O(\exp \{-N \times \text{const}\}). \quad (4.4.2)$$

To verify this, we substitute (4.4.1) into (4.3.80), which yields

$$\begin{aligned} & \left(\frac{\lambda_{\alpha}^n + i(n+2-2j)}{\lambda_{\alpha}^n + i(n-2j)} \right)^N \frac{\lambda_{\alpha}^n + i(n+1+2S-2j) - 1/g}{\lambda_{\alpha}^n + i(n+1-2S-2j) - 1/g} \\ &= \prod_{\beta, m \neq n} \frac{\lambda_{\alpha}^n - \lambda_{\beta}^m + 2i}{\lambda_{\alpha}^n - \lambda_{\beta}^m - 2i} \prod_{j'=1}^n \frac{1-j+j'}{1+j-j'} (\delta_{n,j} - \delta_{n,j+1}). \end{aligned} \quad (4.4.3)$$

The first product on the right-hand side is over all λ 's that do not belong to a given complex, while the second is over the λ 's that belong to it. All cofactors on the right-hand side are finite except the term containing $\lambda^{n,j} - \lambda^{n,j-1}$. On the other hand, the modulus of each cofactor on the left-hand side is less than unity. Therefore, $\delta_{n,j} - \delta_{n,j+1} = O(e^{-N})$. Assuming for the sake of definiteness that $\delta_{n,1} = 0$, we obtain the estimate (4.4.2).

The small quantities $\delta_{n,j}$ can be ignored. We then have equations that include only the real parts λ_α^n . To this end we must multiply Eq. (4.4.3) over $j = 1, \dots, n$.

Suppose that M_n is the number of strings of order n , so that the total number of flipped spins is

$$M = \sum_{n=1}^{\infty} n M_n. \quad (4.4.4)$$

Then the real parts λ_α^n ($\alpha = 1, \dots, M_n$) satisfy the equation

$$\begin{aligned} & \left(\frac{\lambda_\alpha^n + in}{\lambda_\alpha^n - in} \right)^N \prod_{j=1-n}^{n-1} \frac{\lambda_\alpha^n + i2S + i2j - 1/g}{\lambda_\alpha^n + i2S - i2j - 1/g} \\ &= \prod_{m=1}^{\infty} \prod_{\beta=1}^{M_m} \prod_{j=1-n}^{n-1} \prod_{k=1-m}^{m-1} \frac{\lambda_\alpha^n - \lambda_\beta^m + i(j-k)}{\lambda_\alpha^n - \lambda_\beta^m - i(j-k)}. \end{aligned} \quad (4.4.5)$$

In terms of these quantities Eq. (4.3.79) takes the form

$$e^{ik_j L} = \prod_{n, \alpha} \left(\frac{\lambda_\alpha^n + in}{\lambda_\alpha^n - in} \right) e^{iJS}. \quad (4.4.6)$$

Taking logs of Eqs. (4.4.5) and (4.4.6), we obtain

$$Lk_j = 2\pi I_j + JS + \sum_{n=1}^{\infty} \sum_{\alpha=1}^{M_n} \theta_m(\lambda_\alpha^n) - \pi, \quad (4.4.7)$$

$$N\theta_{n,1}(\lambda_\alpha^n) + \theta_{n,2S}(\lambda_\alpha^n - 1/g) = 2\pi J_\alpha^n + \sum_{m=1}^{\infty} \sum_{\beta=1}^{M_n} \Xi_{nm}(\lambda_\alpha^n - \lambda_\beta^m). \quad (4.4.8)$$

Here $2J_\alpha^n$ and $2I_j$ are integers, and $\theta_{n,1}$ and Ξ_{nm} can be interpreted in the following manner: $\theta_{n,1}$ is the momentum of the spin complex (spin $n/2$) that is scattered by the impurity (spin S) with a phase shift $\theta_{n,2S}$ and by other complexes with a phase shift Ξ_{nm} . We can define these two quantities as follows:

$$\theta_{n,1}(\lambda) = 2 \arctan(\lambda/n) \quad (-\pi < \theta < \pi), \quad (4.4.9)$$

$$\theta_{n,m}(\lambda) = \sum_{j=1}^{\min(n,m)} \theta_{n+m+1-2j}(\lambda),$$

$$\Xi_{nm} = 2\theta_{n,m} - \theta_{n+m,1} - \theta_{|n-m|,1} (1 - \delta_{nm}). \quad (4.4.10)$$

Equation (4.4.8) restricts the possible values of the integers $\{J_\alpha^n\}$:

$$|J_\alpha^n| \leq \frac{1}{2} \left\{ N - 2 \sum_{m=1}^{\infty} [\min(n, m) - M_m] + 2M_1 - 1 \right\} \equiv D_{nm}. \quad (4.4.11)$$

Among the numbers J_α^n belonging to one spin complex no two should be equal. Otherwise, it follows from (4.4.8) that some λ_α^n and λ_β^n coincide, and since $\mathbf{B}^2(\lambda)$ is zero (see (4.3.64)), so is the spin part of the wave function. We can show that for any set of integers J_α^n ($n = 1, \dots, \infty$; $\alpha = 1, \dots, M$) such that (1) there are no two equal numbers with the same value of n , (2) $\sum_{n=1}^{\infty} M_n < N/2$, and condition (4.4.11) is met, for such a set there exists a solution of Eq. (4.4.8), and among the λ_α^n with the same n no two are equal.

Hence, the integers J_α^n and I_j are quantum numbers of the system. Each eigenstate of the Hamiltonian is characterized by M_n numbers J_α^n , which can form an integral lattice D_n , and the $2D_n - M_n$ omitted numbers \tilde{J}_α^n (holes). In the ground state and for a given z -component of spin, S^z , only the real λ are nonzero, which implies that $M_n = 0$ for $n > 1$ and the J_α^n must be selected in such a way that

$$J_\alpha^1 = -\frac{N}{2} + \frac{M}{2}, \dots, -\frac{N}{2} + \frac{3M}{2}. \quad (4.4.12)$$

According to Eq. (4.4.8) the rates λ_α^n correspond to the occupied sites in D_n .

Following Gaudin [83], we consider the function

$$Nh^n(\mu) = N\theta_{n,1}(\mu) + \theta_{n,2S}(\mu) - \sum_{m,\beta} \Xi_{mn}(\mu_\beta^n - \lambda_\beta^n).$$

A value of μ_α^n for which $Nh^n(\mu_\alpha^n) = 2\pi\tilde{J}_\alpha^n$ is called the rapidity of a hole.

In the continuous limit $N \rightarrow \infty$, $L \rightarrow \infty$, $N/L = \epsilon_F/\pi = \text{const}$ a state of the system must be described not by a set of rapidities of particles, $\{\lambda_\alpha^n\}$, and holes, $\{\mu_\alpha^n\}$, but by the distribution of the respective densities:

$N\rho_n(\lambda) d\lambda$ = number of particles in interval $d\lambda$,

$$N\tilde{\rho}_n(\lambda) d\lambda = \text{number of holes in interval } d\lambda. \quad (4.4.13)$$

According to this definition, the total number of particles and holes in the interval $d\lambda$ is equal to the number of solutions $Nh^n(\lambda) = 2\pi \times \text{integer}$, which implies that

$$\frac{dh^n(\lambda)}{d\lambda} = 2\pi [\rho_n(\lambda) + \tilde{\rho}_n(\lambda)]. \quad (4.4.14)$$

Then Eqs. (4.4.7) and (4.4.8) can be expressed in terms of ρ_n and $\tilde{\rho}_n$ only:

$$Lk_j = 2\pi I_j - \int_{-\infty}^{+\infty} e_n(\lambda) \rho_n(\lambda) d\lambda, \quad (4.4.15)$$

$$p_n(\lambda) = 2\pi h^n(\lambda) + \int_{-\infty}^{+\infty} \Xi_{nm}(\lambda - \lambda') \rho_m(\lambda') d\lambda', \quad (4.4.16)$$

where

$$e_n = \theta_{1,n} - \pi, \quad (4.4.17)$$

$$p_n = \theta_{1,n} + \frac{1}{N} \theta_{n,2S}. \quad (4.4.18)$$

Differentiating (4.4.16) with respect to λ , we have

$$p'_n(\lambda) = 2\pi \tilde{\rho}_n(\lambda) + \int_{-\infty}^{+\infty} \mathbf{A}_{nm}(\lambda - \lambda') \rho_m(\lambda') d\lambda', \quad (4.4.19)$$

with

$$\mathbf{A}_{nm} = \frac{1}{2\pi} \frac{d\Xi_{nm}}{d\lambda} + \delta(\lambda) \delta_{nm}. \quad (4.4.20)$$

The spin and energy of the system in this case is

$$\frac{S_z}{N} = \frac{1}{2} - \frac{1}{N} \sum_{n=1}^{\infty} n M_n + \frac{S}{N} = \frac{1}{2} - \sum_{n=1}^{\infty} \int_{-\infty}^{+\infty} n \rho_n(\lambda) d\lambda + \frac{S}{N}, \quad (4.4.21)$$

$$E \equiv \sum_{j=1}^N k_j = \frac{2\pi}{L} \sum_{j=1}^N I_j + E_{\text{spin}}, \quad (4.4.22)$$

where

$$\frac{E_{\text{spin}}}{N} = \frac{\epsilon_F}{\pi} \int e_n(\lambda) \rho_n(\lambda) d\lambda. \quad (4.4.23)$$

Formulas (4.4.19), (4.4.21), and (4.4.23) describe all states of the system in the continuous limit.

To keep the formulas simple, we did not go over to the continuous limit in the charge subsystem. As noted before, this subsystem is a gas of free spinless fermions and does not require further study.

In concluding this section, we note an expedient relationship between θ_{nm} and Ξ_{nm} :

$$\frac{1}{2\pi} \frac{d\theta_{nm}}{d\lambda} = \mathbf{A}_{nm} * \mathbf{S}, \quad (4.4.24)$$

with

$$s(\lambda) = [2 \cosh(\pi\lambda/2)]^{-1} \quad \text{and} \quad s * f = \int_{-\infty}^{+\infty} s(\lambda - \lambda') f(\lambda') d\lambda'.$$

The easiest way to verify (4.4.24) is to compare the Fourier transforms of the corresponding functions, e.g.

$$\mathbf{A}_{nm}(\omega) = \coth|\omega| (e^{-|n-m||\omega|} - e^{-(n+m)|\omega|}). \quad (4.4.25)$$

Below we will often use the inverse matrix \mathbf{A}_{nm}^{-1} , which has a very simple form:

$$\mathbf{A}_{nm}^{-1} = \delta_{nm} - (\delta_{n, m+1} + \delta_{n, m-1}) s. \quad (4.4.26)$$

Using (4.4.24) and (4.4.26), we can write Eq. (4.4.16) in compact form:

$$\rho_n + \tilde{\rho}_n = s * (\tilde{\rho}_{n-1} + \tilde{\rho}_{n+1}) + \delta_{n1} s(\lambda) + \frac{1}{N} \delta_{n, 2S} s(\lambda - 1/g). \quad (4.4.27)$$

The spin and energy of the system can be expressed only in terms of hole densities:

$$\frac{S^z}{N} = \sum_{n, m} \int_{-\infty}^{+\infty} n \mathbf{A}_{nm}^{-1}(\lambda - \lambda') \tilde{\rho}_m(\lambda') d\lambda d\lambda' = \lim_{n \rightarrow \infty} \int_{-\infty}^{+\infty} \tilde{\rho}_n(\lambda) d\lambda, \quad (4.4.28)$$

$$E_{\text{spin}} = \frac{N^2}{L} \int_{-\infty}^{+\infty} \arctan e^{-\pi\lambda/2} \tilde{\rho}_1(\lambda) d\lambda + \frac{1}{2} E_0, \quad (4.4.29)$$

where

$$\frac{1}{2} E_0 = \frac{N^2}{L} \int_{-\infty}^{+\infty} \frac{\mathbf{A}_{11}(\omega)}{(\omega + i\delta) \cosh \omega} \frac{d\omega}{2\pi} + \frac{N}{L} \int_{-\infty}^{+\infty} \frac{\mathbf{A}_{1, 2S}(\omega) e^{i\omega/g}}{(\omega + i\delta) \cosh \omega} \frac{d\omega}{2\pi}. \quad (4.4.30)$$

We note that the energy is expressed in terms of the density of holes with real λ . We will show later that in the ground state with a given S^z all the ρ_n are zero at $n > 1$, and for $S^z = 0$ there are no holes with real λ 's, i.e. $\tilde{\rho}_1 = 0$. Whence $E_0/2$ is the ground-state energy of the spin subsystem. The first term on the right-hand side of (4.4.30) refers to the free particles and, which is easily shown, is $\pi N^2/L$, i.e. half the total energy of the free Fermi gas, while the second term is the addition to the ground-state energy due to the impurity. The latter quantity is not universal.

4.4.2 The Equilibrium Distribution

To find the equilibrium distributions ρ_n and $\tilde{\rho}_n$ for a given temperature, we must, according to the general principles of statistical mechanics, find the minimum of the functional of free energy:

$$F[\rho_n, \tilde{\rho}_n] = E - TS - HS^z. \quad (4.4.31)$$

The problem of finding the entropy of a system as the functional of ρ and $\tilde{\rho}$ amounts to determining the statistical weight of a macroscopic state, i.e. the number $\Delta\Gamma$ of microscopic states with close energies. Within a given energy interval dE and segments $(\lambda^n, \lambda^n + d\lambda^n)$ there are $N \prod_{n=1}^{\infty} (\rho_n + \tilde{\rho}_n) d\lambda$ sites. Since we are dealing here with Fermi statistics, there are

$$\Delta\Gamma = \frac{\prod_{n=1}^{\infty} [N(\rho_n + \tilde{\rho}_n) d\lambda]!}{\prod_{n=1}^{\infty} (N\rho_n d\lambda)! (N\tilde{\rho}_n d\lambda)!} \quad (4.4.32)$$

ways in which $\prod_{n=1}^{\infty} N\rho_n d\lambda$ particles can be placed at these sites. Assuming that $N\rho_n d\lambda$ and $N\tilde{\rho}_n d\lambda$ are large and summing over all possible intervals $d\lambda$, we arrive at the usual expression for the entropy of a Fermi gas:

$$S = \frac{N^2}{L} \sum_{n=1}^{\infty} \int d\lambda [(\rho_n + \tilde{\rho}_n) \ln(\rho_n + \tilde{\rho}_n) - \rho_n \ln \rho_n - \tilde{\rho}_n \ln \tilde{\rho}_n]. \quad (4.4.33)$$

In minimizing the free energy we must bear in mind that ρ_n and $\tilde{\rho}_n$ are not independent; they satisfy Eq. (4.4.8). Whence

$$\frac{\delta \tilde{\rho}_n(\lambda)}{\delta \rho_n(\lambda')} = \mathbf{A}_{nm}(\lambda - \lambda'). \quad (4.4.34)$$

Varying the free energy in ρ_n and introducing the notation $\varepsilon_n = T \ln(\tilde{\rho}_n/\rho_n)$, we come to nonlinear equations, which together with Eq. (4.4.8) determine the equilibrium values of ρ_n and $\tilde{\rho}_n$; these

equations are

$$e_n - Hn - T \ln(1 + e^{\varepsilon_n/T}) + T \mathbf{A}_{nm} * \ln(1 + e^{-\varepsilon_m/T}) = 0. \quad (4.4.35)^*$$

The functions $\varepsilon_n(\lambda)$ are the main quantities that emerge when we go over to the continuous limit in Bethe's equations. Their physical meaning is that they are the energies of elementary excitations.

A somewhat more convenient form of Eqs. (4.4.35) can be obtained if we invert the \mathbf{A}_{nm} matrices:

$$\begin{aligned} \varepsilon_n &= s * \ln(1 + e^{\varepsilon_{n+1}/T}) (1 + e^{\varepsilon_{n-1}/T}), \quad n \geq 2, \\ \varepsilon_1 &= s * \ln(1 + e^{\varepsilon_2/T}) - \frac{2}{\pi} \arctan e^{-\pi\lambda/2}, \quad \lim_{n \rightarrow \infty} \varepsilon_n/n = H. \end{aligned} \quad (4.4.36)$$

The free energy can be expressed solely in terms of $\varepsilon_n(\lambda)$. Indeed, according to (4.4.23) and (4.4.33),

$$\frac{F}{N} = \sum_{n=1}^{\infty} \int_{-\infty}^{+\infty} d\lambda \{ \rho_n [e_n - T \ln(1 + e^{\varepsilon_n/T})] - \tilde{\rho}_n T \ln(1 + e^{-\varepsilon_n/T}) \}. \quad (4.4.37)$$

We exclude $\tilde{\rho}_n$ by using the relationship (4.4.19). This yields

$$\frac{F_{\text{spin}}}{N} = \sum_{n=1}^{\infty} \int_{-\infty}^{+\infty} d\lambda \{ \rho_n [\dots] - p'_n T \ln(1 + e^{-\varepsilon_n/T}) \}. \quad (4.4.38)$$

The term in the square brackets is exactly the left-hand side of Eq. (4.4.35). Whence

$$\begin{aligned} \frac{F_{\text{spin}}}{N} &= -T \sum_{n=1}^{\infty} \int_{-\infty}^{+\infty} \ln(1 + e)^{-\varepsilon_n/T}, \\ &\times \frac{d}{d\lambda} \left(\theta_{1,n}(\lambda) + \frac{1}{N} \theta_{n,2s}(\lambda - 1/g) \right) d\lambda - H \left(\frac{1}{2} + \frac{S}{N} \right). \end{aligned} \quad (4.4.39)$$

Another useful formula for free energy can be obtained by excluding ρ_n from (4.4.37). In view of the minimum condition (4.4.35), the coefficient of $\tilde{\rho}_n$ is zero (as in the previous case). This yields

$$\frac{F_{\text{spin}}}{N} = -T \int_{-\infty}^{+\infty} p'_n (\mathbf{A}_{nm}^{-1} * \ln(1 + e^{\varepsilon_m/T})) d\lambda, \quad (4.4.40)$$

* It can be shown that the condition for extremum (4.4.35) determines the minimum of $F[\rho, \tilde{\rho}]$.

which when combined with (4.4.24) yields

$$\begin{aligned} \frac{F_{\text{spin}}}{N} &= -T \int_{-\infty}^{+\infty} s(\lambda) \ln(1 + e^{\varepsilon_1/T}) d\lambda \\ &- \frac{T}{N} \int_{-\infty}^{+\infty} s(\lambda - 1/g) \ln(1 + e^{\varepsilon_2/T}) d\lambda. \end{aligned} \quad (4.4.41)$$

The free energy of the s-d model consists of two parts, the spin and charge free energies:

$$F = F_{\text{charge}} + F_{\text{spin}}. \quad (4.4.42)$$

As noted before, the energy spectrum of the particles from the charge subsystem is unbounded from below. Whence we must assume that in the ground state the particles occupy all levels from 0 to $-\epsilon_F$. This means that

$$F_{\text{charge}} = -NT \int_{-\epsilon_F}^{+\infty} \ln(1 + e^{-\hbar/T}) dk = -\frac{\pi^2}{12} \frac{T^2}{\epsilon_F} + \frac{1}{2} E_0, \quad (4.4.43)$$

which is half the free energy of a gas of free fermions at $H = 0$. Equations (4.4.35), (4.4.36), (4.4.39) and (4.4.41) provide a full thermodynamic description of the s-d model.

4.4.3 The Free Electron Gas ($g \rightarrow 0$ or $S = 0$)

A correct description of the behavior of an impurity requires a very unusual way of representing the gas of free particles. Instead of studying noninteracting fermions with spin "up" and "down", we deal with two different types of fermions. One type transports charge but not spin, while the other does the opposite, i.e. does not change the local distribution of charges. Moreover, excitations in the spin subsystem are linear combinations of different "strings".

The fact that the nonlinear equations (4.4.36), whose solution is practically impossible, together with the first terms in (4.4.39) and (4.4.41) describe free particles is astonishing and requires proof.

In Eqs. (4.4.18) and (4.4.19) we drop the term with $1/N$ or simply put $S = 0$:

$$\frac{d\theta_{1,n}}{d\lambda} = \tilde{\rho}_n + \mathbf{A}_{nm} * \rho_m. \quad (4.4.44)$$

Comparing (4.4.44) with (4.4.35), we find that in the absence of an impurity the ρ_n and $\tilde{\rho}_n$ are linked by simple formulas characteristic

of a free system:

$$\begin{aligned}\rho_n &= \frac{1}{2\epsilon_F} \frac{\partial \epsilon_n}{\partial \lambda} n(\epsilon_n), \\ \tilde{\rho}_n &= \frac{1}{2\epsilon_F} \frac{\partial \epsilon_n}{\partial \lambda} [1 - n(\epsilon_n)], \\ n(x) &= (e^{x/T} + 1)^{-1}.\end{aligned}\quad (4.4.45)$$

This means, for one, that the average number of strings at a given temperature T is

$$\frac{\langle M_n \rangle}{N} = n(\epsilon_n(\infty)) - n(\epsilon_n(-\infty)). \quad (4.4.46)$$

Formulas (4.4.45) also imply that the ϵ_n are monotonically increasing functions, since by their very meaning $\rho_n, \tilde{\rho}_n \geq 0$.

Let us take the free energy in the absence of an impurity:

$$F_{\text{spin}}^0 = T \sum_{n=1}^{\infty} \int_{-\infty}^{+\infty} \ln[1 - n(\epsilon_n)] \frac{d}{d\lambda} \theta_{n,1}(\lambda) - d\lambda \frac{H}{2}. \quad (4.4.47)$$

Finding the derivative of Eq. (4.4.35) with respect to λ and combining the result with (4.4.47), we obtain

$$\begin{aligned}F_{\text{spin}}^0 &= T \sum_{n=1}^{\infty} \int_{-\infty}^{+\infty} \ln[1 - n(\epsilon_n)] \\ &\quad \times \left\{ \frac{d}{d\lambda} \epsilon_n - \Xi''_{nm} * \ln[1 - n(\epsilon_m)] \right\} d\lambda - \frac{H}{2}.\end{aligned}\quad (4.4.48)$$

The second term inside the braces yields zero because Ξ''_{nm} is an odd continuous function. Whence

$$F_{\text{spin}}^0 = \frac{T}{2\epsilon_F} \sum_{n=1}^{\infty} \int_{\min \epsilon_n}^{\max \epsilon_n} d\epsilon_n \ln[1 - n(\epsilon_n)] - \frac{H}{2}. \quad (4.4.49)$$

The easiest way to establish the limits of the ϵ_n is to employ Eq. (4.4.36). Indeed, sending λ to $+\infty$, we have a self-consistent system of equations in $\bar{\epsilon}_n \equiv \max \epsilon_n$:

$$\bar{\epsilon}_n = -\frac{1}{2} \ln[n(\bar{\epsilon}_{n+1}) n(\bar{\epsilon}_{n-1})], \quad (4.4.50)$$

with the conditions that $\lim_{n \rightarrow \infty} (\bar{\epsilon}_n/n) = H$ and $\epsilon_0 = -\infty$.

It is easy to find the solution to these equations [86]. The general solution is

$$\bar{\epsilon}_n = T \ln(\varphi_n^2 - 1), \quad (4.4.51)$$

with

$$\varphi_n = \frac{\sinh(\alpha n + \beta)}{\sinh \alpha}. \quad (4.4.52)$$

To find α and β we must use the boundary conditions for (4.4.50). As a result $\alpha = \beta = H/2T$.

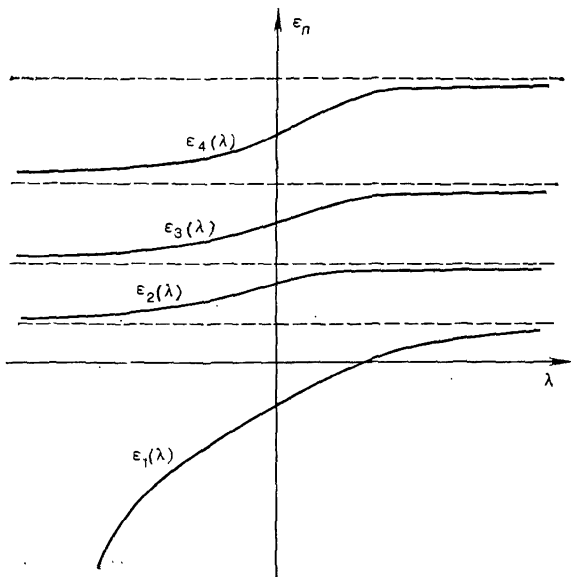


Fig. 4.13. The plot of the functions $\varepsilon_n(\lambda)$ that satisfy Eqs. (4.4.35).

In the other limit, $\lambda \rightarrow -\infty$, we have $\varepsilon_1 \rightarrow -\varepsilon_F \ll -T$. Therefore, if we assume that $n(\varepsilon_1) = 0$, we have an equation for $\tilde{\varepsilon}_n \equiv \min \varepsilon_n$:

$$\tilde{\varepsilon}_n = -\frac{T}{2} \ln [n(\tilde{\varepsilon}_{n+1}) n(\tilde{\varepsilon}_{n-1})]. \quad (4.4.53)$$

Comparing (4.4.50) with (4.4.53), we find that

$$T \ln \left(\frac{\sinh^2 [H(n+1)/2T]}{\sinh^2 (H/2T)} - 1 \right) = \tilde{\varepsilon}_n = \tilde{\varepsilon}_{n+1} \quad (4.4.54)$$

(Fig. 4.13). At $H = 0$ we have

$$F_{\text{spin}}^0 = -\frac{T}{2\varepsilon_F} \int_{-\varepsilon_F}^{\infty} \ln(1 + e^{-\varepsilon/T}) d\varepsilon = -\frac{\pi^2}{12} \frac{T^2}{\varepsilon_F} + \frac{E_0}{2}. \quad (4.4.55)$$

Hence, we see that $F_{\text{spin}}^0 = F_{\text{charge}}^0$ and both are half the free energy of noninteracting fermions at $H = 0$. If a magnetic field is present, it is convenient to calculate not the free energy but directly the magnetic moment of the system, $S^z = -\partial F / \partial H$. Using (4.4.28) and (4.4.46) we obtain

$$S^z = \lim_{n \rightarrow \infty} \ln(1 + e^{-\varepsilon_n/T}) \frac{T}{2\epsilon_F} \Big|_{-\infty}^{+\infty} = \frac{H}{4\epsilon_F}. \quad (4.4.56)$$

Here is an important point. The magnetic susceptibilities of the spin subsystem, χ_{spin} , and the electron gas, χ_{host} , coincide, while the heat capacities differ by a factor of two:

$$\frac{C_{\text{spin}}}{T\chi_{\text{spin}}} = \frac{C_{\text{host}}}{2T\chi_{\text{host}}} = \frac{2\pi^2}{3}. \quad (4.4.57)$$

4.4.4 Universality

According to the general conditions for renormalizability, the impurity parts of thermodynamic functions must be universal functions of T/T_K and H/T_K or functions of the invariant charge $z(T/T_K)$ (sec. 4.2.6) and H/T at $J \rightarrow 0$.

Equations (4.4.36) are the simplest for eliminating nonuniversal terms. Let us everywhere substitute $\lambda = (2/\pi) \ln(\pi T / 2\epsilon_F)$ for λ :

$$\varepsilon'_n(\lambda) = \varepsilon_n \left(\lambda - \frac{2}{\pi} \ln \frac{\pi T}{2\epsilon_F} \right). \quad (4.4.58)$$

In the process the absolute term of (4.4.36) becomes $(2\epsilon_F/\pi) \times \arctan(\pi T e^{-\pi\lambda/2}/2\epsilon_F)$ and the free energy is

$$\frac{F_{\text{spin}}^0}{N} = -T \int_{-\infty}^{+\infty} s \left(\lambda - \frac{2}{\pi} \ln \frac{\pi T}{2\epsilon_F} \right) \ln(1 + e^{\varepsilon'_1/T}) d\lambda, \quad (4.4.59)$$

$$F_{\text{imp}} = -T \int_{-\infty}^{+\infty} s \left(\lambda - \frac{2}{\pi} \ln \frac{T}{T_K} \right) \ln(1 + e^{\varepsilon'_2 S/T}) d\lambda, \quad (4.4.60)$$

$$T_K = \frac{2}{\pi} \epsilon_F e^{-\pi/2J}. \quad (4.4.60a)$$

When $T \ll \epsilon_F$, the main contribution to the integral in (4.4.60) is provided by the region $\lambda \sim \ln(T/T_K) \ll \ln(\epsilon_F/T)$. Therefore, for the term $(2\epsilon_F/\pi T) \arctan(\pi T e^{-\pi\lambda/2}/2\epsilon_F)$ in Eq. (4.4.36) we must substitute $e^{-\pi\lambda/2}/2$. But this can only be done if we wish to calculate the impurity part, F_{imp} . For the function (4.4.39) the important region is just $\lambda \sim \ln(\epsilon_F/T)$. The dimensionless functions

$$\phi_n(\lambda) = \varepsilon'_n/T$$

depend on H/T only as a parameter and satisfy the universal set of equations

$$\begin{aligned}\phi_1 &= -e^{-\pi\lambda/2} + s * \ln(1 + e^{\phi_2}), \\ \phi_n &= s * \ln(1 + e^{\phi_{n-1}})(1 + e^{\phi_{n+1}}), \\ \lim_{n \rightarrow \infty} (\phi_n/n) &= H/T.\end{aligned}\quad (4.4.61)$$

Here F_{imp} is a universal function of H/T and T/T_K :

$$F_{\text{imp}} = -T \int_{-\infty}^{+\infty} \frac{C_S(\omega, H/T) \exp[i\omega(2/\pi) \ln(T/T_K)]}{2 \cosh \omega} \frac{d\omega}{2\pi}, \quad (4.4.62)$$

where

$$C_S(\omega, H/T) = \int_{-\infty}^{+\infty} e^{i\omega\lambda} \ln(1 + e^{\phi_2 s}) d\lambda. \quad (4.4.63)$$

Equations (4.4.61)-(4.4.63) determine the thermodynamics of an impurity in the entire region of universality.

4.4.5 The Limits of Strong and Weak Coupling

Let us send T/T_K to ∞ in Eq. (4.4.60). Since $\ln(1 + e^{2S/T})$ is bounded, we have

$$F_{\text{imp}} \rightarrow -T \ln(1 + e^{2S/T})|_{\lambda \rightarrow +\infty}, \quad (4.4.64)$$

and, according to (4.4.54),

$$F_{\text{imp}}(T \gg T_K) \rightarrow -T \ln \frac{\sinh[H(2S+1)/2T]}{\sinh(H/2T)}. \quad (4.4.65)$$

At high temperatures the interaction of an impurity with the conduction electrons vanishes, as expected. Therefore, (4.4.65) describes the behavior of a free magnetic moment S , and we are dealing with the weak-coupling limit.

Now let us consider the case of strong coupling, i.e. $T/T_K \rightarrow 0$. According to (4.4.54), we have

$$F_{\text{imp}}(T \ll T_K) \rightarrow -T \ln \frac{\sinh(H2S/2T)}{\sinh(H/2T)}. \quad (4.4.66)$$

We can therefore conclude that at absolute zero the impurity ground state is $2S$ -fold degenerate. The impurity's entropy and magnetic moment are $T \ln 2S$ and $S - 1/2$, according to (4.4.46). The conduction electrons cannot compensate for the impurity spin and decrease it by $1/2$. On the basis of qualitative arguments, Mattis [20] arrived at this result as long ago as 1967.

In Sec. 4.4.8 we will show that when S is not $1/2$, the strong-coupling limit is approached logarithmically and the coefficients of inverse powers of $\ln [\max (H, T)/T_K]$ can be found by a perturbation-theory technique.

But if $T \ll T_K$, at $S = 1/2$ the impurity part of the free energy can be expanded in a power series in T/T_K , as noted before. Let us prove this. It suffices to show that $C_1(\omega)$ is analytic in the lower half-plane. Then at $T \ll T_K$ we can bend the integration contour in (4.4.62) into the lower half-plane and determine the integral via the sum of residues of $\cosh \omega$ [36]:

$$F_{\text{imp}}^{1/2} = - \sum_{n=0}^{\infty} \left(\frac{T}{T_K} \right)^{2n+1} (-1)^n C_1(-i\pi(n+1/2)). \quad (4.4.67)$$

Indeed, Eqs. (4.4.61) imply that $\phi_1 \rightarrow -e^{-\pi\lambda/2}$ as $\lambda \rightarrow -\infty$, and the integral (4.4.63) is finite at $\text{Im } \omega < 0$.

To determine the expansion coefficients in (4.4.67), we must know the ϕ_1 versus λ dependence over the entire range for λ , generally speaking. Nevertheless, the heat capacity at $T \rightarrow 0$ can be determined by simple reasoning [36]; namely,

$$C_1(-i\pi/2) \equiv \int_{-\infty}^{+\infty} e^{-\pi\lambda/2} \ln(1 + e^{\phi_1}) d\lambda = \pi^2/3. \quad (4.4.68)$$

To arrive at this result, we note that the formulas for the free energy of the spin subsystem, (4.4.59), and of an impurity with spin $S = 1/2$, (4.4.60), are very similar. In the strong-coupling limit $g \rightarrow \infty$ they coincide completely. Whence

$$\frac{C_{\text{imp}}}{C_{\text{spin}}} = \frac{2\epsilon_F}{\pi T_K}. \quad (4.4.69)$$

This formula together with (4.4.55) yields (4.4.68). It goes without saying that this method can be used only to find the first term in expansion (4.4.67). The point is that the temperature dependence in (4.4.59) and (4.4.60) lies not only in s but in ϵ'_1 as well. Therefore, the formula for the free energy of an impurity, (4.4.60) contains integral powers of T/ϵ_F as well as integral powers of T/T_K . But since $\epsilon'_1/T = \phi_1 + O(T/\epsilon_F)$, terms with T/ϵ_F appear only in the fourth- and higher-order terms. (Note that if we simply substitute $e^{-\pi\lambda/2}$ for ϕ_1 in (4.4.68), the result is half the one we expect.)

The same is true for the magnetic susceptibility at $T = 0$:

$$\frac{\chi_{\text{imp}}}{\chi_{\text{spin}}} = \frac{2\epsilon_F}{\pi T_K}. \quad (4.4.70)$$

Combining (4.4.69) with (4.4.70), we arrive at the Wilson relation:

$$\lim_{T \rightarrow 0} \frac{C_{\text{imp}}}{T \chi_{\text{imp}}} = \frac{2\pi^2}{3}. \quad (4.4.71)$$

This relation has been obtained in various ways [17, 19, 21-23]. All refer in one way or other to the strong-coupling limit.

4.4.6 The Thermodynamics of an Impurity

For further studies we will list the analytic properties of $C_S(\omega, H/T)$. These will be proved in Secs. 4.4.7 and 4.4.8. We start with the asymptotics as $\lambda \rightarrow \pm\infty$:

$$C_n(\omega) = \frac{i \ln(\varphi_n^2)}{\omega + i\delta} + \frac{-i \ln(\varphi_{n-1}^2)}{\omega - i\delta} + D_n(\omega), \quad (4.4.72)$$

where φ_n is defined in (4.4.52), and $D_n(\omega)$ is finite at $\omega = 0$. At $H \ll T$ (a) $D_n(\omega)$ for $n > 1$ has cuts in the lower and upper half-

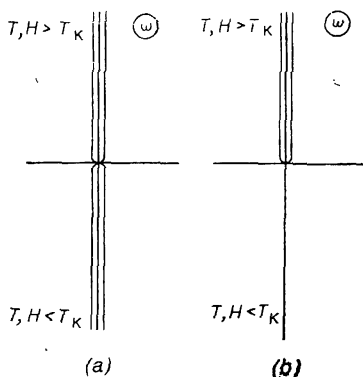


Fig. 4.14. Singularities in the complex ω -plane of $D_n(\omega)$ at $n \neq 1$ (a) and $n = 1$ (b).

planes that start at $\omega = 0$ and which we will place on the imaginary axis (Fig. 4.14); (b) the discontinuities at these cuts are dual:

$$\text{discon } D_{n+1}(i|\omega|) = \text{discon } D_n(-i|\omega|); \quad (4.4.73)$$

for $n = 1$ the situation is different, namely, (c) $D_1(\omega)$ is analytic everywhere in the lower half-plane except at $\omega = \infty$, a point where the function has an essential singularity (Fig. 4.15); it has not yet been proved but there is strong evidence that

$$(d) \text{discon } D_n(i|\omega|) = B_n(|\omega|/\pi) (|\omega|)^{-|\omega|/\pi}, \quad (4.4.74)$$

where $B_n(\omega)$ has an expansion in integral powers of ω ; finally, (e) $B_n(\omega)$ is analytic everywhere except at the cuts and $\omega = \infty$ and has zeros at $\omega = i\pi(k + 1/2)$, $k = 0, 1, \dots$

At $H \gg T$ the same properties are characteristic of $D_n(\omega) \exp \{i\omega [\ln(T/H) - b]\}$, where b is a constant, the only

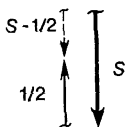


Fig. 4.15. A schematic of the strong-coupling limit at $S \neq 1/2$. The thick solid line represents the impurity spin, the solid line the electron spin, and the dashed line the impurity magnetic moment at $T = H = 0$.

difference being that $\omega = \infty$ is not a singular point. In this case items (d) and (e) are proved.

For an arbitrary magnitude of the ratio T/H there is little hope of finding the $C_n(\omega)$ explicitly. But at $T = 0$ the equations become linear and enable finding $\varepsilon_n = \lim_{T \rightarrow 0} T \phi_n$ analytically (Sec. 4.4.7); the ε_n illustrate the above properties, which determine the dependence of free energy on temperature and magnetic field strength both at $T \gg H$ and at $T \ll H$.

Indeed, at $H \ll T$ and $T \gg T_K$, bending the integration contour into the upper half-plane and by-passing the cut yield

$$F_{\text{imp}} = T \int_0^{\infty} t^{-t} \frac{B_{2S}(t)}{\cos t\pi} e^{-2t \ln(T/T_K)} \frac{dt}{\pi} - T \ln \frac{\sinh[H(2S+1)/T]}{\sinh(H/T)}; \quad (4.4.75)$$

at $\ln(T/T_K) \gg 1$ we arrive at the well-known perturbation-theory expansion in inverse powers of $\ln(T/T_K)$. According to item (e), the poles of $1/\cosh \omega$ are compensated for by the zeros of $B(\omega)$.

Formula (4.4.75) implies that F_{imp} can be expanded in a power series in the invariant charge (4.2.36) for $0 < z \ll 1$:

$$-\frac{1}{z} + \frac{1}{2} \ln |z| = \ln \frac{T_K}{T}. \quad (4.4.76)$$

If we change variables in the integral in (4.4.75), we have

$$T \int_0^{\infty} e^{-tz \ln t - 2t} \frac{B_{2S}(tz, T/H)}{\cos tz\pi} dt = \sum_{n=1}^{\infty} b_n(H/T) z^n. \quad (4.4.77)$$

Below we will use Eq. (4.4.61) to determine the first terms in the expansion in z and compare the result with a perturbation-theory expansion. As usual, the latter, (4.4.77), is an asymptotic expansion

and its coefficients b_n grow like $n!$ as $n \rightarrow \infty$. This readily follows from the fact that the integrand has a finite radius of convergence in t , which is determined by the position of the pole of $1/\cosh tz$.

Now let us turn to the region $T \ll T_K$ and $S > 1/2$. Bending the integration contour into the lower half-plane, we again encounter a cut and poles of $1/\cosh \omega$. At $|z| \ll 1$ the cut plays the main role, while the poles are exponentially small. Whence, according to (4.4.72) and (4.4.73), at $T \ll T_K$ the free energy of the s-d model with $S > 1/2$ is given by an asymptotic expansion in inverse logarithms [33, 38], whose coefficients coincide with those of the expansion at $T \gg T_K$ with $S - 1/2$ substituted for S :

$$F_{\text{imp}}^S = -T \ln \frac{\sinh(SH/T)}{\sinh(H/2T)} + \sum_{n=1}^{\infty} b_n (S - 1/2) z^n (T/T_K) + O(T/T_K). \quad (4.4.78)$$

The logarithmic behavior of the free energy in the strong-coupling limit $g = \infty$ was discovered by Cragg, Lloyd, and Nozieres [58] in the studies of the Hamiltonian (4.2.17) by numerical methods at $n < 2S$.

The duality of the logarithmic expansions in the low- and high-temperature regions can be explained qualitatively in the following way. In each interaction act of a conduction electron with the impurity, the configuration with the electron spin pointing opposite the impurity spin is the most favorable (Fig. 4.15). At high temperatures, when the effective interaction is small, the correlation between the impurity spin and the spin of the electron that has just interacted with the impurity drops off over a time interval that is long compared with the interaction time but still logarithmically small. In the strong-coupling limit (i.e. at $T = 0$) the spins of the impurity and electron "remember" their mutual position after interaction for an infinitely long time. Whence, the actual magnetic moment of the impurity is $S - 1/2$, and we can speak of a ground state of the impurity that is $2S$ -fold degenerate.

The interaction of the electron-impurity system whose spin is now $S - 1/2$ with other conduction electrons can proceed in two ways. First, this may again be the exchange interaction, which produces a "reverse" Kondo effect and leads to logarithmic corrections in (4.4.78). But as (4.4.78) shows, the interaction is now ferromagnetic, i.e. increases with energy. Indeed, an electron whose spin is opposite the impurity spin does not interact with the impurity since its energy level is occupied by the bound electron. But if its spin is parallel to that of the impurity, a spin-flip process is possible (Fig. 4.15). Since this is a second-order process, it leads to a decrease in energy, i.e. the interaction is ferromagnetic [52].

The other possible interaction mechanism is connected with polarization of the electron-impurity system. This mechanism leads to power contributions made by the poles of $1/\cosh \omega$ in (4.4.78). These contributions are exponentially small compared to the contribution provided by integration around the cut.

The situation differs drastically at $S = 1/2$. As we saw in Sec. 4.4.5, $C_1(\omega)$ and, hence, $D_n(\omega)$ are in this case analytic in the lower half-plane, and the logarithmic contribution at $T \ll T_K$ vanishes, $b_n(0) = 0$. Only the poles of $1/\cosh \omega$ contribute, which leads to an expansion in integral powers of T/T_K (4.4.67). However, just as in the case with a Fermi liquid, the expansion is asymptotic:

$$D_1(-i\pi(n+1/2)) \simeq - \int_{-\infty}^{+\infty} e^{-\pi\lambda(n+1/2)} \ln n(e^{-\pi\lambda/2}) d\lambda \simeq n!/\pi.$$

as $n \rightarrow \infty$. We arrive at the same result in the region $H \gg T$; but here the power series in H ($H \ll T_K$, $S = 1/2$) converges. In Sec. 4.4.7 we will obtain an explicit formula for $C_n(\omega)$ at absolute zero; namely (see [30, 32, 33]),

$$\lim_{T/H \rightarrow 0} C_n(\omega, H/T) e^{i\omega(2\pi) \ln(T/H)} = \frac{f_+^n(\omega) f_-^{n-1}(\omega)}{\Gamma(3/2 - i\omega/\pi)(\omega - i\delta)} + 2\pi n \delta(\omega), \quad (4.4.79)$$

where

$$f_{\pm}(\omega) \equiv \left(\frac{i\omega + 0}{e\pi} \right)^{\pm i\omega/\pi} \quad (4.4.80)$$

are functions analytic in the lower and upper half-planes, respectively. Formula (4.4.79) illustrates the analytic properties of $D_n(\omega)$ listed above.

4.4.7 Magnetic Susceptibility at $T = 0$ [30, 32, 33]

Here we will solve Eqs. (4.4.35) and (4.4.36) for $T = 0$ and for an arbitrary magnetic field H .

At $H \neq 0$ the ε_n are finite functions. We introduce the notations

$$\varepsilon_n^+ = \begin{cases} \varepsilon_n & \text{at } \varepsilon_n > 0, \\ 0 & \text{at } \varepsilon_n < 0, \end{cases}$$

$$\varepsilon_n^- = \begin{cases} 0 & \text{at } \varepsilon_n > 0, \\ \varepsilon_n & \text{at } \varepsilon_n < 0. \end{cases}$$

Equation (4.4.36) implies that at $n > 1$ all the ε_n are positive, whence $\varepsilon_n^- = 0$ at $n > 1$. Only ε_1 changes sign, and since it is monotonic, it vanishes at only one point $\lambda = B$, i.e.

$$\varepsilon_1(B) = 0. \quad (4.4.81)$$

As $T \rightarrow 0$,

$$T \ln(1 + e^{\pm \varepsilon_n/T}) \rightarrow \pm \varepsilon_n^\pm \quad (4.4.82)$$

and Eqs. (4.4.35) become linear:

$$\varepsilon_n^+ = nH + \mathbf{A}_{n1} * \varepsilon_1^- + \varepsilon_n. \quad (4.4.83)$$

The fact that all the ε_n^- are zero at $n > 1$ implies that the ground state is a linear combination of only the real solutions to Eqs. (4.3.80). Indeed, according to (4.4.46),

$$\frac{\langle M_n \rangle}{N} = \delta_{n1} \frac{\varepsilon_1^-}{2\epsilon_F} \Big|_{-\infty}^{+\infty} \quad (4.4.84)$$

as $T \rightarrow 0$. It is expedient to write Eqs. (4.4.83) in such a way that ε_n and ε_1^- are expressed in terms of ε_1^+ :

$$\varepsilon_n = (n-1)H + \mathbf{A}_{n1} * \mathbf{A}_{11}^{-1} * \varepsilon_1^+, \quad (4.4.85)$$

$$\varepsilon_1^- = H + \mathbf{A}_{11}^{-1} * \varepsilon_1^+ - \frac{2}{\pi} \epsilon_F \arctan e^{-\pi\lambda/2}. \quad (4.4.86)$$

Just as we did before, we introduce the dimensionless quantity

$$\psi_n(\lambda) = \frac{\varepsilon_n(\lambda - (2/\pi)\ln(H/\epsilon_F))}{H} \quad (4.4.87)$$

and substitute $e^{-\pi\lambda/2}$ for $\arctan e^{-\pi\lambda/2}$ in (4.4.86), so that the region $\lambda \sim \ln(\epsilon_F/H) \gg 1$ provides the main contribution to the integral that determines the impurity part of the energy:

$$E_{\text{imp}}(H) - F_{\text{imp}}(0) = -H \int_{-\infty}^{+\infty} \frac{\psi_{2S}^+(\lambda) d\lambda}{\cosh\{(\pi/2)[\lambda - (2/\pi)\ln(2H/\pi T_K)]\}}. \quad (4.4.88)$$

The function $\psi_1(\lambda)$ satisfies the Wiener-Hopf equation

$$\psi_1(\lambda) = \int_{+b}^{\infty} [R(\lambda - \lambda') \psi_1(\lambda')] d\lambda' + 1 - e^{-\pi\lambda/2}, \quad (4.4.89)$$

where $b = B - (2/\pi)\ln(H/\epsilon_F)$ is an unknown number such that $\psi_1(b) = 0$, (4.4.90)

and the kernel has the form

$$R(\lambda) = \int_{-\infty}^{+\infty} \frac{e^{i\omega\lambda}}{1 + e^{2|\omega|}} \frac{d\omega}{2\pi}. \quad (4.4.91)$$

Equation (4.4.89) can be solved by standard methods (e.g. see [88, 89]).

Let us take the functions

$$\begin{aligned}\psi_1^+(\omega) &= \int_0^\infty e^{i\omega\lambda} \psi_1(\lambda - b) d\lambda, \\ \psi_1^-(\omega) &= \int_{-\infty}^0 e^{i\omega\lambda} \psi_1(\lambda - b) d\lambda,\end{aligned}\quad (4.4.92)$$

which are analytic in the upper and lower half-planes, respectively. Applying the Fourier transform to (4.4.89), we arrive at the boundary-value problem

$$\psi_n(\omega) = e^{-|\omega|(n-1)} \psi_1^+(\omega) + (n-1) 2\pi\delta(\omega), \quad (4.4.93)$$

$$\psi_1^- = \mathbf{A}_{11}^{-1}(\omega) \psi_1^+ + g(\omega),$$

with $\mathbf{A}_{11}^{-1} = \frac{1}{1+e^{-2|\omega|}}$ and $g(\omega) = \frac{e^{-\pi b/2}}{i\omega - \pi/2} - \frac{1}{i\omega - \delta}$. The solution to this problem is given by

$$\psi_1^+(\omega) = \frac{1}{G_+(\omega)} \int_{-\infty}^{+\infty} \frac{d\omega'}{\omega - \omega' + i\delta} \frac{g(\omega')}{G_-(\omega')}, \quad (4.4.94)$$

where the functions G_\pm analytic and without zeros in the upper and lower half-planes, respectively, make the kernel separable:

$$\mathbf{A}_{11}^{-1} = G_+ G_-. \quad (4.4.95)$$

These two functions are equal:

$$G_+(\omega) = G_-(-\omega) = V 2\pi \frac{f_+(\omega)}{\Gamma(1/2 - i\omega/\pi)}, \quad G(\infty) = 1,$$

and the functions $f_\pm(\omega)$ that make $e^{-|\omega|}$ separable,

$$e^{-|\omega|} = f_+(\omega) f_-(\omega), \quad (4.4.96)$$

are defined in (4.4.80).

We can easily evaluate the integral in (4.4.94). Bending the integration contour into the lower half-plane, we have

$$\psi_1^+ = \frac{2\pi}{G_+(\omega)} \left[\frac{1}{\omega + i\delta} \frac{1}{G(0)} - \frac{e^{-\pi b/2}}{\omega + i\pi/2} \frac{1}{G_-(i\pi/2)} \right]. \quad (4.4.97)$$

Now it is easy to find the dependence of the impurity part of the ground-state energy on the magnetic field strength. But first we have to find b . For this we use the formula

$$\psi_1^+(b) = -i \lim_{\omega \rightarrow \infty} \omega \psi_1^+(\omega). \quad (4.4.98)$$

Whence

$$e^{-\pi b/2} = \frac{G_-(i\pi)}{G_-(0)}. \quad (4.4.99)$$

Therefore, according to (4.4.97) and (4.4.99),

$$\psi_n(\omega) = (n-1) \delta(\omega) H + \frac{e^{-(n-1)|\omega|} f_+(\omega)}{G_-(0) G_+(\omega)} \frac{i\pi}{(\omega+i\delta)(\omega+i\pi)} \quad (4.4.100)$$

and, finally, the magnetic moment of the impurity, $M = -dE/dH$, is

$$M_S(H) = S - \frac{1}{2} + \frac{i}{4\pi^{3/2}} \int_{-\infty}^{+\infty} e^{-2i\omega[\ln(2H/\pi T_K) - b]} \times \Gamma(1/2 + i\omega/\pi) \frac{f_+^{2S}(\omega) f_-^{2S-1}(\omega)}{\omega + i\delta} d\omega. \quad (4.4.101)$$

In Sec. 4.4.6 we mentioned the analytic properties of the integrand. We will illustrate these properties by the example of formula (4.4.101).

The integral in (4.4.101) has two different representations, depending on the sign of $\ln(H/\tilde{T}_K)$, with $\tilde{T}_K = (\pi/2)e^b T_K$. At $H > \tilde{T}_K$ the most convenient integration contour includes the cut of f_-^{2S-1} (Fig. 4.14):

$$M_S(H > \tilde{T}_K) = S - \frac{i}{2\pi^{3/2}} \int_0^\infty \Gamma(1/2 + \omega) \left(\frac{\omega}{e}\right)^{-\omega} \times \frac{\sin 2\pi S \omega}{\omega} e^{-2\omega \ln(H/\tilde{T}_K)} d\omega. \quad (4.4.102)$$

If we introduce the invariant charge z , i.e.

$$-\frac{1}{z} + \frac{1}{2} \ln z = \ln \frac{H}{\tilde{T}_K}, \quad (4.4.103)$$

we arrive at an asymptotic series in z :

$$M_S(H > \tilde{T}_K) = S \left[1 + \sum_{n=1}^\infty a_n(S) z^n (H/\tilde{T}_K) \right]. \quad (4.4.104)$$

The first term in this expansion with $a_1 = -1/2$ coincides with the term known from perturbation theory.

At $H < \tilde{T}_K$ the integration contour includes the cut of f_+^{2S} , the poles of the gamma function, and the pole at $i\delta$:

$$M_S(H < \tilde{T}_K) = S - \frac{1}{2} - \frac{1}{2\pi^{3/2}} \int_0^\infty \Gamma(1/2 + z\omega) \times \left(\frac{\omega}{e}\right)^{z\omega} \frac{\sin[(2S-1)\pi z\omega]}{\omega} e^{-2\omega} d\omega + \sum_{n=1}^\infty \left(\frac{H}{\tilde{T}_K}\right)^{2n+1} \gamma_n. \quad (4.4.105)$$

With exponential accuracy,

$$M_S (H < \tilde{T}_K) = \left(S - \frac{1}{2}\right) \left[1 + \sum_{n=1}^{\infty} a_n \left(S - \frac{1}{2}\right) z^n\right]. \quad (4.4.106)$$

All the expansion coefficients in (4.4.106) coincide with those of the high-temperature expansion if we substitute $S - 1/2$ for S . In the ground state the impurity remains magnetic:

$$\lim_{H \rightarrow 0} M(H) = S - 1/2. \quad (4.4.107)$$

If $S = 1/2$, only the poles contribute to the integral in (4.4.101) (see Fig. 4.15) and we have

$$M_{1/2}(H) = \sum_{n=1}^{\infty} \frac{1}{\sqrt{\pi}} \left(\frac{n+1/2}{e}\right)^{-(n+1/2)} (-1)^n \left(\frac{H}{\tilde{T}_K}\right)^{2n}. \quad (4.4.108)$$

Interestingly, the series (4.4.108) is absolutely convergent.

To conclude this section we note that the linear equations built here are the first approximations in a power series in T/H when T is much lower than H . A regular perturbation theory in powers of T/H has been built in [36]. Below we consider the other limiting case.

4.4.8 Solution of Equations (4.4.35) and (4.4.36) by an Iterative Method at $T \gg H$ [36, 38] and Perturbation Theory

In Sec. 4.4.6 we showed that $D_1(\omega)$ is analytic in the lower halfplane. The values of this function at $\omega = i\pi(1/2 - n)$, $n = 1, 2, \dots$, determine the coefficients in the expansion of the heat capacity of an impurity with $S = 1/2$ in powers of T/T_K . Except for $D(-i\pi/2) = \pi^2/3$, there is little hope of finding these quantities analytically.

The situation is quite different for the expansion in inverse logarithms both at $T \gg T_K$ and at $T \ll T_K$ when $S \neq 1/2$ [see (4.4.76) and (4.4.77)]. Indeed, the coefficients of the leading powers of z are determined by the behavior of $D_{2S}(\omega)$ at small values of ω or by the behavior of $\phi_{2S}(\lambda)$ as $\lambda \rightarrow \pm\infty$ and can be found from Eqs. (4.4.36) by an iterative method. Here we will build the first iteration of Eqs. (4.4.36) and show that

$$\begin{aligned} & \text{discon } D_{2S} \left(i|\omega|, \frac{H}{T} \rightarrow 0 \right) \\ &= \frac{2\pi}{3} S(S+1) \left(\frac{H^2}{T^2} - 4\pi\omega^2/\pi \right) (1 - |\omega|/\pi \ln |\omega|/\pi) \end{aligned} \quad (4.4.109)$$

as $|\omega| \rightarrow 0$. This formula, according to Sec. 4.4.6, leads to asymptotic expressions of the type (4.2.38)-(4.2.40) known from perturbation theory.

To build the first iteration we introduce the functions $C_n = -\ln n(\phi_n)$. Then Eqs. (4.4.36) can be written as

$$C_n = \ln \{1 + \exp [s^* (C_{n+1} + C_{n-1}) \delta_{n1} e^{-x\pi/2}]\} \quad (4.4.110)$$

with $C_0 = 0$. The first approximation to the C_n is their asymptotics at $\lambda \rightarrow \pm\infty$:

$$C_n^0 = \begin{cases} 2 \ln \varphi_n & \text{at } x > 0, \\ 2 \ln \varphi_{n-1} & \text{at } x < 0, \quad n \neq 1, \end{cases} \quad (4.4.111)$$

and

$$C_1^0 = \ln (1 + e^{-x\pi} \varphi_1) \text{ at } x < 0.$$

Let us find the next approximation:

$$d_n = C_n - C_n^0.$$

Linearizing Eqs. (4.4.110) and going over to Fourier transforms, we have*

$$d_n^+ \frac{\varphi_n^2}{\varphi_{n-1}\varphi_{n+1}} + d_n^- \frac{\varphi_{n-1}^2}{\varphi_{n-2}\varphi_n} = s^* (d_{n+1} + d_{n-1}), \quad n \geq 3, \quad (4.4.112)$$

$$d_2^+ \frac{\varphi_2^2}{\varphi_1\varphi_3} + d_2^- \frac{\varphi_1^2}{\varphi_2} = s^* (d_3 + d_1^+) + Y_-, \quad (4.4.113)$$

$$d_1^+ \frac{\varphi_1^2}{\varphi_2} = s^* d_2 + Y_+, \quad (4.4.114)$$

where

$$Y_{\pm} \simeq \frac{\pm i}{\omega \pm i\delta}$$

and

$$d^+ = \int_0^{\infty} d(x) e^{i\omega x} dx, \quad d^- = \int_{-\infty}^0 d(x) e^{i\omega x} dx. \quad (4.4.115)$$

We did not write Eq. (4.4.114) for d_1^- because this quantity is not small. Solving the boundary-value problem (4.4.112) and (4.4.114) as $\omega \rightarrow 0$ leads to (4.4.109), since

$$D_n(\omega) = d_n(\omega) + O(\omega^3). \quad (4.4.116)$$

Here we will obtain only the principal order in $|\omega|$ in (4.4.109). To this end we neglect the influence of the regions $\lambda > 0$ and $\lambda < 0$ on each other. In other words in Eqs. (4.4.112) through (4.4.114)

* We employ the identity $\varphi_n^2 - 1 = \varphi_{n+1}\varphi_{n-1}$.

we leave only terms with d^+ or terms with d^- . Then these equations transform into equations for the d_n^\pm , defined on the real axis:

$$\begin{cases} d_n^+ \frac{\varphi_n^2}{\varphi_{n+1}\varphi_{n-1}} = s^* (d_{n+1}^+ + d_{n-1}^+), \\ d_1^+ \frac{\varphi_1^2}{\varphi_2} = s^* d_2^+ + Y_+ \end{cases} \quad (4.4.117)$$

and

$$\begin{cases} d_n^- \frac{\varphi_{n-1}^2}{\varphi_{n-2}\varphi_n} = s^* (d_{n+1}^- + d_{n-1}^-), \\ d_2^- \frac{\varphi_1^2}{\varphi_2} = s^* d_3^- + Y_- \end{cases} \quad (4.4.118)$$

Hence, we see that at least in this approximation $d_n^+(\omega) = d_{n+1}^-(\omega)$ and the duality of the coefficients of the expansion in z at $T \gg T_K$ and $T \ll T_K$ described in Sec. 4.4.6 occurs. It can be proved that this is true for all orders of perturbation theory. The recurrence equations (4.4.117) and (4.4.118) are encountered in studies of high-temperature expansion for the one-dimensional Heisenberg model [85]. Their solution is

$$d_n^+ = -\frac{2 \cosh \omega}{\varphi_1 \varphi_n} \frac{i}{\omega + i\delta} (\varphi_{n+1} e^{-n|\omega|} - \varphi_{n-1} e^{-(n+2)|\omega|}). \quad (4.4.119)$$

This implies that $d_n(\omega)$ and, hence, $D_n(\omega)$ both have a discontinuity that passes through point $\omega = 0$. Retaining in (4.4.119) the leading terms as $\omega \rightarrow 0$, we arrive at (4.4.109).

Therefore, the impurity part of the free energy is

$$\begin{aligned} F_{\text{imp}} = & \left\{ \begin{array}{l} T \gg T_K, \quad -T \ln(2S+1) - T \frac{S(S+1)}{3} \\ T \ll T_K, \quad -T \ln 2S - T \frac{S^2 - 1/4}{3} \end{array} \right\} \\ & \times \left[\frac{H^2}{2T^2} \left(1 - \frac{1}{\ln(T/T_K)} \right) - \frac{\pi^2}{\ln^3(T/T_K)} \right]. \end{aligned} \quad (4.4.120)$$

In conclusion we note that the more precise the iteration the greater the number of function φ_n . Indeed, as n increases, the difference between the asymptotics at $\lambda \rightarrow \pm\infty$ and at $H/T \rightarrow 0$ becomes smaller. Therefore, the parameter in the perturbation-theory approach is not only small $|\omega|$'s but large n 's as well. At $n \gg 1$ we can retain $\ln(T/T_K)$ in (4.4.120). Whence at $S \gg 1$ we have

$$\begin{aligned} F_{\text{imp}} \simeq & -T \ln 2S + \frac{T}{2\pi} \left(\arctan \frac{\pi S}{\ln(T/T_K)} - \frac{\pi \ln(T/T_K)}{\ln^2(T/T_K) + (\pi S)^2} \right) \\ & - \frac{H^2}{6T} S^2 \left(1 - \frac{1}{2S\pi} \ln \frac{\pi S}{\ln(T/T_K)} \right). \end{aligned}$$

This formula is equally suited for $T \gg T_K$ and $T \ll T_K$. The next iterations of Eqs. (4.4.36) are very complex.

4.4.9 Supplementary Discussion

In Chaps. 4.3 and 4.4 we followed the long path from quantum field theory to ordinary integral equations that determine the properties of the system. The nonlinear equations (4.4.36) are, of course, very complex. Nevertheless, we saw how naturally the universality and character of the thermodynamic functions follow from these equations for regions that we could not dream of studying by perturbation-theory techniques, namely $\max(T, H) \ll T_K$. We can hope that numerical solution of these equations would make it possible to determine the function $F_{\text{imp}}(T, H)$ in the entire T, H -plane. And there is no reason why numerical solution should pose any real difficulties.*

As $T \rightarrow 0$, the nonlinear equations become linear on a semiaxis. Fortunately, the problem becomes solvable analytically for any magnetic field strength, and the answer can be expressed as a combination of integrals and be fully investigated.

At $T \ll H$ there exists a simple iteration scheme of finding the coefficients of the power expansion in T/H for any value of H/T_K [36]; we will not discuss this scheme here. The other limiting case, $T \gg H$, as the case with $S \gg 1$, requires a more detailed study than that performed in Sec. 4.4.8. An important task is to prove items (d) and (e) of Sec. 4.4.6.

In this article we do not touch on the s-d model with anisotropic exchange,

$$\mathcal{H}_{\text{int}} = J_{\parallel} \sigma^z S^z + J_{\perp} (\sigma^x S^x + \sigma^y S^y), \quad (4.4.124)$$

at $S = 1/2$, which was solved in [32]. There we studied only the segment $J_{\parallel} > J_{\perp}$. When $|J_{\parallel}| < J_{\perp}$, there appears, besides T_K , another energy scale connected with the anisotropy. One would expect interesting results for this region, but as yet the ground state is not known for this case. Equations (4.4.36) give a correct description of the universal dependencies of the physical quantities on T/T_K and H/T_K ; the coupling constant J enters all final expressions only through T_K , but generally the dependence of T_K on J is nonuniversal because both the dependence of the invariant charge z_0 on J (4.2.28) and the Gell-Mann—Low equation (4.2.35) are nonuniversal. However, the exponential and pre-exponential terms in

$$T_K = \epsilon_F \sqrt{J} e^{-1/J\rho(\epsilon_F)} [1 + O(J)]$$

are always universal. This constitutes the basic difficulty of the above theory: in the formula defining T_K , (4.4.60), the required

*. A good algorithm for solving (4.4.36) numerically appears in problems with anisotropic exchange. Due to strong anisotropy, the number of equations in (4.4.36) becomes finite [36].

pre-exponential factor is absent and, therefore, is no way in which we can expand in powers of J the various physical quantities, which can be expanded in powers of the invariant charge z . Actually, the coupling constant $J_{\text{p.t}}$ of the perturbation theory is not an analytic function of the coupling constant J in formula (4.4.60):

$$\frac{1}{J_{\text{p.t}}} = \frac{1}{J} + \frac{1}{2} \ln J.$$

This fact has no satisfactory explanation as yet. It is clear, however, that this is the result of the linearity of the spectrum. It can be shown that the limit $U \gg V^2$ in Bethe's equations for the Anderson model leads to Eqs. (4.4.7) and (4.4.8) for the s-d model but with a different coefficient of the first term on the left-hand side of Eq. (4.4.8), i.e. with $N\sqrt{J}$ substituted for N . This leads to a correct pre-exponential factor in T_K .

4.5 SOLUTION FOR THE n -FOLD DEGENERATE EXCHANGE MODEL

In Sec. 4.2.5 we saw that Ce and Yb impurities are described by an n -fold degenerate exchange Hamiltonian

$$\mathcal{H} = \sum_{k,j} (k - k_F) c_{kj}^\dagger c_{kj} + \frac{1}{N} \sum_{j=1, \dots, n} J c_{kj}^\dagger c_{k',j} \mathbf{P}_{jj'} + \sum_j E_j \mathbf{P}_j, \quad (4.5.1)$$

where

$$J = -v^2/\epsilon_f,$$

and E_j is the energy separation of the lines in the multiplet characterized by total angular momentum $J = n/2 - 1$ (this energy is due to the presence of a crystal field).

We remark here that we have neglected the anisotropy of the exchange interaction. This can be done if the crystal field is weaker than the energy of the f level: $-\epsilon_f \gg E_j$. Therefore, effects associated with the nonsphericity of the surroundings is accounted for by the last term in (4.5.1).

We apply the Bethe-ansatz technique to the Hamiltonian (4.5.1). The details of such an approach were discussed above using the simple s-d exchange model, which at $S = 1/2$ is a particular case of the Hamiltonian (4.5.1) with $n = 2$. Hence the brevity of our present discussion.

4.5.1 The Bethe Ansatz

When there is no crystal field, the Hamiltonian is invariant under $SU(n)$ -transformations. We introduce the permutation

operator that acts in n -by- n dimensional space; namely,

$$P_{\alpha'\beta'}^{\alpha\beta} = \delta_{\alpha\beta'}, \quad \delta_{\beta\alpha'}, \quad \alpha, \beta, \alpha', \beta' = 1, \dots, n. \quad (4.5.2)$$

Obviously, the scattering matrix of an electron with a total-angular-momentum component α by an impurity in state β is

$$R_{\alpha'\beta'}^{\alpha\beta} = (e^{iJP})_{\alpha'\beta'}^{\alpha\beta}. \quad (4.5.3)$$

As in the case with the s-d exchange model (Sec. 4.3.1), in view of the linearity of the conduction-electron spectrum, the permutation operator can be chosen as the S-matrix of noninteracting particles, so

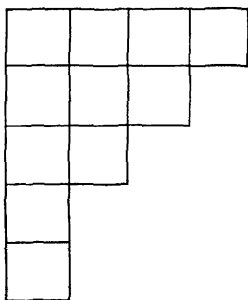


Fig. 4.16. Young's diagram for the representation of the permutation group $[5, 3, 2, 1]$ ($N = 11$, $n = 4$).

that the factorization equations (4.3.46) are valid. Once more Bethe's hypothesis (4.3.25) is valid, but now we must assume that the indices in (4.3.25) and (4.3.46) run through n instead of two values.

The periodic boundary conditions imply diagonalizing the matrix

$$\mathbf{T}_j = \mathbf{P}_{jj+1} \mathbf{P}_{jj+2} \dots \mathbf{P}_{jN} \mathbf{P}_{j1} \dots \mathbf{P}_{jj-1} \mathbf{P}_{j0}. \quad (4.5.4)$$

The diagonalization technique for the \mathbf{T} -operator with an $SU(n)$ -symmetry was developed by Sutherland [90]. His method enabled generalizing the solution with $n = 2$ to include a solution with arbitrary n . Another version of this technique one can find in [91, 92].

The number of particles with a given component of orbital angular momentum j , the impurity included, is obviously conserved in scattering. Therefore, the symmetry of the system's state is described by a Young diagram with vertical columns of length m_j and corresponds to a representation of the permutation group $[n - m_1, m_1 - m_2, \dots, m_{n-2} - m_{n-1}, m_n]$ (see Fig. 4.16). The difference between the heights of adjacent columns, $m_{j-1} - m_j$, gives the number of particles with orbital-angular-momentum component $(n - 1)/2 - j$ (we have put $m_0 = n$ and $m_n = 0$).

Diagonalization of \mathbf{T} leads to the following Bethe-Ansatz hierarchy:

$$\begin{aligned}
 e^{ik_i L} &= \prod_{k=1}^{m_1} \left(\frac{\lambda_k^{(1)} + i/2}{\lambda_k^{(1)} - i/2} \right), \\
 \prod_{p=1}^{m_{j-1}} \left(\frac{\lambda_k^{(j)} - \lambda_p^{(j-1)} + i/2}{\lambda_k^{(j)} - \lambda_p^{(j-1)} - i/2} \right) &\times \prod_{q=1}^{m_{j+1}} \left(\frac{\lambda_k^{(j)} - \lambda_q^{(j+1)} + i/2}{\lambda_k^{(j)} - \lambda_q^{(j+1)} - i/2} \right) \\
 &= - \prod_{l=1}^{m_j} \left(\frac{\lambda_k^{(j)} - \lambda_l^{(j)} + i}{\lambda_k^{(j)} - \lambda_l^{(j)} - i} \right), \quad (4.5.5)
 \end{aligned}$$

where

$$\lambda_p^0 = \delta_{p1} \frac{1}{g}.$$

Here the energy of the state is $E = \sum_j k_j$.

4.5.2 Magnetic Susceptibility at $T = 0$

Just as in the case with $n = 2$, the solutions of Eqs. (4.5.5) lie generally in the complex $\lambda^{(j)}$ -planes. But in the ground state with given $\{m_j\}$ all $\lambda^{(j)}$'s are real and vary in the intervals $(-\infty, B_j)$, where the B_j are functions of the numbers $\{m_j\}$. In the continuous limit ($m_j \rightarrow \infty$, $L \rightarrow \infty$, $m_j/N = \text{const}$, and $\pi N/L = \infty$) the system is described by densities of the number of "particles" $\rho^{(j)}(\lambda)$ in the λ -space (these functions were defined in Sec. 4.4.1). The $\rho^{(j)}$ are nonzero in the intervals $(-\infty, B_j)$ and satisfy the following equations:

$$\begin{aligned}
 \sum_{k=1}^{n-1} \int_{-\infty}^{B_k} a_{jk}(\lambda - \lambda') \rho^{(k)}(\lambda') d\lambda' \\
 = \frac{2}{\pi} \delta_{j1} \left(\frac{1}{4\lambda^2 + 1} + \frac{N^{-1}}{4(\lambda - 1/g)^2 + 1} \right). \quad (4.5.6)
 \end{aligned}$$

The Fourier transform of the kernel a_{jk} is

$$a_{jk}(\omega) = \left[\delta_{jk} - \frac{1}{2 \cosh(\omega/2)} (\delta_{j, k-1} + \delta_{j, k+1}) \right] (1 + e^{-|\omega|}). \quad (4.5.7)$$

The number of particles with the angular-momentum component j is

$$n^{(j)} \equiv m\left(\frac{n-1}{2}-j\right) - n_i\left(\frac{n+1}{2}-j\right) = \int_{-\infty}^{B\frac{n-1}{2}-j} \rho\left(\frac{n-1}{2}-j\right)(\lambda) d\lambda \\ - \int_{-\infty}^{B\frac{n+1}{2}-j} \rho\left(\frac{n+1}{2}-j\right)(\lambda) d\lambda \quad (4.5.8)$$

(we assume that $\rho^{(0)}(\lambda) = \delta(\lambda)$). Equations (4.5.6) and (4.5.8) determine the B_j as functions of $\{n_j\}$.

Before calculating the magnetic susceptibility we must note the following. To the Hamiltonian (4.5.1) we add the term

$$-g_L H J_z, \quad (4.5.9)$$

where $J_z = \sum j n^{(j)}$ is the z -component of the system's total angular momentum, and g_L is the Landé factor of the impurity. We then calculate the dependence of the energy on the magnetic field strength. However, we must bear in mind that (4.5.9) differs from the correct Zeeman term for conduction electrons, which as is known is

$$H(2\mathbf{S} + \mathbf{L}). \quad (4.5.10)$$

The point is that we will be interested only in the impurity part of the magnetic susceptibility, and this part at $J \ll 1$ is a weak function of the magnetism of free electrons. The easiest way to calculate the magnetic susceptibility of an impurity is as follows.

Since Eqs. (4.5.6) are linear, their solution can be written as

$$\rho = \rho_{\text{host}} + \frac{1}{N} \rho_{\text{imp}}, \quad (4.5.11)$$

where ρ_{host} satisfies Eqs. (4.5.6) at $g = 0$, i.e. when the last term on the right-hand side of (4.5.6) is absent. Just as in the case with $n = 2$, it can easily be shown that $\rho_{\text{host}}^{(j)}$ describes correctly a gas of free fermions consisting of particles with n colors. We can therefore readily tell how many particles of each color there are at $T = 0$ in the first (in $1/N$) order:

$$n_{\text{host}}^{(j)} = \frac{Hj + E_j}{4\epsilon_F}. \quad (4.5.12)$$

This formula together with conditions (4.5.8) determine the B_j as functions of H and E_j .

Since we have found (4.5.7) on the condition that the energy is minimal, there is no need to calculate the B_j with a higher accuracy (in $1/N$). If we did this, the energy would change by a quantity of the order $1/N^2$.

Therefore, the magnetic moment of the impurity is

$$J_{\text{imp}}(H) = \sum_{j=-J}^J j \left(\int_{-\infty}^{B_{J-j}} \rho_{\text{imp}}^{(J-j)}(\lambda) d\lambda - \int_{-\infty}^{B_{J-j+1}} \rho_{\text{imp}}^{(J-j+1)}(\lambda) d\lambda \right). \quad (4.5.13)$$

The system of Wiener-Hopf equations (4.5.6) can easily be solved only when the B_j do not depend on j . Even neglecting effects associated with the crystal field (assuming, for instance, that $T_K \gg \gg \max(E_j - E_{j'})$) we still have to deal with different B_j 's. Only when $n = 2, 3$, in view of the symmetry of the Hamiltonian (4.5.1) with respect to the substitution of $-j$ for j , do the limits of integration in Eqs. (4.5.6) coincide. In this case ($n = 2, 3$)

$$J(H) = -\frac{n-1}{4\pi^2} \sin \frac{\pi}{2n} \int_{-\infty}^{+\infty} \frac{d\omega}{i\omega-0} \left(-\frac{i\omega}{4\pi e} \right)^{-i\omega/2\pi} \\ \times \Gamma\left(\frac{1}{2n} + \frac{i\omega}{4\pi}\right) \Gamma\left(1 - \frac{1}{2n} + \frac{i\omega}{4\pi}\right) \exp\left(-\frac{i\omega n}{4\pi} \ln \frac{H}{aT_K}\right), \quad (4.5.14)$$

where

$$a = \frac{4\pi \cos(\pi/2n)}{n-1} \frac{(2en)^{-1/n}}{\Gamma(1/n)}, \quad T_K = \frac{2}{\pi} \epsilon_F e^{-1/gn}. \quad (4.5.15)$$

The integrand in (4.5.14) has a cut in the upper half-plane.

For $n > 3$ the B_j are different and we can hardly hope to solve Eqs. (4.5.6) analytically. Nevertheless, we can establish some of the properties of $J(H)$ for arbitrary n . Namely, at $H \gg T_K$ we have an asymptotic expansion in powers of the invariant charge z , where

$$\frac{1}{nz} - \ln|z| = \ln \frac{H}{T_K}, \\ J_{\text{imp}} = \frac{n-1}{2} [1 - z(H) + O(z^2)]. \quad (4.5.16)$$

At $H \ll T_K$ the function $J(H)$ is analytic in H :

$$J_{\text{imp}} = H \chi_{\text{imp}}(0) + \sum_{n=1}^{\infty} b_n (H/T_K)^{2n+1}. \quad (4.5.17)$$

Formula (4.5.17) means that there is total compensation of impurity angular momentum $J_{\text{imp}}(H \rightarrow 0) \rightarrow 0$, while the magnetic susceptibility remains finite (nonzero). To find its value at $H = 0$ and the solution at $n = 2$, we consider Eqs. (4.5.6) as $g \rightarrow \infty$. We have

$$\chi_{\text{imp}}(H = 0)/\chi_{\text{host}}(H = 0) = \frac{2}{\pi} \epsilon_F/T_K. \quad (4.5.18)$$

The susceptibility χ_{host} of free fermions with the Zeeman term (4.5.9) can easily be calculated. We have

$$\chi_{\text{host}} = \frac{n(n^2-1)}{24\zeta_F} (g_L \mu_B)^2. \quad (4.5.19)$$

Whence

$$\chi_{\text{imp}} = \frac{n(n^2-1)}{12\pi T_K} (g_L \mu_B)^2. \quad (4.5.20)$$

Unfortunately, this line of reasoning does not enable calculating the next (higher-order) terms in (4.5.17). We note that at $n = 3$ it follows from formula (4.5.14) that $b_1 = 0$.

4.5.3 Thermodynamics

The solutions to Eqs. (4.5.5) generally lie in the complex plane and group into strings

$$\lambda_{p, \alpha, k}^{(j)} = \lambda_{p, \alpha}^{(j)} + i(p+1-2k), \quad (4.5.21)$$

$$k = 1, \dots, p.$$

In the continuous limit the distribution of the centers of the strings is described by the densities of "particles" $\rho_p^{(j)}$ and "holes" $\tilde{\rho}_p^{(j)}$ (for $n = 2$ the definition of these quantities is given in Sec. 4.4.1). In terms of these functions Eqs. (4.5.5) must be written as

$$\tilde{\rho}_p^{(j)}(\lambda) + \mathbf{A}_{pq} * a_{jk} * \rho_q^{(k)} = \mathbf{A}_{1p} * s * a_{jl} \sin(\pi l/n),$$

$$j, k, l = 1, \dots, n; \quad p, q = 1, 2, \dots. \quad (4.5.22)$$

Here $*$ stands for the contraction operator, and the indices that appear twice are summed over. The matrices \mathbf{a} and \mathbf{A} are defined in (4.4.25), (4.4.26), and (4.5.7). Curiously, the matrix elements $(\mathbf{A}^{-1})_{jk}$ and a_{jk} are proportional to each other. The difference between the two is that \mathbf{a} is a finite matrix of rank n while \mathbf{A} is infinite.

We minimize the free energy with respect to ρ and $\tilde{\rho}$ and find the equilibrium values of ρ and $\tilde{\rho}$. Calculations that are quite similar to those done in Secs. 4.4.1 and 4.4.2 for $n = 2$ lead to the following results.

We introduce the notation

$$\mathbf{B}_{\alpha\beta}(\lambda) \equiv (\mathbf{A}^{-1})_{\alpha\beta} = \delta_{\alpha\beta} \delta(\lambda) - \frac{1}{2 \cosh \pi \lambda} (\delta_{\alpha, \beta+1} + \delta_{\alpha, \beta-1}) \quad (4.5.23)$$

and the dimensionless function

$$\varepsilon_p^{(j)} = \ln \frac{\tilde{\rho}_p^{(j)} [\lambda - (n/2\pi) \ln(\zeta_F/T)]}{\rho_p^{(j)} [\lambda - (n/2\pi) \ln(\frac{2}{\pi} \zeta_F/T)]}. \quad (4.5.24)$$

Then the $\varepsilon_p^{(j)}$ satisfy the following equations (cf. (4.4.35)):

$$\mathbf{B}_{jk} * \ln(1 + e^{-\varepsilon_p^{(k)}}) = \mathbf{B}_{pq} * \ln(1 + e^{\varepsilon_q^{(j)}}) + \delta_{p1} \frac{\sin(\pi j/n)}{\pi} e^{-2\pi\lambda/n} + O(T/\epsilon_F), \quad (4.5.25)$$

$$\lim_{p \rightarrow \infty} \varepsilon_p^{(j)}/p = H/T.$$

The impurity fraction of the free energy and the free energy of conduction electrons are, respectively,

$$F_{\text{imp}} = -T \sum_{j=1}^{n-1} \int_{-\infty}^{+\infty} d\lambda \rho_0^{(j)} \left(\lambda - \frac{n}{2\pi} \ln \frac{T_K}{T} \right) \ln(1 + e^{\varepsilon_1^{(j)}}), \quad (4.5.26)$$

$$\frac{F_{\text{host}}}{N} = -\frac{T}{2\epsilon_F} \int_{-\epsilon_F}^{\infty} dk \ln(1 + e^{-k/T}) - T \sum_{j=1}^{n-1} \int_{-\infty}^{+\infty} d\lambda \rho_0^{(j)} \left(\lambda - \frac{n}{2\pi} \ln \frac{\epsilon_F}{T} \right) \ln(1 + e^{\varepsilon_1^{(j)}}), \quad (4.5.27)$$

where

$$\rho_0^{(j)}(\lambda) = \frac{1}{n} \frac{\sin(\pi j/n)}{\cosh(2\pi\lambda/n) - \cos(\pi j/n)}. \quad (4.5.28)$$

The first term on the right-hand side of (4.5.27) is the free energy of charge excitations. Just as the case with $n = 2$, it can easily be shown that

$$\frac{F_{\text{host}}}{N} = \frac{\pi^2}{6} \frac{T^2}{\epsilon_F} n, \quad (4.5.29)$$

which is the free energy of a gas of noninteracting fermions of n colors. Equations (4.5.25) and (4.5.26) imply that the integrals

$$\int_{-\infty}^{+\infty} \ln(1 + e^{\varepsilon_1^{(j)}}) e^{-2\pi k\lambda/n} d\lambda \quad (4.5.30)$$

converge. Therefore, at $T \ll T_K$ the impurity fraction of the free energy can be expanded in a power series in T/T_K :

$$\frac{F_{\text{imp}}}{T} = -\gamma \frac{T}{T_K} + \sum_{n=1}^{\infty} b_n \left(\frac{T}{T_K} \right)^{2n+1}, \quad (4.5.31)$$

with the entropy at $T = 0$ being zero. This means that the ground state of the impurity is a singlet. Comparing Eqs. (4.5.27) and (4.5.26), we can easily find the heat capacity as $T \rightarrow 0$. As before,

we see that

$$\frac{C_{\text{imp}}}{C_{\text{host}}} = \frac{\epsilon_F}{T_K} \frac{n-1}{n} \frac{1}{\pi}; \quad (4.5.32)$$

whence, according to (4.5.29), we find that

$$c_{\text{imp}} = \frac{\pi}{3} T \frac{n-1}{T_K} \quad \text{and} \quad \gamma = \frac{\pi}{6} (n-1). \quad (4.5.33)$$

Formulas (4.5.20) and (4.5.33) enable writing a relationship that generalizes the Wilson-Nozieres formula for $n = 2$:

$$\lim_{T \rightarrow 0} \frac{C_{\text{imp}}}{T \chi_{\text{imp}}} = \frac{4\pi^2}{n(n+1)}. \quad (4.5.34)$$

The same result was obtained by Nozieres and Blandin [52]. The approach they used was phenomenological and was developed by Nozieres in [19].

Just as in the case with $n = 2$ (Sec. 4.4.7), the first terms in a perturbation-theory series for $T \gg T_K$ can be found by iterating Eqs. (4.5.25) for an arbitrary n . But the calculations become very cumbersome.

4.5.4 Discussion

The numerical investigation of Eq. (4.5.28) can be used to explain the experimental data. The simplest way to do this would be to verify (4.5.34). Unfortunately, there have been no experiments with dilute alloys with rare-earth impurities, for which the Kondo temperature would be so high that the crystal field could be neglected. High Kondo temperatures were observed in concentrated systems to which the present theory can be applied only for temperatures that are greater than the characteristic energy of RKKY interaction. It would be especially interesting to build an $1/n$ -expansion within the framework of Bethe's method and investigate its convergence.

4.6 CONCLUSION

Although I have named this article "An exact solution of the Kondo problem", it would be more correct to say it clears a path to such a solution. Indeed, the solution of many theoretical problems here is only planned, and a detailed analysis of the experimental situation has yet to come. Still, we will enumerate some striking problems that have yet to be solved.

First, this is the Anderson model. This is a completely integrable model, and Bethe's equations for it were derived in [34]. There are two reasons why we did not include the solution to this problem in the present article. First, we wished to speak only of the Kondo

effect and, second, Bethe's equations for the Anderson model have not been studied except for the case with $U \ll V^2$ [95]. Also, there is no satisfactory derivation of Bethe's equations for the s-d model, which should be obtained in the limit $U \gg V^2$. Nevertheless, it is the author's opinion that the study of these equations is a promising problem that could lead to interesting results.

The complexities in studying these equations at $U \gg V^2$ is due first of all to the uncertainty originating from the approximation of the band-electron spectrum by a linear spectrum unbounded from below. In the s-d model there is no such difficulty because the charge excitations do not interact with the spin excitations, and the spin-excitation spectrum, due to which the Kondo effect is present, is bounded. In the Anderson model the two types of excitation interact and Bethe's equations require completing their definition.

The linear spectrum is also the cause of other difficulties and some remarkable properties. Indeed, the effective Hamiltonian (4.3.22) does not allow for backward scattering. It is easy to understand that as a result all quantities are linear in impurity concentration. In this model there is no RKKY interaction between the impurities, since there is no reflected electronic wave. For the same reason, the electrons in the effective one-dimensional crystal are distributed uniformly over the entire volume and are not localized near the impurity. Indeed, the density of particles with the spin component σ in a one-dimensional system with a single impurity is given by

$$\rho^\sigma(x) = \rho_0 + \text{Im} \int_0^\infty \frac{d\omega}{\pi} G_0(x, \omega + i0) G_0(-x, \omega + i0) t^\sigma(\omega) n(\omega + i0),$$

where ρ_0 is the particle density in the system without the impurity, $t^\sigma(\omega)$ the scattering matrix, $n(\omega)$ the Fermi distribution, and

$$G_0(x, \omega + i0) = \int_0^\infty \frac{e^{i\omega x}}{\omega + i0 - \varepsilon_k} dk$$

the retarded Green function for free particles. For a linear spectrum obviously, $G_0(x, \omega) = 0$ at $x < 0$, whence there is no addition to the density of free particles. Hence the absence of RKKY interaction. In other words, even the low-energy electrons do not stay in the impurity's vicinity, but their spin remains correlated for a long time with the impurity spin.

In a real situation, where the conduction band has a bottom, the density of the electron spin has a maximum at the center of the impurity with a width $r_0 = \varepsilon_F/k_F T_K$, and at $r \gg r_0$ falls off accord-

ing to the law [96]

$$\sigma(r) = \frac{1}{4\pi r^3} \frac{M(H)}{(g\mu_B)^2} \left\{ \cos 2k_F r - \frac{1}{2k_F r} \left[\sin 2k_F r + \frac{4\pi}{(g\mu_B)^2} \chi(H) \varepsilon_F \cos 2k_F r \right] + O(r^{-2}) \right\},$$

where $M(H)$ and $\chi(H)$ are the magnetic moment and susceptibility at $T = 0$.

It would be interesting to build a solution to the Anderson and exchange models with a bounded electron spectrum. Apparently, new ideas are required here, because the solutions presented are based on the assumption that only forward scattering is possible.

Among the methods used earlier in the study of the Kondo problem, Bethe's method proved to be the best suited. But the method is very sensitive to the quantity to be calculated. Thermodynamic functions are relatively easily calculated within the Bethe approach, but the situation is different for transport coefficients and dynamical characteristics of the system. The latter two types of quantities require calculating the Green function, but at present there are no mathematical tools to do this. Even calculating the matrix elements of one-particle operators encounters great difficulties. Progress in this field will be connected with a new mathematical apparatus. For this reason, at present only the transport coefficients that are simply connected with equilibrium quantities or the scattering phase are known. One such quantity is the impurity magnetic reluctance at $T = 0$ and arbitrary H . It is well known that

$$R(H) = R_0 \cos^2 \pi M(H)$$

(e.g. see [24f]).

At $H = 0$ the reluctance attains the unitary limit R_0 and drops as the field grows. The Kondo effect manifests itself in the increase of field strength aiding the current.

An important development in Bethe's method is the search for new separable S -matrices. For our problem it would be most interesting to have separable S -matrices that correspond to the various representations of the $O(3) \otimes O(3)$ group. Such scattering matrices would enable studying exchange Hamiltonians for rare-earth impurities.

The author wishes to express gratitude to A. I. Larkin, who introduced him to Bethe's method, to V. A. Fateev, B. M. Filev, and A. M. Tsvelik for their cooperation, to A. A. Abrikosov and L. P. Pitaevsky for their support, and to B. L. Altshuler, A. A. Belavin, S. A. Bulgadaev, A. A. Gogolin, V. N. Gribov, G. I. Dzhashaparidze, I. E. Dzyaloshinskii, M. I. D'yakonov, A. B. Zamolodchikov, Al. B. Zamolodchikov, V. Korepin, P. P. Kulish, I. B. Le-

vinson, S. V. Maleev, A. E. Meierovich, A. A. Nersesyan, S. B. Pokrovskii, L. A. Takhtadzhyan, D. I. Khomskii, D. E. Khmelnitskii, L. D. Faddeev, and A. M. Finkel'shtein for fruitful discussions.

References

1. C. Rizzuto, *Rep. Progr. Phys.* **37**, 147 (1974).
2. G. Grüner and A. Zawadowski, *Rep. Progr. Phys.* **37**, 1497 (1974).
3. G. Grüner, *Adv. in Phys.* **23**, 941 (1974).
4. G. Grüner and A. Zawadowski, in: *Progress in Low Temperature Physics* [ed. D.F. Brewer], Vol. 7B, North-Holland, Amsterdam (1978).
5. G. Barelus, W.H. Keesom, C.H. Johansson, and J.O. Linde, *Leiden Comm.* **217e** (1932).
6. A.D. Caplin and C. Rizzuto, *Phys. Rev. Lett.* **21**, 746 (1968).
7. J. Kondo, *Prog. Theor. Phys.* **32**, 37 (1964).
8. A.A. Abrikosov, *Physics* **2**, 5 (1965).
9. H. Suhl, *Physics* **2**, 39 (1965).
10. H. Suhl, *Phys. Rev.* **141**, 483 (1966).
11. A.A. Abrikosov and A.A. Migdal, *J. Low Temp. Phys.* **3**, 519 (1970).
12. M. Fowler and A. Zawadowski, *Solid State Commun.* **9**, 471 (1971).
13. Y. Nagaoka, *Phys. Rev.* **138A**, 1112 (1965); *Prog. Theor. Phys.* **41**, 586 (1969).
14. G. Yuval and P.W. Anderson, *Phys. Rev.* **B1**, 1522 (1970).
15. P.W. Anderson and G. Yuval, *J. Phys.* **C4**, 607 (1970).
16. P.W. Anderson, G. Yuval, and D.R. Hamann, *Phys. Rev.* **B1**, 4664 (1970).
17. K.G. Wilson, *Rev. Mod. Phys.* **47**, 773 (1975).
18. P. Nozieres, *J. Low Temp. Phys.* **17**, 31 (1974).
19. K.D. Schotte and U. Schotte, *Phys. Rev.* **B4**, 2228 (1971).
20. D. Mattis, *Phys. Rev. Lett.* **19**, 1478 (1967).
21. P.B. Wiegmann and A.M. Finkel'shtein, *Zh. Éksp. Teor. Fiz.* **75**, 204 (1978) [English transl.: *Sov. Phys.-JETP* **48**, 102 (1978)].
22. P. Lloyd and D.M. Cragg, *J. Phys.* **C12**, 3289 (1979); D.M. Cragg and P. Lloyd, *ibid.* **12**, 3301 (1979).
23. K. Yamada, *Prog. Theor. Phys.* **53**, 970 (1975); *ibid.* **54**, 316 (1975); K. Yosida and K. Yamada, *ibid.* **53**, 1286 (1975).
24. (a) G.J. van den Berg, in: *Progress in Low Temperature Physics* [ed. C.J. Gorter], Vol. 4, North-Holland, Amsterdam (1964), p. 194.
(b) A.J. Heeger, in: *Solid State Physics: Advances in Research and Applications* [eds. H. Ehrenreich, F. Seitz, and D. Turnbull], Vol. 23, Academic Press, New York (1969), p. 283.
(c) J. Kondo, *ibid.*, p. 183.
(d) K. Fischer, in: *Springer Tracts in Modern Physics*, Vol. 54 [ed. G. Höhler], Springer, Berlin (1970), p. 1.
(e) P.W. Anderson, *Comm. Solid State Phys.* **5**, 72 (1972).
(f) K. Yosida and A. Yoshimori, in: *Magnetic Properties of Metallic Alloys*, Volume 5 of *Magnetism: A Treatise on Modern Theory and Materials* [eds. G.T. Rado and H. Suhl], Academic Press, New York (1973), p. 253.
(g) M.D. Daybell, *ibid.*, p. 121.
(h) J. Flouquet, in: *Progress in Low Temperature Physics* [ed. D.F. Brewer], Vol. 7B, North-Holland, Amsterdam (1978), p. 649.
25. A.A. Ansel'm, *Zh. Éksp. Teor. Fiz.* **36**, 863 (1959).
26. A. Luther and V.J. Emery, *Phys. Rev. Lett.* **33**, 589 (1974).
27. P.B. Wiegmann, *Soviet Scientific Reviews* **B2**, 43 (1980).
28. K.D. Schotte, *Z. Physik* **230**, 99 (1970).
29. V.M. Filyov and P.B. Wiegmann, *Phys. Lett.* **A76**, 283 (1980).

30. P.B. Wiegmann, *Pis'ma Zh. Éksp. Teor. Fiz.* **31**, 392 (1980).
31. N. Andrei, *Phys. Rev. Lett.* **45**, 379 (1980).
32. P.B. Wiegmann, *J. Phys.* **C14**, 1463 (1981).
33. V.A. Fateev and P.B. Wiegmann, *Phys. Lett.* **A81**, 179 (1981).
34. P.B. Wiegmann, *Phys. Lett.* **A80**, 163 (1981).
35. A.M. Tsvelik and P.B. Wiegmann, *J. Phys.* **C15**, (1982), to be published; *Landau Institute Preprint* 1981-3 and LT-16; *Physica* **107B**, 379-LT-16 (1981).
36. V.M. Filyov, A.M. Tsvelik, and P.B. Wiegmann, *Phys. Lett.* **A81**, 115 (1981).
37. N. Andrei and J.H. Lowenstein, *Phys. Rev. Lett.* **46**, 356 (1981).
38. V.A. Fateev and P.B. Wiegmann, *Phys. Rev. Lett.* **46**, 1595 (1981).
39. H. Bethe, *Z. Physik* **71**, 205 (1934).
40. L. Hulthen, *Arkiv. Mat. Astron. Fysik* **26A**, No. 11 (1938).
41. R. Orbach, *Phys. Rev.* **112**, 309 (1958).
42. L.R. Walker, *Phys. Rev.* **116**, 1089 (1959).
43. R. Baxter, *Trans. Roy. Soc. (London)* **289**, 315 (1978).
44. A.B. Zamolodchikov and Al.B. Zamolodchikov, *Ann. Phys.* **120**, 253 (1979).
45. A.B. Zamolodchikov, *Sov. Sci. Rev: Phys. Rev.* **2**, 3 (1980).
46. E.K. Sklyanin, L.A. Takhtadzhyan, and L.D. Faddeev, *Teor. Mat. Fiz.* **40**, 194 (1979).
47. L.A. Takhtadzhyan and L.D. Faddeev, *Usp. Mat. Nauk* **34**, 13 (1979).
48. L.D. Faddeev, *Soviet Scientific Reviews* **C1**, 107 (1981).
49. H.B. Thacker, *Rev. Mod. Phys.* **53**, 253 (1981).
50. J.R. Schrieffer, *J. Appl. Phys.* **38**, 1143 (1967).
51. B. Coghlin and J.R. Schrieffer, *Phys. Rev.* **185**, 847 (1969).
52. P. Nozieres and A. Blandin, *J. Phys. (Paris)* **41**, 193 (1980).
53. P.W. Anderson, *Phys. Rev.* **124**, 41 (1961).
54. L. Mihaly and A. Zawadowski, *J. Phys. Lett. (Paris)* **39**, L483 (1978).
55. A.S. Edelstein, R.E. Majewski, and T.H. Blewitt, *Solid State Commun.* **23**, 593 (1977).
56. A.M. Clogston and P.W. Anderson, *Bull. Am. Phys. Soc.* **6**, 124 (1961); P.G. de Gennes, *J. Phys. (Paris)* **23**, 510 (1962); J. Kondo, *Prog. Theor. Phys.* **28**, 846 (1962).
57. J.R. Schrieffer and P. Wolf, *Phys. Rev.* **149**, 491 (1966).
58. D.M. Cragg, P. Lloyd, and P. Nozieres, *J. Phys.* **C13**, 803 (1980).
59. I. Okada and K. Yosida, *Prog. Theor. Phys.* **49**, 1483 (1973).
60. B. Cornut and B. Coghlin, *Phys. Rev.* **B5**, 4541 (1972).
61. W. Felsch, *Physica* **86-88B**, 501, ICM-76 (1977).
62. K. Winzer and K. Samwer, in: *Low Temperature Physics, LT-14*, Vol. 3, Plenum Press, New York (1975), p. 430.
63. E. Lieb and W. Liniger, *Phys. Rev.* **130**, 1605 (1963); *ibid.*, p. 1616.
64. M. Flicker and E. Lieb, *Phys. Rev.* **161**, 179 (1967).
65. J.B. McGuire, *J. Math. Phys.* **5**, 622 (1964).
66. M. Gaudin, *Phys. Lett.* **A24**, 55 (1967).
67. M. Gaudin, thesis (unpublished), University of Paris (1967).
68. C.N. Yang, *Phys. Rev. Lett.* **19**, 1312 (1967).
69. P.P. Kulish and E.K. Sklyanin, *Zap. Nauchn. Sem., Leningrad Branch of Steklov Institute of Mathematics*, **95**, 129 (1980).
70. R.I. Baxter, *Ann. Phys.* **70**, 193 (1972).
71. R.I. Baxter, *ibid.*, p. 323.
72. A.A. Belavin, *Phys. Lett.* **B87**, 117 (1979).
73. E.K. Sklyanin and L.D. Faddeev, *Dokl. Akad. Nauk SSSR* **243**, 1430 (1978).
74. E.K. Sklyanin, *Dokl. Akad. Nauk SSSR* **244**, 1337 (1978).

4. An Exact Solution of the Kondo Problem

75. H.B. Thacker and D. Wilkinson, *Phys. Rev. D* **19**, 3660 (1979).
76. E.K. Sklyanin, *Zap. Nauchn. Sem., Leningrad Branch of Steklov Institute of Mathematics*, **95**, 55 (1980).
77. L.A. Takhtadzhyan, *ibid.* **101**, 121 (1980).
78. A. Zamolodchikov, *Commun. Math. Phys.* **69**, 165 (1979).
79. A.B. Zamolodchikov and V.A. Fateev (unpublished).
80. P.A. Schlottmann, *J. Phys. (Paris)* **39**, CG-1486 (1978).
81. N. Andrei and J.H. Lowenstein, *Phys. Rev. Lett.* **43**, 1698 (1979).
82. C.N. Yang and C.P. Yang, *J. Math. Phys.* **10**, 1115 (1969).
83. M. Gaudin, *Phys. Rev. Lett.* **21**, 1301 (1971).
84. J. Johnson and B. McGoy, *Phys. Rev. A* **6**, 1613 (1971).
85. M. Takahashi, *Prog. Theor. Phys.* **46**, 401 (1971).
86. M. Takahashi, *ibid.*, **50**, 1519 (1973).
87. M. Takahashi and M. Suzuki, *ibid.*, **48**, 2187 (1972).
88. C.N. Yang and C.P. Yang, *Phys. Rev.* **150**, 327 (1966).
89. M.G. Krein, *Usp. Mat. Nauk* **13**, 3 (1962) [English transl.: *Am. Math. Soc. Transl., Series 2*, **22**, 163 (1962)].
90. B. Sutherland, *Phys. Rev. Lett.* **20**, 98 (1967).
91. A. Arinstein, *Phys. Lett.* **B95**, 280 (1980).
92. P.P. Kulish and N.Yu. Reshetikhin, *Zh. Éksp. Teor. Fiz.* **80**, 215 (1981).
93. M. Takahashi, *Prog. Theor. Phys.* **52**, 108 (1974).
94. V.A. Fateev and P.B. Wiegmann (unpublished).
95. N. Kawakami and A. Okiji, *Phys. Lett.* **A86**, 483 (1982).
96. H. Ishii, *Prog. Theor. Phys.* **55**, 1373 (1976).

Author Index

- Aarts, J., 129
 Abragam, A., 66, 217, 235, 237
 Abrikosov, A. A., 235, 241, 277, 311
 Adams, E. D., 67
 Alascio, B., 127f
 Aligia, A., 128
 Allen, A. R., 67
 Allen, J. W., 128
 Allub, R., 128
 Al'tshuler, B. L., 126, 130, 167, 235f
 Anderson, P. W., 81, 126ff, 130, 235, 237, 242, 244, 311f
 Andreev, A. F., 45, 67, 68
 Andrei, N., 277, 312f
 Andres, K., 236f
 Andrianov, A. V., 237
 Andronikashvili, E. L., 69
 Ansel'm, A. A., 311
 Appelbaum, J., 236
 Archie, C. N., 67
 Arinstein, A., 313
 Aronov, A. G., 126, 130, 167, 235f
 Aslamazov, L. G., 236
 Avignone, M., 127
 Avilov, V. V., 66
 Axe, J. D., 128

 Babkin, A., 53f, 57, 68, 69
 Bakalyar, D. M., 67
 Balibar, S., 68
 Bannai, E., 128
 Barabanov, A. F., 127f
 Barelius, G., 311
 Baxter, R. I., 261f, 270, 312
 Belavin, A. A., 277, 312
 Bermon, S., 236
 Bernard, W., 237
 Bethe, H., 244, 257, 277, 312
 Bhatt, R., 237
 Birgenau, R. J., 128
 Birr, G. L., 235
 Bishop, D. J., 236
 Blandin, A., 245f, 251, 312
 Blewitt, T. H., 312
 Blokhin, S. M., 127
 Bogachev, E. N., 206, 237
 Bogoliubov, N. N., 236
 Brandow, B. H., 129
 Bredl, C. D., 129
 Brewer, D. F., 311
 Brinkman, Wm., 40, 68, 127
 Britton, C. V., 67
 Bronevoy, I. L., 236
 Bruysenzaede, Y., 236
 Burton, W. K., 55
 Buschow, K. W. H., 128

 Cardona, M., 128
 Castaing, B., 42, 55, 68
 Chapellier, M., 67
 Chaudhari, P., 236
 Cherkov, A. A., 43, 68
 Chester, G. V., 68
 Chudnovskii, F. A., 127
 Clark, W. G., 67
 Clogston, A. M., 312
 Cochran, B. W., 236
 Cogblin, B., 245, 254, 312
 Cornut, B., 254, 312
 Cragg, D. M., 251, 292, 311f
 Croft, M., 128
 Cyrot, M., 128

 Dahm, A. J., 68
 Davies, R. A., 236
 Davis, E. A., 235
 Daybell, M. D., 311
 de Boer, J., 66
 de Dominicis, C. T., 87, 128
 de Gennes, P. G., 236, 312
 Delrien, J. M., 66f
 Deutscher, G., 236
 Deville, G., 48
 Dingle, R. B., 206, 237
 Dodson, B. W., 237
 Dolan, G. J., 236
 Doniach, S., 128
 Druzhinin, A. A., 91, 119, 127f
 Dyakonov, M. I., 235
 Dynes, R. C., 168, 236f
 Dyson, F., 237
 Dzyaloshinskii, I. E., 68, 235

 Edelstein, A. S., 312
 Efros, A. L., 160, 236
 Ehrenreich, H., 66f, 311
 Emery, V. J., 311
 Entel, P., 93, 128
 Esel'son, B. N., 17, 35, 67
 Esheby, J., 67

 Faddeev, L. D., 312
 Falicov, L. M., 78, 80, 127
 Farberovich, O. B., 127
 Fateev, V. A., 252, 312f
 Ferrell, R. A., 68
 Feynman, R. P., 237
 Fil'kov, V. M., 127, 311f
 Fisher, D. S., 67
 Fischer, K., 311
 Fischer, M. E., 237
 Flerov, V. N., 115, 128
 Fleisch, W., 312
 Flicker, M., 312
 Flouquet, J., 311
- Cabrera, B., 55, 68
 Caplin, A. D., 311

Author Index

- Fowler, M., 311
 Fraass, B. A., 68
 Franciosi, A., 128
 Frank, F. C., 68
 Franz, W., 129
 Freeman, A. J., 127
 Frey, A., 128
 Frossati, G., 67
 Fujita, T., 128
 Fukarawa, H., 237
 Fukuyama, H., 236
- Gachechiladze, I. A., 69
 Garber, M. C., 66
 Garno, J. P., 68, 236
 Gaudin, M., 257, 277, 279, 312f
 Garwin, R. L., 66
 Ghatak, S. K., 127
 Gilson, W., 236
 Giordano, N., 236
 Godfrin, H., 67
 Gogadze, G. A., 206, 237
 Gonsalves Da Silva, C. E. J., 127
 Goodkind, J. M., 67
 Gorkov, L. P., 235
 Gorter, C. L., 311
 Gredeksul, S. A., 68
 Greenbeg, A. S., 30, 67
 Grewe, N., 93, 128
 Grigor'ev, V. N., 17, 35, 67
 Gross, M. C., 67
 Grüner, G., 128, 311
 Güntherodt, G., 120
 Gschneider, Jr., K. A., 126
 Guyer, R. A., 11, 28, 66, 67, 68
- Habermeier, H. V., 236
 Hagström, S. B., 128
 Hajdane, F. D. M., 83, 109, 127f
 Halperin, W. P., 67
 Hamann, D. R., 242, 244, 311
 Harris, A. B., 237
 Harris, I. R., 128, 221, 236
 Hatton, J., 66
 Heald, S. M., 68
 Heeger, A. J., 311
 Heine, V., 128
 Heritier, H., 68
 Herring, C., 127
 Hetherington, J. H., 33, 66ff
 Hewson, A. C., 87, 128
 Hibbs, A. R., 237
 Hikami, S., 235
 Hiki, Y., 69
 Hirst, L. L., 128
 Hirth, J. P., 68
 Holtzberg, F., 128
 Houghton, A., 237
 Huang, W., 67
 Hubbard, J., 73, 107, 127
 Hulthen, L., 244, 312
 Hwang, Y. C., 67
- Ionov, A. N., 236
 Iordanskii, S. V., 48, 66, 68
 Ishii, H., 311
 Ivchenko, E. L., 237
 Izmailyan, N. Sh., 127
- Johansson, L. I., 128
 Johnson, J., 277, 313
 Jullien, R., 113, 128
- Ragan, Yu., 21, 31, 48, 67f
 Kaplan, T. A., 127
 Kasuya, T., 128
 Katz, M. J., 237
 Kaveh, M., 236
 Kawabata, A., 203, 236
 Kawaguchi, Y., 236f
 Kawaji, S., 236f
 Kawakami, N., 313
 Keesom, W. H., 311
 Keldysh, L. V., 84, 127, 237
 Kenway, R. D., 237
 Keshishev, K. O., 34, 53f, 57, 68f
 Khmel'nitskii, D. I., 126, 130, 235
 Khomskii, D. I., 84, 126ff
 Kikoin, K. A., 115, 127f
 Kimball, J. C., 78, 80, 127
 King, E., 128
 Kirk, W. P., 66
 Kirzhnits, D. A., 129
 Kitahara, H., 237
 Klingner, M. I., 24, 31, 67
 Kocharyan, A. N., 84, 127f
 Koelling, D. D., 127
 Kondo, J., 240f, 311f
 Kondratenko, P. S., 68
 Kopaev, Yu. V., 84, 127, 139
 Kozyrev, S. V., 237
 Krein, M. G., 313
 Krishna-Murthi, H. R., 109, 128
 Krivogla, M. A., 68
 Kulik, I. O., 235
 Kulish, P. P., 312f
 Kummer, R. B., 67
 Kuper, C. G., 68
- Lacroix, C., 128
 Laloe, F., 42, 68
 Landau, J., 68
 Landau, L. D., 43f, 47, 66, 67, 68, 126
 Landesman, A., 66ff
 Larkin, A. I., 126, 130, 235f
 Laroche, C., 68
 Lawrence, J. M., 126, 128
 Leder, H. J., 89, 93, 127f
 Lederer, P., 68
 Lee, J. A., 128
 Lee, P. A., 235f
 Leggett, A. J., 68
 Levchenko, V. S., 68
 Lhuillier, C., 42, 68
 Liccardello, D. C., 237
 Lieb, E., 128, 257, 277, 312
 Lieke, W., 129
 Liffle, W. A., 237
 Lifshitz, E. M., 66, 67, 68, 236
 Lifshits, I. M., 48, 68
 Linde, J. O., 311
 Liniger, W., 257, 277, 312
 Lipson, S. G., 68
 Lloyd, P., 251, 292, 311f
 Loethe, J., 69
 Lopez, A., 127
 Lowenstein, J. H., 312f
 Lubensky, T., 221, 237
 Luther, A., 311
- Jackson, K. A., 43, 68
 Jevicki, A., 237
 Johansson, C. H., 311
- Maattenen, L. M., 68
 Mahan, G. D., 128

- Mahanti, S. D., 127
 Majewski, R. E., 312
 Maksimov, L. A., 21, 31, 67, 127
 Marchenko, V. I., 68
 Martin, R. M., 113, 128
 Marty, D., 68
 Mattis, D., 242, 288, 311
 McGoy, B., 277, 313
 McGuire, J. B., 257, 312
 McMahan, A. K., 66
 McMillan, W. L., 169, 236f
 Meierovich, A. E., 67f
 Melik-Shakhnazarov, V. A., 69
 Merlin, R., 128
 Meschede, D., 129
 Meyer, H., 66
 Mezhev-Deglin, L. P., 68
 Migdal, A. A., 311
 Mihaly, L., 246, 312
 Mikheev, V. A., 17, 23, 35, 67
 Mikhin, N. P., 67
 Mineev, V. P., 68
 Mizuquchi, K., 237
 Mochel, J., 169, 236f
 Mook, H. A., 128
 Motizuki, K., 128
 Mott, N. F., 73, 107, 126f, 235
 Müller-Krumbhaar, H., 68
 Mueller, R. M., 67
 Müschlegel, B., 127
 Mulhern, J. E., 237
 Mullin, W. J., 28, 66f
- Nagaev, E. L., 68
 Nagaoka, A., 40, 68
 Nagaoka, N., 235
 Nagaoka, Y., 242, 311
 Naskidashvili, I. A., 69
 Nasledov, D. N., 237
 News, D. M., 101, 127
 Newson, A. C., 101, 127
 Nicklow, R. M., 128
 Nosanow, L. H., 66
 Nozieres, P., 42, 55, 68, 87, 112, 128, 242f, 245f, 251, 292, 311f
- Obrach, R., 312
 Okada, I., 312
 Okiji, A., 313
 Olmedo, C. F. E., 127
 Orbach, R., 244
 Osgood, E. B., 66
 Osheroff, D. D., 67, 236
 Ovchinnikov, Yu. N., 235
 Ovnyanyan, P. S., 127f
- Paderno, Yu. B., 127
 Parks, R. D., 126, 237
 Penney, T., 128
 Pepper, M., 236
 Perel, G. E., 235
 Petukhov, B. V., 48, 66, 68
 Pfenty, P., 128
 Pickett, W. E., 127
 Peierls, R., 73
 Pikus, G. E., 235, 237
 Pitaevsky, L. P., 236
 Pokrovskii, V. L., 48, 66, 68
 Polyakov, A. M., 213, 237
 Polyanskaya, G. A., 237
 Pope, J., 30, 67
 Prewitt, T. C., 67
 Prober, D. E., 236
- Pruisken, A. M. M., 237
 Pushkarov, D. I., 23, 67
- Rado, G. T., 311
 Ramakrishnan, R., 235, 237
 Ramirez, R., 80, 127
 Rasulov, R. Ya., 237
 Reich, H. A., 66
 Reshetikhin, N. Yu., 313
 Rice, T. M., 40, 68, 127
 Richards, M. G., 17, 27, 30, 66f
 Richardson, R. C., 31, 66f
 Riseborough, P. S., 87, 126, 128
 Rizzuto, C., 311
 Roberts, M., 129
 Robinson, J. M., 126
 Roger, M., 66f
 Rosenbaum, T. F., 236f
 Rotar, 205
 Roth, H., 237
 Rowel, J. M., 236
 Rukhadze, A. A., 235
 Rushussen, F. B., 67
- Sacco, J. E., 28, 67
 Sadovskii, M. V., 126
 Sai-Halasz, G. A., 68
 Sakurai, A., 127
 Samwer, K., 312
 Sasaki, W., 204, 237
 Schaefer, L., 237
 Schafer, H., 129
 Schlottmann, P., 86f, 127f
 Schotte, K. D., 243f, 311
 Schotte, U., 243, 311
 Schrieffer, J. R., 127, 245, 312
 Seitz, F., 66, 67, 311
 Shafer, M. W., 128
 Shal'nikov, A. I., 34, 68
 Shapiro, S. M., 96, 128
 Sharvin, D. Yu., 237
 Sharvin, Yu. V., 237
 Sherrington, D., 128
 Shil'shtein, A. A., 128
 Shirokov, D. V., 236
 Shklovsky, B. I., 160, 236
 Shul'man, Y. E., 17, 67
 Silin, V. P., 235
 Simmons, R. O., 68
 Sklyanin, E. K., 312f
 Smith, J. H., 67
 Smith, T. F., 128
 Smoluchowski, R., 126
 So, C. K., 236
 Somenkov, V. A., 128
 Spivak, B. Z., 237
 Steglich, F., 129
 Stewens, K. W. H., 129
 Straub, W., 237
 Strom-Olsen, J. O., 236
 Sugiyama, K., 236
 Suhl, H., 241, 311
 Sullivan, N., 68
 Sutherland, B., 313
 Suzuki, H., 69
 Suzuki, M., 277, 313
- Takahashi, M., 277, 313
 Takegahara, K., 128
 Takhtadzhyan, L. A., 312f
 Tanaka, T., 128
 Thacker, H. B., 312f

Author Index

- Thomas, G. A., 236f
Thomblison, W. C., 31, 67
Thompson, R., 236
Thouless, D. J., 66, 235
Thouloure, D., 67
Tofts, P. S., 67
Tolmachov, V. V., 236
Tsui, D. C., 236
Tsuruoka, F., 69
Tselik, A. M., 127f, 312
Tsymbalenko, V. L., 69
Turnbull, D., 66, 67, 311
- Uren, M. J., 160, 236
- Vainstein, E. E., 127
Vaks, V. G., 126
van Daal, H. J., 128
van den Berg, G. J., 311
van den Dries, L., 236
Van Haesendouck, G., 236
Varlamov, A. A., 236
Varma, C. M., 66, 74, 126, 128
Vonsovskii, S. V., 127
- Walker, L. R., 244, 312
Weaver, J. H., 128
Weeks, J. D., 68
Wegner, F., 237
Widom, A., 17, 28, 30, 67
Wiegmann, P. B., 127f, 252, 311f
Wigner, E., 73, 127
Wilkins, J. M., 66, 128
- Wilkinson, D., 313
Wilks, J., 67
Willard, F. D. C., 66
Williams, F. I. B., 68
Wilson, K. G., 128, 237, 242f, 311
Winter, J. M., 67
Winzer, K., 312
Wolf, P., 312
Wolff, P. A., 127
Wu, F. Y., 128
- Yamada, K., 243, 311
Yamanouchi, C., 237
Yamashita, Y., 67
Yang, C. N., 257, 261, 270, 277, 31
Yang, C. P., 277, 313
Yaroshetskii, I. D., 237
Yefetov, K. B., 235
Yemelyanenko, O. V., 237
Yoshimori, A., 311
Yosida, K., 67, 243, 311f
Yu, W. N., 66
Yuval, G., 242, 244, 311
- Zaitsev, P. O., 127
Zakharchenya, B. P., 127
Zamolodchikov, Al. B., 312f
Zane, L. I., 66f
Zawadowski, A., 128, 246, 311f
Zel'dovich, Ya. B., 73, 116, 126
Zharkov, 74
Zinichik, Yu. S., 237
Zuckermann, M. J., 236

Subject Index

- Anderson lattice, 109ff, 117ff
- approximation
 - Born, 132f
 - Hartree-Fock, 115
 - Heitler-London, 72
 - Hubbard, 83
 - ladder, 138, 176
 - mean-field (MFA), 79ff, 91, 95, 99f, 103
 - generalized, 88
 - strong-binding, 31, 113
 - weakly non-ideal gas, 157
 - ARM, 199, 204, 212f, 225
- Bethe Ansatz, 244, 257, 259, 277
- for s-d exchange model, 264f
- Bloch waves, 72, 75
- Bose crystals, 38
- coefficient(s),
 - Clebsch-Gordan, 253
 - damping, 53
 - Slater, 246
- conditions, periodic boundary, 269
- conductivity,
 - Drude, 224
 - Hall, 187f
 - of interacting electrons, 170ff, 232
 - Mott minimal metallic, 222
 - quantum corrections, 199f
 - temperature dependence, 176, 179ff
- constant,
 - Coulomb coupling, 177
 - electron-electron scattering, 158
- Cooper channel, 136, 166, 175f, 208f
- Cooper diagrams, 192
- cooperon, 134, 136, 138f, 141f, 148f, 157, 197, 199, 206
- in external field, 229f
- Cooper pole(s), 157, 161, 226
- Cooper propagator, 176
- correction to conductivity,
 - Aslamazov-Larkin, 176
 - Hartree, 182f
 - localization, 199
 - Maki-Thompson, 151, 176, 187, 197ff, 203f, 212
- correlation(s),
 - electron-electron, 160ff
 - Coulomb gap, 160
- cross-section, of vacancy-impurity inelastic scattering, 34, 36
- coupling,
 - strong, 288ff
 - weak, 288ff
- crystal faceting, critical temperature, 60
- crystal-liquid interface, 42f
- crystal-liquid phase equilibrium, 42
- crystallization, 48ff
- crystallization waves, 51f
- delocalization,
 - of dislocations, 64ff
 - of particles, 12, 14
- diagrams,
 - Feynman, 136
 - ladder, 154
 - Maki-Thompson, 175
 - parquet, 241
 - Young, 302
- diagrammatic technique,
 - Keldysh, 226
 - Matsubara, 227
- dielectric,
 - Anderson (AD), 224
 - classical (CD), 223
 - Mott-Hubbard, 116
- diffusion,
 - of isotopic impurities, 35
 - spin, 17
 - of strongly interacting impurities, 17
 - thermoactivation, 20, 33f
- diffusion coefficient, 15, 17ff, 34, 155, 219, 224
- dependence on impurities, 17
- kink, 65
- temperature dependence, 22f
- disordered solids, 41
- distribution equilibrium, 282ff
- drift velocity, 36f
- effect,
 - Aharonov-Bohm, 206ff, 225
 - coherent, 130ff
 - suppression of, 146ff
 - excitonic, 84, 123
 - Hall, 108, 130, 186ff
 - for interacting electrons, 189f
 - for noninteracting electrons, 188f
 - Kondo, 71, 75, 124, 166, 244, 254, 292, 308f
 - local,
 - excitonic, 99
 - polaron, 99f, 123
 - nearest-neighbor blocking, 104
 - Pomeranchuk, 42
- electron-electron collision time, 151f
- electron localization, 213ff
- Anderson, 213
- energy
 - characteristic interaction, 12, 16
 - Hund interaction, 249
- EPT, 77, 79, 89ff
- equation(s),
 - Bethe, 275ff, 283, 301, 308f
 - Boltzmann, 21f
 - diffusion, 142
 - factorization (triangle), 257f, 270
 - Gell-Mann-Low, 216, 256, 300
 - Laplace, 52
 - renormalization group, 216
 - Schrodinger, 265f, 268

- equation(s),
 - self-consistency, 90, 93
 - state, 97
 - Wiener-Hopf, 294, 305
- excitonic correlations, 117ff
- faceting transitions in crystals, 55
- factor, Landé, 304
- Fermi crystals, 39
- Fermi liquid, 51, 53, 106ff, 110, 122, 124f, 151, 160, 293
- Fermi-liquid renormalization, 130
- Fermi surface, 51
- fluctuations, 55
- formula, Drude, 131f, 134
- free electron gas, 284ff
- function, Gell-Mann-Low, 218
- graphs,
 - Feynman, 188
 - Hartree-type, 173f
- ground-state energy, 11
- Hall coefficient, correction to, 191
- Hall current, 187
- Hamiltonian,
 - Anderson, 245ff, 253
 - effective exchange, 248ff, 263ff
- Hartree term, 164
- homogeneous strain, 91f
- Hubbard model, 40
- Hund rule, 247f, 250ff
- hybridization,
 - excitonic, 92
 - f-s, 70, 89, 91
- hybridization amplitude, angular dependence, 246f
- impuritons (mass fluctuation waves), 14ff
 - one-dimensional, 24ff
 - two-dimensional, 24ff
- impuriton gas, 15
- impuriton-impuriton scattering cross section, 15f
- impurity thermodynamics, 290ff
- insulator, excitonic, 117
- interaction,
 - Coulomb f-s, 92f, 119, 123
 - electron-electron, 101, 104, 130
 - electron-impurity, 137f, 151ff, 208
 - electron-lattice, 91ff, 119
 - electron-phonon, 91, 94, 102
 - exchange, 14
 - antiferromagnetic, 242
 - ferromagnetic, 241
 - exciton-exciton, 122
 - Hartree, 174
 - Hund, 246
 - phonon-impuriton, 20ff
 - RKKY, 75, 78, 308
 - Ruderman-Kittel, 119
 - via short-wave phonons, 102ff
- interaction Hamiltonian, 17f, 78
- interaction potential, retarded electron-electron, 153
- interaction radius, 15f
- kink,
 - band width, 46
 - isolated, 46
 - localized, 46
 - quasimomentum, 65
- kink-kink interaction radius, 65
- Kondo impurity, 110f, 117
- Kondo lattice, 106, 109ff, 117
- Kondo problem, exact solution, 238ff, 242
- Kondo spin compensation, 78
- Kondo temperature, 78, 109, 238, 241, 242, 252, 254, 308
- law,
 - Curie, 238
 - Curie-Weiss, 106
 - Gauss δ -correlated, 132
 - Gaussian, 13
 - of mass conservation, 52
- Lindemann criterion of melting, 120
- liquid helium, 41
- local (excitonic) correlations, 84ff, 88f
- localization of electrons, 72ff
 - in magnetic field, 222ff
 - in one and three dimensions, 219ff
 - in percolating structures, 223ff
- magnetic semiconductors, 41
- magnetic susceptibility, 242, 293
 - at $T=0$, 303
- magnetoconductivity, 223
 - effect of spin-orbit scattering, 199ff
- magnetoresistance,
 - anomalous (AMS), 191ff
 - in many-valley semiconductors, 197f
 - of non-interacting electrons, 191
 - and scattering by superconducting fluctuations, 196
 - in thin films and wires, 194ff
- Matsubara energy, 161
- Matsubara frequency, 176f, 232
- McDonald function, 208
- melting, 48ff
- method,
 - Baxter, 261
 - Bethe, 257ff, 261ff
 - Gennes, 194
 - iterative, 297f
 - NMR, 17
 - quantum, of inverse scattering problem 272
 - renormalization group, 109, 111, 219
 - strong binding, 37
 - X-ray scattering, 39
- mixed valence (MV), 70ff, 91
- mixed-valence phase, 76f
- mixed-valence state, 105ff
- model,
 - Anderson, 78, 109, 243f, 245ff, 301, 311
 - asymmetric, 77, 124
 - lattice, 78, 89
 - Anderson-Falikov, 117
 - exchange, 301ff
 - excitonic-insulator, 112
 - Falikov-Kimball, 77, 80ff, 85, 87, 95, 99, 111
 - Heisenberg one-dimensional, 276, 299
 - Hubbard, 74, 112f, 115
 - impurity (local), 79, 87, 89, 92, 94f
 - Ising, 103
 - isolated impurity, 117, 124
 - jellium, 73
 - Kondo, 77, 86, 109, 111f
 - n-fold degenerate exchange, 252f
 - periodic, 87, 89ff, 94
 - s-d exchange, 239f, 242, 244, 251, 252, 257, 263, 292, 301, 309
 - Bethe equations, 270, 277f
 - thermodynamics, 275ff
 - spinless, 89
 - two-level, 87ff, 97, 99, 103
- Mott insulators, 72

- nesting, 74
- nucleus production, 48
 - probability, 50
- Nyquist noise, 160, 186
- orbital singlet, 250f
- order parameter, 74
- parameter, quantum de Boer, 12f
- phase transitions
 - Anderson, 70
 - electronic (EPT), 70ff
 - in rare-earth compounds, 75ff
 - ferroelectric, 70
 - insulator-insulator, 90
- phase transitions,
 - isostructural, 70
 - Mott metal-insulator, 70
 - valence, 70, 97ff
- phonon distribution function, 22
- phonon-impuriton scattering cross section, 21
- polaron band narrowing, 99
- polaron shift, 102
- principle, Yoffe-Regel-Mott, 130
- pseudofermions, 277
- Q-Hamiltonian, 214
- quantum corrections to conductivity, 130ff, 134ff, 142, 144ff
- quantum crystals, 11ff, 45
- quantum effects in crystals, 12ff
- quantum tunneling, 31
- quasimomentum, 18
- rapidity, 26
- relation,
 - cooperon-current, 226f
 - Einstein, 134, 170, 220
- rotons, 51
- Ruderman-Kittel exchange, 112
- spatial correlations, 119ff
- spatial ordering, 71
- spin-flip, 14
- spin-flip, 137
- spin scattering, 137
- stability criterion, 60
- superconducting fluctuations, 176ff
- superconductivity, 71
- supercrystallization, 42
- superfluidity, 38
- supermelting, 42
- surface phenomena, 42ff
- symmetry axis,
 - 4-fold, 61ff
 - 6-fold, 60ff
- technique, impurity diagrammatic, 131f
- theorem,
 - Luttinger, 114
 - Nernst, 122
- theory,
 - Drude, 183
 - of excitonic insulators, 86
 - Landau,
 - of Fermi liquids, 243
 - of phase transitions, 56, 61
 - mean-field, 221
 - perturbation, 254f, 297f
 - scaling, 214
- thermodynamic potential, 58
- thermodynamic relations, 58
- transformation,
 - canonic Schrieffer-Wolf, 250, 253
- transition(s),
 - discontinuous, 95
- in insulator-metal (Mott-Hubbard), 72ff
 - 75, 114ff, 119
 - Mott, 73f
 - valence, 80, 114ff
- tunneling conductivity, 167f
- tunneling integral, 73
- tunneling probability, 13
- universality, 287f
- vacancies,
 - in ^3He crystals, 40
 - in ^4He crystals, 32ff
 - zero-point, 37f
- valencedensity wave (VDW), 103
- Wigner crystal, 107, 120ff, 126
- Wigner crystallization, 71, 120
- zero-bias anomalies, 166

ERRATUM

p. 283, formula (4.4.39) instead of $\ln (1+e)^{-}$
 read $\ln (1+e^{-\varepsilon_n/T})$